This project has received funding from the European Union's Horizon 2020 research and innovation programme under the Marie Sklodowska-Curie grant agreement No 722642

An investigation into the mechanisms underlying the Plant Growth Promoting Properties of *G. diazotrophicus*

Michele Pallucchini

Thesis submitted to the University of Nottingham for the degree of Doctor of Philosophy

The University of Nottingham

Division of Plant Sciences

School of Biosciences

Sutton Bonington Campus

Loughborough, LE12 5RD, UK

July 2023

Contents

1. ABSTRACT 5
2. INTRODUCTION 7
2.1. Overuse of nitrogen fertilizers and sustainable alternatives 7
2.2. Non-nodulating diazotrophic bacteria as biostimulants 10
2.3. Inoculation methods 14
2.4. Gluconacetobacter diazotrophicus, a versatile PGPB 19
2.5. Nitrogen metabolism of *G. diazotrophicus* 22
AIMS 29
3. MATERIALS AND METHODS 30
3.1. Media preparation for bacterial cultures 30
3.2. Strains and growth conditions 31
3.3. Electroporation 32
3.4 Biparental mating 33
3.5. Seed sanitation 33
3.6. Bacterial inocula preparation for hydroponic systems or seed coating 34
3.7. Plant growth and bacterial inoculation in hydroponic systems 34
3.7.1. Tomato 35
3.7.2. Rice 35
3.8. Bacterial re-isolation from treated plants 36
3.9. Evaluation of $^{15}N/^{14}N$ incorporation 36
3.10. Seed coating, MS agar and glasshouse growth conditions 37
3.11. Histochemical GUS assay 38
3.12. Microscopy and image analysis 38
3.13. Protoplast isolation 39
3.14. Callus culture 39
3.15. qPCR analyses 40
3.16. RT-qPCR analyses 41
3.17. Primers table 41
3.18. Salkowski's test for IAA detection 42
3.19. Statistical testing 43
4. RESULTS AND DISCUSSION 44
4.1 Plant growth promotion evaluation 44
4.1.1 PGP evaluation in tomato plants inoculated with *G. diazotrophicus* 45
4.1.1a Rationale and former G. diazotrophicus inoculation attempts 45

4.1.1b Seed coating and in soil growth induced a cultivar and formulation dependent PGP effect....48
4.1.1c Hydroponic systems provided a highly controllable setup and revealed an enhanced PGP in WT-inoculated plants compared to the BNF-impaired mutant....62
4.1.1d Evaluation of BNF contribution to the PGP could not detect significant incorporation of N2 into treated plants....76
4.1.2 PGP evaluation in rice plants inoculated with *G. diazotrophicus*....80
4.1.2a Rationale and former G. diazotrophicus inoculation attempts....80
4.1.2b Seed coating and in soil growth induced a PGP effect dependent on the bacterial load, carbon source and inoculation duration....82
4.1.2c Hydroponically grown rice exhibited PGP when treated with G. diazotrophicus WT through either seed coating, direct inoculum in NS or seedling dipping, especially under N-replete conditions....90
4.1.3 PGP evaluation in *A. thaliana* inoculated with *G. diazotrophicus*....98
4.2 Mutants and mutagenesis tools creation....115
4.2.1 Electroporation optimisation and expression vector selection....119
4.2.1a pBBR1MCS-5_GFP plasmid characterisation and testing for *in planta* detection....120
4.2.1b Generation of pICH47751_DsRed plasmid and derivative expression vectors....127
4.2.1c Electroporation and media optimisation....137
4.2.2 Conjugation and genomic integration for reporter genes expression....145
4.2.2a Conjugation as a transformation tool and application to *G. diazotrophicus*....145
4.2.2a pRGS561 characterisation and *GGG* creation for *in planta* detection....148
4.2.2b Conjugation optimisation for reporter genes integration....156
4.2.2c nifHDK reporter genes integration....169
4.2.2d Tn5 mutagenesis to find negative regulator of BNF....174
4.2.3 CRISPR/Cas9 for G*. diazotrophicus* mutagenesis....177
4.2.3a Native CRISPR/Cas I-C system *in silico* characterisation....180
4.2.3b Native CRISPR/Cas II-C system *in silico* characterisation....186
4.2.3c Transient CRISPR/Cas9 system development....193
4.2.3d Future prospective for Native CRISPR/Cas system in *G. Diazotrophicus*....202
4.3 Colonisation imaging....209
4.3.1 Colonisation imaging in tomato and *A. thaliana*....210
4.3.1a Tomato and *A. thaliana* colonisation in MS agar setup....212

4.3.1b Tomato inoculation in hydroponic setup - Root colonisation 226
4.3.1c Tomato inoculation in hydroponic setup - Shoot colonisation 243
4.3.1d Tomato colonisation in hydroponic setup - bacterial quantification by qPCR 248
4.3.1e Foliar application 251
4.3.2 Colonisation imaging in rice and colonisation model 255
4.3.2a Rice colonisation in hydroponic setup - Root 256
4.3.2b Rice colonisation in hydroponic setup – Shoot 264
4.3.3 *G. diazotrophicus* colonisation model and additional considerations 269
4.3.4 Cytoplasmic invasion in protoplast and callus systems 287
4.4 PGP metabolism investigation and engineering 292
4.4.1 Colonisation establishment 294
4.4.2 Nitrogen metabolism 302
4.4.3 IAA production and PGP metabolism overview 323
4.4.4 PGP engineering 333
5. CONCLUSIONS AND FUTURE PERSPECTIVES 337
6. ACKNOWLEDGEMENTS 343
7. REFERENCES 344

1. ABSTRACT

The indiscriminate use of synthetic nitrogen fertilisers to support intensive farming in the last decades has been one of the leading causes of soil degradation, greenhouse gases emission, eutrophication and ecosystem unbalance. Plant growth promoting bacteria (PGPB) have the potential to alleviate this environmental damage by providing a more sustainable alternative for enhancing crop productivity, but require careful optimisation as their physiology remain elusive. In this study, the PGP activity of the non-nodule forming diazotroph *Gluconacetobacter diazotrophicus* was assessed in monocot and dicot systems through the comparison of different inoculation strategies and experimental setups. In particular, two of the main contributors to the PGP capability of this bacterium, i.e., nitrogen fixation and hormonal production, were investigated through the use of mutants and gene expression analyses, and were further evaluated in relationship to the bacterial colonisation dynamic under different nutrient conditions. The study unveiled a multifaceted root invasion strategy, encompassing root hair colonisation, crack entry, and the ability for intracellular invasion and cytoplasmic transmission, followed by the migration into the shoot through xylem vessels and the occupation of stomata and trichomes. A complex and delicate balance between bacterial PGP factors and the carbon and nitrogen metabolism was uncovered. The presence of ammonium in the system had a negative impact on the PGP effect, while the lack of a nitrogen source highlighted the beneficial bacterial stimulation, although the bacterium itself was not sufficient for normal plant development. Bacterial genes responsible for hormonal production were expressed during early symbiosis stages in the root system of plants grown in nitrogen-replete conditions; as time progressed, nitrogen fixation genes were upregulated, primarily in the aerial parts of the plant, while the bacterial genes conferring protection against the plant's immune response were switched off as the symbiosis established. The introduction of an external carbon source enhanced the expression of nitrogen fixation genes *in planta*. These findings may have a potential implication on the application strategies in agricultural

settings. Furthermore, novel tools for genetic manipulation and metabolic engineering of *Gluconacetobacter diazotrophicus* are described.

2. INTRODUCTION

2.1. Overuse of nitrogen fertilizers and sustainable alternatives

The evolution and application of technology in agricultural systems has been the driving force of human development throughout the centuries, shifting the layout of societies worldwide from primary to tertiary sector-based economies with as low as 1% of the population being currently employed in agriculture in the most advanced countries [1] [2]. However, the technological breakthroughs which made such a progress possible, have also opened the way to an increasing land consumption and anthropogenic pressure on aquatic and terrestrial ecosystems, with deleterious impact on the environment; over the last decades, agricultural practices have been considered one of the primary causes of soil degradation and biodiversity loss [3].

Nitrogen (N), as one of the most important elements in biological systems and a limiting nutrient for higher plants, plays a major role in the ability to exploit the full potential of agriculture [4].

In nature, nitrogen is mostly found in the form of the nonreactive diatomic gas dinitrogen (N_2) - which forms about 78% of Earth atmosphere. However, the strength of the triple bond characterizing the elemental nitrogen, makes energetically demanding its conversion in other nitrogen-based chemically and biologically reactive species (N_r) [5].

At industrial level, the transformation of N_2 into N_r, or nitrogen fixation, is mainly obtained through the Nobel Prize-winning Haber-Bosh process; this method allows to directly synthesise ammonia (NH_3) by reacting atmospheric dinitrogen with hydrogen (H_2) using a metal catalyst under high temperatures and pressures [6]. The process, discovered in 1909 and largely relying on fossil fuels as energy source ever since, is nowadays responsible for 1.2% of CO_2 emission worldwide and consumes around 2% of the global primary energy supply [6] [7] [8]. As of 2018, the Haber process produced 230 Tg year $^{-1}$ of ammonia [9]; at least 80% of it is used in the production of agricultural

fertilisers, the global consumption of which is around 108 Tg year $^{-1}$ [7] [10]. Strikingly, recent studies estimated that around 80% of the nitrogen in the average human body originally derived from the Haber-Bosch process [11].

In nature, N_2 is converted to N_r biotically or, to a lesser extent, abiotically. The abiotic N_2 conversion route consists in the reaction with oxygen under high heat conditions, typically powered by lightning, volcanoes and biomass burning, and is estimated to account for less than 10 Tg N_r year $^{-1}$[12]. To the larger extent, however, it is the microbial activity to be responsible for the reduction of N_2 to the soluble nontoxic cation ammonium (NH_4^+) through a process known as biological nitrogen fixation (BNF) [13]. This process is carried out by the activity of the nitrogenase enzymatic complex, and is thought to be exclusively performed by bacteria and archaea (mostly methanogens) [11]. Before the nitrogen cycle modification of the industrial era, BNF was estimated to create 90-195 Tg N_r year^{-1} on land and 200-300 Tg N_r year $^{-1}$ in the oceans by the action of cyanobacteria, for a total production of 300-500 BNF-associated Tg N_r year $^{-1}$ [11].

The biosphere has evolved over the millennia by relying on the limited amount of nitrogen provided by this natural process; however, the colossal increase of human associated N_r creation (accounting for 165 Tg year $^{-1}$, mostly in the form of NH_3 for agricultural applications [11]), has doubled the total annual input of N_r into global terrestrial ecosystems [14]. This had a significant impact on the natural nitrogen cycle and detrimental effects on the environment, posing a threat to human health and food security.

On one hand, the cheap ammonia synthesis and the consequent ten-fold increase of nitrogen fertilisers usage over the last century - along with other technological achievements of the “Green revolution” - have dramatically enhanced agricultural productivity: crop yield has increased up to 50%, with one hectare of arable land supporting 4.3 persons in 2008, against 1.9 persons in 1908 [7] [10].

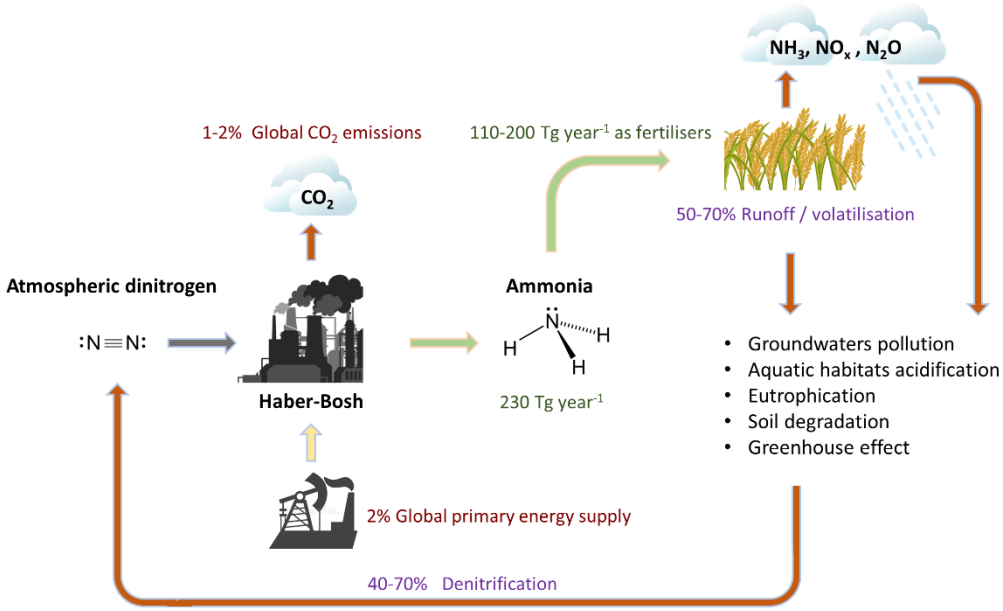


Fig. 2.1. Simplified representation of the anthropogenic nitrogen cycle.

On the other hand, only 30 [15] to 50% of the applied N_r is estimated to be taken up by crops [14]. Being highly mobile, the rest of the excess N_r (in particular nitrates) escapes into the environment through leaching (with 60 Tg N_r $year^{-1}$ estimated to runoff in oceans [16]), volatilisation (involving 30% of the applied NH_3 [17]) and animal waste. Eventually, 40 to 70% of the escaped N_r is denitrified back to unreactive atmospheric N_2, highlighting an extremely low nitrogen-use efficiency and the waste of about 1% of the global energy supply [7] [18][11].

Moreover, NH_3 and nitrogen oxides (NO_x) emitted from agricultural systems (as well as from fossil fuel combustion) and released in the atmosphere, act as potent greenhouse gases, increasing radiative forcing in the troposphere through the photochemical production of ozone, smog and particulate matter [19] [18]. In particular, nitrous oxide (N_2O, known as laughing gas), which is mostly emitted during microbial denitrification of nitrate runoff from agricultural systems, has 300 times the global warming potential of CO_2, and is the most impactful greenhouse gas after carbon dioxide and methane [20]. In addition to concurring in the climate change crisis, these molecules have a direct toxicity effect on both humans and crops [21].

Atmospheric N_r, along with nitrate (NO_3)-based mineral fertilisers leaching from agricultural applications, cascades in nitrogen-limited ecosystems and accumulate in groundwater, surface water and soil [10]. This causes the acidification of aquatic habitats, along with costal eutrophication and the consequent emergence of "dead zones", i.e. hypoxic or anoxic areas in the ocean and surface water that suffer from profound reduction in biodiversity (see the case of hypoxia in the Gulf of Mexico due to nitrogen runoff in the Mississippi river drainage [22]). Similarly, on land, soils undergo acidification and degradation [21].

Historically, in addition to the environmental damage, the economic importance of nitrogen proved to have the potential to escalate in dramatic social turmoil, as in the case of the War of the Pacific in 1879 between Chile, Bolivia and Peru, broken out over a series of guano deposits tax disputes [23]. More recently, the severe price increase of chemical fertilisers (+78% in 2021 [24]) in consequence of global trade instability aggravated by events such as the 2022 Russian invasion of Ukraine (with Russia and Belarus supplying more than 20% of the world's fertilisers), exposed the fragility of a N_r production chain that depends deeply on natural gas-derived energy and can be affected by geopolitical factors [25].

To mitigate the noxious impact that the overuse of chemical fertilisers, along with other intensive agricultural practices characteristic of the "Anthropocene era" [26], are having on the environment, while at the same time being able to increase by 56% the food production required to feed a population projected to reach 10 billion by 2050 [27], alternative strategies are needed.

Among the most promising approaches for an integrated and sustainable agriculture development, biostimulants are increasingly emerging as a subject of research interest [28].

2.2. Non-nodulating diazotrophic bacteria as biostimulants

Bacteria capable of preforming BNF (diazotrophs) have been used as natural occurring enhancers of crop productivity since the beginning of the agricultural

practice itself. Broadly speaking, they are classified as Plant Growth-Promoting Bacteria or Microorganisms (PGPB/M), an expression that refers to a diverse group of microorganisms that establish symbiotic relationships with plants without eliciting pathogenic effects, leading to improved plant nutrition and health [29]. These bacteria, archaea and fungi inhabit the rhizosphere (rhizobacteria or rhizospheric bacteria), the aerial parts (phyllospheric bacteria) and the seed, and can establish themselves on the surface (associative PGPB or epiphytes) or in the interior (endophytes) of plant tissues [30] [31].

Historically, most research efforts have been devoted to studying symbiotic interactions between legumes (or *Parasponia* species) and nitrogen-fixing bacteria from the Rhizobia group, thanks to the formation of macroscopic nodules in plant roots which have facilitated their isolation and subsequent investigations. These specialised organs supply the rhizobial bacteroids with carbohydrates and other nutrients, and produce the oxygen-carrying phytoglobin leghemoglobin to restrict oxygen flow, which inhibits BNF [32]. The legume-rhizobia symbiotic systems coevolved around 60-70 Mya [33] based on a much older and less specific signalling mechanism developed by symbiotic arbuscular mycorrhizal fungi in the Early Devonian period around 400 Mya [34] [35]. Fascinatingly, the last common genetic toolkit for symbiotic establishment, also involved in eukaryogenesis, seems to include a Type IVB secretion system, possibly dating back as far as 1.9 Bya [36]. Similarly to rhizobia, diazotrophic actinomycetes of the genus *Frankia* establish symbiotic associations with the so-called actinorhizal plants via nodule formation, although they usually do not produce the Nod factors that in rhizobia are instrumental for the chemical crosstalk leading to plant invasion and nodule formation [37].

In parallel to these highly efficient symbiotic nitrogen-fixation systems, other types of non-nodular symbioses, more enigmatic and challenging to investigate due to their lower short-term impact in plant nutrition and more discreet interaction dynamics, have been progressively discovered in both associative/endophytic and free-living diazotrophic bacteria [38]. Some of these non-nodulating diazotrophs, similarly to *Rhizobia* and *Frankia*, establish a mutualistic relationship with a limited number of hosts which they coevolved

with. For instance, nitrogen-fixing cyanobacteria from the genus *Nostoc* (but also *Anabaena*, *Trichormus*, *Calothrix* and *Chlorogloeopsis*) can colonise intracellularly plants from the Gunneraceae family, or extracellularly various species of liverworts, hornworts, *Azolla* and Cycadaceae [39]. The mutualism between diazotrophic cyanobacteria and plants or algae represents the most widespread N-fixing symbiosis [39].

On the other hand, diazotrophs from genera including *Acetobacter*, *Azoarcus*, *Azospirillum*, *Azotobacter*, *Bacillus*, *Burkholderia*, *Enterobacter*, *Herbasprillum*, *Glucenobacter*, *Gluconacetobacter*, and *Pseudomonas* (notably, all Gram-negative except for *Bacillus*) form associative and/or endophytic relationships with a wide variety of plants [38]. In these symbioses, plants provide an ecological niche rich in carbon-based nutrients and compatible with BNF, in exchange for fixed ammonia and other bacterial derived metabolites [38]. Members of the *Poaceae* family, including rice, maize, wheat, and sugarcane can derive a substantial part of their nitrogen from associative and endophytic diazotrophs [35] [40]. The colonisation establishment of these non-nodulating bacteria has never been fully elucidated, but it is known that the rhizosphere hosts the greatest abundance (10^5-10^8 cells per root gram) and diversity of microorganism compared to aboveground organs (10^3-10^4 cells per shoot gram) [41]. In symbiotic *Azoarcus* species, the colonisation process starts by chemotaxis toward root exudates via type IV pili and twitching motility [42]. In rhizobia, *A. brasilense* and *H. seropedicae* species, this step is mediated by flavonoid chemoattractants [43]. Non-rhizobial PGPB colonise root epidermis, root hair and secondary root emergence sites, aided by the secretion of extracellular polymeric substance, lipopolysaccharides and rhamnose to promote biofilm formation, stress resistance, chemical signalling and root adhesion [35]; once inside the root, thanks to the production of plant cell wall-degrading enzymes, some species can reach and move through the plant's vascular system, enabling the invasion of various above-ground organs, including stems, leaves, and flowers [41], [44], [45].

The inoculation of PGPB usually elicits a significant immune response in the host during early colonisation stages, which microbes evade by modulating the

plant's defence mechanisms through a still elusive process [46]. Conflict between host and guest is common in all symbiotic relationships; interestingly, in the symbiosis between *Paramecium bursaria* and the green algae *Chlorella*, this contrast is managed via RNA–RNA interactions, in a mechanism termed "RNAi collisions" that is mediated by specific RNAi factors and suggests a previously overlooked level of regulation [47].

The interactions between PGPBs and plants are multifaceted and mediated by a range of mechanisms which results in increased biomass production and fruit yield. In addition to nitrogen fixation, another pivotal function exerted by PGPM is the production of plant growth-regulating hormones such as auxins, cytokinins, gibberellins, NO and ACC (1-aminocyclopropane-1-carboxylate) deaminase activity for promoting plant growth by lowering ethylene levels; other PGP activities include solubilisation and uptake of phosphates, production of siderophores for iron uptake, synthesis of vitamins (thiamine, biotin, riboflavin, niacin), osmotic adjustment, stomatal regulation, changes in phospholipid content in the cell membranes, resistance against abiotic stresses like drought, salt, oxidation and heavy metal pollution, and induction of systemic resistance against phytopathogens [45], [48], [49] [50].

Crucially, carefully selected PGPB can be cheap and easy to self-produce and apply as biostimulants, potentially allowing developing countries to alleviate their dependency from more expensive and energy consuming agricultural technologies often monopolised by first world nations. Biostimulants are defined by the EU Regulation 2019/1009 as "products stimulating plant nutrition processes independently of the product's nutrient content with the sole aim of improving one or more of the following characteristics of the plant or the plant rhizosphere: nutrient use efficiency, tolerance to abiotic stress, quality traits, availability of confined nutrients in soil or rhizosphere" [51].

However, the efficacy of PGPM when applied as biostimulants can be greatly influenced by various factors, including environmental conditions, plant genotype, and microbial community dynamics [38], [52]. For instance, it was observed that the "hybrid vigour" effect typical of hybrid maize cultivars was strongly dependent on the genotype-specific recruitment and establishment of

rhizospheric PGPB communities from the soil [53]. In fact, bacterial symbiotic or associative relationships exists with virtually any living organism, from protists to mammals, but the crucial role that they play ultimately responds to the laws of community ecology theory, including ecological niche compatibility, inter/intraspecific competition, and predator-prey populations cycles [54]. This apparently trivial statement underlies an inherent limit in forcing functional symbiosis in non-native hosts. Furthermore, it must be emphasised that the introduction of non-native microbial species and the modification of crops rhizosphere in field or natural habitats, have the potential for negative environmental consequences that are hard to predict, but have already been observed [55], [56]. Therefore, ongoing research aims to explore the potential of specific PGPB strains and their interactions with different plant species, with the goal of optimising their use in agricultural and environmental management strategies [52]. Furthermore, the concurrent coordination with a regulatory and legislative framework is essential to ensure a scientifically sound approach [57].

One of the ultimate goals of this research field is the engineering of crops and PGP diazotrophs in order to establish highly efficient artificial symbiotic associations that provide substantial amount of nitrogen and modulate the metabolic composition of plants [52]. While the road is still long due to the complexity and diversity of the molecular mechanisms that control symbiotic nitrogen fixation [52], the knowledge gained from basic research in plant-bacterial interactions can serve as a basis for these long-term efforts and open new avenues for achieving such goal.

2.3. Inoculation methods

While the identification of bacteria with PGP potential has been rapidly expanding thanks to the combination of traditional approaches and metagenomics analyses, their efficient application as bioinoculants to crops still poses a non-trivial challenge. When using microbial inoculants, especially in field conditions, a poor survival rate is usually the limiting factor for a

successful establishment of the beneficial symbiosis [58]. Notably, the delivery of a threshold number (that differs among species) of viable bacteria cells in good physiological conditions is key for the effectiveness of the inoculum [59]. For this reason, it is crucial to optimise both the application method and the formulation in which the bacterium is handled and delivered to its crop target. The formulation is the process of manufacturing the final product, the "inoculant", by incorporating the PGPM in a "carrier", i.e., a substrate capable of supporting and promoting the bacterial survival and providing protection against biotic and abiotic threats [60]. The main causes of the rapid bacteria population decline observed for most inoculants in traditional agricultural systems are 1) external: the complexity of the soil environment, where the inoculated PGPM usually face the competition with native microorganisms and pathogens better adapted to the local ecological niche, and may encounter water stress, salinity, nutrient-poor zones, temperature shocks and high pollutant levels [61], and 2) internal: poor carrier choice and/or suboptimal formulation.

The formulation of a valid inoculant should consider both manufacturers' and farmers' interests, and meet as much as possible the following criteria: 1) prolonging the survival of the PGPM long enough for it to exert a biologically significant effect on the targeted crop; 2) being nontoxic and non-polluting, with a low carbon footprint and no negative impact on the native microflora and microfauna of the application site; 3) being easy to manufacture and compatible with routine field practices and equipment; 4) relying upon the upstream selection of a strain (or a combination of strains) suitable for the specific crop and environment on which the inoculant will be applied, also taking into consideration strain specific parameters such as the optimal growth phase of the PGPM culture when mixing it with the carrier; 5) using a carrier with the appropriate chemical and physical properties [60].

The most common carriers for inoculants can be classified in: 1) Inorganic substrates and inert soils. These were among the first to be utilised, and include coal, lignite, clays, talc, perlite, vermiculite and, more recently, synthetic polymers. 2) Organic carriers. "Nitragin", the first inoculant to be ever commercialised, in 1896, was initially using gelatine as carrier, replaced

shortly after by a nutrient medium, and finally by peat, which rapidly become the most common substrate up until the 1990s [61]. Being rich in organic matter it was considered a valid nutrient source for the PGPB, and was routinely added with 10% sucrose to help bacterial adhesion [62] and, later, amended with vermiculite or charcoal [63]; however, it was eventually discontinued because of the environmental implication of the peat bogs exploitation. From the 1980s, peat alternatives, often trying to recycle industrial waste, started being explored; some examples include coco peat, higher in water holding capability, animal manure, earthworm compost, compost from cork industry, sugarcane bagasse, sawdust, olive mill wastewater, lignin from Kraft pulping process (validated for *A. Vinelandii* inoculation), and banana waste (used for co-inoculation of *Azotobacter* and *Azospirillum* spp.) [64]. All these methods, although valid in laboratory conditions, are difficult to scale up for bigger industrial productions due to the limited availability of the carriers. 3) Carrier-less lyophilised microbial cultures. Removing intracellular water reduces the metabolic activity of the inoculant, therefore increasing the product lifetime, but implies high production costs and a careful evaluation of the suitable rehydration protocol. 4) Liquid carriers. This formulation is the evolution of the older "no formulation" option, which simply consisted in keeping the selected PGPM in its growth medium. The method was later improved by resuspending the microbial culture in water-based solutions amended with nutrients and chemicals to improve stickiness, stability, protection and to confer surfactant proprieties [65]. Among the advantages of the liquid state inoculants compared to the other carrier types (mostly formulated in slurry, granular or powdered form [66]) are: being suitable for cost effective sterilisation procedures, which are considered to be critical for the long term survival of the inoculant; being easy to formulate with a high cell count [67]; being compatible with machinery such as seed augers, and reportedly being more effective in field than peat.

Other emerging methods for inoculant application involve the bioencapsulation of live microorganisms in slowly biodegradable polymeric matrices, such as alginate or calcium chloride; this provides shelter to the microorganisms and gradually release them in the soil or seedbed, where the bioencapsulated

PGPM are usually directly applied in the form of granules or micro and macro beads [60]. Another inoculation method, often favoured by both farmers and the PGPM industry for its practicality, is the seed inoculation, or "seed coating", which is usually coupled with liquid inoculants. In this technique seeds are dipped in or sprayed with the inoculant, dried, and finally sowed. To improve the survival of the microorganisms, sucrose is typically added, along with adhesive agents such as gum Arabic or carboxymethyl cellulose, and, when required, calcium carbonate to balance soil acidity [68]. This method is convenient because a limited amount of inoculant is needed to treat a large number of seeds, and is compatible with other practices such as spraying the inoculant on germinated shoots ("foliar application", [69]). When seed coating is coupled with liquid inoculants, it is sometimes referred to as "biopriming", since it combines the application of PGPM and the advantages of seed priming. Seed priming is a practice known since the ancient Greece [70] which nowadays consists in the imbibition of the seeds in water or chemicals such as hormones and nutrients prior to their sowing, to prime the germination and activate a subset of biochemical processes in the seed; subsequentially, seeds are re-dried before the emergence of the radicle, and this procedure ensure a higher and more homogeneous germination rate, along with enhanced resistance to biotic and abiotic stress of the seeds after germination [71]. The main drawback of the seed coating or biopriming inoculation technique is the limited amount of the inoculant exposed to the seed surface, especially for small seeds; moreover, the thin layer of inoculant enclosing the seed must rely on the effectiveness of the adhesive agents not to be lifted out during sowing and germination.

A way to overcome the intrinsic criticalities of bioinoculants coupled with in soil growing, is the employment of hydroponic systems. Hydroponic farming is believed to be dating back as early as the Hanging Gardens of Babylon in 600 BCE [72], but was confined to academic research and was not commercially widespread until, in early 1900s, the work of William Frederick Gericke pointed out its promising application in the horticultural sector [73]. Hydroponic farming is now regarded as indoor high-tech controlled environment agriculture, which gives to farmers higher controls over

environmental variables [74]. It is a soil-less method of growing plants in inert substrates or artificial supports in which nutrients are delivered through a water based nutrient solution (NS), and provides several advantages over traditional farming: faster growth times due to greater availability of the nutrient in the NS and optimised artificial light systems, up to 90% less water consumption, lower fertilisers use and higher yield, along with the independence from soil and climate geographical characteristics [75]. While all 17 elements essential for plant growth are routinely supplied as inorganic nutrients in the NS, the integration of PGPM in such systems is increasingly being investigated for their potential to alleviate some of the main drawback of hydroponics, such as biotic stress from pathogens recirculating in water, and to increase yield. An extensive review about the application of PGPM to hydroponic systems was done by Stegelmeier et al. [75], who reported numerous examples of how the main advantages of bioinoculants application were also found in hydroponic farming. Notably, the direct inoculation of the inoculant in the NS circumvents some of the main seed coating drawbacks by providing a consistent amount of PGPM in contact with the root system and offering a controlled and stable medium devoid of the stressors and microbial competitors found in soil [75]. Recently, as soils were found to be more important than plant genotype in shaping the microbiome, a metagenomic study on hydroponically grown tomato reported a lower microbial diversity compared to in-soil cultivation [76], also suggesting that bioinoculants made with PGPB isolated from soil are not always suitable for this type of farming. Interestingly, due to their practicality, controllability, and higher yield per unit area, hydroponic horticultures are being investigated by the space industry as promising on-site food source in bioregenerative life support systems for the future deep space missions; even in this context, PGPB inoculants are pointed out as one of the best strategies to relieve the nutritional stress of plants grown in micro-gravity environment by enriching their nutrient uptake and availability [77].

2.4. Gluconacetobacter diazotrophicus, a versatile PGPB

Between 1960 and 1980, a major interest in identifying symbiotic diazotrophs had arisen in the context of sugarcane plantations in Brazil, after it was pointed out how the intensive cropping, traditionally carried out with modest N fertilisation and followed by the removal of plant biomass at each harvest, did not result in the decline in yield or in soil nitrogen content as expected [78]. This nitrogen input-output unbalance, together with various ^{15}N-aided N incorporation studies [78] [79] and the isolation of diazotrophic bacteria from the rhizosphere of sugarcane (mostly from the genus *Beijerinckia* [80]), led to the conclusion the BNF was responsible for the surprisingly high productivity of this crop [81] [82].

In 1987, Cavalcante and Dobereiner described a new N_2-fixing bacterium associated with roots and stems of sugarcane plants collected in various regions of Brazil, which was identified as one of the main actors in sugarcane nutrition [83]. Originally classified as *Saccharobacter nitrocaptans* and later *Saccharobacter nitrobacter*, this bacterium was recognised as a Gram-negative, aerobic species, described as straight rods about 0.7 x 2 µM, motile by 1 to 3 lateral flagella [83]. Other particularly interesting features included: 1) the nitrogenase activity was not inhibited by nitrate due to the lack of a nitrate reductase, indicating the potential for application in highly fertilised soils; 2) the maximum nitrogenase activity occurred under 10% sucrose at 30 °C, but persisted in the presence of up to 1 g L^{-1} yeast extract, at pH levels of 3 or below, and under up to 30% sucrose and 10 mM NH_4 [84]; 3) sucrose was preferred as a carbon source, but glucose, fructose and galactose were also used, as well as 1% mannitol, glycerol and ethanol (the latter being oxidized to acetic acid); 4) 10^3 to 10^7 CFUs g^{-1} were isolated between the rhizosphere and the shoots, but no isolation was obtained from soil, indicating this bacterium as an obligate associative organism [83]. Later studies reclassified *Saccharobacter nitrocaptans* as *Acetobacter diazotrophicus* from the *Acetobacteraceae* family (*alpha proteobacteria*), sub-genus "*Gluconoacetobacter*", which had been recently made to contain the Acetobacters with ubiquinone Q10; the sub-genus was elevated to genus in

1997 [85] and renamed *Gluconacetobacter* [86]. *Gluconacetobacter diazotrophicus* was the first nitrogen fixing Acetobacteraceae species described and is the only species in this family employed in agricultural applications [87].

The Acetobacteraceae family comprises, to date, 46 validly published genera [88], among which, ten genera form the acetic acid bacteria (AAB) clade [89]. AAB are mesophilic obligate aerobes that can oxidize sugars, sugar alcohols, and ethanol at low pH, with acetic acid as the major product. In nature they occur in sugar- and alcohol-enriched environments, and are industrially involved in the production of vinegar (mainly *Acetobacter* and *Gluconacetobacter* genera), cocoa and kombucha [89]. Only 11 species from the Acetobacteraceae family are known for nitrogen fixation capabilities, among which 9 species are AAB belonging to the genera *Gluconacetobacter* (*G. diazotrophicus*, *G. johannae* and G. *azotocaptans*), *Acetobacter*, *Asaia* and *Swaminathania*.

Following its isolation from sugarcane and characterisation, *G. diazotrophicus* was isolated from many other hosts and locations, such as *Pennisetum purpureum* cv. Cameroon [90], sweet potatoes [91], sugarcane plantations in Australia [92] [93], Coffea arabica [94], millet [95], Ananas comosus [96], rice [97] and more, for a total of at least 19 plant species from 15 plant families [98]. Such extensive range of hosts suggested a versatile colonisation mechanism and highlighted the potential for utilising this bacterium as a PGPB in crops.

During 1990s and early 2000s, *G. diazotrophicus* was therefore extensively investigated and tested in many possible hosts (see section 4.1), mostly for its nitrogen fixation capability. In addition to BNF, other PGP properties emerged, including phosphate solubilisation capability [99], gibberellins and auxin production [100], [101], resistance to drought [102], and more uncommon features such as the production of betalain, which is recognised as a unique occurrence in microbiology and is mediated a novel dioxygenase enzyme previously believed to be restricted to plants and fungi [103].

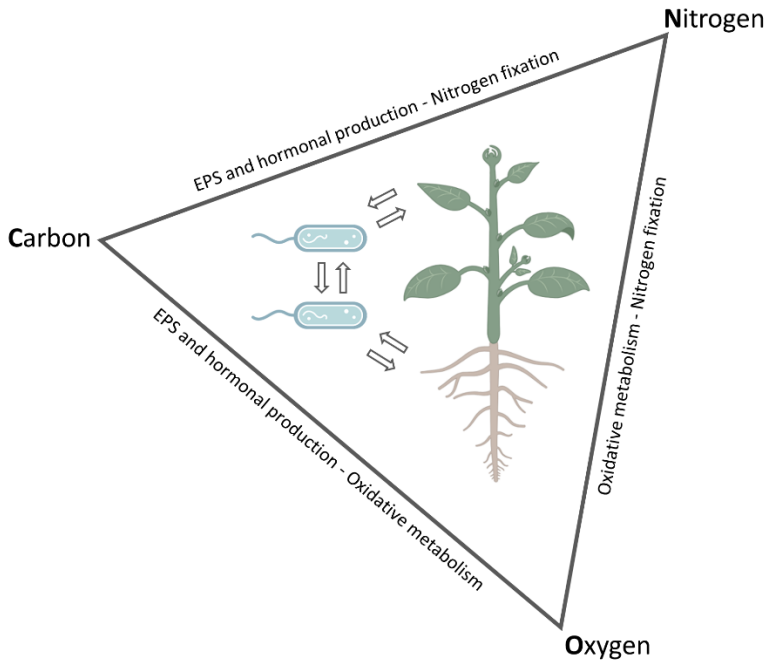


Fig. 2.2. Graphical abstract depicting the interrelation of foundational physiological traits that shape the interactions between G. diazotrophicus and its plant hosts, indicating the main pillars on which past and future research will need to focus in order to fully characterise this bacterium and unlock its full potential as a biostimulant. Arrows represent the occurrence of chemical signalling.

In the metabolic landscape of *G. diazotrophicus*, two pivotal enzymes play a crucial role: the levansucrase and the pyrroloquinoline quinone-linked glucose dehydrogenase (PQQ-GDH). Levansucrase, a fructosyltransferase exoenzyme, compensates for the bacterium's inability to transport sucrose intracellularly by hydrolysing this sugar in the extracellular space, producing glucose for the oxidative metabolism; furthermore, it polymerises fructoses into fructooligosaccharides and levan, providing a mucilaginous coating which is essential for biofilm formation, colonisation, oxidative stress protection and tolerance to desiccation and NaCl [104]–[107].

PQQ-GDH is responsible for the oxidation of glucose to gluconic acid in the extracellular space. It acts as a primary energy producer during nitrogen-fixing conditions, providing the consistent energy needed for dinitrogen conversion by the nitrogenase enzyme [108], [109]. In fact, the nitrogenase enzyme is oxygen labile, but while aerobic diazotrophs like *G. diazotrophicus* require ATP and reductants from aerobic respiration to sustain its activity, they cannot

benefit from nodule formation to limit oxygen flow. In solid and semi-solid medium, this bacterium was reported to be able to grow on N_2 as the sole nitrogen source at up to 20 kPa pO2, relying on the combination of ROS scavenging activity [110], enhanced respiration rates [111] and physical protection by mucilaginous coating [112] to prevent oxidative damage. The pivotal points of *G. diazotrophicus'* physiology in symbiotic systems (Fig. 2.2) include carbon metabolism, nitrogen metabolism and oxidative metabolism, all equally contributing to shaping bacteria-bacteria and plant-bacteria signalling and interactions.

In 1993, Fuentes-Ramirez isolated 18 strains of *G. diazotrophicus* from roots and, particularly, apical stems of sugarcane from Mexico plantations [100] [113]. One of these strains, named UAP5541, was tested by the University of Nottingham and further sub-cultured until the isolation of a new strain, named AZ0019, which was used in this study. The main objective of this work was to elucidate the role of nitrogen metabolism in the colonisation and PGP properties of *G. diazotrophicus*, although carbon metabolism and hormonal production were also taken into account.

2.5. Nitrogen metabolism of *G. diazotrophicus*

To date, a comprehensive understanding of the nitrogen metabolism of *G. diazotrophicus* is still lacking. Thus, shedding light into this pivotal node of the bacterium's physiology implicates the comparison with other related diazotrophs. Identifying unique traits in the nitrogen metabolism of *G. diazotrophicus* could be crucial for optimising growth conditions in agricultural settings and, ultimately, fostering the beneficial mutualistic interaction.

Bacteria, including diazotrophs, can take up and utilise nitrogen in various forms to support their growth, including biomolecules such as amino acids, nucleotides, and urea; however, most of these molecules are ultimately decomposed in aerobic environments by the combined action of microbial

communities (e.g. the bacterial genera *Clostridium*, *Proteus*, *Pseudomonas* and *Bacillus*) through the sequential activity of proteinases, peptidases, decarboxylase and deaminase or urease to finally yield ammonium (NH_4^+) in a process named ammonification or mineralisation [114]. Alternatively, ammonium is produced by BNF or by dissimilatory nitrate reduction to ammonium (DNRA), a process by which, in anaerobic environments such as the upper layers of marine sediments, prokaryotes like benthic sulphur bacteria (but also fungi and diatoms) use nitrite as an electron acceptor in place of oxygen, reducing it to ammonium [115], [116]. Ammonium, being the simplest form of bioavailable nitrogen, is the primary and preferred nitrogen source for bacterial growth in most habitats and, in contrast to plants, is minimally toxic at molar concentrations [117]. It is exchanged as a building block during amino acids synthesis and is central in the nitrogen metabolism regulation [114]. At low NH_4^+/NH_3 concentrations, the uptake of this molecule is enhanced by upregulating dedicated ammonium channels (named AmtB in *E. coli* and NrgA in *B. subtilis*) which are usually cotranscribed with the regulatory protein GlnK At increasing NH_4^+/NH_3 concentrations, *amtB*/*nrgA* are downregulated since ammonia can diffuse freely through biological membranes [118] (Fig. 2.3b). Once imported, ammonium is incorporated into keto acids from glycolysis and TCA cycle to form glutamate (Glu) and glutamine (Gln). At increasing ammonium levels, the enzyme glutamate dehydrogenase (GDH) consumes reducing power to incorporate one molecule of ammonium in the TCA intermediate 2-oxoglutarate (2-OG) (Fig. 2.3a), a central molecule that connects carbon and nitrogen metabolism; this mechanism has been also observed in *G. diazotrophicus* [119]. Glutamate serves as nitrogen storage unit and act as ammonium donor or intermediate during the synthesis of other amino acids and various metabolite such as GABA, which is involved in acid and oxidative stress response [120]. Then, a second molecule of ammonium is incorporated in glutamate by the enzyme glutamine synthetase (GS), encoded by the gene *glnA*, which has been characterised in *G. diazotrophicus* [121] (Fig. 2.3a). GS activity is coupled with the glutamate synthase, also called glutamine-2-oxoglutarate-amido transferase (GOGAT), which uses the amide group of glutamine to reductively aminate 2-OG, generating two molecules of glutamate [122] (Fig. 2.3a).

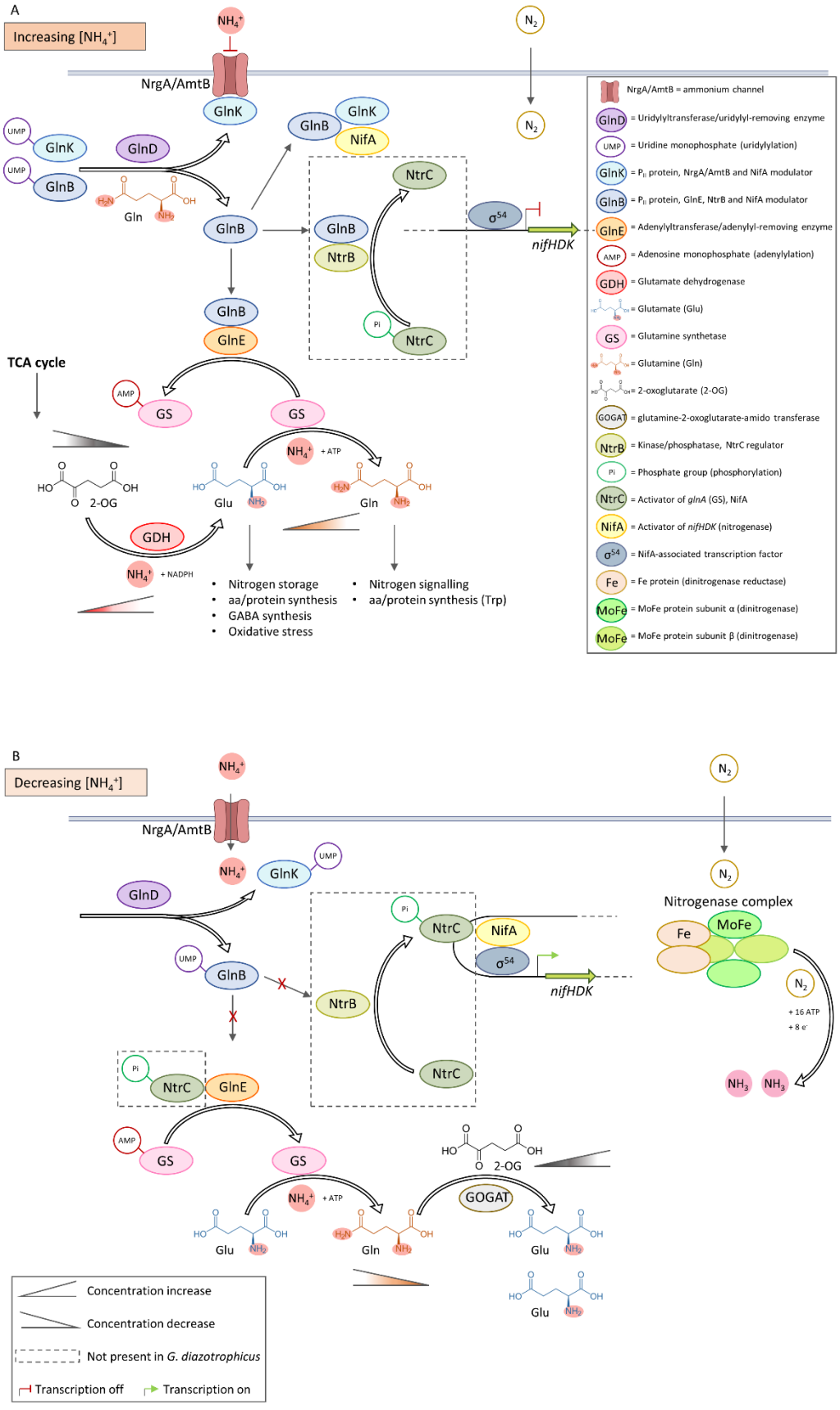


Fig. 2.3. Simplified representation of proposed G. diazotrophicus' nitrogen metabolism regulation, based on the available literature and integrated with data from phylogenetically close diazotrophs. ***(A)*** *At increasing ammonium levels, glutamate dehydrogenase (GDH)*

incorporates ammonium into 2-oxoglutarate (2-OG) from the tricarboxylic acid (TCA) cycle, creating one glutamate (Glu) molecule [119]. Glutamine synthetase (GS) then adds a second ammonium to glutamate, increasing intracellular glutamine (Gln) levels [121]. The bifunctional uridylyltransferase/uridylyl-removing protein GlnD senses the increasing Gln levels [122] [123] and promotes the deuridylylation of the PII-like nitrogen signalling proteins GlnB and GlnK [124]. Deuridylylated GlnB interacts with the bifunctional adenylyltransferase/adenylyl-removing enzyme GlnE to inactivate GS, reducing Gln accumulation [118]. In most proteobacteria (but not in G. diazotrophicus), deuridylylated GlnB also modulates the NtrB/NtrC regulatory system that further regulate BNF effector genes such as nifA [125, 126]. Deuridylylated GlnK interacts with the ammonium channel NrgA/AmtB, inducing its closure [118]. In R. capsulatus, deuridylylated GlnK and GlnB sequester the BNF activator NifA, preventing the expression of the nitrogenase genes nifHDK [130]; similarly, in G. diazotrophicus, the deletion of both GlnK and GlnB induced nifHDK transcription even in high N condition but had no effect under low ammonium [124]. ***(B)*** *As intracellular ammonium decreases and 2-OG increases, glutamate synthase (GOGAT) reconvert Gln in two Glu molecules via the GS/GOGAT pathway [121], and GlnD promote the uridylylation of GlnB and GlnK. Uridylylated GlnB cannot interact with GlnE and NtrB which, in turn, promote the dedenylation of the GS and the phosphorylation of NtrC, respectively [126]. Uridylylated GlnK detaches from the ammonium channel, allowing NH_4^+ influx [124]. The uridylylation of GlnB and GlnK prevent the sequestration of NifA, which, together with phosphorylated NtrC in some diazotroph species, activate the transcription of the nitrogenase genes nifHDK [126].*

This second step of the so-called GS/GOGAT pathway (which is the main ammonium incorporation process under physiologic conditions in most species, including *G. diazotrophicus* [121] [123]) is predominant when intracellular ammonium levels start to decrease and Gln needs to be reconverted into Glu for physiological functions (Fig. 2.3b). GS activity is crucial as the whole nitrogen metabolism regulation depends on glutamine sensing: at high intracellular ammonium levels, corresponding to high Gln availability and decreasing 2-OG, glutamine binds to the bifunctional uridylyltransferase/uridylyl-removing (UTase/UR) protein GlnD and stimulates its uridylyl-removing activity [123] (Fig. 2.3a). The role of GlnD, which is constitutively expressed [123], is to sense the intracellular nitrogen level and regulate accordingly the P_{II}-like nitrogen signalling proteins, which can be divided into the three subfamilies GlnB, GlnK and NifI [122]. In *G. diazotrophicus*, one *glnB* and two *glnK* genes have been found, the latter being associated with a *nrgA*-like ammonium channel (*glnK1/nrgA* operon) and an *amtB*-like ammonium channel (*glnK2/amtB* operon) [124]. Similarly, *Azoarcus* and *Rhodospirillum rubrum* both possess two *glnK*/ammonium channel operons [125]. The deuridylylated P_{II} protein GlnB interacts with the bifunctional adenylyltransferase/adenylyl-removing enzyme GlnE which, in turn, inactivates GS by covalent transfer of an adenylyl group from ATP, in

order to reduce the accumulation of glutamine [118] (Fig. 2.3a). In parallel, the deuridylylated P_{II} protein GlnK binds to NrgA/AmtB and induces the channel closure [118]. In most proteobacteria (e.g. *E. coli* and *Klebsiella Pneumoniae*), deuridylylated GlnB also modulate the nitrogen regulatory system NtrB/NtrC by binding NtrB and promoting its dephosphorylation activity toward NtrC, which becomes unable to activate the expression or activity of nitrogen fixation genes/proteins such as NifA [126]. When intracellular ammonium decrease and 2-OG from the respiratory metabolism increases, Gln levels diminish, favouring the UTase activity of GlnD which uridylylates GlnB (GlnB-UMP) and GlnK (GlnK-UMP) (Fig. 2.3b); consequently, GlnK-UMP detaches from the channels which reprises its ammonium uptake, while GlnB-UMP detaches from NtrB and GlnE, resulting in the reactivation of GS by deadenylation activity and in the NtrC phosphorylation by NtrB activity, respectively [118] [126] (Fig. 2.3b). The phosphorylated NtrC binds with a σ^{54} transcription factor-associated polymerase and NifA, driving the transcription of genes related to low nitrogen metabolism such as *nifHDK*, *glnA* and directly activating the GS [118] [126] (Fig. 2.3b).

In *G. diazotrophicus* [127] and other diazotrophs such as *Azospirillum brasilense* and *Azotobacter vinelandii* however, this second level of control does not seem to be present or required, and *nif*-specific regulation is exerted at the level of NifA activity [126]. In these alphaproteobacteria, the absence of the NtrB/NtrC system is compensated by the ability of the P_{II} proteins GlnK and GlnB to interact directly with NifA, which has a similar architecture to NtrC [118] and a "GAF" N-terminal domain for binding such proteins [128]. In some species such as *A. vinelandii* and *K. Pneumoniae* NifA is further controlled by the anti-activator NifL, which under N-replete condition sequesters NifA in concert with deuridylylated GlnB; however, this ulterior control is not present in *G. diazotrophicus* either [129]. In *Rhodobacter capsulatus* and *Azorhizobium caulinodans*, which also lacks a NifL regulator, NifK and NifB both concur in sequestering NifA under N-replete conditions to inhibit nitrogenase transcription [130] [118]. Interestingly, a study on the P_{II} protein of *G. diazotrophicus* reported that the combined (but not individual) deletion of *glnB*, *glnK1* and *glnK2* resulted in the nitrogenase transcription

even under high ammonium concentration, while under N-limiting conditions the deletion of the three P_{II} protein did not affect the *nifHDK* transcription [124]. This study may have been limited by the bicistronic nature of *glnK* and *amtB*, since the mutation of the former would have likely also affected the transcription of the latter, with consequent ammonium sensing and import imbalance. Nevertheless, based on the available data, it is reasonable to hypothesise a nitrogen regulation model similar to what observed in *R. capsulatus* (Fig. 2.3). According to this model, under N-replete and deuridylylation conditions, GlnB and possibly GlnK (although the latter may impact this mechanism mainly indirectly by regulating the ammonium import) would sequester NifA, thereby preventing the nitrogenase activation. The σ^{54}-dependent transcriptional activator NifA can also be regulated transcriptionally or post-translationally; in *G. diazotrophicus*, its expression was 18-65 fold higher under 1 mM ammonium compared to 20 mM [128]. In addition to direct GlnK and GlnB binding via GAF domain, NifA is also modulated by inherent sensitivity to oxygen damage in a Cys-aa4-Cys motif in its interdomain linker region, although oxygen did not also influence *nifA* transcription [128]. Similarly, the nitrogenase complex is sensitive to oxygen, although paradoxically optimal BNF in this bacterium requires high respiration rates and oxygen levels of 0.2 kPa, with up to 30 kPa pO_2 being tolerated [131] [132]. To explain this apparent paradox, *G. diazotrophicus* was proposed to undergo a 'respiratory protection' strategy during BNF in cultures, i.e., to consume high amount of oxygen via respiration (the respiratory rate during BNF was among the highest ever reported for aerobic bacteria) and alter its electron transport chain and terminal oxidase composition to optimize ATP production and preserve nitrogenase activity [111]. However, such mechanism has never been investigated *in planta*. This more tolerant nitrogen sensing modulation, deprived of the NtrB/NtrC control level, seems to mainly rely on NifA post-transcriptional regulation, which, together with the high respiration rate, may explain why *G. diazotrophicus* performs BNF at up to 20 mM NH_4 under high sugars, with the optimal fixation rate being at 1.6 mM NH_4 [133]; in contrast, in other diazotrophs such as *Herbaspirillum seropedicae, Rhodospirillum rubrum, Azospirillum brasilense* and *Azospirillum Lipoferum* this process is reversibly inhibited already at 0.2 mM NH_4 [134]. However, this also suggests

that engineering NifA may be sufficient for constitutively activating the *nifHDK* operon and boosting the BNF capability of *G. diazotrophicus* in agricultural settings. Similar strategies, encompassing *nifHDK* overexpression by NifA deregulation, are being attempted with other non-nodulating diazotrophs [135].

The nitrogenase complex is the effector of BNF and the main target of its tight regulation. It consists of two essential subunits: the Fe-protein NifH and the α2β2 heterotetrameric MoFe-protein NifDK. NifH is responsible for transferring electrons to the MoFe-protein, which hosts the catalytic site of the reduction of N_2 to NH_3 [136] [137], [138]. Understanding the role and regulation of this enzyme, which is the heart of the nitrogen availability on the Earth's biosphere, is crucial for exploiting BNF in agricultural and industrial processes.

At the end of the nitrogen cycle of symbiotic diazotrophs, a portion of the reduced ammonia (which diffuse away from the bacterial cell and can be protonated into ammonium in reducing environments such as the rhizosphere) is transferred to the plants in exchange for carbon-rich photoassimilates. Plants absorb nitrogen primarily in the form of ammonium and nitrate [139], whose ratio depends on environmental factors: nitrite and nitrate are the prevalent forms in well-aerated, aerobic soils (e.g. agricultural fields or riparian areas) due to the action of nitrifying such as *Nitrosomonas* or the comammox *Nitrospira*, while ammonium is more common in anaerobic or microaerobic soils, such as flooded rice paddies, grassland ecosystems or permanent forests, where it is produced by the ammonification of organic material and BNF performed by methanogenic archaea or various non-nodulating diazotrophs [140]–[142]. Additionally, to a lesser extent, plant can uptake organic molecules such as proteins and amino acids through the use of endocytosis and proteolytic enzymes [143], [144]. The imported ammonium is directly incorporated into amino acids via the GS-GOGAT pathway in root plastids (although significant quantities of ammonium have also been reported to be transported to the shoot via xylem vessels [145]), while nitrate is mostly xylematically translocated to the aerial parts, where it is stored in vacuoles or reduced to ammonium inside plastids [146].

AIMS

The project was organised into four primary objectives, spanning from a fundamental exploration of *G. diazotrophicus* physiology to its practical application in diverse crops and optimization through genetic engineering.

Objective One: To assess the PGP capabilities of the bacterium in monocots vs. dicots model systems across various settings and nutritional conditions, aiming to identify effective inoculation strategies scalable for industrial applications.

Objective Two: To investigate genetic engineering tools and synthetic biology modules for constructing a toolkit conducive to efficient and tailored *G. diazotrophicus* mutagenesis.

Objective Three: To describe the colonisation process of *G. diazotrophicus* in monocots vs. dicots model systems under different nitrogen conditions, seeking insights into the precise dynamics of plant invasion.

Objective Four: To scrutinize the bacterium's physiology in relation to nitrogen and carbon metabolism, both *in planta* and *in vivo*, utilising gene expression analyses and mutants. The aim is to unravel the nitrogen metabolism regulatory network and, based on this understanding, create mutant strains with enhanced PGP capabilities.

3. MATERIALS AND METHODS

3.1. Media preparation for bacterial cultures

All the *G. diazotrophicus* strains were routinely grown at 28°C in:

- ATGUS medium [glucose 2.7 g L^{-1}; mannitol 1.8 g L^{-1}; yeast extract 2.7 g L^{-1}; K_2HPO_4 4.8 g L^{-1}; KH_2PO_4 0.65 g L^{-1}; MES hydrate 4.4 g L^{-1}; final pH 6.5 with acetic acid].
- DYGS [glucose 2 g L^{-1}; Pepton 1.5 g L^{-1}; Yeast extract 2 g L^{-1}; K_2HPO_4 0.5 g L^{-1}; $MgSO_4 \cdot 7H_2O$, 0.5 g L^{-1}; Sodium L-glutamate monohydrate 1.5 g L^{-1}].

E. coli β2163 strains were grown in

- LB-Miller medium [yeast extract 5 g L^{-1}, peptone 10 g L^{-1}, NaCl 10 g L^{-1}] at 37°C with the addition of the appropriate antibiotics and diaminopimelic acid (DAP) 0.3 mM.

G. diazotrophicus cells were re-isolated from plant tissues on:

- ace-LGIP medium [sucrose 100 g L^{-1}; yeast extract 0.025 g L^{-1}; KH_2PO_4 0.75 g L^{-1}; CH_3CO_2K 0.35 g L^{-1}; $MgSO_4 \cdot 7H_2O$ 0.2 g L^{-1}; $CaC1_2 \cdot 2H_2O$ 0.02 g L^{-1}; $Na_2MoO_4 \cdot 2H_2O$ 0.002 g L^{-1}; $FeCI_2.6\ H_2O$ 0.01 g L^{-1}; bromothymol blue 0.5% solution in 0.2 N KOH 5 mL; agar 15 g L^{-1}; final pH 4.0 with acetic acid].

When grown on solid (agar 1.5%), semisolid (agar 0.7%) or liquid medium for *nif* expression analyses or IAA detection, *G. diazotrophicus* was cultured in LGI-P medium in which nitrogen or carbon were added at the desired concentrations in the form of ammonium and sucrose, respectively.

- LGI-P medium [K_2HPO_4 0.2 g L^{-1}; KH_2PO_4 0.6 g L^{-1}; $MgSO_4 \cdot 7H_2O$ 0.2 g L^{-1}; $CaC1_2 \cdot 2H_2O$ 0.02 g L^{-1}; $Na_2MoO_4 \cdot 2H_2O$ 0.002 g L^{-1}; $FeCI_2.6\ H_2O$ 0.01 g L^{-1}; bromothymol blue 0.5% solution in 0.2 N KOH 5 mL; agar 15 g L^{-1}; final pH 4.0 with acetic acid].

3.2. Strains and growth conditions

Bacterial strain	**Relevant characteristics**	**Media and selection (μg mL^{-1})**	**Source**
***G. diazotrophicus* AZ0019**			Azotic Technologies Ltd.
G. diazotrophicus nifD$^-$	nifD$^-$ [Kan^R]	Kan$_{75}$ in ATGUS Kan$_{100}$ in DYGS	R. Fray Lab, University of Nottingham
***E. coli* DH5α**	F- Φ80lacZΔM15 Δ(lacZYA-argF) U169 recA1 endA1 hsdR17(rk-, mk+) phoA supE44 thi-1 gyrA96 relA1 λ-		Thermo Fisher Scientific
E. coli β2163	(F-) RP4-2-Tc::Mu ΔdapA::(erm-pir) [Km^R; Em^R]	LB Kan$_{50}$ + diaminopimelic acid (DAP) 0.3 mM. (+ Cm$_{25}$ if transformed with pSW23t)	R. Fray Lab, University of Nottingham
G. diazotrophicus GGG	pBBR1MCS5 [Gent^R,Cm^R] for constitutive *gfpmut3*;* pRGS561 [Spe^R; St^R; Kan^R] for constitutive *gusA* expression	Kan$_{75}$ + Ste/Sp$_{100}$ in ATGUS Kan$_{200}$ + Ste/Sp$_{500}$ in DYGS	This study
GdRed	pICH47751_DsRed for constitutive dsRed expression	Kan$_{100}$ in ATGUS Kan$_{200}$ in DYGS	This study
GdRed_nifHp::GFP	pICH-DsR-*nifHDK*p::GFP for *nif*-reporter GFP activity	Kan$_{100}$ in ATGUS Kan$_{200}$ in DYGS	This study
Gd_nifHDK::GFP	*nifHDK*::*gfpmut3** reporter	Ste/Sp$_{100}$ in ATGUS Ste/Sp$_{500}$ in DYGS	This study
GdRed_nifHDK::GFP	*nifHDK*::*gfpmut3** reporter + pICH47751_DsRed	Kan$_{75}$ + Ste/Sp$_{100}$ in ATGUS Kan$_{200}$ + Ste/Sp$_{500}$ in DYGS	This study
Gd_nifHDK::GUS	*nifHDK*::*gusA* reporter	Ste/Sp$_{100}$ in ATGUS Ste/Sp$_{500}$ in DYGS	This study
GdnifAoe_nifHDK::GUS	*nifHDK*::*gusA* reporter + pICH47751_NifA for constitutive *nifA* expression	Kan$_{75}$ + Ste/Sp$_{100}$ in ATGUS Kan$_{200}$ + Ste/Sp$_{500}$ in DYGS	This study

Table 3.1. List of relevant strains used in this study. E. coli plasmid carrier intermediates used during cloning and transformation procedures were not included. The number after each antibiotic indicates its working concentration in µg mL^{-1}. Cm = chloramphenicol; Kan = kanamycine; Gent = gentamycin; Ste = streptomycin; Sp = spectinomycin.

3.3. Electroporation

To prepare electrocompetent *G. diazotrophicus* cells, a fresh streak from solid medium was cultured overnight in 25 mL of liquid ATGUS until exponential phase. The pre-culture was reinoculated into a new culture (final volume 200 mL in a 1L flask) and grown at 200 RPM until OD_{600} ~ 0.3, corresponding to the peak exponential phase. The culture was then chilled on ice for 15 mins and aliquoted in four 50 mL Falcon tubes. Cells were harvested by centrifugation at 4000g for 7 mins at 4°C. The supernatant was discarded, and the cells resuspended in 30 mL ice-cold 10% glycerol. Cells were pelleted again at 4°C for a total of 3 washes in cold 10% glycerol. After the third wash, the pelleted cells were resuspended in 1 mL of ice cold 10% glycerol. 200 µL of electrocompetent bacteria were aliquoted on ice in 1.5 mL tubes and snap-frozen in liquid nitrogen.

For electroporation, one aliquot was thawed on ice for 10 mins. 5 to 10 µL of plasmid, corresponding to 1 to 5 µg of DNA, were resuspended in the aliquot, and the mix was transferred into a pre-chilled 2 mm-cuvette. Electroporation was performed with a Gene Pulser apparatus (Bio-Rad) at 2.2 kV pulse, corresponding to a field strength of 11 kV/cm. Immediately after electroporation, 1mL ice-cold ATGUS or DYGS medium was added to the cuvette, and cells were gently resuspended and transferred to a 2mL tube. The transformed cells were incubated at 29°C for 3 h at 100 RPM, then rested at room temperature for 4 more hours and finally plated in selective medium and incubated at 28°C for 2-3 days.

3.4 Biparental mating

Cultures of *G. diazotrophicus* and *E.coli β2163* carrying the appropriate vector were grown overnight at suitable temperature until exponential phase. 2 mL of each culture were pelleted at 4000 rpm/3800 g at room temperature for 4 mins and washed once with sterile water. Once discarded the water supernatant, cells were mixed in 5 mL of sterile water or $MgSO_4$ 10 mM, vortexed briefly and transferred into a sterile syringe coupled with a previously sterilised filter apparatus (Swinnex Filter Holder, 25mm) containing a Millipore membrane (25 mm MF-Millipore® Membrane Filter, 0.45 µm pore size). The solution was carefully squeezed and discarded, and the membrane was then carefully transferred face up on a non-selective plate (PDA+ 0.3 mM DAP + 100 mM phosphate buffer pH 6.9) and incubated at 28 °C for maximum 30 hours. After the incubation, the filter was placed in a 50 ml tube filled with 5% ethanol, and further incubated at room temperature for 1 h in gentle agitation. 100-200 µL of the bacterial suspension were then plated on selective media and incubated at 28 °C until colonies were sufficiently big for screening (usually 2 to 3 days). Where possible, to further eliminate any *E.coli β2163* carryover, Kan200 and Gent25 were added to the selective medium.

3.5. Seed sanitation

Seeds of *Solanum lycopersicum* cv. MoneyMaker (Mole's Seeds, UK; Just Seed, UK) were surface sanitised by soaking in 5% sodium hypochlorite for 10 mins, followed by several rounds of vigorous washing in sterile distilled water; then, seeds were soaked in 70% ethanol for 5 mins in agitation followed by vigorous washing with sterile distilled water.

Unhusked seeds of *Oryza sativa* cv. BT7 or BC15 were surface sanitised by soaking in 50 sodium hypochlorite for 1 h in agitation, followed by several rounds of vigorous washing in sterile distilled water; then, seeds were soaked in 70% ethanol for 10 mins in agitation followed by vigorous washing with sterile distilled water. Alternatively, if the husk was removed, seed were

sanitised under 10% sodium hypochlorite for 15 mins followed by 70% ethanol for 5 mins.

Arabidopsis thaliana Col-0 seeds were surface sanitised by soaking in 5% sodium hypochlorite for 5 mins followed by several rounds of vigorous washing in sterile distilled water.

3.6. Bacterial inocula preparation for hydroponic systems or seed coating

A pre-inoculum of *G. diazotrophicus* WT or *nifD*$^-$ was prepared as in section 3.3 and used to re-inoculate 500 mL of liquid ATGUS in a 1 L flask. Alternatively, in preparation of microscopy analyses, the tagged strains were grown with appropriate antibiotic concentration (Table 3.2). Growth was carried out overnight at 28° at 200 rpm. Bacteria were aliquoted in sterile 50 mL tubes and pelleted at 4000 x g (Thermo Scientific™ TX-400 4 x 400 mL Swinging Bucket Rotor), at 21 °C for 10 mins. The cultures were washed and re-pelleted twice with sterile distilled water. After washing, bacteria were re-suspended in the hydroponic nutrient solution to a concentration of OD_{600} = 0.3, corresponding to 10^7 CFUs mL^{-1}.

3.7. Plant growth and bacterial inoculation in hydroponic systems

Both tomato and rice were grown in the following modified "Hoagland" nutrient solution (NS). Nitrogen sources were added separately in the form of potassium nitrate or ammonium nitrate at the desired concentration.

Nutrients	**mM in NS 1x**
K_2SO_4	1.5
$MgSO_4.7H_2O$	1.5
KH_2PO_4	1
NaCl	0.5
$Ca(H_2PO_4)2.H_2O$	0.5
$CaCl_2.2H_20$	2
$FeSO_4.7H_20$	0.020035971
EDTA $2Na.2H_20$	0.020013969
Micronutrients	
Cu$SO_4.5H_2O$	0.002002483
Zn$SO_4.7H_2O$	0.010431154
Mn$SO_4.4H_2O$	0.008966125

$H_3\mathbf{BO}_3$	0.064693514
$Na_2\mathbf{Mo}O_4.2H_2O$	0.002066392
$Cl_2\mathbf{Co}.6H_2O$	0.002101458

Table 3.2. Nutrient solution (NS) for hydroponic systems.

3.7.1. Tomato

Sanitised tomato seeds were sown in sterile hydroponic boxes (10/15 seeds per box) filled to the top with half strength (0.5x) modified "Hoagland" nutrient solution (NS; Table 3.2). The N replete condition was set at 2 mM KNO_3 and 2 mM KNO_3 + 0.2 mM $(NH_4)_2SO_4$. Germination and growth were performed in a growth chamber (Conviron / Binder kbwf720, Bohemina, NY, USA) set at 80% humidity, 16 hours photoperiod, at a temperature of 28 °C. Five days after seed germination, plants exhibiting the same developmental stage and root length were kept, while outliers were discarded, and the same number of plants were kept in each system. The bacterial suspension was added to the growth solution (section 3.6) and incubated for 48 h, after which it was poured off from the hydroponic systems and replaced with fresh nutrient solution. This was defined as the first day post inoculum (dpi), after which all the other timepoints of collection for imaging, maceration, phenotyping, qPCR and RT-qPCR analyses were counted.

3.7.2. Rice

Santitised rice seeds were pregerminated at 28 °C in dark for 3 to 5 days on sterile Whatman paper placed in a Petri dish and covered with a thin layer of sterile water. Then, seeds at the same developmental stage (radicle of around 1 cm and emerging coleoptile of 1 to 2 mm) were selected and submerged in the bacterial inoculum prepared as in section 3.6. After an overnight incubation at 28 °C in dark, seedling were transferred on the hydroponic system.

3.8. Bacterial re-isolation from treated plants

To verify the bacterial colonisation, untreated and inoculated plants were collected at the desired timepoints, and each plant was washed twice with 10 mM MgCl2 to remove loosely attached/non-adhering bacteria. Roots and shoots samples were separated, weighted and ground in a mixer-mill disruptor (MM 400, Retsch, Haan, Germany) at 25 Hz for 1 min (or until completely macerated). Samples were then re-suspended in 500 µL of sterile water and carefully vortexed. Each suspension was serially diluted and 10 µL aliquots were plated in triplicate on ace-LGIP medium. After incubation at 28° C for three days, the most probable number (MPN) of colony forming units (CFUs) per unit of plant fresh weight (CFUs g^{-1}) were calculated. Colony PCR was performed on bacterial colonies employing strain specific primers 11 and 12 (Primers Table 3.3) to confirm bacterial identification after re-isolation from plants.

3.9. Evaluation of $^{15}N/^{14}N$ incorporation

G. diazotrophicus WT and *nifD*$^{-}$ were streaked from frozen glycerol stock to LGI-P medium in which the N source was 2 mM $(^{15}NH_4)_2SO_4$. The strains were subsequently cultured in liquid ATGUS medium in which the yeast extract had also been substituted with 2 mM $(^{15}NH_4)_2SO_4$, and prepared for hydroponic inoculation as described above. Plants grown under zero N, $K^{15}NO_3$ or $K^{15}NO_3$ + $(^{15}NH_4)_2SO_4$ were inoculated and grown as in section 3.5. Treated and untreated control samples were collected at 20 dpi. Chlorophyll was then extracted from three biological replicates of each treatment (uninoculated, *G. diazotrophicus* WT and *G. diazotrophicus nifD*$^{-}$ treated). Chlorophyll extraction was adapted from Loh et al. [147]. For each treatment, around 0.1 g of freeze-dried tomato plants aerial parts (leaves and shoots) were finely pulverized using a sterilised mortar and pestle and mixed with 30 ml of hexane/ethanol/acetone/toluene (10:6:7:7, v/v/v/v) in a flask. The mixture was then shaken at room temperature for 1 h, followed by the addition of 15 ml of hexane, further shaking for 10 min and a final addition of

15 ml of 10% anhydrous sodium sulphate solution for partition. The upper phase containing chlorophylls was collected, and the lower phase was repeatedly extracted with 15 ml of hexane until the supernatant became colourless. Samples were then stored at -20 °C and sent for LC-MS analyses (Mass Spectrometry and Chromatography Services, School of Chemistry, University of Nottingham).

3.10. Seed coating, MS agar and glasshouse growth conditions

Bacterial inocula prepared as in section 3.6 were resuspended at the desired concentration in either water or in an aqueous solution containing 3% sucrose (87 mM), 0.3% gum Arabic and 0.1% (v/v) polysorbate 80. For the seed coating technique, seeds were incubated in the solution for the desired amount of time, then dried under lamina flow hoods for around 15 min. For the vacuum infiltration protocols, seeds were incubated under a vacuum of 800 mbar until bubbling of the solution.

For MS-agar based experiments, seeds were then sown in ammonium-free MS agar (2.2 g L^{-1} of Sigma-Aldrich Murashige and Skoog Modified Basal Salt Mixture, M2909) and or half-strength MS agar (2.2 g L^{-1} of Sigma-Aldrich Murashige and Skoog Basal Salt Mixture, M5524). Due to the percentage of the various salts in the MS salt mixture used, the concentration of potassium nitrate was 15 mM KNO_3 in ammonium-free MS agar (M2909) and 20 mM in half-strength MS agar (M5524), which also contained 10 mM NH_4; however, the concentration of the other macro and micro elements was around 50% higher in the ammonium-free MS medium.

For in soil experiments, tomato seeds were sown into Levington® Potting & Bedding R-M3 Compost - High Nutrient soil (premixed with the biocontrol agent *Trichoderma asperellum* T34, as per manufacturer (Fargro®) instructions) and incubated in a glasshouse with a 16-8 light-dark photoperiod at 24 °C during the day and 20 °C at night. One month after germination, plantlets were transferred from germination trays into 10 L pots filled with Klasmann Traysubstrate mixed with Silver Sand (50:50) and routinely watered with N-free feeding. Rice seeds were sown into a mix containing 70% v/v

Kettering loam, 25% v/v John Innes number 2 and 5% v/v horticultural sand and grown in a glasshouse as described above but with a temperature of 26°C during the day. Plants were watered with rainwater.

3.11. Histochemical GUS assay

To visualise the *gusA* gene expression in the pRGS561 tagged strain *GGG in planta*, plant samples and untreated controls were incubated for 1 to 2 days in dark at 28 °C in GUS staining solution [potassium ferricyanide 1 mM, potassium ferrocyanide 1 mM, phosphate buffer pH 7 100 mM, EDTA pH 8 1 mM, Triton X-100 1% v/v, 5-bromo-4-chloro-3-indolyl-beta-D-glucuronic acid, cyclohexyl ammonium salt (X-Gluc) 500 μg mL^{-1} (1.2 mM)]. After the incubation, the staining solution was discarded and substituted with 70% ethanol and stored at room temperature until chlorophyll was completely removed from samples allowing blue signal visualization. To visualize the *Gd_nifHDK::GUS* strain *in planta*, X-Gluc concentration was increased to 750 μg mL^{-1} (1.7 mM); to visualize it in solid or semi-solid medium, X-Gluc concentration was reduced to 130 μg mL^{-1} (0.29 mM).

3.12. Microscopy and image analysis

Widefield fluorescence imaging of samples at the mm-scale level was carried out with a Modular Stereo Microscope for Fluorescent Imaging Leica MZ10 F coupled with Chroma's ET GFP LP (ET480/40x, ET510 LP), allowing for excitation and detection of both GFPmut3* and DsRed-Express2 reporter proteins, or with Chroma's ET dsRed (ET546/10x, ET595/50m). For widefield fluorescence microscopy at the μm-scale level, a Leica DM5000 B Automated Upright Microscope was employed, coupled with a L5 filter set for GFPmut3* detection (BP480/40x, BP527/30) and a N2.1 filter set for DsRed-Express2 BP detection (BP515-560, LP 590). For confocal fluorescence microscopy and z-stacks, a Leica TCS SP5 confocal microscope was employed, with a 488nm

laser and “Leica/EGFP” software pre-set for imaging GFPmut3* and a 633nm laser to image plastidial chlorophyll. Sample sectioning was carried out with a 7000smz-2 Vibrotome (Campden Instruments) as in Atkinson and Wells [148]. Z-stacks, 3D models and composite images were processed with the Fiji software using the Z Project, 3D Project and Merge Channels algorithms, respectively, leaving default settings. ET = enhanced transmission due to magnetron sputtered exciter or emitter. x = excitation (filter). m = emission (filter). LP = long-pass. BP = band-pass.

3.13. Protoplast isolation

Young, terminal leaves of untreated tomato plants grown hydroponically were cut in strips approximately 5 mm wide. The strips were incubated in dark for 5 hours at 28 °C in a solution of *G. diazotrophicus* (cultured and washed as described for hydroponic inoculation) resuspended in water to an OD_{600} = 0.3. After the incubation, the leaf strips were washed twice by swirling in sterile water, transferred to the digestion solution (0.1 g leaf tissue in 2 mL digestion solution) and put in gentle agitation at room temperature for one hour. The digestion solution was made by dissolving 0.3% of Cellulase “Onozuka R-10” (Duchefa Biochemie) and 0.4% of Macerozyme R-10 (Duchefa Biochemie) in Plant Protoplast Digest/Wash Solution (Sigma-Aldrich, Merck) for 10 minutes at 50 °C, then adding 10% v/v Viscozyme® L (Sigma-Aldrich, Merck) and 1% BSA. After the incubation, the protoplasts were pelleted at 500 G for 4 minutes; the pellet was carefully removed from the digestion solution by pipetting and transferred to some fresh Plant Protoplast Digest/Wash Solution (Sigma-Aldrich, Merck). The protoplasts so obtained were directly observed under bright field microscopy.

3.14. Callus culture

The young apical leaves of tobacco plantlets grown in sterility on MS agar were inoculated with *GGG* or *G. diazotrophicus* WT prepared as in section 3.6

and resuspended in water to OD_{600} = 0.3. After an overnight incubation in growth chamber (Conviron / Binder kbwf720, Bohemina, NY, USA) at 23 °C, 5 x 5 mm squares were cut from treated and untreated leaves and placed on Shoot Regeneration Medium [MS 4.4 g L^{-1}; sucrose 30 g L^{-1}; thiamine-HCl 0.9 mg L^{-1}; agar 4 g L^{-1}; IAA 0.1 mg L^{-1}; BAP 1 mg L^{-1}]. Calli were grown in the growth chamber at 23 °C with 16 hours photoperiod for 25 days before X-Gluc staining.

3.15. qPCR analyses

Tomato plantlets were collected from hydroponic systems and samples were prepared as in section 3.7, but divided into 5 different anatomical zones (see section 4.3.1d). The total DNA was extracted with the following protocol. 0.1 g of plant material from three biological replicates of each treatment were macerated in liquid nitrogen as in section 3.8. 600 µL of DNA extraction buffer [for 100 mL, add 20 mL of 1M TrisHcl pH 7.5, 6.25 mL of 4M NaCl, 5 mL of 0.5M EDTA, 5 mL 10% SDS] were added to each sample, incubated for 5 mins at room temperature and spun at 13k x G for 10 minutes. 500 µL of the supernatant was mixed with 500 µL of isopropanol and incubated at room temperature for 3 mins. Samples were spun at 20k x G for 10 mins and the supernatant was discarded. Pellets were washed once in 70% ethanol, air-dried, resuspended in 50 µL of distilled water and brought to the same concentration after NanoDrop DNA quantification. qPCR reactions of each biological replicate were carried out in three technical replicates with the cycling protocol reported in the section below, using one primer combination from the tomato genome as reference (from the *ard2* gene) and one primer combination from the bacterial genome (from the *nifD* gene, see Primers Table 3.3).

3.16. RT-qPCR analyses

Tomato plantlets were collected from untreated controls or *G. diazotrophicus* WT-inoculated hydroponic systems in the different N conditions at 1 and 20 dpi. Roots and shoots were separated and processed as distinct samples. After swirling samples twice in a plate with 10 mM MgCl2 to remove loosely attached bacteria, roots or shoots tissue from at least three biological replicates were aliquoted in 0.1 mg samples. The total RNA (plant and bacterial) was extracted with the RNeasy® Plant Mini Kit Kit (Quiagen) according to the manufacturer instruction, using RLT buffer and adding a DNase incubation step (RNase-Free DNase Set, Quiagen) between the points 6 and 7 of the manufacturer RNA extraction protocol. The RNA samples so obtained were brought to the same concentration using Qubit BR assay (ThermoFisher Scientific), and cDNA libraries were produced using SuperScriptTM III Reverse Transcriptase Kit (Invitrogen). Each RT-qPCR reaction was set up using 5 µL SensiMix SYBR Lo-ROX Kit (Meridian Bioscience®), 1 µL primer forward 10 µM, 1 µL primer reverse 10 µM, 200 ng cDNA, sterile water to 10 µL. The qPCRs were performed on a LightCycler® 480 System apparatus at the following conditions: 10 min at 95 °C followed by 40 cycles with steps of 95°C for 15 s, 60°C for 15 s, 72°C for 15 s, and a final 2 min amplification at 72 °C. All the amplicons were designed to be between 80 and 130 bp in length. Data analysis was carried out as in Banani et al. [149]. The expression of the investigated genes was normalised against the bacterial *rho* gene as advocated by Galisa et al [150].

3.17. Primers table

Primers specific to AZ0019 for colony PCR	
11 Fw	5’-TCGAGCAGCCGTTTCATCCA-3’
11 Rv	5’-TCAGGGCAATCACTAGCCGG-3’
12 Fw	5’-TGATGCGCTTGTTCGTGACG-3’
12 Rv	5’-CGTTCGCCCTTGTCGTCATG-3’
Bacterial primers for RT-qPCR	
rho Fw	5’-GCAACTCGGAACTCATCCTC-3’
rho Rv	5’-GGACCCACATCTTCGACAGT-3’
nifD Fw	5’-AGTTCACGTCCGATTTCCAG-3’

nifD Rv	5’-CGGAAAGAGCTCATCGATTT-3’
nifA Fw	5’-GATGTCTGCCTCCTGTCGAT-3’
nifA Rv	5’-CTGTCGTGCAGCAGGTTTTC-3’
nifE Fw	5’-TTCCGGACCGAAACTGTATC-3’
nifE Rv	5’-CCTTGATGGCCTTGTACAGC-3’
nrgA Fw	5’-CGTCACGATTGTCTGGATGG-3’
nrgA Rv	5’-GCATGAAGCGGGACAGAT-3’
cccA Fw	5’-CCGATCTATGTCGTGCTGAA-3’
cccA Rv	5’-GAAATGGCTGCGGACATAGT-3’
lsdA Fw	5’-GTTCAGCTATAACGGCTGGGA-3’
lsdA Rv	5’-ACGATAGAAGAAGCCGATGC-3’
katE Fw	5’-AACGATATTCCGGTCTTCGTC-3’
katE Rv	5’-CGGACAGGAAAGGCCCTAT-3’
Reference tomato primers for qPCR	
ard2 Fw	5’-TGTTCATCAGTGTGCTAGTG-3’
ard2 Rv	5’-GCTGTCCTTCCTTCTGAATC-3’
Primers for tentative constitutive *gfp*/*gusA* integration screening	
GFP 3’ F	5’-GCGTTCAACTAGCAGACCAT-3’
GFP 5’ R	5’-GTTGCATCACCTTCACCCTC-3’
GUS 3’ F	5’-CAACAACTCTCCTGGCGC-3’
GUS 5’ R	5’-TTCACGGGTTGGGGTTTCTA-3’
CheckTagGd LF	5’-GGTCTCTTTCACTCCCCTCGT-3’
CheckTagGd RR	5’-AGTCGTAACAAGGTAGCCGT-3’
Primers for reporter *nifHDK*::*gfp*/*gusA* integration screening	
CheckNifGd LF	5’-GGCTACGACAACATGCTCAA-3’
CheckNifGd LF	5’-TTCCTCCTCCGCGATCAG-3’

Table 3.3. List of relevant primers used in this study for in vivo detection of the strains and verification of the correct plasmid assembly or cassette integration. Primers used for fragments preparation and plasmid construction via HiFi assembly or GoldeGate cloning were not included. Primers were routinely validated in silico through the website bioinformatics.org leaving settings as default to minimize GC clamps, self-annealing and hairpin formation [151].

3.18. Salkowski's test for IAA detection

G. diazotrophicus WT and *nifD*$^{-}$ strains were grown in triplicate in LGI-P medium supplemented with 100 µg/mL Tryptophan (Trp) under 10% sucrose and 1.5 mM (fixing-condition) vs 15 mM NH_4Cl (non-fixing condition). In parallel, the two strains were cultured under the same conditions but without Tryptophan. The Salkowski’s Reagent for the colorimetric test was prepared under the fume hood by mixing 2 ml 0.5M $FeCl_3$, 49 ml water and 49 ml 70% perchloric. Bacterial cultures were brought to the same OD_{600} using the Trp-depleted cultures (that had grown at the same OD_{600} of their +Trp

correspondants). 1 ml of each normalised culture was pelleted, and the supernatant was transferred into a new 2ml Eppendorf tube. 1 ml of Salkowski's Reagent was added to each sample, vortexed for 5s and incubated for 30 mins in the dark. The same procedure was carried out on Trp-depleted cultures. After the incubation in dark, the red pigment formation was spectrophotometrically measured at OD_{536}, with the Trp-depleted samples being used as blank. Reference samples for Standard Curve were produced by proper dilution from a 1mg mL^{-1} stock of IAA dissolved in acetone at 100-50-20-10-5 µg mL^{-1}, and the estimation of IAA concentration in the analysed samples was calculated accordingly.

3.19. Statistical testing

Statistical data analysis was performed with the open access online tools at www.socscistatistics.com and www.statskingdom.com, leaving all the default settings unaltered. Data with a non-normal distribution relative to plant growth promotion phenotype, colonisation rate and plasmid stability were analysed according to non-parametric tests. For the comparison of two groups, the Mann-Whitney *U* test was applied, set as 2-tailed hypothesis with a significance level of $p \leq 0.05$. For the comparison of ≥ 3 groups, the Kruskal-Wallis test was performed, with a significance level of $p \leq 0.05$. Measurements from the $^{14}N/^{15}N$ balance experiment (section 3.9), which only showed a moderate violation of the normal distribution assumption (as calculated based on the Shapiro-Wilk Test, $\alpha = 0.05$), were subjected to a One-Way ANOVA test with a significance level set at $p \leq 0.05$. Significance assessments for the One-Way ANOVA analyses relative to qPCR and RT-qPCR data were conducted using Tukey's Honestly Significant Difference (HSD) test in R, with letter assignments implemented through the 'agricolae' package.

4. RESULTS AND DISCUSSION

4.1 Plant growth promotion evaluation

Since *G. diazotrophicus* was shown to substantially contribute to sugarcane nutrition in field [81] and was isolated as a natural host of both monocots and dicots with different physiologic characteristics [98], its plant growth promotion potential was tested with great interest in other crops of commercial value such as sweet potato [152], maize [3] [4] [154], wheat, sorghum [155][156], beet [157], carrot [157][158], strawberry [159], cassava [160], bean [161], lettuce [162] and more. These studies generally reported a growth or yield benefit induced by the bacterial application, although with great variability in terms of efficacy and type of PGP effect elicited, especially when the tested crops were grown in unsterile soil setups [163]. A general paradigm for an effective inoculation strategy is yet to be found, and the question of whether it is feasible to efficiently apply *G. diazotrophicus* to agricultural systems and induce an active bacterium-crop symbiosis still needs further investigations. In this study, two host plant models were selected, tomato and rice, belonging to the dicotyledon and monocotyledon clades respectively; the aim of this work was to investigate *G. diazotrophicus'* application potential in both *in vitro* and *in vivo* systems, and to evaluate any substantial difference in the PGP effect elicited or colonisation dynamic observed between the two species as indicators of each clade. Furthermore, as a popular and convenient model system due to its limited dimension and fast life cycle, *Arabidopsis thaliana* was also selected as a host organism for a subset of *G. diazotrophicus* tests in which a larger sample size was desirable.

4.1.1 PGP evaluation in tomato plants inoculated with *G. diazotrophicus*

4.1.1a Rationale and former G. diazotrophicus inoculation attempts

Tomato, the berry-producing dicotyledon plant *Solanum lycopersicum*, was introduced in Europe in 16th century during the colonization of the Americas by the Spanish Empire *conquistadores* and was first described by the Italian botanist Pietro Andrea Mattioli in 1544. Since then, its production has been constantly growing; it is now the second most important vegetable crop globally, and in 2020 accounted for 186 Tg of tomatoes harvested worldwide (Fig. 4.1), with China and India being the major producers (Fig 4.2) [164] and Europe and the United States being the greatest consumers [165]. Least developed countries (as ranked by FAO) are also emerging, although at a slower rate, in the tomato market (Fig 4.2), the global revenue of which amounted to $190.4 billion in 2018, with an average annual value increase of +3.1% from 2007 to 2018 [166].

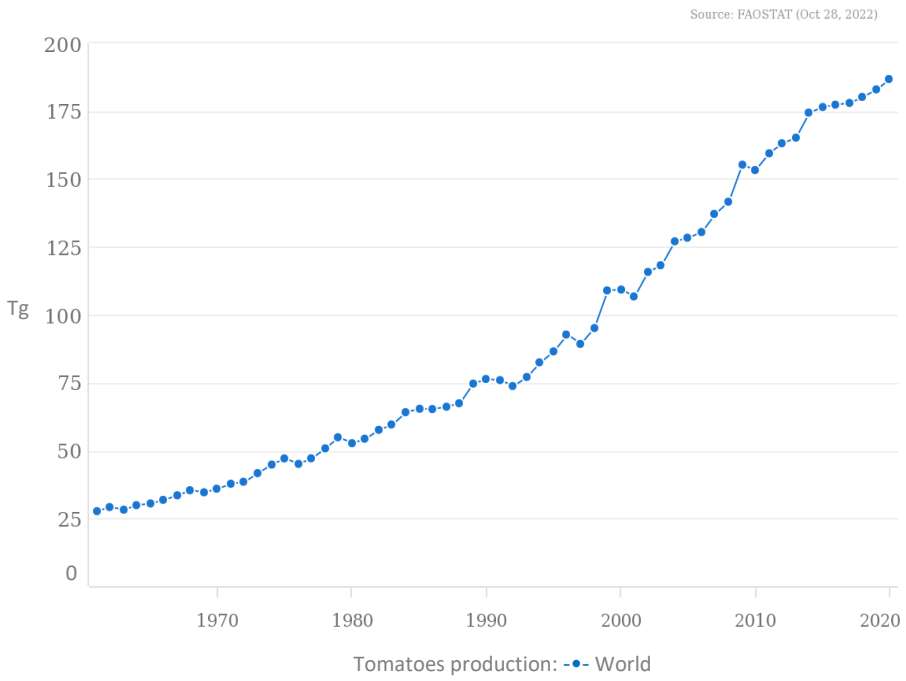


Fig. 4.1. Tomatoes production worldwide between the year 1961 and 2020, Tg year $^{-1}$. Source: FAOSTAT.

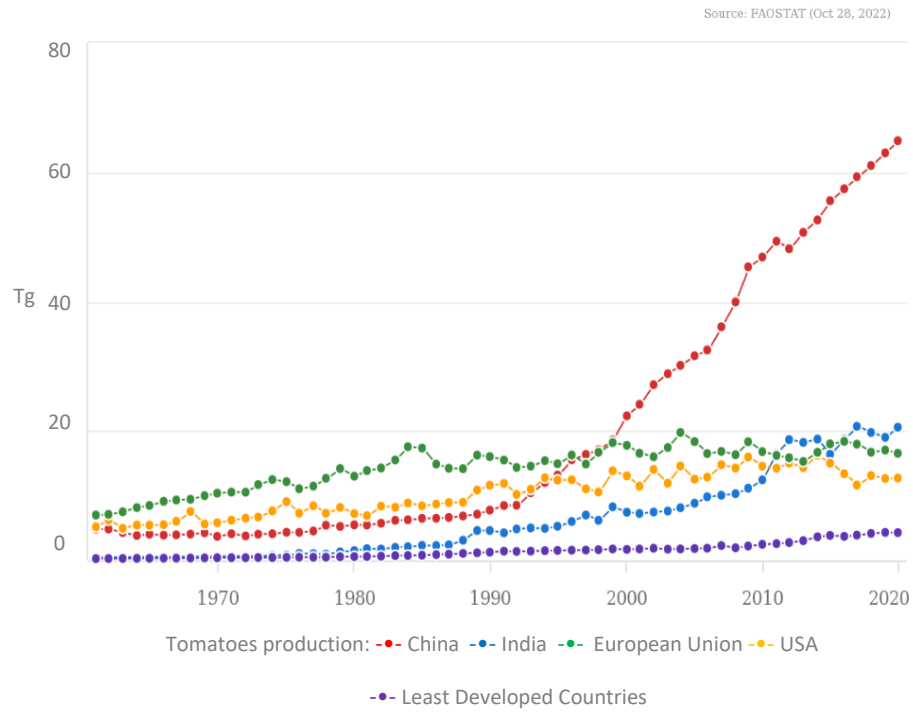


Fig 4.2. Tomatoes production in the four top producer countries and the least developed countries between the year 1961 and 2020, Tg year $^{-1}$. Source: FAOSTAT.

In particular, hydroponic based tomato production in Europe accounted for a 45 % share of the global tomato revenue in 2017 [167]. While Italy is the largest tomato producer within the EU through conventional farming, the Netherlands leads the production of greenhouse-grown tomatoes, and account for the highest production intensity in the world thanks to the use of state-of-the-art integrated hydroponic systems [168]. This makes the use of hydroponically grown tomato a convenient model for both its practical and commercial interest and for the possibility of precisely controlling growth parameters. Cheap and sustainable agricultural technologies such as biostimulants have the potential to boost the tomato production in developing countries without the need to relying on expensive and energy intensive fertilisation practices. Furthermore, tomato yield is primarily limited by availability of nitrogen and water and is therefore often associated with high N fertilisation inputs, highlighting the need for a sustainable fertilisation management [169].

The tomato microbiota has been described to naturally possess a more rich and diverse microbial community in the rhizosphere (with the most abundant bacterial phylum represented by *alpha-protobacteria*) compared to the endosphere, in accordance with other plant model systems [170], but with the most distinctive community features found in the endosphere [171]. The natural association with nitrogen fixing bacteria belonging to the *Burkholderia* sp. was also reported [172], increasing the confidence on the practicability of the application of the *alpha-protobacterium G. diazotrophicus* AZ0019.

Following its discovery in sugarcane, *G. diazotrophicus* was also isolated from dicot species such as coffee [94], carrot, radish, and beet [173]. In 2011, Luna et al. [174] reported for the first time an enhanced growth phenotype in tomato plants treated with *G. diazotrophicus* (Pal5 strain) in glasshouse experiments. In their setup, the bacterium was inoculated at 10^9 CFU mL^{-1} on the sterile vermiculite where the seedling had been germinated in nitrogen replete condition for 4 weeks at 28 °C. After an overnight incubation, the treated seedlings were transferred in soil and moved to the glasshouse, where they were maintained with no feed. The study reported an increase in fruit yield of *G. diazotrophicus* Pal5 treated plants compared to uninoculated controls. Shortly after, in 2013, Dal Gallo's et al. inoculated *Lycopersicon esculentum* (cherry tomato) seedlings for 20 min with 10^8 *G. diazotrophicus* Pal5 CFU mL^{-1} and grew them for 30 days in MS agar or 60 days in soil; they reported an improved root and aerial biomass production when grown *in vitro* but not in soil, in which in fact a lower yield was observed compared to controls, unless other diazotroph species were co-inoculated in the system [175]. Interestingly, in 2017, a study reported for the first time the isolation of *G. diazotrophicus* from the stem of tomato plants in a 150-day-old crop in Colombia, further reinforcing the choice of this crop as a model plant host [176].

No other attempt of confirming the PGP provided by *G. diazotrophicus* to tomato is mentioned in literature, until in 2015-2016, in the University of Nottingham, the *G. diazotrophicus* strain AZ0019 was tested on the tomato varieties "MoneyMaker" and "Ailsa Craig" through the seed coating inoculation method followed by in soil growth (as described in section below and in Material and Methods section 3.10). This preliminary experiment

showed promising results in terms of significant shoot growth enhancement, chlorophyll content and yield increase (unpublished), thus encouraging further analyses with this model system. It is worth noting that, in this setup, *Trichoderma asperellum (T34)* was routinely premixed as a biocontrol agent in the soil used for germinating both treated and mock-treated control plants. Several species of *Trichoderma* fungi are known to establish symbiotic relationship with plants, and are frequently used as bioinoculant for their well-documented ability to promote plant growth, nutrient uptake and resistance against abiotic stress or phytopathogens in different crops, including tomato [177] [178]. Additionally, there is evidence suggesting that *Trichoderma* strains may have a synergic effect with bacterial biostimulants, including diazotrophs [179] [180], but the investigation of such interaction was beyond the aim of this study.

4.1.1b Seed coating and in soil growth induced a cultivar and formulation dependent PGP effect

The experiment that had previously led to an obvious PGP phenotype, carried out in the University of Nottingham by applying *G. diazotrophicus* to tomatoes through the seed coating method (unpublished), was reattempted with the same method (described in section 3.10 and below) to confirm the positive results. Furthermore, the parameter of the growth stage of *G. diazotrophicus* at the time of the formulation was investigated. While this aspect it is commonly accepted to be important for the success of the inoculum [60], not much research has been conducted on the topic, especially regarding bacteria growing as biofilm or colonies in a solid agar matrix. Compared to planktonically cultured bacteria, colonies on agar base show a heterogeneous metabolic profile due pH, O_2, and both nutrients and catabolites micro gradients caused by the nature of the bacterial growth and diffusion when constrained in a solid support [181]. This physiological diversity could enhance the chances of acquiring the adaptations needed by the bacteria to survive during the seed coating process. Moreover, bacteria grown as biofilm or colonies are embedded in extracellular polymeric substances, a mixture of

polysaccharides and proteins with physical properties similar to gums which are central in the biofilm structure, provide protection against desiccation or predation, and act as a nutrient trap [182]. In particular, exopolysaccharides (EPSs), the sugar-based components of extracellular polymeric substances, are known to be involved in biofilm formation, adherence to surfaces, resistance to extreme temperature, osmotic shocks and other abiotic stress factors [107]; furthermore, they are thought to have an active role in the plant-bacterial molecular crosstalk during early colonisation stages of both Rhizobia and non-nodulating associative diazotrophs [183]. EPSs production was namely observed in *G. diazotrophicus* colonising sugarcane plants and was proposed as a recognition signal during the plant-bacterial interaction [163]. Furthermore, the genus *Gluconacetobacter* is known to produce large amounts of EPSs, especially in the case of *G. diazotrophicus* Pal5 grown with mannitol as a carbon source [184]: mannitol was indeed one of the carbon sources, along with glucose, in the ATGUS growth medium employed to culture *G. diazotrophicus* AZ0019 in this experiment.

Hence, the experiment was carried out under two distinct conditions. In the first condition, as already done during the former attempt, *G. diazotrophicus* wild-type (Gd WT) was grown in liquid ATGUS and pelleted around the end of the exponential growth phase, then mixed with a liquid carrier to a density of $OD_{600} = 2$, corresponding to $\approx 10^8$ CFUs mL^{-1}. In the second condition, the bacterium was scraped from a five-day old plate of agarized ATGUS where it had grown to confluency, and likewise resuspended in the liquid carrier to a density of $OD_{600} = 2$. Another dilution of bacteria, one order of magnitude less dense, was also applied in the second condition, to test whether a dose dependent effect was relevant for the success of the treatment. The liquid carrier was developed by Azotic Technologies ltd. and consisted in a sterile aqueous solution containing 3% sucrose (87 mM), 0.3% gum Arabic and 0.1% (v/v) polysorbate 80. Sucrose is a common additive in liquid inoculants, and is used to improve both bacterial survival and adhesion to the seed surface [185]; it was also selected since *G. diazotrophicus* is best adapted to sucrose-rich environments. Gum Arabic, a polymer extracted from acacia trees, is also frequently used as an adhesive agent for *rhizobia* formulations, and was shown

to confer protection against desiccation [186] [187]. Polysorbate 80 is a non-ionic surfactant and emulsifier often employed as a stabiliser and solubiliser in food and pharmaceutical products; it was also reported to promote biomass, growth rate and biofilm formation increase of certain bacterial strains and to decrease the effect of antimicrobial compounds [188].

The tomato seeds (MoneyMaker variety) were incubated in the inoculants for 30 min at room temperature, dried for 15 min in sterile environment and sown in soil. Mock-treated control seeds (Ctrl) were imbibed in the same carrier solution depleted of bacteria. To encourage a vigorous germination and create a rhizosphere rich in nutrients that could better sustain the bacterial growth in the initial colonisation stages, seeds were sown in the "Levington® M3 - High Nutrient" compost mix (beginning of May). In sugarcane, *G. diazotrophicus*-mediated PGP comes into play as the rapid growth of plantations deplete the nutrients from the soil [81]. To mimic this condition, the one-month-old tomato plants were re-potted in a lower-nutrients soil (Klasman tray substrate) and mixed with equal volume of sand; plants were routinely watered with nitrogen-free feeding. After another month of growth in the poorer substrate, i.e., after a total of 60 days post inoculum (dpi) the plant phenotype and yield were assessed. The results of the experiments are reported in figures 4.3 and 4.4.

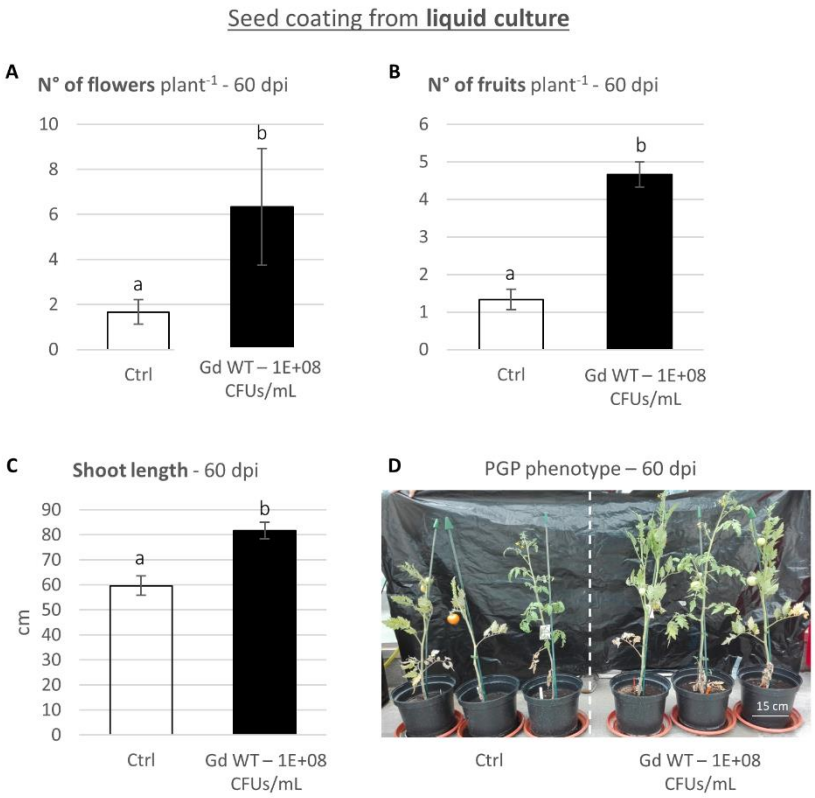


*Fig. 4.3. Growth promotion phenotype 60 days post inoculum (dpi) of tomato MoneyMaker plants inoculated through the seed coating technique with G. diazotrophicus WT (Gd WT) grown in liquid medium (**D**). Mock-treated controls plants (Ctrl) are shown as comparison. Average number of flowers per plant (**A**), average number of fruits per plant (**B**) and shoot length (**C**) are reported (N = 7). The standard error of the mean (SEM) is shown. Bars marked with the same letter within each chart do not differ by Mann–Whitney U test (P ≤ 0.05).*

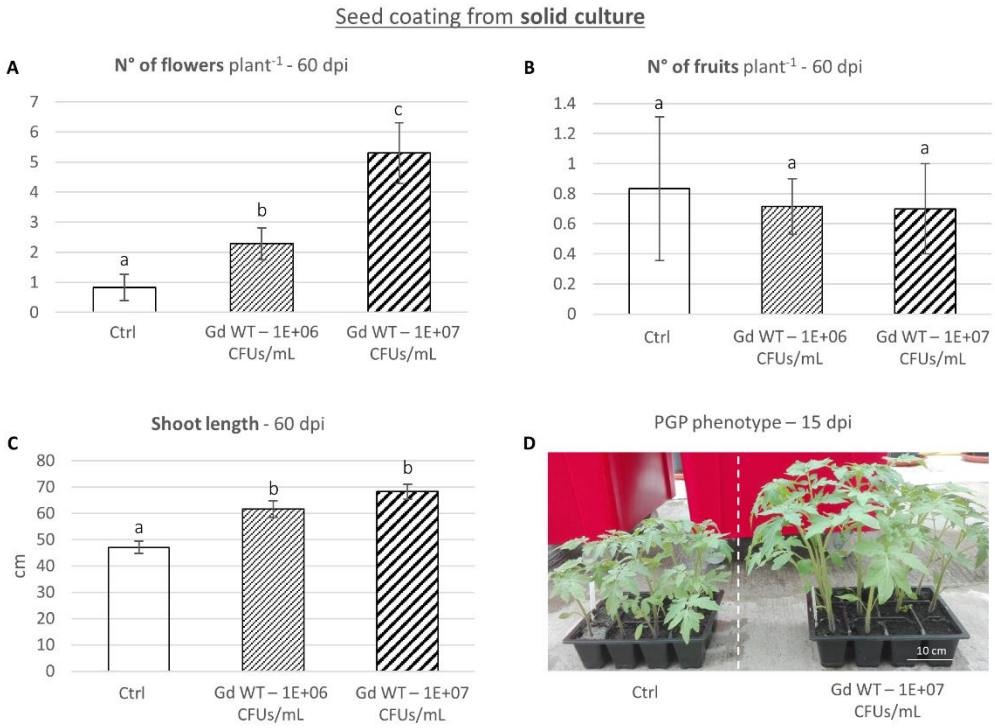


*Fig. 4.4. Growth promotion phenotype 60 days post inoculum (dpi) of tomato MoneyMaker plants inoculated through the seed coating technique with G. diazotrophicus WT (Gd WT) scraped from solid medium and resuspended at two different densities (**D**). Mock-treated controls plants (Ctrl) are shown as comparison. Average number of flowers per plant (**A**), average number of fruits per plant (**B**) and shoot length (**C**) are reported (N = 7). The standard error of the mean (SEM) is shown. Bars marked with the same letter within each chart do not differ by Kruskal-Wallis test (P ≤ 0.05).*

The phenotype elicited to tomato plants by the inoculant cultured in liquid ATGUS medium seemed to confirm the positive results previously observed in the same model system (Fig 4.3). This was visible in terms of the shoot length, with treated plants being 20 cm higher than controls on overage after two and up to four months post sowing (Fig 4.3c) and, mostly, in both floral and fruit yield per plant, almost tripled after 2 months compared to mock-treated controls (Fig 4.3a, b). As for the seeds inoculated with the two concentrations of *G. diazotrophicus* scraped from solid medium, however, the PGP evaluation was less in magnitude (Fig 4.4). First, the bacterial cell count from the inoculant applied to seeds in this experiment was found to be around one order of magnitude lower than the inoculant from liquid culturing, although diluted at the same OD_{600} = 2 during the formulation. Therefore, while the inoculant of *G. diazotrophicus* grown in liquid medium contained 10^8 CFUs mL^{-1}, the two

concentrations of the bacteria from the solid culture condition had, respectively, 10^7 CFUs mL^{-1} and 10^6 CFUs mL^{-1}. This is likely due to the fact that a percentage of bacterial cells embedded in the extracellular polymeric substances of the colonies grown on a solid support were non-viable. Nevertheless, despite of the lower cell concentration, a PGP was still visible, especially in the early plant growth stages. In fact, after 10 to 20 days post inoculum (dpi), the shoot of plants treated with the highest concentration of bacteria from solid culture were visibly longer than the controls (Fig 4.4d), to an extent that the plants treated with bacteria from liquid medium, although at a higher cell concentration, did not show at the same growth stage. After two months, this phenotype become less striking, although shoots were still consistently 10 to 20 cm longer than controls, regardless of the concentration of bacteria in the applied inoculant (Fig 4.4c). The average number of flowers per plant was also higher in the treated plants compared to the mock-treated, in a dose-dependent manner (Fig 4.4a), but this did not correspond to a higher fruit yield (Fig 4.4b).

This data suggests that the concentration of the bacteria applied to the seed surface is critical for the success of the inoculum in terms of the significance of the PGP induced, since a dose dependent effect was observed. The most striking phenotype elicited by the highest concentration of bacteria from solid medium during the early plant growth stages, could be the result of an efficient early tomato-bacteria cross talk, possibly mediated by the EPSs present in the inoculant, that could have primed a hormonal signalling in the plantlets. However, the lack of a sufficiently numerous bacterial population in the system may have not supported an enhanced plant growth in the long term, resulting in the aborted floral development to fruits. On the other hand, soaking the seeds with 10^8 CFUs mL^{-1} of *G. diazotrophicus* cultured in liquid ATGUS medium, resulted in a positive PGP effect, although not sufficient for a normal plant development in no nitrogen feed (as evidenced by the paler and fewer leaves of *G. diazotrophicus*-treated plants compared by routinely fertilised uninoculated ones at the same growth stage, not shown).

As the bacterial inoculant grown in liquid ATGUS medium proved to be a valid strategy for the tomato seed coating at 10^8 CFUs mL^{-1}, it was maintained as a standard for the following experiments.

Another parameter of this method, the carrier composition, was subsequently investigated. The sucrose present in the liquid carrier employed in the former experiments was used at 3% (87 mM). However, historically, sucrose has been used to improve inoculant adhesion to peat carriers at a concentration of up to 10% (292 mM) [60]. This is also the amount of sucrose present in the LGI-P medium, in which *G. diazotrophicus* is routinely grown [83], and grossly equals the concentration found in sugarcane parenchyma [189]. Therefore, to test whether an increased concentration of sucrose would favour the bacterial adhesion to the seed surface and ultimately support an improved colonisation and PGP, the liquid carrier composition was amended by increasing sucrose concentration to 10%. Polysorbate 80 was also increased to 0.5% (v/v) and gum Arabic to 1.5% to further support the adhesion of a higher number of bacterial cells to the seed surface. This new more concentrated carrier solution was compared with the former one, as well as with the use of sterile water with no other nutrient or adhesive agents. Furthermore, the inoculants so formulated were applied to both MoneyMaker (MM) and Ailsa Craig (AC) tomato varieties. Instead of focusing on the yield, the early growth promotion phenotype was assessed. Plants were grown as reported for the previous experiment and phenotyped one month after the germination (Fig 4.5, 4.6).

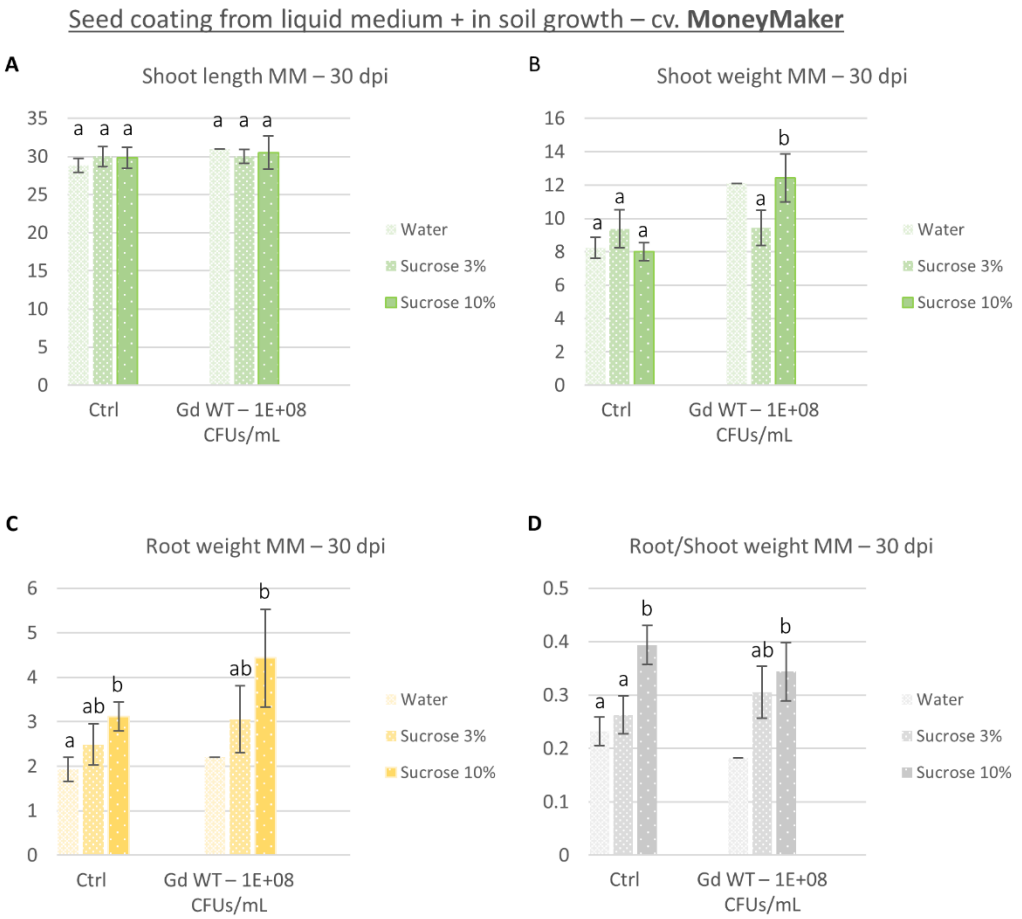


*Fig. 4.5. Phenotype at 30 dpi of tomato MoneyMaker plants (MM) inoculated through the seed coating technique with G. diazotrophicus WT (Gd WT) resuspended in either sterile water, 3% sucrose carrier or 10% sucrose carrier. Mock-treated controls plants (Ctrl) are shown as comparison. Shoot length (**A**), shoot weight (**B**), root weight (**C**) and root to shoot weight ratio (**D**) are reported. N = 7 for all the parameters tested. The standard error of the mean (SEM) is shown. Bars marked with the same letter within each chart do not differ by Kruskal-Wallis test ($P \leq 0.05$).*

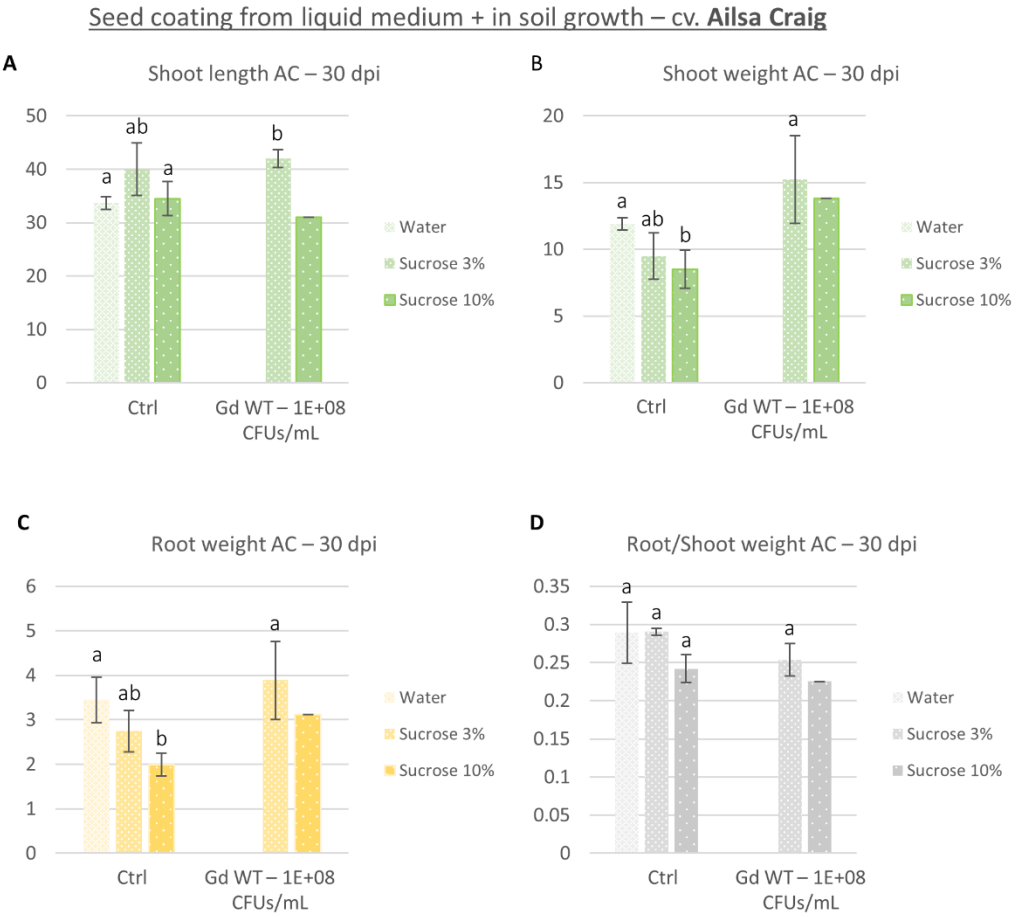


*Fig. 4.6. Phenotype at 30 dpi of tomato Ailsa Craig plants (AC) inoculated through the seed coating technique with G. diazotrophicus WT (Gd WT) resuspended in either sterile water, 3% sucrose carrier or 10% sucrose carrier. Mock-treated controls plants (Ctrl) are shown as comparison. Shoot length (**A**), shoot weight (**B**), root weight (**C**) and root to shoot weight ratio (**D**) are reported. N = 7 for all the parameters tested. The standard error of the mean (SEM) is shown. Bars marked with the same letter within each chart do not differ by Kruskal-Wallis test ($P \leq 0.05$).*

None of the inoculants tested elicited an increase in the shoot length after 30 dpi in MoneyMaker plants compared to mock treated controls (Fig. 4.5a), as already observed in the previous experiment at the same growth stage (*G. diazotrophicus* cultured in liquid medium condition). However, the highest sucrose concentration promoted an increased shoot biomass in the treated MoneyMaker tomatoes (Fig. 4.5b). The root weight also seemed to be increased at the highest sucrose concentration, although a great variability was observed between samples (Fig. 4.5c). Interestingly, the 10% sucrose inoculants promoted in both controls and *G. diazotrophicus*-treated plants a higher root-to-shoot ratio (Fig. 4.5d), a parameter know to increase in response

to stress or nutrient scarcity but also to hormonal alterations [190]. Conversely, no such effect was observed in the Ailsa Craig plants where, in fact, sucrose seemed to induce a decrease in the root biomass, regardless of the bacteria presence (Fig. 4.6c, d). It is possible that this observation reflects a differential early immune response of the two tomato varieties to other soil microorganisms feeding on the sucrose present on the seeds during the root emergence, toward which Ailsa Craig may be more susceptible. No obvious shoot biomass increase was observed either in the Ailsa Craig plants (Fig. 4.6a, b). This data show that, similarly to what observed in early *G. diazotrophicus* colonisation and BNF contribution experiments in sugarcane [191] [192], the tomato genotypes tested responded differently to the nutrients and bacteria in the inoculant. In this case, the cultivar MoneyMaker seemed to have a more positive response to the bacterial inoculant, even if at 30 dpi the PGP effect was not as obvious as after 60 dpi (Fig. 4.3). In support of this observation, a recent metagenomic analysis on 8 tomatoes genotypes, including the MoneyMaker variety, reported a very different response to bioinoculants application in terms of root and shoot growth and a differential modulation of the root microbiome assembly [193]; a similar cultivar-specific effect was also reported for Archaea-based inocula [194]. Contrary to the Ailsa Craig variety, in the cv. MoneyMaker the highest sucrose concentration in the carrier enhanced root and shoot growth compared to plain water regardless of the bacterial presence, and it increased the shoot biomass of treated plants compared to the control (Fig. 4.5b). This result highlights the importance of testing the variety-specific effect of bioinoculant application and of tailoring the concentration of nutrients and additives in the formulation accordingly.

Finally, the inoculant application method was investigated. The main drawbacks of the seed coating technique for bioinoculant applications are: 1) the limited amount of space available in the seeds surface for the PGPB to take contact with, and 2) the high chances of the inoculant film encapsuling the seed to be lifted out and dislodged during sowing and germination [68]. To address these disadvantages, a vacuum infiltration protocol was attempted. Vacuum infiltration consists in applying a vacuum to plant tissues submerged in a bacterial solution, causing the air entrapped in the plant to bubble off and

be replaced by the liquid inoculant. While this is a well-known method for enhancing the efficiency of *Agrobacterium* transformations [195], the vacuum infiltration application to seeds has been rarely reported in literature for plant-bacterial interactions studies [196]. In this experiment, *G. diazotrophicus* was grown in liquid ATGUS medium as already done in the previous setups, but was resuspended in sterile water instead of using the liquid carrier employed thus far; this was done, in spite of the worse PGP performance under plain water condition observed in the preceding experiment, to prevent any physical or osmotic damage to the embryo caused by the sucrose and the other sticky agents. For the same reason, the bacterium was resuspended at three different concentrations: the highest density, which already proved to be the most effective, corresponding to 10^8 CFUs mL^{-1}, along with two other concentrations one and two order of magnitude lower, i.e., respectively, 10^7 CFUs mL^{-1} and 10^6 CFUs mL^{-1}. Seeds were treated for 1 hour, dried and sowed in early September. The phenotype was evaluated at two (Fig. 4.7) and four (Fig. 4.8) months after sowing (60 and 120 dpi).

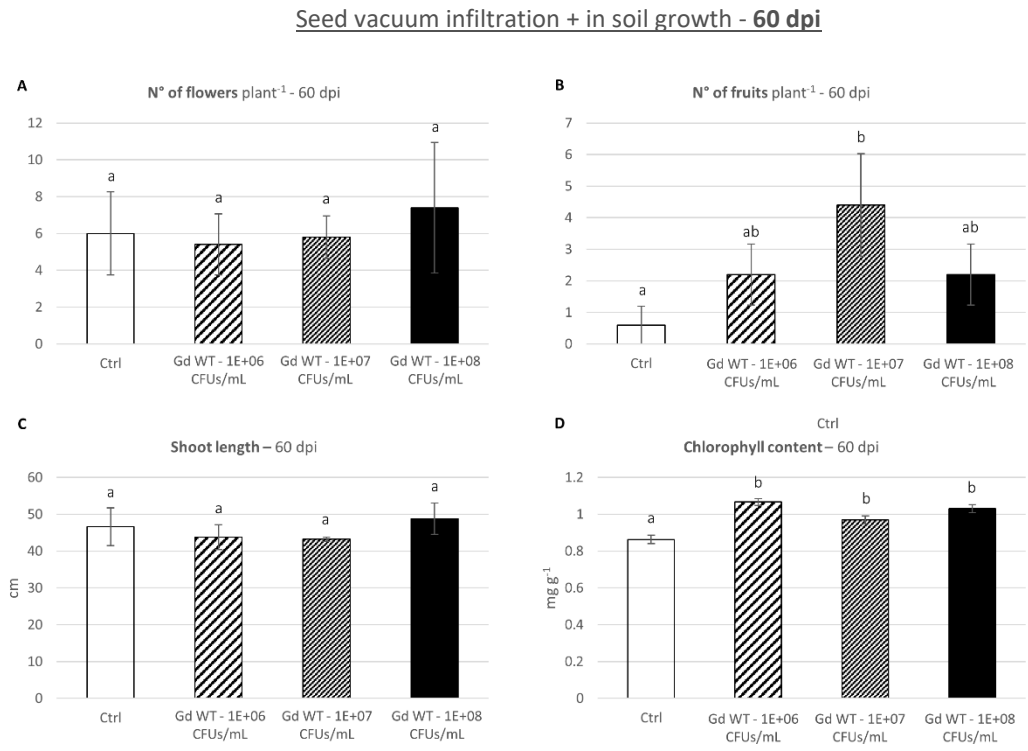


*Fig. 4.7. Phenotype at 60 dpi of tomato MoneyMaker plants inoculated through the seed vacuum infiltration technique for 1 hour at 800 mbar with G. diazotrophicus WT (Gd WT) grown in liquid medium and resuspended in water at three different densities. Mock-treated control plants (Ctrl) are shown as comparison. Average number of flowers per plant (**A**), average number of fruits per plant (**B**), shoot length (**C**) and chlorophyll content (**D**) are reported. N = 35 for SPAD measurements and 7 for all the other parameters tested. SPAD measurement conversion to chlorophyll content was calculated as in Jiang et al. (2017)* [197]. *The standard error of the mean (SEM) is shown. Bars marked with the same letter within each chart do not differ by Kruskal-Wallis test ($P \leq 0.05$).*

At 60 dpi, no difference was observed in the flower abundance per plant (Fig. 4.7a) or in the shoot length (Fig. 4.7c) but there was a significant fruit yield increase compared to controls, especially in the seed treated with 10^7 CFUs mL^{-1} (Fig. 4.7b). Furthermore, the chlorophyll content, that was measured through a SPAD meter, was found to be significantly higher in all the treated plants, regardless of the bacterial concentration (Fig. 4.7d). Since chlorophyll content is found to be correlated with nitrogen availability [198] [199] these data suggest that the presence of *G. diazotrophicus* under low N conditions may confer an advantage in terms of nitrogen metabolism, either by providing fixed N_2 or by enhancing nutrients uptake.

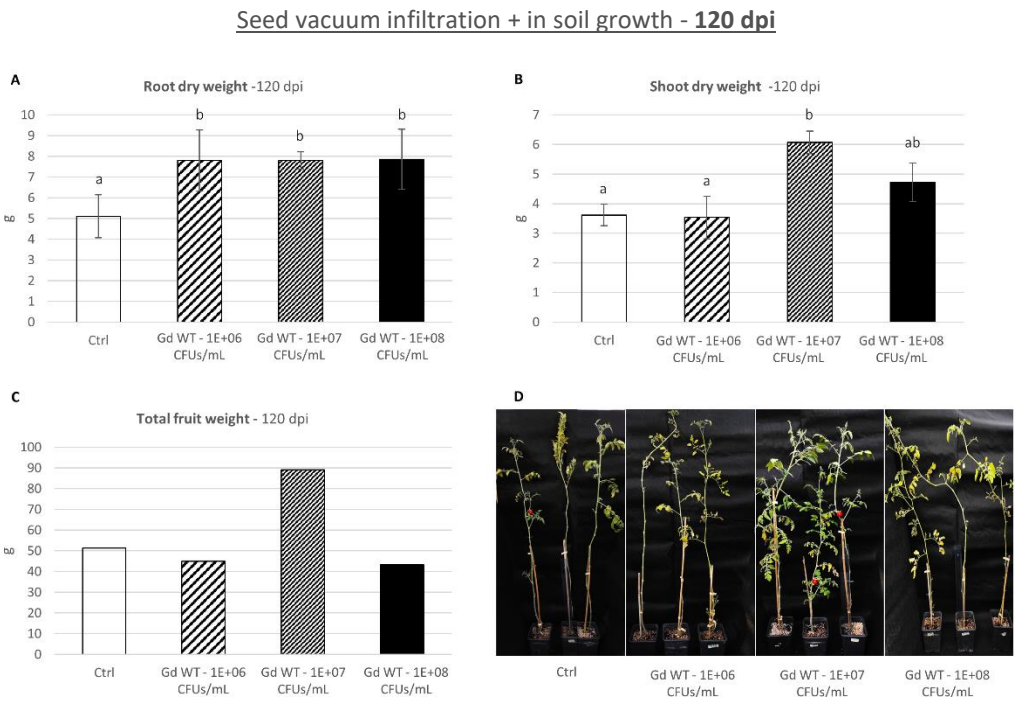


*Fig. 4.8. Phenotype at 120 dpi of tomato MoneyMaker plants inoculated through the seed vacuum infiltration technique for 1 hour at 800 mbar with G. diazotrophicus WT (Gd WT) grown in liquid medium and resuspended in water at three different densities (**D**). Mock-treated controls plants (Ctrl) are shown as comparison. Root dry weight (**A**), shoot dry weight (**B**) and total fruit weight (**C**) are reported. N = 7 for all the parameters tested. The standard error of the mean (SEM) is shown. Bars marked with the same letter within each chart do not differ by Kruskal-Wallis test ($P \leq 0.05$).*

In support of the latter hypothesis, the measurement of the root dry weight at 120 dpi revealed an increased biomass in all the treated plants (Fig. 4.8a), although a corresponding increase in the shoot dry weight was only observed in the 10^7 CFUs mL^{-1} inoculated plants (Fig. 4.8b). The same samples produced the highest yield in terms of total weight of fruits harvested 120 dpi (Fig. 4.8c).

The PGP effect elicited by *G. diazotrophicus* when applied through the seed vacuum infiltration technique seemed to mostly increase at the specific concentration of 10^7 CFUs mL^{-1}, while higher or lower bacterial densities were not equally effective. The results show that, with further similar tests, an ideal concentration of bacterial could be experimentally determined for this inoculation method. In particular, these data suggest that such concentration needs to be high enough for establishing a successful growth promoting colonisation, but not to the point of affecting the plant development and,

therefore, negatively counterbalancing the PGP effect; this seemed to be the case for the 10^8 CFUs mL^{-1} inoculant being less effective than the 10^7 CFUs mL^{-1}. Considering the importance of the seed endosperm tissue for germination and embryo development, is unsurprising that excessive bacterial infiltration can partially compromise plant growth in the long term [200].

These data combined proved that *G. diazotrophicus* AZ0019, applied to tomato seeds (cv. MoneyMaker), is able to exert a PGP effect to plants grown in soil. This finding highlights the ability of the bacterium to colonise its host and proliferate at least to the point of reaching the critical biomass needed to elicit a biologically relevant effect. It is possible that the combined effect of the mannitol-induced EPSs produced in the growth media and the sucrose present in the liquid carrier offered a niche that, even in the harsh soil environment, could favour *G. diazotrophicus* survival in the seedling long enough to mediate a PGP effect. Although not critical, the amount of sucrose in the inoculant was ascertained to mediate a more effective PGP compared to a nutrient-free carrier (Fig 4.5). The tomato cultivar MoneyMaker was found to respond better than the Ailsa Craig variety (Fig 4.6), and a bacterial dose-dependent effect was also observed. While this concentration effect may impart the idea of using the highest possible cells count when using the seed coating method (Fig.4.3, 4.4), a more complex dynamic was observed after the vacuum infiltration technique (Fig. 4.7); the phenotypic data obtained, together with the observation through microscopy that in vacuum infiltrated seeds the bacterial cells penetrate deeper in the seed endosperm (section 4.3.1, Fig. 4.50), highlight the potential risk of this method and the need for further and finer protocol optimisations. The positive effects induced by *G. diazotrophicus* to tomato plants included enhanced yield (Fig. 4.3b, 4.7b, 4.8c), shoot biomass (Fig. 4.3c, 4.4c, 4.5b, 4.8b), root biomass (Fig. 4.5c, 4.8a) and chlorophyll content (Fig 4.8a). The larger root system suggests a more effective nutrient uptake capability, and the increased chlorophyll concentration could indicate an advantage in the nitrogen availability or uptake, possibly mediated by *G. diazotrophicus* BNF. Despite of a similar root biomass increase, only some treatments resulted in an equally enhanced shoot biomass production (Fig. 4.8a, b): this may indicate that, for a full PGP, the *G. diazotrophicus*-induced growth stimulation from the

rhizosphere needs to be combined with a successful establishment of the bacterium in the aerial parts of the plants, resulting in a more complete interaction that ultimately leads to the desired yield increase.

However, in all the afore mentioned experiments, a considerable variability between biological replicates was experienced. The improved phenotype was observed up to four months post-inoculum in at least two experimental replicates for each test and was present to some extent in subsequent repetitions. However, the PGP was primarily noticeable during a specific, and often heterogeneous, plant growth stage, and became less pronounced during later stages of plant maturation. This variability is consistent with what previously reported for similar trials [201], and is due to the intrinsic complexity of the soil and other environmental factors impacting plant growth in field or glasshouse. The success of colonisation establishment, not investigated in this setup, is likely to be instrumental in causing the phenotypic discrepancies observed: in fact, even when investigating sugarcane, the natural host of *G. diazotrophicus*, the lack of colonisation has often been reported in greenhouse experiments conducted with non-sterile soils, presumably due to rapid death of the bacteria [163].

To overcome the variability of in-soil experiments and gain fine control over crucial variables in the plant-bacteria interaction, a hydroponics setup was developed for further investigations.

4.1.1c Hydroponic systems provided a highly controllable setup and revealed an enhanced PGP in WT-inoculated plants compared to the BNF-impaired mutant

Commercially, hydroponic tomatoes are primarily grown through the drip irrigation system, which was found to improve tomato nutritional value and antioxidant levels [202]. However, for practical reasons, the system adopted in this study was ascribable to a deep-water setup, in which plants are grown on suspended supports above the nutrient solution, where the roots are submerged

and grow unconstrained. Given the short-term duration of the experiments conducted with this setup (never exceeding one month post inoculum) and to ulteriorly reduce the variables of the system, no mechanical aeration was added; however, this is a parameter that will have to be investigated in the future, considering the different diffusion and solubility dynamics of BNF relevant gases such as O_2 and N_2 in water as compared to soil substrates [203]. The NS employed was previously adapted in the University of Nottingham (unpublished) from the commonly utilised Hoagland's solution [204]; the differences include a lower amount of potassium and calcium (respectively 97.75 mg L^{-1} and 100.20 mg L^{-1}) and a slightly higher concentration of micronutrients, among which molybdenum is essential for the nitrogenase functioning (see Table 3.2). Conveniently, the temperature in the growth chamber was kept at 28 °C, which is optimal for both tomato and *G. diazotrophicus* growth.

In the first hydroponic test, the vacuum infiltration technique was utilised to treat tomato cv. MoenyMaker seeds and verify whether, in this setup, a PGP effect could be observed. The formulation was carried out in a plain water carrier as already performed for the in-soil vacuum infiltration trial; after 30 minutes under vacuum, seeds were briefly dried and placed on the NS-filled cavities of the plant support structure. Due to the seeds being directly submerged in the NS, a higher chance of washing off the bacterial coating from the seeds during their deposition and germination was expected, possibly resulting in a poorer colonisation which would entirely rely on the bacteria infiltrated inside the seed tissues. This experiment was conducted parallelly with two different nitrogen concentrations. The first test was conducted in nutritional stress condition, with no nitrogen source added to the NS (zero N condition); in the second test, a source of nitrogen was provided in the form of 0.2 mM KNO_3. Potassium nitrate is a valuable and widely employed nitrogen source for plants, which was proved to be particularly beneficial for tomato growth [205]. Crucially, *G. diazotrophicus* is unable to utilise nitrate directly as a N source due to the lack of a nitrogen reductase [83], and, unlike other diazotrophs, its nitrogenase enzyme does not seem to be inhibited even in high nitrate concentrations [206] [207]. Therefore, it was hypothesised that in such

hydroponic setup the absence of a nitrogen source available to the bacterium (apart from N traces in the root exudates) could encourage BNF.

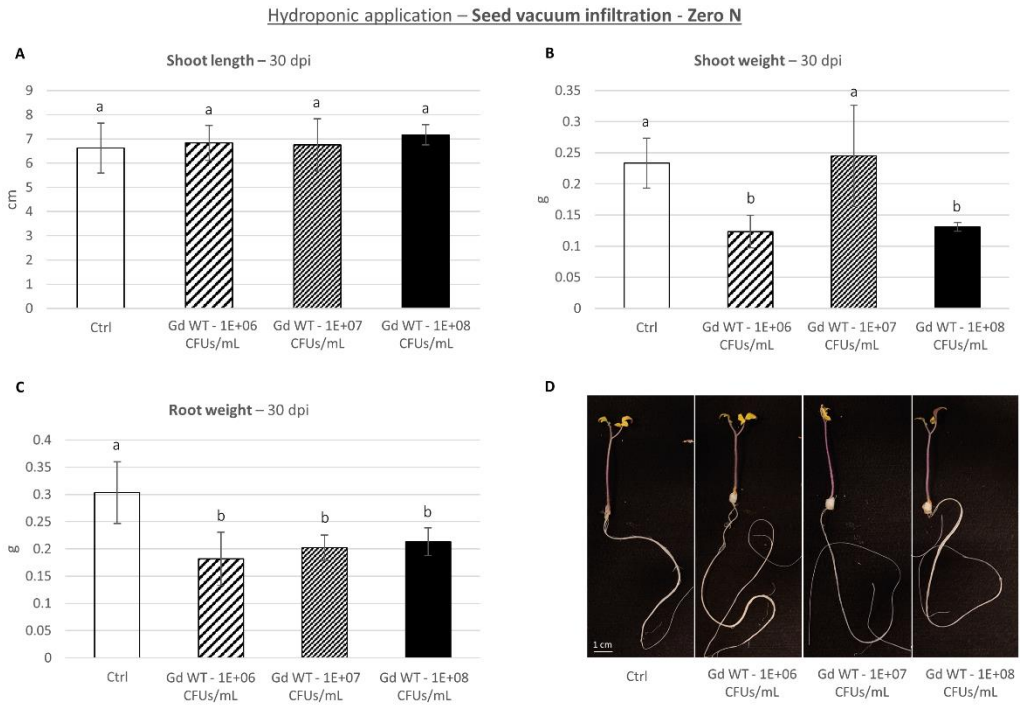


*Fig. 4.10. Phenotype at 30 dpi of tomato MoneyMaker plants hydroponically grown in zero N condition (**D**). Plants were inoculated through the seed vacuum infiltration technique for 3o min at 800 mbar with G. diazotrophicus WT (Gd WT) resuspended in NS at three different densities. Mock-treated controls plants (Ctrl) are shown as comparison. Shoot length (**A**), shoot weight (**B**) and root weight (**C**) are reported. N = 10 for all the parameters tested. The standard error of the mean (SEM) is shown. Bars marked with the same letter within each chart do not differ by Kruskal-Wallis test (P ≤ 0.05).*

At 30 dpi, no difference was observed in the zero N condition in terms of shoot length, while shoot fresh weight decreased under the lowest and highest bioinoculant densities (Fig. 4.10a, b). The root system, on the other hand, seemed to be inhibited by the bacterial presence (Fig. 4.10c). In the 0.2 mM KNO_3 condition, however, a significant biomass increase was observed in both shoots and roots, especially in the case of seed vacuum infiltrated with 10^7 CFUs mL^{-1} (Fig. 4.11).

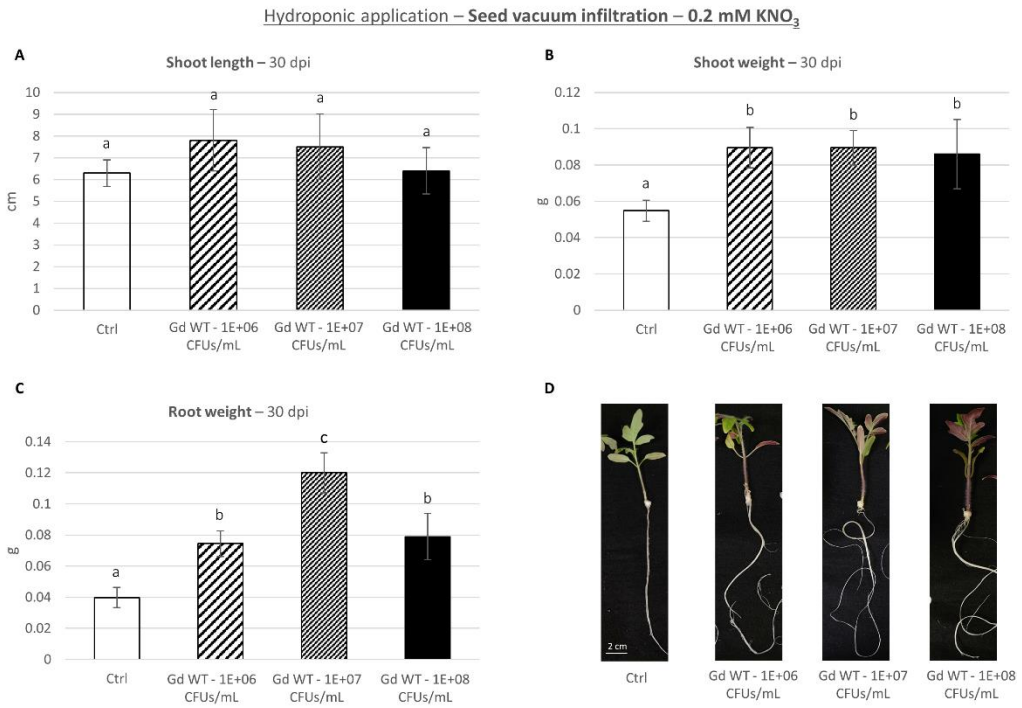


*Fig. 4.11. Phenotype at 30 dpi of tomato MoneyMaker plants hydroponically grown in 0.2 mM KNO_3 condition (**D**). Plants were inoculated through the seed vacuum infiltration technique for 30 min at 800 mbar with G. diazotrophicus WT (Gd WT) resuspended in water at three different densities. Mock-treated controls plants (Ctrl) are shown as comparison. Shoot length (**A**), shoot weight (**B**) and root weight (**C**) are reported. N = 10 for all the parameters tested. The standard error of the mean (SEM) is shown. Bars marked with the same letter within each chart do not differ by Kruskal-Wallis test ($P \leq 0.05$).*

The phenotype observed in this preliminary experiment showed that, in zero N condition, the seed vacuum infiltration did not produce any advantage in terms of PGP, and, in fact, resulted in a smaller root system. It is possible that the bacterial presence within the seed tissues, in a context of nutritional stress induced by the absence of nitrogen, may negatively affect the roots emergence. To corroborate the assumption that the effect observed was elicited by the bacterium, its presence was screened in shoots and roots via plant tissue maceration, followed by plating in ace-LGIP selective medium and colony PCR with *G. diazotrophicus* AZ0019 specific primers (see Primers table 3.3): the successful migration of the bacterium from the seed to plant tissues was confirmed, and the cell count was estimated to be around 10^4 CFUs g^{-1} in roots and 10^3 CFUs g^{-1} in shoots, although with a great variability between biological replicates (data not shown). On the other hand, the presence of a low amount of nitrate in the NS could counterbalance any negative consequence of the application method, and sustain a bacteria-mediated plant growth

promotion effect in the treated seeds. In accordance with what observed in the seed vacuum infiltration trial coupled with in-soil growing (Fig. 4.8), the intermediate density of bacteria seemed to induce the most positive response. These results indicated that, even though *G. diazotrophicus* was proven to be able to migrate from the vacuum infiltrated seeds to plant tissues, in light of the negative effects in zero N condition and of the great variability among replicates that was observed, this application method may not optimal for the hydroponic setup. Therefore, a new inoculation protocol, in line with other routinary application methods of bioinoculants in hydroponic systems, was developed and adopted in University of Nottingham (for further details refer to M. Franchini's PhD thesis [208]).

Briefly, *G. diazotrophicus* was grown on liquid ATGUS, washed once to remove any trace of growth medium, and resuspended in water. It was then directly inoculated to a final optical density of OD_{600} = 0.3 (corresponding to around 10^7 CFUs mL^{-1}) in the NS of the hydroponic system, in which tomato cv. MoneyMaker plants had been pregerminated for 5 to 10 days. At the time of the inoculation, the primary roots were 3 to 5 cm long. Outlier plantlets with abortive germination or longer roots and shoots were removed prior to the inoculum, and the same number of samples was kept in each hydroponic unit to reduce errors caused by a differential bacterial response to different root density per unit area. The inoculant was kept in the system for 48 hours, following which the NS was removed and replaced with a fresh, non-inoculated solution. Through this setup, the interplay between the N source in the nutrient solution and the bacterium-elicited PGP was investigated. Along with the "zero N" stress condition, a "N replete" condition was tested, with the nitrogen level set at 2 mM KNO_3 as in Jensen and Malter, 1995 [209] (although other guidelines for open soilless greenhouse tomato production suggest a NO_3 use of up to 16 mM [210]). Furthermore, a third condition was evaluated, in which the 2 mM KNO_3, available for the plant but not for the bacterium, was supplemented with 0.2 mM $(NH_4)_2SO_4$; this small amount of ammonium, bioavailable for the bacterial usage, was added to assess whether the presence of a N source external to the tomato-*G. diazotrophicus* system would have sustained a more vigorous bacterial growth and stimulated N_2-

fixation. This experiment was conducted with both *G. diazotrophicus* AZ0019 wild type (Gd WT) and *G. diazotrophicus* AZ0019 *nifD*$^{-}$ (*Gd nifD*$^{-}$), a mutant strain previously developed in the University of Nottingham in which the *nifD* gene was disrupted by partial deletion and insertion of a kanamycin resistance cassette; the loss of nitrogen fixation capability was confirmed through acetylene reduction assay (ARA) [208]. The aim of this experiment, parallelly to investigating the differential PGP effect elicited by the wild-type bacterium as compared to the nitrogen fixation impaired strain in different N conditions, was also to estimate the amount of BNF-derived nitrogen incorporated in the plant tissues. To achieve this, the afore mentioned hydroponic system was set up as a ^{15}N isotope dilution experiment (see section "4.2.1c Evaluation of N-fixation contribution"), and the nitrate and ammonia were added in the form of 2 mM $K^{15}NO_3$ and 0.2 mM $(^{15}NH_4)_2SO_4$. During the experiment, N-free NS was used to top up the hydroponic systems in all the conditions, to favour a gradual decrease of nitrogen and encourage BNF. After 20 days of growth at 29 °C in a growth cabinet, samples were collected, and phenotype was evaluated (Fig. 4.12 - 4.14).

In the zero N condition, the wild-type strain led to a significant increase of root (Fig. 4.12c) and aerial (Fig. 4.12b) biomass, along with an enhanced shoot height (Fig. 4.12a). The *nifD*$^{-}$ mutant strain elicited a similar effect (Fig. 4.12b, c), although to a lower extent and with no shoot length promotion (Fig. 4.12a). In the N replete condition, the same pattern was observed for roots biomass increase (Fig. 4.13c) and shoot length (Fig. 4.13a), with the WT strain having the most beneficial effect and the *nifD*$^{-}$ promoting a lower root growth; however, no significant shoot biomass promotion could be detected in either treatment as compared to uninoculated controls (Fig. 4.13b).

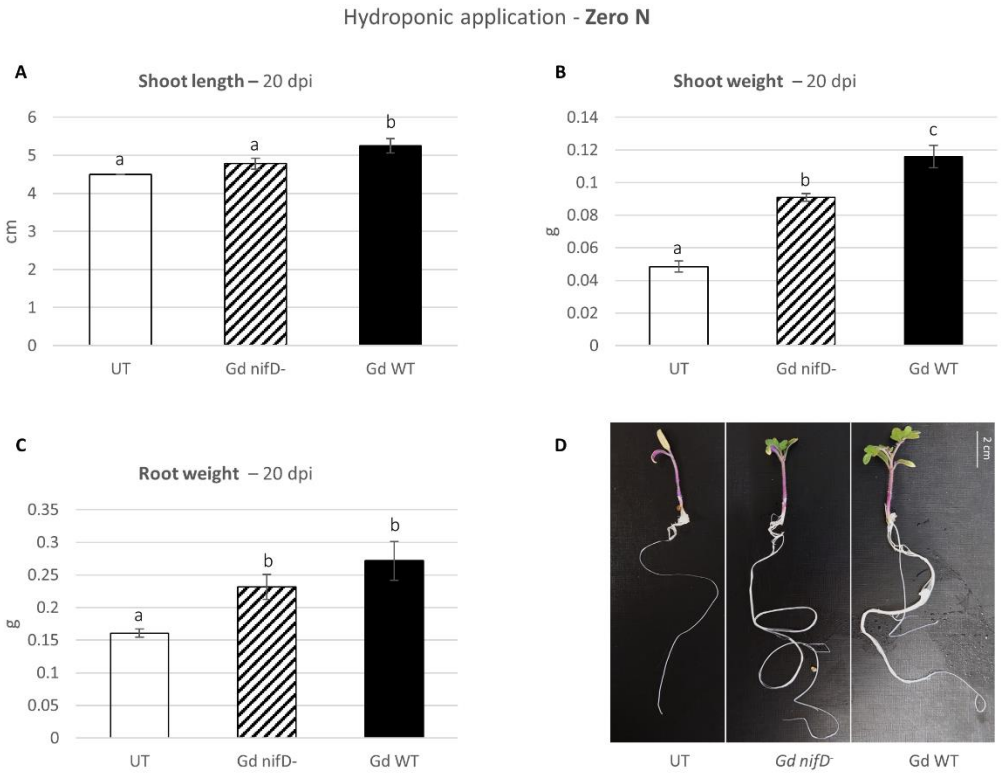


*Fig. 4.12. Phenotype at 20 dpi of tomato MoneyMaker plants hydroponically grown in zero N condition (**D**). G. diazotrophicus WT (Gd WT) or nifD- (Gd nifD-) strains were inoculated in the hydroponic NS at OD_{600} = 0.3 and kept for 48 h. Uninoculated controls plants (UT) are shown as comparison. Shoot length (**A**), shoot weight (**B**) and root weight (**C**) are reported. N = 10 for all the parameters tested. The standard error of the mean (SEM) is shown. Bars marked with the same letter within each chart do not differ by Kruskal-Wallis test ($P \leq 0.05$).*

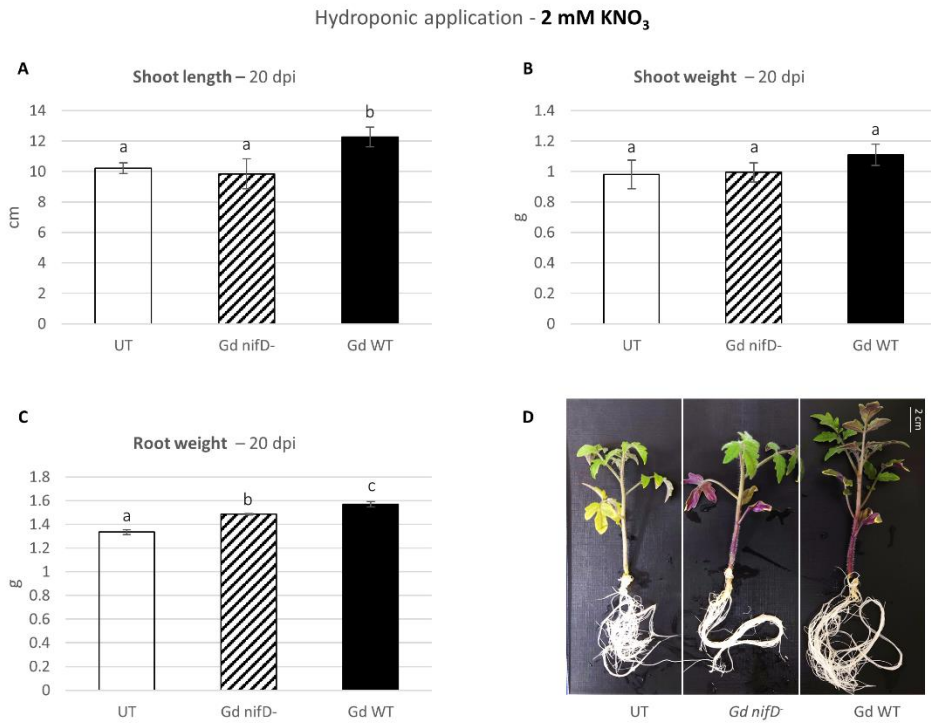


*Fig. 4.13. Phenotype at 20 dpi of tomato MoneyMaker plants hydroponically grown in 2 mM KNO_3 condition (**D**). G.diazotrophicus WT (Gd WT) or nifD$^-$ (Gd nifD$^-$) strains were inoculated in the hydroponic NS at OD_{600} = 0.3 and kept for 48 h. Uninoculated controls plants (UT) are shown as comparison. Shoot length (**A**), shoot weight (**B**) and root weight (**C**) are reported. N = 10 for all the parameters tested. The standard error of the mean (SEM) is shown. Bars marked with the same letter within each chart do not differ by Kruskal-Wallis test ($P \leq 0.05$).*

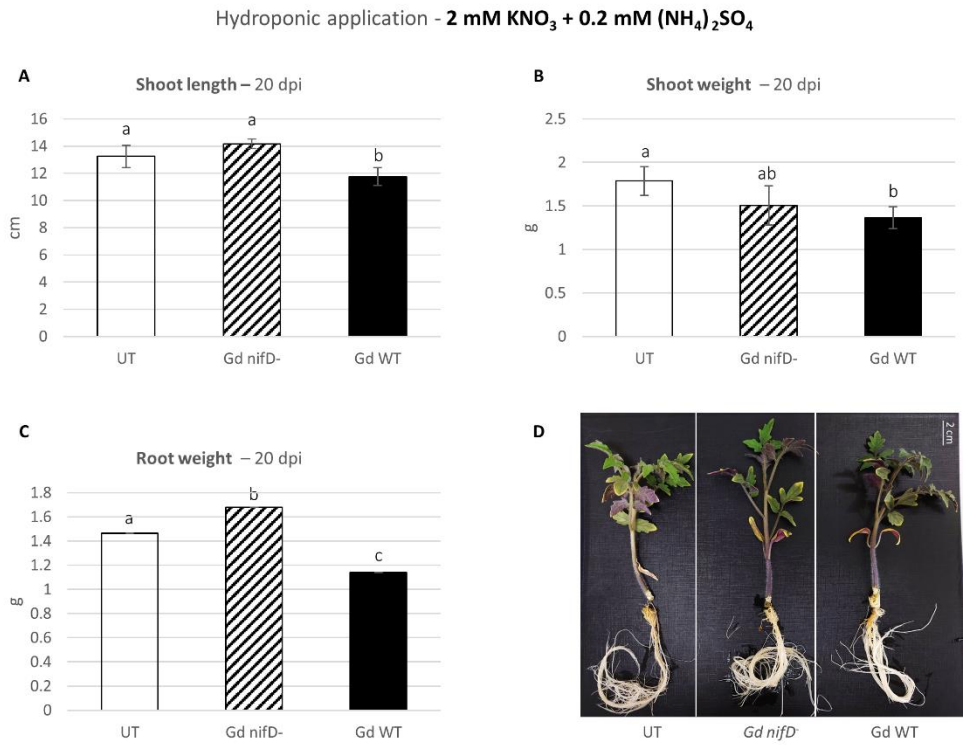


*Fig. 4.14. Phenotype at 20 dpi of tomato MoneyMaker plants hydroponically grown in 2 mM KNO_3 + 0.2 mM $(NH_4)_2SO_4$ condition (**D**). G. diazotrophicus WT (Gd WT) or nifD$^-$ (Gd nifD$^-$) strains were inoculated in the hydroponic NS at OD_{600} = 0.3 and kept for 48 h. Uninoculated controls plants (UT) are shown as comparison. Shoot length (**A**), shoot weight (**B**) and root weight (**C**) are reported. N = 10 for all the parameters tested. The standard error of the mean (SEM) is shown. Bars marked with the same letter within each chart do not differ by Kruskal-Wallis test ($P \leq 0.05$).*

Unexpectedly, when some ammonium was introduced in the system (Fig. 4.14), the WT strain seemed to cause a reduction of all growth parameters tested (Fig. 4.14a.c), while the mutant strain had no impact on shoots but induced a moderate root biomass increase (Fig. 4.14c).

To verify whether the phenotypes observed across the three N conditions were dependent on different colonisation patterns, and to estimate the bacterial presence in plant tissues over time, root and shoot samples were collected at one and twenty dpi (beginning and ending of the experiment, respectively), macerated, and plated in ace-LGIP medium. This method, known as the Most Probable Number (MPN), allows the reisolation and counting of culturable diazotrophic bacteria per gram of plant sample, upon their maceration and serial dilution in selective medium [211]. The ace-LGIP was adapted from the widely employed LGI-P medium [212] by amending it with a buffer at pH 4

(see Materials and Methods); although the hydroponic cultures were kept in only partially gnotobiotic conditions (the growth cabinet was thoroughly sanitised before starting the experiment, seeds were surface sterilised prior to germination, NS was autoclave-sterilised, and no other sample was introduced in the cabinet for the duration of the trial, however the environment was not strictly sterile due to the need of periodically topping up the system with fresh NS), the high concentration of sucrose (100 g L^{-1}) and low pH make this medium selective for *G. diazotrophicus*, in which it grows forming characteristic orange colonies [83]. However, it is important to mention that, in comparison to more sensitive assays such as qPCR or ELISA, the MPN is known to underestimate the diazotrophs population due incomplete bacteria release from plant tissues and non-homogenous suspension before plating, as also shown in the case of *G. diazotrophicus* [213].

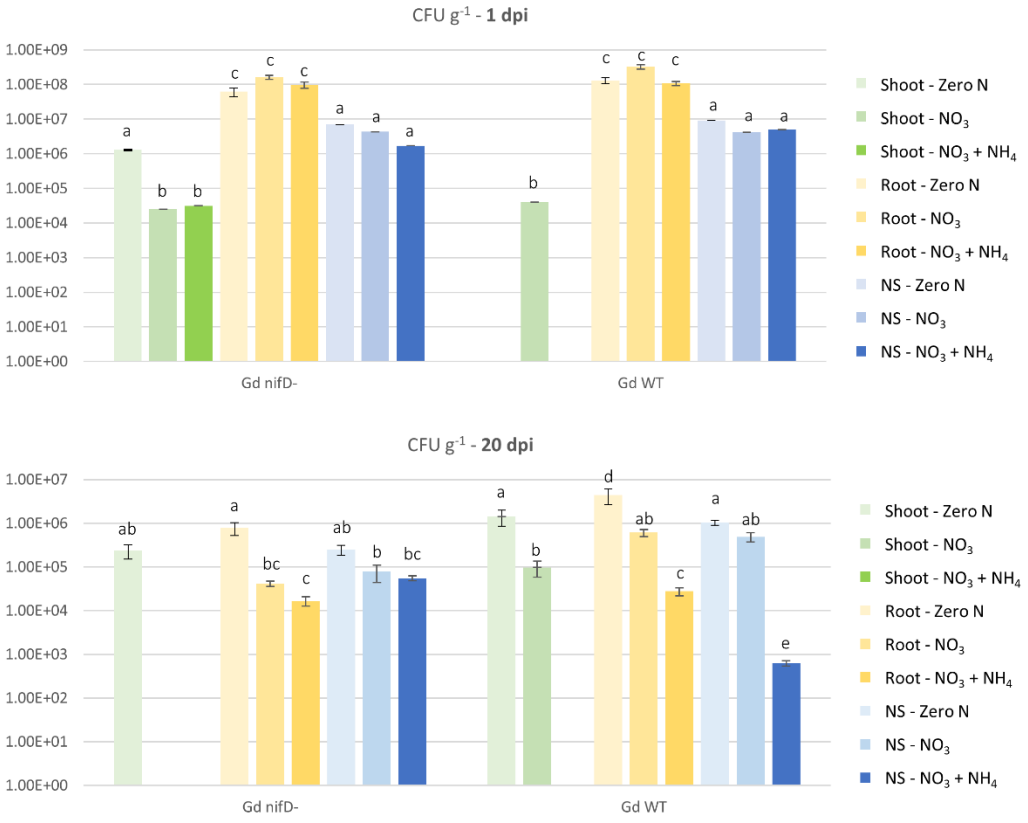


Fig. 4.15. G. diazotrophicus WT (Gd WT) or nifD⁻ (Gd nifD⁻) colonisation rate of tomato MoneyMaker plants hydroponically grown in either zero N, 2 mM KNO_3 ("NO_3") or 2 mM KNO_3 + 0.2 mM $(NH_4)_2SO_4$ ("NO_3 + NH_4") conditions. CFUs plant g^{-1} at 1 and 20 days post inoculum (dpi) are reported as distinguished in shoot, roots and hydroponic nutrient solution (NS). No bacteria were isolated from uninoculated controls. Bars marked with the same letter within each chart do not differ by Kruskal-Wallis test ($P \leq 0.05$, $N = 3$).

For this assay, any bacteria that remained associated with the plant samples after washing them in a 10 mM $MgCl_2$ solution to remove loosely attached, non-interacting cells were collectively considered to be actively colonising tomato tissues, without distinguishing between epiphytic and endophytic colonisation. This approach was taken to ensure that no potential PGP mechanisms related to the two different colonisation strategies were excluded. The presence of free-living bacteria in the NS was also screened by serial diluting and plating NS samples. Results are reported in Fig 4.15.

The data obtained indicate how *G. diazotrophicus* can promote tomato growth when applied as an inoculum in the hydroponic nutrient solution. When grown in zero N, tomato seemed to benefit the most from the bacterial-induced PGP, with the WT strain inducing a significantly more positive effect compared to the nitrogen fixation impaired mutant (Fig. 4.12). Colonisation data estimated 10^6 *GD nifD*$^-$ CFUs g^{-1} from shoot tissues at 1 dpi and around 10^8 CFUs g^{-1} in the root system for both strains (Fig. 4.15); no WT cells were recovered from aerial tissues at 1 dpi, but this could be due to a technical artifact such as uneven maceration or sampling, since after 20 days 10^6 GD WT CFUs g^{-1} were found in the same N condition.

In the N replete condition, no shoot biomass increase promoted by the either strain was observed (Fig. 4.13b), although a small but statistically significant increase in root material was present. This result is in contrast with what previously described by similar analyses conducted with the same setup and N input, in which an enhanced aerial biomass accumulation was reported to be induced by both strains, with a stronger effect from the WT bacterium [208]. The colony count at 20 dpi (when the phenotype was evaluated) in the N replete condition showed, for the Gd WT treatment, 10^6 CFUs root g^{-1} and around 10^5 CFUs shoot g^{-1}, suggesting a good colonisation, although an order of magnitude lower than in the zero N setup. Therefore, the lack of an obvious PGP phenotype in terms of fresh shoot weight, conversely to what reported before in similar trials, could be explained by *G. diazotrophicus* contribution to the plant nutrition being neglectable after 20 dpi in N replete condition (previous analyses were conducted at 14 dpi [208]); alternatively, it can be hypothesized that a slight but somehow impactful difference in the use of the

^{15}N isotope by the plant could result in a different host-bacterial nutrients exchange dynamic [214]. It is also worth mentioning that, in the previous afore mentioned trials [208], the hydroponic cultures were routinely topped up with NS containing the same N source and level of the corresponding treatment, whereas in this experiment all the N conditions were refilled with zero N nutrient solution to encourage BNF. Altogether, the data obtained seem to suggest the need for a minimum amount of N to be constantly supplemented in the system. In the zero N condition, the presence of *G. diazotrophicus* could significantly alleviate the N starvation phenotype (Fig. 4.12) to an apparently superior extent compared to the N replete conditions, and both strains exhibited a higher colonisation rate; however, such nutritional stress did not allow long term plant growth without any exogenous nitrogen. Therefore, to fully benefit from the bacterial PGP, it seems to be particularly favourable a condition in which the N level (yet to be precisely determined) is relatively low (as compared to modern greenhouse standards [215]), but high enough to guarantee a healthy plant development in the long term and at the same time ensuring adequate root exudate levels to promote bacterial growth. As for the N replete condition amended with 0.4 mM NH_4, the negative response of tomato to the inoculants (Fig. 4.14) could be explained by a direct effect of ammonium on the bacterial metabolism, and by the inefficient root colonisation revealed by the colony count (Fig. 4.15). On one hand, the presence of a N source available for the bacterium could have discouraged BNF and reduced its dependency on roots exudates. Theoretically, *G. diazotrophicus* nitrogenase was reported to decrease activity at 1 mM NH_4 and stop it completely at 10 mM NH_4 in some studies [216], and to be still active up until 20 mM NH_4 in other studies [217]; however, all these previous evaluations were conducted in plates with high carbon conditions, and never on hydroponic setups, where nutrients and gases diffuse in an enclosed water based system. On the other hand, the presence of ammonium as low as 1 mM was reported to negatively affect *A. thaliana* roots development by decreasing cell length, columella cells number, root meristem size and number of dividing cells [218], and to upregulate genes associated with plant defence and immunity [219]. All these factors combined could have caused an impairment of the bacterium establishment on plant tissues, and could therefore explain the

decrease of both strains reisolation rate, found to be absent in shoot tissues at 20 dpi and only around 10^4 CFUs g^{-1} in roots (Fig. 4.15). In support of this, Munoz-Rojas and Caballero-Mellado observed a decline in *G. diazotrophicus* population of micro propagated sugarcane plants even upon the addition of 0.35 mM $NH_4 NO_3$ [191].

As a general trend, Gd WT treatments seemed to result in slightly higher bacterial cell counts compared to *GD nifD*$^-$ treated plants, in contrast with previous studies with sugarcane [220] and hydroponically grown tomato [208], in which wild type and *nifD*$^-$ *G. diazotrophicus* strains were reported to colonise plants to the same level. CFUs g^{-1} were always lower in the aerial parts than in roots, as already reported for both tomato-*G. diazotrophicus* models and other endophytic population [201]. At the beginning of the experiment, the number of bacteria found in the root system was unsurprisingly similar between treatments regardless of the N condition, suggesting a stochastic adhesion to root tissues during early colonisation stages; however, the increase of this number by around one order of magnitude at 1 dpi (10^8 CFUs plant g^{-1}) compared to the amount of cells inoculated in the NS (10^7 CFUs mL^{-1}) hints at an active migration and concentration of bacteria in plant tissues. 10^6 CFUs mL^{-1} of both strains were recovered from the medium at 1 dpi in all N conditions, probably due to carryover and cells washed off the roots during the removal of the inoculum-containing NS and its substitution with fresh non-inoculated solution after the 48 hours of incubation. The number of bacteria in the NS decreased over time, especially in the presence of ammonium, suggesting a faster drop of bacterial population in the system in which the interactions with the host plant were reduced. After 20 days, a clear colonisation pattern emerged, with a lower number of bacterial cells reisolated from plant tissues as the N input in the system increased; this is consistent with the general observation that *G. diazotrophicus* colonisation rates fall at increasing fertilisation levels [100]. The gradual decline in bacterial population overtime is commonly reported for non-pathogenic endophytes, including *G. diazotrophicus*, the concentration of which was found to decline after early colonisation stages, especially when host plants were grown or transferred in to pots under greenhouse conditions [221]. This

probably reflects the effect of dilution and spatial limitation of these microorganism's ecological niches as the plants grow beyond the seedling stage [222]. In 2012, upon the treatment of tomato seedling with 10^9 *G. diazotrophicus* UAP5541 CFUs mL^{-1} and their cultivation in semi solid Fahräeus medium (0.5% agar) [174], Luna et al. reported the reisolation of 10^7 CFUs g^{-1} from the rhizoplane, of which 10^5-10^6 CFUs g^{-1} endophytically colonising roots at 7 dpi, and decreasing to 10^4-10^6 CFUs g^{-1} at 25 dpi; similarly, bacteria reisolated from shoots varied between 10^3 and 10^5 CFUs g^{-1} between 7 to 25 dpi [174], confirming the numbers found in this study.

Overall, considering the discrepancies of this data with similar trials conducted on hydroponically grown MoneyMaker tomato plants and *G. diazotrophicus* AZ0019 [208] and the opposite outcomes of vacuum infiltration tests vs direct inoculations under zero N condition, it appears evident how even a minor variation in the inoculation method can lead to divergent phenotypes, highlighting the importance of fine tuning every parameter of the system. Although variability was greatly reduced compared to in soil growth, the inherently high complexity of investigating the interaction between two organisms suggests the adoption of measures to further reinforce the confidence on the biological effects observed. In particular, greatly increasing the number of repetitions and biological replicates could realistically be the most efficient method for discriminating between stochastic fluctuations and biologically relevant mechanisms. However, the high number of tests conducted with the hydroponic setup in this and previous studies [208] permitted to conclude beyond any reasonable doubt that 1) the application of *G. diazotrophicus* to hydroponic tomato horticultures in zero N and N replete conditions through the inoculation method described above, results in some growth promotion; 2) in zero N and N replete conditions without ammonium, the PGP effect elicited by the nitrogen fixation impaired mutant is less pronounced than the WT bacterium (as previously reported in sugarcane model systems [223]). To complement these observations, the nature of the PGP difference between the two strains was further investigated through a ^{15}N isotope dilution experiment (section 4.2.1c) and *G. diazotrophicus* gene expression analyses (see Chapter 4.4).

4.1.1d Evaluation of BNF contribution to the PGP could not detect significant incorporation of N2 into treated plants

To evaluate the BNF-derived nitrogen presence in plant tissues, ^{15}N isotope dilution experiments are commonly carried out. In this assay, nitrogen is added to the investigated system in the ^{15}N form, and its presence as ratio with the natural ^{14}N is subsequently verified through gas or liquid chromatography–mass spectrometry (GC-MS, LC-MS) techniques [224]. In ^{15}N-fed hydroponic setup, where no ^{14}N input is present in the system except in seed reserve tissues, any ^{14}N increase detected in the treated plants would necessarily derive from atmospheric $^{14}N_2$ and thus have a BNF origin. The ^{15}N isotope dilution technique was utilised in early sugarcane-*G. diazotrophicus* studies, in which ^{15}N-marked soil was used to estimate the BNF contribution in pots [225]; but while a significant $^{14}N/^{15}N$ increase was observed in treated sugarcanes compared to controls, severe methodology biases and issues were reported due to the complexity of the setup [226]. The use of hydroponic systems greatly reduced this uncertainty, allowing complete control over the N input. To guarantee a complete penetration of ^{15}N in both plant and bacteria tissue, *G. diazotrophicus* WT and *nifD*$^{-}$ were streaked from frozen glycerol stock to LGI-P medium in which the N source was 2 mM $(^{15}NH_4)_2SO_4$. For the same reason, the strains were subsequently cultured in liquid ATGUS medium in which the yeast extract had also been substituted with 2 mM $(^{15}NH_4)_2SO_4$, thus ensuring that no ^{14}N source was ever available to the bacterium during its growth for the inoculum preparation: any BNF-derived $^{14}N_2$ incorporation during culturing in liquid medium with vigorous shaking and 2 mM $(^{15}NH_4)_2SO_4$ (implying 4 mmol NH_4 L^{-1}) is implausible if not at negligible levels. Upon the inoculation procedure described in section 4.2.1b, the experiment was prolonged as much as possible in order to dilute any ^{14}N carryover from seed tissues by allowing the bioaccumulation of the ^{15}N feed in plants; 20 days of growth was found to be the endurance limit of the uninoculated tomatoes in zero N condition due to the severe nutritional stress (Fig. 4.12d), therefore all samples were collected at that timepoint. Chlorophyll was then extracted from three biological replicates of each treatment (uninoculated, Gd WT and *Gd nifD*$^{-}$ treated) and N conditions (zero N, N replete and N replete plus

ammonium) and sent for LC-MS analyses (Fig. 4.16). Chlorophyll, accounting for 0.5–1.5% of total leaf N content (with great variations among species and fertilisation level), was selected for the ease of extraction and purification, and for its correlation with the nitrogen content of leaf tissues [227].

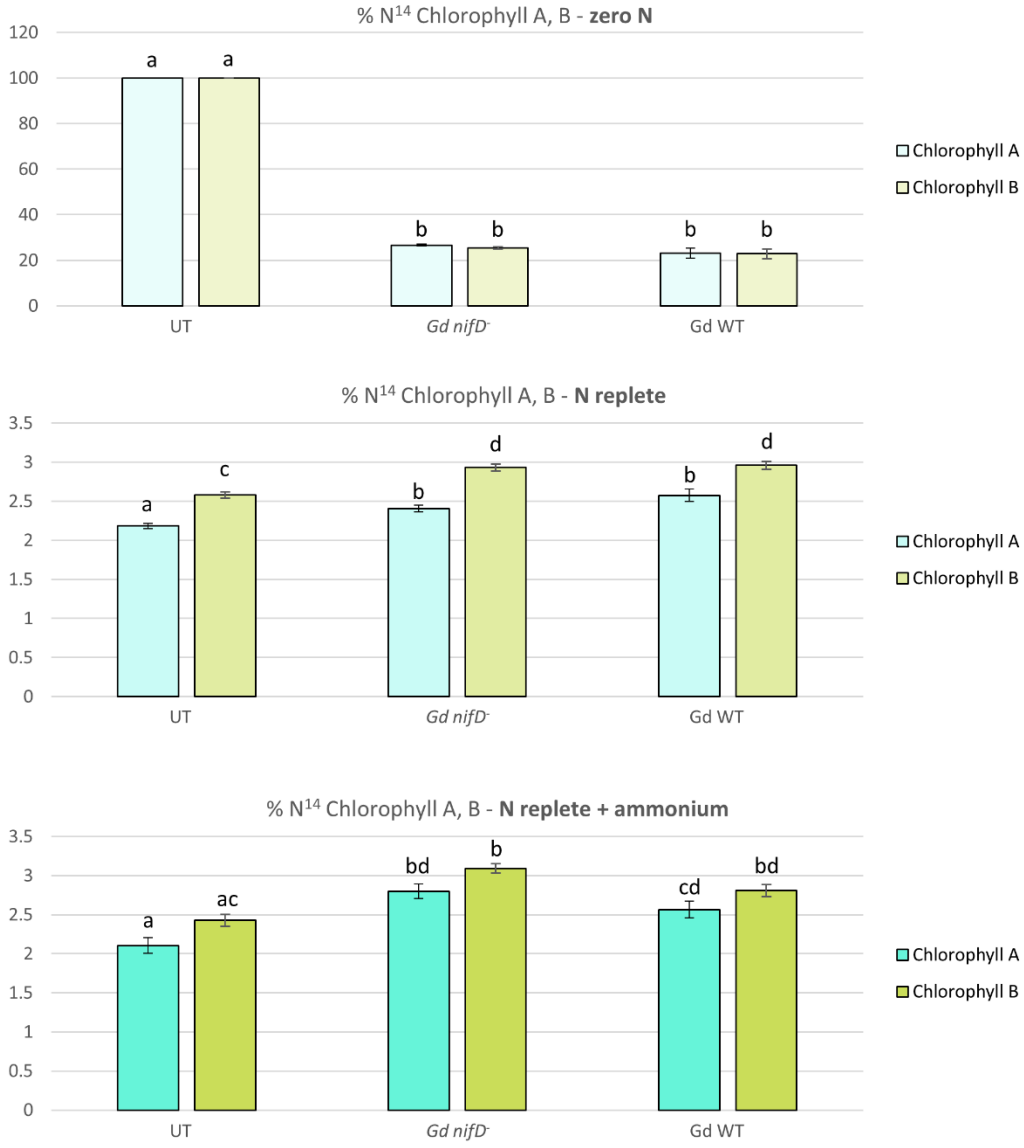


Fig. 4.16. ^{14}chlorophyll A and B percentage detected through LC-MS in uninoculated (UT), G. diazotrophicus WT (Gd WT) or nifD$^-$ (Gd nifD$^-$) treated tomato MoneyMaker plants, hydroponically grown in either zero N, 2 mM $K^{15}NO_3$ ("N replete") or 2 mM $K^{15}NO_3$ + 0.2 mM $(^{15}NH_4)_2SO_4$ ("N replete + ammonium") conditions (N = 12). The standard error of the mean (SEM) is shown. Bars marked with the same letter within each chart do not differ by One-Way ANOVA test ($P \leq 0.05$).

As a general trend, a significant amount of ^{14}chlorophyll A and B was detected in treated plants grown in zero N condition (around 25% of the total chlorophyll pool analysed), whereas samples grown in the two N replete conditions only showed a ^{14}chlorophyll baseline of around 2.5%. Crucially, no ^{14}N incorporation difference was ever detected between Gd WT and *Gd nifD*$^{-}$ treated plants, regardless of the nitrogen condition. Therefore, this trace amount of ^{14}chlorophyll detected, comparable between the two treatments although slightly higher than in the uninoculated controls, is unlikely to have a BNF origin.

In the zero N condition, the presence of ^{14}chlorophyll from untreated plants was found to be 100% as expected, since the only nitrogen source ever introduced in the system came from the seed tissue reserves; therefore, the ≈ 75% of ^{15}chlorophyll found in both Gd WT and *Gd nifD*$^{-}$ treatments must derive from assimilated debris of *G. diazotrophicus* cells, which were cultured on ^{15}N before the inoculation. The remaining ≈ 25% of ^{14}chlorophyll, being equally represented in the WT and BNF-impaired mutant strain, most likely comes from the seed endosperm; the value difference with the uninoculated control is explained by the fact that the data presented are ^{14}N/^{15}N ratios and are not normalised on the total amount of chlorophyll extracted (a parameter not covered by the analyses conducted). For the same reason, in the N replete conditions, the ^{14}chlorophyll weight on the ratio may be smaller than in the zero N condition due to a higher absolute amount of chlorophyll in the fertilised systems, but the result is substantially the same across all the N conditions: the ^{14}N found in the treated plant tissues, being similar between Gd WT and *Gd nifD*$^{-}$ treatments, probably derives from seed tissues. The small ^{14}chlorophyll increase observed in the *G. diazotrophicus* treated plants compared to controls in N replete condition could apparently suggest a BNF origin, but the presence of the same ^{14}chlorophyll level in the *Gd nifD*$^{-}$ treatment contrasts this idea. Other explanations of this paradox could involve the natural fluctuation in seed dimension, and thus ^{14}N reserve, that could have biased the experiment from the start; furthermore, it must be underlined that the ^{15}N labelled reagents used did not guaranteed 100% of isotope presence, but 98% ^{15}N in $(^{15}NH_4)_2SO_4$ and 99% ^{15}N in $K^{15}NO_3$. Nitrogen isotope

fractionation is also known to greatly vary between different nitrogen forms, such as nitrate and ammonium, in response to various physiological and metabolic processes involved in nitrogen assimilation [228]. Finally, it is possible that chlorophyll, although conveniently correlated with nitrogen presence, is not the optimal N sink metabolite in this type of analyses: photosynthetic proteins, accounting for 50% of total nitrogen allocation in leaves [227], could be a more representative candidate for future experiments.

Regardless of the biological interpretation of the modest difference observed between treatments, these data suggest that, in the context of *G. diazotrophicus* applied to deep water hydroponic cultivation with a single initial inoculum, the amount of nitrogen fixed and released as a N source for the plant after 20 dpi may be negligible. Similar conclusions, in contrast with the acknowledged importance of *G. diazotrophicus* for the nitrogen nutrition of its host plant, have been drawn before even in sugarcane [191] [221] and sweet potato [229] models (both natural hosts of the bacterium), highlighting the elusiveness of rigorously assessing the biological impact of *G. diazotrophicus* mediated BNF. It has also been proposed that the abundance of this bacterium within plant tissues may not be sufficient to sustain BNF-derived N-nutrition [191]. In conclusion, the PGP effect observed in this setup seems to be primarily attributed to other mechanisms, such as the direct assimilation of bacterial debris as a N source (particularly important in the nutritional stress condition, as shown in Fig. 4.12), a bacterial-driven mineralisation of organic detrita from root tissues (a well-documented bacteria-mediated PGP in hydroponic cultures [230]), or a bacteria-driven hormonal stimulation effect. Additionally, the deep-water hydroponic setup employed in this study, due to the lack of water circulation, on one hand may not have provided the adequate distribution of nutrients and oxygen or nitrogen gases to both plants and bacteria, and on the other hand may have caused the dispersal into the NS of the nitrogen fixed at the rhizosphere level. Crucially, sub-optimal oxygenation levels, along with the accumulation of organic debris in non-sterile conditions, are likely to have generated an anaerobic environment, restraining the remarkably high oxygen demand which *G. diazotrophicus* was reported to need for its physiological functions, including nitrogen fixation [111]. These complications could be

prevented by adding a water recirculation mechanism and by increasing the duration of the experiment, therefore allowing the build-up of significant amount of BNF-derived nitrogen in the medium and ultimately in the plant tissues. Additionally, studies on sugarcane have indicated that, although the lack of a carbon source in the medium would still allow high colonisation levels [231], *G. diazotrophicus* displays a significant increase in its capacity for nitrogen fixation when cultured in a high-sugar environment (10% sucrose) as opposed to a low-sugar one [232]. There is also evidence, in other non-nodulating diazotrophs, that *in vivo* BNF is only achievable upon the addition of an external carbon source to the system [233]. It can thus be speculated that also in the setup tested in this study a higher sugar concentration could be needed to better sustain BNF and provide a significant level of fixed nitrogen.

4.1.2 PGP evaluation in rice plants inoculated with *G. diazotrophicus*

4.1.2a Rationale and former G. diazotrophicus inoculation attempts

Rice (*Oryza sativa*), a cereal grain from the Poaceae family (which it shares with sugarcane), native from Asia and Africa, is a staple food that provides to more than half of the world's population over one-fifth of its daily calorie intake and micronutrients [234]. It accounts for more than 40,000 varieties [235], and 90% of its total global production comes from Asian countries. It is usually cultivated in flooded paddy soils, where the O_2 released from the rice aerenchyma tissues creates an oxic-anoxic interface between the roots and the bulk soil, resulting in great abundance and diversity of bacterial, archaeal, and fungal communities. This rich microbiota is shaped by soil type, plant genotypes, agricultural management, and rice growth stage, and includes, among others, methanogenic archaea and bacteria from the *alpha-*, *beta-* and *delta-protobacteria* classes [236]. Paddy ecosystems are known to favour N loss, due to a bacterial-driven nitrification/denitrification nitrogen flow in which the NO_2^-/NO_3^- produced from ammonia by aerobic nitrifiers is denitrified back to nitric oxide (NO), nitrous oxide (N_2O) and N_2 by heterotrophic denitrifiers, and ammonia is oxidised to N_2 by anammox bacteria

[236]; for this reason, the uptake of chemical fertilisers is below 40%, and their use is in constant growth [237]. On the other hand, several studies have reported a significant presence of BNF from rice systems [238] and the association between rice and diazotrophs such as *Azoarcus* [239], *Burkholderia* [240], *Serratia* [241], *Rhizobium* [242] and more [243]. In controlled systems, increase in BNF-derived N content from rice inoculated with *Herbaspirillum sp*., *Burkholderia sp*., or *Azospirillum sp*. was claimed to reach up to 31% of the total [244]. A study reported that only 1.5% to 2.5% of the microbial community composition variation is attributable to rice genotype [245], although taxonomic composition doesn't necessarily reflect variation in functions elicited by the PGPM, toward which genotype could be crucial [170]. In fact, great variability was reported in regard to BNF contribution to the N nutrition among different rice genotypes [246].

A few attempts of applying *G. diazotrophicus* to rice had been conducted after its isolation, with mixed results. For example, in 1997, Rolfe et al showed that the colonisation and PGP of one of the two rice cultivars tested on agar and perlite was only effective upon the addition of exogenous synthetic auxin [247]. Shortly after, Sevilla and Kennedy inoculated pregerminated rice seedlings (cv. Maratelli) on sucrose-free MS agar with 100 µL of *G. diazotrophicus* at OD_{600} = 0.6, and after 10 days transferred the plantlets in sterile sand. After 30 days, they reported a PGP (in terms of shoot, but not roots, length) only in rice grown in N-free conditions and treated with *G. diazotrophicus* WT, while no positive effect was observed after the treatment with a *G. diazotrophicus nifD*$^-$ mutant. In contrast to sugarcane, in N-replete MS agar, no PGP was detected in either strain, and in both N conditions colonisation was restricted to roots epidermis, where 10^3 CFUs g^{-1} were recovered at 40 dpi [248].

In 2003, however, Loganathan & Nair isolated for the first time a nitrogen-fixing, NaCl-resistant strain of *G. diazotrophicus* from wild rice (*Porteresia coarctata*) growing in a mangrove forest [97]. Subsequently, in 2005, Muthukumarasamy reported the natural association of *G. diazotrophicus* with four different wetland rice varieties cultivated in the state of Tamilnadu, India [249]. It was the first isolation of nitrogen fixing acetic acid bacteria from rice;

later, the same association was reported from temperate regions of South Korea, where sugarcane was not cultivated, revealing a wider geographic distribution of the bacterium [250]. Therefore, since its novel designation as a natural host of this crop, *G. diazotrophicus* has been applied to rice on more occasions to test its PGP abilities, showing potential for yield increase [251] and drought resistance [102].

In this study, rice was selected as a monocotyledon model system, in contrast to tomato belonging to the dicotyledon clade. It is acknowledged that the compositions of endophytic microbiomes vary among host plant species and genotypes, a difference related to distinctive plant physiologic traits, such as metabolites composition, nutrients availability or requirement, and root exudates, anatomical structure and architecture, with monocots having fibrous roots and dicots taproots [252]. The use of rice as a second model system was aimed to 1) investigate whether an efficient application of *G. diazotrophicus* was possible and could provide an obvious growth benefit, contributing to the quest for nitrogen fixation on rice [248], and 2) describe any variations as compared to the dicotyledon tomato system in terms of PGP effect promoted, colonisation dynamic and different application methods outcome.

4.1.2b Seed coating and in soil growth induced a PGP effect dependent on the bacterial load, carbon source and inoculation duration

Similarly to what already tested in tomato, the first application attempt in rice (BC15 variety) was carried out through the seed coating method. *G. diazotrophicus* was cultured as described in the tomato seed coating section and resuspended in the afore mentioned liquid carrier containing 3% sucrose (87 mM), 0.3% gum Arabic and 0.1% (v/v) polysorbate 80. Compared to tomato, more literature is available regarding similar inoculation protocols on rice; for example, the diazotroph *Rhodobacter capsulatus* was successfully applied to rice using gum Arabic as an adhesion coadjutant [253]; similarly, sucrose was added in the formulation of in field co-inoculation trials in

Vietnam [185]. However, the application of PGPM on rice is often carried out through pregerminated seedling inoculation, rather than seed coating, as it was proposed for other endophytic diazotrophs that the emerging rice coleoptile could be an entry point for such bacteria [254]. Therefore, in this preliminary in soil experiment, surface sterilised dehulled seeds were pregerminated directly in the liquid carrier alone (mock-treated controls) or containing *G. diazotrophicus* at either 10^7 CFUs mL^{-1} or 10^8 CFUs mL^{-1}. After four days of incubation in dark at 28 °C, germinated seeds were transferred in pots containing a mix of loam, sand and soil routinely used as a rice substrate, and grown in glasshouse conditions. As in the tomato trials, no feed was applied to the plants. The phenotype at 60 dpi is reported in Fig. 4.17.

Since it was not possible to isolate the root system from the growth medium without major ruptures, only the shoot length and chlorophyll content were measured. Interestingly, also with this inoculum application method, a dose-dependent effect was observed: similarly to what already recorded in the tomato trials, the intermediate (in this case lowest) bacterial concentration (10^7 CFUs mL^{-1}) elicited the most beneficial effect in terms of shoot length (Fig. 4.17a) and chlorophyll content (Fig. 4.17b).

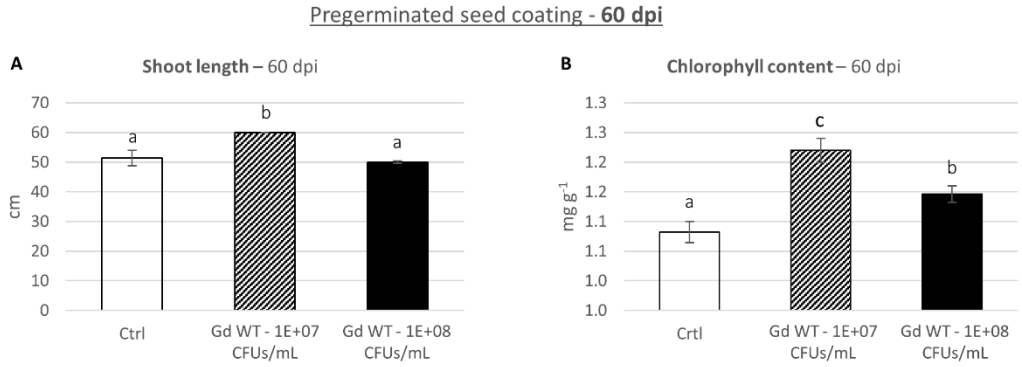


*Fig. 4.17. Growth promotion phenotype 60 days post inoculum (dpi) of BC15 rice plants pregerminated in liquid carrier containing G. diazotrophicus WT (Gd WT) at two different densities. Mock-treated controls plants (Ctrl) are shown as comparison. Shoot length (**A**) and chlorophyll content (**B**) are reported. N = 35 for SPAD measurements and 7 for all the other parameters tested. SPAD measurement conversion to chlorophyll content was calculated as in Jiang et al. (2017)* [197]. *The standard error of the mean (SEM) is shown. Bars marked with the same letter within each chart do not differ by Kruskal-Wallis test ($P \leq 0.05$).*

In light of this experiment, the bacterial concentration of 10^7 CFUs mL^{-1} was maintained as a standard for the following trials in soil.

One parameter which is likely to have an impact on the inoculation outcome and was not accurately investigated in the tomato system, is the incubation time of the seeds in the inoculum. Arguably, this factor could influence the bacterial adhesion to the seeds in a similar manner to the inoculum density: less cells incubated for a longer time frame could perform similarly to a higher number of bacteria applied for shorter. Therefore, in the attempt of finding an optimal inoculation protocol for inducing rice growth promotion, the impact of the inoculum application duration was evaluated along with its interplay with bacterial density and sucrose concentration (Fig. 4.18). The aim of this experiment was primarily to assess whether bacteria in contact with the seed surface for longer times could induce a significantly different PGP to rice, in a similar way to what observed in experiments with different bacterial or sucrose concentrations. Rice seeds were incubated with the bacterial inoculum for either one hour or overnight. Two bacterial densities were tested: due to the beneficial effect reported in Fig. 4.17, the 10^7 CFUs mL^{-1} concentration was maintained and compared to a second, lower, density, corresponding to 10^6 CFUs mL^{-1}. The bacteria were resuspended in either sterile water, the sucrose-containing liquid carrier or the same but more concentrated solution with 10% sucrose, as already tested in tomato (Fig. 4.5, 4.6). In this case, the inoculants were applied to surface sterilised seeds and not to germinating seedlings, in order to avoid biases caused by different germination stages at the time of sowing. It is worth mentioning that, in order to test *G. diazotrophicus* colonisation capability in conditions as faithful to natural environments as possible, seeds were not dehulled in any of the in-soil experiments; not forcing the contact with the endosperm by maintaining this first physical barrier between the bacterium and the seed, could allow a more natural and gradual, although less vigorous, bacterial establishment, resulting in a more realistic interaction dynamic.

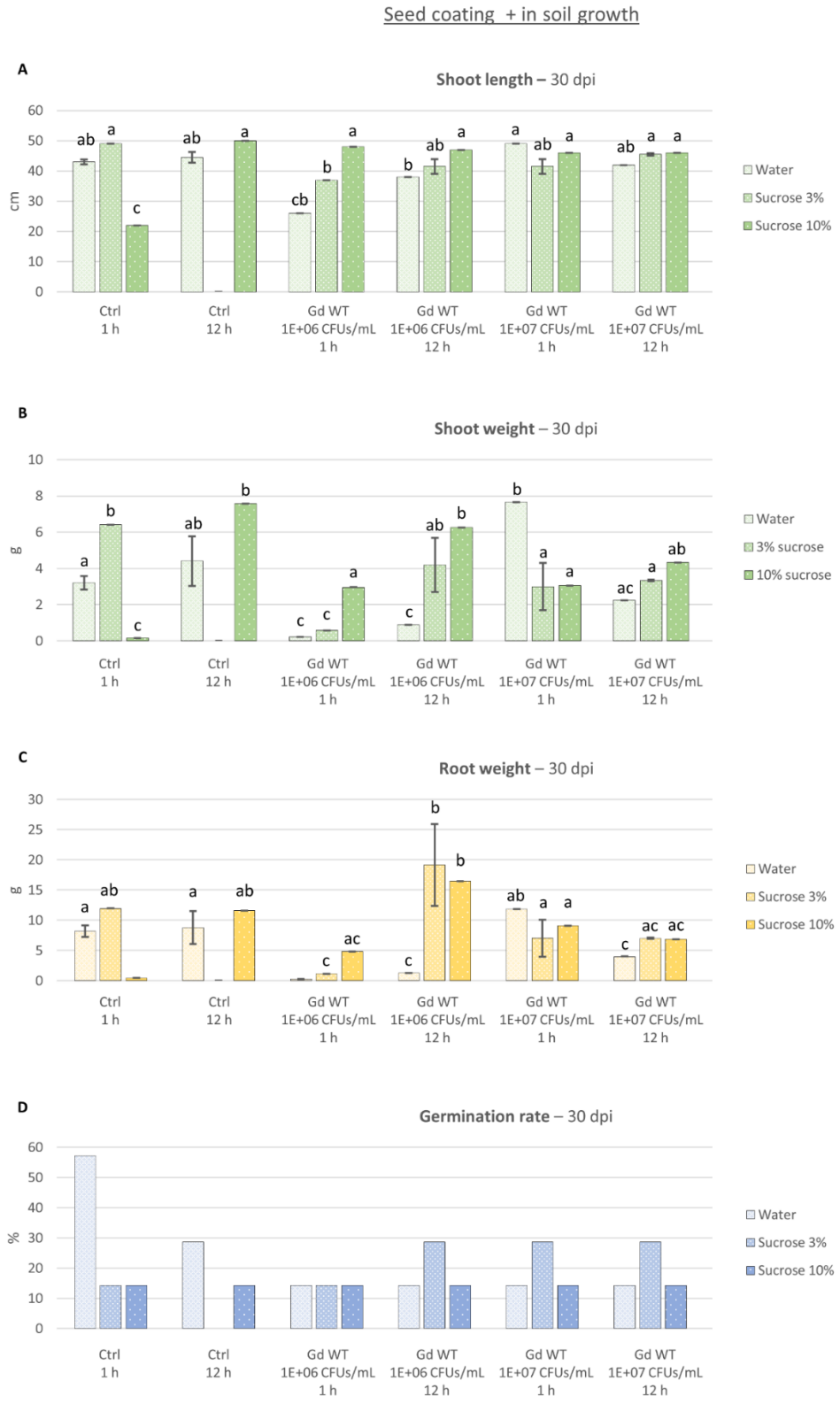


*Fig. 4.18. Growth promotion phenotype 30 days post inoculum (dpi) of BC15 rice plants inoculated through the seed coating technique with G. diazotrophicus WT (Gd WT) resuspended at three different densities in either sterile water, 3% sucrose carrier or 10% sucrose carrier. Seeds were inoculated for one hour (1h) or overnight (12 h). Mock-treated control plants (Ctrl) are shown as comparison. Shoot length (**A**), shoot weight (**B**), root weight (**C**) and germination rate (**D**) are reported. N = 7 for all the parameters tested. The standard error of the mean (SEM) is shown.*

Despite the complexity of interpreting the combination of three variables (inoculation time, bacterial density, and sucrose concentration) in the same experiment, a trend could be inferred from the phenotypic data obtained. The germination rate in general was low (Fig. 4.18d), as expected from rice seeds sown without removing the husk [255]. The shoot height of treated plants increased with the concentration of sucrose in the carrier, but only when using the lowest bacterial concentration, and it never surpassed the untreated controls (Fig. 4.18a). The same pattern appeared for shoot and root weight (Fig. 4.18b, c) and at both incubation times, but was more pronounced with the 12 hours incubation, where the addition of sucrose induced a greater root development compared to controls (Fig. 4.18c). Interestingly, at this lowest bacterial density, the water-based treatment inoculated for one hour did not elicit a positive effect compared to untreated controls in any of the parameter examined, and in fact caused a biomass decrease unless 10% sucrose was added; on the other hand, the overnight incubation promoted a beneficial effect even with 3% sucrose present in the inoculation medium (Fig. 4.18a-c). The application of the higher bacterial concentration (10^7 CFUs mL^{-1}) promoted a more beneficial effect at both incubation times compared to the one-hour treatment with 10^6 CFUs mL^{-1} in terms of shoot and root biomass accumulation (Fig. 4.19a-c), even with the water-based inoculum. However, with the 12 hours application, the phenotypic traits evaluated were still less pronounced if compared to the untreated controls or the sucrose-amended 12 hours treatment with 10^6 CFUs mL^{-1}, regardless of the carbon concentration. The one-hour application in water seemed to promote the most pronounced plant growth improvement among the 10^7 CFUs mL^{-1} treatments.

This data, similarly to what was previously observed in the tomato model (Fig. 4.3, 4.4, 4.7, 4.8, 4.11), corroborates the idea that if the colonisation process is too vigorous, there can be a negative impact on plant growth. Such effect, possibly caused by some germination hindrance, appears to be linked with the "bacterial load", here defined as either bacterial count, incubation time or bacterial growth rate induced by the carbon source in the inoculum. It is indeed recognised that plants exposed to microbial cells, either belonging to pathogen or mutualistic species such as rhizobia, initially recognize the microorganisms

as intruders and activate defence response mechanisms - which PGPM are eventually able to evade [256]. The dynamic described above has also been observed in the interaction between *G. diazotrophicus* and rice [257], where the activation of the jasmonic acid/ethylene defence pathway was reported [258]. Similarly, in sugarcane, *G. diazotrophicus* treatment was found to induce expression of the same defence pathway [259] and result in the accumulation of polysaccharides and tannins in the parenchymal cells surrounding the metaxylem [221] [260]. Furthermore, in *A. thaliana* it was reported the protective role of *G. diazotrophicus* against the phytopathogenic bacterium *R. solanacearum* through the activation of the defence system [261]. It is therefore unsurprising that a high bacterial load during the seed germination can results in an acute biotic stress and virulence response such to affect plant development; growth inhibition by activation of plant immune response has indeed been reported in several studies [262]. Conversely, a lower or slow-growing bacterial population seems advantaged in finding a natural balance between the minimal threshold number of bacteria required to elicit the beneficial PGP, without the drawback of inducing a biotic stress by excessive proliferation. However, when the bacterial load was too low, no positive effect was elicited and, in fact, a growth impairment was observed compared to untreated controls, as in the case of the one-hour 10^6 CFUs mL^{-1} treatment or the overnight treatment in water at the same density. This may be explained by the initial biotic stress induced by the bacterium not being counterbalanced by later association and PGP, due to insufficient bacterial load. If the bacterial load is quantified by assigning an arbitrary value to each condition, i.e. a number increasing as the carbon concentration, incubation time and bacterial density increase, and this number is plotted with a PGP parameter such as shoot or root weight, this proposed model can be easily visualised (Fig. 4.19).

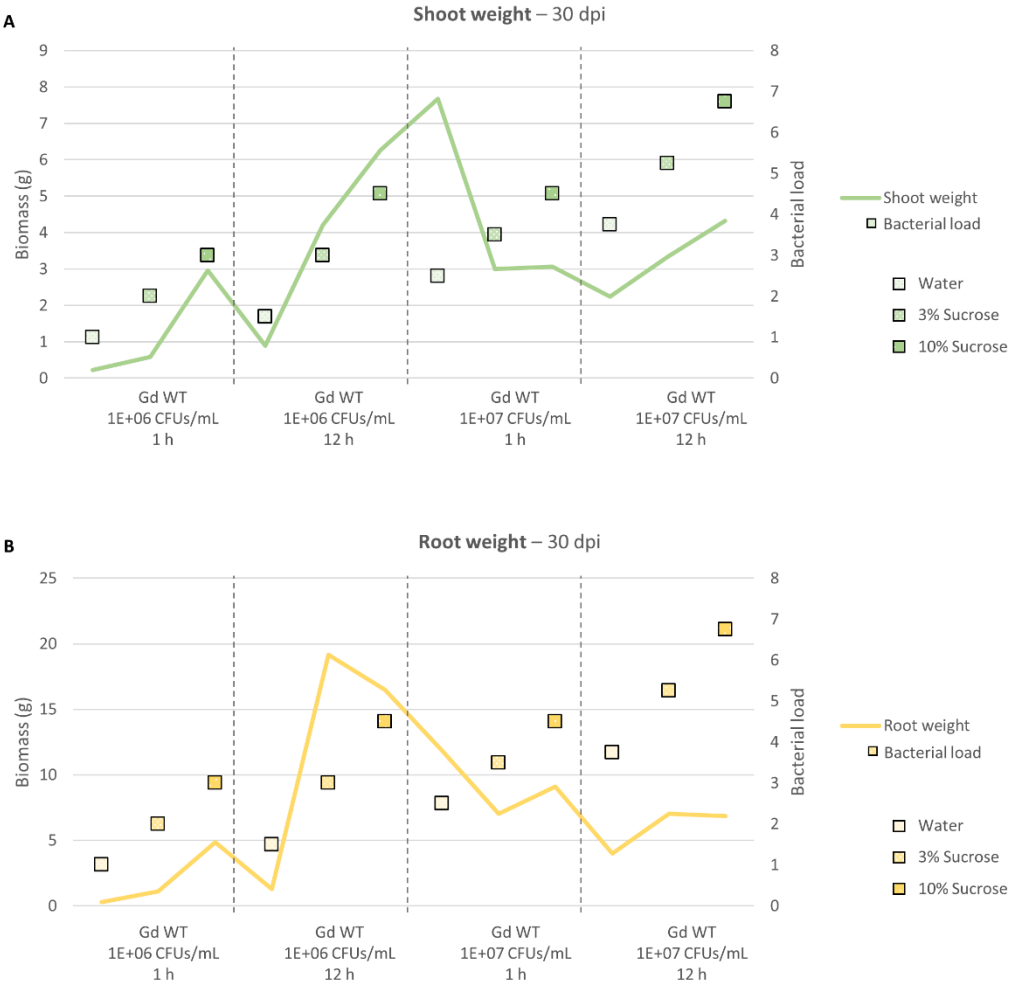


*Fig. 4.19. Correlation between growth promotion phenotype of G. diazotrophicus-treated BC15 rice plants and bacterial load during seed inoculation. A number expressing the bacterial density, incubation time and sucrose-mediated growth rate was assigned to each of the twelve conditions examined in order to quantify the bacterial presence and plot it with shoot (**A**) or root (**B**) weights: the smallest value, arbitrarily assigned as "1" to the lowest bacterial density inoculated in water for one hour, was multiplied by a constant (K_1 = 2.5) to obtain the correspondent value at the highest bacterial density. Then both values were progressively increased by the same factor (+1) to obtain the values for the two sucrose concentrations. Finally, both value sets were multiplied by a constant to obtain the correspondent value set in the twelve-hours incubation conditions.*

The maximal beneficial effect in terms of biomass accumulation, peaks in the centre of the bacterial load values, i.e. where an intermediate amount of bacteria (in terms of either cell density, sucrose concentration or incubation time) was inoculated in the seeds. Interestingly, this "the dose makes the poison" dynamic was observed in tomato only when the inoculants were applied through the more forceful vacuum infiltration method (Fig. 4.7, 8, 10,

11), and not with the seed coating technique (Fig. 4.4). This difference may be explained by either a species-specific higher sensitivity of germinating rice seedling to the presence of exogenous bacterial cells, or by the different dimension of tomato and rice seeds: the wider surface area of rice, along with the presence of the husk and the micro cavities beneath it, could allow a greater accumulation of bacteria, therefore causing a more acute immune reaction.

On the other hand, these results concur with tomato seed coating experiments in highlighting how an external carbon source can modulate the bacterial growth, inducing different growth promotion phenotypes which are most likely dependent on the bacterial growth during the seed inoculation and early germination stages: different bacterial growth rates are accompanied by changes in the cell cycle and metabolism [263], which according to the results collected in this study may be crucial for the successful establishment of a functional PGPB-plant symbiosis. The great variability between biological replicates and the inherent stochasticity of in soil colonisation experiments discussed above, dictate cautiousness in handling the results obtained through these trials: more than providing the ideal carbon or bacterial concentration, the data presented hereby mainly show a rice growth promotion trend induced by *G. diazotrophicus* in glasshouse condition which varies according to the bacterial load that seeds are exposed to. Before inferring a statistically solid application method, a meticulous and systematic screening of suitable nutrient sources for *G. diazotrophicus* formulation (in particular carbon sources) along with the accurate evaluation of plant species-specific inoculation protocols, are recommended for future developments of this bacterium as a commercial biostimulants.

4.1.2c Hydroponically grown rice exhibited PGP when treated with G. diazotrophicus WT through either seed coating, direct inoculum in NS or seedling dipping, especially under N-replete conditions

The seed coating application of *G. diazotrophicus* to rice followed by in soil growth confirmed the great phenotype variability already observed in tomato, exacerbated by a low germination rate (Fig. 4.18d). The hydroponic system set up in this and previous studies [208] already proved to be a valid tool to decrease environmental fluctuations and enhance consistency among replicates. Therefore, subsequent rice colonisation experiments were carried out in the hydroponic setup described for tomato.

As previously done with tomato, the first hydroponic rice culture was coupled with the seed coating method. Based on the data obtained from the seed coating followed by in soil growth (Fig. 4.17, 4.18), *G. diazotrophicus* WT or *nifD*$^{-}$ strains were resuspended in water at a concentration of 10^7 CFUs mL^{-1} and incubated for one hour with the surface sterilised rice seeds. They were then germinated and grown in the hydroponic system with zero nitrogen and the phenotype was evaluated at 20 days after germination (Fig. 4.20). The growth promotion elicited through this application method was visible in terms of root and shoot length (Fig. 4.20a, b). However, no PGP was observed in the rice plants treated with the *G. diazotrophicus nifD*$^{-}$ mutant strains; this confirmed the trend previously observed with tomato treated through seed vacuum infiltration in zero N hydroponic system (Fig. 4.12) and also reported in sugarcane [223], according to which, in absence of a nitrogen source, the wild type strain induces a significantly higher biomass increase compared to the nitrogen fixation impaired mutant. This effect seemed somehow more extreme to what observed in tomato, where the *nifD*$^{-}$ strain could still significantly alleviate the nutritional stress phenotype, reinforcing the predictable occurrence of species-specific PGP mechanisms.

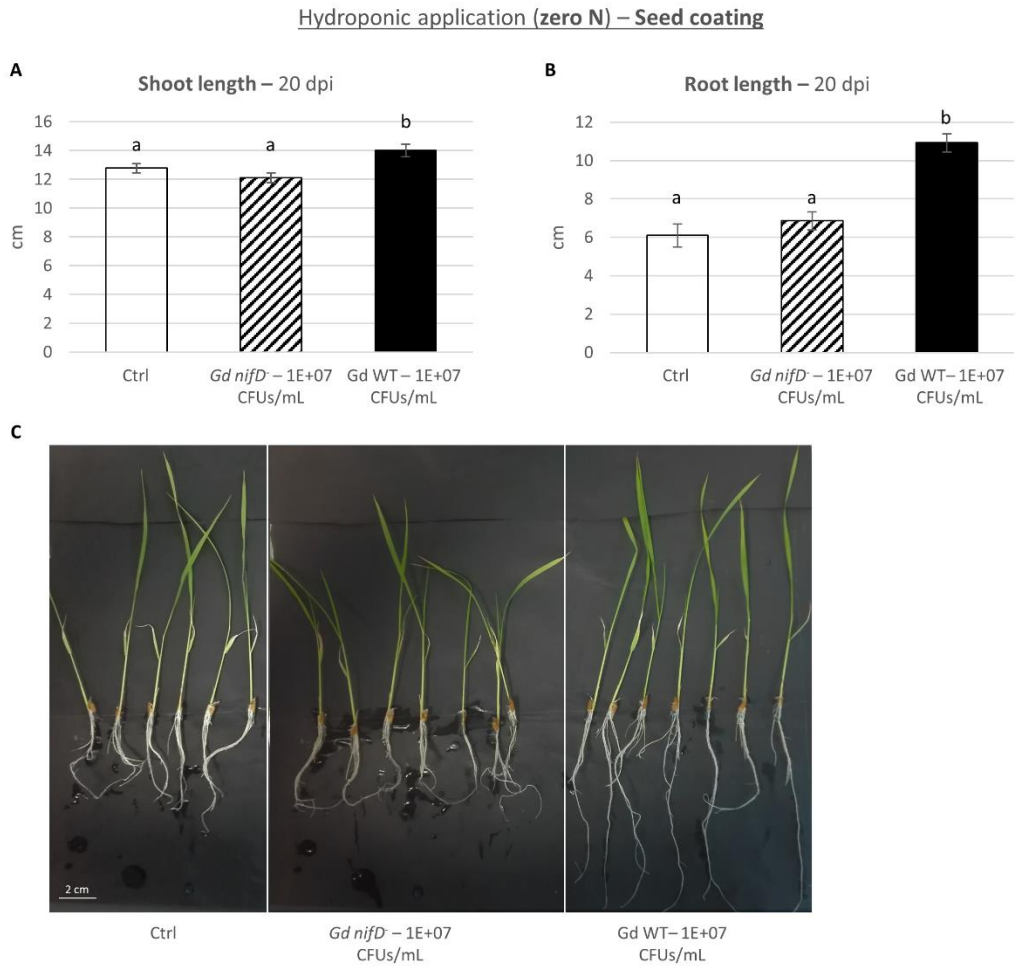


*Fig. 4.20. Growth promotion phenotype at 20 dpi of BC15 rice plants hydroponically grown in zero N condition (**C**). Plants were inoculated through the seed coating technique for one hour with G. diazotrophicus WT (Gd WT) or nifD- (GD nifD-) resuspended in water. Mock-treated controls plants (Ctrl) are shown as comparison. Shoot (**A**) and root (**B**) length are reported. N = 7 for all the parameters tested. The standard error of the mean (SEM) is shown. Bars marked with the same letter within each chart do not differ by Kruskal-Wallis test (P ≤ 0.05).*

Once confirmed the possibility to induce a PGP phenotype to hydroponically grown rice through the seed coating method, the bacterium was tested by direct inoculation in the NS (Fig. 4.21), as already done for tomato.

It is worth noting that, when grown hydroponically for a short period, rice plantlets tent to exhibit an elongated root morphology, somehow different from the fibrous architecture found in soil cultivation. Thus, for simplicity, only the root length is reported in Fig 4.20 and Fig. 4.21: for both shoot and roots, length and weight were found to be linearly correlated (not shown).

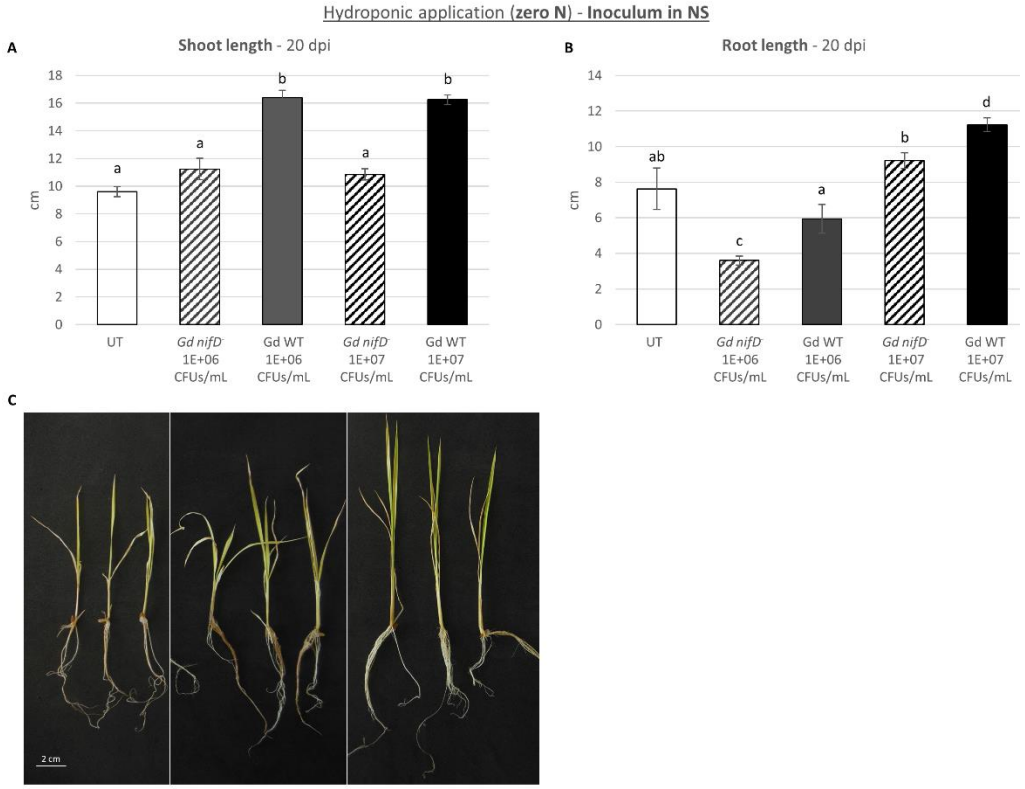


*Fig. 4.21. Growth promotion phenotype at 20 dpi of BC15rice plants hydroponically grown in zero N condition (**C**). Gd WT or GD nifD- strains were inoculated in the hydroponic NS at OD_{600} = 0.3 or 0.03 and kept for 48 h. Uninoculated controls plants (UT) are shown as comparison. Shoot length (**A**) and root length (**B**) are reported. N = 10 for all the parameters tested. The standard error of the mean (SEM) is shown. Bars marked with the same letter within each chart do not differ by Kruskal-Wallis test ($P \leq 0.05$).*

Even with this application method, carried out as already reported for tomato (Fig. 4.12-4.14) the wild-type strain inoculated in the NS for two days at OD_{600} = 0.3, corresponding to 10^7 CFUs mL^{-1}, could induce the PGP to the N-starved plantlets (Fig. 4.21c), as revealed by the enhanced root and shoot length at 20 dpi (Fig. 4.21c). The lower bacterial density could still increase the shoot length, but none of the *G. diazotrophicus nifD*- concentrations could elicit a positive effect. On the contrary, the lowest density of the mutant strain seemed to cause a reduction of the root length. Once again, this finding was different from what observed in tomato, where the *nifD*- inoculation in zero N condition could partially revert the N starvation phenotype; similarly to the previous rice

trials (Fig. 4.18, 4.20), this could speculatively be explained by the biotic stress induced by the bacterium not being counterbalanced by the PGP elicited by an adequate cell number, and, in this case, by the lack of an active N-fixation process. This points out again at the need of a functional nitrogen fixation machinery for exerting a full PGP effect, either because of the direct use of fixed nitrogen in rice nutrition, or for its role in the bacterial metabolism.

Finally, a different application technique was tested. It is acknowledged in other endophytic diazotrophs models that the inoculation method can affect the success of the bacteria establishment on rice: in particular, dipping the seedling root in the bacterial solution was found to be more efficient than the PGPM inoculation on the growth substrate [264], and is one of the most widely adopted method for rice biotreatment [265]. Therefore, for the following trial, seeds were pregerminated in sterile conditions and incubated at 28 °C overnight with the bacterium, previously cultured in liquid ATGUS to exponential phase, washed, and resuspended in water at three densities: 10^6, 10^7 and 10^8 CFUs mL^{-1}. This technique combines the mechanical advantages of the seed coating method and the dynamics of the hydroponic application. On one hand, only a minimal volume of bacterial culture is needed for evenly sprinkling the inoculant over the germinated seedlings, as opposed to the large volume required for the inoculation in the hydroponic NS. On the other hand, the direct contact of the bacteria with the emerging radicles, without the physical barrier of the seed husk which qualify the seed coating technique, replicates the interaction dynamic characteristic of the inoculation in the hydroponic NS.

The experiment (Fig. 4.22) was carried out in nitrogen starvation (zero N), nitrogen replete condition (2 mM KNO_3) and an intermediate amount of N (0.2 mM KNO_3), which had been already tested for vacuum infiltrated tomato seeds and was found to promote a biomass increase only in the root system and with certain bacterial densities (Fig. 4.11). This third nitrogen condition was introduced in order to probe how low could the nitrogen be kept in the system without causing a nutritional stress phenotype capable of nullifying the PGP effect.

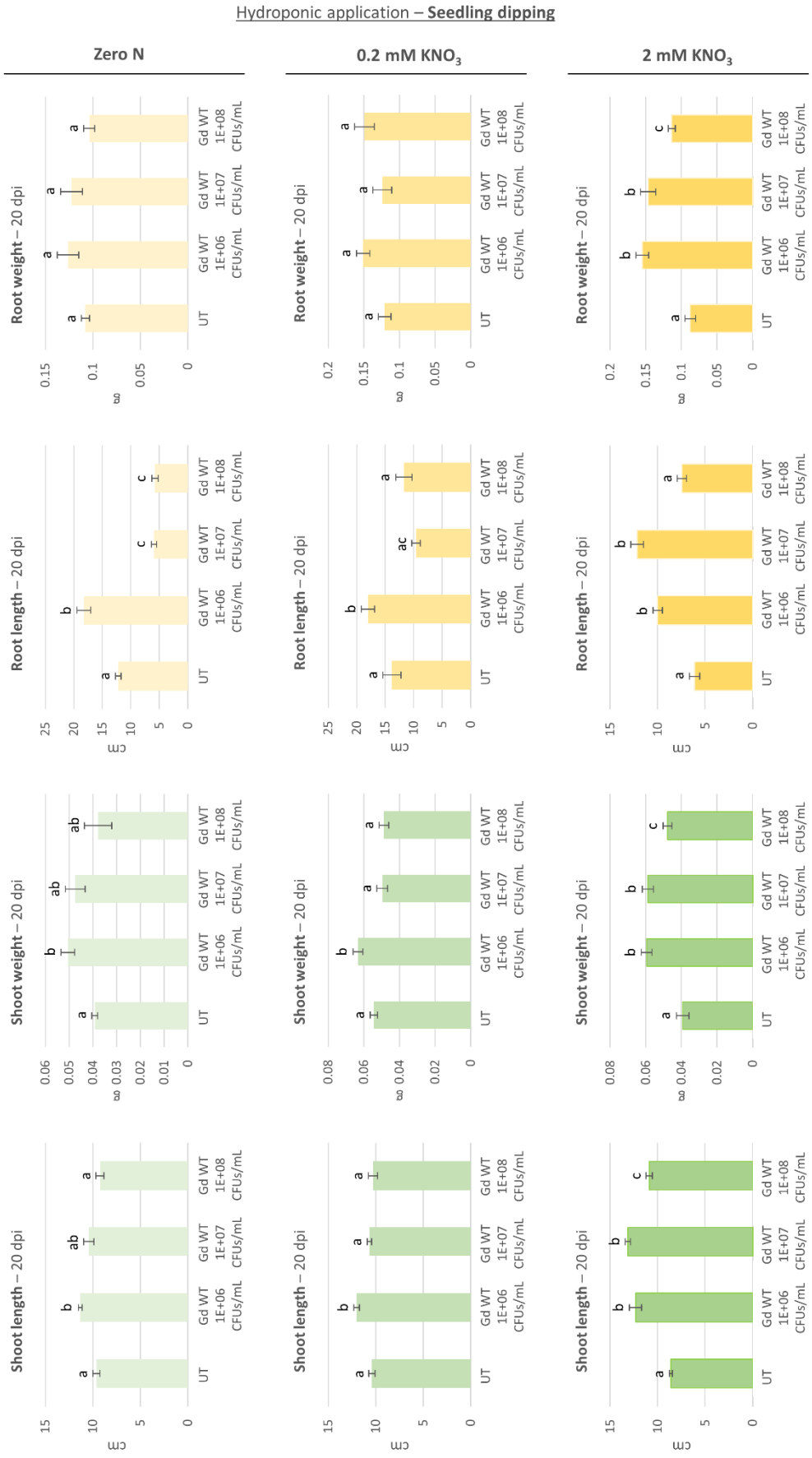

Hydroponic application – Seedling dipping
Zero N
0.2 mM KNO3
2 mM KNO3
Root weight – 20 dpi
Root length – 20 dpi
Shoot weight – 20 dpi
Shoot length – 20 dpi
UT
Gd WT 1E+06 CFUs/mL
Gd WT 1E+07 CFUs/mL
Gd WT 1E+08 CFUs/mL

Fig. 4.22. Growth promotion phenotype 20 days post inoculum (dpi) of BC15 rice plants hydroponically grown in three different N condition. Seeds were pregerminated in water, and seedling at the same developmental stage of similar dimension were sprinkled with Gd WT at three different densities and inoculated overnight. Uninoculated controls plants (UT) are shown as comparison. N = 10 for all the parameters tested. The standard error of the mean (SEM) is shown. Bars marked with the same letter within each chart do not differ by Kruskal-Wallis test ($P \leq 0.05$).

The first conclusion that can be drawn from the phenotypic data obtained is that the zero N condition and the 0.2 mM KNO_3 condition induced substantially the same result: the only growth promotion effect was in both cases obtained only with the lower bacterial treatment, in terms of shoot biomass increase and root elongation. This confirms that 0.2 mM KNO_3 is not sufficient for sustaining a regular plant growth and is in fact assimilable to the N starvation condition. The lack of a PGP phenotype upon higher bacterial densities treatments in zero or low nitrogen conditions, indicates that without a threshold amount of nitrogen available for the plant growth, the application of *G. diazotrophicus* in high cell number poses a biotic stress which reverses the PGP benefit, resulting in no neat gain in biomass accumulation at 20 dpi. The root architecture was also affected, with the partial loss of the linear correspondence between length and weight previously observed, and the favouring of a more fibrous root system (not shown). On the contrary, in the N replete condition, the bacterial presence was better tolerated (Fig. 4.23) and could elicit a growth advantage with all three treatments, though the biomass accumulation was more pronounced at10^6 and 10^7 CFUs mL^{-1}. In this context, it is likely that an adequate concentration of nitrogen in the system could provide the plants with enough energy to cope with the biotic stress provoked by the bacterium. To assess how these different phenotypes were affected by the colonisation dynamics, plants were macerated, and the reisolated bacteria were counted as described above (Fig. 4.23). The root system of plants treated with the highest bacterial density could support up to 10^6 CFUs g^{-1} but only in N replete condition, whereas at lower nitrogen concentrations the bacterial cell count at 20 dpi was almost two orders of magnitude lower (Fig. 4.23b). Conversely, the lower density bacterial inoculants established themselves in the root tissues at a concentration of around 10^5 CFUs g^{-1} regardless of the nitrogen presence.

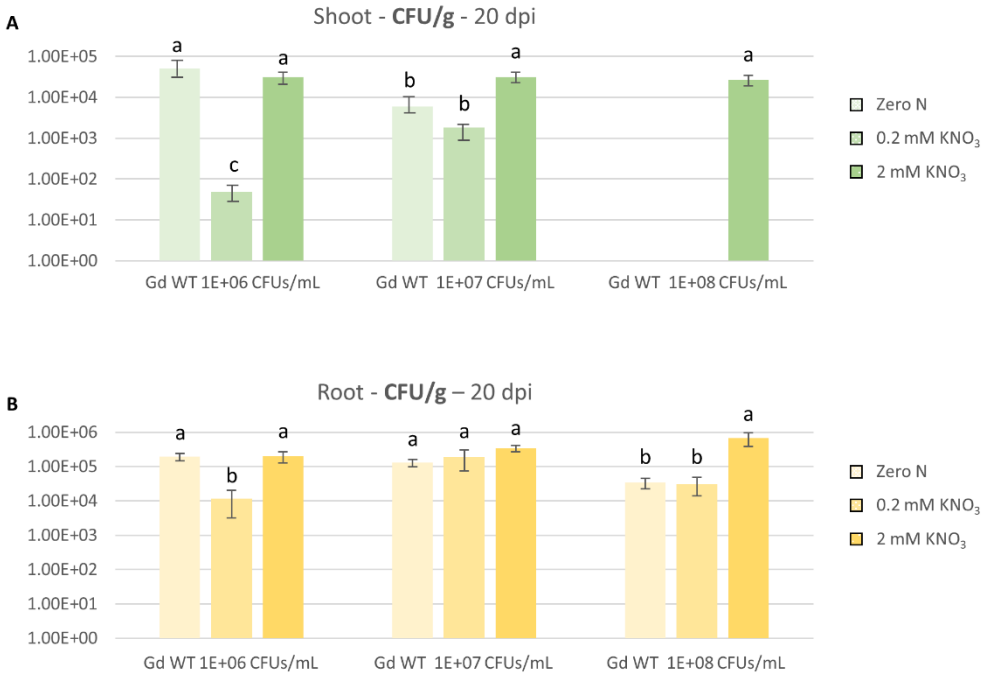


Fig. 4.23. G. diazotrophicus WT (Gd WT) colonisation rate of BC15 rice plants hydroponically grown in either zero N, 0.2 mM KNO_3 or 2 mM KNO_3 conditions. CFUs plant g^{-1} at 20 dpi are reported as distinguished in shoot and roots. No bacteria were isolated from uninoculated controls. Bars marked with the same letter within each chart do not differ by Kruskal-Wallis test ($P \leq 0.05$, $N = 3$).

A similar but more extreme effect was found in the shoots, where plants treated with the most concentrated inoculum supported endophytic colonisation in aerial parts only in N replete condition (Fig. 4.23a). With such nitrogen availability, the bacterial density at 20 dpi in shoots was between 10^4 and 10^5 CFUs g^{-1} regardless of the initial inoculum density. Similarly, in the root system, the N replete condition induced grossly the same level of colonisation at 20 dpi regardless of the initial bacterial concentration (between 10^5 and 10^6 CFUs g^{-1}), confirming the numbers found in hydroponically grown tomato and suggesting this amount of cells to be the physiological limit of CFUs g^{-1} achievable in this type of setup. As for the lower N conditions, the apparent drop or even complete lack of colonisation in some of the samples, always encountered in this type of analyses, can be due to technical artifacts (e.g., uneven maceration or sampling) during the maceration and plating process. The number of *G. diazotrophicus* cells found at 20 dpi in the tissues of both tomato and rice grown in hydroponic setup in N replete condition are in line with what normally expected from non-pathogenic endophytes, typically

ranging from 10^4 to 10^8 in roots and 10^3 to 10^7 in shoots [266]; compared to the 10^4 to 10^5 CFUs per root gram and 10^2 to 10^7 CFUs per shoots gram previously reported relatively to the population dynamics of *G. diazotrophicus* in sugarcane [191], the microorganism natural host, the reisolation rate obtained through this setup suggest an efficient colonisation level. It should be noted that hydroponically grown rice was shown to have reduced root exudation between 7 and 28 dpi in response to organic matter accumulation and lack of aeration, influencing endophytic dynamics [267].

In conclusion, these results show that *G. diazotrophicus* can promote growth in rice plants when applied through seed coating, seedling dipping and hydroponic inoculation methods, but with differences relative to the bacterial densities required for the different applications. The wild-type strain was found to be more effective than the *nifD*$^-$ mutant (Fig. 4.20, 4.21), indicating that a functional nitrogen fixation machinery is necessary for the full plant growth promotion effect. The presence of an external carbon source during the formulation was also found to influence the effectiveness of the treatment, probably through the modulation of the bacterial growth rate (Fig. 4.18). No general paradigm was found about the ideal application method or bacterial density, since every setup produced distinctive outcomes. However, as a thumb rule, the "law of diminishing returns" seemed to apply. Such economic principle states that as more units of a variable input (in this case the bacterial load) are added to a system, the marginal output (the rate of profit of the system, in this case the PGP effect) will eventually decrease if other variables remain at a constant [268]. In the context of this study, the variable input is the *G. diazotrophicus* cell number, which was found to elicit growth promotion effect in soil cultivation only beyond a certain threshold density, while a lower bacterial load would cause a phenotype deterioration (Fig. 4.18); this is speculated to be due to the biotic stress caused by the bacterium during seed germination not being counterbalanced by the later successful symbiosis establishment and PGP induction. However, increasing the bacterial load was effective only to a certain extent, after which, eventually, the growth promotion effect levelled off or was even negative (Fig. 4.17, 4.18), as the system (both hydroponic and soil) couldn't sustain a higher bacterial presence.

This negative effect was contrasted by either decreasing the input (lowering the bacterial load by shorter application times, less carbon sources in the formulation or less concentrated inoculants) (Fig. 4.18) or, in hydroponics, through the addition of nitrogen (Fig. 4.22), which would increase the system capacity to counterbalance the biotic stress and sustain a higher bacterial load. Indeed, it was reported that the gene expression profile of rice roots supplied with high levels of nitrate presents an up-regulation of plant resistance genes, nitrogen assimilation and hormone metabolism, suggesting a healthier growth and interaction dynamic with the bacteria [269]. For this reason, the nitrogen replete condition could sustain a higher and more consistent colonisation in hydroponics (Fig. 4.23) and promoted the growth effect even with denser inoculants (Fig. 4.22). These findings suggest that *G. diazotrophicus* has the potential to be used as a plant growth-promoting microbe in rice cultivation, but more research is needed to fully understand the species-specific PGP mechanisms and the best application methods.

4.1.3 PGP evaluation in *A. thaliana* inoculated with *G. diazotrophicus*

The ultimate goal of this and other *G. diazotrophicus* studies is investigating its potential as a PGPB in commercially relevant crops. For this reason, the model systems employed in this work were chosen to represent monocot and dicot crops which can be crucial to address the objective of ensuring worldwide food security with sustainable agricultural practices. However, the target of greatly increasing the number of replicates to enhance the statistical power of the PGP effect investigated, as discussed above, becomes hardly achievable in species with substantial size and relatively long life cycles. For this reason, the small sized, fast-growing, and well characterised *Arabidopsis thaliana (A. thaliana* Col-0*)* was utilised in this work for further testing how the bacterium-induced PGP would be affected by some of the growth parameters, such as nitrogen and carbon concentration in the substrate. Confirming the suitability of *A. thaliana* as a model system for *G. diazotrophicus* AZ0019-induced PGP evaluation may facilitate basic research

on this bacterium, with valuable implications for advancing crop-related studies.

Although this species was successfully used before as a model system for studying the interaction between plants and beneficial microbes [270], very limited literature is available relatively to the application of *G. diazotrophicus* to *A. thaliana*. In 2006, Cocking et al. reported for the first time that *G. diazotrophicus* AZ0019 embedded in MS agar (0.8% w/v) with 3% sucrose (87 mM) at the concentration of around 10^7 CFUs mL^{-1} (1 mL of bacterium grown in ATGUS and resuspended in water at 10^9 CFUs mL^{-1} mixed with 14 mL of cooled MS agar) could intracellularly invade *A. thaliana* plants growing on that substrate [271]. However, the study also reported that when the bacterium was directly inoculated on the germinating seedling at any concentration between 10^1 to 10^{10} CFUs mL^{-1}, its extensive growth on the sucrose-replete MS agar surface would inhibit and eventually overgrowth the plantlets. Only as low as 5 CFUs mL^{-1} were found to cause no phenotype deterioration compared to the untreated controls. A similar outcome had been reported before in sugarcane, which led to amending the plant growth conditions by decreasing sucrose concentration from 20 to 2 g L^{-1} (58 to 5.8 mM) [231]. Ten years after Cocking's paper, it was reported the successful colonisation and growth promotion of *A. thaliana* plants pregerminated on MS agar, treated for 3 hours with 10^6 CFUs of *G. diazotrophicus* Pal5 mL^{-1} (OD_{600} = 0.01) and potted in commercial substrate [262]. The PGP was found in terms of increased photosynthetic rate, water-use efficiency (due to reduced stomatal conductance), number of leaves, as well as dry and fresh weight of shoot and roots. However, an initial deterioration of plants phenotype caused by the activation of the plant defence system was reported until 28 dpi, after which the PGP effect manifested for up to 50 dpi. It was also reported the beneficial effect of metabolites exuded by *A. thaliana* grown on half-strength MS medium with 0.5% (14.5 mM) sucrose in promoting the growth of *G. diazotrophicus* Pal5 (inoculated on pregerminated seedlings at 10^7 CFUs mL^{-1}) and modulating its protein expression [272].

In this study, *A. thaliana* (Columbia-0) plants were grown on MS agar (0.8% w/v) upon seed coating treatment with *G. diazotrophicus* AZ0019 wild type or

nifD^{-} mutant. As a preliminary experiment, the effect of the addition of sucrose in the medium was investigated (Fig. 4.24).

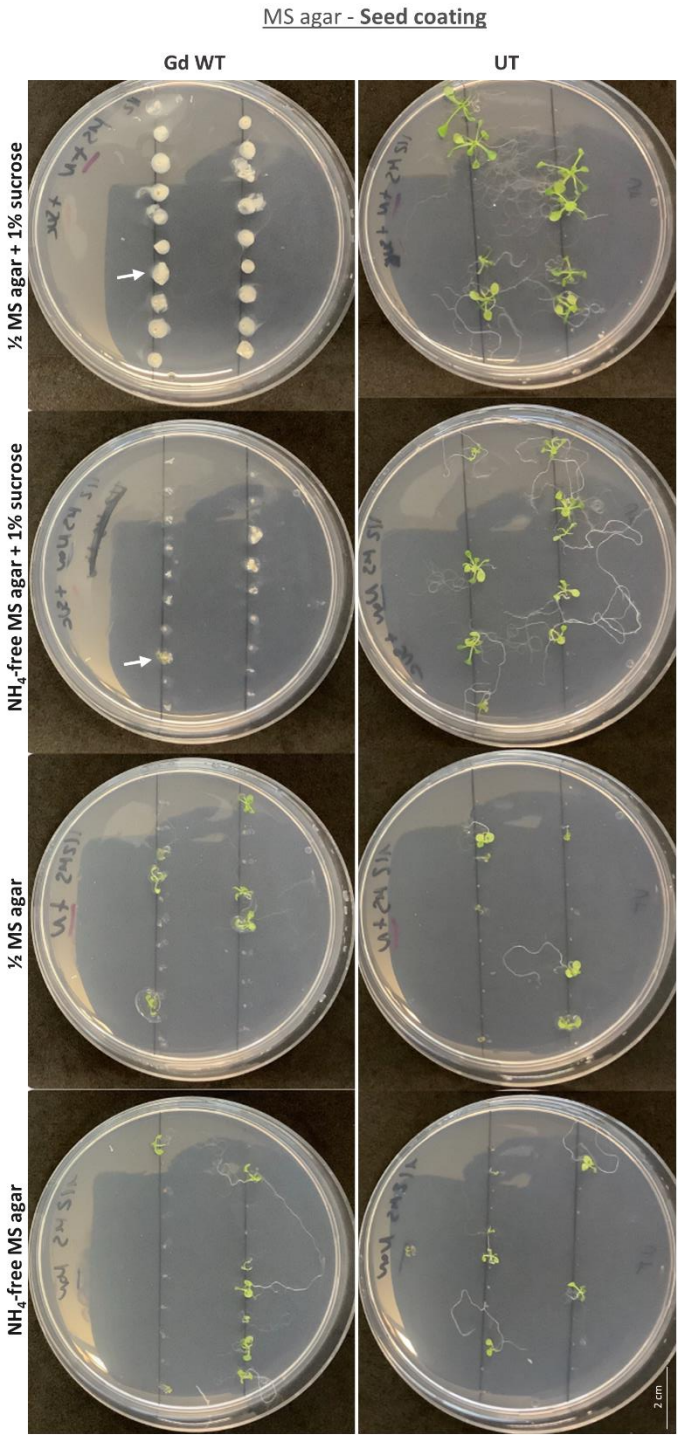


Fig. 4.24. Effect of G. diazotrophicus on A. thaliana (Columbia-0) 15 days post inoculum (dpi). Plants were inoculated through the seed coating technique with G. diazotrophicus WT (Gd WT) resuspended in water at 10^8 CFUs mL^{-1} for one hour, and grown on either half-strength MS agar (½ MS agar) or ammonium-free MS agar, with or without 1% sucrose (29 mM). Bacterial growth around seeds is indicated by white arrows. Untreated control plants (UT) are shown as comparison.

In light of the strong growth inhibition effect of inoculated *A. thaliana* under 3% sucrose reported by Cocking et at. [271], the sugar concentration in this setup was decreased to 1% (29 mM). Seeds were coated with the water based bacterial solution at the density of 10^8 CFUs mL^{-1} for one hour, quickly dried in sterile condition and sowed on plates containing either half-strength MS agar or ammonium-free MS agar. As shown in Fig. 4.24, the growth inhibition reported by Cocking et al. [271] was confirmed in both media tested when supplemented with sucrose, despite its concentration being reduced from 3% to 1%. The bacterial growth was evident around the seed sowing sites (white arrows), where it completely suffocated the plant germination, and was more vigorous in the half-strength MS agar medium. Since *G. diazotrophicus* was shown to be unable to utilise nitrate as nitrogen source due to the lack of a nitrate reductase [83], the increased growth compared to the ammonium-free MS agar is likely due to the ammonium, which would provide an available nitrogen source for the bacterium. Due to the low germination rate and lack of growth in sucrose-supplemented media, no phenotyping was carried out; however, in light of these results, further *A. thaliana* colonisation experiments were conducted decreasing the sucrose concentration in MS agar to 1 mM. Similarly, previous research on sugarcane grown on MS agar had set the suitable sucrose concentration for both plant and *G. diazotrophicus* growth and colonisation to $2\ g\ l^{-1}$ (= 5.8 mM) [231], which here was further reduced according to the different model plant requirements. Furthermore, when untreated and treated seeds were sowed on agar containing the same salts used in the hydroponic nutrient solution (similar in composition and concentration to the Murashige and Skoog Basal Salt Mixture apart from the N source, see Table 3.2), including 2 mM KNO_3 as in the hydroponic N replete condition, no plant growth was observed in either case (not shown). This suggested that, probably due to a different diffusion in the agarised medium compared to the liquid NS, the minimal amount of nitrogen needed for a healthy plant development in agar is at least 15 mM KNO_3, as present in the ammonium-free MS agar tested. Therefore, the ammonium-free MS agar (2.2 g L^{-1} of Sigma-Aldrich Murashige and Skoog Modified Basal Salt Mixture, M2909) was adopted as the standard agarised medium for *A. thaliana* cultivation.

The effect of *G. diazotrophicus* AZ0019 wild type or *nifD*$^-$ on *A. thaliana* growth was then tested on the ammonium-free MS agar medium. Sucrose 1 mM and ammonium at two concentrations (1 mM $(NH_4)_2SO_4$ or 20 mM $(NH_4)_2SO_4$, equivalent to 2 and 40 mmoles of ammonium, respectively) were added to the medium to test 1) the influence of a carbon source to the bacterial growth, and thus the colonisation capability and PGP effect elicited, 2) the influence on the PGP of a nitrogen source available for the bacterial use, at the concentration of 2 mM, i.e. allowing nitrogen fixation (see section 4.4.2), or 40 mM, i.e. suppressing nitrogen fixation [216], and 3) the interplay between carbon and nitrogen in influencing the bacterial PGP capability. The concentration of 40 mM ammonium was chosen to ensure maximum inhibition of nitrogenase activity. In fact, while 10 mM ammonium has been considered sufficient for this purpose in some studies [216], other research has suggested that concentrations over 20 mM [217] are needed for complete nitrogenase inhibition, and is not uncommon to find in literature the non-fixing condition set at 20 mM [124], 30 mM [121] or even 80 [111] mmoles of ammonium. The two bacterial strains, cultured on ATGUS medium, were washed and resuspended in water at the concentration of 10^7 and 10^8 CFUs mL^{-1}. The inoculum was applied through the seed vacuum infiltration technique for 30 min to ensure maximum penetration despite of the small seed surface; seeds were then dried in sterile conditions before sowing. The root and shoot biomass were measured at 20 days post sowing (Fig. 4.25). Other vacuum infiltration conditions had been evaluated preliminarily to this experiment: the infiltration time, tested at 30, 60 and 120 min, did not obviously affect the colonisation level up until 30 dpi as assessed through microscopy (not shown), although at 60 dpi the shortest treatment seemed to result in a poorer root colonisation compared to the 120' treatment (section 4.3.1, Fig. 4.52). The inoculum concentration, on the other hand, showed no apparent difference in terms of bacterial abundance on root tissues when applied in the range of 10^6 to 10^8 CFUs mL^{-1} (section 4.3.1, Fig. 4.52), but prevented germination at 10^9 CFUs mL^{-1}, possibly due to embryo damage or biotic stress response at excessive bacterial densities (not shown). This is consistent with the observation that tomatoes treated through seed vacuum infiltration with 10^8 CFUs mL^{-1} for either 30' (Fig. 4.11) or 60' (Fig. 4.7, 4.8) and grown with a N

source showed a lower or absent PGP effect compared to seeds that were vacuum infiltrated with 10^7 CFUs mL^{-1}. Therefore, a 30' infiltration time coupled with inocula of 10^7 and 10^8 CFUs mL^{-1} were selected as experimental conditions to strike a balance between an effective and yet non-disruptive treatment.

The outcome of the experiment showed that, out of the five different growing conditions, the only one with an increase of shoot biomass compared to the untreated controls was the ammonium-free MS agar without the supplement of neither sucrose nor ammonium (Fig. 4.25a). The other conditions confirmed the lack of PGP until 28 dpi reported by de Souza et al. [262]. Similarly, other studies conducted on sugarcane grown on MS agar setups have reported the lack of *G. diazotrophicus*-induced PGP [163] [221]. It was not possible to isolate the roots of the single plants due to the entanglement of the root systems within the same petri dish, therefore the total weight of the roots present in each petri dish, corresponding to a specific treatment, was measured and divided by the number of plants present. Despite the lack of statistics due to this technical artifact, which must be taken into consideration, some observation can still be inferred.

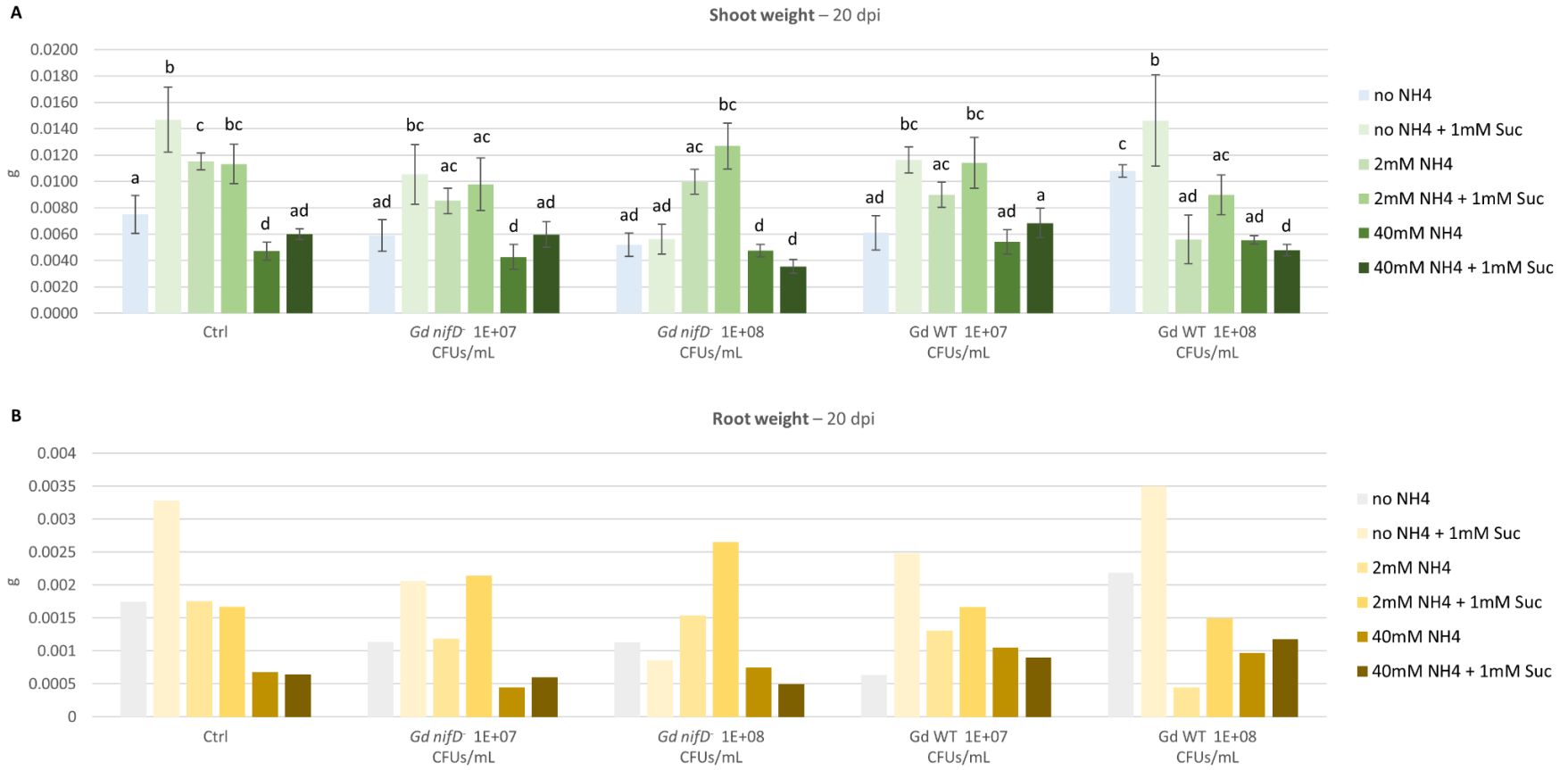

A
Shoot weight – 20 dpi
g
0.0200
0.0180
0.0160
0.0140
0.0120
0.0100
0.0080
0.0060
0.0040
0.0020
0.0000
a
b
c
bc
d
ad
bc
ac
ac
d
ad
ad
ad
bc
ac
bc
d
d
ad
bc
ac
bc
ad
a
c
b
ad
ac
ad
d
Ctrl
Gd nifD- 1E+07 CFUs/mL
Gd nifD- 1E+08 CFUs/mL
Gd WT 1E+07 CFUs/mL
Gd WT 1E+08 CFUs/mL
no NH4
no NH4 + 1mM Suc
2mM NH4
2mM NH4 + 1mM Suc
40mM NH4
40mM NH4 + 1mM Suc
B
Root weight – 20 dpi
g
0.004
0.0035
0.003
0.0025
0.002
0.0015
0.001
0.0005
0
Ctrl
Gd nifD- 1E+07 CFUs/mL
Gd nifD- 1E+08 CFUs/mL
Gd WT 1E+07 CFUs/mL
Gd WT 1E+08 CFUs/mL
no NH4
no NH4 + 1mM Suc
2mM NH4
2mM NH4 + 1mM Suc
40mM NH4
40mM NH4 + 1mM Suc

Fig. 4.25. Growth promotion phenotype 20 days post inoculum (dpi) of A. thaliana (Columbia-0) grown in ammonium-free MS agar supplemented with or without 1 mM sucrose (Suc) and with different levels of ammonium (no NH4 = no ammonium added). Seeds were inoculated through the vacuum infiltration technique for 30 min at 800 mbar with G. diazotrophicus WT (Gd WT) or nifD$^-$ (GD nifD$^-$) strains resuspended in water at two different densities. Shoot (A) and root (B) weight are reported. In the case of roots, the total weight in each condition was measured and divided by the plants number. Untreated controls plants (Ctrl) are shown as comparison. N = 10 for all the parameters tested. The standard error of the mean (SEM) is shown. Bars marked with the same letter within each chart do not differ by Kruskal-Wallis test ($P \leq 0.05$).

In most of the plant-endophyte models studied, the root system and rhizosphere has been shown to harbour the majority of microorganisms compared to the aboveground portions of the plant, in terms of both diversity and abundance [273]. The present study confirmed this trend relatively to the colonisation abundance and distribution of *G. diazotrophicus* in tomato (Fig. 4.15, see section 4.3.1d) and rice (Fig. 4.23). As a result, expectedly, the phenotypic alterations induced by the bacteria (in both positive and negative terms) were usually found to be more pronounced and significant in the root system compared to the aboveground plant organs (Fig. 4.5, 4.6, 4.8, 4.10, 4.11, 4.12, 4.13, 4.14), probably due to a more direct and thus impactful interaction and modulation of those plant tissues. This experiment corroborates such finding, since the effect of *G. diazotrophicus* on *A. thaliana* roots seemed to follow the same trend of shoots while being more accentuated (Fig. 4.25b). As observed in the shoots, in the absence of both ammonium and sucrose, only the highest concentration of wild type bacteria seemed to induce a growth promotion. The addition of 1 mM sucrose produced a similar but more marked outcome, with plants presenting a reduction in root biomass only when exposed to the nitrogen fixation impaired mutant, while the wild-type strain had no negative effect, and, in fact, seemed to elicit a biomass increase at the highest bacterial density. This trend was similar, although less pronounced, in the shoots. The presence of sucrose, boosting the bacterial growth, seemed to have magnified the phenotype elicited by the two strains, with the mutant causing a biotic stress response in the plant and not counterbalancing it with PGP factors, due to lack of N_2 fixation or a nitrogen source.

It is important to note that the *nifD*$^-$ strain would not be able to survive in the long term without any external nitrogen source, but its presence in the seeds (possibly sustaining itself through the endosperm nutrients) was still able to provoke the biotic stress which impaired the plant growth. When the medium was supplemented with 2 mmol of ammonium, however, the inhibition effect caused by the *nifD*$^-$ strain disappeared in both shoots and roots, while the highest concentration of wild type bacteria led to biomass reduction. This result is consistent with the growth inhibition recorded in tomato plants hydroponically grown in the presence of ammonium and *G. diazotrophicus* WT (Fig. 4.14), where, likewise, the *nifD*$^-$ strain kept exerting a positive PGP effect. Although in accordance with the general observation that *nif* mutants of *G. diazotrophicus* are capable of promoting the growth of inoculated plants when nitrogen is not limiting [223], this finding does not explain the negative effect exerted by the wild-type strain. However, since this phenomenon was observed with two different crops and cultivation setups, it suggests that the presence of a nitrogen source available for the bacterium in the form of ammonium can differentially impact the nitrogen metabolism of the wild type and the *nifD*$^-$ mutant. Interestingly, the addition of sucrose in the 2 mM NH_4 condition maintained the mutant-mediated beneficial effect in roots, while alleviating the detrimental effect elicited by the WT strain; thus, it is possible that the presence of a carbon source could provide the wild-type strain with the metabolic energy required to alleviate the mechanism causing the plant growth inhibition in presence of ammonium. Although this interplay between the nitrogenase mutant and the ammonium remains elusive, some hypotheses can be formulated. First, it must be emphasized that no carbon source was available in this particular growth condition of *A. thaliana*. Similarly, no carbon source was added in the tomato hydroponic setup in which the same inhibition effect was observed: the only carbon source available to the bacterium would have been via root exudates [274], which would have varied based on the plant's photosynthetic rate that, in turn, would have been influenced by the nitrogen level in the medium. The carbon availability in root exudates was not investigated; however, in the case of tomato, the amount of nitrogen provided (2 mM KNO_3 + 0.4 mM NH_4), although sufficient for a healthy plant growth, does not meet the levels considered optimal in

greenhouse conditions [215], suggesting a sub-optimal metabolic rate and arguably a scarcity in carbon-rich roots compounds. Therefore, on one hand, a growth condition such to induce a nitrogen-fixing state in *G. diazotrophicus* (i.e. over 0.2 and below 10 mM NH_4, see section 4.4.2), could lead to a local build-up of ammonia in the bacterial infection sites in addition to the ammonium already present in the medium, causing an ammonium toxicity phenotype [218] [219]. Additionally, the limited carbon available to fuel the N_2-fixation process (otherwise derived from seed nutrient reserves and root exudates) may induce the bacteria to consume plant resources as a carbon source for sustaining the energetically demanding reaction. Finally, the bacterial intracellular accumulation of both ammonium from the surroundings and ammonia from the N_2-fixation, may on one hand exacerbate the need for a carbon backbone from the TCA metabolism for NH_4^+ incorporation into glutamate (Glu) [275], and on the other hand it may increase the ammonia diffusion from the bacterial cells to the plant tissues, leading to the above-mentioned ammonium toxicity on plants. Intriguingly, this stress phenotype in *A. thaliana* was recently shown to be mediated by the action of a plastid-based glutamine synthetase (GS) which, converting the ammonium-derived glutamate in glutamine (Gln) at high rates, would favour the acidification of the medium, with detrimental effects for plant metabolic processes [276]. It is tempting to draw an analogy between this plastid enzymatic activity and the action of endophytic (and possibly intracellular) *G. diazotrophicus* cells in the particular condition of coping with excess ammonium production in scarcity of carbon sources. This mechanism would not occur in the nitrogenase mutant, which, in turn, could invest the metabolic energy saved from N_2-fixation, along with the ammonium captured from the medium, in producing beneficial phytohormones and other growth factors. Furthermore, in the *nifD*$^-$ mutant strain, the *nifD* gene was disrupted through the insertion of a kanamycin resistance cassette [208]. This targeted integration impaired the expression of the *nifHDK* polycistronic transcript, resulting, theoretically, in the transcriptional termination of the genes downhill the insertion locus, i.e. *nifD* and *nifK* (while possibly leaving the *nifH* expression unaltered). Recently, a proteomic study reported that, in Nostoc sp. PCC 7120 grown in nitrogen-fixing conditions, *nifD* and *nifK* can partner with the bacterial glutamine

synthetase, and that the downregulation of such genes could affect the process of ammonium incorporation [277]. It is therefore possible that the lack of this putative interaction with the bacterial GS, due to the *nifDK* transcript disruption, may cause an ammonium assimilation unbalance in the *G. diazotrophicus nifD*$^-$ mutant, resulting in the preservation of its PGP function while growing in the particular N to C ratio described. Finally, the last condition investigated contained 40 mM NH_4 (Fig. 4.25), which caused an unsurprisingly pronounced plant growth inhibition compared to the other media, regardless of the presence of sucrose, to the point of almost obscuring other phenotype examinations. However, some bacteria-mediated growth divergences were still observed. Without the addition of sucrose, the *nifD*$^-$ mutant performed worse than the wild type, and in fact seemed to cause a reduction in root biomass (Fig. 4.25b). Similarly, in the carbon amended medium, the mutant strain did not elicit any visible phenotype amelioration, and caused a biomass decrease at the highest bacterial density; the wild-type strain, on the other hand, could still stimulate the root growth, although it also caused a shoot reduction at the densest inoculum. In other words, in non-diazotrophic conditions (i.e. in the presence of nitrogenase-inhibiting levels of ammonium), the effect observed in low NH_4 was reverted, and the advantage of the wild type strain over the mutant was restored. This finding reinforces the idea that the PGP capability of *G. diazotrophicus* are affected by its metabolic state, with a delicate balance between ammonium uptake and nitrogen-fixation being required for its successful adaptation to various environmental condition. The paradoxical consequences of the *nifD*$^-$ mutant being able to outperform the wild type in specific growth conditions, motivates further research and genetic engineering efforts aimed at uncoupling nitrogen and carbon metabolism, in order to gain deeper understanding of the regulation of nitrogen metabolism and optimize the bacterium for PGP in various field conditions.

In conclusion, the interplay between different environmental and physiological factors such as the availability of nitrogen and carbon can shape both the bacterial PGP efficacy and the plant response to the mutualistic relationship. From the plant's perspective, the trade-off between the energetic burden induced by the bacterium through the defence activation, and the beneficial

growth factors provided by *G. diazotrophicus*, can influence its metabolism according to the availability of nutrients, as recently shown in a work in which the nutrient variable was substituted with light intensity variations [278]. In a similar manner, the availability of nitrogen and carbon sources in the growth medium, from both inorganic and plant exudate origins, could impact the balance between nitrogen fixation, ammonium uptake, and carbon metabolism in the bacterium, leading to differing interactions and PGP capabilities.

In addition to investigating the *G. diazotrophicus*-mediated PGP effect, these experiments have confirmed the suitability of the *A. thaliana* model for microscopy analysis (see section 4.3), allowing for further examination of intracellular bacteria and their role in plant-microbe interactions.

In Table 3.4 the PGP effect and phenotypic modifications induced by the application of *G. diazotrophicus* to tomato and rice are summarised.

Reference	Model system	Inoculation strategy	Inoculum carrier	Inoculum concentration	Inoculum incubation time and T	Plant growth substrate	N source	Floral abundance	Fruit yield	Shoot length	Shoot weight	Root weight	Root length	Chlorophyll content
Fig. 4.3	Tomato cv. MoneyMaker	seed coating (LC)	3% sucrose, 0.3% gum arabic, 0.1% Tween 80	1E+08 CFUS mL^{-1}	30 min, RT	30 days Levington M3 soil + 30 days 50:50 Klasman soil:sand	soil	+	+	+				
Fig. 4.4	Tomato cv. MoneyMaker	seed coating (SC)	3% sucrose, 0.3% gum arabic, 0.1% Tween 80	1E+07 CFUS mL^{-1}	30 min, RT	30 days Levington M3 soil + 30 days 50:50 Klasman soil:sand	soil	+	/	+				
Fig. 4.4	Tomato cv. MoneyMaker	seed coating (SC)	3% sucrose, 0.3% gum arabic, 0.1% Tween 80	1E+06 CFUS mL^{-1}	30 min, RT	30 days Levington M3 soil + 30 days 50:50 Klasman soil:sand	soil	+	/	+				
Fig. 4.5	Tomato cv. MoneyMaker	seed coating (LC)	Water	1E+08 CFUS mL^{-1}	30 min, RT	30 days Levington M3 soil	soil			/	/	/		
Fig. 4.5	Tomato cv. MoneyMaker	seed coating (LC)	3% sucrose, 0.3% gum arabic, 0.1% Tween 80	1E+08 CFUS mL^{-1}	30 min, RT	30 days Levington M3 soil	soil			/	/	/		
Fig. 4.5	Tomato cv. MoneyMaker	seed coating (LC)	10% sucrose, 1.5% gum arabic, 0.5% Tween 80	1E+08 CFUS mL^{-1}	30 min, RT	30 days Levington M3 soil	soil			/	+	/		
Fig. 4.6	Tomato cv. Ailsa Craig	seed coating (LC)	Water	1E+08 CFUS mL^{-1}	30 min, RT	30 days Levington M3 soil	soil			/	/	/		
Fig. 4.6	Tomato cv. Ailsa Craig	seed coating (LC)	3% sucrose, 0.3% gum arabic, 0.1% Tween 80	1E+08 CFUS mL^{-1}	30 min, RT	30 days Levington M3 soil	soil			/	/	/		

Reference	Model system	Inoculation strategy	Inoculum carrier	Inoculum concentration	Inoculum incubation time and T	Plant growth substrate	N source	Floral abundance	Fruit yield	Shoot length	Shoot weight	Root weight	Root length	Chlorophyll content
Fig. 4.6	Tomato cv. Ailsa Craig	seed coating (LC)	10% sucrose, 1.5% gum arabic, 0.5% Tween 80	1E+08 CFUS mL^{-1}	30 min, RT	30 days Levington M3 soil	soil			/	/	/		
Fig. 4.7, 4.8	Tomato cv. MoneyMaker	seed vacuum infiltration (LC)	Water	1E+06 CFUS mL^{-1}	60 min at 800 mbar, RT	30 days Levington M3 soil + 90 days 50:50 Klasman soil:sand	soil	/	/	/	/	+		+
Fig. 4.7, 4.8	Tomato cv. MoneyMaker	seed vacuum infiltration (LC)	Water	1E+07 CFUS mL^{-1}	60 min at 800 mbar, RT	30 days Levington M3 soil + 90 days 50:50 Klasman soil:sand	soil	/	+	/	+	+		+
Fig. 4.7, 4.8	Tomato cv. MoneyMaker	seed vacuum infiltration (LC)	Water	1E+08 CFUS mL^{-1}	60 min at 800 mbar, RT	30 days Levington M3 soil + 90 days 50:50 Klasman soil:sand	soil	/	/	/	/	+		+
Fig. 4.10	Tomato cv. MoneyMaker	seed vacuum infiltration (LC)	Water	1E+06 CFUS mL^{-1}	30 min at 800 mbar, RT	30 days in hydroponic system	0			/	-	-		
Fig. 4.10	Tomato cv. MoneyMaker	seed vacuum infiltration (LC)	Water	1E+07 CFUS mL^{-1}	30 min at 800 mbar, RT	30 days in hydroponic system	0			/	/	-		
Fig. 4.10	Tomato cv. MoneyMaker	seed vacuum infiltration (LC)	Water	1E+08 CFUS mL^{-1}	30 min at 800 mbar, RT	30 days in hydroponic system	0			/	-	-		
Fig. 4.11	Tomato cv. MoneyMaker	seed vacuum infiltration (LC)	Water	1E+06 CFUS mL^{-1}	30 min at 800 mbar, RT	30 days in hydroponic system	0.2 mM KNO_3			/	+	+		
Fig. 4.11	Tomato cv. MoneyMaker	seed vacuum infiltration (LC)	Water	1E+07 CFUS mL^{-1}	30 min at 800 mbar, RT	30 days in hydroponic system	0.2 mM KNO_3			/	+	+		

Reference	Model system	Inoculation strategy	Inoculum carrier	Inoculum concentration	Inoculum incubation time and T	Plant growth substrate	N source	Floral abundance	Fruit yield	Shoot length	Shoot weight	Root weight	Root length	Chlorophyll content
Fig. 4.11	Tomato cv. MoneyMaker	seed vacuum infiltration (LC)	Water	1E+08 CFUS mL^{-1}	30 min at 800 mbar, RT	30 days in hydroponic system	0.2 mM KNO_3			/	+	+		
Fig. 4.12	Tomato cv. MoneyMaker	direct inoculation in NS	NS	1E+07 CFUS mL^{-1}	2 days in NS, 29 °C	20 days in hydroponic system	0			+, /	+, +	+, +		
Fig. 4.13	Tomato cv. MoneyMaker	direct inoculation in NS	NS	1E+07 CFUS mL^{-1}	2 days in NS, 29 °C	20 days in hydroponic system	2 mM KNO_3			+, /	/, /	+, /		
Fig. 4.14	Tomato cv. MoneyMaker	direct inoculation in NS	NS	1E+07 CFUS mL^{-1}	2 days in NS, 29 °C	20 days in hydroponic system	2 mM KNO_3 + 0.2 mM $(NH_4)SO_4$			-, /	-, /	-, +		
Fig. 4.17	Rice cv. BC15	pregerminated seed coating (LC)	3% sucrose, 0.3% gum arabic, 0.1% Tween 80	1E+07 CFUS mL^{-1}	4 days in carrier, 28 °C	60 days in loam:soil:sand	0			+				+
Fig. 4.17	Rice cv. BC15	pregerminated seed coating (LC)	3% sucrose, 0.3% gum arabic, 0.1% Tween 80	1E+08 CFUS mL^{-1}	4 days in carrier, 28 °C	60 days in loam:soil:sand	0			/				+
Fig. 4.18	Rice cv. BC15	seed coating (LC)	Water	1E+06 CFUS mL^{-1}	60 min, RT	30 days in loam:soil:sand	0			/	-	-		
Fig. 4.18	Rice cv. BC15	seed coating (LC)	3% sucrose, 0.3% gum arabic, 0.1% Tween 80	1E+06 CFUS mL^{-1}	60 min, RT	30 days in loam:soil:sand	0			-	-	-		
Fig. 4.18	Rice cv. BC15	seed coating (LC)	10% sucrose, 1.5% gum arabic, 0.5% Tween 80	1E+06 CFUS mL^{-1}	60 min, RT	30 days in loam:soil:sand	0			+	+	+		

Reference	Model system	Inoculation strategy	Inoculum carrier	Inoculum concentration	Inoculum incubation time and T	Plant growth substrate	N source	Floral abundance	Fruit yield	Shoot length	Shoot weight	Root weight	Root length	Chlorophyll content
Fig. 4.18	Rice cv. BC15	seed coating (LC)	Water	1E+07 CFUS mL^{-1}	60 min, RT	30 days in loam:soil:sand	0			/	+	/		
Fig. 4.18	Rice cv. BC15	seed coating (LC)	3% sucrose, 0.3% gum arabic, 0.1% Tween 80	1E+07 CFUS mL^{-1}	60 min, RT	30 days in loam:soil:sand	0			/	-	/		
Fig. 4.18	Rice cv. BC15	seed coating (LC)	10% sucrose, 1.5% gum arabic, 0.5% Tween 80	1E+07 CFUS mL^{-1}	60 min, RT	30 days in loam:soil:sand	0			+	+	+		
Fig. 4.18	Rice cv. BC15	seed coating (LC)	Water	1E+06 CFUS mL^{-1}	12 hours, RT	30 days in loam:soil:sand	0			/	-	-		
Fig. 4.18	Rice cv. BC15	seed coating (LC)	10% sucrose, 1.5% gum arabic, 0.5% Tween 80	1E+06 CFUS mL^{-1}	12 hours, RT	30 days in loam:soil:sand	0			/	/	/		
Fig. 4.18	Rice cv. BC15	seed coating (LC)	Water	1E+07 CFUS mL^{-1}	12 hours, RT	30 days in loam:soil:sand	0			/	/	-		
Fig. 4.18	Rice cv. BC15	seed coating (LC)	10% sucrose, 1.5% gum arabic, 0.5% Tween 80	1E+07 CFUS mL^{-1}	12 hours, RT	30 days in loam:soil:sand	0			/	/	/		
Fig. 4.20	Rice cv. BC15	seed coating (LC)	Water	1E+07 CFUS mL^{-1}	60 min, RT	20 days in hydroponic system	0			+, /			+, /	
Fig. 4.21	Rice cv. BC15	direct inoculation in NS	NS	1E+06 CFUS mL^{-1}	2 days in NS, 29 °C	20 days in hydroponic system	0			+, /			/, –	
Fig. 4.21	Rice cv. BC15	direct inoculation in NS	NS	1E+07 CFUS mL^{-1}	2 days in NS, 29 °C	20 days in hydroponic system	0			+, /			+, /	

Reference	Model system	Inoculation strategy	Inoculum carrier	Inoculum concentration	Inoculum incubation time and T	Plant growth substrate	N source	Floral abundance	Fruit yield	Shoot length	Shoot weight	Root weight	Root length	Chlorophyll content
Fig. 4.22	Rice cv. BC15	seedling coating	Water	1E+06 CFUS mL^{-1}	12 hours, 28 °C	20 days in hydroponic system	0			+	+	/	+	
Fig. 4.22	Rice cv. BC15	seedling coating	Water	1E+07 CFUS mL^{-1}	12 hours, 28 °C	20 days in hydroponic system	0			/	/	/	-	
Fig. 4.22	Rice cv. BC15	seedling coating	Water	1E+08 CFUS mL^{-1}	12 hours, 28 °C	20 days in hydroponic system	0			/	/	/	-	
Fig. 4.22	Rice cv. BC15	seedling coating	Water	1E+06 CFUS mL^{-1}	12 hours, 28 °C	20 days in hydroponic system	0.2 mM KNO_3			+	+	/	+	
Fig. 4.22	Rice cv. BC15	seedling coating	Water	1E+07 CFUS mL^{-1}	12 hours, 28 °C	20 days in hydroponic system	0.2 mM KNO_3			/	/	/	/	
Fig. 4.22	Rice cv. BC15	seedling coating	Water	1E+08 CFUS mL^{-1}	12 hours, 28 °C	20 days in hydroponic system	0.2 mM KNO_3			/	/	/	/	
Fig. 4.22	Rice cv. BC15	seedling coating	Water	1E+06 CFUS mL^{-1}	12 hours, 28 °C	20 days in hydroponic system	2 mM KNO_3			+	+	+	+	
Fig. 4.22	Rice cv. BC15	seedling coating	Water	1E+07 CFUS mL^{-1}	12 hours, 28 °C	20 days in hydroponic system	2 mM KNO_3			+	+	+	+	
Fig. 4.22	Rice cv. BC15	seedling coating	Water	1E+08 CFUS mL^{-1}	12 hours, 28 °C	20 days in hydroponic system	2 mM KNO_3			+	+	+	/	

Table 3.4. Summary of the phenotype modification induced by the inoculation of G. diazotrophicus to tomato and rice with all the application methods tested. The red colour refers to the G. diazotrophicus nifD- mutant. LC = bacteria grown in liquid cultures; SC = bacteria scraped from solid medium. / = no difference from the controls; + = increase compared to the control; - = decrease from the control; no symbol = not assessed.

4.2 Mutants and mutagenesis tools creation

Bacterial mutagenesis, the art of manipulating the genetic material of prokaryotes, is an essential tool in molecular biology, with applications ranging from research in gene function to metabolic engineering. However, due to the frequent lack of solid species-specific theoretical foundations or universally valid principles, the techniques employed for this purpose can be challenging, as they require careful design, precise execution, and time-consuming validations.

Habitually, most areas of basic research in microbiology employ model organisms such as *E. coli* [279] or *B. subtilis* [280] (representing Gram-negative and Gram-positive bacteria, respectively) thanks to their well-characterized physiology and the large genetic toolbox available from decades of technical and practical knowledge, which allows relatively effortless genetic engineering. Although *E. coli* is an excellent host for the physical assembly of DNA fragments and cloning methods, it is often not the optimal platform for developing specific biological features or biotechnologies which requires the releasing of the bacterium into the environment [281].

Studies in the environmental biotechnology field have increasingly shifted their attention to non-model organisms that natively exhibit desirable phenotypes for specific purposes, as in the case of the PGP capabilities of *G. diazotrophicus*. These non-domesticated organisms can be difficult to genetically modify due to the lack of genetic tools and limited knowledge about the organism's physiology; nevertheless, advances in next-generation sequencing techniques have made accessible the genomic knowledge which can be used as a basis for systems-level biological analyses and mutagenesis design [282].

Successful transformation of bacteria for genetic engineering is usually hindered by four primary barriers: cellular uptake of foreign DNA, evasion of native immune system that degrade exogenous genetic material, transformant selection, and retention of the transformed DNA by the targeted organism [283].

In this study, different transformation techniques were evaluated to overcome such obstacles and develop a reliable transformation method for the creation of *G. diazotrophicus* mutants. In the context of the present research, the goal was to tag the bacterium with reporter proteins for *in planta* detection or gene expression analyses, either in the form of constitutive plasmids or through genomic integration.

In the preliminary evaluations of the genes of interest for this work, the mutagenesis design had been based on the published genome sequences of *G. diazotrophicus* publicly accessible on NCBI. Unusually, two genomes are available for the same *Gluconacetobacter diazotrophicus* PAl5 strain, both published between 2009 and 2010. The genome with accession number AM889285.1 was published by the RioGene group in Brazil, who submitted a 3,944,163 bp chromosomal sequence accompanied by two plasmids (plasmid pGDIPal5I: AM889287.1, plasmid pGDIPal5II: AM889286.1) [284]. The second genome, with accession number CP001189.1, is a direct submission by the US DOE Joint Genome Institute (JGI) in California, USA, and describes a 3,887,492 bp sequence with one plasmid (CP001190.1). Although reportedly deriving from the same PAl5 type strain (ATCC 49037), a study analysing the differences between the two genomic sequences by optical mapping validation, identified 168 and 187 unique coding sequences (CDS) in the RioGene and JGI genomes respectively (approximately 5% of the CDS), with zero percent identity between each other, and found only 90% of the CDS predicted in each genome to share more than 90% identity [285]. A high level of chromosomal rearrangements was found in the AM889287.1 sequence, possibly explained by the presence of 110 transposase genes, while the JGI sequence only contained 59. Other possible explanations of this unexpected discrepancy are either the natural strain divergence due to rapid evolution during culturing, or the different bioinformatic approaches and presence of inverted repeated regions that may have caused errors in the sequence assembly [285].

To ensure maximal accuracy for this study, the *Gluconacetobacter diazotrophicus* AZ0019 wild type and the *Gluconacetobacter diazotrophicus* AZ0019 *nifD*$^{-}$ mutant strains were sent for genome sequencing (Deep Seq Centre for Genetics and Genomics, University of Nottingham), via the

combination of Nanopore Technology and Illumina sequencing for optimal fidelity. The sequencing service produced around 300 contigs for each strain. Each contig represents a long, continuous fragment of a genomic region and, as so, is an accurate and theoretically error-free rendition of the actual sequence. However, the operation of assembling the contigs into a single sequence in the correct order require additional bioinformatic processing, since the simple juxtaposition of the fragments would result in a random alignment order and with gaps and mismatches between the contig ends [286]. Therefore, an assembly was attempted using the software Mauve [287], a multiple alignment bioinformatic tool which, for the purpose of this study, was used to reorder the contigs using the published *Gluconacetobacter diazotrophicus* PAl5 "AM889285.1" sequence as a scaffold. Although this method could not ensure an error-proof end-joining of the contigs, it allowed their assembly and rearrangement in accordance with the scaffold provided, ultimately yielding a sequence amenable for further downstream analyses. In Fig. 4.26 is shown the visual comparison between the reordered genome of *G. diazotrophicus* AZ0019 and the two available genomic sequences of *G. diazotrophicus* Pal 5, i.e. AM889285.1 and CP001189.1. The comparison was performed with the software BLAST Ring Image Generator (BRIG) [288]. Expectedly, the *G. diazotrophicus* AZ0019 sequence closely matches the AM889285.1 genome, since it was used as a scaffold for its assembly. However, the presence of nonaligned white gaps between the two sequences, representing regions with 0 to 50% bp identity, highlights a divergence that most likely is not only due to an imperfect end joining of the 300 contigs, but to strain-specific genomic variations. This is not surprising, since *G. diazotrophicus* AZ0019 was originally isolated from a sub-culture of the strain *G. diazotrophicus* UAP5541, first isolated in Mexico [113].

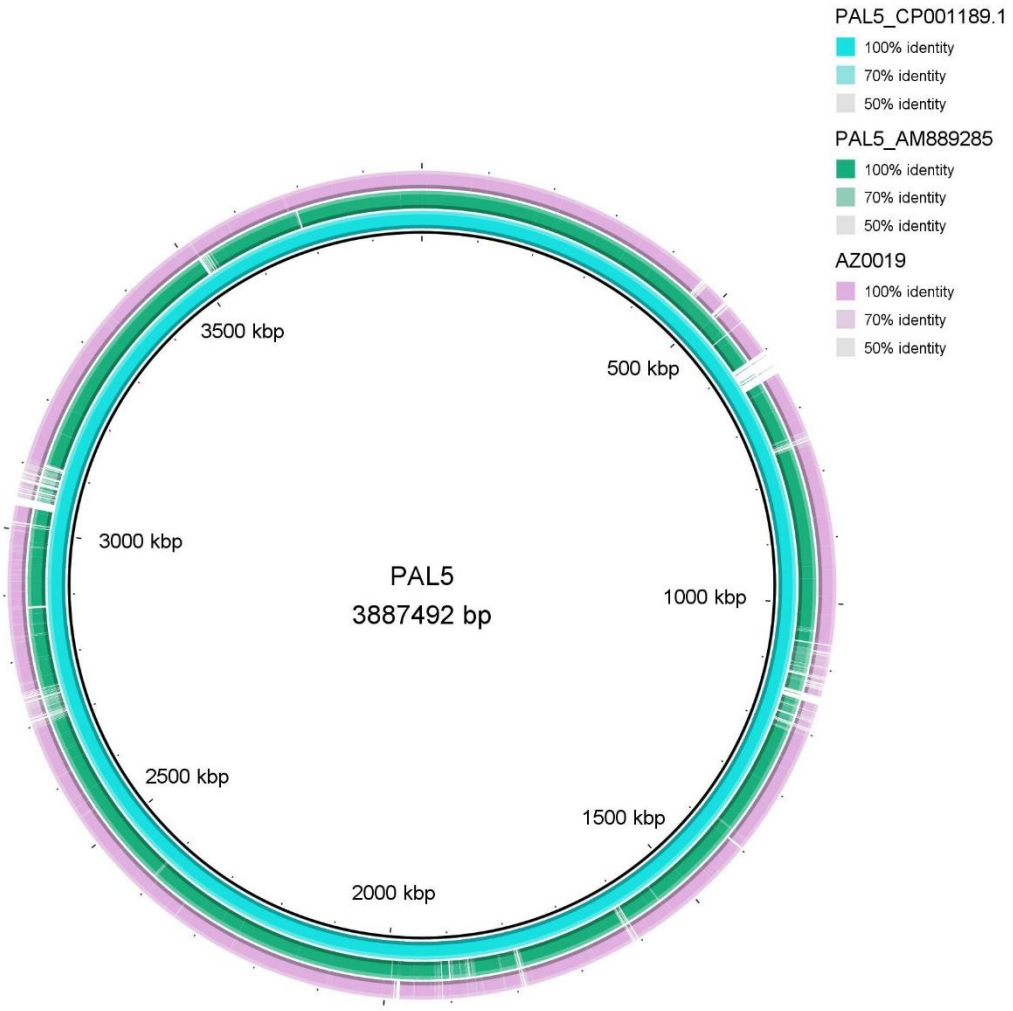


Fig. 4.25. Visual comparison between the two published G. diazotrophicus Pal 5 genomic sequences and the assembled G. diazotrophicus AZ0019 genome. The G. diazotrophicus Pal 5 "CP001189.1" genome was used as reference for the comparison between the G. diazotrophicus AZ0019 and the G. diazotrophicus Pal 5 "AM889285.1" genomic sequences. The upper identity threshold (in a lighter shade of the corresponding ring colour) was set at 70% bp identity, while the lower identity threshold (in grey) was set at 50% bp identity. White gaps represent 0 to 50% identity. The image was generated with BRIG (BLAST Ring Image Generator).

The natural occurrence of numerous *G. diazotrophicus* strains with intraspecific genetic variation (as shown by the analysis of genome islands in 19 *G. diazotrophicus* strains [284]) suggest part of the genomic discrepancies observed between AZ0019 and AM889285.1 to be the result of evolutionary divergence, with possible implications in the physiological characteristics of the strain. Indeed, it cannot be ruled out that the software's algorithm may have forced the contigs assembly on the AM889285.1 scaffold to some degree, therefore losing some of the genetic diversity due to the biased trimming of

unfitting sequencing data; however, such bioinformatic issues were beyond the main scope of this work and were not further investigated. Future work should focus on creating a coherent and error-proof assembled genomic sequence in order to compare it with the other published *G. diazotrophicus* strains and precisely assess unique genetic traits of *G. diazotrophicus* AZ0019.

The wild-type genome obtained through the assembly of the contigs was used as a base for all the downstream applications, such as cloning strategies and primers design, while also referring to both the *G. diazotrophicus* AZ0019 *nifD*$^{-}$ genome (similarly sequenced and assembled) and the publicly available Pal 5 sequences for validation.

4.2.1 Electroporation optimisation and expression vector selection

One of the aims of this study was the establishment of a suit of vector backbones allowing replication and gene expression in *G. diazotrophicus*. This process requires the identification of strain-compatible functional elements, such as suitable origin of replication (*ori*, sometimes referred to as *oriV*, where V stands for vegetative), allowing stable and chromosome-independent replication of plasmids in the bacterial host, and promoters granting significant gene expression. Furthermore, in the case of transformation with multiple plasmids, the choice must fall on compatible *ori* belonging to different incompatibility groups, i.e. replicons with different replication control machineries, to prevent plasmid loss due to uneven partitioning [289] or disproportionate iteron/antisense RNAs negative regulation [290]. To deliver the foreign DNA in *G. diazotrophicus* cells, different techniques were attempted. The electroporation method, although quicker and more versatile than other transformation techniques such as conjugation, and nominally up to 10-fold more efficient than chemical transformation [291], still suffers from some drawbacks. In this technique, a high-voltage electric pulse is applied to carefully prepared electrocompetent cells, creating nm-wide transient, aqueous pores in the membrane, which ultimately allow the entry of the DNA molecules [292]. During this process the cellular uptake of the molecules

continue until the pore resealing, which can take milliseconds to minutes. However, this procedure also bears the risk for cell damage or death, since inadequate experimental conditions can induce the transient pores to expand beyond a critical threshold radius and cause membrane rupture, and therefore requires careful optimisation [293]. The research for an optimised electroporation protocol and the pursuit of functional plasmid elements suitable for *G. diazotrophicus* were carried out in the attempt to establish a valid transformation method for constitutive plasmid delivery.

4.2.1a pBBR1MCS-5_GFP plasmid characterisation and testing for *in planta* detection

Firstly, a green fluorescent protein (*gfp*)-bearing plasmid named pBBR1MCS-5_GFP was tested. The origin of this plasmid's backbone dates back to the isolation of a 2.6 kb cryptic plasmid from *Bordetella bronchiseptica*, named pBBR1 [294]. Later, the plasmid was modified by Kovach et al. by the addition of a multiple cloning site (MCS) within a *lacZα* gene from the pBluescript® II KS vector and a chloramphenicol-resistance (Cm^R), and was renamed pBBR1MCS [295]. It was described as a broad-host-range vector for its ability to be stably maintained in *Bordetella*, *Brucella*, *Escherichia*, *Vibrio*, *Pseudomonas* and *Rhizobium* species for up to 10 days without antibiotic selection, and was found compatible with IncP, IncQ, and IncW group plasmids and with ColE1- and p15A-based replicons [295]. pBBR1MCS carries an *ori* named $oriV_{pBBR1}$ which requires the pBBR1 Rep protein for replication, and is currently not classified in any particular incompatibility group [296]. Subsequently, the plasmid was further diversified into four derivatives, named pBBR1MCS-2 to 5, in which the Cm^R was substituted with different antibiotic resistances; in particular, the pBBR1MCS-5 carries a gentamicin resistance ($Gent^R$) [297]. Interestingly, the study also validated these vectors in *Acetobacter xylinum*, suggesting their use in the Acetobacteraceae family. Consistently with this indication, during the years 2000s, pBBR1MCS-based plasmids have become among the most frequently employed in AAB, especially in the *Gluconobacter* species but with some

examples in *G. diazotrophicus* too [298]. This plasmid family is described as medium [299] to low copy number (around 30 copies per cell in *P. fluorescens* 13525) and wasn't found to affect the bacterial host growth rate or glucose utilization [300].

In this work, the presence of a functional *gfp* gene in pBBR1MCS-5_GFP, kindly provided by professor P. Hill (Food Sciences, University of Nottingham), was optically verified through fluorescence microscopy upon transformation on *E. coli* DH5α cells; however, no specific information on the reporter gene cassette was available, therefore the plasmid was sequenced, and its history was reconstructed in order to gain some insights about its optimal use. It was found to contain a *gfpmut3** gene, created by Andersen et al. in 1998 and described as a *gfpmut3b* with an accidental mutation at position 2 (S2R) that does not affect its function [301]. *gfpmut3b* is a *gfp* variation with two mutations in the chromophore region (S65G, S72A) that under 488 nm excitation light makes it 20 times more fluorescent than the wild-type variant in *in vitro* protein assay and 100 times more fluorescent when expressed *in vivo* from *E. coli* host [302] [303]. This amelioration is believed to depend on a folding advantage that makes GFPmut3b entirely soluble, while part of the wild-type protein is normally accumulated in inclusion bodies in a non-fluorescent form [303]. Additionally, the excitation maximum (i.e. the peak of the light absorption spectrum) is red-shifted at 500 nm compared to the 395 nm of the parental GFP, while the emission maximum is essentially unchanged (513 nm), making GFPmut3b a more convenient target for the popular 488 nm line of an argon laser [304]. This protein was reported to have a 10-hour half-life in *B. subtilis* [305] and more than one day in *E. coli* MV1190 (λ-pir) [301]. The pBBR1MCS-5_GFP plasmid sequencing showed *gfpmut3** to be part of the $P_{A1/04/03}$-RBSII-*gfpmut3**-T0-T1 cassette generated by Andersen et al. in their 1998 study [301] (Fig. 4.26). $P_{A1/04/03}$ is a modified *lac*-repressible promoter reportedly obtained from Lanzer and Bujard's work, although no such name appears in the cited paper [306]. However, the sequence revealed it to be a fusion between the promoter $P_{A1/04}$ (a modified version of the *E. coli* P_{lac} promoter, with different -33 and -10 elements and a *lac* operator inserted in between) and the 3' end of the promoter $P_{A1/03}$ (only including its *lac* operator),

resulting in a chimeric promoter with two *lac* operators. The RBSII-T0-T1 cassette cloned next to $P_{A1/04/03}$ by Andersen et al. includes a ribosomal binding site (RBSII) followed by a phage lambda T0 terminator and a T1 terminator from the *rrnB* operon of *E. coli*; although not mentioned in the publication, between the two terminators lies a chloramphenicol acetyl transferase gene (*cat*) cassette, conferring resistance to chloramphenicol (Cm^R). The RBSII-T0-T1 cassette, that should be renamed RBSII-T0-*cat*-T1, derives from the Qiagen pQE-70 vector, which, in turn, is based on the pDS56/RBSII and pDS781/RBSII-DHFRS vectors described by Stüber et al. [307] (for a more detailed report see the QIA*expressionist*^{TM} manual [308]). The origin and characterisation of the RBSII itself, apart from being described as a strong synthetic RBS [308], is unclear, but the work from Stüber et al. refers to a previous publication in which the RBSII was reportedly integrated upstream the T0-*cat*-T1 cassette to drive recombinant protein expression [309]. The *cat* gene itself is described in the same publication as promoter-free but with its own ribosomal binding site, allowing expression via transcriptional readthrough from any upstream "Promoter-RBSII-gene of interest" expression cassette; the presence of the T0 terminator between the expression cassette and the *cat* gene is said to reduce transcription of *cat* 10-fold, therefore preventing growth inhibition by CAT overproduction, but allowing sufficient synthesis of this protein to select for intermediate levels of chloramphenicol resistance [309]. Although no details about the RBSII discussed herein were provided by the above-mentioned studies, more recent research evaluating the activity of 13 RBSs driving the expression of *gfpmut3b* in cyanobacterium *Synechocystis sp*. PCC 6803, found it to perform at about half of the maximum activity of the best RBS tested [310]. In summary, in order to create the "$P_{A1/04/03}$-RBSII-*gfpmut3**-T0-*cat*-T1" cassette, Andersen et al. [301] fused the $P_{A1/04}$ and $P_{A1/03}$ (Lanzer and Bujard, 1988 [306]) into the chimeric and theoretically tight promoter "$P_{A1/04/03}$" bearing two *lac* operators; $P_{A1/04/03}$ was inserted upstream the RBSII-T0-*cat*-T1 cassette from Bujard et al. 1987 [309] for granting maximum translation efficiency, and finally the *gfpmut3** gene from Cormak et al. [303] was cloned between the RBSII and the T0 terminator. The whole construct was cloned in the *lacZα*MCS of pBBR1MCS_5, a broad-host-range, medium-low copy plasmid [297], resulting in a ~ 6800 bp vector (Fig. 4.26).

1 µg of vector was electroporated into electrocompetent *G. diazotrophicus* cells (see Materials and Methods) and selected in ATGUS + gentamicin 25 µg mL^{-1} medium (Gent 25). Transformants were screened under fluorescent stereo microscope with GFP excitation light. Only one colony out of several hundred was found to fluoresce, highlighting an extremely low transformation and/or selection efficiency. The strain was named "*GG*" (from GFP Gd). As in the case of *E. coli* DH5α cells transformed with the same vector, strong fluorescence was detected under appropriate excitation light.

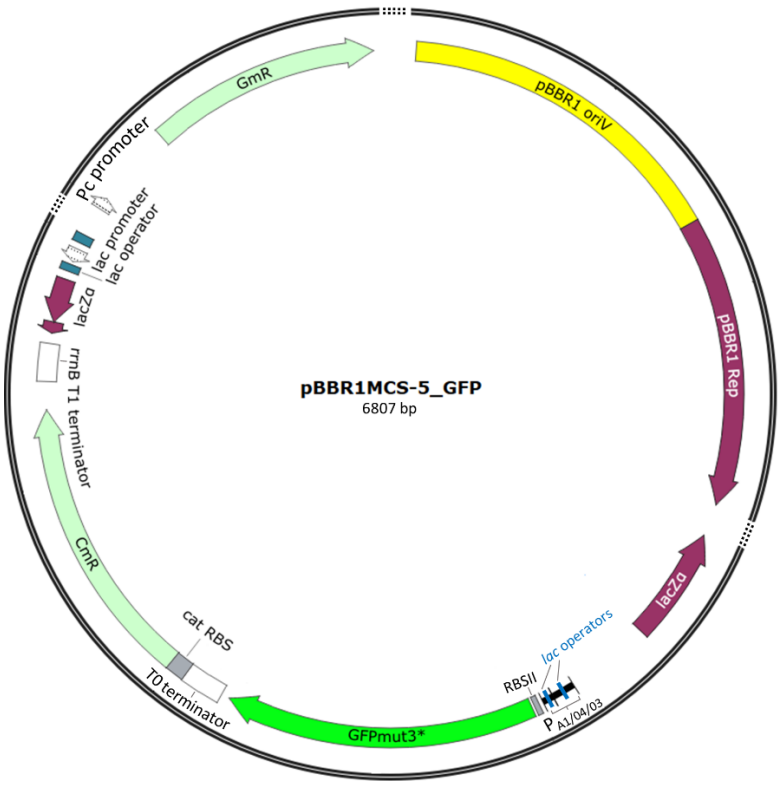


Fig. 4.26. Visual representation of the pBBR1MCS-5_GFP plasmid generated from sequencing data. Relevant vector components are shown, while featureless backbone regions are omitted (double dashed line). Image was generated with the software SnapGene [311].

Gentamicin (Gent 25), chloramphenicol (Cm 25) or the combination of the two, each at the concentration of 25 µg mL^{-1}, were all found suitable for both

bacterial species growth and GFP expression (Fig. 4.27). The use of Cm 25 alone in *E. coli* seemed to induce higher GFP expression, as indicated by the intense yellow colour of the colonies (Fig. 4.27c) and by a stronger fluorescent signal under GFP excitation light (Fig. 4.27a, e). The Gent 25 selection, on the other hand, produced a seemingly mixed population of *E. coli*, with colonies exhibiting a fainter shade of yellow (resulting in a dimmer fluorescence) intermingled with more vibrant CFUs which were also more luminous under fluorescent illumination (Fig. 4.27a, d, f). *GG*, however, did not show the same obvious correlation between fluorescence intensity and the selection used, and no yellow colour was observed in any antibiotic condition under daylight, implying a lower plasmid replication rate or less efficient protein expression. *GG* CFUs within the same plate or the same culture showed slightly different fluorescence intensity among each other (Fig. 4.27i), probably due to a phase variation mechanism [312], and some of the colonies occasionally exhibited stronger fluorescence in Gent 25 compared to Cm 25 (Fig. 4.27 g). To assess the plasmid stability, *GG* was grown in liquid ATGUS medium with no antibiotic selection until stationary phase and plated in selective or non-selective ATGUS medium. The fluorescent cell count showed 96% of the CFUs to be still expressing *gfp* when plated in the selective medium, and around 90% when plated in non-selective medium, denoting a high plasmid stability (Fig. 4.27h). It should also be emphasized that these experiments can artificially inflate the apparent plasmid loss rate because the growth rate of plasmid-free cells may be higher [313]. As a comparison, *E. coli* cells were observed to lose any trace of GFP expression when plated in non-selective LB medium (Fig. 4.27b). When streaked on a larger area of selective medium, *GG* green fluorescence mostly originated from the border regions, suggesting the synthesis of the fluorescent protein to be associated with the fastest-growing cells localized in the periphery of the colonies, possibly due to antibiotic depletion in the central area (Fig 4.27g).

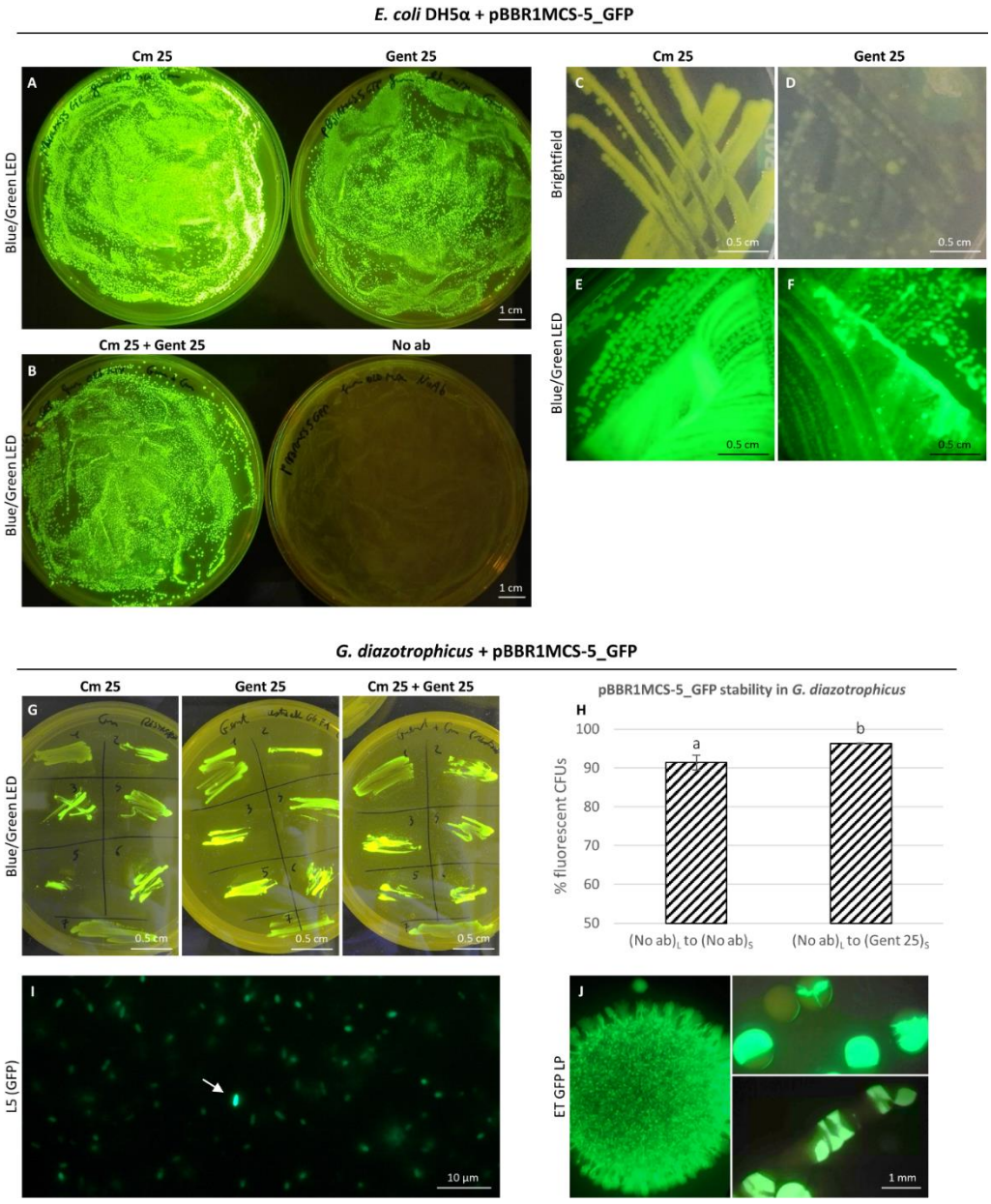


*Fig. 4.27. Strain phenotype upon transformation with pBBR1MCS-5_GFP in E. coli DH5α (A-F) or G. diazotrophicus "GG" (G-I). (**A**-**F**): A single CFU of transformed E. coli was grown overnight in LB + Gent 25 and plated in LB in different antibiotic (ab) conditions, leading to different fluorescence intensity. (**G**): Seven GG subclones from the original single transformant obtained through electroporation, showing different fluorescence intensity, were restreaked from ATGUS + Gent 25 to ATGUS with different antibiotics. CFU 3, showing the brightest signal in each condition, was selected and grown for -80 °C glycerol stocks. (**H**) The same clone was grown in liquid ATGUS until the end of the exponential phase with no selection ($(No\ ab)_L$) and plated in either solid ATGUS with no selection ($(No\ ab)_S$) or solid ATGUS + Gent 25 ($(Gent\ 25)_S$), in triplicate, and fluorescent CFUs were counted and normalised on the total colony number to assess plasmid stability.(**I**) Phase variation in GG culture (AGUS + Gent 25), with some cells exhibiting a stronger GFP signal (white arrow). (**J**) A single 10 µL drop of GG culture was either laid (J, left) or spread (J, right) on ATGUS + Gent 25, and after 10 days, a mixed population of non-fluorescent subcolonies (J, left) or non-fluorescent stripes in individual CFUs (J, right) was observed. A FastGene Blue/Green LED Gel Illuminator, emitting between 470 nm and 520 nm, was used to detect fluorescence at the plate level (A-G); a Modular Stereo Microscope for Fluorescent Imaging Leica MZ10 F with Chroma's ET GFP LP filter was used for imaging at the single colony level (J); a Leica*

DM5000 B Microscope coupled with a L5 filter set (BP480/40x, BP527/30) was used to detect fluorescence at the single-cell level (I).

Although a stable fluorescent signal was observed after weeks of incubation in both strains tested (in accordance with other studies employing *gfpmut3** [301]), when grown on a single antibiotic selection, single colonies would occasionally show a stripe pattern with fluorescence only coming from some defined sublocations, suggesting plasmid loss, a quick adaptation to antibiotic, and a rapid divergence or function partitioning mechanism within the same clonal population (Fig. 4.27j).

Overall, the reporter gene seemed to led to a more intense fluorescent signal when expressed from the *E. coli* strain compared to *GG*, although the plasmid was found to be more stable in *G. diazotrophicus* (Fig. 4.27b, h). This may indicate a less efficient use of the plasmid *ori* by *GG*, resulting in a lower copy number and reduced metabolic burden, which could promote a more stable plasmid retention. Additionally, the host-specific transcription machinery affinity to the promoter and RBS are likely to contribute to the different protein expression levels. Normally, in *E. coli*, in the absence of inducers such as lactose or IPTG, the *lac* operator recruits the lac repressor protein, inactivating P_{lac} (and derivatives); however, no correlation between repressibility and promoter strength was reported *in vivo*, indicating the promoter strength to be influenced by other factors, such as the RNA polymerase affinity with the other promoter elements or the half-life of lac repressor-operator complexes [306]. In fact, although the insertion of the 17 bp *lac* operator between the -33 and -10 elements in $P_{A1/04}$ was shown to result in a stronger repression effect *in vitro* compared to the wild-type P_{lac}, the high RNA polymerase affinity with the promoter was found to have a stronger impact in the overall promoter strength [306], suggesting $P_{A1/04/03}$ to potentially show the same characteristic. In support of this, in the present study, the chimeric promoter was found to be very active in *E. coli* despite of the two *lac* operators, which may have been expected to provide an even tighter regulation in non-induced condition [301]. On the other hand, it is important to note that most of the *E. coli* strains do not provide enough repressor proteins to

completely repress the function of a promoter present in a plasmid [307]. These observations are corroborated by an independent investigation from the iGEM Foundation, which characterised $P_{A1/04/03}$ as strong and leaky, to the point of inhibiting inducted *E. coli* cells growth due to metabolic stress; the authors suggested to regard this promoter as constitutive unless used in *lacIq* strains [314]. As for *G. diazotrophicus*, these hypotheses to explain the $P_{A1/04/03}$ strength in *E. coli* may also apply, but, most importantly, no *lacI* repressor homologue was described in *G. diazotrophicus* literature, nor it was found in the genome sequenced in this study. Therefore, the apparent lack of a repressor binding to the two operators is likely to concur to enhance the promoter strength in *GG* despite its *E. coli* origin [306]. Finally, the stronger fluorescence observed in *E. coli* under Cm selection suggests a positive feedback expression mechanism between *gfpmut3** and *cat*; therefore, for further applications, *GG* was selected in both Gent 25 and Cm 25 in order to maximise the fluorescence output.

Following to the creation of the *GG* strain, the pBBR1MCS-5_GFP vector was also transformed in the *G. diazotrophicus* AZ0019 *nifD*$^{-}$ mutant strain [208], which, in regard to the fluorescence expression, exhibited the same phenotype and characteristics of the wild-type strain.

4.2.1b Generation of pICH47751_DsRed plasmid and derivative expression vectors

Once verified the compatibility of the pBBR1MCS vector family with *G. diazotrophicus*, another class of plasmid was tested in the pursuit of expanding the plasmid repertoire for diverse applications and enhancing the versatility of genetic manipulations within the bacterium.

pICH47751, a plasmid with a backbone derived from pBIN19 and pUC19, is commonly used as a level 1 destination vector in Golden Gate cloning [315]. This technique allows for the seamless directional assembly of multiple DNA fragments into a larger construct by single-stranded overhangs joining, employing a standardized system of modular and hierarchically organized

recipient vectors that contain type IIS restriction enzyme recognition sites (such as BsaI) [316]. In this work, pICH47751 was used as a destination vector to Golden Gate assemble a new reporter cassette. To expand the range of available fluorescent reporter genes for bacterial tagging, a red-emitting fluorescent protein (FP) was selected, thereby broadening the available colour spectrum in addition to *gfpmut3** for diverse applications. In particular, a variant of the *dsRed* gene, named *dsRed-Express2*, was chosen. In 2002, Bevis and Glick created a derivative of the red fluorescent protein DsRed, named DsRed.T1 and later known as DsRed-Express, to overcome its slow chromophore maturation and poor solubility [317]. Building on this work, Strack et al. further engineered *dsRed-Express* into *dsRed-Express2*, a rapidly maturing tetrameric red FP with improved solubility, photobleaching half-time and photostability in bacterial and mammalian cells and with reduced cytotoxicity, which is often associated with red FP [318]. With excitation/emission maxima at 554 and 591, respectively, the protein can be excited efficiently by either a dedicated green DsRed filter set or, conveniently, by a wide band-pass blue excitation filter also suitable for GFP excitation, if coupled with an appropriate long-pass emission filter (Fig. 4.29d) [319]. Being a tetramer, DsRed-Express2 is best suited for whole cells labelling rather than creating fusion proteins. More recently, Wilton et al. described a suite of plasmids for tagging and imaging *Pseudomonas* colonising plant roots [320], including a *dsRed-Express2*-based vector that they kindly provided for the purpose of this work. In the vector, named pSW002-Pc-DsRed-Express2, the red FP was inserted in a constitutive expression cassette including a P_c promoter, a RBS and a T4 transcription terminator. The P_c promoter was derived from a class 3 integron of *Delftia acidovorans* C17 [321]. Integrons are genetic elements encoding a site-specific recombination system that can capture gene cassettes in tandem arrays, inserting them next to an integrase gene (*intI*) and its associated integration site (*attI*): when an exogenous cassette carrying an *attC* site is incorporated in the integron via integrase-mediated *attI*-*attC* recombination, the cassette is then transcribed by a strong constitutive promoter, named P_c, that lies within the 5'-terminal of the *intI* gene [322]. The strength of this class 3 P_c promoter was tested in *E. coli,* in which the concentration of streptomycin required to reduce the plating efficiency to 50%

(IC_{50}) by P_c-driven streptomycin resistance was found to be 340 μg ml^{-1}, a relatively high value that lies within the range of the class 1 P_c in similar trials (IC_{50} of streptomycin, 65 to 1200 μg ml^{-1}) [323]. The choice of the P_c promoter is based on the widespread occurrence of integrons, which increases their likelihood of functioning in a wide range of bacterial species [324]. A study comparing this class 3 P_c strength with other promoters in *Pseudomonas*, found P_c-driven expression to be about 2-fold higher than the strong inducible P_{tac} promoter (a fusion of the *trp* and *lac* promoters), 2.9-fold higher than P_{Tet} (from the tetracycline resistance gene) and 52.0-fold higher than P_{Gm} (from the gentamicin resistance gene) [324]. The RBS that Wilton et al. cloned downstream P_c was derived from the gene *10* of bacteriophage T7, and was found by the authors who first characterised it to enhance the translation efficiency in *E. coli* more than 40-fold times when compared to a 'consensus' RBS [325]. In this work, pSW002-Pc-DsRed-Express2 was tested on *G. diazotrophicus*, but no transformants could be recovered. Therefore, the pICH47751 vector was selected as a destination vector for the assembly of a new expression cassette, including: 1) the "P_c-RBS-*dsRed-Express2*-T4 transcription terminator" cassette from the pSW002-Pc-DsRed-Express2 plasmid; 2) a kanamycin resistance cassette (Kan^R) from the level 2 destination vector pAGM4723 [316], with its medium-strength AmpR promoter, derived from the β-lactamases transcriptional regulator *AmpR* of *Citrobacter freundii* [326]; 3) a β-glucuronidase (*gus*) gene with its native promoter from the pRGS561 vector (see section 4.2.2a). However, during the Golden Gate cloning, instead of the PCR fragment containing the GUS gene, a small but more abundant 37 bp PCR by-product with compatible ends was accidentally assembled, resulting in a plasmid containing only the *dsRed-Express2* cassette and the Kan^R cassette. The vector was named pICH47751_DsRed (Fig. 4.28). Although the original experimental design envisaged the subsequent cloning of the so obtained expression cassette in a broad-host-range plasmid, pICH57751_DsRed was successfully electroporated and expressed into *G. diazotrophicus*, originating the *GdRed* strain. The electroporation conditions were similar to those employed in creating the *GG* strain, which led to a comparable low transformation efficiency. The plasmid was found to be stably maintained, and to provide a constitutive *dsRed-Express2* expression.

pICH47751 features two *ori*: an *oriV*$_{RK2}$, typically associated with plasmids from the IncP family, and a ColE1 origin of replication; additionally, the plasmid harbours a *trfA* gene. The *oriV*$_{RK2}$ found in this construct derives from the RK2 plasmid belonging to the IncP-1α subgroup [327]), which is known to include large, broad-host-range conjugative plasmids, capable self-maintaining in most Gram-negative bacteria [328]. The 60,099 bp IncP-1α, broad host range plasmid RK2 [329], was first isolated during an outbreak of antibiotic-resistant *Pseudomonas aeruginosa* in Birmingham in 1969 and is essentially the same as the RP4 plasmid [330] [331]; therefore, in this work, it will be referred to as RP4/RK2. The origins of replication from this plasmid group contain multiple iterons (short repeated sequences) that are recognised by one or more replication initiation proteins (Rep); in RK2 plasmid and derivatives, the replication initiation protein is cis-encoded by the *trfA* gene [332]. ColE1-like *ori*, on the other hand, including pUC, pBR322 (also called pMB1) and the more distant p15A, need no replication initiation genes, as they rely on a two sense/antisense RNAs system for priming the replication process, and are typically high copy number, narrow-host-range *ori* specific for enteric bacteria [333]. Therefore, it is likely that in the case of *G. diazotrophicus*, the 632 bp, low-copy number *oriV*$_{RK2}$ is responsible for the plasmid maintenance. It is worth noting that, along with the P$_c$-RBS-*dsRed-Express2*-T4 transcription terminator cassette, the last 151 bp from the 3' end of a p15A *ori* (830 bp long) were copied as a carryover from the pSW002-Pc-DsRed-Express2 vector, along with a cryptic origin of transfer (*oriT*) retained within p15A; theoretically, this trait could either enable intended plasmid transfer via conjugation or cause undesired plasmid mobilization when used in complex environments or mixed microbial communities [320]. However, it is unlikely that such functions would be still retained in pICH57751_DsRed, considering that only a fraction of the p15A *ori* is present.

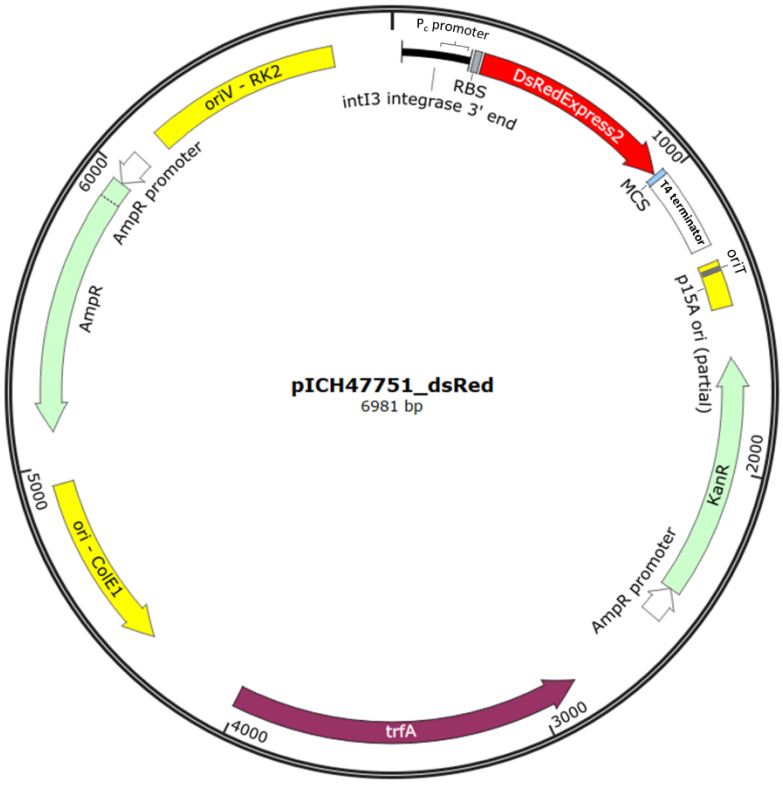


Fig. 4.28. Visual representation of the pICH47751_DsRed plasmid generated from sequencing data. Relevant vector components are shown. The image was generated through the software SnapGene [311].

Despite of *oriV*$_{RK2}$ being described as very-low copy number, with only 2 to 7 copies per cell in *E. coli* [333], the fluorescence from *GdRed* was sufficiently bright for obvious detection with the imaging systems used in this study (Fig. 4.29d, f, g). Furthermore, the fluorescent signal was found to be stable for months without appreciable loss of expression or sub colonial divergence in ATGUS + Kan 50, possibly due to the superior DsRed-Express2 photostability or to the more efficient kanamycin selection. However, the same non-fluorescent stripe pattern observed for the *GG* strain in inadequate antibiotic conditions was observed for *GdRed* when grown in non-selective medium (Fig. 4.29f), corroborating the importance of an adequate selection for unbiased FP detection. The *GdRed* strain itself showed a faint pink hue under ambient light compared to the WT, (Fig. 4.29b, c), indicating a relatively high FP presence, although it did not exhibit the bright red colouration observed in *E. coli* (Fig. 4.29a), which can rely on the high copy number ColE1 *ori*.

Stability analysis, conducted as described for the pBBR1MCS-5_GFP vector, showed a comparable 90% plasmid retention rate when plated in non-selective medium from non-selective culture, but no plasmid loss when plated from non-selective ATGUS to Kan 50 medium, indicating the suitability of the antibiotic concentration used (Fig. 4.29e). As in the case of *GG*, single *GdRed* cells exhibiting an enhanced fluorescent signal compared to the surrounding clonal population were occasionally observed (Fig. 4.29f), reinforcing the idea that this organism is capable of quick phenotypic divergence, possibly through a phase variation mechanism to maximise its environmental adaptation capability. Interestingly, a site-specific recombinase involved in phase variation was found to be involved in plant colonization by *Pseudomonas fluorescens* WCS365 [334].

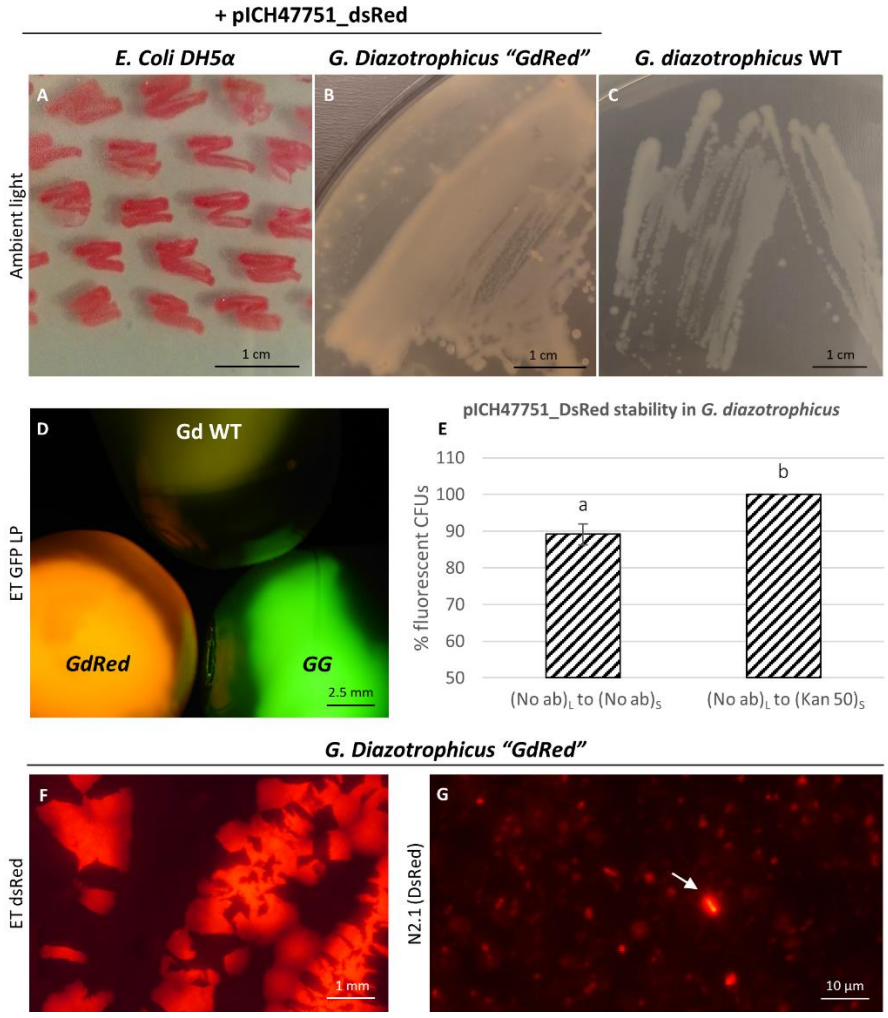


*Fig. 4.29. Strain phenotype upon transformation with pICH47751_DsRed in E. coli DH5α (A) or G. diazotrophicus "GdRed" (B-G). (**A**): E. coli clones transformed with the Golden Gate assembled pICH47751_DsRed vector exhibiting a high FP concentration in LB + Kan 50. (**B**-*

***C**): Pink coloration of GdRed compared to the WT strain. (**D**) Use of ET GFP LP filter (ET480/40x, ET510 LP) for simultaneous visualisation of both GFP and DsRed signal (pelleted overnight cultures grown with appropriate selection and showed in comparison with non-fluorescent WT strain). (**E**) One GdRed clone was grown in liquid ATGUS until the end of the exponential phase with no selection ($(No\ ab)_L$) and plated in either solid ATGUS with no selection ($(No\ ab)_S$) or solid ATGUS + Kan 50 ($(Kan\ 50)_S$), in triplicate, and fluorescent CFUs were counted and normalised on the total colony number to assess plasmid stability. (**F**) GdRed plated on non-selective ATGUS, showing non-fluorescent stripes within individual CFUs after 4 days of incubation. (**G**) Phase variation in GdRed culture (AGUS + Kan 50), with some cells exhibiting a stronger DsRed signal (white arrow). A Modular Stereo Microscope for Fluorescent Imaging Leica MZ10 F with Chroma's ET GFP LP filter or ET dsRed (ET546/10x, ET595/50m) was used for imaging at the single colony level (D, F); a Leica DM5000 B Microscope coupled with a N2.1 filter set (BP515-560, LP 590) was used to detect fluorescence at the single-cell level (G).*

The putative low copy number coupled with the efficient *ori*V_{RK2}-TrfA replication and partitioning system, could be instrumental in providing stable expression of the desired genetic function while at the same time preventing biased observations due to metabolic stress induced by plasmid overproduction. Additionally, the presence of an ampicillin resistance (Amp^R) in the plasmid proved to be convenient for facilitating the transformants selection during the cloning steps in E. *coli* DH5α. *G. diazotrophicus*, on the other hand, was found to be naturally resistant to ampicillin up until 500 µg mL^{-1}, as suggested by a previous report [335].

For these reasons, the pICH57751_DsRed plasmid was selected as a platform for building new constructs for further cloning and mutagenesis applications.

In particular, the *nif* operon expression was investigated by the use of vectors harbouring promoter-less *gfp* or *gus* genes cloned under the promoter region of polycistronic transcripts within the *nif* operon (see Chapter 4.4). As an example, the archetypical *nifHDK*-sfGFP reporter cassette is illustrated (Fig. 4.30). A promoter-less super folder *gfp* (sfGFP), exhibiting improved folding kinetics and tolerance of circular permutation [336], was codon optimised for *G. diazotrophicus* according to the Codon Usage Database [337] and cloned downstream the 248 bp promoter region preceding the *nifHDK* polycistron in *G. diazotrophicus* AZ0019. The plasmid, named pICH-DsR-*nifHDK*p::GFP, was transformed into *G. diazotrophicus*, giving origin to the strain named *GdRed_nifHp::GFP* in which the GFP expression is induced by nitrogen fixation. In a variant of this construct, the 70 bp promoter region upstream the

nifENXQ polycistronic mRNA [129] was used in place of the *nifHDK* promoter to activate the sfGFP expression, leading to the generation of the plasmid pICH-DsR-*nifENXQ*p::GFP and the strain *GdRed_nifEp::GFP*.

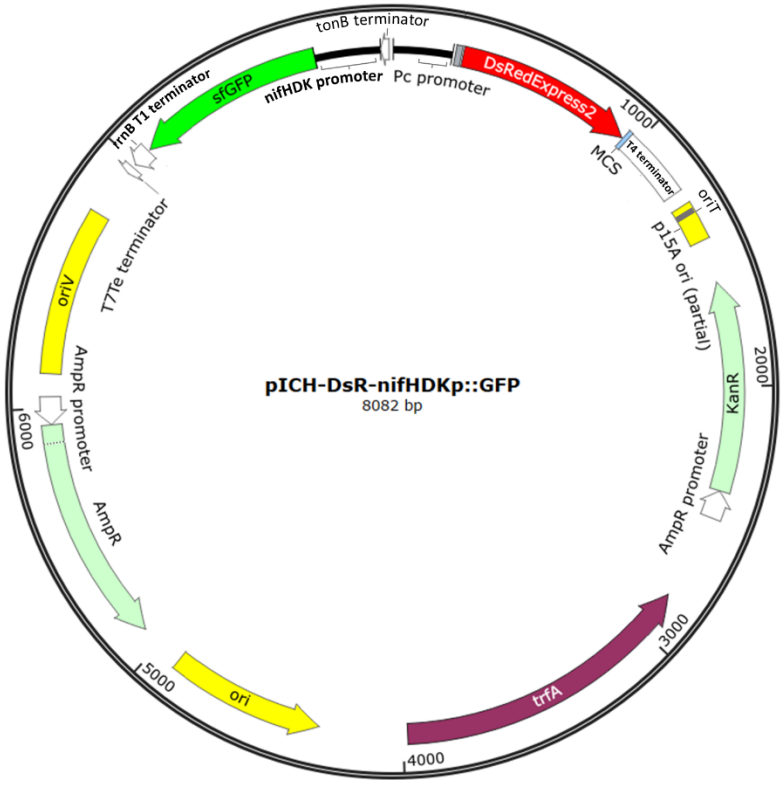


Fig. 4.30. Visual representation of the pICH-DsR-nifHDKp::GFP plasmid generated from sequencing data. Relevant vector components are shown. More variants of this vector, featuring the nifENXQ promoter in place of the nifHDK promoter, or gus in place of gfp as a reporter gene, were designed with identical structure. The image was generated through the software SnapGene [311].

Similarly, a codon-optimised *gus* reporter gene was used in alternative to *sfgfp* to investigate the nitrogenase expression dynamics without the drawbacks of fluorescence imaging, giving origin to the pICH-DsR-*nifHDK*p::GUS vector. In this set of plasmids, all the reporter cassettes were cloned between the *oriV*$_{RK2}$ and the "P$_c$-RBS-*dsRed-Express2*-T4" elements, leaving unaltered any pICH57751_DsRed feature. Additionally, they were flanked by the bidirectional *E. coli tonB-P14* transcription terminator [338] [339] in their 5' end, and by the terminator T1 from the *E. coli rrnB* gene [340] [341] and the early transcription terminator from phage T7 [342] in their 3' end. These Rho-

independent terminators were added to isolate the transcription cassettes by preventing any transcriptional read-trough from adjacent plasmid elements that could confuse the observations. For the same reason, the reporter genes were arranged in a head-to-head configuration with *dsRed-Express2*, with their coding sequences transcribed in opposite directions to each other. The vectors were designed this way to allow constitutive red FP expression for bacterial localisation and concomitant nitrogen fixation dependent GFP activation. Harbouring both the FPs in the same vector should eliminate any *ori*-dependent expression bias.

Finally, in order to investigate the role of the transcriptional activator *nifA* in regulating nitrogen fixation, the *dsRed-Express2* gene in the pICH47751_DsRed plasmid was replaced with the promoter-less *nifA* CDS from *G. diazotrophicus* AZ0019. The vector was named pICH47751_NifA. The *Gd_nifHDK::GUS* mutant (see section 4.2.2c) was transformed with pICH47751_NifA to obtain a strain overexpressing *nifA* from the constitutive P_c promoter named *GdnifAoe_nifHDK::GUS* (See Chapter 4.4). All the plasmids inserted via electroporation are listed in Table 3.5.

Name	**Ab^R**	**Cargo**	**Purpose**	**Reference**
pICH47751_DsRed	Amp^R, Kan^R	dsRed-Express2	Constitutive bacterial tagging (red)	Section 4.2.1b
pICH_DsR-*nifHDK*p::GFP	Amp^R, Kan^R	dsRed-Express2, *nifHDK*p::sfGFP	Constitutive bacterial tagging (red), GFP reporter for *nifHDK* expression	Section 4.2.1b
pICH_DsR-*nifENXQ*p::GFP	Amp^R, Kan^R	dsRed-Express2, *nifENXQ*p::sfGFP	Constitutive bacterial tagging (red), GFP reporter for *nifENXQ* expression	Section 4.2.1b
pICH_DsR-*nifHDK*p::GUS	Amp^R, Kan^R	dsRed-Express2, *nifHDK*p::GUS	Constitutive bacterial tagging (red), GUS reporter for *nifHDK* expression	Section 4.2.1b
pICH47751_NifA	Amp^R, Kan^R	*nifA*	*nifA* overexpression	Section 4.2.1b, 4.4.4

Table 3.5. List of all the generated plasmids transformed into G. diazotrophicus via electroporation.

4.2.1c Electroporation and media optimisation

In order to optimise the electroporation method in *G. diazotrophicus*, the process was broken down into its main barrier steps (electrocompetent cell culture conditions, plasmid concentration, electric pulse parameters, medium and selection during post-electroporation recovery), which were addressed individually.

Normally, after the electro-permeabilisation that forces the foreign DNA uptake, cells are cultured on a rich liquid medium for a few hours to allow the production of the antibiotic resistance before plating in the selective substrate [343]. The choice of the recovery and plating medium plays an important role in furnishing enough nutrients for the microorganism recovery after the transient membrane permeation, while at the same time providing stringent growth conditions for selecting the transformants over wild-type cells carryover [344]. Therefore, as a first step, an adequate recovery and selection medium was investigated. Among the various media employed for *G. diazotrophicus* growth, LGI-P is probably the most mentioned in literature. LGI-P is a minimal medium that provides enough essential nutrients to selectively support the bacterium growth when reisolated from non-gnotobiotic samples, and is therefore used in determining the MPN or for liquid culturing before colonisation or metabolic studies [83] [212] [211]. However, its minimal composition would not probably satisfy the bacterium need for a rich nutrient medium to recover from the stress of the electroporation process. Additionally, the high sucrose concentration in this medium induces *G. diazotrophicus* to grow in semi-translucent, viscous colonies which were found to greatly reduce the GFP fluorescence. As shown in Fig. 4.31, the acidified LGI-P used in this study for the MPN technique (see Chapter 4.1), either full or deprived of nitrogen (in the form of yeast extract), was tested together with ATGUS for its suitability in selecting the *GG* strain.

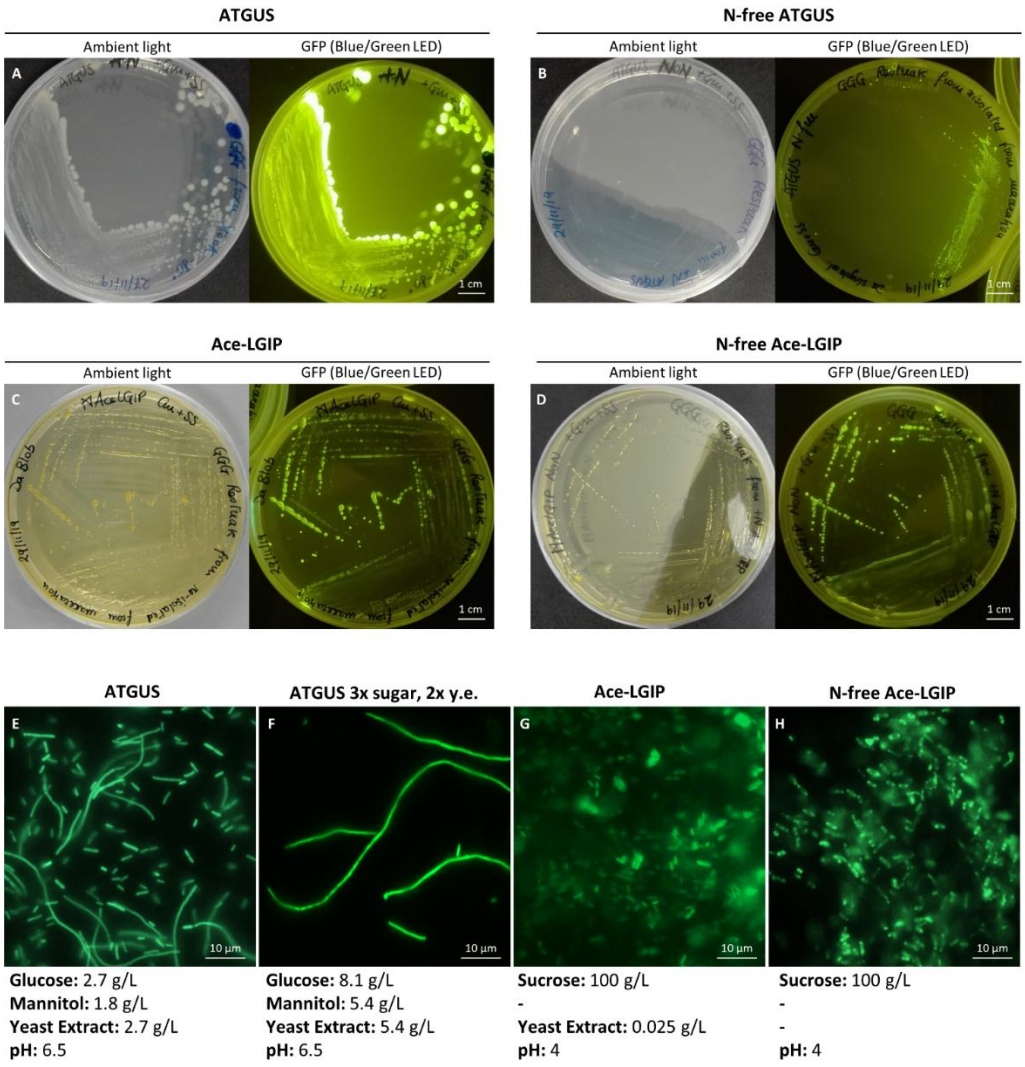


*Fig. 4.31. GG phenotype on different media, in either their complete formulation or in absence of nitrogen (N-free), obtained through the omission of yeast extract (y.e.). (**A-D**) Plates are shown at 5 days after streaking. All CFUs grown in N-free media (**B, D**) showed a contraction of the colony diameter, although in ace-LGIP this effect was partially obscured by the semi-liquid and sticky structure of the bacterial aggregates, resulting in the apparent expansion of the CFUs due to passive diffusion of the sugary material. The FastGene Blue/Green LED Gel Illuminator, emitting between 470 nm and 520 nm, was used to detect fluorescence at the plate level. (**E-F**) GG cultured in different liquid media, with the main nutrients reported underneath. A diffuse green hue due to the sugary substance is observed among the GG cells in ace-LGIP media. A Leica DM5000 B Microscope coupled with a L5 filter set (BP480/40x, BP527/30) was used to detect fluorescence at the single-cell level. All the media were supplemented with Gent 25, Cm 25.*

Compared to the full ATGUS medium, *GG* grown in ace-LGIP exhibited a dim fluorescence that completely disappeared after one week. This does not seem to be related to the acidity of the environment, since ace-LGIP is buffered at pH 4 and GFP fluorescence was visible in the first 2 to 3 days; on the other hand, the fluorescence disappearance seems to be correlated with the

production of the sugary matrix, which may create a condition incompatible with the FP folding, possibly by reducing the oxygen diffusion which is essential in the chromophore maturation [345]. The elimination of nitrogen from both media, which was tested to verify whether the induction of a nitrogen fixation state would influence the plasmid retention capacity, caused a great reduction in the colony surface area and an even fainter fluorescence (Fig. 4.31B, D), suggesting a metabolic stress that would likely further decrease the plasmid uptake and retention rate upon electroporation. Furthermore, the low concentration of yeast extract in ace-LGIP (Fig. 4.31g) and its absence in N-free ace-LGIP (Fig. 4.31h) seemed to cause a reduction in the cell length, with a nonhomogeneous intracellular *gfp* expression pattern (Fig. 4.31h) which may contribute to explain the decreased fluorescence observed at the colony level. ATGUS, on the other hand, allowed the isolation of definite colonies displaying a strong GFP fluorescence, as previously illustrated (Fig. 4.27). However, when used in liquid state for culturing *GG*, ATGUS induced the bacteria to assume a filamentous phenotype or possibly to aggregate (Fig. 4.31e); these pleomorphic cells seemed to increase in number with the concentration of nutrients, as observed when doubling the sugars and tripling the yeast extract of ATGUS (Fig. 4.31f). Filamentation was first observed in *G. diazotrophicus* by Muthukumarasamy et al. [134] in diverse semi solid media (LGIP, SYP and MS agar) supplemented with different nitrogen sources, but not in N-free media; in particular, Muthukumarasamy reported that ammonium nitrate (NH_4NO_3) 25 mM and ammonium chloride (NH_4Cl) 25 mM resulted in 21 to 22% of pleomorphic cells, while potassium nitrate 25 mM and urea 500 ppm resulted in 6 to 6%, suggesting this phenotype to be mainly induced by ammonium [134]. Bacterial autoaggregation is a poorly understood phenomenon, believed to occur for protection against environmental stresses or for initiating biofilm formation [346]. Similarly, conditional filamentation, a phenomenon in which cells continue to elongate but do not divide, is a highly context dependent environmental adaptation in response to various stressors or nutrients unbalance [347]. The long *GG* filaments do not appear to be a stress defence mechanism against the high media osmolarity, since no pleomorphism was observed in aceLGIP (which contains sucrose 292 mM, i.e., an order of

magnitude higher than in both normal and enriched ATGUS, Fig. 4.31g, h); additionally, *G. diazotrophicus* is known for its adaptation to high osmolarity environments such as sugarcane tissues [348]. Therefore, it is possible that this phenotype was indeed induced by the nitrogen, although no ammonium salts was directly used in the aforementioned media, in which nitrogen derived from yest extract (typically containing ≥11% total nitrogen). Autoaggregation and filamentation are also observed under exposure to sub-lethal concentrations of antibiotics, which can reduce bacterial fitness and induce the transition from a planktonic lifestyle to microcolonies formation [346] [347], possibly suggesting an inadequate gentamicin and chloramphenicol concentration in ATGUS. However, filamentation in some bacteria is also associated with the stationary phase [349]; therefore, it cannot be ruled out that the elongated phenotype is not directly caused by the presence of nitrogen, but rather arises because the bacteria reach the stationary phase earlier in nutrient-rich media compared to minimal media. Remarkably, the pleiomorphic cells seemed to be the only one to be retaining the plasmid in enriched ATGUS, highlighting an accelerated plasmid loss in rich media. In addition to these observations, ATGUS performed poorly when used to recover and select *GG* transformants after electroporation, with only 1 to 3 positive CFUs per DNA μg per 50 μL of electrocompetent cells at OD_{600} = 2 (grossly corresponding to 10^6 total cells) out of hundreds of recovered CFUs (not shown). The reason for the high number of FP-negative cells recovered after the electroporation is unclear. It could be caused by a Restriction-Modification (RM) system, selectively retaining the resistance cassette from the plasmid while cleaving the rest of the foreign DNA (see section 4.2.3), or, alternatively, by a natural quick adaptation to suboptimal antibiotic concentrations. The ATGUS medium was first described by Cocking et al. [271], and based on the current literature, its use does not seem to have been documented elsewhere. The presence of mannitol as one of the carbon sources was speculated in this work to increase colonisation capacity via exopolysaccharide production enhancement (see section 4.1). However, crucially, the electro-transformation efficiency can be hindered by the presence of surface EPSs, which have been reported to act as a major barrier in successful DNA delivery [350]. Therefore, the mannitol-

induced EPSs overproduction is conjectured to be one of the causes for the extremely low electroporation efficiency found in this study when using ATGUS for recovery and selection medium and for electrocompetent cell preparation. DYGS, in contrast, is a rich medium developed in 1986 for *Xanthomonas* spp. and later modified and repurposed for the purification of diazotrophic bacteria [211]; it contains glucose as the main carbon source, along with yeast extract for nitrogen and peptone and glutamic acid as an extra source of nutrients. It is often found in studies involving *G. diazotrophicus* mutagenesis [351], and was thus used as a comparison to ATGUS in this work. To test the two media, *G. diazotrophicus* was electroporated with 1.5 μg of pICH47751_DsRed plasmid; the same 50 μL aliquot of electrocompetent cells was split and recovered in 975 μL ATGUS or 975 μL DYGS for three hours, after which the cultures were plated on selective ATGUS + Kan 75 μg mL^{-1} or DYGS + Kan 100 μg mL^{-1}. The kanamycin concentration was increased by 1.5-fold in ATGUS compared to the standard recommended working dose to lower the amount of false positive CFUs found in previous trials, while it was doubled in DYGS, in light of its increased nutrients availability which could favour plasmid loss (Fig. 4.31f) and the carryover of wild-type clones.

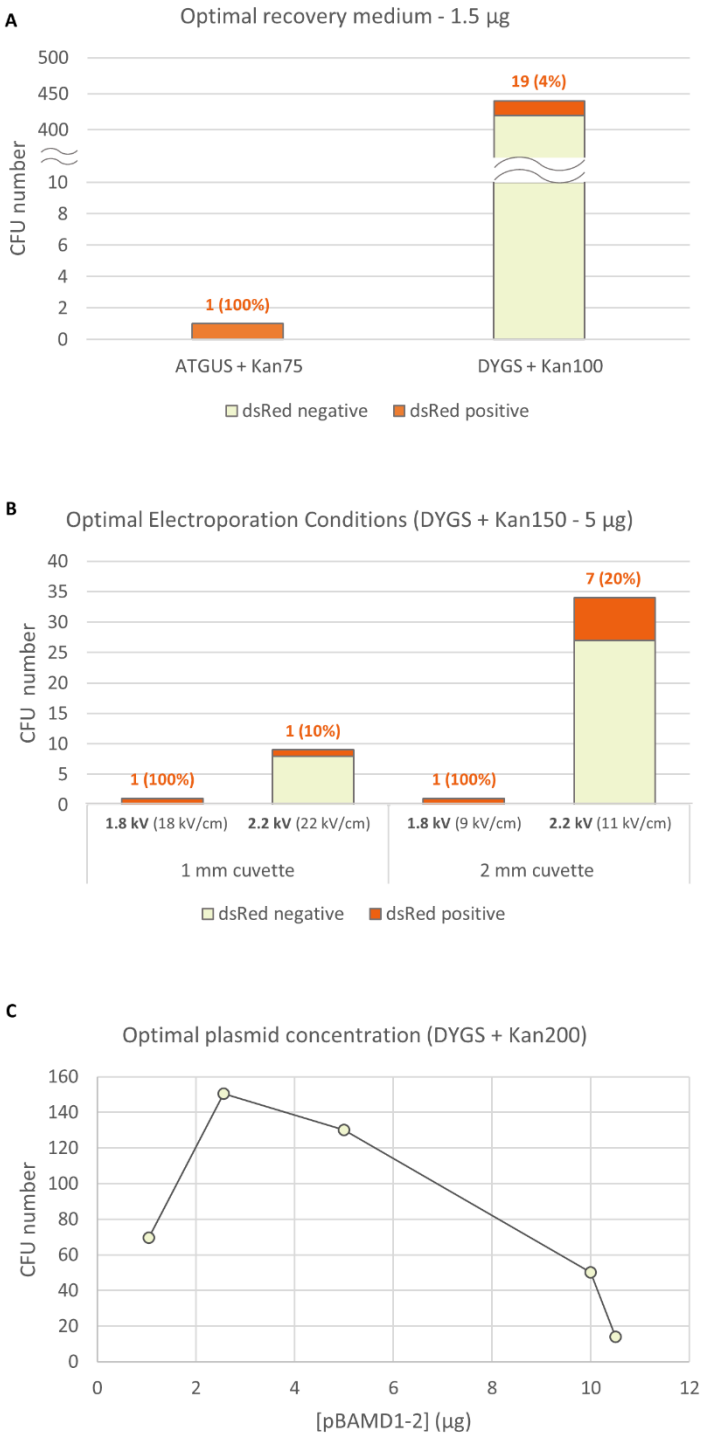


*Fig. 4.32. Electroporation optimisation. (**A**) Recovery and selection media comparison (ATGUS + Kan 75 µg mL^{-1} vs DYGS + Kan 100 µg mL^{-1}) upon electroporation with 1.5 µg of pICH47751_DsRed. (**B**) Cuvette and voltage combination tested for optimal field strength upon electroporation with 5 µg of pICH47751_DsRed and selection in DYGS + Kan 150 µg mL^{-1}. (**C**) Optimal plasmid concentration assay upon electroporation with pBAMD1-2 and selection in DYGS + Kan 200 µg mL^{-1}. In all the tests above, the recovery was carried out for 3 hours in agitation at 200 rpm in 950 µL of antibiotic-free medium corresponding to the solid medium used for the selection.*

As shown in Fig. 4.32a, the DYGS medium increased the number of true positive transformants by around an order of magnitude compared to ATGUS. However, it also greatly increased the false positive CFUs, indicating an inadequate antibiotic concentration. Kan 75 μg mL^{-1}, on the other hand, eliminated the false positive cell carryover in ATGUS, but only one transformant was recovered. When screening for mutants, especially in the case of selection markers such as FPs which are easily detectable even amidst a multitude of wild-type cells, the absolute number of true positives is more important than the true to false positive ratio, as the highest possible number of transformants is desirable. Therefore, DYGS was adopted as favoured transformation medium.

Next, the cuvette and electric pulse conditions were investigated. Among the electroporation critical variables, the distance between the cuvette electrodes, or "gap size", plays an important role, as it determines the field strength. The field strength, expressed as kV/cm, is measured as the voltage delivered across the electrode gap, and is key for surpassing the electrical potential of the cell membrane and induce the reversible pore formation [352]. Typically, the field strength for bacteria and yeast ranges between 3-24 kV/cm, and is calculated as a function of the cell diameter: smaller cell sizes require higher voltages while larger cell diameters require lower voltages. However, the smaller the gap between the electrodes, the higher the chances of arcing. Bacteria such as *E. coli* usually requires 1 mm gap cuvettes, while other bacterial or yest species are routinely transformed with 2 mm gap cuvettes [353]. In this study, a combination of 1- and 2-mm cuvettes and different voltages (1.8 kV and 2.2 kV) were evaluated for the highest number of *GdRed* colonies upon transformation with 5 μg of pICH47751_DsRed. As shown in Fig. 4.32b, the combination of the 2 mm cuvette and a 2.2 kV pulse, corresponding to a field strength of 11 kV/cm, was found to be the most effective in terms of both absolute number of colonies recovered and true positive transformants, and was therefore adopted in the optimised electroporation protocol. Other parameters such as pulse length, shape and number were not further investigated. In this assay, the kanamycin concentration was increased to 150

µg mL^{-1} to further reduce the number of false positives, which, however, remained high.

Next, the optimal plasmid concentration was investigated. The amount of plasmid employed for electroporation in literature greatly vary with species and applications, ranging from 10-50 pg of DNA per electrocompetent aliquot of highly competent *E. coli* [291], to 100 ng -10 µg in *Pseudomonas* spp. [354] [355]. It must also be taken into consideration that the efficiency of electroporation is reported to decrease as the DNA molecule size increases, and large plasmids usually requires lower voltages with longer pulse lengths compared to smaller molecules [291] [352]. As for *G. diazotrophicus*, only a few studies have employed the electroporation technique for the mutagenesis of this bacterium, and they all refer to a method first described by Teixeira et al.: the paper reports the use of 1 µg of plasmid, a field strength of 12.5 kV/cm (similar to the optimal 11 kV/cm found in this study), and a rich recovery and selection medium supplemented with chloramphenicol 150 µg mL^{-1} or kanamycin 200 µg mL^{-1} [128]. In the present work, several electroporations were carried out with different amount of plasmid, ranging from 1 to 11 µg per 50 µL of electrocompetent cell (Fig. 4.32c). Instead of pICH47751_DsRed, the pBAMD1-2 vector [356] from the SEVA collection [299] was used. This is a small 4.5 kb vector for Tn5 mutagenesis, featuring a kanamycin cassette transposon, a transposase gene and a π protein dependent ori_{R6K}, which makes it a suicide vector in *G. diazotrophicus* (see section 4.2.2). The antibiotic concentration in DYGS was increased to 200 µg mL^{-1}, consistently to other studies [128] [351], and Kan 200 µg mL^{-1} was adopted as a standard in selective DYGS medium. In light of the increased stringency of the antibiotic and considering the impossibility of pBAMD1-2 replication in *G. diazotrophicus*, the number of CFUs recovered in this assay should be devoid of any false positive carryover. The highest number of transformants was obtained when using 2 to 4 µg of plasmid, above which the transformation efficiency dropped linearly (Fig. 4.32c).

In all the test discussed above, the electrocompetent cells preparation was carried out similarly to Teixeira et al. [128] (see Materials and Methods); the electro-transformation was carried out keeping the cells in ice during the entire

process until the inoculation in the recovery medium, and, as a final adjustment, the electrocompetent cells aliquots were increased from 50 to 200 µL.

The vector listed in Table 3.5 were transformed into electrocompetent *G. diazotrophicus* cells using the optimised transformation parameters described in this chapter.

4.2.2 Conjugation and genomic integration for reporter genes expression

4.2.2a Conjugation as a transformation tool and application to *G. diazotrophicus*

Conjugation is a natural mechanism for horizontal gene transfer (HGT) among bacteria which is widely used as a transformation method in bacterial mutagenesis research. Among the three main types of transfer of genetic material (also comprehending transformation with exogenous DNA and transduction of viral nucleic acids), conjugation is the only one to involve direct cell-to-cell contact. It requires a specialized structure called conjugative pilus, through which a single-stranded copy of the mobilizable plasmid from the donor cell is delivered to a recipient cell [357]. This process is ubiquitous in bacterial communities, and is a major drive of genome evolution and quick adaptation to hostile environmental conditions through the exchange of advantageous metabolic traits [358]. Given the limited number of bacterial species naturally competent for DNA transformation and the low efficiency of transformation methods such as electroporation in non-model organisms, exogenous DNA delivery is frequently achieved via conjugation with broad host range plasmids, often based on the IncP-1α plasmid RP4/RK2 transfer functions [359]. The F plasmid and the RP4/RK2 plasmid have been widely investigated as model systems for bacterial conjugation research. The main components of the conjugation machinery are encoded by the transfer genes *tra* (also referred to as MOB genes) harboured in these conjugative plasmids

[358]. The *tra* operon includes: 1) the proteins forming the conjugative pilus, which mediates the establishment of the mating pair through wall-to-wall contact and possibly serves as a channel for the single strand DNA transfer [360]; 2) a type IV secretion system (T4SS), which was proposed to inject the genetic material using the pilus as a needle [361] independently from the presence of specific receptors on the recipient cell membrane [358]; 3) the relaxosome, i.e. a protein complex needed for the processing of the plasmid prior to transfer, including the single strand cut at a 100–400 bp "origin of transfer" region (*oriT*) by a relaxase [362], the binding of the 5′-phosphate end of the nicked strand (T-strand), and its recruitment and extrusion through the conjugative pore with the mediation of the Type IV Coupling Protein (T4CP) [358]. Plasmids carrying an *oriT*, a relaxase, a T4CP and a T4SS are defined as conjugative, while plasmids without an in cis T4SS are defined mobilizable, and are classified into six MOB families [363]. Interestingly, *G. diazotrophicus* itself carries 4 complete T4SS in its chromosome, which are similar to bacterial conjugation machines of *Agrobacterium* [284]. To turn these features into a molecular biology tool, the *oriT* from the RP4/RK2 plasmid [329], has been cloned in other derivative plasmids to make them mobilizable between Gram-negative and even some Gram-positive bacteria, provided the in trans expression of the RP4 delivery machinery [364]. For this purpose, in 1983, Pühler et al. integrated in the chromosome of *E. coli* an RP4 derivative, the RP4-2-Tc::Mu plasmid (with the RP4 tetracycline resistance gene interrupted by a Mu temperate prophage), giving origin to the strains SM-10 (kanamycin resistant) and S17-1 (kanamycin sensitive and streptomycin/trimethoprim resistant following the inactivation of the RP4-associated kanamycin resistance gene by Tn7 insertion) [365]. Subsequently, a prophage λ derivative carrying the *pir* gene from plasmid R6K (from the IncX family) [366] was integrated into both strains to enable the replication of Π-dependent vectors, creating the strains SM10 λpir and S17-1 λpir [367]. Vectors carrying the R6K minimal γ origin of replication from the 39.9-kb plasmid R6K ($ori\mathrm{V}_{\mathrm{R6K}\ \gamma}$) require the Rep protein Π for replication initiation, which is encoded by the *pir* gene [368]. Due to this characteristic, conditionally replicative $ori\mathrm{V}_{\mathrm{R6K}\ \gamma}$ conjugative vectors have been turned into the most popular system for random mutagenesis or allelic exchange for (but

not limited to) Gram-negative species [359]. Indeed, plasmids referred to as "suicide vectors" can be designed with an *ori*$V_{R6K\ \gamma}$ to only replicate in the donor strain, which provides in trans the *pir* function and the RP4 conjugation machinery [364]. Once delivered in the recipient cell, the suicide vector can not replicate due to the lack of Π and is selectively eliminated with antibiotics or other selection markers, facilitating the insertion of the desired DNA cassette from the suicide vector into the genome through homologous recombination or transposon-mediated integration [364]. Conjugation-based methods however have limitations, including difficulty in selecting the recipient transconjugant. Antibiotic-resistant recipient mutants can used to select against the sensitive donor strain, but this strategy is laborious and limits the number of markers that can be used [359]. In 2005, Demarre et al. partially circumvented this limitation by creating *E. coli* donor strains auxotrophic for diaminopimelic acid (DAP) [359]. This molecule is an intermediate precursor in the biosynthetic pathway of lysine from aspartate, and is found incorporated as a crosslinking agent in the peptidoglycan of the bacterial cell wall. Crucially, neither animals nor fungi possess the metabolic pathway leading to its synthesis; therefore, DAP auxotrophy is not alleviated by compounds found in rich media based on yeast or animal extracts, which can be employed for the transconjugants counterselection [359].

In this work, the donor strain named β2163 described from the aforementioned study [359], coupled with the mobilizable suicide vector pSW23t, has been adopted for transferring desired genetic constructs to *G. diazotrophicus.* In particular, β2163 cells carry a chromosomal RP4 mobilisation machinery from the SM10 strain (the RP4-2-Tc::Mu which include a kanamycin resistance), and a ΔdapA::(erm-pir) allele in which the *dapA* gene for DAP synthesis has been disrupted by a cassette including an erythromycin resistance rRNA methylase (*erm*) from Tn1545, and the *pir* gene expressed from the *erm* promoter. This strain only grows if supplemented with DAP 0.3 mM, and can sustain the replication and mobilization of the 1818 bp pSW23t suicide vector.

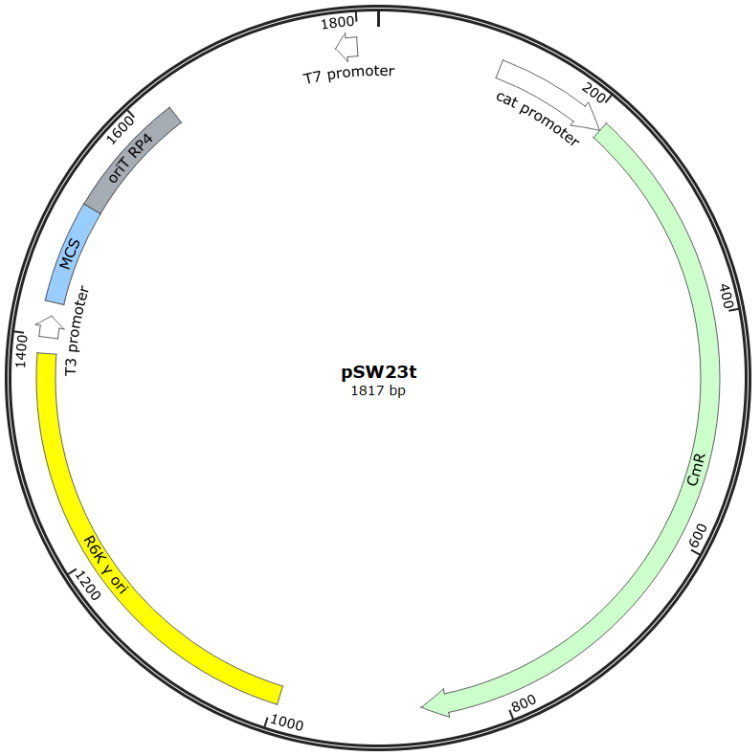


Fig. 4.33. Visual representation of the pSW23t plasmid. Relevant vector components are shown.

This vector carries an *oriV*$_{R6K\gamma}$ from pGP704, a *cat* gene from pSU18 as a selection marker and the *oriT*$_{RP4}$ from RP4 [359] (Fig. 4.33), enabling efficient mobilisation and selective elimination in the recipient bacterium when delivered via conjugation into *G. diazotrophicus*. Thus, in this study, the pSW23t suicide vector was used as a platform for the assembly of various expression cassettes, which were delivered through β2163-mediated conjugation.

4.2.2a pRGS561 characterisation and *GGG* creation for *in planta* detection

One of the first plasmids ever tested for tagging *G. diazotrophicus* with the purpose of visualising the process of plant colonisation, was the *gus*-harbouring vector pRGS561 [207]. In the study by Fuentes-Ramírez et al., the plasmid, allegedly featuring a *gusA-NPTII* fusion construct under a double 35S CaMV promoter, was conjugatively mobilized from *E. coli* to *G. diazotrophicus* UAP5541, and was found to provide a stable GUS signal, with a remarkable claimed plasmid maintenance rate of over 95% after 7 months in

plant tissues [207]. Due to these promising characteristics, pRGS561 was used in this work for tagging *G. diazotrophicus* AZ0019 and to explore the possibility of another usable plasmid platform archetype for *G. diazotrophicus* genetic engineering. However, no sequencing data about the vector were available in literature. Therefore, in this study, the history of pRGS561 construction has been elucidated, following a similar approach used for the pBBR1MCS-5_GFP vector, in order to characterise the plasmid and gain a better understanding of its potential applications.

In the late 1980s, Richard A. Jefferson described for the first time the use of the *E. coli* β-glucuronidase *(gusA*) gene as a reporter system in plants [369]. Since then, the CDS of *gusA* (syn. *Gus*, *uidA*) from the *E. coli uidA* locus, first characterised by Novel and Novel in the early 1970s [370], has been used in various molecular applications, but has remained substantially unchanged in the vectors used over the decades. The β-glucuronidase enzyme is a hydrolase that catalyses the cleavage of a wide variety of β-glucuronides (a type of glycoside composed of a glucuronic acid attached to an aglycone molecule) [371]. In particular, the 5-bromo-4-chloro-3-indolyl glucuronide (X-Gluc) is hydrolysed by GUS into glucuronic acid and 5-bromo-4-chloro-indoxyl, which in presence of oxygen undergoes a spontaneous oxidative dimerization, resulting in the product 5,5'-dibromo-4,4'-dichloro-indigo (diX-indigo); this molecule appears as a blue precipitate under light microscopy, and is stable through fixation, dehydration and embedding [372]. Other desirable characteristics of this enzyme include a great stability in plant extracts and cells, tolerance for large amino-terminal fusions without loss of activity and lack of toxicity in transgenic plants [369]. For these reasons, the GUS system is widespread as a biochemical and histochemical marker, alone or as a transcriptional reporter for studying developmental patterns of gene expression in plants [373]. Critically, only low levels of endogenous GUS activity are present in most higher plants (including tomato, rice and *A. thaliana*), providing a null background for such histochemical GUS assay [369] if the X-Gluc staining conditions are appropriately optimised [374]. These same features make *gus* an ideal reporter gene for bacterial tagging in plant-microbial interaction studies, and, as so, it has been frequently employed in

different plant systems for investigating the colonisation process of *G. diazotrophicus* itself (including sugarcane [207], rice [97], tomato [174], sorghum and wheat [155]) and other endophytic diazotrophs such as *H. seropedicae* [375] or *Azoarcus* spp. [254].

In 1987, Jefferson et al. cloned the *gus* CDS under the strong, constitutively active promoter CaMV 35S (a promoter from the Cauliflower Mosaic Virus, vastly employed for transgene expression in plants) in the large *Agrobacterium* binary vector pBIN19, creating the pBI121 plasmid [369]. Subsequently, Datla et al. cloned a neomycin phosphotransferase II gene (*ntp-II*, another popular plant reporter system in transcriptional and translational fusions, conferring kanamycin resistance) at the 3' end of *gus*, creating a bifunctional fusion peptide with the configuration NH_2-GUS::NPTII-COOH [373]. This construct was found to provide both GUS and Kan^R functions in plants and *E. coli* systems, and was then used to replace the *gus* gene in pBI121 [373]; the resulting "CaMV 35S-*gus::ntp-II*" cassette was cloned in the *Agrobacterium* binary vector pMON806, giving origin to pBIN405 [373]. In the aforementioned study by Fuentes-Ramírez et al. [207], a wild-type *gus* gene from the broad-host range cosmid pRG960SD [376], was allegedly replaced with a *gus::ntp-II* construct under the control of a double CaMV 35S promoter plus a leader sequence from Alfalfa Mosaic Virus (AMV), resulting in the final pRGS561 [207]. The parental plasmid harbouring the "CaMV35S-CaMV35S-AMV-*gus::ntp-II*" cassette is referred by Fuentes-Ramírez et al. as pBI426, and the paper cited for its creation is the study by Datla et al. that, however, only described pBIN405, while pBI426 was described elsewhere [377]. Ultimately, due to a non-standardised annotation and citation system (that have characterised decades of chaotic development of cloning vectors [299]), it was not possible to conclude whether the *gus::ntp-II* gene expression is driven by the "CaMV 35S" promoter from pBIN405 [373] or by the "CaMV35S-CaMV35S-AMV" promoter cassette from pBI426 [377].

The final pRGS561 plasmid used by Fuentes-Ramírez et al. and also employed in this work for tagging *G. diazotrophicus*, proved to be problematic to sequence, possibly due to the presence of repeated regions within the plasmid which resulted in different sequencing outputs from the same primer, although

supposedly unique (data not shown). Nevertheless, after various attempts combining Sanger-sequencing and publicly available sequences of the pRGS561 parental vectors, a highly plausible sequence (although possibly not 100% accurate) was generated (Fig. 4.34).

pRGS561 features both a ColE1 and a pVS1 origins of replication, an incomplete *cos* element for packaging into phage λ particles [378], a Rop protein for keeping the copy number of ColE1 family plasmids low [379], a *bom* (basis of mobility) site from pBR322 [380] along with *traI* and *traJ* genes, providing relaxase and helicase functions in cis for plasmid mobilisation [358], and an aminoglycoside adenylyl-transferase (*aadA* gene), conferring resistance to streptomycin and spectinomycin (Sm^R) [381]. The Sm^R, present in the pRG960SD cosmid backbone [376] in which the *gus* expression cassette was cloned, derives from a 2.3 kb *Bam*HI fragment of the pR702 vector [382], which the sequencing showed to include an integrase *intI* gene. The $oriV_{pVS1}$ origin of replication in pRGS561 was found to be part of the entire replicon from the 29-kb *Pseudomonas* plasmid pVS1, including the partitioning genes *par*, the stability protein StaA and the replication initiation protein RepA [383]. Plasmids based on the pVS1 replicon cannot replicate in *E. coli*, but are stably maintained in many proteobacteria genera, such as *Pseudomonas*, *Agrobacterium*, *Rhizobium*, *Burkholderia*, *Aeromonas*, *Comamonas* and more [383]. These vectors have been demonstrated to be retained in several plant-associated, Gram-negative bacteria for many generations even under non-selective conditions, making them suitable for studying bacterial colonization in plant systems or other experiments in which the use of antibiotics is hardly achievable [320] [384].

This enhanced stability was also observed in this study and allowed efficient plasmid maintenance *in planta* (see section 4.3), making pRGS561 a valuable tool for assessing *G. diazotrophicus* colonisation and gene expression in all the plant model systems utilised in this study.

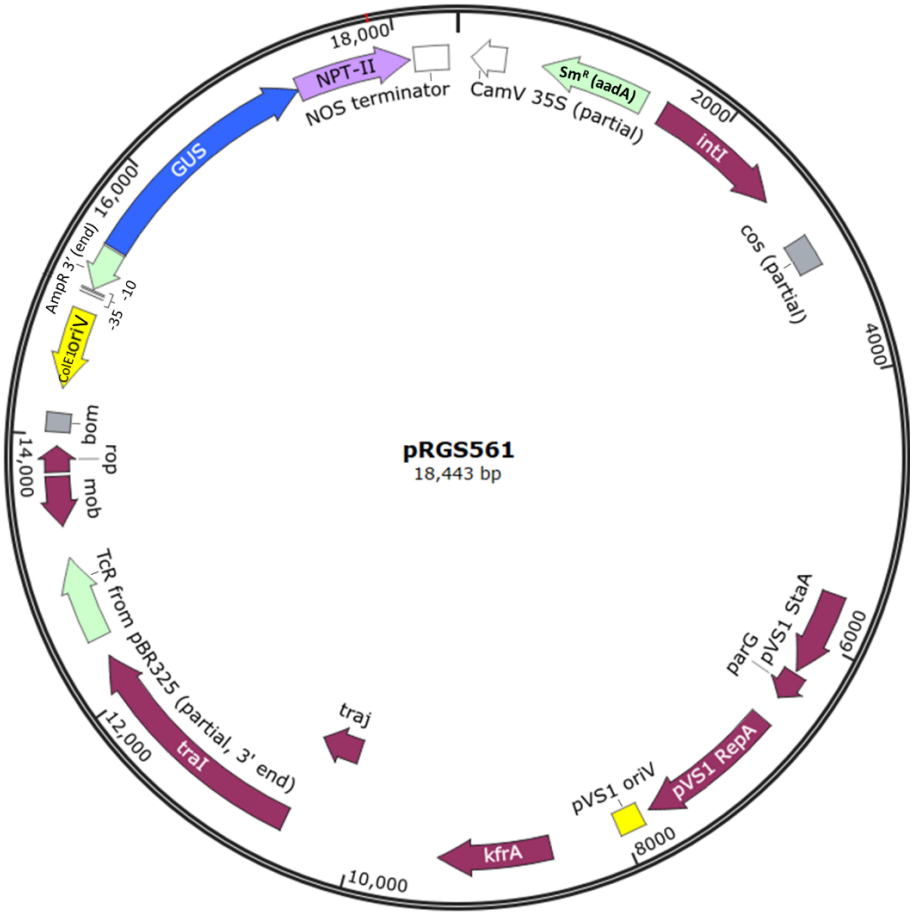


Fig. 4.34. Visual representation of the pRGS561 plasmid generated from sequencing data and validated on publicly available sequence of the parental vectors. Relevant vector components are shown, while other genes encoding for hypothetical proteins of unknown function present in the pRG960SD backbone cosmid are hidden. ColE1 and pVS1 ori = dual origins ensuring versatile replication capabilities; Rop protein = regulates copy number; Incomplete cos element = facilitates packaging into phage λ particles; Bom = basis of mobility, along with traI and traJ genes providing relaxase and helicase functions; SmR = confers resistance to streptomycin and spectinomycin; NPT-II = confers resistance to kanamycin.

Bizarrely, the *gus::ntp-II* gene was found not to be driven by "CaMV 35S", nor by "CaMV35S-CaMV35S-AMV" promoters: instead, it seems to have been cloned within an Amp^R cassette, in what appears to be a fragment from the pBR325 vector [385] (including the 3' end of a tetracycline resistance) that was used during the construction of pRG960SD [376]. An incomplete CaMV 35S promoter, however, was found downstream the COOH end of *gus::ntp-II*, in opposite orientation and separated by a *nos* terminator, therefore inoperative. It remains uncertain whether this apparently non-functional plasmid configuration was the result of a flawed cloning procedure during the plasmid reconfiguration over the decades, or if it is due to spontaneous

rearrangements, possibly induced by the recombinase function of IntI. Irrespective of the answer, the plasmid was still found to provide a strong GUS activity in both *E. coli* DH5α cells and *G. diazotrophicus* AZ0019 WT and *nifD*$^{-}$, in which it was conjugated as described elsewhere [208].

Briefly, the plasmid was introduced in β2163 cells through electroporation, and was subsequently mobilised from β2163 to *G. diazotrophicus* AZ0019 WT and *nifD*$^{-}$ via conjugation [208]. Normally, even in the absence of an in-trans β-glucuronidase function, the endogenous GUS activity of *E. coli* can react with X-Gluc and yield the blue stain; however, it was found that by incorporating the β-glucuronide to LB medium at the threshold concentration of 60 μg mL^{-1} (135 μM), the X-Gluc reaction was only induced in the *E. coli* CFUs transformed with pRGS561, resulting in a blue coloration, while non-transformed colonies did not exhibited any staining. *G. diazotrophicus* WT, on the other hand, showed no GUS activity up until the presence of X-Gluc 500 μg/mL, and no *gus* homologue nor β-glucuronidase function were found in the bacterial genome. The presence of a β-glucuronidase activity provided by the pRGS561 despite of the apparent lack of a functional promoter could be explained by read-through from upstream genes. Furthermore, the analyses of the plasmid sequence between the *ori*V_{pVS1} and the truncated *Amp*^{R} using bacterial promoter predicting tools such as BPROM [386] [387], revealed more than one set of -35/-10 regions from putative cryptic promoters, potentially explaining the GUS expression. Moreover, between *Amp*^{R} and the first ATG codon of the *gus* CDS, lies an 8 bp sequence which have been carried over since the first *gus* plasmid version from Jefferson et al., and that derive from the original *E. coli* K-12 *uidA* locus [388], suggesting the presence of the endogenous *gusA* Shine-Dalgarno (SD) sequence for translation initiation. Ultimately, the difficulty in manipulating the pRGS561 vector (as already experienced with the problematic *gus* PCR during the construction of the pICH47751_DsRed vector), possibly caused by its imperfect sequencing data, discouraged the use of this plasmid as a platform for further cloning projects. However, its analysis still enriched the list of usable plasmid elements for *G. diazotrophicus* mutagenesis (Fig. 4.36) by indicating a usable *ori*V_{pVS1} and an effective *gus* expression cassette.

In this work, the pRGS561 was conjugated into the *GG* strain, in order to obtain a double tagged mutant strain providing both GFP expression for colonisation imaging at the single cell level, and GUS activity for bacterial detection at the plant organ level. The complementary approach of the two different tagging systems was pursued to circumvent the limitations that are inherently associated to each strategy, while maintaining a simple setup by the use of a single strain for investigating the colonisation process (see section 4.3).

The conjugation method previously developed for *G. diazotrophicus* AZ0019 [208] and adopted in this work is based on the filter conjugation protocol described by De Lorenzo and Timmis [389] and the use of PDA supplemented with DAP 0.3 mM as a conjugation medium, which allows the growth of both strains. After two days of incubation at 28 °C (the optimal *G. diazotrophicus* growth temperature, also compatible with strong *E. coli* growth) the filter, in which the strains are concentrated, is resuspended in 5% ethanol and incubated in gentle agitation for two hours at room temperature: this step was found to facilitate the elimination of the donor *E. coli* strain [208], for which ethanol starts to become toxic at 1 to 2% [390], whereas *G. diazotrophicus*, as an acetic acid bacterium, can oxidatively ferment ethanol to acetic acid and is therefore less sensitive to it [391]. When the conjugation mix was plated in selective ATGUS + Sm 100 in the presence of X-Gluc 60 µg/mL (135 µM) and in absence of DAP to counter-select the transconjugants over any β2163 carryover, some blue CFUs could be isolated from the background (Fig. 4.35a). The NPTII function cannot be used for counter-selection since β2163 are kanamycin-resistant. Therefore, the blue CFUs were restreaked in ATGUS + Sm 100, Gent 25 to confirm the presence of both GUS and GFP activity. The presence of gentamicin eliminated any residual β2163 carryover.

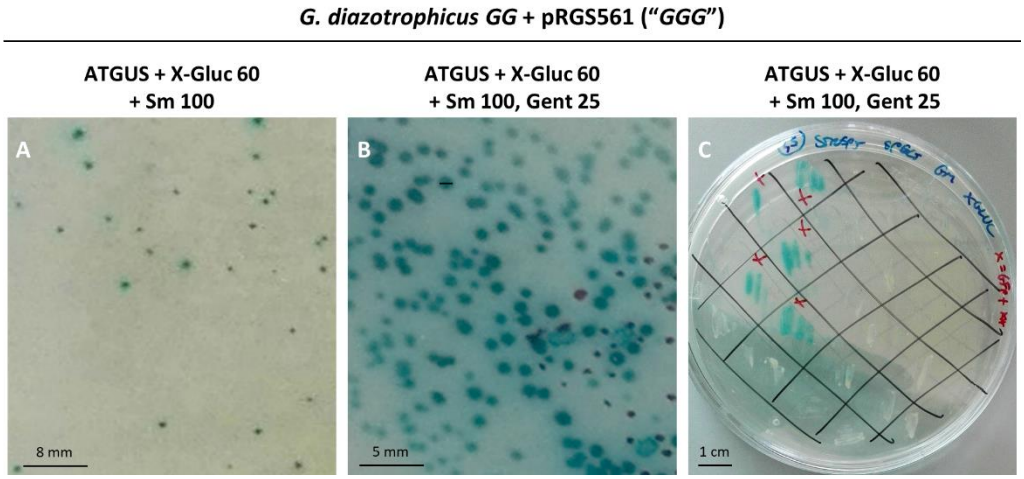


*Fig. 4.35. GGG strain selection upon conjugation between GG and β2163 carrying the pRGS561 plasmid. The transconjugants were first selected in ATGUS + Sm 100 and X-Gluc to isolate the blue GUS-expressing clones (**A**, 3 days after plating the transconjugants in selective medium) and, subsequently, in ATGUS + Sm 100, Gent 25 (**B, C**) to also confirm the presence of pBBR1MCS-5_GFP and GFP expression through fluorescence microscopy (not shown). Red crosses mark restreaked colonies showing bot GUS activity and GFP fluorescence. Despite of the lack of DAP, a background of β2163 seemed to still be present in the selection plates. The GUS activity was screened by incorporating in the ATGUS medium X-Gluc 60 µg/mL (X-Gluc 60).*

The strain so obtained was named *GGG* (as in *GG* + GUS), and showed the same features of *GG*, including analogous fluorescence levels, plus the pRGS561 functions. It was routinely cultured in ATGUS + Gent 25, Cm 25, Kan 50, Sm 100 or, alternatively, in DYGS + Gent 50, Cm 50, Kan 100, Sm 200.

The successful co-maintenance of the two plasmids by *G. diazotrophicus*, on one hand showed the compatibility of *ori*V_{pVS1} and *ori*V_{RK2}-based plasmids, and on the other hand provided a powerful tool for the advancing genetic engineering research on this bacterium, highlighting its capacity for supporting the metabolic burden of multiple expression vectors and exogenous in trans functions. A double expression system can be used to introduce multiple genes or pathways simultaneously into a single bacterial strain, allowing for complex metabolic engineering and providing a more versatile platform for gene editing. Ultimately, this possible mutant configuration can have promising implications for both basic research and practical applications in the agricultural industry.

Fig. 4.36 summarizes the key plasmid elements identified in this study as suitable for stable expression of genes of interest in *G. diazotrophicus*. These features can be taken into consideration in situations where the multi-copy expression from plasmid vectors is preferable over the more stable but less impactful genomic integration approach for gain-of-functions research.

	pBBR1 MCS 5 (GFP)		pRGS561 (GUS)		pICH47751 (dsRed)	
		Function		**Function**		**Function**
ori	$oriV_{pBBR1}$	Stable plasmid maintenance *in vitro* and *in planta*	$oriV_{pVS1}$	Stable plasmid maintenance *in vitro* and *in planta*	$oriV_{RK2}$	Stable plasmid maintenance *in vitro* and *in planta*
Promoters/ RBS	lac-repressible promoter PA1/04/03 + strong synthetic RBSII (designed for *E. Coli*)	Strong constitutive gene expression in *G. diazotrophicus*	Putative cryptic promoter + putative *uidA* SD	Strong constitutive gene expression in *G. diazotrophicus*	Pc promoter + RBS from gene *10* of bacteriophage T7 (designed for *Pseudomonas*)	Strong constitutive gene expression in *G. diazotrophicus*

Fig. 4.36. Summary of the key plasmid elements identified in this study as suitable for gene expression in G. diazotrophicus. In particular, ori, promoters and ribosomal binding sites (RBS) are showed. For simplicity, the elements are organised in correspondence of the parental archetypical plasmid platforms from which they were identified.

4.2.2b Conjugation optimisation for reporter genes integration

Although plasmid-mediated bacterial mutagenesis is a powerful and time-effective tool for conferring new functions to the investigated organism, it suffers from one main drawback: the necessity for selective pressure, which can be particularly challenging for *in vivo* studies where antibiotics may be harmful to the model system. The risk of plasmid loss or unwanted recombination events limit the reliability of plasmids as mutagenesis tools. In contrast, the genomic integration of foreign DNA allows for stable and heritable genetic modifications without the need for antibiotic selection. The integration of an exogenous DNA fragment is usually achieved by the conjugative transfer into the target recipient strain of an integration cassette carried by a conditionally replicative suicide vector. Specifically, the $oriV_{R6K\,\gamma}$-based vectors employed in this study are rapidly lost after their RP4-mediated delivery in the *G. diazotrophicus* recipient, but the passenger exogenous DNA

can be designed to be integrated in the chromosome through transposition or homologous recombination [364]. Homologous recombination (HR) is a conserved and naturally occurring DNA repair mechanism that plays a crucial role in maintaining genomic stability in bacteria. It involves the exchange of DNA strands between two homologous DNA molecules, allowing for the repair of single or double-strand breaks, the correction of replication errors, and the formation of genetic diversity in bacterial populations [392]. The process is usually mediated by the conserved RecBCD nuclease-helicase complex that recognize and process DNA ends, promote strand invasion and DNA synthesis, and resolve the recombination intermediates [393]. The analysis of *G. diazotrophicus* AZ0019 genome, and its comparison with the two publicly available Pal5 genomic sequences, revealed the recombination machinery of this bacterium to include a number of identifiable Rec proteins (RecA, D, F, G, J, N, O, Q, R, X), the XerC and XerD site-specific tyrosine recombinases [394] the RuvA resolvase [395], and some auxiliary putative resolvases varying between the three strains. No RecB and C genes could be identified from either of the three genome sequences, suggesting the alternative RecF pathway, which involves the other member of the Rec family listed above, to be the main recombination mechanism in *G. diazotrophicus* [396]. Interestingly, *recD*, the only identifiable gene from the RecBCD complex, showed 97% amino acid identity between AZ0019 and the two Pal5 strains, which in turn only showed 96% aa identity between each other. As a comparison, the RecA protein, essential for recruiting the foreign single-stranded DNA during the transformation process and its alignment to the homologous chromosomal region [397], showed 100% of identity in all three genomes available. This may suggest the divergence of a vestigial RecBCD system among *G. diazotrophicus* strains and a possible residual RecBCD function with strain-specific recombination efficiency.

The homologous recombination mechanism can be exploited to induce targeted genome modifications such as gene knockout, gene knock-in, and site-directed mutagenesis. This is achieved by designing a donor DNA molecule that carries an *in vitro*-modified allele, usually including a selectable marker, flanked by sequences homologous to the upstream and downstream regions of

the targeted gene [398]. These sequences are often around 500–1000 bp each [399]. The homologous recombination machinery can integrate the whole plasmid through a cross-over event between the first homology arm and the correspondent chromosome sequence (a state defined as merodiploid), followed by its excision via a second cross-over event with the other homology arm, resulting in the allelic exchange [400]. With this method, the investigated gene or genomic region can be replaced with virtually any synthetic construct. The double cross-over event can arise naturally, although an antibiotic selection marker will allow for direct selection of the construct integration and increase the chance of recovering a true positive transformant; alternatively, it can be facilitated by a counter selection system in which a negative selection marker present on the suicide vector will cause toxicity on appropriate medium, creating a favourable condition for the vector excision through the second crossing over event [401]. In either case, this system, although extremely powerful, is not very efficient because of low integration rates and illegitimate recombination events, and while a counter selection strategy can increase the positive transformants yield to a certain extent, it also greatly lengthens the process by introducing an additional step of colony restreaking and screening [401].

In this study, the strategy chosen for genomic cassette integration relied on the natural occurrence of double crossing over events, focusing on optimising the upstream conjugation conditions to maximise the chances of efficient plasmid delivery, and fine-tuning the selection conditions for minimising the number of false positive transformants. Nevertheless, the β2163 auxotrophy for DAP can be considered a counter-selection per se.

First, a cassette for constitutive *G. diazotrophicus* tagging was HiFi-assembled in the pSW23t vector (Fig. 4.37a) in order to genomically integrate both *gfp* and *gus* genes and overcome plasmid maintenance limitations. Two homology arms, named A and B, of 671 bp and 506 bp, respectively, were cloned from one of the four rRNA clusters in *G. diazotrophicus* genome (Fig. 4.37b). This region was selected to increase the chances of integration, since the sequence covered by the two homology arms is present in four copies in the bacterial chromosome; additionally, the rRNA-rich region was speculated to confer to

the integrated cassette the high transcription rate which is characteristic of ribosomal RNA genes [402]. The $P_{A1/04/03}$-RBSII-*gfpmut3** expression cassette was copied from the pBBR1MCS-5_GFP vector, while the *gus-NPTII* gene was copied from pRGS561 along with its putative SD element and 100 bp of the upstream sequence. Due to the uncertainty about the putative *gus-NPTII* cryptic promoter efficiency (section 4.2.2a), the construct was assembled in such a way to favour transcriptional readthrough from the $P_{A1/04/03}$ promoter.

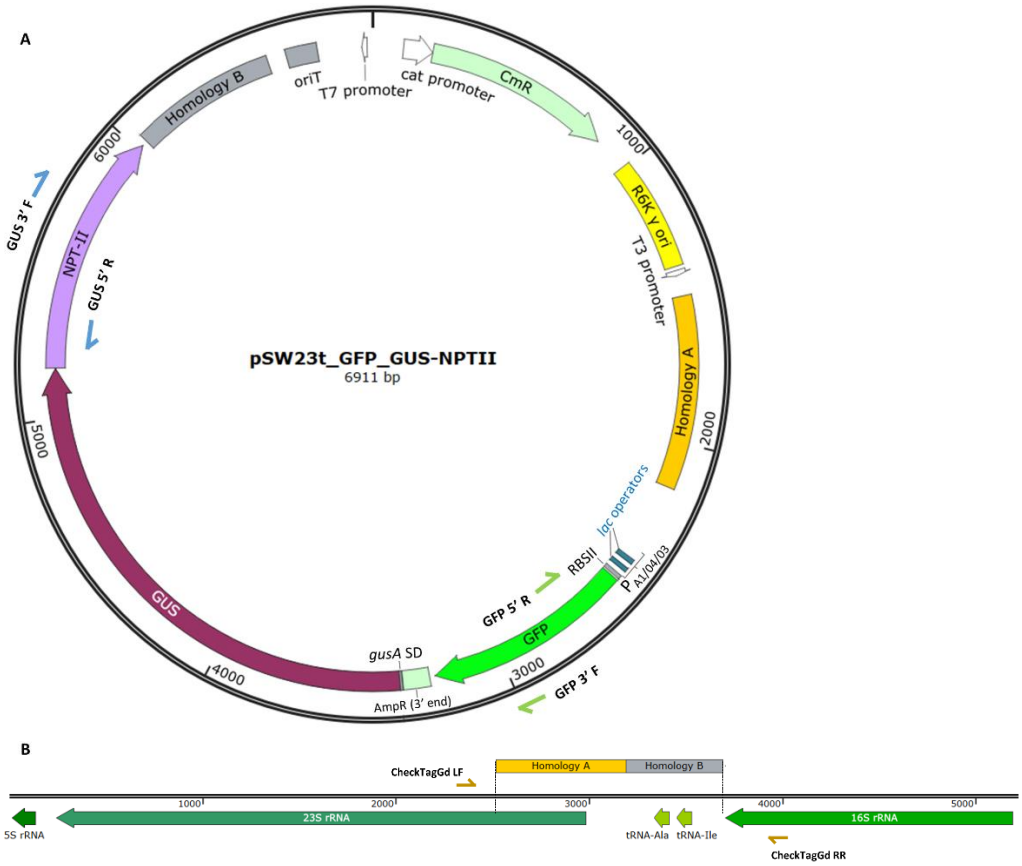


Fig. 4.37. (A) Visual representation of the pSW23t_GFP_GUS-NPTII vector generated from sequencing data; relevant vector components are shown. (B) rRNA cluster from G. diazotrophicus AZ0019 genomic sequence designated for the cassette integration; the homology arms A and B are shown. The primers annealing internally to the construct (GFP 3' F, GFP 5' R, GUS 3' F, GUS 5' R) and externally in the chromosome (GFP 5' R, GFP 3' F, CheckTagGd LF and CheckTagGd RR) for colony PCR screening are also shown.

The conjugation between *G. diazotrophicus* WT and the donor β2163 strain carrying the pSW23t_GFP_GUS-NPTII suicide vector (named *β2163_pSWgg*), was performed as previously described for the mobilisation of pRGS561 into *G. diazotrophicus* WT, *G. diazotrophicus nifD*$^{-}$ [208] and *GG*

(see section 4.2.2a). However, the analysis through fluorescence microscopy of the transconjugants recovered in selective ATGUS + Kan 50 or ATGUS + Kan 75, showed no sign of GFP expression in any of the colonies screened. Surprisingly, it was noted that during the biparental filter mating procedure, the initial fluorescence from the donor/recipient mix on the Millipore membrane (emitted by the *β2163_pSWgg* cells), was lost after around 24h of incubation in PDA + DAP. On the contrary, the *β2163_pSWgg* strain showed bright and stable fluorescence for up to one week when singularly plated on the same non-selective medium (Fig. 4.38b). This suggested some inhibitory effect of *G. diazotrophicus* on the *E. coli* strain, resulting either in an accelerated plasmid loss or in growth inhibition. To test this hypothesis, *G. diazotrophicus* was cross streaked with the *β2163_pSWgg* strain. This microbiological technique is usually employed for studying the communication and behaviour of bacteria in complex microbial communities by assessing the production of quorum sensing (QS) signalling molecules. A test strain is streaked on an agar plate perpendicularly to a second "biosensor" strain, known to produce a visible phenotype (such as the production of a pigment) in response to QS factors diffused in the medium from the test strain [403]. In this case, *G. diazotrophicus* was crossed streaked against the donor *E. coli* strain and the GFP fluorescence intensity was regarded as an indicator of the inhibitory effect of *G. diazotrophicus* on *β2163* (Fig. 4.38a). The experiment showed a significant reduction in GFP fluorescence intensity that emanated from the point of the cross streak closest to *G. diazotrophicus*; this was already visible after an overnight incubation at 28 °C and progressed until complete loss of GFP signal at 3 to 4 DPI (Fig. 4.38a). *G. diazotrophicus* is known to rapidly acidify its growth medium to a pH as low as 3.5, while exhibiting no adverse effects on its metabolic activity [111]; therefore, the PDA medium acidification was speculated to be a key factor contributing to the inhibition of *E. coli* growth. An alternative hypothesis for the observed reduction in GFP signal could be attributed to the susceptibility of this protein to low pH conditions. GFP has a pK_a of around 6 [404], and under acidic pH values below this point, the electron-rich, light-absorbing part of its chromophore exists in a protonated form that cause the fluorescence to quench [405]. However, while the specific pK_a of GFPmut3* is unknown [406], the

fluorescent signal observed in the *GG* strain in different media, including the acidified L-GIP (Fig. 4.31), may partially discredit this hypothesis, although the intracellular pH condition and protein localisation may be different between the two species. More importantly, the *E. coli* growth inhibition due to medium acidification hypothesis was supported by the observation that the *G. diazotrophicus* streak continued to enlarge overtime while the *β2163* one maintained a constant length and diameter, suggesting a reduced growth rate (Fig. 4.38a).

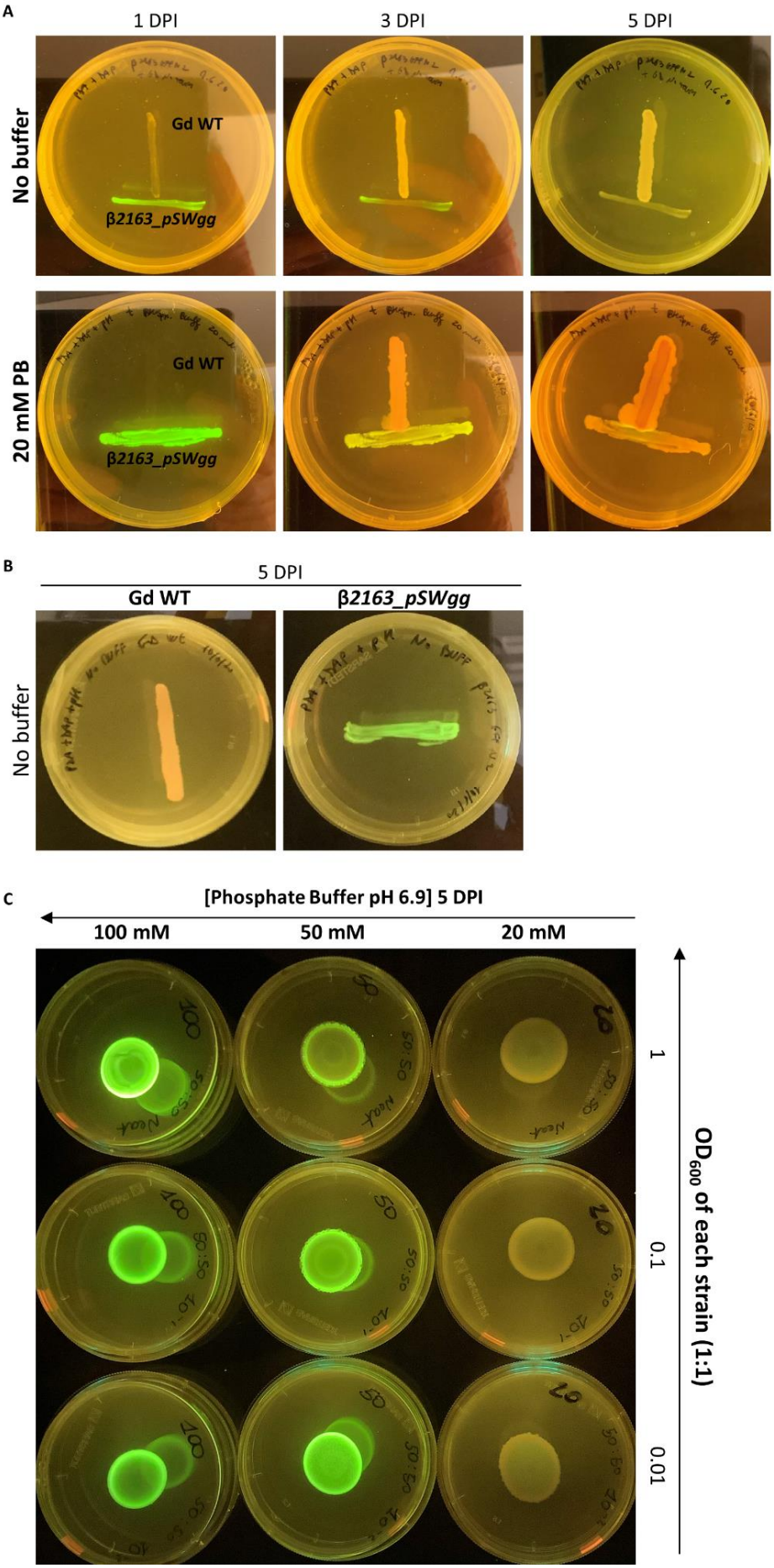

A
1 DPI
3 DPI
5 DPI
No buffer
20 mM PB
Gd WT
β2163_pSWgg
B
5 DPI
Gd WT
β2163_pSWgg
No buffer
C
[Phosphate Buffer pH 6.9] 5 DPI
100 mM
50 mM
20 mM
1
0.1
0.01
OD600 of each strain (1:1)

*Fig. 4.38. (**A**) Cross streaks between G. diazotrophicus and β2163_pSWgg in PDA + DAP in no buffer or 20 mM phosphate buffer (PB) pH 6.9 after 1, 3 and 5 days of incubation (DPI) at 28 °C. (**B**) G. diazotrophicus and β2163_pSWgg strains singularly streaked in unbuffered PDA + DAP. (**C**) Mock conjugation test: the two strains, cultured in appropriate media and washed twice, were resuspended in water at different OD_{600} (0.01, 0.1 and 1) and mixed at the ratio of 1:1 before being inoculated in PDA + DAP as a single drop with different concentrations of PB pH 6.9. The same experiment was conducted with the recipient:donor ratios of 1:5 and 1:10, with similar results (not shown).*

To test this theory, 20 mM phosphate buffer (PB) at pH 6.9 was added to the PDA (Fig. 4.38a). In this pH condition the fluorescence decrease was attenuated as expected compared to the unbuffered medium, but ultimately the quenching effect was only delayed of 24 to 48 hours (Fig. 4.38a). Therefore, different buffer concentrations were tested until no fluorescence reduction was observed for up to 5 DPI in a mock conjugation experiment (Fig. 4.38c). In this assay, *G. diazotrophicus* and *β2163_pSWgg* were mixed and plated in a single drop on PDA + DAP medium, mimicking the biparental mating protocol, with different concentrations of phosphate buffer at pH 6.9. The two bacterial species, both collected towards the end of their exponential phase and washed twice to avoid antibiotic carryover, were resuspended at three different densities to eliminate any dose-dependent observation bias during the PB screening. In fact, for some Gram-negative conjugation systems (e.g., in the case of the conjugative tumour-inducing plasmid pTi of *Agrobacterium*), the expression of the mobilisation machinery genes *tra* was found to be regulated by bacterial concentration-dependent quorum-sensing mechanisms [358]. Finally, the same experiment was repeated with three different *G. diazotrophicus: E. coli* ratios of 1:1, 1:5 and 1:10; this was done to test whether progressively decreasing the concentration of the recipient strain in the mix would result in a corresponding decrease in its inhibitory effects. The results showed that neither the bacterial density (Fig. 4.38c), nor the *G. diazotrophicus: E. coli* ratio (not shown), had an obvious impact on the fluorescence stability. The pH and buffer concentration, on the other hand, was instrumental in maintaining a bright GFP signal for up to 5 days of incubation at 28 °C (Fig. 4.38c), with the highest PB concentration tested (100 mM) being the most effective. While the experiment did not establish with certainty that the stable fluorescence achieved in PB 100 mM was a result of the unconstrained donor strain growth in the buffered medium rather than an

improved protein maturation resulting from a less acidic pH, it is plausible that an optimal pH condition for *E. coli* could stimulate its growth and metabolic processes, including the expression of the conjugation machinery. It must also be taken into consideration that *G. diazotrophicus* was reported to produce a Linocin M18-like bacteriocin named Gluconacin, i.e., a small protein with antimicrobial activity toward sugarcane phytopathogens and other bacteria [407], which may have contributed to the *β2163* growth inhibition. Nevertheless, the ultimate goal of optimizing the conjugation protocol was to ensure the survival of the donor strain long enough for it to transfer the conjugative vector to the recipient strain, which the addition of 100 mM PB pH 6.9 seemed to achieve to a certain extent. Therefore, the modified conjugation medium was adopted as a standard in the conjugation protocol.

This protocol optimisation provided new insights about the interaction between the two bacterial species during the conjugation process. The stabilised fluorescence allowed the visualisation of *β2163_pSWgg* cells or sub-colonies adhering or colocalising within *G. diazotrophicus* CFUs in selective ATGUS medium (Fig. 4.39). Despite of the lack of DAP, which prevented any growth of *β2163* when singularly plated in DAP-free LB or PDA medium, the presence of *G. diazotrophicus* allowed the survival of the *E. coli* strain, possibly by providing a source of DAP or DAP intermediates. The *β2163_pSWgg* strain was observed to survive in this condition either in the form of small background CFUs, about 1/10 of the diameter of a colony in DAP-amended medium (Fig. 4.39d, e) and appearing semi-transparent under light microscopy (Fig. 4.39f, g), or as sub-colonies directly adhering to the broader *G. diazotrophicus* colonies borders (Fig. 4.39a-d) or even coexisting as single cells inside them (Fig. 4.39c-e). Small *E. coli* sub-colonies growing in proximity of a *G. diazotrophicus* CFU, would initially take contact with it by sticking on its surface (Fig. 4.39a), with one *G. diazotrophicus* colony supporting one (Fig. 4.39a) or more (Fig. 4.39c, d) "guest" sub-colonies (phase 1). Subsequently, the guest sub-colonies were observed to lose their defined shape by injecting themselves inside the "host" *G. diazotrophicus* CFU through a protrusion (phase 2), penetrating the colony boundaries in a specific point instead of homogeny diffusing along the contact surface (Fig. 4.39b, c).

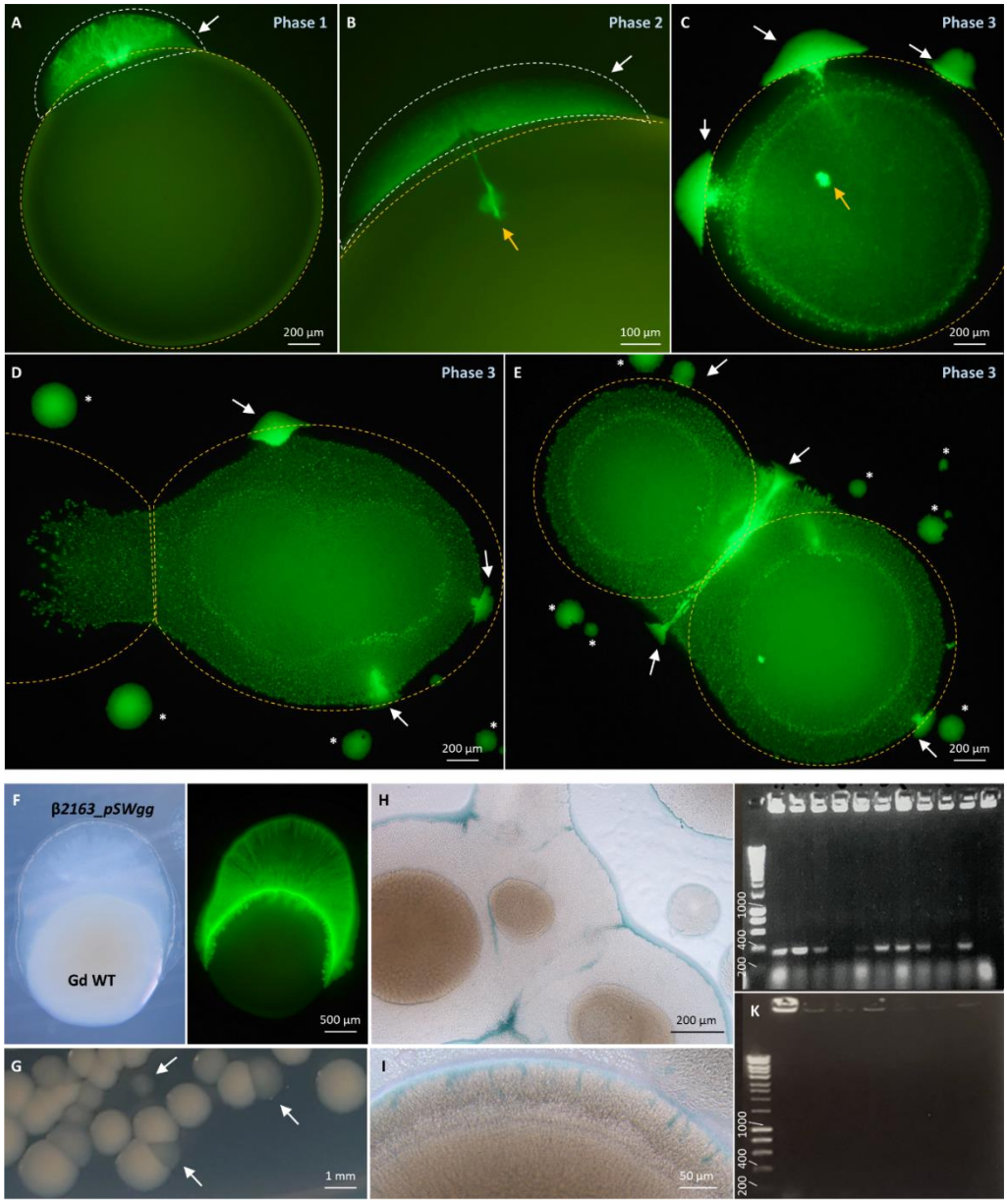


*Fig. 4.39. G. diazotrophicus interaction with β2163_pSWgg during conjugation. (**A**) Contact between a β2163_pSWgg sub-colony (marked in white dashed line and/or white arrows) and G. diazotrophicus colonies (orange dashed line) in ATGUS + Kan 75 (phase 1). (**B**) Injection of β2163 (orange arrow) inside the G. diazotrophicus colony (phase 2). (**C-E**) Diffusion of β2163_pSWgg from multiple contact points (white arrows) to the whole volume of the G. diazotrophicus single or conglomerated colonies, marked in orange dashed line (phase 3). The grainy green signal represents single β2163_pSWgg cells evenly distributed. Small β2163_pSWgg colonies were also observed detached from G. diazotrophicus (D, E, white star). Occasionally, β2163_pSWgg sub-colonies were found to colocalise directly inside the host colony (C, orange arrow) and initiating the colonisation process from the inside. (**F, G**) Semi-transparent β2163_pSWgg sub-colonies (white arrows) attached to G. diazotrophicus colonies after 15 days in ATGUS + Kan 75, Amp 100, light and fluorescence microscopy. (**H, I**) β2163_pSWgg cell layer surrounding the borders or penetrating G. diazotrophicus colonies (phase 1 and 2) after5 days in N-free ATGUS + Kan 75, Amp 100, X-Gluc 100. (**J**) Colony-PCR screening of G. diazotrophicus colonies recovered in ATGUS + Kan 75, Amp 100, using the primer combination internal to the cassette ("GFP 3' F" + "GUS 5' R"); the expected 350 bp band, present in almost all samples, is visualised against the 1 kb HyperLadder from LIFEGENE. (**K**) Colony-PCR screen of G. diazotrophicus colonies recovered in ATGUS + Kan 75, Amp 100, using the primers combination "2)" ("CheckTagGd LF" + "GFP 5' R). None of the clones transconjugant screened showed the band corresponding to the cassette*

integration. The same result was obtained when using the primer combinations "3)" and "4)" (not shown).

After the self-inoculum in the host colony, single *β2163_pSWgg* cells would eventually permeate the whole host colony volume with an even distribution (Fig. 4.39d, e) (phase 3). In the case of two or more merged *G. diazotrophicus* colonies in which the *E. coli* colonisation had taken place in only one of the conglomerated CFUs, phase-3 guest cells were seen to colonise the whole host volume by diffusing from the entry host cell (Fig. 4.39d) until the complete phase-3 colonisation of the host conglomerate (Fig. 4.39e). Noteworthily, the otherwise even distribution of phase-3 fluorescent *β2163_pSWgg* cells, localised at a higher concentration in a ring-like formation, seemingly dividing the *G. diazotrophicus* colony into two sub-regions (Fig. 4.39d, e). Interestingly, a similar phenotypic gradient within the *G. diazotrophicus* colonies was also observed when analysing the *nifHDK*-driven GFP expression patterns (see section 4.4.2), highlighting a particular structural colony organisation characterised by discrete micro-environments and possibly associated with divergent bacterial functions. Due to this unexpected flow in the DAP auxotrophy counter-selection system, and considering the impossibility to efficiently use kanamycin as a selection marker (against which *β2163* are naturally resistant), Amp 100 was added to the selective ATGUS medium to eliminate any *β2163* carryover. This addition seemingly allowed the elimination of the *E. coli* strain, as indicated by the disappearance of any background fluorescence. No GFP-positive *G. diazotrophicus* CFU could still be detected. However, upon addition of X-Gluc 100 in the selective medium, a blue halo was observed in the surroundings of the *G. diazotrophicus* colonies (Fig. 4.39h), occasionally penetrating through the colony border (Fig. 4.39i). Furthermore, after around 10 days in selective ATGUS + Kan 75, Amp 100, new small fluorescent and semi-transparent colonies started to appear in proximity of the ivory-coloured *G. diazotrophicus* colonies, from which they become obviously distinguishable after two weeks (Fig. 4.39g). This suggested that the presence of the *β2163* sub-colonies was in fact merely concealed, while still being included within the host biomass, in which *β2163_pSWgg* could be sheltered against the ampicillin until its complete catabolisation by *G.*

diazotrophicus. The same behaviour was observed in selective nitrogen-free ATGUS, in which the addition of X-Gluc 100 and the action of either the *gus::nptII* gene from the pSW23t_GFP_GUS-NPTII vector, or the endogenous *β2163_pSWgg* GUS activity, revealed a layer of guest *E. coli* attached to *G. diazotrophicus*.

In all these experiments, the transconjugant *G. diazotrophicus* colonies recovered were PCR-screened, using four different combinations of primers internal and external to the integration cassette (see Fig. 4.37): 1) "GFP 3' F" + "GUS 5' R", with both primers internal to the cassette; 2) "CheckTagGd LF" + "GFP 5' R", with one primer annealing in the bacterial chromosome just upstream the left homology arm and one inside the 5' end of the cassette; 3) "CheckTagGd RR" + "GUS 3' F", with one primer annealing in the bacterial chromosome just downstream the right homology arm and one inside the 3' end of the cassette; 4) "CheckTagGd LF" + "CheckTagGd RR", with both primers external to the cassette, resulting in a band of different length compared to the wild-type in case of cassette integration (see Primer table 3.3). The majority of the colonies screened exhibited the expected 350 bp band with the internal primers combination, but no clone produced a positive signal when using the other 3 primer combinations for cassette integration (Fig. 4.39j, k; see Fig. 4.37 for primers allocation). The same result was obtained when the pSW23t_GFP_GUS-NPTII suicide vector was electroporated in competent *G. diazotrophicus* cells: the CFUs recovered in ATGUS + Kan 75 showed the presence of the cassette by the use of the internal primers (Fig. 4.39j), but no GFP nor GUS signal was detected from the screened colonies. These results suggest the persistence of the plasmid genetic material either as randomly integrated in the chromosome, or retained by carryover *β2163_pSWgg* cells coexisting amidst *G. diazotrophicus* colonies. The lack of integration may have different explanations. On one hand, the rRNA targets selected, due to their housekeeping importance, may be less prone to mutations and more tightly controlled by the bacterium RM system; in fact, it has been recently acknowledged that mutation rates are biased across genomic positions, with certain loci being particularly prone or insensitive to DNA modifications [408]. Furthermore, although four distinct copies of the designated rRNA

homology region were found in the two available Pal5 genomes, only one could be located in the *G. diazotrophicus* AZ0019 chromosome, thus nullifying the putative advantage of the four possible integrations sites; however, this finding may be a mere artifact due to the imperfect assembly of the genome sequencing data (see section 4.2). On the other hand, the putative presence of the other three homology regions may be preferred as a recombination template over the foreign DNA provided.

It is also possible that neither of the two reporter genes can be efficiently transcribed when put outside the context of the plasmid from which they were copied, indicating that the strong GFP and GUS phenotype obtained in the *GGG* strain depended more on the plasmid's multiple copy number than on the effectiveness of the promoter and RBS themselves: in the latter case, the presence of a single cassette copy, regardless of it being in an actual double-recombinant mutant or in a merodiploid one, may not be sufficient for detectable reporter gene expression.

What was more surprising in the conjugation dynamic characterised, was the propensity of the two strains to engage in a seemingly symbiotic relationship. The otherwise impossible survival of *E. coli* in ampicillin-replete or nitrogen-free media was allowed by the direct interaction with *G. diazotrophicus*, which, speculatively, provided fixed nitrogen and an antibiotic-deplete environment in exchange for the kanamycin resistance activity from the *ß2163_pSWgg* strain, affecting the conjugation process. A similar mutualistic relationship has been described before with yeast cells nourished by the BNF activity of *G. diazotrophicus* [232]. Therefore, far from hindering the interaction with *E. coli* by bacteriocins production, *G. diazotrophicus* seemed to be naturally inclined to physically and functionally engage with this other bacterial species, corroborating its reputed intimate nature of symbiotic organism [98].

4.2.2c nifHDK reporter genes integration

One of the aims of this work was investigating the BNF process in *G. diazotrophicus* in relationship to the environmental conditions. Transcriptional fusions represent a valuable tool for studying gene expression patterns in prokaryotic systems. They consist in the fusion of a promoter-less reporter gene to a gene of interest, allowing the measurement or visualisation of the targeted gene expression by monitoring the reporter gene activity [409]. Conveniently, this approach can be applied *in vivo*, providing valuable insights into the regulation of gene expression in response to environmental cues. In this study, the fusion of promoter-less *gfp* or *gus* genes to the *nifHDK* polycistronic transcript has been used as a means of studying nitrogen fixation in *G. diazotrophicus* (see section 4.4.2). Among the many genes participating in the nitrogen fixation process, the *nifHDK* operon encodes for three structural components of the nitrogenase complex, and is transcribed as a single polycistronic mRNA unit [129]. In particular, the homodimeric dinitrogenase reductase Fe-protein NifH is associated with the transfer of electrons to the $\alpha_2\beta_2$ heterotetrametric MoFe-protein NifDK, which contains the molybdenum–iron cofactor that catalyse the reduction of N_2 to NH_3 [136]. The strategy adopted for the reporter gene integration was similar to what illustrated in the section 4.2.2b. The promoter-less reporter genes were designed to be inserted at the 3' end of the *nifK* gene, in order to be co-transcribed with the *nifHDK* polycistronic transcript upon activation of the *nifHDK* promoter (Fig. 4.40). To ensure efficient translation, the 18 bp RBSII from the *gfpmut3** gene of the pBBR1MCS-5_GFP plasmid was maintained. The cassette was designed to be integrated at the end of the polycistronic unit in order to reduce the risk of insertional frameshift, nonsense or antisense disruption of the operon's ORFs or other so-called polar effects which can potentially affect upstream or downstream gene expression in addition to the targeted gene [401]. The left and right homology arms were designed to target the last 768 bp of *nifK* 3' end, and the *nifENXQ* operon promoter plus the first 821 bp of *nifE* 5' end, respectively (Fig. 4.40a, b).

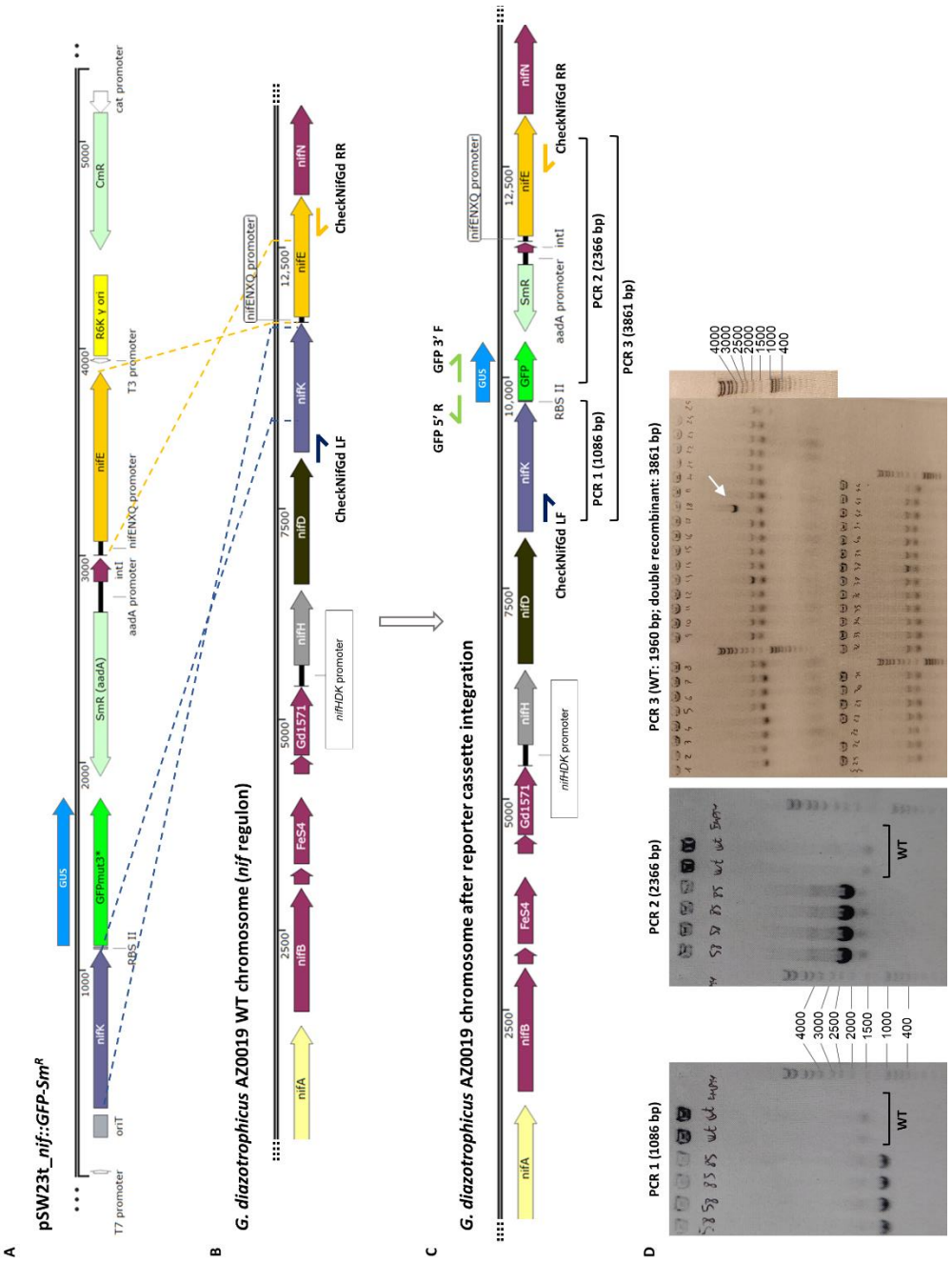


*Fig. 4.40. nifHDK reporter gene integration. (**A**) Visual representation of the pSW23t_NifK::GFP-Sm^R plasmid generated from sequencing data. The codon optimised gus gene, used as an alternative to the gfpmut3* in the vector pSW23t_NifK::GUS-Sm^R, is also shown. The dashed lines represent the two crossing-over events between the homology arms and their corresponding genomic regions in the chromosomic nif locus of G. diazotrophicus AZ0019 (**B**). (**C**) Visual representation of the reporter cassette integration generated from sequencing data of the Gd_nifHDK::GFP strain. The primers used for the colony-PCR screening are shown. (**D**) Colony-PCR screening of G. diazotrophicus colonies recovered in ATGUS + Sm 100, Amp 100 after optimised biparental filter mating conjugation with β2163_pSWNifK::GFP. The primers combination "1)" ("CheckNifGd LF" + "GFP 5' R", named PCR 1) "2)" ("CheckNifGd RR" + "GFP 3' F", named PCR 2) and "3)" ("CheckNifGd LF" + "CheckNifGd RR", named PCR 3) are shown. Four out of the five double recombinants isolated are shown as screened through PCR 1 (1086 bp band expected) for left homology arm integration and PCR 2 (2366 bp band expected) for right homology arm integration. One out of the five double recombinants isolated is shown as screened through PCR 3 (3861 bp band expected against 1960 bp band in wild-type loci) for both homology arms integration (white arrow).*

As a selection marker, the Sm^R from the pRGS561 plasmid was chosen, including its putative promoter sequence and the 3' end of the class I integrase flanking the *aadA* gene in pRGS561, which possibly contains a cryptic antisense promoter driving the transcription of *aadA* [322]. The antibiotic cassette was oriented in a tail-to-tail configuration against the reporter gene in order to prevent any read-through of the *nifENXQ* operon from the *aadA* gene constitutive promoter. The integration cassette was assembled in the pSW23t vector backbone, giving origin to the pSW23t_NifK::GFP-Sm^R vector. β2163 cells transformed through electroporation with the pSW23t_NifK::GFP-Sm^R vector were named *β2163_pSWNifK::GFP*. Alternatively, the *gfpmut3** CDS was substituted with the codon-optimised *gus* gene from the pICH-DsR-*nifHDK*p::GUS plasmid, while leaving the RBSII an all the other plasmid features unchanged, originating the pSW23t_NifK::GUS-Sm^R vector and the relative donor strain *β2163_pSWNifK::GUS*.

The conjugation between *G. diazotrophicus* and the donor strain *β2163_pSWNifK::GFP* was carried out through biparental mating, using the filter mating protocol optimised as described in the section above. The transconjugants were selected in ATGUS + Sm 100, Amp 100 and screened through colony-PCR using a combination of primers conceptually identical to what illustrated in section 4.2.2b (Fig. 4.40c): 1) "CheckNifGd LF" + "GFP 5' R", with one primer annealing in the bacterial chromosome just upstream the left homology arm and one inside the 5' end of the cassette; 2) "CheckNifGd RR" + "GFP 3' F", with one primer annealing in the bacterial chromosome just downstream the right homology arm and one inside the 3' end of the cassette; 3) "CheckNifGd LF" + "CheckNifGd RR", with both primers external to the cassette, giving a 1960 bp band from the wild-type locus and a 3861 bp band after a double homologous recombination event (Fig. 4.40c, d and Primer table 3.3). The integration efficiency obtained with the optimised conjugation protocol was around 2%, with a mean of 1 positive colony every 50 colonies screened (Fig. 4.40d). Five double-recombinant *G. diazotrophicus* clones with the correct integration were recovered, as shown by colony-PCR with all the three primers combinations (Fig. 4.40d) followed by Sanger-sequencing of the genomic *nif* operon. The mutant was named *Gd_nifHDK::GFP*. This double-

recombinant isolation rate, although extremely low, was more than double to what previously obtained when a similar strategy was applied for the creation of the *G. diazotrophicus nifD*$^{-}$ strain (< 1%).

Although the addition of Amp 100 to the selective medium delayed the growth of β2163 residual colonies, their concealed presence amidst the biomass of *G. diazotrophicus* (Fig. 4.39) still introduced the potential for false positives and misinterpretations of the PCR screening. Therefore, during the construction of a *nifHDK::GUS* reporter system via biparental mating with the *β2163_pSWNifK::GUS* strain, the conjugation protocol was further adjusted. The filter conjugation was performed with 1 mL of donor and recipient strains each, both cultured until the exponential phase with appropriate antibiotics in LB or DYGS medium, respectively, and washed twice in water before being mixed and filtered on the Millipore membrane. Considering the faster growth rate of *E. coli* compared to *G. diazotrophicus*, this corresponded to a donor:recipient ratio of around 2:1. The filter membrane was incubated at 28°C in PDA + 0.3 mM DAP + 100 mM PB pH 6.9 for a maximum of 36-48 hours, to reduce the risk of plasmid loss and β2163 growth inhibition by *G. diazotrophicus* antagonistic effect. Furthermore, as an ulterior counter-selection method during the *G. diazotrophicus* mutants screening in selective medium, Gent 25 was added. This antibiotic concentration was previously found to have no impact in *G. diazotrophicus* growth whilst being lethal for *E. coli* (Fig. 4.35). Finally, instead of ATGUS, DYGS was used as a selective medium to recover the transconjugants, in light of its beneficial properties observed during the electroporation protocol optimisation. The optimal concentration of spectinomycin to be coupled with the DYGS medium was found to be 500 μg mL^{-1}, while the ampicillin concentration was raised to 200 μg mL^{-1} (Fig. 4.41b).

The implemented modifications in the conjugation protocol led to a considerable improvement in the efficiency of transconjugant isolation, as reflected by the reduced formation of background false-positive colonies, absence of *E. coli* carryover and increased double-recombinants isolation rate. Out of 11 screened CFUs, 5 were identified to harbour the reporter cassette correctly integrated in the bacterial chromosome, demonstrating an integration

efficiency of nearly 50% (Fig. 4.41a). The use of these methodologies underscores their significance in enhancing the accuracy and precision of the experimental outcomes, while significantly reducing the time required for transconjugant screening. To further validate the *gus* reporter mutants, named *Gd_nifHDK::GUS*, the chromosomic integration was confirmed through Sanger-sequencing. Furthermore, some of the CFUs recovered in DYGS + Sm 500, Amp 200, Gent 25 (Fig. 4.41b), including the 11 PCR-screened CFUs (Fig. 4.41a), were restreaked in N-free ATGUS + Sm 150, Amp 150, X-Gluc 120 (Fig. 4.41c). As expected in N-starvation conditions, the *nif* operon expression was visualised by the appearance of GUS-mediated blue stains around the 5 double recombinants that had been confirmed through colony-PCR, although the intensity of the blue signal diverged across the five clones (see section 4.4.2). Specifically, clones 1 and 2 only developed a faint blue hue, while clones 3, 4 and 6 where associated with a more obvious coloration (Fig. 4.41c).

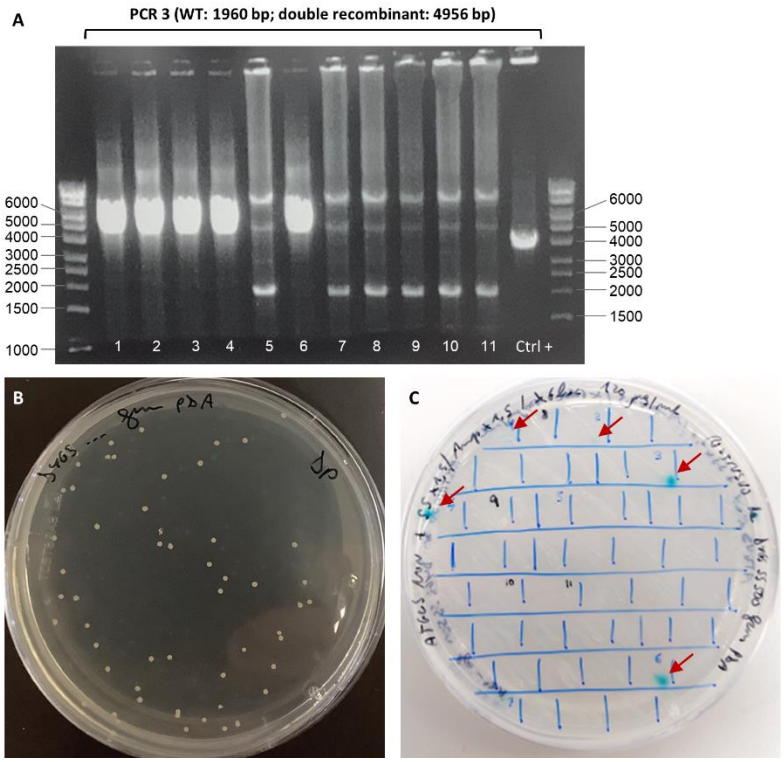


Fig. 4.41. nifHDK::GUS reporter gene integration. (A) Colony-PCR screening of G. diazotrophicus colonies recovered in DYGS + Sm 500, Amp 200, Gent 25 (B) after optimised biparental filter mating conjugation with β2163_pSWNifK::GUS. Eleven CFUs from the selective DYGS medium (B) were randomly selected and screened through colony-PCR 3 ("CheckNifGd LF" + "CheckNifGd RR", Fig. 4.40) for both homology arms integration (4956 bp band expected against 1960 bp band in wild-type loci). The Gd_nifHDK::GFP strain,

giving a 3861 bp band with the same primer combination and PCR program, was used as positive control (Ctrl +). The CFUs 1, 2, 3, 4, and 6 exhibited the 4956 bp band corresponding to a double recombination event, while the other colonies showed the 1960 bp band of the wild-type locus. (C) Some of the CFUs recovered in DYGS + Sm 500, Amp 200, Gent 25 (B), including the 11 PCR-screened CFUs, were restreaked in N-free ATGUS + Sm 150, Amp 150, X-Gluc 120. The CFUs 1, 2, 3, 4, and 6 all exhibited GUS activity (red arrows).

None of the colonies that tested negative by colony-PCR produced a blue stain, while some of the unscreened CFUs did (although with a fainter GUS signal, similar to the weak coloration developed by clones 1 and 2).

It should be emphasized that the method described in this study for mutant creation through biparental mating with an auxotrophic donor strain is more time-efficient compared to other conventional approaches, such as the *sacB* counterselection system [401]. By optimizing various aspects of the conjugation conditions and the stringency of the selective media, it was possible to obtain a knock-in *G. diazotrophicus* mutant strain in less than one week, with as little as less than 20 clones required for colony-PCR screening. This streamlined approach has the potential to expedite the process of *G. diazotrophicus* mutant creation, thereby facilitating the advancement of non-model bacteria in agricultural biotechnologies research.

4.2.2d Tn5 mutagenesis to find negative regulator of BNF

Tn5 mutagenesis is a powerful tool used in bacterial genetics for the creation of mutants by the random integration of a mobile genetic element (MGE), specifically a Tn5 transposon, into the bacterial chromosome, with no required homology sequences. The insertions can induce mutations throughout the genome by disrupting or altering gene expression. This mutagenesis technique has been extensively used to study gene function, gene regulation, and bacterial physiology, as it allows for the rapid generation of large collections of mutants that can be screened for specific phenotypes or used for functional genomics studies [356]. The Tn5 transposon is usually mobilised from a suicide vector that also provides in cis the transposase gene activity (*tnpA*). The transposase recognises specific DNA sequences at the ends of the transposon (sometimes used in a minimised variant referred to as mini-

transposon), excises the element and integrate it in a random genomic position, although some "hotspots" can be favoured [399]. The transposon typically contains an antibiotic resistance cassette or other markers. Since *tnpA* is lost after each transposition event, mini-Tn5 do not provoke DNA rearrangements once inserted in a target sequence, unlike natural transposons, and are stably inherited; this characteristic enables the use of multiple transposons on the same genotype regardless of previous insertions, if coupled with different selection markers [389].

In this study, the $oriV_{R6K\gamma}$-based mini-Tn5 vectors pBAMD1-2 and pBAMD1-4, described by Martínez-García et al. [356] and obtained from the SEVA collection [299], were used for *Gd_nifHDK::GUS* mutagenesis. These vectors harbour transposons with a Kan^R and Sm^R cassette, respectively, flanked at both sides by the minimal 19 bp inverted repeat "ME" elements (hyperactive mosaic ends [410]). Additionally, the vectors' backbone contains the *tnpA* gene, an Amp^R cassette for plasmid maintenance, and an $oriT_{RP4}$. Tn5 elements are usually mobilised through conditionally replicative vectors delivered via biparental mating or electroporation, or by direct electroporation of the functional transposome pre-assembled *in vitro* [411]. This strategy has been successfully applied to *G. diazotrophicus* for the characterization of a flagellar mutant [412]. In this work, the pBAMD1-2 vector has been used on *G. diazotrophicus* AZ0019 wild-type for calibrating the optimal plasmid concentration in electroporation experiments, and allowed the recovery of around 100 CFUs per vector μg in DYGS + Kan 200 (Fig. 4.32c).

Following the creation of the *Gd_nifHDK::GUS* reporter strain, the Tn5 system was employed in the attempt of identifying a negative regulator of the nitrogen-fixation machinery. The strategy consisted in transferring the pBAMD1-2 and pBAMD1-4 suicide vectors to the *Gd_nifHDK::GUS* reporter strain, either by conjugation or electroporation, and recover the transformed strain in DYGS + Kan 200 or DYGS + Sm 500, respectively, in the presence of X-Gluc 130 μg mL^{-1} (290 μM). The appearance of any blue stain in the nitrogen replete DYGS medium would indicate the disruption of a gene involved in repressing the nitrogen fixation process in nitrogen-rich environments. In fact, while the NifA protein is usually regarded as the

transcriptional activator of the nitrogenase genes [128], the regulation system of the *nifA* gene itself was never fully elucidated in *G. diazotrophicus*, although it was proposed to be associated with the P_{II} nitrogen regulatory proteins GnlB and GnlK [124].

Around 2000 colonies of *Gd_nifHDK::GUS-Tn5* mutants were recovered in selective DYGS medium following the transformation with the two aforementioned Tn5 vectors, delivered using both conjugation and electroporation approaches. However, none of the colonies displayed detectable GUS activity indicative of *nif* operon transcription under the N-replete conditions of the DYGS medium. There may be several explanations for the underwhelming outcome of this experiment. First, the number of mutants generated may not be sufficient for pinpointing the gene involved in the negative regulation of nitrogen fixation. Furthermore, the disruption of a single gene may not be enough to suppress this regulatory function in case of a multi-enzymatic complex: a similar scenario was reported during the identification of GnlB and GnlK [124]. On the other hand, due to the high energy demand associated with the nitrogen fixation process, the elimination of a putative negative regulator of such mechanism may be lethal, or cause growth inhibition, therefore impairing the mutant isolation. Similarly, the researched locus may be in linkage with other housekeeping genes, or lay in genomic regions more protected from mutagenesis [408] and far from the Tn5 integration hotspots [413]. Finally, the mutagenesis conditions used, including transposon delivery method and selection conditions, may not have been optimal for generating the desired mutant and phenotype.

While the initial attempts to identify a negative regulator of the nitrogen-fixation machinery were not successful, the use of the *Gd_nifHDK::GUS* mutant strain in combination with the Tn5 transposon or other forms of random mutagenesis, still holds potential for further optimization and testing. Overall, this system may be a valuable tool for improving the current understanding of nitrogen fixation regulation in *G. diazotrophicus*, and could ultimately aid in the development of strains with enhanced nitrogen-fixation efficiency under nitrogen-replete agricultural conditions.

4.2.3 CRISPR/Cas9 for G. *diazotrophicus* mutagenesis

Genomic modifications strategies relying on the homologous recombination mechanism are often limited by low efficiency, as this method requires extensive optimisation of both the integration cassette design and the screening conditions to identify desired mutants, and ultimately is characterised by an intrinsic degree of stochasticity (see sections above). Furthermore, the process is laborious and technically challenging. In contrast, the CRISPR-Cas9 system, a type of prokaryotic immune system that has been adapted for genome engineering purposes, is regarded as a powerful, quick, and accurate approach for targeted mutagenesis [399].

In nature, CRISPR-Cas is a type of adaptive immune system used in parallel to the innate RM system as a defence mechanism to neutralise endogenous MGEs and HGT from bacterial conjugation and viral transduction [414]. During the immunisation (or adaptation) phase, a clustered set of *cas* genes (CRISPR associated proteins) works in concert to: 1) recognise exogenous or endogenous MGEs (including plasmids and phage DNA and RNA) and binding to so called "protospacer" sequences often flanked by a specific protospacer adjacent motif (PAM); 2) cleave the foreign genetic material in 26-72 bp protospacer fragments; 3) integrate the protospacers without the PAM in a chromosomal CRISPR array (clustered regularly interspaced palindromic repeats [414] [415]. CRISPR arrays contain previously assimilated protospacer fragments, now called spacers (Fig. 4.45a), which are stored as genetic memory of the exogenous invasion by conferring acquired immunity, and are arranged in alternation with 21-48 bp partially-palindromic direct repeats (DRs); new spacers are usually inserted at the 5' end of the array, downstream a CRISPR leader sequence which act as a promoter [416]. During subsequent immune reactions following the invasion of the same foreign genetic material, the transcribed CRISPR locus is processed by Cas proteins or RNase III into CRISPR RNAs (crRNAs); these short RNA molecules include a spacer and part of the flanking DRs sequences that form a scaffold secondary structure. The crRNA guides a Cas protein complex with endonuclease activity to its complementary sequence in the invading nucleic acids, resulting in their

silencing [415]. The crRNA distinguishes the invading protospacer from the self CRISPR spacer thanks to the presence of the DR-derived secondary structures in the crRNA, and for the absence of PAMs [417].

Several thousands of CRISPR-Cas systems, classified in two classes, 6 types and many subtypes, have been identified in 45% of all bacterial and 84% of all archaeal genomes [418], each characterised by a specific set of genes and immunity mechanism [419]. Types I, II, and III systems are the most prevalent in both bacteria and archaea, and are differentiated by the presence of the signature effector genes *cas3*, *cas9*, or *cas10*, respectively, which have endonuclease activity [420].

The analysis of *G. diazotrophicus* genome carried out in this study through software such as CRISPRCasFinder [421] revealed three CRISPR-Cas systems: a type I-C system, a type II-C1 system, and a type I-E system. While the type I-C and II-C1 systems were identified in *G. diazotrophicus* AZ0019 as well as in both publicly available *G. diazotrophicus* Pal5 genomes (Fig. 4.42), the type I-E system could only be located in Pal5 chromosome but not in the AZ0019 one, and will not be discussed further. The CRISPR arrays of both the I-C and II-C1 systems were found to be identical between *G. diazotrophicus* AZ0019 WT and *G. diazotrophicus* AZ0019 *nifD*$^{-}$, indicating that no spacer was assimilated in the mutant strain's genome during the transformation and homologous recombination process. This finding, along with the high double recombination efficiency obtained using the optimised protocol for the *Gd_nifHDK::GUS* strain creation (Fig. 4.41) suggest that the CRISPR-Cas system may not be instrumental in blocking invading DNA material transferred via conjugation. In fact, native CRISPR systems have been considered unlikely to act as a major barrier to artificial DNA transformation, as the presence in the host genome of endogenous spacers targeting the conjugated plasmid is improbable [399].

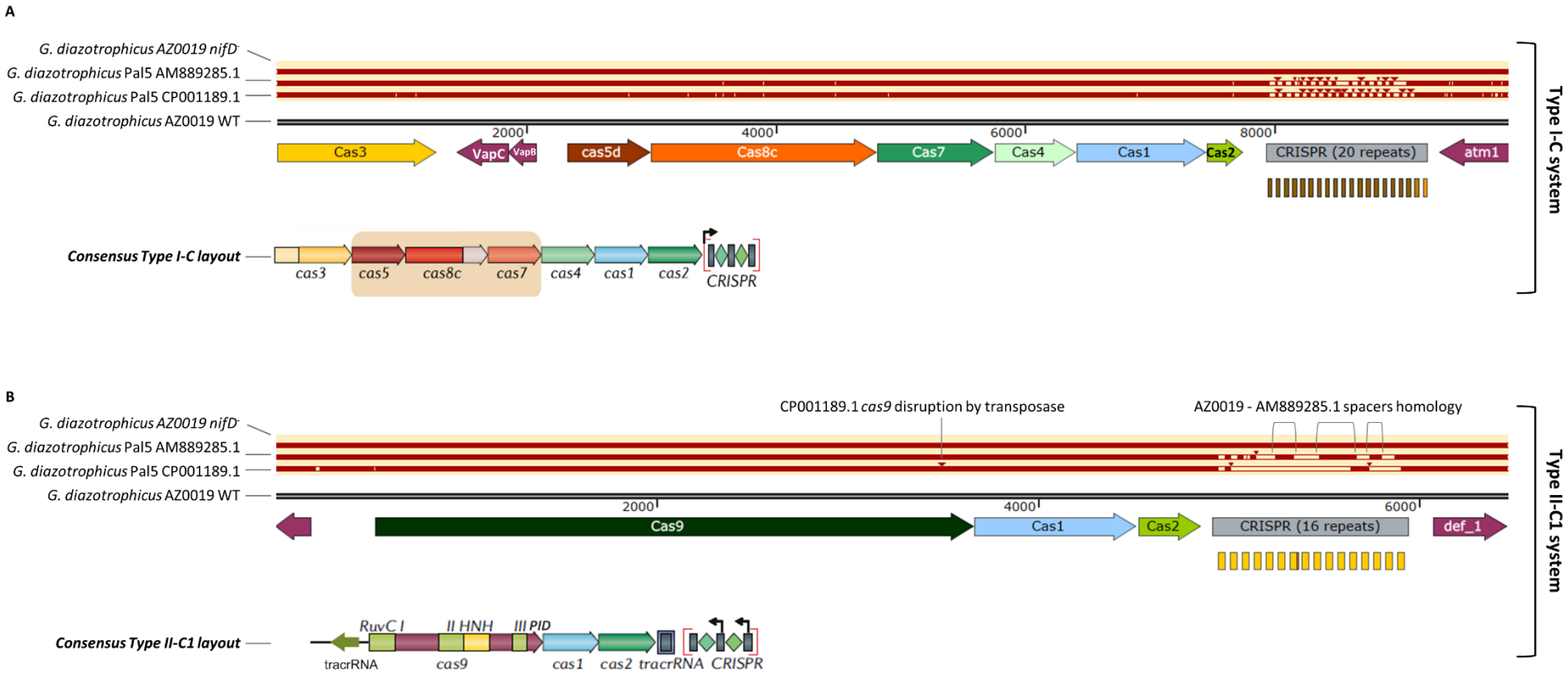

A
G. diazotrophicus AZ0019 nifD-
G. diazotrophicus Pal5 AM889285.1
G. diazotrophicus Pal5 CP001189.1
G. diazotrophicus AZ0019 WT
2000
4000
6000
8000
Cas3
VapC
VapB
cas5d
Cas8c
Cas7
Cas4
Cas1
Cas2
CRISPR (20 repeats)
atm1
Consensus Type I-C layout
cas3
cas5
cas8c
cas7
cas4
cas1
cas2
CRISPR
Type I-C system
B
CP001189.1 cas9 disruption by transposase
AZ0019 - AM889285.1 spacers homology
G. diazotrophicus AZ0019 nifD-
G. diazotrophicus Pal5 AM889285.1
G. diazotrophicus Pal5 CP001189.1
G. diazotrophicus AZ0019 WT
2000
4000
6000
Cas9
Cas1
Cas2
CRISPR (16 repeats)
def_1
Consensus Type II-C1 layout
RuvC I
II HNH
III PID
tracrRNA
cas9
cas1
cas2
tracrRNA
CRISPR
Type II-C1 system

Fig. 4.42. Visual representation of the type I-C (A) and type II-C1 (B) CRISPR-Cas systems found in G. diazotrophicus AZ0019 genome. The two systems from AZ0019 are aligned against their homologous regions from the two publicly available Pal5 genomes and the G. diazotrophicus AZ0019 nifD- strain. A continuous red bar indicates 100% sequence identity; a gap in the red bar indicates misalignment or mismatch; small red triangles on top of the red bar indicate the presence of a sequence absent in the reference AZ0019 genome. The alignment was generated with the SnapGene software. In the type I-C system, an alternation of short homologous fragments (corresponding to the DR) and gaps (corresponding to the diverse spacers) is present between the three genomes. In the type II-C1 system, larger homologous regions between AZ0019 and Pal5 CRISPR arrays are shown. The AZ0019 WT and nifD- sequences show 100% identity. The AZ0019 CRISPR-Cas systems layout are shown in comparison to their consensus architectures as classified and adapted from Makarova et al. [419]. *The HNH domain and the three RuvC subdomains of the Cas9, with endonuclease activity, are shown. The crRNA transcription direction is indicated as a black arrow. Note that the two possible but mutually excluding arrangments of the tracrRNA are displayed.*

To the best of the current knowledge, there have been no prior investigations into the CRISPR systems of *G. diazotrophicus*. In this work, the endogenous CRISPR-Cas loci as well as the artificial Cas9 genome editing method were investigated to explore the potential of this tool for *G. diazotrophicus* mutagenesis.

4.2.3a Native CRISPR/Cas I-C system *in silico* characterisation

The type I-C system, which is the most widespread among bacteria, was found in *G. diazotrophicus* to be composed of the canonical set of seven genes plus a *vapBC* toxin-antitoxin (TA) operon, nested within the I-C cluster and transcribed in opposite orientation (Fig. 4.42a). This widespread bi-cistronic TA system is known to be involved in bacterial environmental adaptation by balancing a ratio of translation-inhibiting VapC toxin, expressed in unfavourable conditions to induce a "energy saving" state, and the antitoxin VapB, which counteracts VapC in normal growth conditions [422]. TA systems, which can also promote enhanced plasmid maintenance, have occasionally been found associated with CRISPR systems, and have been proposed to increase the stability of local chromosomic DNA regions that might otherwise be liable to loss [423]. Recently, a TA operon was reported for the first time to prevent the loss of CRISPR-Cas loci by making them addictive to the host cell [424], suggesting that similar mechanism may occur in *G. diazotrophicus* I-C system. The *cas1* and *cas2* nucleases-integrases,

almost ubiquitous in all CRISPR-Cas types, are involved, along with *cas4* (often fused with *cas1*), in PAM recognition and protospacers cleavage and insertion into the CRISPR array during the immunisation phase [425] [426]; the Cas5d subunit (where "d" stands for *D. vulgaris*) serves as an endoribonuclease for pre-crRNA maturation instead of the typical type I RNA endonuclease Cas6 [427]; the Cas8c subunit (possibly nesting an internal RBS at the C terminus which encodes a separate small subunit Cas11c [428]) is responsible for PAM recognition, initial dsDNA unwinding and non-target strand (NTS) stabilisation during the R-loop formation [429]; the backbone subunits Cas7 form a caterpillar-like heptamer stretching along the heteroduplex to accommodate the annealing of the DNA target strand (TS) to crRNA [429] (Fig. 4.43a). Together, these proteins form the crRNA-guided surveillance complex "Cascade/I-C" that can pair with complementary foreign DNA target sequences and trigger their degradation [430]. The NTS displacement following the annealing of the crRNA with the TS, promotes a Cascade conformational change and creates an R-loop which is targeted by Cas3, the effector 3'-5' ssDNA helicase-nuclease enzyme; this protein nicks the NTS of the invading DNA, generating a single strand break (SSB), and subsequently unwinds and processively degrades the target protospacer in 5'-3' direction [431] [430] [432] (Fig. 4.43a). The TS is also eventually degraded by Cas3, although the exact mechanism remains unclear [433]. Differently to the most renowned type II Cas9 systems, the PAMs recognised by Cas3 are located upstream the protospacer, and the enzyme nicks the NTS complementary to the PAM identified on the TS [434] [435] (Fig. 4.43a). In the extensively studied type I–E CRISPR-Cas system of *E. coli* K12, Cascade recognises a 3'-TAC-5' or 3'-TTC-5' PAM in the TS [436] (although other PAMs are tolerated [437]) and a mature 61 nt crRNA, including a 32 nt spacer, anneals to the TS [438]; the protospacer is then nicked by Cas3 between the 7th and 11th nucleotide into the NTS [431] [434].

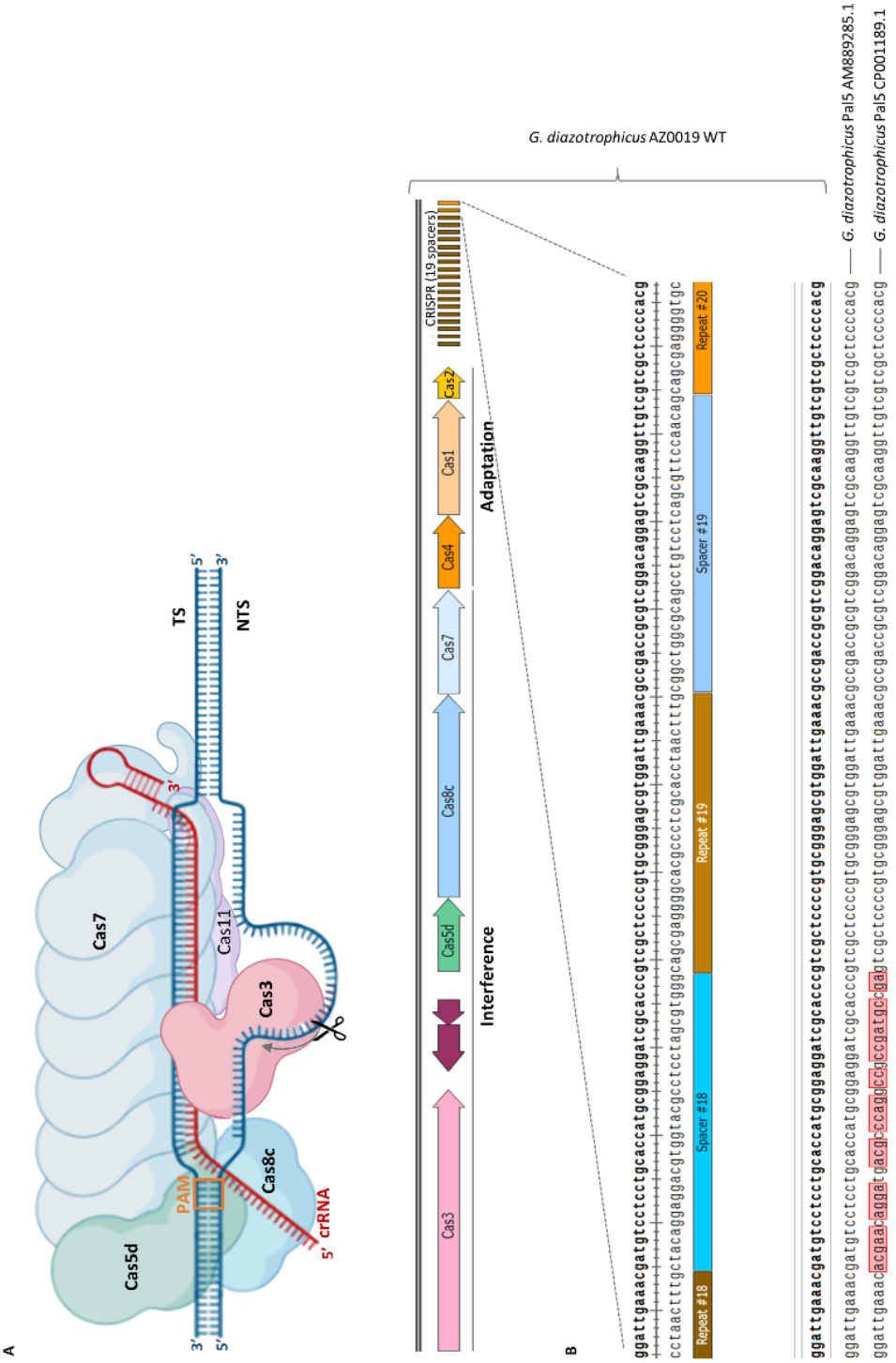


*Fig. 4.43. Visual representation of the type I-C CRISPR-Cas system of G. diazotrophicus. (**A**) Hypothetic I-C interference mechanism, adapted from* [433] [439] [429]. *The Cas8 subunit takes contact with the PAM and initiate the cascade complex recruitment as the dsDNA is unwound and a single crRNA anneals with the TS. Seven Cas7 and two Cas11 subunits stretch along the duplex from the 5' to the 3' "handle" of the crRNA. The Cas3 further contributes to the R-loop formation by NTS displacement and nicks the NTS strand, subsequently proceeding to its degradation in 3'-5' direction (grey arrow). (**B**) Sequence comparison of the last (#19) and penultimate (#18) spacers in AZ0019 vs AM889285.1 and CP001189.1; the nucleotides highlighted in red represent a mismatch. The illustration was created with BioRender.com.*

In this study, the CRISPR loci of the publicly available genomes of the Pal5 strain and the sequencing data from the AZ0019 strain were analysed through the CRISPRCasFinder online tool [440]. The number of the spacers present in the I-C CRISPR locus of *G. diazotrophicus* varied greatly among the three genomes analysed. The AM889285.1 I-C array was found to contain 29 spacers, while the CP001189.1 sequence showed 48 + 11 spacers, interrupted by a transposase gene. In the AZ0019 strain, both WT and *nifD*$^{-}$, 19 spacers were identified. The length of the spacers varied between 33 and 37 bp among the three I-C loci analysed, in accordance with the 32-44 bp length of the other known type I system spacers [441]. In contrast, the 32 bp DRs sequence in the array showed 100% identity in the three genomes (5'-GTCGCTCCCTGTGCGGGAGCGTGGATTGAAAC-3'), including a characteristic sequence variation in the last two repeats, occurring in all the three strains regardless of the total DR number (penultimate DR: 5'-GTCGCTCCCCGTGCGGGAGCGTGGATTGAAAC-3'; last DR: 5'-GTCGCTCCCCACGCGGAAGCGGGGATTAAAAC-3'). The number of DRs, as expected, equalled the spacers number + 1, due to the duplication of the first 5' repeat downstream the leader sequence after each new spacer integration [414]. Although no strict bioinformatic analysis was carried out relatively to the DRs, the 32 bp sequence showed high identity with other type I-C DRs, including the signature "ATTGAAA(C/G)" motif at the 3' end of the DR (Fig. 4.48c, d) [442]; this analogy suggest a similar crRNA processing mechanism (see section 4.2.3d), as expected between I-C systems orthologs.

The majority of spacer sequences in the type I-C array showed no significant identity between the three genomes available, apart from AZ0019 WT and *nifD*$^{-}$, which exhibited 100% identity between each other. The only exception was the last spacer (i.e. the oldest integration event), which was identical in AZ0019, AM889285.1 and CP001189.1 regardless of the total number of spacers. Similarly, the penultimate spacer showed 100% identity between AZ0019 and AM889285.1, but diverged in CP001189.1 (Fig. 4.43b).

This finding reveals an active CRISPR array which, from a last common spacer, diverged overtime among the strains. This CRISPR divergence among closely related strains is not surprising, since, due to the stochasticity of the protospacer acquisition process, the same bacterial population is likely to

generate a diverse set of spacers against the same threat [443]. Early analyses of CRISPR arrays belonging to multiple bacterial species reported that 65% of the spacer homologs correspond to bacteriophages or conjugative plasmids, while the remaining 35% to chromosomal sequences of other bacteria [444]. To find protospacer sequences targeted by *G. diazotrophicus* I-C CRISPR array, the spacers of AZ0019 were blasted with the nucleotide collection database of NCBI through the BLASTn alignment tool [445] and via specific bioinformatic tools for CRISPR analyses, such as CRISPRCasFinder [421] and CRISPRTarget [446], using the databases PHAGE, PHAST and REFSEQ_PLASMID (containing sequences from bacteriophages, prophages and bacterial plasmids, respectively). In all the aforementioned tools, the search parameters were left at their default settings or lowered in stringency when zero hits were obtained. Regardless of the search parameters, a hit was only considered when showing ≥ 80% sequence identity with the spacer.

In addition to various hits targeting phage and prophage sequences, the matched bacterial plasmid sequences belonged to the species *Serratia marcescens* (a plant-associated microbe with phytopathogen activity [447]), *Rhizobium bangladeshense* and *Ensifer adhaerens* (a bacterial predator from the *Rhizobiales* family with PGP capabilities [448] [449]); the majority of the hits, however, targeted different strains of *Ralstonia solanacearum* (Table 3.6). Interestingly, *G. diazotrophicus* has been reported to have antagonistic effect against this phytopathogen [261]. Additionally, some spacers showed partial complementarity to chromosomal sequences of bacteria belonging to the species *Gordonia*, *Sphingomonas* and *Novosphingobium*, and of archaea found in highly saline environments such as *Natronomonas* and *Halorubrum*. While *G. diazotrophicus* and the targeted archaea are known to inhabit vastly different environments, making their potential encounter difficult to interpret, it is possible to speculate that the other bacterial genera found shared a similar ecological niche. For example, some *Sphingomonas* strains inhabit the rhizosphere of rice and show growth-promoting activities [450] [451] [452]; *Novosphingobium sp.*, which includes free-living, diazotrophic strains, has been frequently characterised as a plant endophyte with PGP capabilities even in sugarcane hosts [453] [454] [40].

N° (tot 19)	Repeat	Spacer	Organism description	Spacer per. Identity	3'-5' TS	Spacer alignment
1	gtcgctccctgtgcgggagcgtggattgaaac	tttgccggcctgaagcacaatatcacgaagatcaa				
2	gtcgctccctgtgcgggagcgtggattgaaac	cggtcgaatggatggagagggtgaaggccgctccg	Gordonia sp. KTR9	88%	GATCACGC	|||||| |||||||| |||||||||||||||||| ||
3	gtcgctccctgtgcgggagcgtggattgaaac	tcggcatgggaccttggatggtcagatatgacct				
4	gtcgctccctgtgcgggagcgtggattgaaac	acggtcgccacgtcggaaacgtggaaggatcggca	Sphingomonas sp. AP4-R1/Sphingomonas donggukensis strain RMG20 (x2)	80%	TCGAACTG	|||||||||||| |||||||||||||||
			Novosphingobium sp. EMRT-2	80%	GCAACCTG	|||||||||||||||||||||||||||| || |
			Escherichia phage Skarpretter	80%	CGTTGGAA	||| ||||||| ||||||| ||||| ||| |||
5	gtcgctccctgtgcgggagcgtggattgaaac	tccagatccaacgatcctcacgggttcgagcat				
6	gtcgctccctgtgcgggagcgtggattgaaac	gccggacccggccagtcctatccgatccccgacaa	Vibrio_VvAW1	80%	CACTGAAA	||||| ||| || ||||| |||||||| |||||
7	gtcgctccctgtgcgggagcgtggattgaaac	ctcgatatcgtcgcaaaccgaagactggcggcag				
8	gtcgctccctgtgcgggagcgtggattgaaac	cccgcctggacattttgtcgtggctgaagcgcct				
9	gtcgctccctgtgcgggagcgtggattgaaac	tgctccaggccggcgccgacatccacgccgttcggaa	Serratia marcescens strain 9580 map unlocalized plasmid p9580-818 tig00000287	81%	CCTAGTCG	| ||||||||||||||| |||||||| |||||
			Rhizobium bangladeshense strain PLR8-1a	80%	ACTTTTTT	|| |||||||| |||||| | ||| | || || |||
			Gemmatirosa kalamazoonensis strain KBS708	80%	ACGGGCCG	|| |||| ||| |||||| ||||||| ||||||
			Vibrio_VvAW1	95%	AAGGTAAG	|||||||||||||| ||||||||||| ||||||||||
10	gtcgctccctgtgcgggagcgtggattgaaac	aagggtggtttaatcgagcaaatgggagcggagc				
11	gtcgctccctgtgcgggagcgtggattgaaac	acgggccggccgccggttgcgaccaaagggtcgac				
12	gtcgctccctgtgcgggagcgtggattgaaac	ccggagggagcagaatgaccgacgaaacctggcc				
13	gtcgctccctgtgcgggagcgtggattgaaac	ccggccgacatgctcgacgttgctccgcttctgga	Ralstonia solanacearum (x26)	80%	ACCTGCCG	| ||||||||||||||| |||||| |||| ||
			Ensifer adhaerens strain Casida A plasmid pCasidaAB	80%	CGCCCGAC	|| |||| |||| ||| ||||| |||||||||
			Erwinia phage pEa_SNUABM (x 7)	80%	GTTAGCAT	| ||||||||||||||| ||| | || |||| ||
14	gtcgctccctgtgcgggagcgtggattgaaac	aaggcgtggcgccatcacccggtgtcgcgggcagt				
15	gtcgctccctgtgcgggagcgtggattgaaac	ctgacgattccgatgaattggccgccattgctc	Enterobacter sp. LU1 plasmid unnamed	82%	AACGATAA	||| ||||||| ||||| |||||||||| |
16	gtcgctccctgtgcgggagcgtggattgaaac	cgggatcgtcagaatcacagcgtccgcgccacca	Natronomonas salina strain YPL13	88%	TTGGTCGC	||||| ||||||||||||| |||||||
			Shewanella phage vB_Sb_QDWS (x2)	82%	AGCTAGAG	|||||||| || ||||| ||||||| ||| |||
			Gordonia phage (x3) Delrey21, Verity, DoctorFroggo)	80%	TCGCCATA	|| ||||| ||| | ||||||| ||||| ||||
17	gtcgctccctgtgcgggagcgtggattgaaac	tgtgatcaatctctcgatgcgctcgacacagga				
18	gtcgctccctgtgcgggagcgtggattgaaac	gatgtcctcctgcaccatgcggaggatcgcaccc	Ralstonia solanacearum (x32)	80%	TTCCGCTG	|||| |||||||| | |||||| | ||||| ||
			Pseudo_F10_NC_007805(51) (x3)	80%	CGTACGTC	| |||||||||| |||||||| ||||| |||
19	gtcgctcccgtgcgggagcgtggattgaaac	gccgaccgcgtcggacaggagtcgcaaggttgtc				

Table 3.6. List of spacers and repeats of the type I-C CRISPR system of G. diazotrophicus AZ0019. The percentage identity (Spacer per. Identity) and the alignment with the closest characterised spacer (a space between bars indicates a mismatch), as identified by the CRISPRTarget software (see section 4.2.3d) are shown, along with the putative corresponding PAMs in the target strand (TS) in 3'-5' direction. The cutoff score of CRISPRTarget for alignment identification was set at 20. The colour of the identified organism, which yielded a match by aligning with G. diazotrophicus spacers, corresponds to the database in which the identification was made; blue = blastn; black = REFSEQ_PLASMID/plasmid.fa; red = PHAGE/phage.fa; green = PHAST/PHAST.fa.

Similarly, the spacers from the AM889285.1 strain aligned against plasmids from the rice-PGPB *Burkholderia vietnamiensis* [455], the sugarcane-PGP diazotroph *Azospirillum brasilense* [456], as well as the phytopathogens X*anthomonas citri*, *Ralstonia solanacearum* and other halophilic archaea (see Supplementary Table 1). Previous studies have documented the antagonistic and biocontrol capacity of *G. diazotrophicus* against *Xanthomonas* spp. in sugarcane [407] [457]. Since some of these bacterial genera and species co-occur in certain environments and may therefore interact with each within their common plant hosts, it is intriguing to speculate that these analyses may provide potential hints regarding *G. diazotrophicus* environmental and functional associations with other microorganisms, such as antagonistic interactions or competition for the same ecological niche. However, it should be noted that these findings are not conclusive and require further experimental validation, since the bioinformatic analysis of spacer sequences is still challenging due to the elusiveness of their alignments in available databases [458].

4.2.3b Native CRISPR/Cas II-C system *in silico* characterisation

The more compact type II-C1 system [419] is only composed of the *cas1* and *cas2* nucleases-integrases and the large effector Cas9 endonuclease protein (Fig. 4.42b). Type II Cas9s, especially from the II-A family, have been extensively characterised in other bacterial species and successfully repurposed as a genome editing tool [459]. Differently to most CRISPR-Cas systems, in which the whole CRISPR locus is transcribed from the leader region as a single pre-crRNA transcript and is successively processed into individual

crRNAs, type II-C arrays seem to possess internal, independent promoters within each DR sequence, yielding sets of pre-crRNAs of varying length [460] [461]. This finding, which was subsequently experimentally validated, originated from the discovery of a -10 box element nested in the downstream end (relatively to the *cas* genes transcription direction) of each DR of *Neisseria* spp. and *Campylobacter jejunii* [460]. Similarly, the analyses of *G. diazotrophicus* type II-C CRISPR/Cas locus through the promoter prediction tool BPROM revealed the presence of a -10 and a -35 box within each DR (Fig. 4.44b), although no sequence identity was observed with the DRs of *Neisseria* spp.. Furthermore, another putative promoter was detected at the downstream end of the CRISPR array, following the last DR, suggesting the presence of the leader sequence; on the other hand, an obvious loop-stem structure, presumably indicating a Rho-independent transcription terminator, was identified upstream the first DR (Fig. 4.44b). These findings strongly suggest the same functional organisation of *Neisseria* spp. type II-C system [460], with independent crRNAs transcribed in opposite orientation to the *cas* genes.

The immunisation process in the type II-C system has not been fully elucidated [461], and the type II-A systems of *Streptococcus pyogenes* and *Streptococcus thermophilus* remain to date the best characterised adaptation mechanisms [462]. Although a PAM is strictly required in all II systems for recognizing protospacers in invading genetic material, the PAMs and PAM-interacting domains (PIDs) of type II-C Cas9 orthologs vary greatly even among closely related species, with long PAM sequences that can extend for up to 8 bp [461]. Longer PAMs limit the number of possible targets but are believed to increase the targeting accuracy [463].

In type II systems, during the immunity/interference phase, a "trans-activating crRNA" (tracrRNA), transcribed from a locus upstream the CRISPR array, hybridises with the pre-crRNA through a DR-derived complementary sequence (anti-DR, Fig. 4.44e, f, Fig. 4.45b): the so formed dsRNA is processed by an RNase III in association with Cas9, which cleaves the duplex leaving short overhangs at the 3′ ends [464]. However, in type II-C systems, the RNase III enzyme doesn't seem to be essential in this process [460].

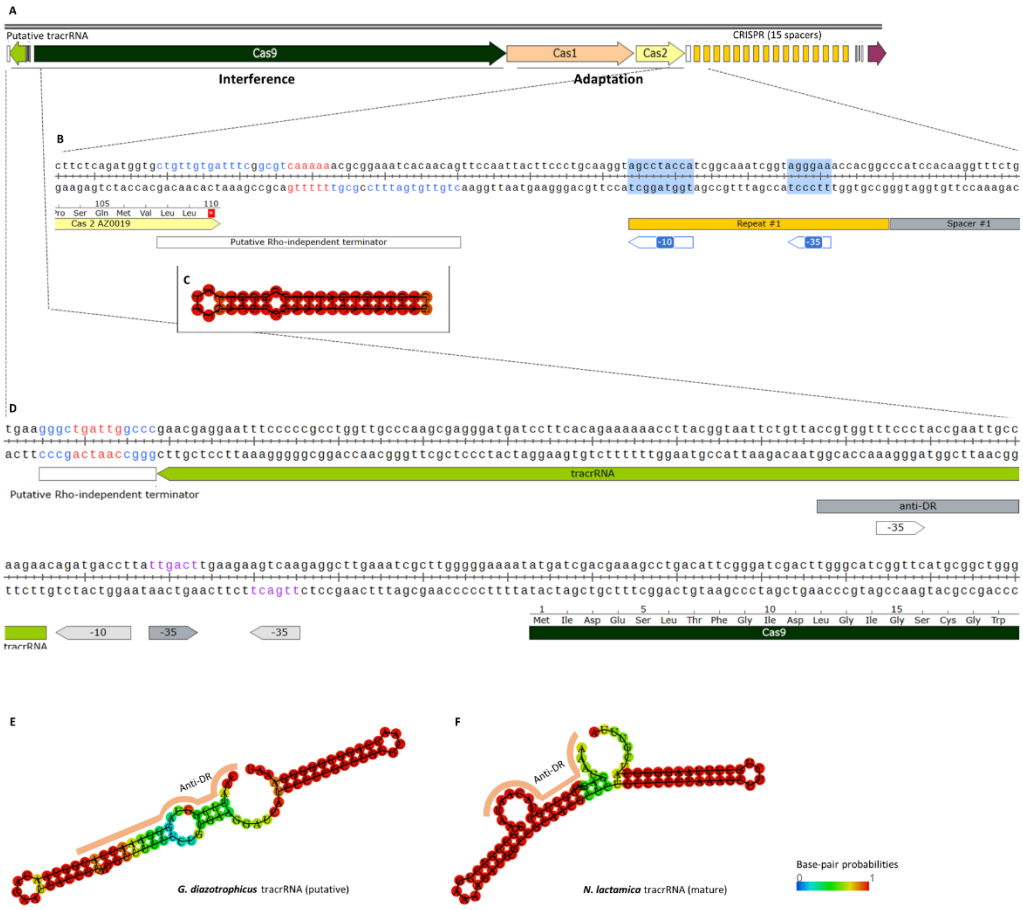


*Fig. 4.44. Visual representation of the type II-C1 CRISPR-Cas system of G. diazotrophicus AZ0019. (**A**) Locus layout. (**B**) Close-up view of the intergenic region between the Cas2 ORF and the beginning of the CRISPR array. The -35 and -10 boxes within each DR are highlighted in blue, and the orientation of the arrow corresponding to each element indicates the putative crRNA transcription direction. The putative Rho-independent terminator is depicted with blue nucleotides of the inverted repeats corresponding to the stem and red nucleotides corresponding to the loop. (**C**) Predicted 2D folding of the putative CRISPR Rho-independent terminator according to the RNAfold software* [465]. *The red color indicates a base-pair probability of 100% (see the bottom right corner for the full legend). (**D**) Close-up view of the intergenic region upstream the cas9 gene, containing: two -35 boxes in opposite orientation (purple nucleotides), with one presumably driving the cas9 expression and the other one driving the putative tracrRNA expression, together with the -10 box (light grey); the putative tracrRNA; a Rho-independent terminator delimiting the tracrRNA end, depicted with the same colour code as in (B). (**E-F**) Predicted 2D folding of the putative tracrRNA of G. diazotrophicus (assuming a 91 nt mature form ranging from the anti-DR to the terminator) compared to the experimentally validated II-C tracrRNA of N. lactamica. The anti-DR in highlighted in pink.*

During the pre-crRNA maturation the trimming of the 5’ end of the crRNA reduces the length of the spacer sequence to 20 nt in type II-A systems or 22-24 nt in the known type II-C systems which have been investigated and validated for genome editing [461]. The ribonucleoprotein complex, formed by the mature crRNA:tracrRNA duplex and Cas9, recognises the PAM downstream its complementary protospacer sequence through the Wedge and

PID domains, and enable a dsDNA crRNA-guided cleavage of the TS and NTS through a HNH (His-Asn-His) and three RuvC endonuclease domains, respectively [466] [467] (Fig 4.42b, 4.45b). While type II-A Cas9 of *Streptococcus pyogenes* (spCas9) only recognises the NTS PAM [468], type II-C Cas9 require both DNA strands to recognize PAM and trigger cleavage [469]. The Cas9 catalyses a blunt double-stranded DNA break (DSB) between the third and fourth nucleotide counting from upstream the PAM-proximal end of protospacers [470] (Fig. 4.45b); the same mechanism was described for the II-C Cas9 of *Neisseria* spp. [471].

The analyses of *G. diazotrophicus* type II-C CRISPR/Cas locus revealed the presence of a partial anti-DR sequence (a 24 bp sequence, excluding the DR - 10 box) upstream the *cas9* gene (Fig. 4.44d). Furthermore, such element was encased between a putative promoter (composed of two – 35 boxes and one -10 box) and a Rho-independent terminator, as predicted by the ARNold tool [472] (Fig. 4.44d). This configuration strongly hints at the presence of a tracrRNA gene, transcribed in opposite orientation to the *cas* genes and arranged almost exactly as previously described in *Neisseria* spp. [460]. The two -35 boxes are arranged as inverted repeats, implying that one is driving the tracrRNA expression in "antisense" direction (relatively to the *cas* genes), while the other is possibly driving the *cas9* gene "sense" transcription. Although the precise location of the tracrRNA transcription starting site (TSS) cannot be determined without experimental validation, if the TSS is assumed to lie between the -10 box and the anti-DR element (as demonstrated in *Neisseria* spp.), a 102 to 108 bp sequence would be transcribed before encountering the terminator; intriguingly, the unprocessed form of the tracrRNA in *Neisseria* was shown to be 107 nt long [460], further corroborating the nature of this putative *G. diazotrophicus* tracrRNA. Moreover, the comparison of the predicted secondary structure of both species' tracrRNAs through the RNAfold software [465] revealed a similar conformation, with two loop-stem motifs flanking the anti-DR element (Fig. 4.44e, f), which was also predicted in the other characterised type II-C systems [461].

N° (tot 19)	Repeat	Spacer	Organism description	Spacer per. Identity	5'-3' NTS	Spacer alignment (5'-3')
1	agcctaccatcggcaaatcggtagggaaaccacggc	ccatccacaaggtttctgaatgcgcgctgg	SEQ_15774_2_2739399-2765770_NC_011365_PHAGE_Bordet_1	99%	CCGGGCAA	|||\

Table 3.7. List of spacers and repeats of the type II-C CRISPR system of G. diazotrophicus AZ0019. The percentage identity (Spacer per. Identity) and the alignment with the closest characterised spacer (a space between bars indicates a mismatch), as identified by the CRISPRTarget software (see section 4.2.3d) are shown, along with the putative corresponding PAMs in the non-target strand (NTS) in 5'-3' direction. The cutoff score of CRISPRTarget for alignment identification was set at 20. PAM marked in red were not considered for the PAM consensus analyses (see section 4.2.3d). The colour of the identified organism, which yielded a match by aligning with G. diazotrophicus spacers, corresponds to the database in which the identification was made; blue = blastn; black = REFSEQ_PLASMID/plasmid.fa; red = PHAGE/phage.fa; green = PHAST/PHAST.fa; purple = IMGVR; orange = REFSEQ_ARCHAEA; grey = REFSEQ_VIRAL.

The type II-C clade of the Cas9 family is considered to include orthologs with naturally higher fidelity compared to other Cas9 variants [461], and in the last decade it has therefore started to be investigated and applied [471] as a candidate to mitigate the relatively high off-target rate of the spCas9 [459].

The type II-C Cas9 ORF of *G. diazotrophicus* (gdCas9) was found to be 3141 bp long (1047 aa), confirming the compact size that characterises II-C Cas9s (<1100 aa) compared to the widely employed spCas9 (1368 aa) [461]. This can be an obvious advantage in *in vivo* applications utilising vectors with limited cargo capacity, such as adeno-associated virus vectors [473]. In the CP001189.1 genome, the *cas9* ORF was interrupted by a transposase (Fig. 4.42b), a phenomenon believed to occur to escape self-targeting [463].

Similarly to what observed in the type I-C system of *G. diazotrophicus*, a different number of spacers and DRs was found in the three genomic sequences: the analyses revealed 11 DRs/10 spacers in the AM889285.1 genome, 5 DRs/4 spacers in the CP001189.1 genome, and 16 DRs/15 spacers in the AZ0019 strains, both WT and *nifD*$^{-}$ (Fig. 4.42b). The AZ0019 WT and *nifD*$^{-}$ arrays exhibited 100% identity between each other.

All the spacers were found to be 30 bp long. This is consistent with the 30 bp spacers found in the best characterised II-C system of *Neisseria* spp. [460]. Another common characteristic with *Neisseria* spp. was the spacer arrangement, with conserved spacers that are shared among the three *G. diazotrophicus* strains being enriched at the downstream end of the array (relative to the to the *cas* genes direction of transcription) (Fig. 4.45a). This architecture suggest that new spacers are integrated at the opposite end of the

array compared to the putative leader sequence, which is contrary to what reported in the majority of the other CRISPR systems [420]. While only one spacer was shared between AZ0019 and CP001189.1 in the type II-C CRISPR array, AM889285.1 and AZ0019 shared a large portion of the locus (Fig. 4.42b, 4.45a), confirming AZ0019 to be phylogenetically closer to AM889285.1 than to CP001189.1, as suggested by the genome assembly (Fig. 4.25). Some of the bacterial genomes or plasmids targeted by the spacers with >80% identity included PGP diazotrophs from the rhizobia family such as *Mesorhizobium onobrychidis* [474] or *Rhizobium acidisoli* strain FH23, recently isolated from common bean nodules in Mexico [475], as well as the noduling diazotroph *Cupriavidus necator* [476], some halophilic archaea and, in the case of AM889285.1, *Ralstonia solanacearum* (Table 3.7).

The DRs were found to have the same 36 nt consensus sequence in all three genomes investigated (5'-AGCCTACCATCGGCAAATCGGTAGGGAAACCACGGC-3'). The same length of 36 nt was reported in *Neisseria* spp. [460], although no sequence identity was shared between the two species, confirming the great diversity which characterise the II-C systems.

The presence of homologous regions within the three II-C1 loci and the lower number of spacers in the type II-C1 CRISPR array of all three genomes compared to the type I-C system, may suggest the former to be less active than the latter, with spacer being added at a slower rate or with less efficiency. The *cas9* gene disruption by transposase integration in the CP001189.1 genome may reinforce the speculatively secondary role of this system in *G. diazotrophicus*.

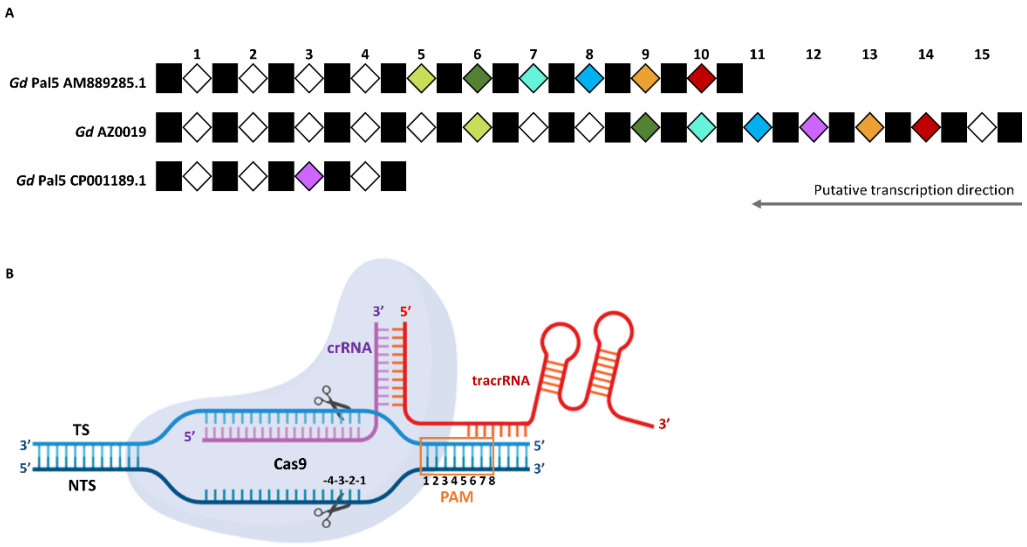


Fig. 4.45. (A) Schematic representation of CRISPR II-C loci from the three G. diazotrophicus genomes. Repeats and spacers are shown as rectangles and diamonds, respectively, with white unique spacers and color-coded common spacers. The spacers are numbered relatively to the cas gene orientation, i.e. opposite to the putative crRNA and tracrRNA transcription direction (grey arrow). (B) Hypothetic II-C1 interference mechanism, adapted from [461] [477] [460] [471]. *Upon the crRNA-tracrRNA-guided recruitment of Cas9 on the targeted protospacer, allowed by the recognition of a 8 bp PAM, an R-loop is formed along the annealing between the 22-24 nt spacer of the crRNA (purple) and the corresponding protospacer TS, while the anti-DR portion of the crRNA hybridises in a stem structure with the tracrRNA (red). A DSB is carried out between the -3 and -4 nt upstream the PAM (numbered from 1 to 8). The illustration was created with BioRender.com.*

4.2.3c Transient CRISPR/Cas9 system development

Among the various types of CRISPR/Cas systems and thousands of *cas9* genes discovered, the Cas9 protein from the type II-A systems of *Streptococcus pyogenes* (spCas9), from which this gene was first identified, has emerged as the best understood and most widely used system for genome editing [399] [461] [477]. When expressed in trans, spCas9 can be guided on its target by a programmable single guide RNA (sgRNA), which was designed as the fusion between the type II crRNA and tracrRNA [466]. In order to recognise and bind to its target site, the spCas9-gRNA complex requires a 5'-NGG-3′ PAM on the NTS [478], the presence of which allows the cleavage of the DNA three nucleotides upstream of the PAM element [466] [479].

While in eukaryote organisms a DSB can be repaired by either non-homologous end joining (NHEJ, which often results in random indels) or HR-

directed repair, only a quarter of prokaryotes are estimated to harbour a NHEJ machinery, which involves the Ku and LigD proteins [480]. Consequently, a DSB in a bacterial chromosome is either quickly repaired via RecA-mediated HR or proves lethal to dividing cells [481], resulting in a powerful counterselection system against non-edited cells [482]. Interestingly, the analysis of *G. diazotrophicus* AZ0019 carried out in this work revealed a bicistronic operon harbouring the two NHEJ-associated *ku* and *ligD* genes (annotated in AM889285.1 as GDI0168 and GDI0169, respectively); this suggest that a HR-mediated DSB repair mechanism may be competing with the NHEJ machinery.

To date, the use of CRISPR as a genome editing tool has been mainly tested, optimised and employed on eukaryote systems; conversely, its implementation in bacteria remains relatively limited and has not consistently yielded favourable outcomes [433] [482] [463]. CRISPR-mediated DSBs are believed to undergo less efficient repair in prokaryotes, due to the need of maintaining an effective immune reaction against exogenous DNA [483]; this, along with Cas9 off-target cleavage and transient binding of random PAMs, may explain the high lethality rate reported in prokaryotic cells transformed with self-targeting crRNAs of active systems or even spCas9 with no sgRNA [433].

Therefore, considering the aforementioned limitations, the practicality of a CRISPR-mediated genome editing strategy was first tested through the use of the popular spCas9 system. In light of the relatively high recombination efficiency obtained by optimised non-replicative vector conjugation (Fig. 4.41), no heterologous recombinase gene was introduced in the system, although such strategy has been previously adopted to improve Cas9-mediated bacterial mutagenesis [482]. In order to compare the efficiency of this strategy with the previously tested mutagenesis systems, the *nifHDK* locus was chosen again as a target for the insertion of the same GFP-Sm^R cassette used for the *Gd_nifHDK::GFP* strain construction. The suicide plasmid pSW23t_NifK::GFP-Sm^R was used as a backbone for assembling an all-in-one non-replicative spCas9 plasmid system which could couple the benefit of the optimised conjugation protocol and the putative advantages of CRISPR-

mediated genome editing. Including the recombination cassette in the same plasmid harbouring the sgRNAs, is generally regarded as the most efficient strategy [483]. In particular, three different vectors were assembled (Fig. 4.47), all including the pSW23t_NifK::GFP-Sm^R backbone (Fig. 4.40), the spCas9 (as in Jiang et al. [484], Addgene plasmid # 62225) and two sgRNA composed of a 20 nt guide spacer and the scaffold sequence as in Wang et al. [484] [485] (Addgene plasmid # 62226). Some unique restriction sites were introduced in the plasmid to allow subsequent modifications (Fig. 4.46a, in red), in particular around the Cas9 promoter, around the recombination cassette and close to the sgRNAs for streamlined guide protospacer substitution. Two sgRNA, targeting opposite DNA strand in close proximity, were employed in order to enhance the probability of Cas9-induced DSB in the designated region. The two sense and antisense 20 nt guide spacers were designed to anneal in the chromosome astride the conjunction of *nifK* and the *nifENXQ* operon promoter, in order to prevent self-targeting in the vector homology arms (Fig. 4.46a, b). The guide sequences were designed with the software CHOPCHOP [486] and CCTop [487].The "sense" sgRNA (sgRNA1) was put under the control of the $P_{A1/03/04}$ promoter, while the "antisense" sgRNA (sgRNA2) was driven by the strong synthetic promoter "J23119SpeI", which had been successfully applied before for driving sgRNA expression in *E. coli* ([484], Addgene plasmid # 62226). The selection of one promoter already validated for gene expression in *G. diazotrophicus* and one promoter validated for sgRNA expression, although in another model system, was speculated to minimise the risk of unsuccessful protospacer targeting by suboptimal sgRNA transcription. At the same time, the use of a suicide vector was hypothesised to provide enough expression to elicit the desired editing while also reducing the potential toxic effects associated with excessive Cas9 presence thanks to the limited plasmid retention in the cells.

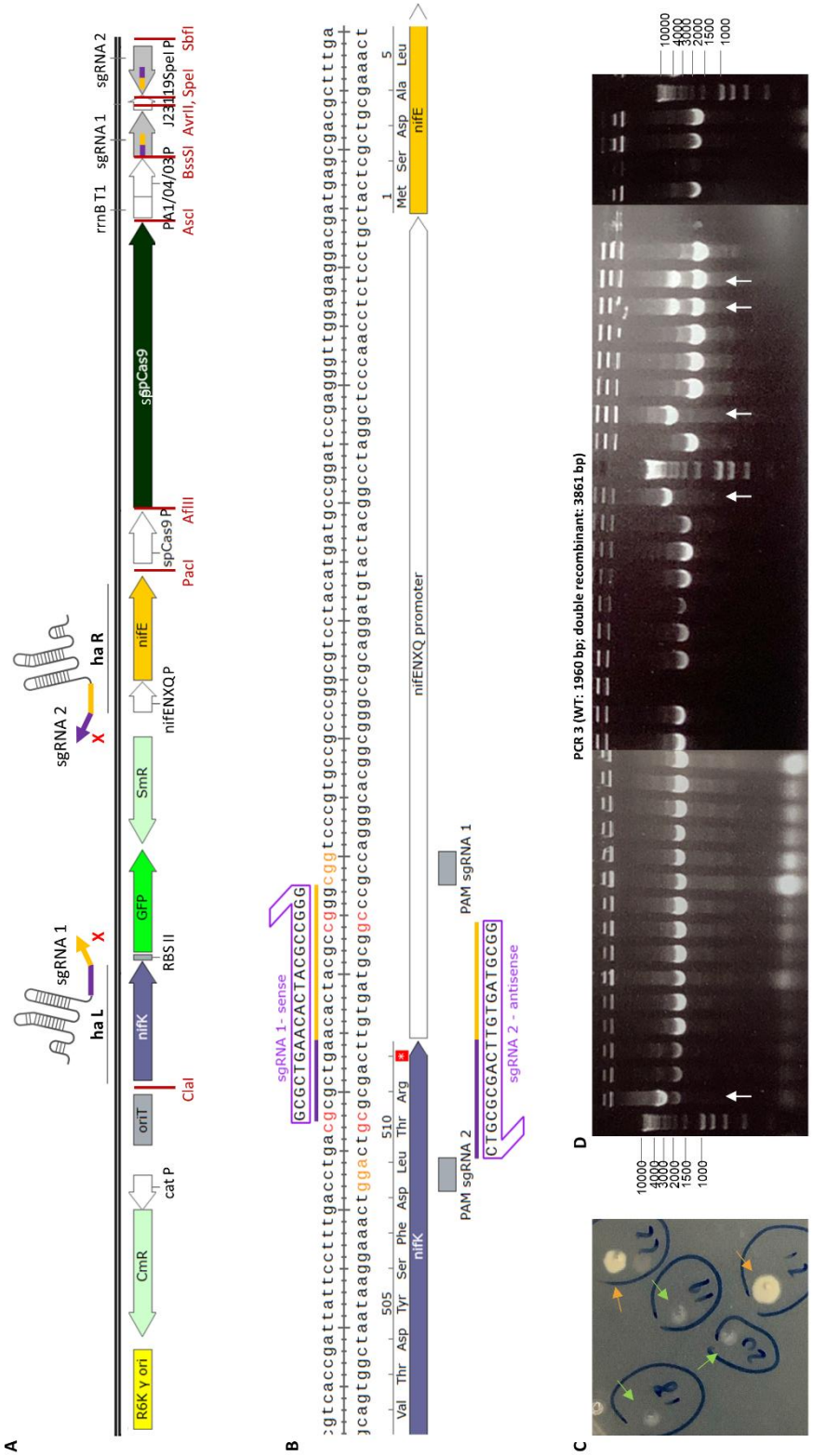
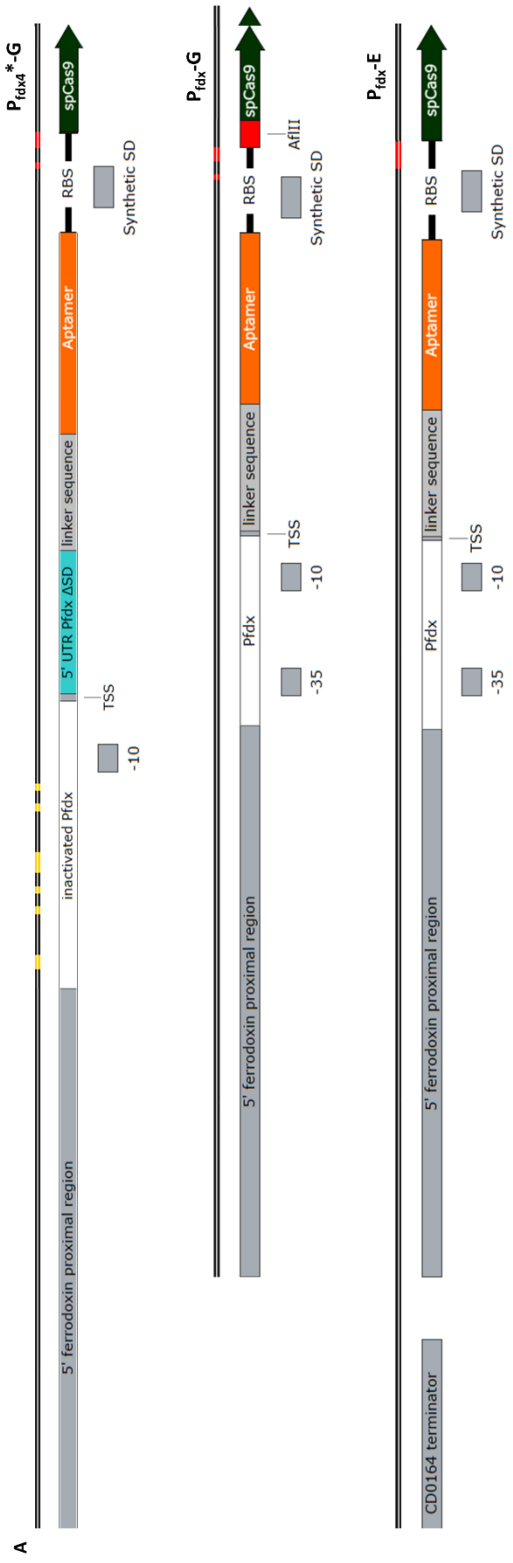


Fig. 4.46. (A) Schematic representation of the pSW23t_NifK::GFP-SmR_sg2Cas9 suicide vector. The two sgRNAs are represented with their guide protospacers (yellow/purple) which are unable to anneal (red crosses) with the two homology arms (ha, L = left, R = right), preventing self-target of the recombination cassette. The unique restriction sites inserted for downstream applications are shown in red. P = promoter. (B) Representation of the two guide protospacers target site in the chromosome of G. diazotrophicus AZ0019. The NTS PAMs are marked in yellow, while the Cas9 DSB sites (between the 3rd and the 4th nt upstream the PAM) are marked in red. (C) β2163_pSWNifK::GFPcas9 colonies (green arrows) showing an

abnormal growth compared to wild-type colonies (orange arrows). (D) Colony-PCR screening of G. diazotrophicus colonies recovered in ATGUS + Sm 100, Amp 150 after biparental filter mating conjugation with β2163_pSWNifK::GFPcas9. The primers combination "3)"is shown (see Fig. 4.40). 5 double recombinants (white arrow) were obtained out of 35 screened colonies (3861 bp band expected against 1960 bp band in wild-type loci) for both homology arms integration.

In the first vector prototype (Fig. 4.46a), named pSW23t_NifK::GFP-SmR_sg2Cas9, the Cas9 was put under its endogenous promoter form *S. pyogenes*, as in Jiang et al. [484] (Addgene plasmid # 62225). However, working with this plasmid proved problematic from the outset as both the assembly process and subsequent transformation in β2163 showed unprecedented low efficiency. Eventually, a few mutant β2163 colonies (named *β2163_pSWNifK::GFPcas9*) carrying the desired plasmid (confirmed by Sanger sequencing) were obtained, but they exhibited abnormal and slower growth, characterised by a semi-transparent phenotype (Fig. 4.46c). This finding is reminiscent of similar observations reported in other CRISPR-mediated bacterial mutagenesis studies [488] and strongly indicates the cytotoxicity of SpCas9, possibly exacerbated in the β2163 genotype. In support of this hypothesis, sequencing analysis uncovered that the colonies displaying a wild-type phenotype (as observed in terms of colour and growth, Fig. 4.46c) harboured plasmids with incomplete assembly, either entirely lacking the *spcas9* gene or containing truncated segments of it. Nevertheless, a conjugative vector transfer in *G. diazotrophicus* was attempted, applying the same conditions as in Fig. 4.40. Out of 35 PCR-screened *G. diazotrophicus* transformant colonies, 5 were found to possess the integrated cassette, indicating the presence of around 15% double recombinants (Fig. 4.46d); thus, the result suggests this technique to perform better than the simple vector conjugation (Fig. 4.40) but not as efficiently as the fully optimised conjugation protocol (Fig. 4.41). Crucially, however, subsequent attempts of further modifying the plasmid, either by restriction cloning or by HiFi assembly, were all unsuccessful, both in terms of PCR and plasmid extractions often resulting in smeared product, and in terms of poor to null transformation rates in the *E. coli* intermediates. This may be caused by a self-endonuclease activity due to the sgRNAs partially targeting the vector HAs.

To overcome such drawbacks, one of the most commonly employed cloning strategies involves the use of an inducible promoter to regulate the expression of Cas9 and restrict its residence time in the cell in order to decrease the toxic and off target effects [482]. Therefore, the vector was reassembled with the spCas9 under the control of theophylline-inducible riboswitches (RS), i.e. ligand-responsive genetic elements that sequester the RBS of the mRNA's 5'-UTR in a stem-loop structure until the ligand is added [489]. Cañadas et al. described an array of theophylline-inducible RSs giving different levels of translation repression, which were found to greatly improve the genome editing efficiency of spCas9 in *Clostridium* spp. by decreasing the enzyme toxicity [490]. The RSs are fused by default to the core region (−35 and −10) of P_{fdx}, a strong promoter of the *C. sporogenes* ferredoxin gene, and were further diversified by altering the SD sequence or other upstream promoter elements: these modifications resulted in four RS classes, sorted according to both the repression strength in the "off state" (no ligand added) and the expression level in the "on state" (ligand added) [490]. In this study, three RSs were tested for their ability to mitigate the detrimental effects of the spCas9 (Fig. 4.47a). To induce the enzyme translation, the theophylline was added at different concentrations (2, 4 or 10 mM, Fig. 4.47b) to the biparental mating PDA medium, in order to trigger the endonuclease activity as soon as the vector was delivered to the recipient cells. The first element tested, named P_{fdx4}*-G, belonged to the class of RSs showing extremely tight control in the off-state and low-to-no expression in the on-state, due to a disruptive mutation of the P_{fdx} promoter (Fig. 4.47a). Using this element allowed effortless cloning and transformation in the β2163 recipient strain, that reverted to the wild-type-like phenotype in terms of growth and colour. This confirmed that the technical difficulties previously encountered were indeed attributed to spCas9 as the underlying cause; as expected, however, no double transformant was recovered upon conjugative vector transformation, due to the complete translation suppression provided by P_{fdx4}*-G. Subsequently, the P_{fdx}-G and P_{fdx}-E RSs were evaluated, both belonging to the group provisioning moderate-to-tight translation suppression in the off-state and medium-to-high activation in the on-state, characterised by unique RBS sequences (Fig. 4.47a).



B

	β2163 wild-type phenotype	Transconjugant CFUs/plate (in ATGUS Sm 100, Amp 150)	Double recombinants
P_{fdx4}*-G	Y	2 mM Theo. ~ 60; 4 mM Theo. ≥ 1000	0/30
P_{fdx}-G	Y	2 mM Theo. ~ 60; 4 mM Theo. ≥ 1000	2/30 (2 mM); 0/30 (4 mM)
P_{fdx}-E	Y	4 mM Theo. ≥ 1000 ; 10 mM Theo. ≥ 1000	0/30

		Transconjugant CFUs/plate (in DYGS Sm 500, Amp 200, Gent 25)	
P_{fdx}-E	Y	4 mM Theo. = 0	

Fig. 4.47. (A) Schematic representation of the RSs used to substitute the native spCas9 promoter in the pSW23t_NifK::GFP-SmR_sg2Cas9 suicide vector. The different RS element are represented, including: a shared 5' sequence upstream the promoter element; the core P_{fdx} promoter region (in white), which was inactivated in the P_{fdx4}-G RS (yellow lines); a 5' UTR sequence depleted of the SD element from the native ferredoxin promoter, originally inserted in the P_{fdx4}*-G RS to allow a basal expression level (still reported as close to zero* [490]*); a linker sequence joining the P_{fdx} promoter and the aptamer element of the RS, i.e., the sensing*

component that undergoes conformational changes upon binding to the inducer molecule; a RBS, including a strong synthetic SD and some unique nucleotides (red lines) resulting in different translation efficiencies. The TSS and AlfII site, were present, are indicated. (B) Table showing the main results upon conjugative transfer of the RS-amended pSW23t_NifK::GFP-SmR_sg2Cas9 vectors. The reversion to a wild-type phenotype (as in Fig. 4.46c, orange arrows) is indicated with Y/N (Yes, No); the total number of transconjugants per plate recovered, along with the number of colonies exhibiting double recombination as determined by PCR screening, is indicated alongside the respective theophylline concentration employed in the conjugation medium.

In particular, P_{fdx}-G was reported to be leakier in the off-state while allowing higher protein expression when induced compared to P_{fdx}-E, which, in turn, was classified as tighter but more specific [490]. In addition to the sequence differences in the RBSs, the two RSs were hereto further diversified. The vector containing the P_{fdx}-G RS was depleted of one of the two sgRNA cassette, leaving only the $P_{A1/04/03}$-driven sgRNA1, in order to investigate how the recombination efficiency would be affected by a decreased guide RNA presence. On the other hand, the AflII restriction site preceding the *spcas9* gene was removed from P_{fdx}-E to prevent its potential interference with the RBS functionality; additionally, a terminator from *C. difficile* was inserted upstream the P_{fdx}-E RS to block any unwanted readthrough from upstream plasmid elements (Fig. 4.47a). Contrary to what expected, the number of transconjugants recovered in ATGUS + Sm 100, Amp 150, increased with the theophylline concentration (Fig. 4.47b); this suggested that in sublethal selection conditions *G. diazotrophicus* was putatively able to escape the spCas9-mediated counterselection, with a background bacterial population (named "escaper colonies" [482]) accounting for surviving transformants [483]. The only two double recombinants identified through PCR screening were obtained by the use of the single sgRNA, P_{fdx}-G RS-containing vector (Fig. 4.47b). Thus, considering the results observed using the RS-less vector, there seems to exist a correlation between spCas9-mediated recombination efficiency and the spCas9 expression level, with the sgRNA concentration also playing a role. Whether the poor double recombination rate and high escaper colonies occurrence was caused by suboptimal plasmid architecture, inefficient vector transfer, inadequate selection conditions or heterologous CRISPR machinery deactivation [482] (a process occasionally reported to be extremely

common [491] [492]) remains to be defined. It should be also taken into account the possibility that Ku and LigD may have played a significant role in repairing any DSBs, which could be confirmed by screening for indels in colonies exhibiting a wild-type-like band through PCR3 testing; this characteristic could transition from a drawback to a valuable tool, as previously demonstrated in a separate study [493]. However, interestingly, when the P_{fdx}-E RS-containing vector was conjugated into *G. diazotrophicus* using the optimised conjugation and selection conditions (as in Fig. 4.41), no colony was recovered in the selective DYGS (Fig. 4.47b). This finding indicates that by increasing the stringency of the transconjugant selection, the spCas9 counterselection worked as expected, leading to death of all the unedited cells. The absence of colonies, which has been reported before in Cas9-mediated bacterial genome editing [494], suggests that the double recombination event did not occur prior to the onset of spCas9 activity. As previously mentioned, it has been hypothesised that CRISPR-harbouring prokaryotes may have evolved to block the repair of Cas-induced DNA cleavage, possibly even through the action of a Cas3 [483]. It should also be taken into consideration that the endogenous type II-C CRISPR system may partially overlap with the heterologous spCas9 function, and possibly even interact with the sgRNAs, leading to unpredicted interference. Furthermore, the endogenous AZ0019 II-C spacers were found to possess 11 bp complementary to the vector haR (targeting *nifE*, spacer #7) and 14 bp to the haL (targeting Sm^R, spacer #13), which, although probably too short to guide a direct attack against the invading suicide vector, may still contribute to the system instability.

However, the Cas9-mediated genome editing strategy demonstrates potential for further improvement, for example by adjusting the expression of either the Cas9, the sgRNAs, or the plasmid's copy number, which have been previously shown to alleviate the aforementioned (see section 4.2) genome editing barriers [482]. Additionally, modulating the conjugation conditions may prove beneficial to allow sufficient time for the double recombination event to take place before the DSB-induced cell death.

Alternatively, the utilization of native CRISPR systems may provide an alternative avenue for unexplored genome editing strategies (section 4.2.3d).

4.2.3d Future prospective for Native CRISPR/Cas system in *G. Diazotrophicus*

Given the encountered complexities and ongoing optimization challenges associated with the heterologous expression of spCas9 in *G. diazotrophicus*, alternative strategies that capitalise on the host endogenous CRISPR systems were evaluated. Harnessing and repurposing the host's native CRISPR machinery have gained considerable attention, since it allows to leverage the existing cellular mechanisms for efficient genome editing without the drawbacks of exogenous Cas effectors' intrinsic toxicity and transformation difficulty in poorly genetically accessible prokaryotes [433].

In this study, the CRISPR systems of *G. diazotrophicus* were subjected to preliminary investigation to evaluate their suitability for potential future applications as genome editing tool.

The I-C system appeared particularly interesting due to the abundance of spacers and the presence of the *vapBC* TA module (see section 4.2.3a), suggesting its active involvement and significance in the bacterium physiology and environmental adaptation. The presence of a native type I system implies that all the necessary protein components are already available within the cells, and crRNAs or even entire CRISPR arrays can be processed in situ for multiplexed genome editing without additional engineering efforts. The first and often challenging step in adapting a native CRISPR system is the identification of the required PAM [463]. PAMs can exhibit species-specific differences, with varying degrees of degeneracy being tolerated from the *bona fide* sequence to provide a certain level of flexibility to the system [495]. The best characterised *E. coli* I-E system recognises at least four different PAMs (TS 3'-TTC, TAC, TCC, and CTC-5' [437] [431]), most commonly referred to as TS 3'-TTC-5' [496]. Interestingly, despite of the striking structural and

functional analogies between I-E and I-C systems [433], the type I-C Cas3 was consistently reported to require a TS 3'-AAG-5' [478] [446], as confirmed in *Desulfovibrio vulgaris* [429], *Neisseria lactamica* [497], *Bacillus halodurans* [498] and *Xanthomonas oryzae* [499]. In other words, I-C PAMs correspond to the reverse complementary sequence of the I-E PAM, possibly indicating an evolutionary divergence based on the recognised protospacer strand [500]. To uncover *G. diazotrophicus*' *bona fide* PAM, the spacers from AZ0019 and AM889285.1 genomes were blasted on CRISPRTarget against all the available databases, and a consensus sequence was sought in the 8 nt upstream the TS, numbered from -8 to -1 in 3'-5' direction (Table 3.6, Fig. 4.48a). While PAM mutations result in a broad spectrum of interference efficiencies but remain restricted by a limited range of permissible combinations, the pairing of crRNAs on the targeted protospacer showed a remarkable flexibility, with up to 13 mismatches being tolerated [496]. Hence, among the putative protospacer targets identified by CRISPRTarget, those exhibiting ≥ 80% complementarity with the spacers screened were consider significant. However, within the range of 32 to 44 bp which characterise type I spacers, a seed region encompassing the first 8-9 nt (depending on the specific type I classes) downstream of the PAM, was found to be crucial for the early crRNA-protospacer annealing and, as such, not to tolerate any mismatch, except at the +6 position [436] [441]. Therefore, the identified protospacers which showed more than one mismatch in the +1 to +9 position were discarded (Table 3.6). The WebLogo [501] in Fig. 4.48b represent the consensus sequence derived from the alignment of the first 8 bp on the protospacers' TS in 3'-5' direction (18 sequences aligned from AZ0019 (Table 3.6) and 32 from AM889285.1 (not shown)). The TS 3'-AAG-5' PAM was confirmed, although the consensus was weak, probably due to the low stringency of the bioinformatic parameters applied. Alternatively, it is possible that *G. diazotrophicus* exhibits a higher tolerance for promiscuous PAM recognition, as it was recently proposed that a *bona fide* I-C PAM may be more crucial during the acquisition stage rather than the interference stage [429] and more promiscuous during plasmid transformation than during phage infection [438].

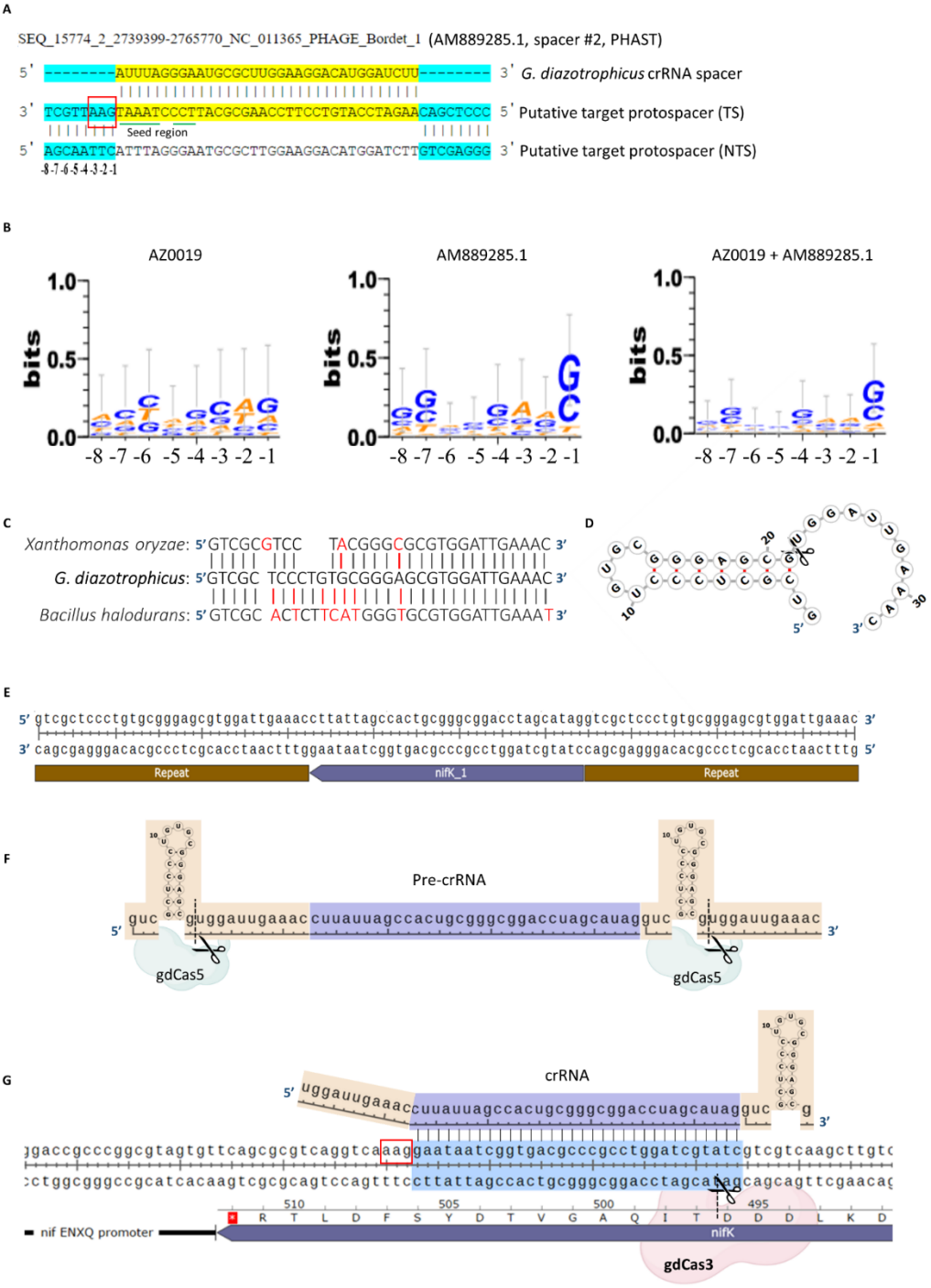


*Fig. 4.48. (**A**) Representation of type I-C PAM determination by the CRISPRTarget software. One of the hits from the PHAST database, exhibiting 100% complementarity with the spacer #2 of AM889285.1, is shown. The putative PAM is marked in red, and the seed region is underlined in green. (**B**) WebLogos representing the 8 nucleotides (-8 to -1) upstream of the identified protospacers, containing the predicted 3'-5' TS PAM. A total of 18 sequences aligned from AZ0019 (left panel) and 32 sequences from AM889285.1 (central panel) were included, resulting in a combined dataset of 50 sequences (right panel). (**C**) Alignment of the DR sequence of G. diazotrophicus with DRs from the best characterised I-C systems, i.e. X. oryzae and B. halodurans. Mismatches are indicate in red. (**D**) Secondary structure of the DR sequence of G. diazotrophicus as predicted by RNAFold, showing the same characteristics reported by Zheng et al. for other type I DRs* [433]. *The Cas5-mediated cleavage site by during pre-crRNA maturation is shown according to Nam et al.* [427]. *(**E-G**) Hypothetical strategy for editing the nifK gene via heterologous crRNA expression and native I-C*

machinery exploitation. The picture shows the designed mini- CRISPR element (E) as expressed from a conjugative vector, along with the unprocessed (F) and mature crRNA (G) upon Cas5-mediated trimming; the putative Cas3 nick site, according to Nimkar et al. [439]*, is depicted. The PAM is marked in red box.*

Crucially, out of the only three protospacer hits showing 100% sequence identity with I-C spacers, two possessed a TS 3'-AAG-5' PAM, reinforcing the robustness of the analysis (Fig. 4.48a). Once the PAM was identified, the putative crRNA structure was investigated by integrating the available information on other known type I-C systems with the I-C CRISPR features discovered during the analysis of *G. diazotrophicus* conducted in this study. The I-C DRs sequence of *G. diazotrophicus* showed high identity with the repeats of *B. halodurans* and *X. oryzae*, especially at the highly conserved 3' end (Fig. 4.48c), which plays a crucial role in pre-crRNA maturation by Cas5d [427]. Structural analyses through RNAfold further predicted the presence of a conserved 7-bp stem-loop structure towards the 5' end of the repeat (Fig. 4.48d), which was observed in mature I-C crRNA associated with the Cas5d subunit during the formation of the cascade complex [427]. This element was found to be highly conserved in other I-C systems [433], suggesting its importance for the functionality of CRISPRs and suggesting the structural analogy with different species I-C crRNAs [442]. Assuming an analogous pre-crRNA maturation mechanism as the one experimentally validated in *B. halodurans* [427], due to the remarkable similarities of the two species I-C CRISPRs, the model of a possible genome editing application employing the native *G. diazotrophicus* machinery was hypothesised (Fig. 4.48e-g). The technique would only require the transformation of one spacer (or more) nested between two DRs (Fig. 4.48e) along with the recombination cassette depleted of the PAM sequence to prevent subsequent self-targeting, if necessary; in the example, a 32 bp spacer was designed to target the 3' end of *nifK* in order to induce the same genome modification endeavoured in the previous sections. The strategy of expressing a 32 bp spacer in between two DRs has been successfully applied in both I-E [431] [438] and I-C [497] systems, while the only study to date to have efficiently repurposed *Pseudomonas* I-C system for both endogenous and heterologous bacterial genome engineering employed 34 bp spacers [492]. Upon Cas5d-mediated cleavage of the pre-crRNA repeats at

the 3′ base of the stem-loop structure between the conserved residues G21 and U22 (Fig. 4.48d, f, as demonstrated in *B. halodurans* I-C system [427]), the mature crRNA, left with a 21 bp 3' stem-loop handle (as demonstrated in *E. coli* I-E system [438]), is predicted to target the protospacer as shown in Fig. 4.48f. Cas3/I-C is then expected to nick the NTS at ~30–35 nt from the PAM (as demonstrated in *B. halodurans* I-C system [439]).

Interestingly, the repurposing of type-I systems as genome editing tools has revealed that Cas3-mediated degradation of the NTS can extend over thousands of base pairs, thus rendering this tool highly valuable for large-scale genomic deletions [502]. This characteristic has been confirmed for I-C systems repurposed for both eukaryotic [497] and prokaryotic [492] genome engineering. The potential limitation of exploiting native type I systems include: endogenous crRNAs outcompeting the heterologously expressed ones, which can be mitigated by Cas5 deletion [503]; spacer loss by DR recombination, that can be prevented by modification of one of the two repeats [492]; the necessity for empirical validation of both the bioinformatically determined consensus PAM [504] and of the environment-independent activity of the repurposed CRISPR system [482].

Despite these factors which may require some fine tuning, the utilization of the native type I-C system may be a valuable tool to explore for convenient engineering of *G. diazotrophicus*.

Similar analyses were performed on the type II-C CRISPR system of *G. diazotrophicus*. Although poorly characterized and less frequently employed compared to the II-A systems, Cas9s from the type II-C class have recently gained attention due to their smaller size, higher specificity [505] (possibly attributed to the longer 22-24 nt gRNA and 8 bp PAM [322]) and independence from RNase III processing, the overexpression of which can be toxic in bacterial systems [506]. Due to the smaller set of II-C spacers existing in *G. diazotrophicus*, the tentative PAM identification was conducted simultaneously on all the spacers of the three genomes, using the same strategy applied for the I-C system (Fig. 4.49a) and assuming the CRISPR transcription direction described in section 4.2.3b. The seed sequence in type II systems includes the 10-12 nucleotides proximal to the PAM [441]; thus, putative

protospacers containing more than one mismatch in that region were discarded, as previously described [460]. Out of the 22 unique spacers blasted in CRISPRTarget, only 21 hits fitted the set parameters (Supplementary Table 1), and no protospacer with 100% sequence identity was found. This limit, along with the restricted dataset, reduces confidence in the validity of the identified consensus sequence. As depicted in Fig. 4.49b, such putative consensus exhibits no similarities to the well-characterized II-C systems PAMs found in *Neisseria* spp., *Campylobacter jejuni*, or *Geobacillus stearothermophilus* [461]. However, II-C systems have also been reported to allow multiple PAMs alternatively to the *bona fide* sequence [505]; furthermore, as depicted in Fig. 4.49c, the gdCas9 is not phylogenetically close to any of the aforementioned II-C Cas9s, possibly justifying the diversity of its required PAM. These observations suggest that further experimental validation of the identified potential *G. diazotrophicus* II-C PAM may be warranted to explore its functional relevance and potential utility. Conveniently, II-C systems has been previously adapted for eukaryote editing [461], resulting in the availability of synthetic sgRNA scaffolds of either 101 nt [507] [508] or 121 nt [509] which have been already successfully employed in II-C Cas9-mediated editing upon insertion of 24 nt guide spacer sequences [505].

Overall, these findings suggest that harnessing the host's endogenous machinery offers a promising avenue for efficient genome editing without the drawbacks associated with exogenous Cas effectors. The identified PAM sequence and proposed editing model for the native I-C system present a potential strategy for large-scale genomic deletions, while for the type II-C system further experimental validation is needed. The native systems characterisation opens new possibilities for convenient and efficient genome editing in *G. diazotrophicus*, holding implications for genetic engineering applications.

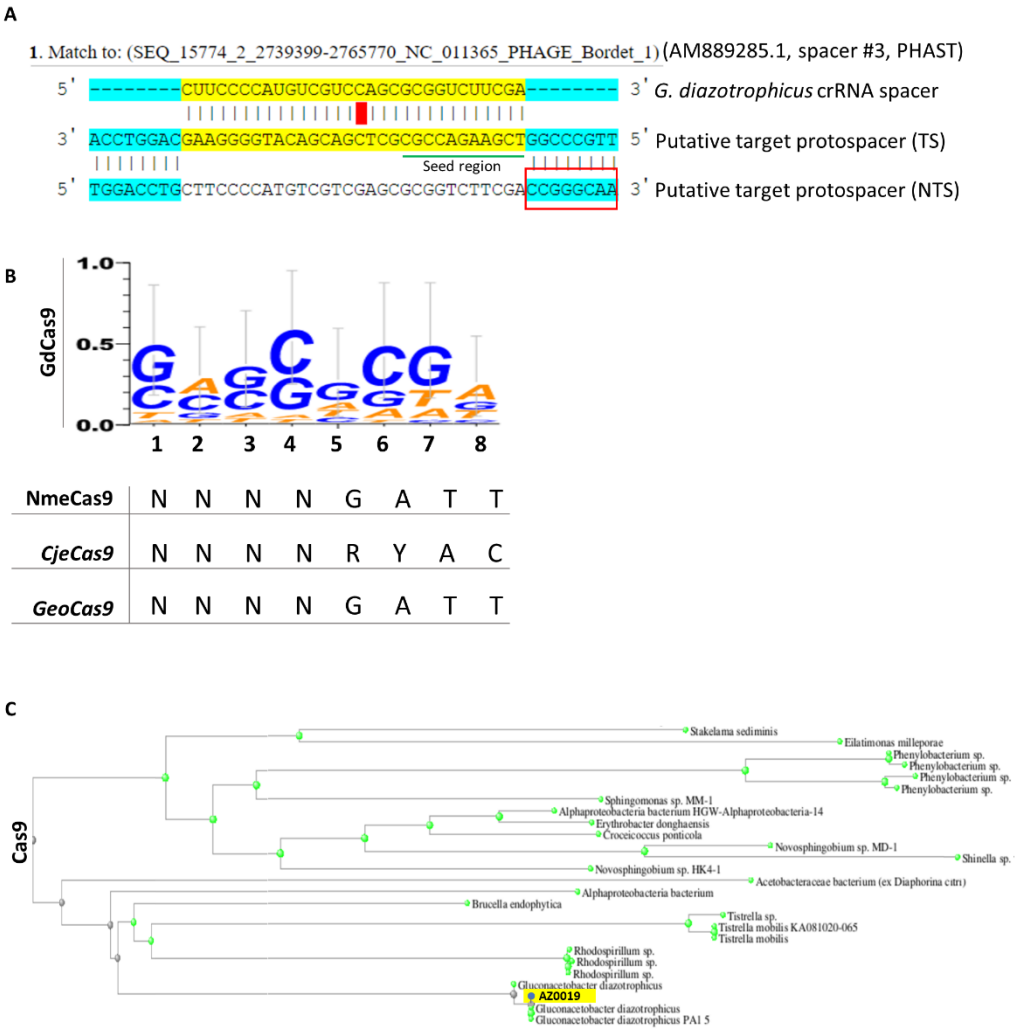


*Fig. 4.49. (**A**) Representation of type II-C PAM determination by the CRISPRTarget software. One of the hits from the PHAST database, exhibiting 97% complementarity with the spacer #3 of AM889285.1, is shown. The putative PAM is marked in red, and the seed region is underlined in green. (**B**) WebLogos representing the 8 nucleotides (1 to 8) downstream of the identified protospacers, containing the predicted 5'-3' NTS PAM. A total of 21 sequences aligned from AZ0019, AM889285.1 and CP001189.1 were included. The result is shown in comparison with other experimentally validated II-C PAMs from Neisseria spp.(NmeCas9), Campylobacter jejuni (CjeCas9), or Geobacillus stearothermophilus (GeoCas9)* [461]. *(**C**) Proximal vicinity of the gdCas9 protein (marked as AZ0019 in yellow) phylogenetic tree as visualised by Blast Tree View from the blastp database. Green dots correspond to a-proteobacteria species.*

4.3 Colonisation imaging

Despite an extensive array of biomolecular techniques that enable indirect targeting of the microorganisms under examination, microscopy still offers an advantageous investigation method due to the tantalizing possibility of direct observation with minimal sample disruption and artifact formation. In this study, fluorescence and light microscopy were employed to detect FP and GUS tagged *G. diazotrophicus* strains (see section 4.2.1 and 4.2.2) inoculated in the model systems tomato, rice and *Arabidopsis*, using the experimental setups described in section 4.1. The treated plant samples analysed were mostly derived from hydroponic and MS agar setups due to the technical difficulties of imaging plant tissues grown in soil, which, while being more realistic, often contain biological and physical contaminants that can interfere with the process of imaging bacteria.

During the microscopic analyses, it was observed that the expression of GFP from tagged bacteria appeared to be localized mainly on the external tissues, or, at most, within the cells of the first root epidermal and cortex layers, and almost exclusively from rod-shaped or elongated bacteria. In contrast, the GUS-tagged bacteria were also observed to reach deeper plant tissue regions, with apparent intracellular colonization (as shown in the sections below) and frequently showed a filamentous morphology. Since the majority of these samples were collected from plants grown under axenic conditions, minimizing the occurrence of cross-contamination with other microorganisms possessing GUS activity (which were never observed in untreated samples), this apparent discrepancy may be explained by an issue with GFP maturation when expressed by intracellularly established bacteria. This issue has been documented ever since Sevilla and Kennedy successfully tagged *G. diazotrophicus* for the first time using broad-host-range plasmids carrying *uidA*, *gfpmut2*, and *cobA* (a red FP): upon sugarcane, rice, and maize inoculation, only GUS activity could be consistently detected, indicating the limited success of FPs expression in these plants [248]. This difficulty suggests that the intracellular microenvironment of colonised plant cells may cause degradation or misfolding of the GFP protein. This occurrence, especially in

root tissues, may be due to low oxygen concentration and excessively acidic pH, both of which can hinder correct protein maturation (see section 4.2.1a). Another explanation may involve a lower stability of the pBBR1MCS-5_GFP plasmid in non-selective, intracellular environments (in contrast to the artificial media in which the stability tests were carried out) compared to the pRGS561 cosmid, which was previously validated to be endophytically retained in sugarcane for up to seven months [207]. However, Sevilla and Kennedy did confirm the plasmid presence in the investigated samples, reinforcing the hypothesis of a GFP folding issue [248]. Speculatively, differences in bacterial metabolism during intracellular vs epiphytic growth may also result in altered affinities for crucial plasmid elements such as *oriVs* or promoters. Interestingly, the issue with intracellular FP expression seemed to be less severe when using dsRed tagged mutants.

Taking into consideration the aforementioned limitations of the developed tagged strains, the following sections describe the colonization dynamics of *G. diazotrophicus* obtained by complementing different mutants, imaging methods, and setups in the attempt to provide a comprehensive understanding of the process.

4.3.1 Colonisation imaging in tomato and *A. thaliana*

First, the *GGG* mutant was employed to gain visual insight into the effectiveness of one type of *G. diazotrophicus* application strategy tested on tomato, i.e. seed treatment followed by growth on solid substrate (see section 4.1.1a). In particular, the seed coating method was compared with the seed vacuum infiltration (Fig. 4.50), which proved to be a promising technique for inducing a more consistent PGP effect (see section 4.1.1a).

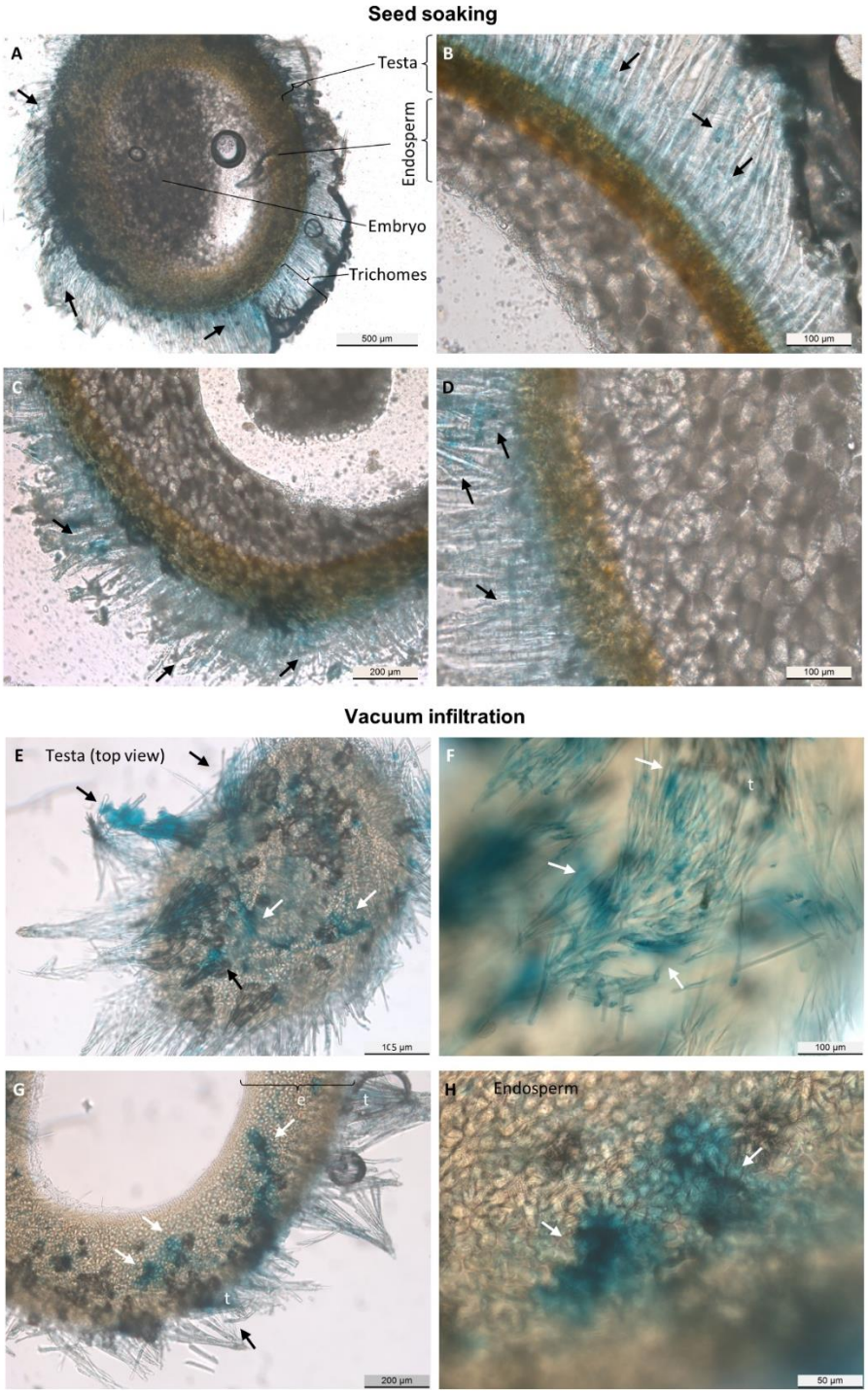


*Fig. 4.50. Comparison of seed treatment methods upon inoculation with GGG resuspended in water at a concentration of 10^8 CFU mL^{-1} for 60 minutes at room temperature, longitudinal sections; samples where quickly dried, as in preparation of a colonisation experiment, and subjected to GUS staining. (**A-D**) Seed coating method: GGG (blue stains, indicated by arrows) primarily localizes on the seed testa and trichomes. (**E-F**) Vacuum infiltration method, applying 800 mbar: in addition to the testa (E, whole seed overhead view, and F, trichomes close-up) GGG penetrates in the endosperm tissues (G-H, seed sections). t = seed testa; e = endosperm*

The seeds were treated for one hour with *GGG* resuspended in water at the concentration of OD_{600} = 2, corresponding to around 10^8 CFUs mL^{-1}. This bacterial concentration had been found to be optimal for the seed soaking application method followed by in soil growth (Fig. 4.3) but not ideal for the vacuum infiltration method followed by hydroponic cultivation (Fig. 4.7, 4.8). The treated seeds were quickly dried and subjected to X-Gluc staining to expose the bacterium presence. The results showed that both seed soaking and seed vacuum infiltration techniques resulted in the noticeable presence of *GGG* among the trichomes of the seed's testa (Fig. 4.50, black and white arrows). Only the vacuum infiltration managed to deliver bacteria in the seed endosperm tissue (Fig. 4.50b). This deeper penetration may confer an obvious advantage in terms of colonisation efficiency during the seed germination, but at the same time highlights the need of a careful optimisation to prevent embryo damage due to a too aggressive inoculation protocol (not shown).

4.3.1a Tomato and *A. thaliana* colonisation in MS agar setup

Following the investigation of the colonisation within seed tissue upon seed soaking and seed vacuum infiltration, the inoculated seeds were sown and grown in ½ MS agar (2.2 g L^{-1} of Sigma-Aldrich Murashige and Skoog Basal Salt Mixture "M5524", containing 20 mM KNO_3 + 10.5 mM NH_4) to emulate the nutrient-rich environment of the soil used for seed germination in glasshouse experiments. The presence of *GGG* and *GdRed* was screened for through fluorescence microscopy. To date, there has been limited investigation into the colonization process of *G. diazotrophicus* Pal5 when applied to tomato plants, with only one article providing preliminary insights. In their study, Luna et al. [174] treated 4 day-old tomato seedlings with high densities (10^9 CFUs mL^{-1}) of *G. diazotrophicus* UAP5541 carrying the pRGS561 plasmid and evaluated its colonisation level in semi solid Fahräeus medium through GUS staining; they reported colonisation in the root epidermal layer, primarily localising in root-stem junctions (occasionally including sub-stomatal cavities),

lateral root emergence sites, root hairs and rarely root tips. In the present work, such observations were assessed by the use of FP-tagged mutants, thus enabling a more direct imaging procedure without the potentially perturbing step of GUS staining. Furthermore, *A. thaliana* was parallelly investigated and compared as an alternative dicot model system due to its simpler and more accessible anatomical structure, facilitating superior imaging capabilities in comparison to tomato.

When seeds were grown on ½ MS agar vertical plate cultures, a biofilm of bacteria was observed growing on and around the root system as it developed over the course of 30 days (Fig. 4.51). The biofilm extended from the root-stem junction (Fig. 4.51a), along the maturation/elongation zone (Fig. 4.51b, c, white stars) and up until the root tip (Fig. 4.51g-i), which showed a lower bacterial presence. This observation suggest that bacteria followed the physical channel left by the elongating root on the agar surface with a small lag; in other words, the bacterial spreading along the roots boundaries was not only the result of an active chemotaxis toward the plant tissue, but also the physical passive diffusion on the negative space created in newly opened root-agar interfaces. However, the biofilm always remained confined in close association with the roots without any detectable growth on other area of the agar surface, most likely due to the lack of a carbon source; in contrast, the addition of sucrose 10 mM in an analogous setup involving *A. thaliana* allowed the bacterium dispersal across the plate and the consequent colonisation of untreated plantlets that were growing in proximity to treated ones (Fig. 4.52g). Such observations suggested the establishment of an active symbiosis, with both organisms depending on plant-mediated carbon fixation unless in the presence of a carbon-rich environment, which permitted the partial uncoupling of the binary system and further bacterial spreading. This scenario may also be applicable in soil systems, where bacterial transmission between different plant individuals or even across different species could occur in the rhizosphere through carbon-rich microenvironments acting as corridors for bacterial diffusion.

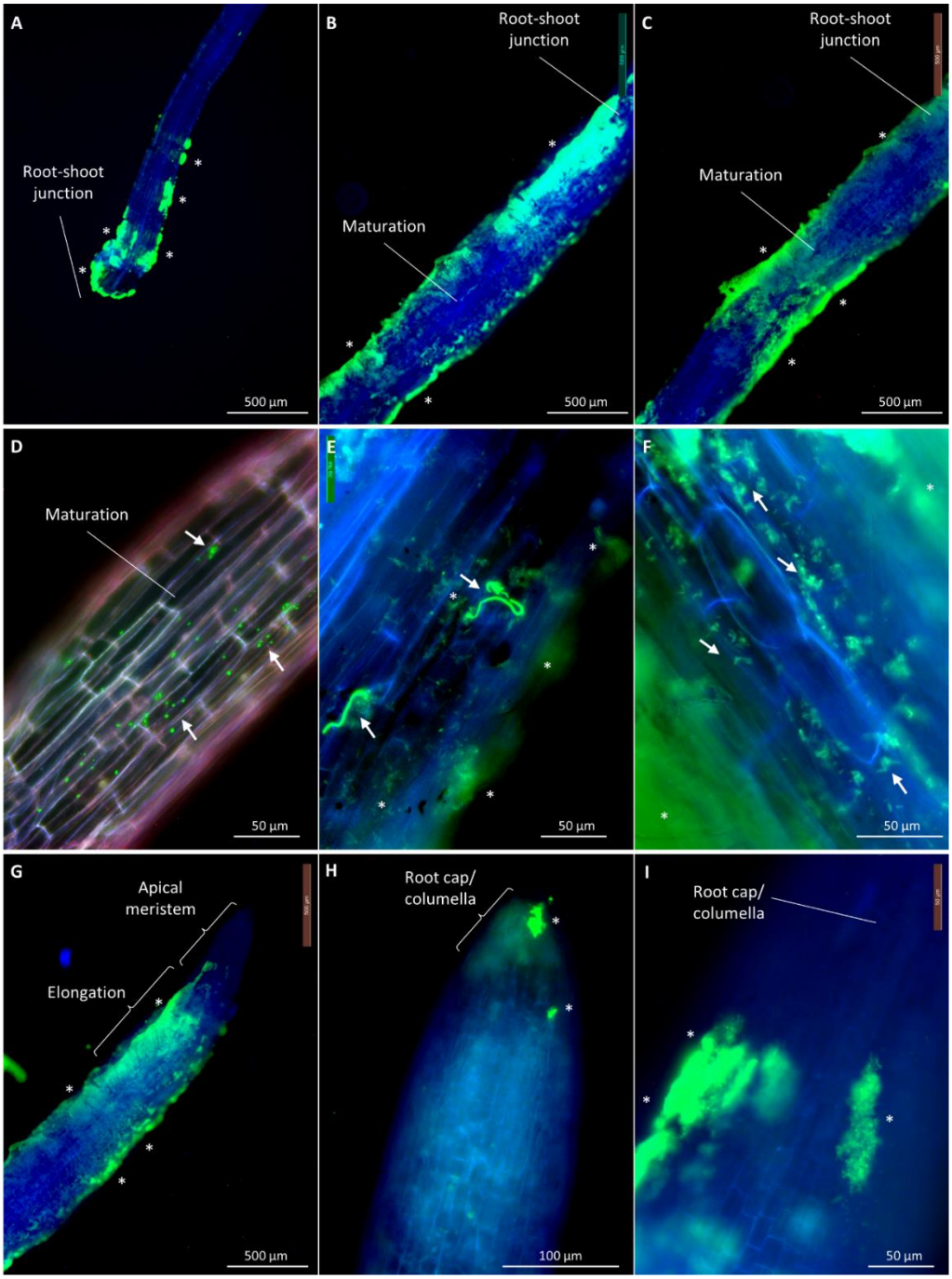


*Fig. 4.51. Tomato (cv. "MoneyMaker") grown on ½ MS agar vertical plate cultures upon seed vacuum infiltration treatment with GGG resuspended in water at a concentration of 10^8 CFU mL^{-1} for 60 minutes at room temperature, fluorescence microscopy (green = bacterial GFP fluorescence; blue to violet = root tissue autofluorescence). (**A-C**) GGG biofilm (white stars) coating the root from the stem-root junction (A) to the maturation and elongation zones (B, C). (**D-E**) Single bacterial cells (white arrows) interspersed among the root epidermis surface; some GGG cells exhibited a filamentous phenotype (E, white arrow). (**G-I**) GGG biofilm (white stars) coating the root tip, usually around the elongation zone (G, I) but occasionally colonising the apical meristem (H).*

Occasionally, bacteria were spotted in the root cap (Fig. 4.51h), possibly finding a carbon-rich but unstable niche among the sloughed off cellular debris. In the maturation/elongation zone, the close-up view of the root surface revealed a high density of bacteria colonising the root epidermis, possibly endophytically (Fig. 4.51d-f), with some cells exhibiting the filamentous phenotype (Fig. 4.51e, white arrow) showed in Fig. 4.31.

This filamentation behaviour, characteristic of proteobacteria and other bacterial phyla [347], was previously reported by Muthukumarasamy et al. [134] [510] to be induced by high ammonium (25 mM), and to a lesser extent by other N sources such as nitrate or urea; the author suggested this morphological change to cause reduced bacterial growth and possibly to explain the low re-isolation rate of *G. diazotrophicus* in highly fertilised agricultural systems. Cocking et al. agreed with this hypothesis after discovering the same pleomorphic cells colonising the root cortex of inoculated maize grown on MS agar supplemented with 3% sucrose [271]. However, in the present study, the same filamentous phenotype was also detected among the root system of *A. thaliana* grown on ammonium-free MS agar (2.2 g L^{-1} of Sigma-Aldrich Murashige and Skoog Modified Basal Salt Mixture, M2909) vertical plate cultures, containing 15 mM KNO_3 but no ammonium nor sucrose (Fig. 4.53). *A. thaliana* seeds were vacuum infiltrated for either 30 minutes or two hours with three different concentrations of *GGG* resuspended in water (Fig. 4.52, 4.53). The bacterial GFP signal co-localised with the roots, confirming what observed with tomato despite of the lack of ammonium in the medium. Considering the inability of *G. diazotrophicus* to reduce and use nitrate as a nitrogen source [83], this strict spatial association supported the hypothesis of a commensal and possibly mutualistic symbiosis, with bacteria feeding on carbon from root exudates and speculatively releasing some of the fixed ammonium in the surroundings.

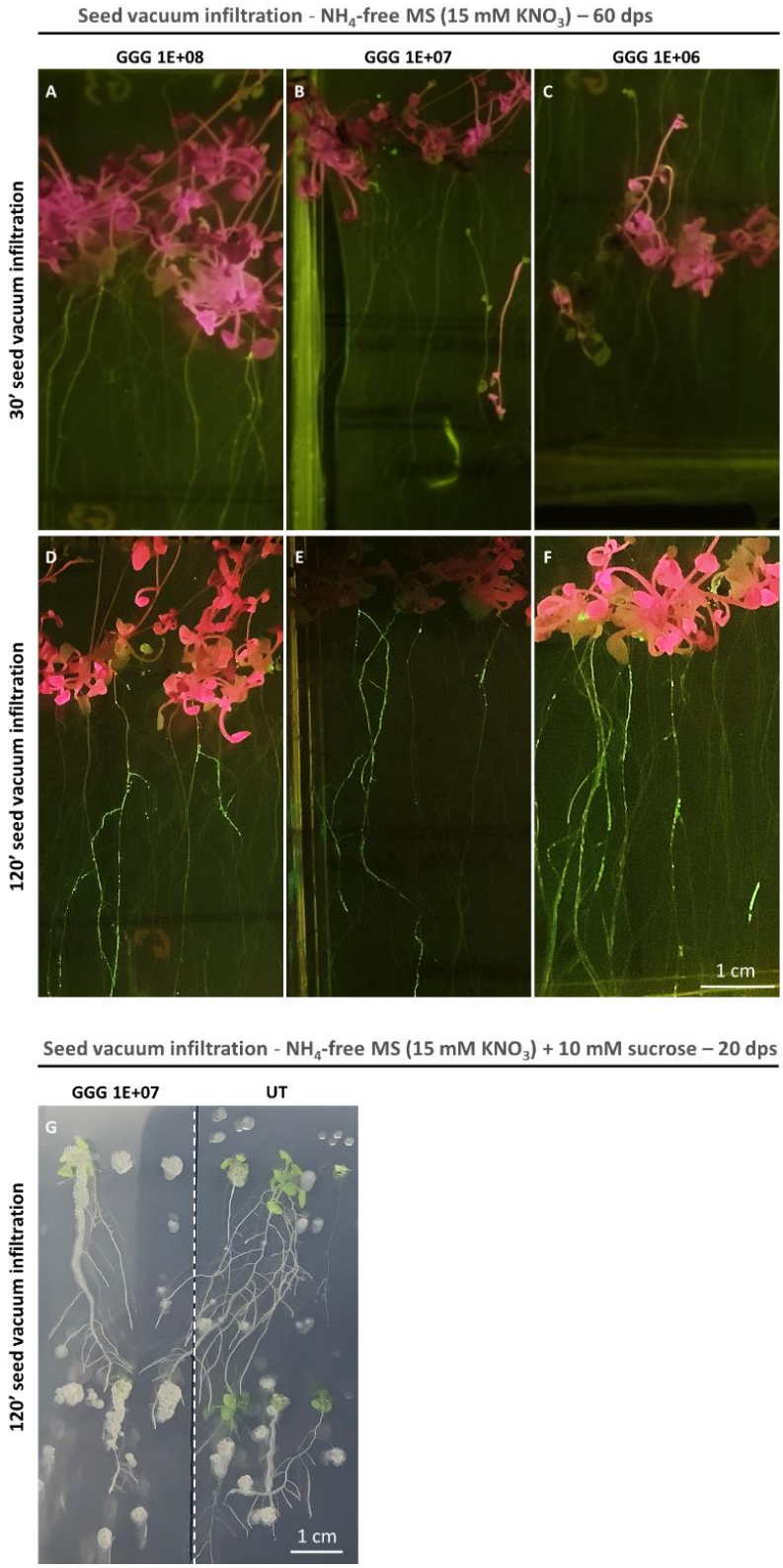


Fig. 4.52. A. thaliana (Col-0) grown on NH_4-free MS agar vertical plate cultures upon seed vacuum infiltration treatment with GGG resuspended in water at a concentration of 10^6 to 10^8 CFU mL^{-1} for 30 (A-C) vs 120 minutes (D-F) at room temperature. The FastGene Blue/Green LED Gel Illuminator, emitting between 470 nm and 520 nm, was used to detect fluorescence at the whole-plant level (green = bacterial GFP fluorescence localising on the roots; red = chlorophyll autofluorescence). (G) GGG biofilm (white colonies) spreading from the treated plants (left) to both the agar surface and the tissues of untreated controls (UT) germinated on NH_4-free MS agar + sucrose 10 mM.

Remarkably, following the two hours seed treatment, this relationship lasted for as long as to two months post-sowing within the limited enclosed system of a 12x12 cm square Petri dish (Fig. 4.52a-f), after which the experiment was suspended due to excessive agar desiccation. In contrast, the 30-minute inoculum resulted in an accelerated decline in root-associated *GGG*, likely attributable to a suboptimal initial bacterial establishment, as evidenced by a gradual attenuation of the GFP signal after 10-15 days post-sowing (not shown). On the other hand, the inoculant density did not obviously affect neither the GFP signal level and distribution across the root system, nor the bacterial morphology (Fig. 4.53). In fact, the filamentous phenotype was observed regardless of the seed treatment density and in spite of the lack of ammonium, therefore weakening the direct correlation between *GGG* filamentation and presence of ammonium salts in the medium (Fig. 4.53).

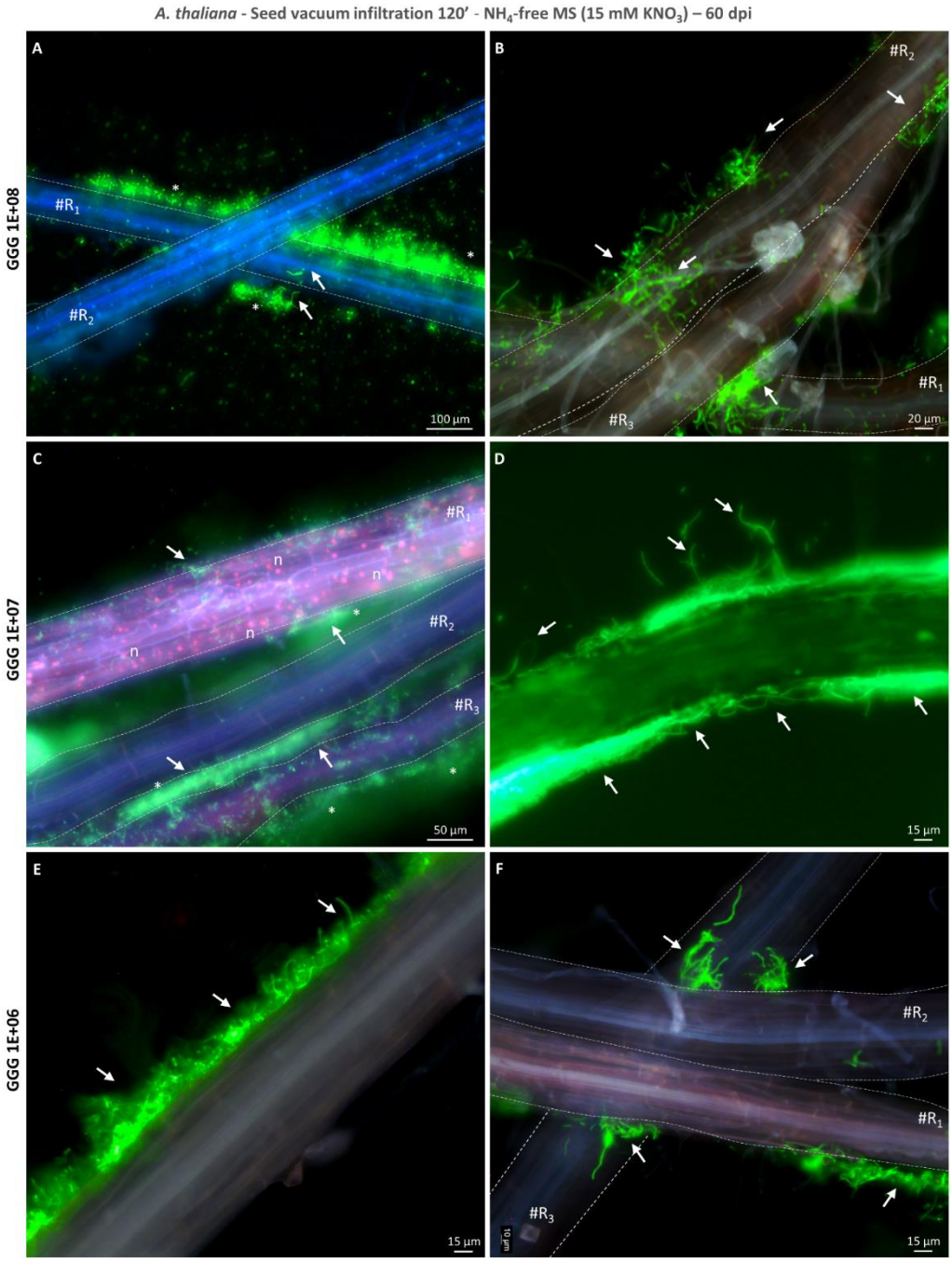
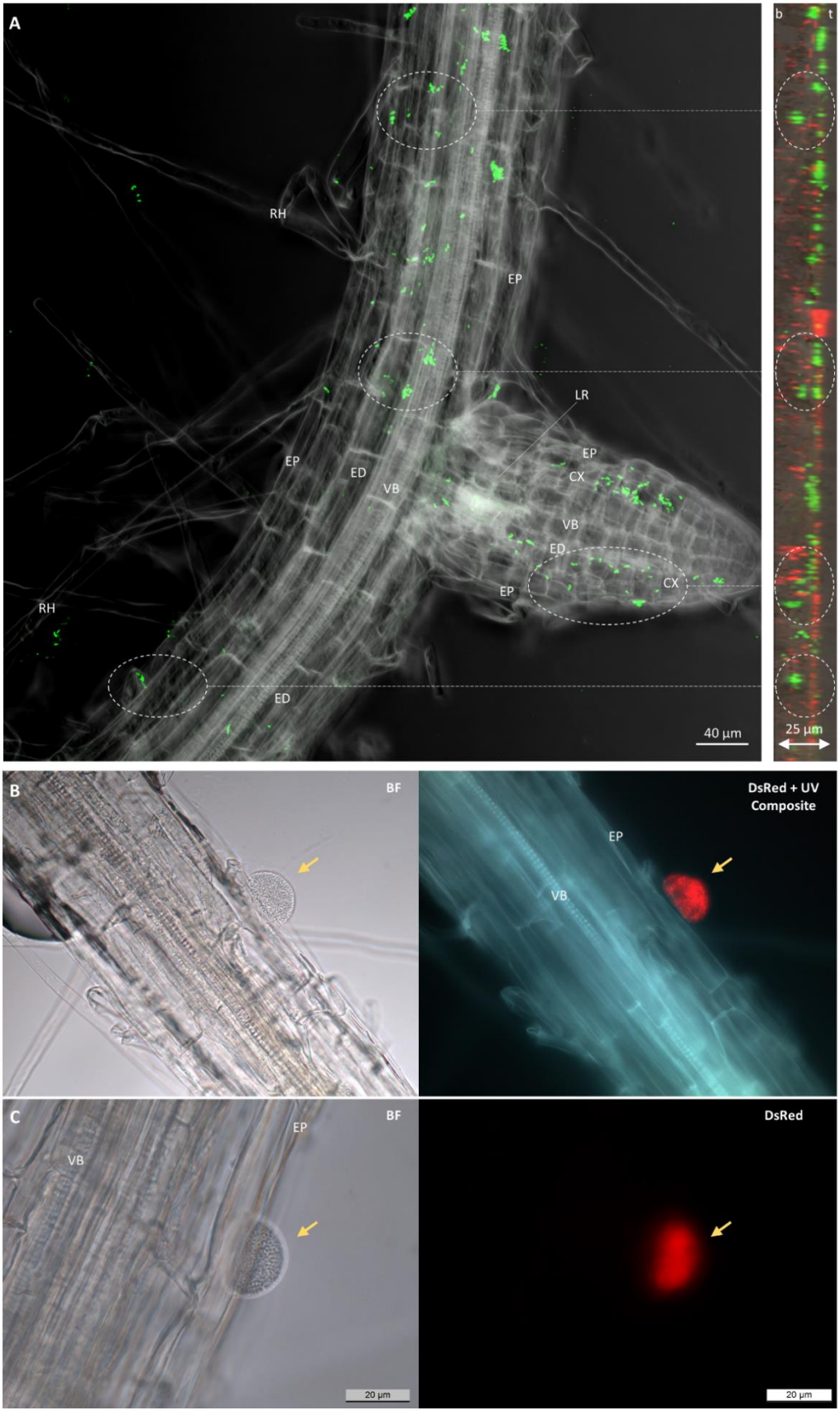


Fig. 4.53. Close-up view of Fig. 4.52d-f, showing only A. thaliana treated for 120 minutes at 60 dps, fluorescence microscopy. Green = bacterial GFP fluorescence localising on the roots; blue/brown/purple = root autofluorescence. Different filters and white balance settings were applied to consistently highlight the root autofluorescence considering the variations in sample thickness and arrangement. In contrast, the same GFP settings and filter were used for imaging the fluorescent bacteria. All images are composites of different colour channels, except for (D), which was captured exclusively using the GFP filter. The pink dots in (C) indicate the nuclei of root cells (marked as n). Filamentous bacteria are marked with a white arrow. Biofilm of rod-shaped bacteria are marked with a white star. When multiple roots were present in the same image, they were demarcated individually with white dashed lines to facilitate precise identification and labelled as #R_n.

The filamentous morphology seemed to affect a high percentage of the total *GGG* cells, that was estimated to be over 50% of the bacterial population (Fig. 4.53a-f). However, most of GFP-tagged bacteria, despite adopting a rod-shape or filamentous phenotype, seemed to be mainly colonising the roots epiphytically (Fig. 4.53e-f). This behaviour may simply reflect a more energetically cost-effective distribution: the root-agar interface, enriched with root exudates in addition to the MS agar micronutrients, would offer a valuable growth medium for the bacteria, rendering the energy-demanding endophytic colonisation of plant tissues less convenient.

To reduce the number of bacteria colonising the agar surface in the root-agar interface and encourage endophytic colonisation, tomato and *A. thaliana* seeds, after being vacuum infiltrated as described above, were germinated and grown in ammonium-free semisolid agar flasks, allowing the roots to penetrate the medium as in traditional pot-based cultivation. With a reduced surface area available as a growth substrate for the bacteria, confined to the agar below surface surrounding the roots, this setup was anticipated to facilitate the colonisation of deeper root tissues. The experiment was also conducted employing the *GdRed* mutant. As expected, this setup reduced the number of loosely interacting bacteria and possibly facilitated an endophytic behaviour (Fig. 4.54, 4.55). The confocal microscopy and 3D modelling of *A. thaliana* roots (Fig, 4.54a) revealed the presence of epiphytic rod-shaped bacteria spread along the maturation zone epidermis, but also endophytic cells penetrating in the cortex and endodermis of emerging lateral roots (Fig. 4.54a). The use of the *GdRed* mutant enabled the bacterial distribution to be seen among the root system similar to what observed with the *GGG* mutant in Fig. 4.53 and 4.54a (not shown); additionally, it allowed the visualisation of a peculiar biofilm structure, with cells enclosed in a round or drop-like matrix (Fig. 4.54b, c). The regular shape of these formations makes them unlikely to be an artifact from unwashed agar remnants, suggesting that they may be composed of an EPS-based matrix and act as specialised biofilm structures. However, a similar phenomenon could not be traced in the scientific literature, making its interpretation challenging.

A. Thaliana - Seed vacuum infiltration 120' - *GGG/GdRed* 1E+07 - NH_4-free MS (15 mM KNO_3) – 10 dpi



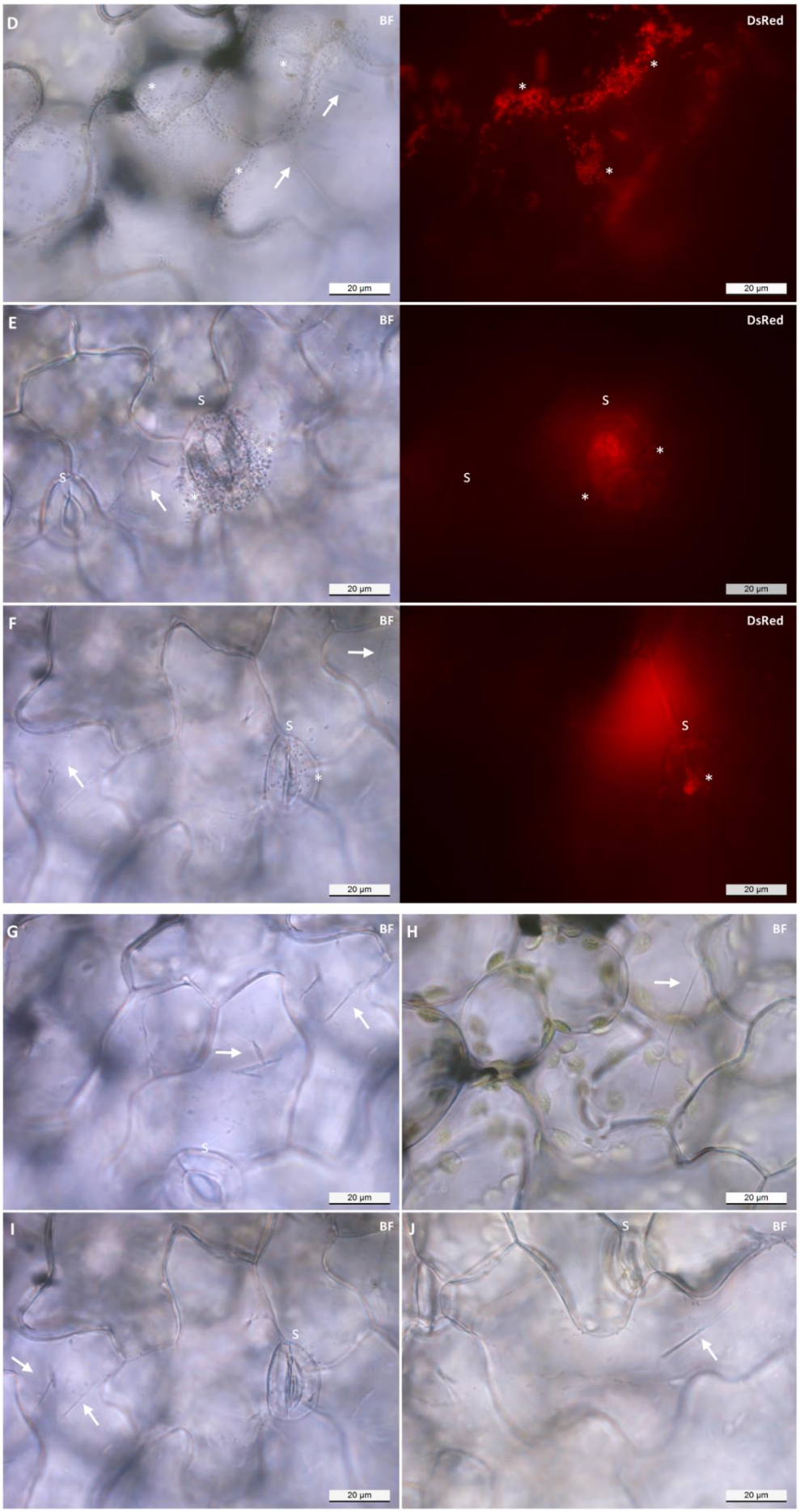

D
BF
DsRed
E
F
G
H
I
J
S
20 µm

Fig. 4.54. A. thaliana (Col-0) grown on NH_4-free MS agar medium upon seed vacuum infiltration treatment with GGG or GdRed resuspended in water at a concentration of 10^7 CFU mL^{-1} for 120 minutes at room temperature. (A) Differentiation/maturation zone of GGG-treated Arabidopsis, showing the emergence of a lateral root at 10 dps, confocal microscopy. The main image displays the maximum projection of a 25 images z-stack, for a total of 25 µm depth. On the right, the lateral view of the 3D modelling of the z-stack is included, with its right side corresponding to the top (t) of the z-stack (root surface) and the left side corresponding to the z-stack bottom (b, root interior). GGG clusters (green) exhibiting penetration within root tissues are demarked in dashed line and linked to their correspondents in the 3D side view. In red are shown some chlorophyll-containing plastids as excited by a 633 nm laser (which were removed from the main picture) to serve as a reference for evaluating the penetration of GGG cells into the root tissue. The closer to the left side of the 3D lateral view image (b), the deeper the penetration. (B-C) Spheroid biofilm (orange arrows) on the surface of GdRed-treated Arabidopsis roots (cyano), containing fluorescent coccoidal cells (red) at 7 dps, fluorescence microscopy. (D-J) GdRed colonising the shoot of treated plants 10 dps. Bacteria were observed either as fluorescent coccoidal cells (D-F, white stars) or as non-fluorescent elongated cells often found in proximity to stomata (D-J, white arrows). (D) GdRed epiphytically colonising the leaf epidermis, mainly localising around the epidermis cell boundaries. (E) GdRed entering (or exiting from) an opened stoma (labelled as s). (F) GdRed colonising the sub-stomatal chamber of a semi-closed stoma. CX = cortex; EP = epidermis; ED = endodermis; LR = lateral root; RH = root hair; S = stoma; VB = vascular bundle.

Intriguingly, the bacterial cells confined inside the round biofilm exhibited a spherical/ovoid phenotype. The differentiation from rod to coccus shape is a poorly understood adaptation typically associated with a slower growth or entrance into the stationary phase and possibly induced by a change in the nutritional status [349]. However, this scenario is further complicated by the fact that, as discussed in section 4.2.1c, bacteria in the stationary phase can also adopt a filamentous morphology [349]. Furthermore, it must be emphasized that bacterial polymorphism is a highly environment dependent trait which, in the case of endophytic diazotrophs such as rhizobia or *Nostoc* cyanobacteria, is also influenced by the plant species, anatomical district and metabolic status, and by the bacterial strain, nitrogen fixation activity and bacteroid differentiation stage [349] [511] [512]. These variables have yet to be connected in a definite cause-effect model [349].

The thinness of Arabidopsis leaves, contrarily to tomato, allowed the direct visualization of *GdRed* cells colonising the aerial tissues of the plant (Fig. 4.54d-j). Fluorescent bacteria exhibiting the same coccoidal phenotype described above were detected to epiphytically colonise the leaves, mostly localising in proximity to the epidermal cell boundaries. The epidermal cell wall junctions, and the indentation that characterises these regions, may offer a more easily accessible interface to the internal environment, as well as a

physical protection against biotic and abiotic stressors such as light and shear forces. In support of this observation, epiphytic bacteria have previously been reported to preferentially colonise this particular niche of the leaf [31]. Coccoidal *GdRed* cells were also observed to enter through opened stomata (Fig. 4.54e) and to subsequently occupy substomatal chambers (Fig. 4.54f). It is unclear, however, whether these structures serve as the primary entry point for bacteria living epiphytically in the cuticle/epidermis, or if they represent the outlet of a colonisation process initiated from the root system and progressed upward via apoplastic and symplastic pathway or through xylem vessels (as suggested by Dong et al. [260] and James et al. [221]), ultimately reaching the shoot. It is also possible that, upon seed vacuum infiltration, bacteria may be transported and undergo passive dissemination throughout the differentiating embryo as the plant tissues grow, resulting in an evenly colonised plant. *G. diazotrophicus* has been reported to reduce stomatal conductance in *Arabidopsis*, possibly by inducing the stomata closure, with a beneficial effect for the canopy water-use efficiency [262]. This is consistent with the observation that salicylic acid-mediated stomatal closure is part of *Arabidopsis* immune response to limit bacterial invasion [513]. It was therefore surprising to observe bacteria swarming across a fully (Fig. 4.54e) or partially (Fig. 4.54f) opened stoma. This finding suggests a complex dynamic in which the chemical cross-talk between the two organisms may result in a transitory stomata aperture. A similar mechanism has been described for the phytopathogen *Pseudomonas syringae*, which counteracts stomatal closure by modulating the abscisic acid-mediated mechanical regulation of guard cells [513]. Interestingly, the majority of the shoot samples analysed were colonised by non-fluorescent filamentous *GdRed* cells (Fig. 4.54d-j, white arrows), mostly localised in proximity to stomata and apparently established either intracellularly or in the apoplast space parallel to the periclinal wall. The plasmid loss or failed FP maturation were possibly influenced by the combination of the morphological transition and the endophytic behaviour, since fluorescent filamentous bacteria were observed colonising epiphytically the root epidermis (Fig. 4.53).

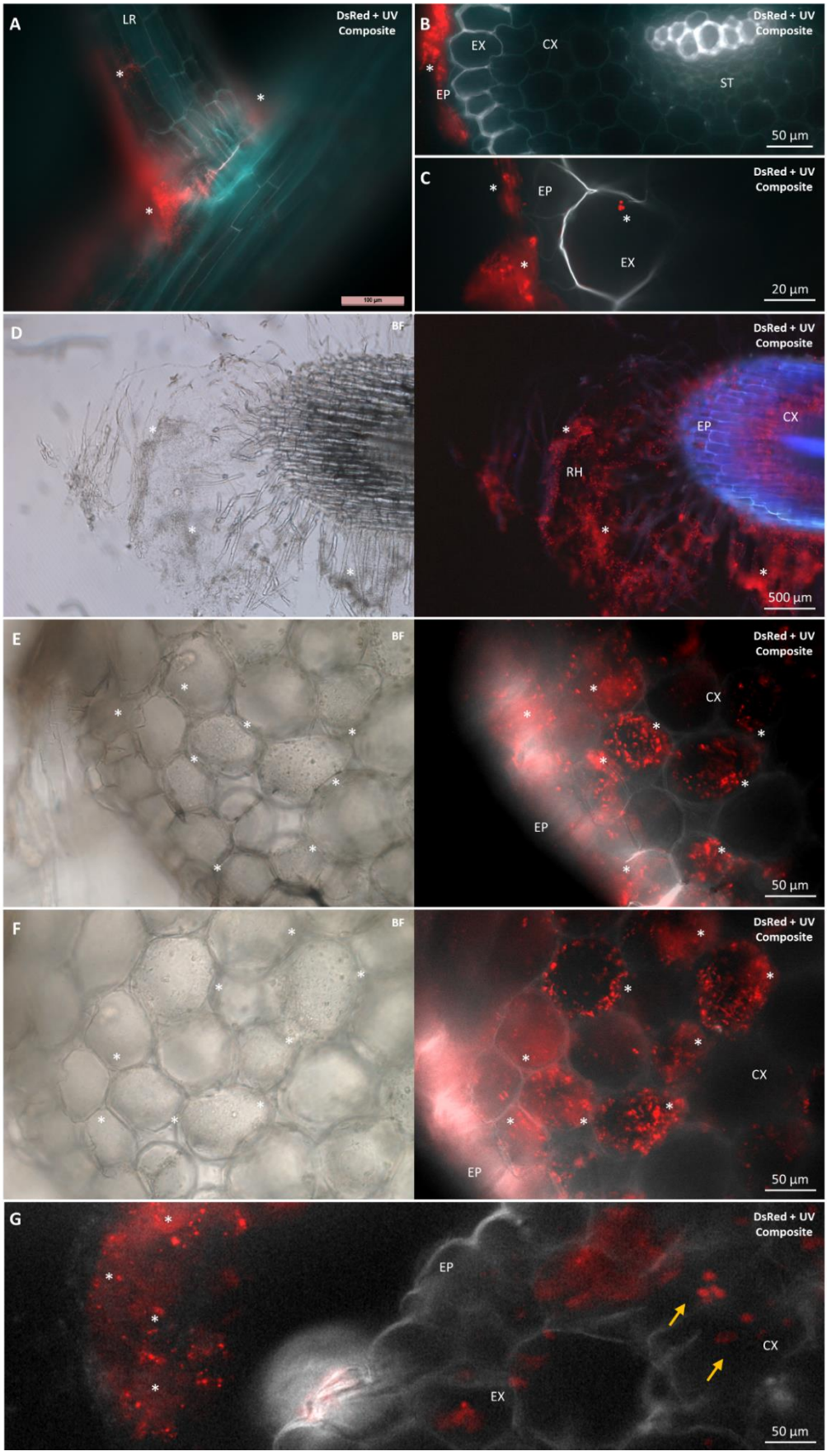

A
LR
DsRed + UV Composite
B
EX
CX
ST
EP
50 µm
DsRed + UV Composite
C
EP
EX
20 µm
DsRed + UV Composite
D
BF
DsRed + UV Composite
EP
CX
RH
500 µm
E
BF
DsRed + UV Composite
CX
EP
50 µm
F
BF
DsRed + UV Composite
CX
EP
50 µm
G
DsRed + UV Composite
EP
CX
EX
50 µm

Fig. 4.55. Tomato (cv. "MoneyMaker") grown on NH_4-free MS agar medium upon seed vacuum infiltration treatment with GdRed resuspended in water at a concentration of 10^7 CFU mL^{-1} for 60 minutes at room temperature, 7 dps, fluorescence microscopy (red = bacterial dsRed fluorescence; grey/cyan/blue = root tissue autofluorescence). (A) GdRed entering root tissue from a lateral root emergence site. (B-C) Close-up view of GdRed colonising the root epidermis epiphytically with some rod-shaped cell (white stars) intracellularly established in the exodermis, cross section. (D) Cross section from the maturation zone of a colonised root showing densely-colonised root hairs. (E-F) Cross section from the root-shoot junction of a colonised root showing putative intracellular colonisation of the cortical parenchyma cells. (G) Cross section from the root-shoot junction of a colonised root showing the difference in dimension between GdRed cells epiphytically colonising the root epidermis (the biofilm appears detached due to a cross-sectioning artifact) in comparison with chlorophyll-containing plastids (orange arrow). CX = cortex; EP = epidermis; EX = exodermis; LR = lateral root; RH = root hair; ST = stele.

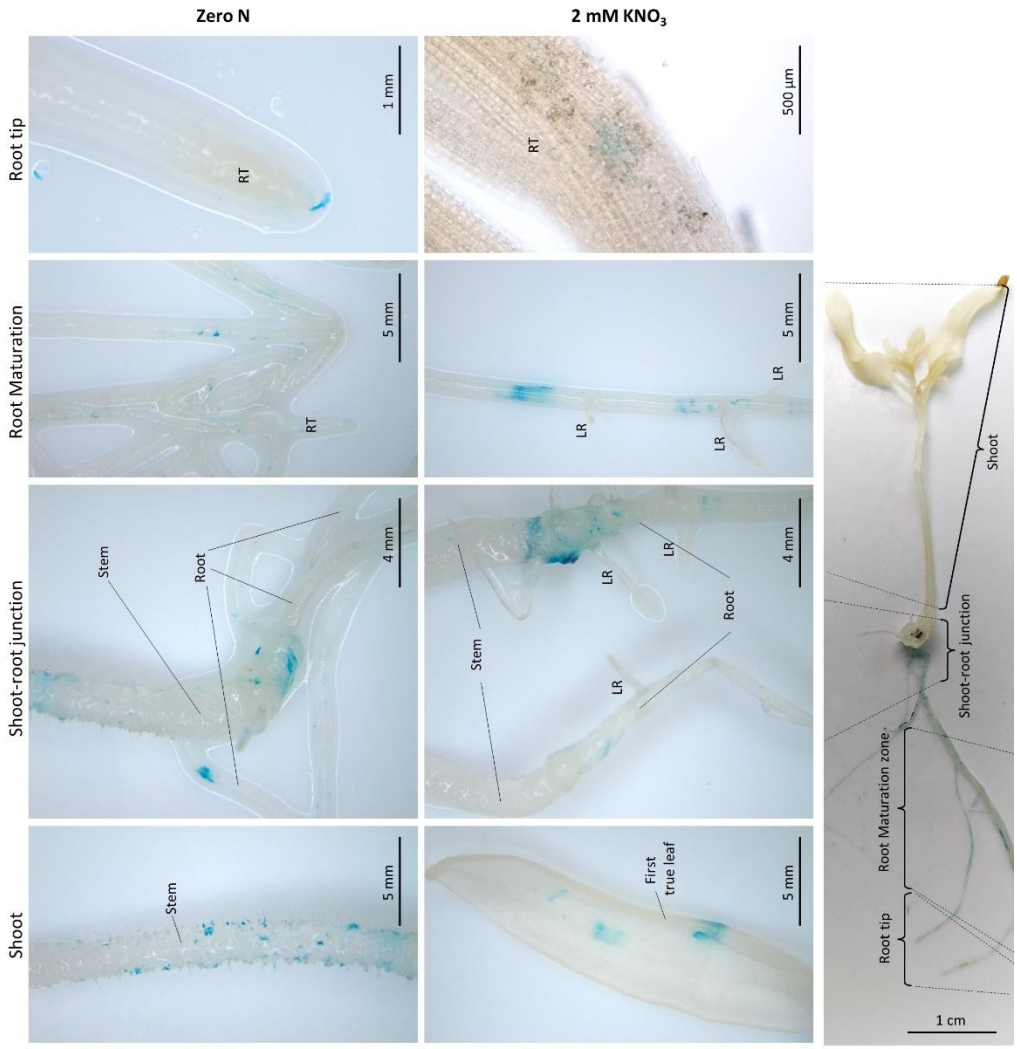
When the same experiment was repeated with tomato, no fluorescent filamentous bacteria could be detected, and the organizational complexity and thickness of the samples did not allow an obvious visualisation of bacterial cells with simple brightfield illumination. Rod-shaped bacteria were observed entering plant tissues through lateral root emergence sites (Fig. 4.55a) and to extensively colonise the agar rhizosphere and the root hairs of the maturation zone (Fig. 4.55d), similarly to what described in *A. thaliana* but with a lower number of filamentous cells. Cross sections of the roots generally showed an epiphytic biofilm of rod-shaped bacteria surrounding the epidermis (Fig. 4.55b), with a minority of ovoid cells penetrating in the epidermal or exodermal layer (Fig. 4.55c). However, one sample had an extraordinarily substantial intracellular colonisation of the cortical parenchyma cells in the root-shoot junction (Fig. 4.55d, e). It should be noted that the filter set used for detecting the DsRed-Express2 protein can also excite chlorophyll molecules, thus introducing a potential for misinterpretation when some elements of the analysed sample were not clearly inferable from the cellular context. Nevertheless, chlorophyll-containing plastids were easily discernible from bacteria due to the obvious dimensional and shape differences, with rod-shaped bacteria being approximately one order of magnitude smaller than plastid organelles. This difference is shown in Fig. 4.55g, where an epiphytic layer of bacteria (white stars) is showed next to chlorophyll-containing organelles, possibly chloroplasts (orange arrow). Furthermore, no green coloration, implying chlorophyll presence, was observed under brightfield illumination (Fig. 4.55d, e, left images). Even though a better-defined image at higher

magnification could not be obtained due to the thickness of the section, it was still possible to distinguish some rod-shaped bacteria among the red-tagged matter. Therefore, it seems that some plantlets can sustain a more substantial intracellular colonisation, although it is not clear whether this capacity is restricted to some specific plant growth stage and anatomic area or if such observation is just the fortunate result of a stochastic process in which the endophytic infection of some specific plant individuals take place more efficiently.

4.3.1b Tomato inoculation in hydroponic setup - Root colonisation

Next, the colonisation of hydroponically grown tomato was investigated. While the bacterial dynamics in plants grown in solid or semisolid agar substrates may provide a more accurate approximation of a natural colonisation mechanism, one of the scientific aims of this study was to describe *G. diazotrophicus* behaviour in artificial and commercially applicable setups. Therefore, tomato plants treated with *GGG* as described in section 4.1.1b (Fig. 4.12, 4.13, 4,14) and grown with different nitrogen concentrations were collected at different time points (from 1 to 21 dpi) and subjected to GUS staining or direct fluorescence microscopy. Specifically, plants were cultivated in N-free and 2 mM KNO_3 NS conditions to evaluate the impact of a nitrogen source accessible solely by the plant on the colonisation dynamics. This approach aimed to explore the boundaries of the symbiotic relationship, resembling the NH_4-free MS agar experiment, and the GUS staining was employed to capture the overall bacterial diffusion at the whole plant level.

GGG localisation in tomato – Hydroponics 3 dpi



GGG localisation in tomato – Hydroponics 20 dpi

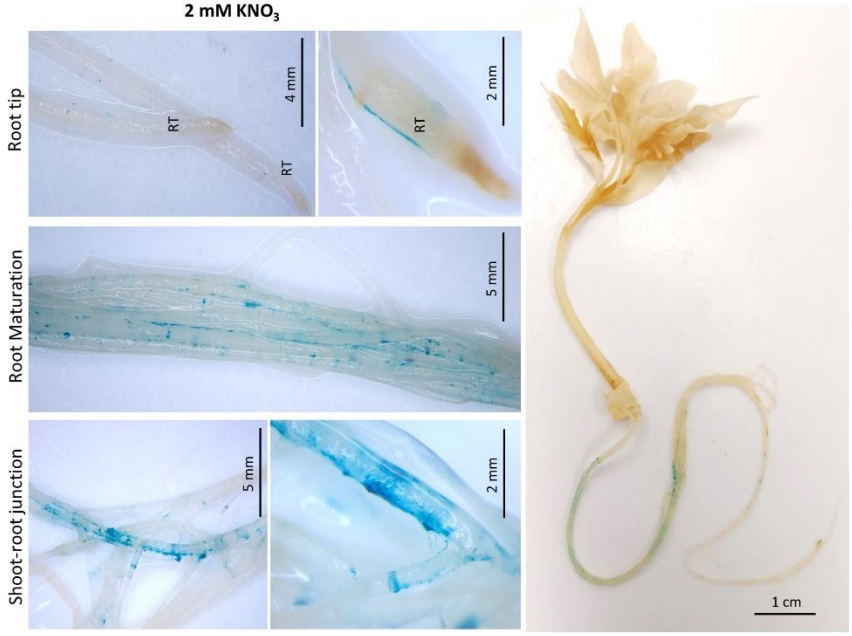


Fig. 4.56. Tomato (cv. "MoneyMaker") grown hydroponically in zero N or 2mM KNO_3 NS inoculated with GGG at OD_{600} = 0.3 and of (10^7 CFU mL^{-1}) kept for 48 h., 3 dpi (top panel) vs 20 dpi (bottom panel), brightfield microscopy/stereoscopy. Plants were rinsed in water to discard loosely adherent bacteria and subjected to X-Gluc staining overnight at 28 C°. One whole representative GUS-stained plantlet is shown at the right side of both panels, while the anatomical zones analysed are depicted separately on the left side. LR = lateral roots; RT = root tip.

At three dpi (meaning one day after substituting the inoculated NS), *GGG* had colonised the root system regardless of the N condition with roughly the same pattern observed in agar, i.e., a predominance of interspersed or clustered bacteria in the root-shoot junction and elongation zone, and a less dense bacterial population in the root tip except for sporadic colonies in the root cap (Fig. 4.56, top panel). A similar distribution was maintained up until 20 dpi (Fig. 4.56, bottom panel; only the plants grown in N-replete conditions are shown due to the deteriorated phenotype of the plants grown in absence of synthetic nitrogen). Remarkably, the shoot was found to be already colonised at 3 dpi, as shown by punctate stains along the stem and rare blue areas in the leaves (Fig. 4.56, bottom-right corner of the top panel). This finding rules out the hypothesis of a mere passive diffusion from the inoculated seeds driven by the germinating embryo (although this dynamic may still play a role in the overall colonisation model), since in this setup the inoculum is added to the NS with no direct contact with the shoot. Therefore, a rapid migration to the aerial tissues is likely to take place, but whether such event is the result of passive circulation via xylem sap upon endophytic root penetration or whether there is an active bacterial chemotaxis toward the shoot via apoplastic or symplastic route, or both, remains to be ascertained.

A more detailed analysis of *GGG*-treated samples collected from both zero N and N-replete conditions at different timepoints through fluorescence microscopy, revealed a dynamic similar to what was described in the MS agar setup. Initially, the root surface was colonized by individual bacterial cells with an even distribution, although slightly skewed around the boundaries of root cells (Fig. 4.57a, c) and occasionally clumped in large clusters (Fig. 4.57b). Within these biofilms, some filamentous cells were distinguishable among a majority of rod-shaped bacteria (Fig. 4.57b, white arrow).

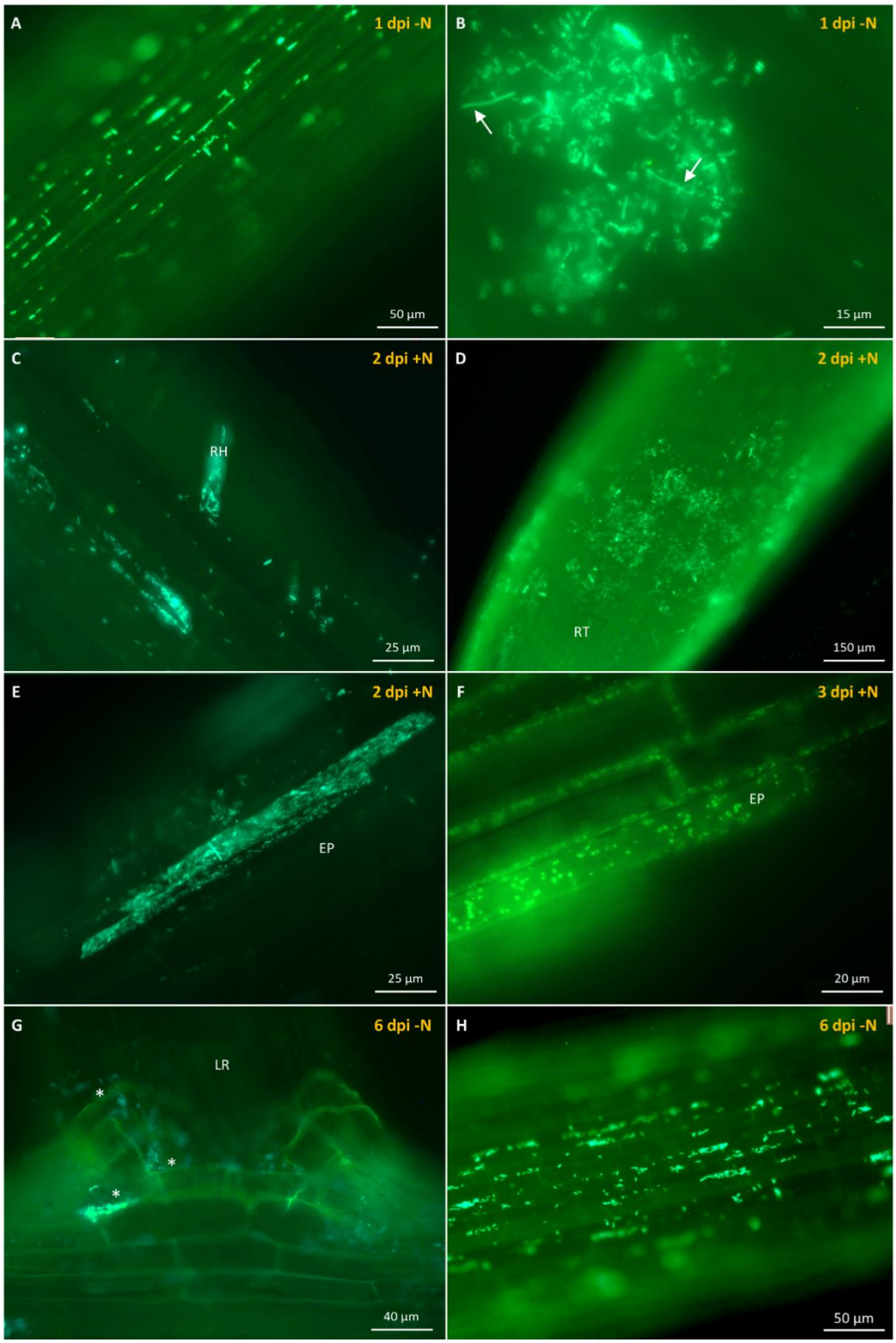


Fig. 4.57. Tomato (cv. "MoneyMaker") grown hydroponically in zero N ("-N", in orange) or 2mM KNO_3 NS ("+N", in orange) inoculated with GGG at OD_{600} = 0.3 and collected at different time points (in orange), fluorescence microscopy. (A, H) Individual interspersed cell evenly distributed on the root epidermis of the maturation zone, with a preference for the cell wall junctions. (B) Bacterial aggregates exhibiting both rod and filamentous (white arrow) morphology. (C) GGG colonising a root hair and initiating the colonisation of an epidermis cell. (D) GGG colonising root tip, similarly to what described for A and H. (E) Bacterial cell colocalising within the area of the periclinal cell wall of some specific epidermal cells. (F) Globular bacteria-like organelles localised in intercellular spaces and within the cytoplasm of

one epidermal cell. (G) GGG cells (white stars) entering plant tissues through the cracks created by an emerging lateral root. EP = epidermal cells; LR = lateral roots; RH = root hair; RT = root tip.

Already after 1-2 dpi, root hairs appeared to be colonised (Fig. 4.57c). Additionally, as new lateral roots emerged, some cells were observed entering through the cracks left by the ruptured or displaced epidermal cells (Fig. 4.57g). The interplay of interspersed individual cells and biofilm aggregates was observed in both the maturation/elongation zone (Fig. 4.57a-c) and in the root tip (Fig. 4.57d), and remained stable throughout the duration of the experiment (note the similarity between Fig. 4.57b and Fig. 4.57h, captured with a 6-day interval). This suggests that the root surface could serve as an "operational base" for a continuous process of bacterial multiplication and subsequent invasion of plant tissues, most likely through epidermis cell wall junctions, lateral root emergence sites and possibly root hairs. No obvious colonisation differences were detected between the two different growth media.

Rarely, a phenotype as the one showed in Fig. 4.57f was observed, with green-fluorescing globular particles localised in the epidermis cell walls and inside the cytoplasm. These formations, with their regular round shape, were reminiscent of organelles, possibly amyloplasts-statoliths (which are also excited when using a GFP filter set); however, they did not localise in the root cap and seemed to mostly occur intercellularly, between the anticlinal cell walls. The similarities of these images with statolith-rich areas found in untreated root tips (not shown) prevents a conclusive characterisation of these fluorescent bodies as either organelles or a specialised endophytic *GGG* morphology. Similar observations, however, were relatively frequent in early studies of *G. diazotrophicus* employing immunogold labelling [221] or other form of bacterial staining [271] coupled with electron microscopy, although all these detection techniques are prone to artifacts due to the sample processing. Furthermore, a similar phenotype was reported in parallel investigations conducted on rice by another research group at Durham University, utilizing the same *GGG* strain produced in this study (Unpublished). Nevertheless, these findings remain inconclusive.

Another intriguing finding was the precise co-localization of bacteria with the outer periclinal cell wall of some epidermal cell (Fig. 4.57e). This behaviour was further investigated in light of its apparent linkage with intracellular colonisation, employing both *GGG* and *GdRed* strains (Fig. 4.58). Some of the root epidermis cells, independently from the bacterial presence and the N condition, exhibited a higher autofluorescence, possibly due to a denser lignin concentration or, more probably, because of a different refraction of the excitation light due to a dissimilar (or absent) cytoplasmic content. (Fig. 4.58a, UT sample). This phenotype likely discloses the formation of aerenchyma, i.e., a degenerate cellular tissue that plants produce to facilitate gas exchange in submerged tissues as a response to flooding stress [514]. Tomato have been reported to be prone to aerenchyma formation, which would be consistent with the deepwater hydroponic setup employed, although very limited research is available in this regard [514].

Interestingly, the process is known to be driven by the accumulation of ethylene in the submerged root system, resulting in ROS-mediated programmed cell death (PCD) [514]; if confirmed, this mechanism would indicate that the lack of aeration in the hydroponic setup may result in a particularly hostile root environment, with oxidative stress coupled with hypoxic condition and low gas circulation (possibly including gaseous nitrogen), which may contribute to the lack of detectable BNF-derived nitrogen in plant tissues and the putative plant immune response discussed in section 4.1. On the other hand, the formation of aerenchyma cells culminates with the action of cell wall loosening enzymes such as cellulases, expansins and xyloglucan endo-transglycosylase [514], creating a convenient entry point for bacteria, without the energetic burden of cell wall degradation (if any) and providing a perfect ecological niche to be used as a "wedge" for subsequent colonisation of deeper tissues.

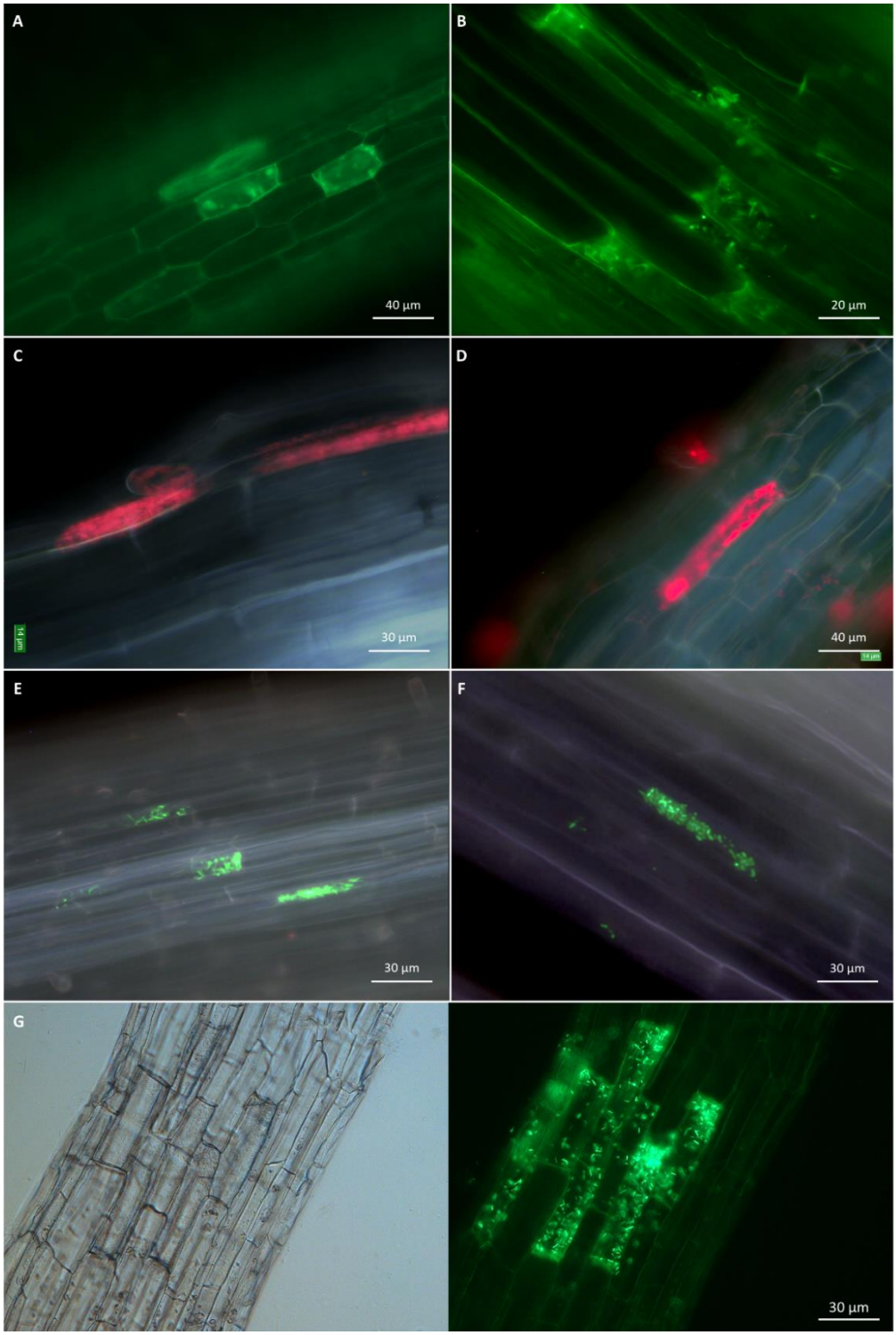


Fig. 4.58. Root epidermis cell colonisation of tomato grown hydroponically in 2mM KNO_3 NS inoculated with GGG or GdRed. (A) Untreated root showing a degenerate cell with a higher autofluorescence, speculatively as the result of flooding stress-induced aerenchyma formation. (B-G) Rod-shaped GGG (green) and GdRed (red) colonising intracellularly some specific epidermal cells, possibly taking advantage of the aerenchyma formation process. Samples were collected between 2 to 15 dpi, and no apparent divergence in this colonisation mechanism was observed throughout this period.

This model was also proposed by a study investigating the colonisation of rice by the non-nodulating diazotroph *Herbaspirillum seropedicae*, which was found to densely colonise the large cells committed to transitioning into lysigenous aerenchyma, typical of wetland rice [254]. While this hypothesis has not been experimentally validated and cannot be assumed as true, it is evident that *G. diazotrophicus* concentrates its efforts on certain root epidermis cells (Fig. 4.58b-g) as the initial entry point for either apoplastic or symplastic colonization. The FP-tagged bacteria observed engaging in such behaviour predominantly exhibited a rod shape (Fig. 4.58g), occasionally displaying some degree of elongation (Fig. 4.58b), and appeared to reside within the same plane, suggesting their presence between the cell wall and the plasma membrane rather than within the cytoplasm.

Another favoured entry point, as also suggested by the MS agar setup (Fig. 4.55d), were the root hairs, which were found to be epiphytically and endophytically colonised at all stages of the experiment (Fig. 4.59). Even this mode of action did not show any obvious mechanistic differences between N-replete (Fig. 4.59) and N-free conditions (not shown). The colonization process seemed to either initiate at the base of the emerging hair (Fig. 4.59a) upon endophytic invasion of the trichoblast and subsequent progress along the length of the hair (Fig. 4.59c), or by direct epiphytic colonization of the hair following biofilm formation on its surface (Fig. 4.59d, g, f). Most of the time, both mechanisms were observed to occur simultaneously (Fig. 4.59b, d). In scenarios such as in Fig. 4.59c, it cannot be ruled out that the trichoblasts are colonised as a consequence of prior root hair entrance.

In either case, the result was an obvious endophytic colonisation of the hair structure by bacteria exhibiting an elongated (but not filamentous) or rod shape (Fig. 4.59 b, e, h, i, j). In contrast, the concurrent epiphytic colonisation observed on the hair surface (Fig. 4.59b, d, g, f) was characterised by a biofilm composed of a majority of rod/coccoidal-shaped bacteria and some rare filamentous cells.

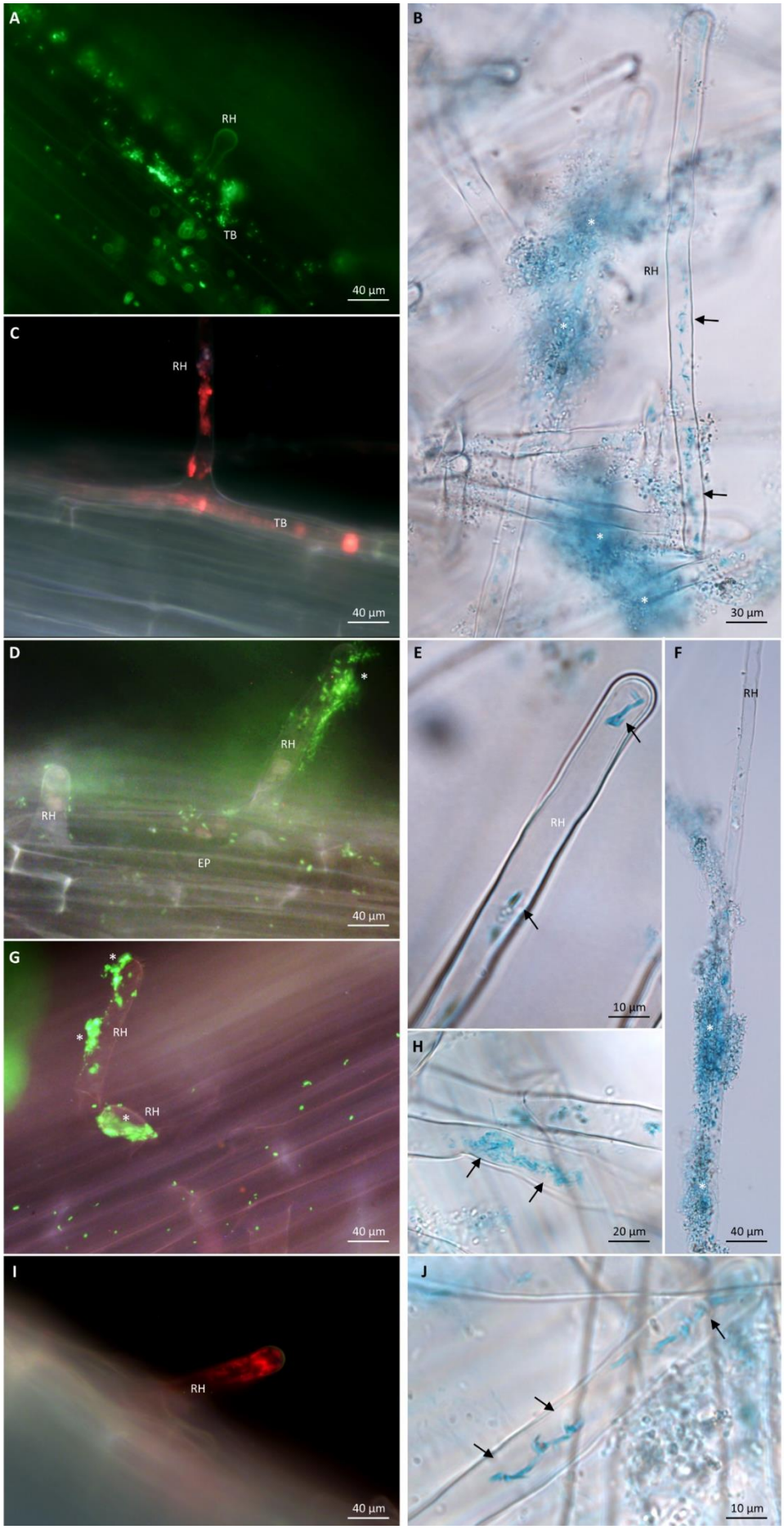

A
RH
TB
40 µm
B
RH
30 µm
C
RH
TB
40 µm
D
RH
RH
EP
40 µm
E
RH
10 µm
F
RH
40 µm
G
RH
RH
40 µm
H
20 µm
I
RH
40 µm
J
10 µm

Fig. 4.59. Root hairs colonisation of tomato grown hydroponically in 2mM KNO_3 NS inoculated with GGG or GdRed. GGG-treated samples shown in brightfield illumination upon GUS staining (B, E, F, H, J) were collected at 3 dpi. GGG (green) or GdRed (red)-treated samples shown through fluorescence microscopy (A, C, D, G, I) were collected between 7 and 21 dpi. (A, C) Colonisation extending from the root hair to its epidermal cell (with unclear temporal direction). (B, D, G, F) Epiphytic colonisation of root hairs by coccoidal/rod-shaped bacteria aggregated in biofilms (white stars). (E, H, I, J) Intracellular colonisation of root hairs by rod-shaped G. diazotrophicus (black arrows). EP = epidermis; RH = root hair; TB = trichoblast.

Root hairs are usually assumed to play a significant role in establishing plant-microbiota interactions: studies investigating the endophytic behaviour of *G. diazotrophicus* reported root hairs colonisation in tomato [174], sorghum [155], *A. thaliana* [262] and sugarcane [510]. Similarly, other PGP diazotrophs such as *Herbaspirillum seropedicae* have been observed among root hairs of rice [254] and pineapple [516] (for a comprehensive review see Mercado-Blanco and Prieto, 2012 [515]). However, there is limited research about the role of root hairs in non-rhizobial microbe uptake, and scarce evidence for their intracellular colonisation [515], except for a few studies involving *Pseudomonas* spp. in olive trees [517] and reed grass [520], and endophytic communities inhabiting corn [518] or rice [519].

In the extensively characterised process of rhizobial colonisation, flavonoids such as luteolin attract the bacteria to root hairs and initiate a crosstalk with bacterial *nod* factors that, together with EPS-mediated colonisation, induce the root hair to form an infection thread; this structure consists in a closed channel [521] of growing plant cell wall that, elongating uninterruptedly from the root hair into the apoplastic space, deliver the bacteria in deeper cell layers, where they are endocytosed by plant plasma membrane vesicles into symbiosomes [522]. This specialized process is believed to have emerged as recently as 60 million years ago, when legumes evolved, and is restricted to 75% of leguminous plants; the remaining species, primarily from tropical biomes (but with temperate exceptions such as *Lupinus*), rely on the older strategy of direct epidermis colonisation and passive invasion of lateral root emergence sites [33].

While non-nodulating diazotrophs such as *G. diazotrophicus* may share this older and more generalist colonisation mechanism with rhizobia species that do not form infection threads, it is still plausible that root hairs may offer a privileged entry point for endophytic colonisation, due to the high exudation of nutrients and chemoattractants [523] and to the thinner cell wall in the vesicle-dense region of the root hair apex [524]. It is conceivable, as previously proposed [515], that active endocytosis of endophytes may occur along the root hair (possibly at the root hair tip, Fig. 4.59e) allowing the entrance of beneficial bacteria for plant growth modulation or even the uptake of free-living bacteria to be degraded and assimilated as a nutrient source [520], in a type of mixotrophy (the use of nutrients of both photosynthetic and organic origin) named "rhizophagy" [525].

Further investigations along the longitudinal plane of the root surface, allowed the definition of four main colonisation behaviours: 1) single interspersed bacteria, often occupying the wall junction of root epidermis cells (Fig. 4.57a, c, d, h); 2) large aggregates of bacterial biofilm emerging with no apparent pattern across the rhizoplane (Fig. 4.57b, Fig. 4.60e, f); 3) confined apoplastic (and possibly symplastic) colonisation of specific root epidermis cells, some of which may offer a favoured niche due to cytoplasm degeneration following aerenchyma formation, used as entry point for further colonisation (Fig. 4.57e, f, Fig. 4.58); 4) diffused colonisation of root hairs all along the root maturation zone (Fig. 4.57c, Fig. 4.59, Fig. 4.60g, h). The passive diffusion through lateral root emergence sites, which is frequently reported as the preferred entry point for non-nodulating endophytes [266] including *G. diazotrophicus* [526], was only occasionally observed (Fig. 4.57g), indicating that in the hydroponic setup this mechanism may lose its advantages; this may be due to the liquid medium in which the symbiotic system is submerged, that may partially alter the outcome of the bacterial chemotaxis toward the root system compared to a solid or semisolid substrate. Interestingly, while epiphytic biofilms were mostly composed of rod or ovoidal bacteria in both the epidermis cells and the root hairs, a more thorough examination of colonised epidermal root cells revealed the endophytic bacterial cells to be almost entirely elongated or filamentous (Fig. 4.60a-d).

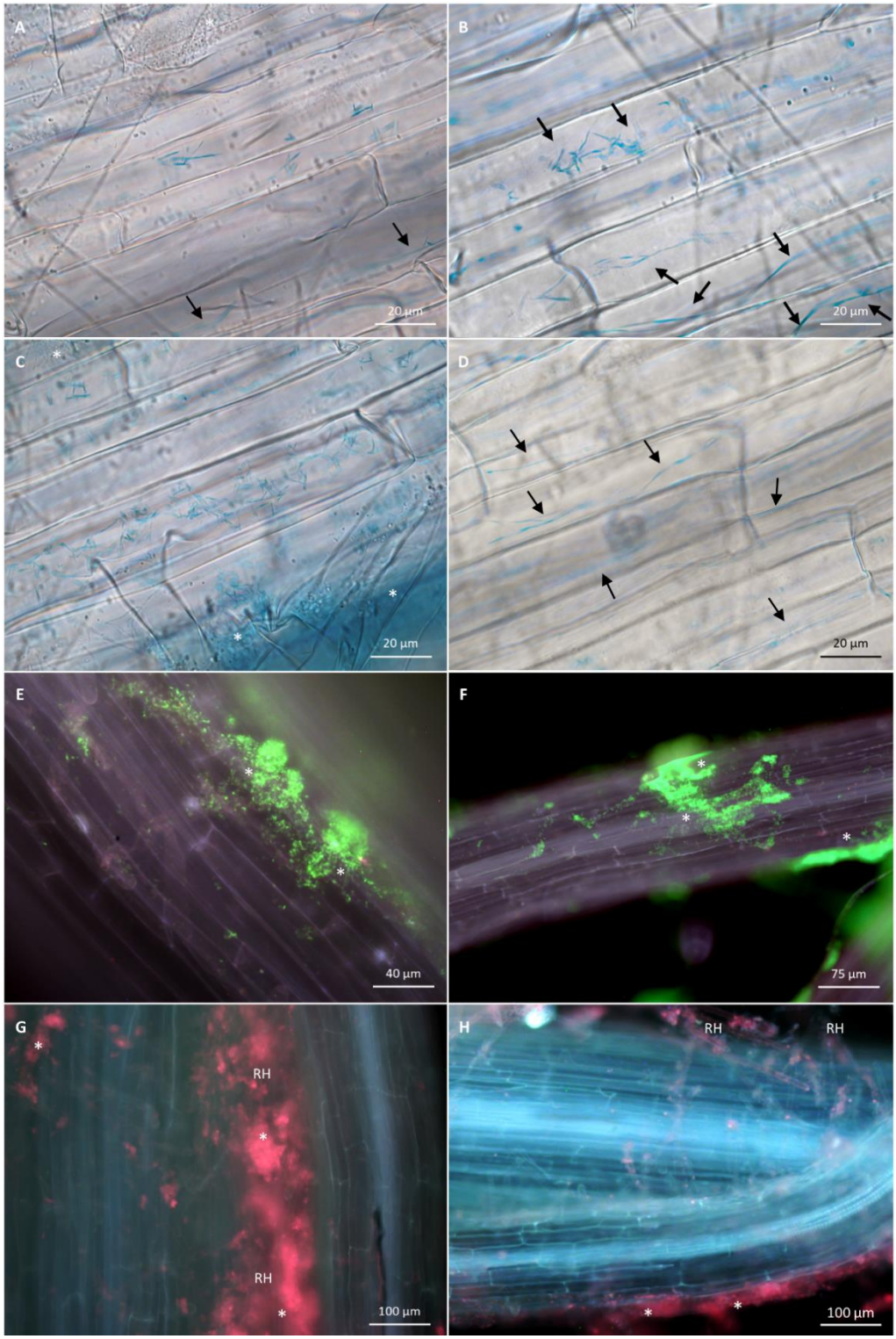
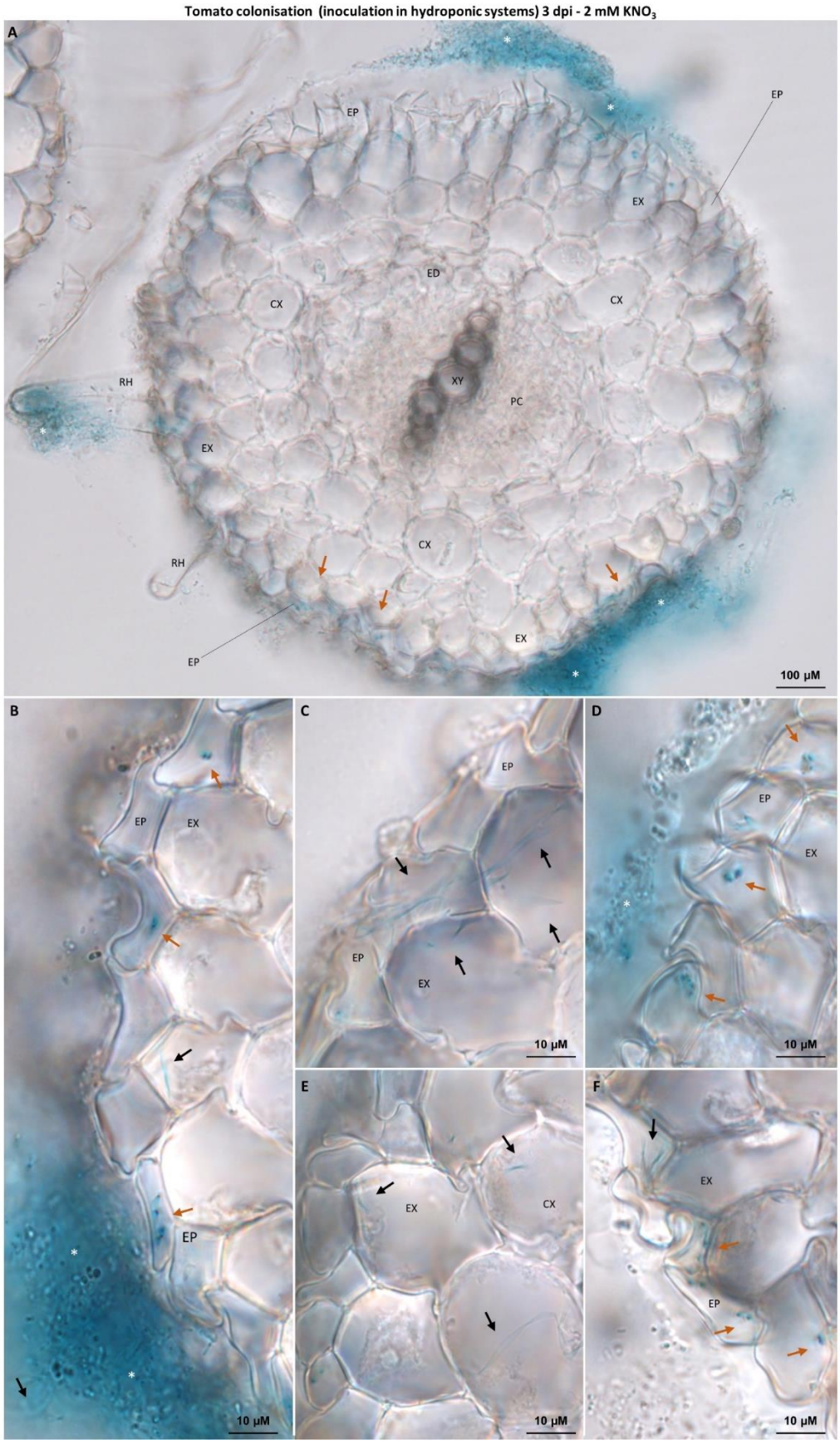


Fig. 4.60. Root epidermis colonisation of tomato grown hydroponically in 2mM KNO_3 NS inoculated with GGG or GdRed, longitudinal plane. GGG-treated samples shown in brightfield illumination upon GUS staining (A, B, C, D) were collected at 3 dpi. GGG (green) or GdRed (red)-treated samples shown through fluorescence microscopy (E, F, G, H) were collected between 15 and 25 dpi. (A-D) Elongated and filamentous GGG cells (black arrows) colonising endophytically epidermal root cells. (E, F) Bacterial biofilm composed of rod/coccoidal cells aggregating on the root surface (white stars). (G, H) Rod-shaped GdRed cells colonising the root hairs all along the maturation zone. RH = root hairs.

These cells exhibited a filamentous morphology with different degrees of elongation, ranging from extending along the entire length of the epidermal root cell (Fig. 4.60a, b, d, black arrows) to slightly elongated rod-shaped cells and a spectrum of intermediate forms (Fig. 4.60a-c). The degree of elongation appeared to be inversely proportional to the number of bacteria present within a single root cell (Fig. 4.60a-d).

The presence of filamentous cells and their level of penetration in the root tissues was verified through cross sectioning of treated plants at different time points and N levels (Fig. 4.61). No difference in colonisation patterns was observed between N-replete (Fig. 4.61a-f and l-q) and N-free (Fig. 4.61g-k) conditions. In accordance with previous observations, no obvious shift in the colonisation dynamic was observed over the duration of the experiment (up to 30 dpi) and all the different mechanisms seemed to occur simultaneously at every investigated time point, as if the same colonisation course was occurring continuously in a cyclic manner. Fig. 4.61a summarises the main colonisation phenotypes encountered along the maturation/differentiation zone in the hydroponic (and MS agar) setups: epiphytic biofilms covering the root epidermis and hairs (white stars), with some obvious intracellular colonisation on the epidermal layer by elongated rod-shaped bacteria (orange arrows). The combination of brightfield illumination and fluorescent microscopy at higher magnifications showed bacteria tightly adhering to the root epidermis (Fig. 4.61g, h) along with bacterial cells intracellularly colonising the epidermal layer, typically ranging between 2 and 6 bacteria per epidermal cell (Fig. 4.61a, b, d, f, m). These bacteria, regardless of the staining or visualisation method employed, usually appeared as round dots, indicating the cross sectioning of the elongated cells arranged parallelly to the periclinal wall described in Fig. 4.60a-d. Some *GGG* cells were found in the exodermal layer (Fig. 4.61b, c, i, h) and even within the cortex tissues (Fig. 4.61e, j, k, h, l, o, p).


Tomato colonisation (inoculation in hydroponic systems) 3 dpi - 2 mM KNO_3
A
EP
EP
EX
ED
CX
CX
XY
PC
RH
EX
CX
RH
EP
EX
100 µM
B
EP
EX
EP
10 µM
C
EP
EP
EX
10 µM
D
EP
EX
10 µM
E
EX
CX
10 µM
F
EX
EP
10 µM

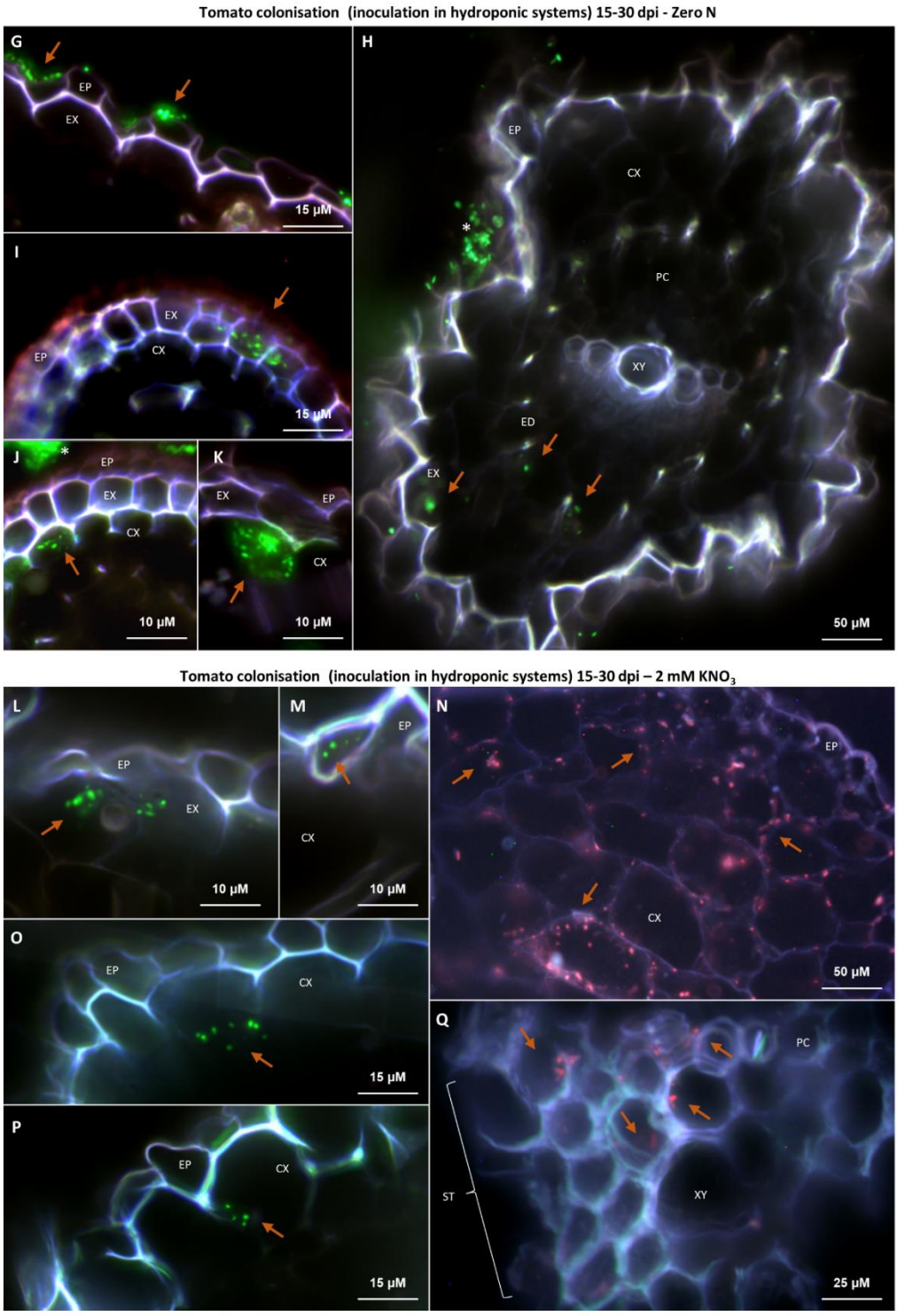


Fig. 4.61. Root epidermis colonisation of tomato grown hydroponically in zero N (G-K) or 2mM KNO_3 (A-F and L-Q) NS inoculated with GGG or GdRed, cross sections. GGG-treated samples shown in brightfield illumination upon GUS staining (A-F) were collected at 3 dpi. GGG (green) or GdRed (red)-treated samples shown through fluorescence microscopy (G-Q) were collected between 15 and 25 dpi. Rod-shaped intracellular bacteria or cross section of filamentous bacterial cells (appearing as circles) are indicated by orange arrows, while filamentous intracellular bacteria captured in their longitudinal plane are indicated by black arrows. (A) Comprehensive view of a root cross section from the maturation zone showing X-Gluc stained biofilm (white stars) surrounding the root epidermis and hair and some elongated

rod-shaped cells occupying intracellularly the epidermal layer, showed in detail in B, D, F, M. (G) Epiphytic colonisation of the epidermis by rod-shaped GGG cells. (B) Detail of the epidermis and exodermis layers in proximity to a biofilm composed of coccoidal/rod-shaped cells, with the exception of a filamentous cell (black arrow). Sectioned elongated rod-shaped bacteria and filamentous cells are also shown (orange arrow). (C, F) Filamentous GGG cells extending between the exodermis and the epidermis through the cell wall. (I, L) rod-shaped cells colonising intracellularly the exodermis layer in the maturation zone (L) and in the root tip (I). (E, H, O, P) Filamentous (GUS staining) and rod-shaped (fluorescence) cells colonising the cortex without extending pass the endodermis. (J, K) Rod-shaped cells colonising the cortex of the root tip. (N, Q) Mixed GdRed and chlorophyll signal diffused throughout the whole apoplastic root space (N) and the xylem vessels (Q) in the root-shoot junction. CX = cortex; ED = endodermis; EP = epidermis; EX = exodermis; PC = procambium; RH = root hair; ST = stele; XY = xylem.

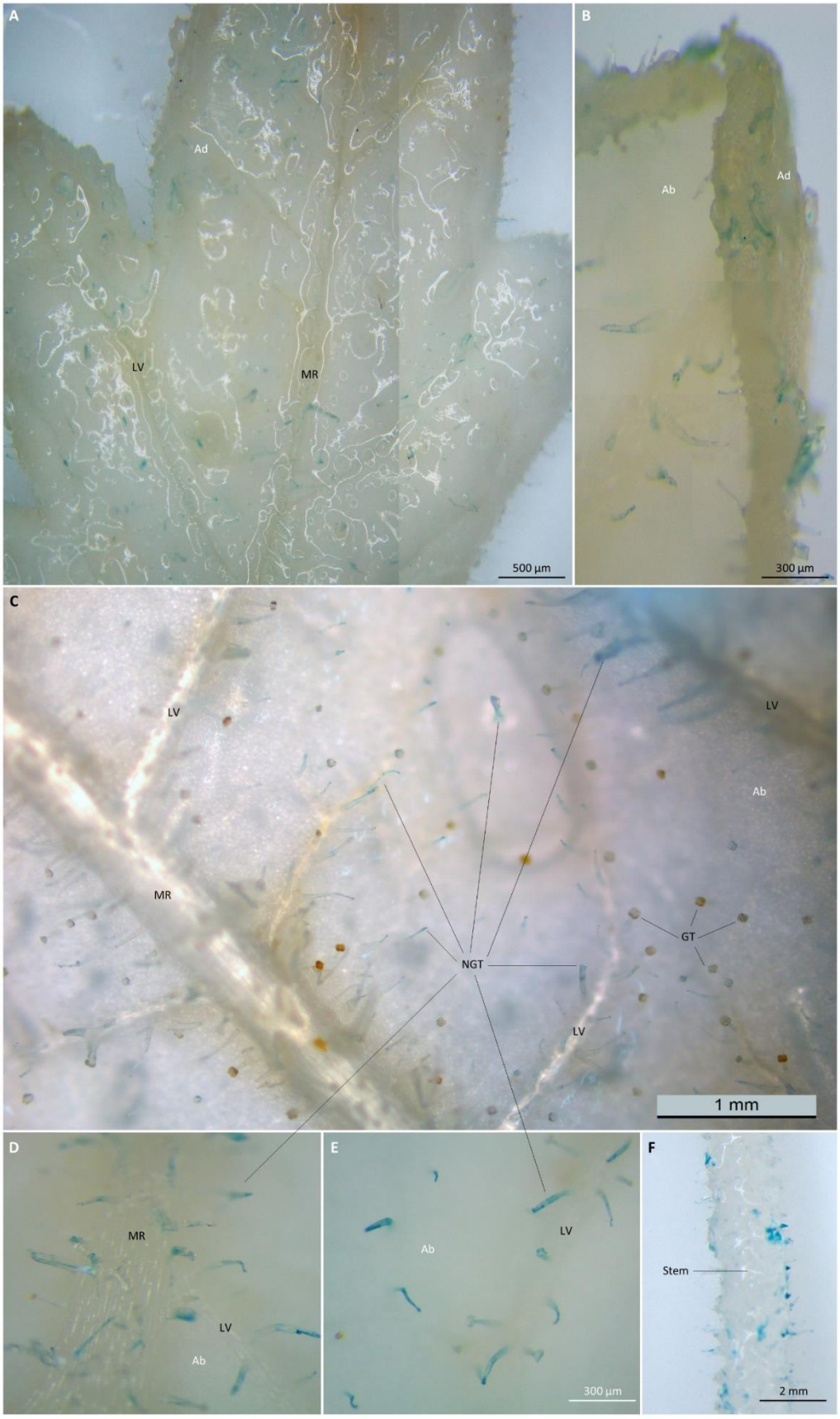
As for the stele, no bacteria were observed unless plants were inoculated with *GdRed*, the excitation of which, as previously discussed, overlaps with chloroplasts and was also detected in untreated samples (not shown); in images such as Fig. 4.61n, the red signal is emitted from chlorophyll and, possibly, from bacteria, distinguishable only for their smaller size. However, the size comparison does not exclude the presence of partially degraded chlorophyll-containing organelles debris, and the absence of GFP or GUS-tagged bacteria past the endodermis/pericycle (Fig. 4.61a, h) seems to weaken the hypothesis of a full endophytic root pervasion suggested by the *GdRed* mutant application. Nevertheless, the shape and dimension of red-marked organelles among the procambium and xylem vessels in Fig. 4.61q were compatible with *G. diazotrophicus* cells. The distribution of these putative bacterial cells adhering on the inner cortical and vascular cell walls (Fig. 4.61n, q) closely resembles the images produced through scanning electron microscopy by Fuentes-Ramìrez et al. in their study on sugarcane colonisation [207]. The use of GFPmut3* circumvented the complete lack of intracellular fluorescence experienced by Sevilla and Kennedy in GFPmut2-tagged *G. diazotrophicus* [248] or *H. seropedicae* [516] as a result of chromophore protonation in environments acidified by the bacterial metabolism; however, it cannot be ruled out that such issue may have been mitigated not suppressed, and that it may persist in some intracellular environment or be associated with a specific bacterial metabolic state. Rouws et al. also employed GFPmut3* in their investigation of rice colonisation by *G. diazotrophicus* and, similarly, obtained detailed images of tagged bacteria on the root surface but relied on GUS tagging and light microscopy for the detection of endophytic bacteria in cross

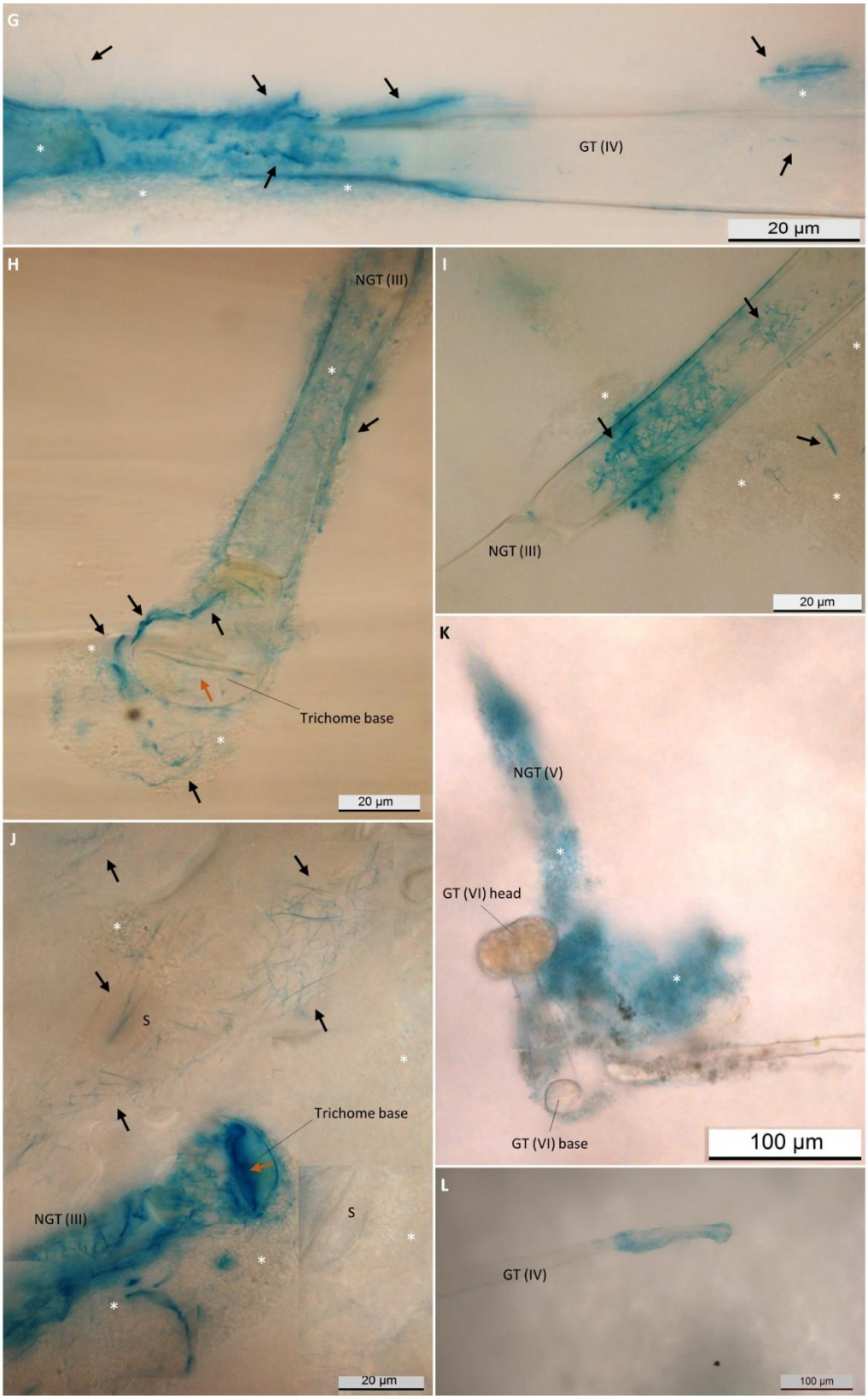
section analyses [526]. The DsRed-Express2 protein, on the other hand, is likely to possess greater stability, as explained in section 4.2.1b. To support the hypothesis that different tagging proteins may possess varying folding efficiencies based on their localization within plant tissues or the physiology of the tagged bacteria, thereby explaining their different distribution patterns, the GUS tagging not only disclosed bacteria in deeper cortical layers compared to the GFP signal (Fig. 4.61e) but, crucially, also stained intracellular filamentous *GGG* cells (Fig. 4.61a-f, black arrows) that were never observed through fluorescence microscopy. This finding confirms that different metabolic state or microenvironments inhabited by *G. diazotrophicus* can affect the expression of the tagging protein *in vivo*, reinforcing the necessity of complementing microscopy observations with different visualisation strategies. The GUS-stained filamentous *GGG* cells were found to extend from the epidermis (Fig. 4.61f) to the cortex layer proximal to the endodermis (Fig. 4.61e), although no blue signal was detected past the Casparian strip. Occasionally, the filamentous cells were observed extending from one cortex/exodermis cell to the adjacent root cell (Fig. 4.61c), suggesting a potential symplastic connection, although this may be an artifact of the sectioning procedure. Passage through plasmodesmata (PD) may seem unlikely, since these channels are occupied by cytoskeletal proteins and the endoplasmic reticulum, leaving only narrow cytoplasmic sleeves of 3-4 nanometres in diameters [527] [528] [529]. However, if *G. diazotrophicus* possesses the ability to penetrate the cell wall and reach the cytoplasm, as suggested by the microscopy analyses illustrated above, PD may still represent a preferred crossing point between plant cells. Cell wall regions around PD are thinner and characterised by an enrichment in distinct pectic polysaccharides and callose and by a reduction in cellulose content, and can be rearranged in their structure and aperture by modulating their composition [529]; for example, pectin degradation can lead to the PD channel destabilisation [530]. Furthermore, not only viruses but even fungi have been shown to diffuse through remodelled PD [527], while phytopathogenic bacteria can modulate PD-mediated cell-to-cell communication in plants by the production of non-cell autonomous effectors proteins [531] [532] [527]. This information supports the idea of *G. diazotrophicus* diffusing through adjacent root cells upon endophytic

colonisation, although it is not clear whether this mechanism can extend to the stele.

4.3.1c Tomato inoculation in hydroponic setup - Shoot colonisation

The leaves of hydroponically grown tomatoes were analysed in more detail through X-Gluc staining, due to the difficulty of distinguishing FP fluorescence from the auto fluorescent background of the thick and chlorophyll-rich leaf samples. At a first glance, the shoots appeared mostly unstained compared to the roots except for some confined areas (Fig. 4.56). However, a closer inspection showed that the vast majority of the non-glandular trichomes in the stem and leaves were densely colonised by *GGG* cells (Fig. 4.62), usually in the elongated or filamentous morphology (black arrows). Trichomes were colonised along the stem (Fig. 4.62f) and on the adaxial (upper) surface (Fig. 4.61a, b) and the abaxial (lower) surface (Fig. 4.61b-e) of the leaf. Interestingly, trichomes arising in correspondence of primary (Fig. 4.61d) and secondary (Fig. 4.61e) veins on the abaxial leaf surface showed the highest rate of colonisation (Fig. 4.61c-e). This may suggest that bacteria are transported through the xylem sap via vascular bundles and subsequently secreted or "stored" within the non-glandular trichomes. The apparent lack of blue staining inside the four-disc-cells head of type VI glandular trichomes [533] (Fig. 4.61c, k) may be either an artifact caused by their natural orange coloration, or, most likely, may reflect the unsuitability of this particular niche for bacterial invasion due to the high concentration of antimicrobial compounds such as terpenoids [534] [535] or myricetin [533] [536].


A
Ad
LV
MR
500 µm
B
Ab
Ad
300 µm
C
LV
LV
Ab
MR
GT
NGT
LV
1 mm
D
MR
LV
Ab
E
LV
Ab
300 µm
F
Stem
2 mm


G
GT (IV)
20 µm
H
NGT (III)
Trichome base
20 µm
I
NGT (III)
20 µm
K
NGT (V)
GT (VI) head
GT (VI) base
100 µm
J
S
Trichome base
NGT (III)
S
20 µm
L
GT (IV)
100 µm

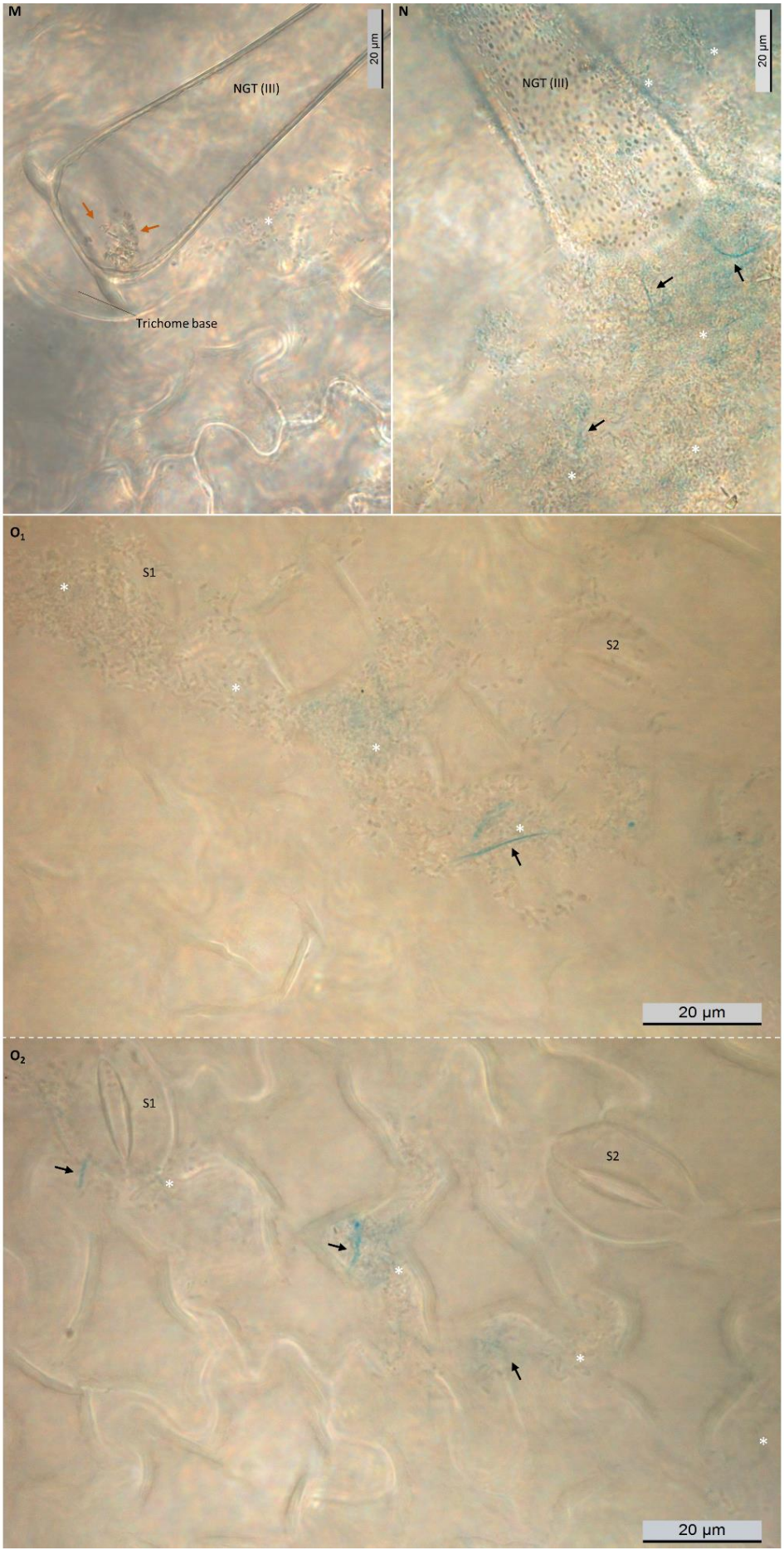

M
20 µm
NGT (III)
Trichome base
N
20 µm
NGT (III)
O1
S1
S2
20 µm
O2
S1
S2
20 µm

Fig. 4.62. Shoot epidermis colonisation of tomato grown hydroponically in 2mM KNO_3 NS inoculated with GGG, 20 dpi. GGG-treated samples are shown in brightfield illumination upon GUS staining. Filamentous and elongated GGG cells are labelled with black arrows; rod/coccoidal-shaped GGG biofilms are labelled with white stars; GGG cells colonising the interface between the trichome bases and underlying epidermal cells are indicated by orange arrows (A) Colonised non-glandular trichomes (blue) disseminated on the adaxial leaf surface. (B) Colonised non-glandular trichomes disseminated on the abaxial leaf surface, particularly in correspondence to the primary (D) and secondary (E) vascular bundles. The head of type VI glandular trichomes appears in orange. (F) Colonised non-glandular trichomes and epidermal cells on the stem. (G) Type IV glandular trichome epi and endophytically colonised by filamentous and elongated GGG cells, z-stack composite. (H-J) Non-glandular trichomes epi and endophytically colonised by filamentous and elongated GGG cells, z-stack composites. The orange arrows indicate the interface between the basal cell of the trichome stalk and the underlying epidermal cell colonised by filamentous or rod-shaped bacteria bacteria; filamentous bacterial cells colonising the leaf epidermal cells around the trichome are indicated by black arrows. (K) Uncolonised type VI glandular trichome close to a densely colonised hairy non-glandular trichome. (L) Type IV glandular trichome colonised by GGG cells on the stalk head. (M-N) Unstained biofilm of rod-shaped bacteria, including a minority of stained filamentous cells, endophytically (M) and epiphytically (N) invading type III non-glandular trichomes (usually 0.4–1.0 mm in length [534]*) from the unicellular base. (O_1-O_2) Unstained biofilm of rod-shaped bacteria (white stars), including a minority of stained filamentous cells (black arrows), colonising epidermal subsidiary cells around stomata on the abaxial leaf surface, z-stack from top (O_1) to bottom (O_2). Ab = abaxial leaf surface; Ad = adaxial leaf surface; GD = glandular trichome (the type is indicated in brackets); LV = lateral or secondary vein; MR = midrib, or primary vein; NGD = non-glandular trichome; S = stoma.*

Occasionally, colonisation was found in type I and IV glandular trichomes, which are similar in content and shape to non-glandular ones except for a small terminal globe-shaped storage/secretion unit (Fig. 4.62g, l) [533]. In general, trichomes were colonised both on the inside (Fig. 4.62h-j) by elongated bacterial cells, and on the outside (Fig. 4.62g-l, black arrows) by filamentous cells (Fig. 4.62g-j) or, more rarely, by epiphytic rod/globular shaped cells (Fig. 4.62 g-l, n, white stars). The symplastic transport of bacteria into the trichome stalk from the underlying epidermal cell is suggested by their presence in the interface that separates these two environments (Fig. 4.62j, m, orange arrows). Alongside reaching trichomes via xylem sap as the endpoint of a transport route initiated in the root system, it is also possible that trichomes are colonised externally (Fig. 4.62k, l, n) by bacteria emerging from adjacent stomata, which were frequently observed in close proximity to colonized trichomes. (Fig. 4.62j). However, this mechanism still implies prior bacterial convey to stomatal chambers via xylem or phloem flow. Alternatively, the presence of epiphytic bacteria alongside the trichome stalks (Fig. 4.62g-l) or around their bases (Fig. 4.62h, j, n) may be the result of exocytosis or secretion of the bacteria from the trichomes in response to environmental condition or

physical damage. It was also observed that a higher concentration of bacteria was present in the epidermal cells around the trichomes (Fig. 4.62i, j, n) or stomata, including the subsidiary cells (Fig. 4.62o) compared to other featureless epidermis cells. These bacterial cells were usually filamentous (Fig. 4.62h-o, black arrows) or rod/coccoid-shaped (Fig. 4.62h-o, white stars). However, it is important to note that the biofilm of rod-shaped bacteria surrounding stomata or trichome bases often did not stain blue (Fig. 4.62h-o, white stars), whereas the filamentous ones did (Fig. 4.62g-o, black arrows), suggesting a distinct plasmid retention capacity corresponding to the acquired morphology, as discussed in section 4.2.1c. Overall, trichomes and stomata seemed to be the preferred shoot colonisation sites in the same way that root hairs and degenerated epidermal root cells or cell wall junctions were the hot spots for root colonisation.

4.3.1d Tomato colonisation in hydroponic setup - bacterial quantification by qPCR

To complement the imaging data illustrated above and obtain a quantification of the relative distribution of *G. diazotrophicus* throughout the plant tissues, qPCR analyses targeting the bacterial genome were conducted on the hydroponically grown tomatoes. The colonisation of tomato inoculated with either *G. diazotrophicus* AZ0019 WT or *G. diazotrophicus* AZ0019 *nifD*$^{-}$ was investigated in order to gain insight into the potential influence of nitrogen fixation on the bacterial endophytic behaviour (see section 4.41). Plants were grown in zero nitrogen, 2 mM KNO_3 or 2 mM KNO_3 + 0.2 mM $(NH_4)_2SO_4$ conditions (see section 4.1.1b) and collected at 1 and 20 dpi. Each plant was divided into five main anatomical regions: leaves (including the compound and terminal leaflets, rachis and petiolules), stem (also including the basal region of the main petioles), shoot-root junctions, maturation/differentiation zones, and root tips (see Fig. 4.56, top panel). To ensure accurate quantification and unbiased comparison, the DNA was extracted from each sample in three biological replicates and brought at the same concentration, and the fold change (FC) of the amplicons obtained from the targeted unique *G.*

diazotrophicus genomic site were normalised against the amplicons from the tomato *ard2* gene.

The qPCR data revealed a consistent trend in the bacterial distribution, regardless of the N condition or BNF ability (Fig. 4.63). In general, colonisation in the shoot decreased by around one order of magnitude compared to the root system, confirming the trend observed through the MPN method (see section 4.1.1b, Fig. 4.15).

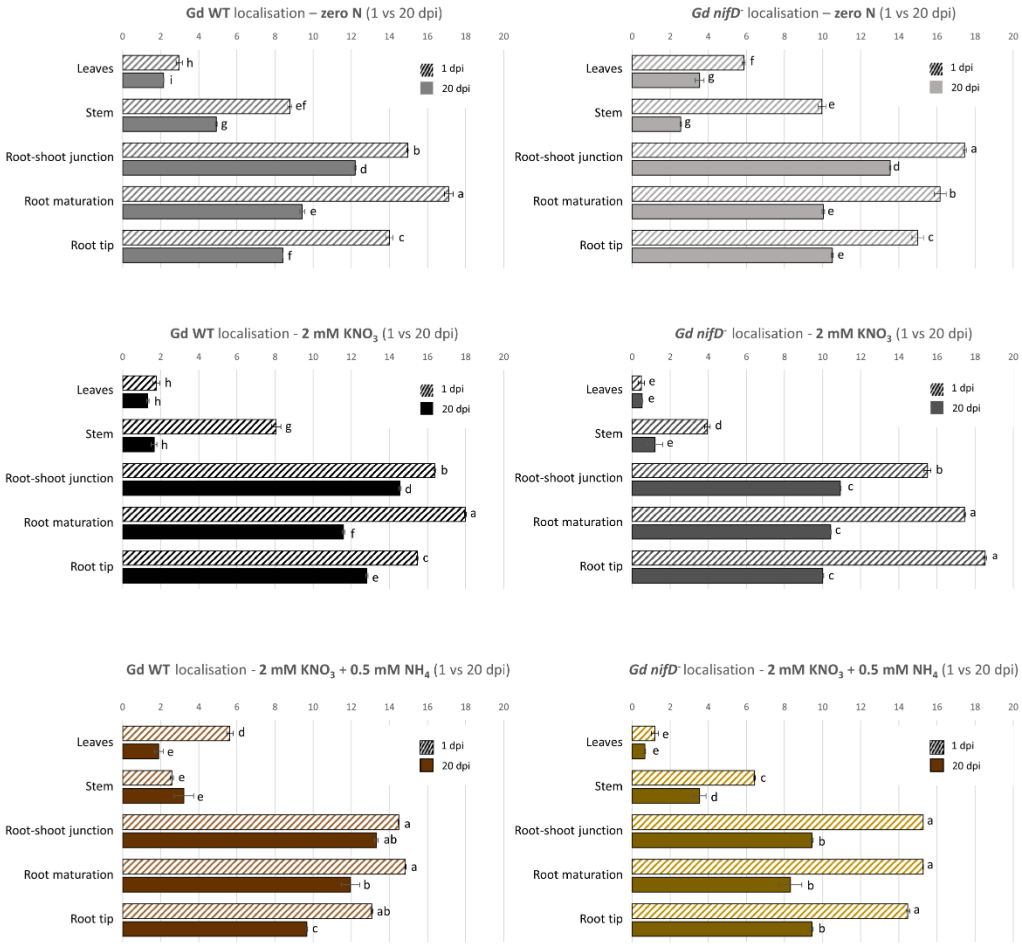


Fig. 4.63. qPCR analyses on tomatoes hydroponically grown in three different nitrogen conditions (zero nitrogen, 2 mM KNO_3 or 2 mM KNO_3 + 0.2 mM $(NH_4)_2SO_4$) inoculated with G. diazotrophicus WT or nifD- strains. Samples were collected in triplicate at 1 and 20 dpi and divided into five anatomical regions (leaf, stem, shoot-root junction, maturation/differentiation zone, and root tips). The graph represents the fold change of the amplified bacterial template (from the nifD gene) as normalised on the tomato amplicons (amplified from the ard2 gene). The standard error of the mean (SEM) of the biological replicates is shown. Bars marked with the same letter within each chart do not differ by One-Way ANOVA test ($P \leq 0.05$); significantly different pairs were identified using Tukey's HSD test..

Another trend common to all samples was the decrease of bacterial population over time, as also evidenced through maceration and plating techniques (Fig. 4.15). At 1 dpi the root colonisation did not show a distinct pattern and seemed to be stochastically distributed, except for a trend of lower bacterial presence around the root tips which persisted up to 20 dpi. This finding confirmed what observed through microscopy in this study (Fig. 4.51, 4.56) and what reported by Luna et al. in their tomato colonisation study conducted through whole plantlet inoculation and growth in MS agar [174]. At 20 dpi there seemed to be an enrichment of bacteria in the root-shoot junction, in accordance with the high bacterial presence observed in this point through microscopy (Fig. 4.55e, f). The increased colonisation of such region may depend on a higher nutrient concentration in this transition zone; also, speculatively, it may reflect that this area is a primary accumulation point of bacteria during their continuative migration toward the shoot. Is should also be taken into consideration that the root-shoot junction was in direct contact with the small piece of cotton wool used for sowing and germinating the seed in the hydroponic system, constituting a possible substrate for bacterial adhesion and subsequent root-shoot junction invasion. However, the same enrichment of *G. diazotrophicus* in the root-shoot junction was also reported by Luna et al. in the afore-mentioned study [174], confirming the bacterial preference for this specific area. In general, the stems exhibited higher colonisation compared to the leaves, with the exception of the *nifD*$^{-}$ strain under zero N condition and the WT strain under ammonium-supplemented condition. Interestingly, these two conditions also demonstrated the highest level of leaf colonisation among all the samples. No major differences were observed between the distribution of the two strains, except for this unexpectedly high level of leaves colonisation by the *nifD*$^{-}$ mutant at 1 dpi; such finding may be explained by the bacterial research for N-rich compounds in the shoot or, alternatively, by an enhanced NS uptake by the roots due to the lack of both mineral and BNF-derived nitrogen in the environment. In contrast, the efficient establishment of the WT strain in the phylloplane may be the result of faster BNF initiation triggered by the ammonium assimilated in the NS before the migration to the shoot. Crucially, the phyllospheric bacteria discovered through light microscopy at 20 dpi were found to be already colonising both stem and leaves at higher

concentrations at 1 dpi, regardless of the N condition. Therefore, although no conclusive direct evidence of bacterial transport through xylem vessels was collected through microscopy (except for Fig. 4.61q), qPCR data strongly suggests that such mechanism may play a central role in transferring *G. diazotrophicus* to the aerial parts of the plant, as neither apoplastic nor symplastic ascent via root cortex or epidermis appears to be sufficiently efficient to explain such rapid relocation.

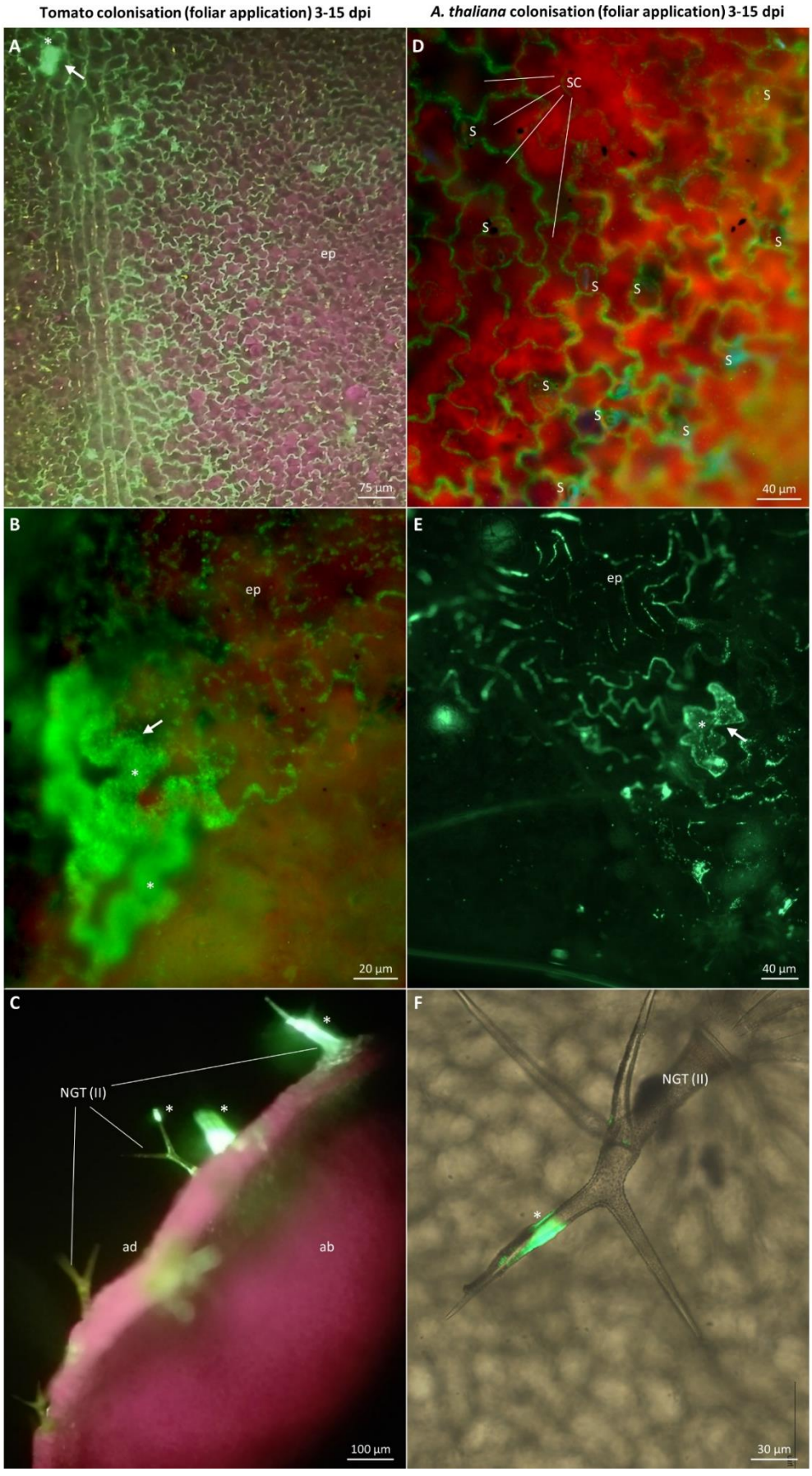
4.3.1e Foliar application

To gain additional insight into the phyllospheric potential of *G. diazotrophicus*, foliar application was tested. Foliar spraying of PGPB on aerial plant tissues is garnering growing interest as a biofertilisation method, since it can bypass the criticalities of seed coating and low bacterial survival during the first days of plant growth in agricultural settings, provided that the bacterium under consideration is capable of direct shoot colonisation [537]. The foliar application of non-nodulating PGP diazotrophs such as *Azotobacter* and *Azospirillum* has already proven successful in mulberry [538], maize [539], wheat [540] and canola [541]. However, the understanding of this colonisation mechanism remains scarce [537].

In this study, tomato (cv. “MoneyMaker”) and *A. thaliana* grown in axenic conditions in hydroponic setups or MS agar, respectively, were inoculated with 10^7 CFU mL^{-1} (OD_{600} = 0.3) of *GGG* directly on the leaves, including both terminal leaflets and younger leaves close to the apical bud but avoiding older basal leaves in the case of tomato. After an overnight incubation at room temperature, the leaves were washed thoroughly with sterile water or 10 mM $MgCl_2$ three times to remove loosely attached, non-interacting cells and conserved in the cold room in an airtight container with high humidity for up to two weeks, during which the bacterial GFP signal remained stable (Fig. 4.64).

The colonisation pattern was consistent between the two treated dicot species, and, intriguingly, resembled the dynamic observed in the root system of hydroponically grown tomatoes. Bacterial cells were primarily detected at the junctions of the epidermal cell walls (Fig. 4.64a, b, d, e), including abaxial stomata and subsidiary cells (Fig. 4.64d), confirming the preference of this grooves as advantageous entry points and protective niches against physical stresses. Some epidermal cells had a denser bacterial presence (Fig. 4.64a, b, e, white arrows), similar to what discussed relatively to the roots. This finding either indicates that certain cells may be a preferred colonisation site due to a higher exudation rate or nutrient presence, or it may confirm that *G. diazotrophicus* exerts targeted efforts for endophytic invasion on specific plant cells, possibly taking advantages micro ruptures in the corresponding cuticle or wall. Trichomes were confirmed to be hot spots for colonisation in both plant species (Fig. 4.64c, f). The confocal scanning of colonised leaves revealed the presence of leaf adaxial areas with bacteria occupying the epidermal cell wall junctions (Fig. 4.64g), aggregating in biofilms (Fig. 4.64h) or both (Fig. 4.64i). The endophytic penetration seemed to stop at the palisade mesophyll, as shown in reference to the chloroplasts localisation in the 3D modelling of the confocal z-stacks (Fig. 4.64g-i); however it is not clear whether this observation may suffer from the GFP limitation discussed earlier.

Overall, the foliar application of *G. diazotrophicus* on tomato and *A. thaliana* showed successful leaf colonisation with low levels of endophytic presence on the upper epidermis (although stomata were not analysed in detail) and an intriguing resemblance to the root invasion dynamics observed in the hydroponic setup. The collected evidence suggests the presence of a dual mechanism involving the combined action of individual bacterial cells colonising the cell wall junctions, and sparse biofilm aggregations serving as epiphytic “encampment” for subsequent expansion. Further investigation is necessary to elucidate the precise mechanisms underlying foliar colonisation, as well as its potential interaction with the root system and effect on the PGP potential.


Tomato colonisation (foliar application) 3-15 dpi
A. thaliana colonisation (foliar application) 3-15 dpi
A
ep
75 µm
D
SC
S
40 µm
B
ep
20 µm
E
ep
40 µm
C
NGT (II)
ad
ab
100 µm
F
NGT (II)
30 µm

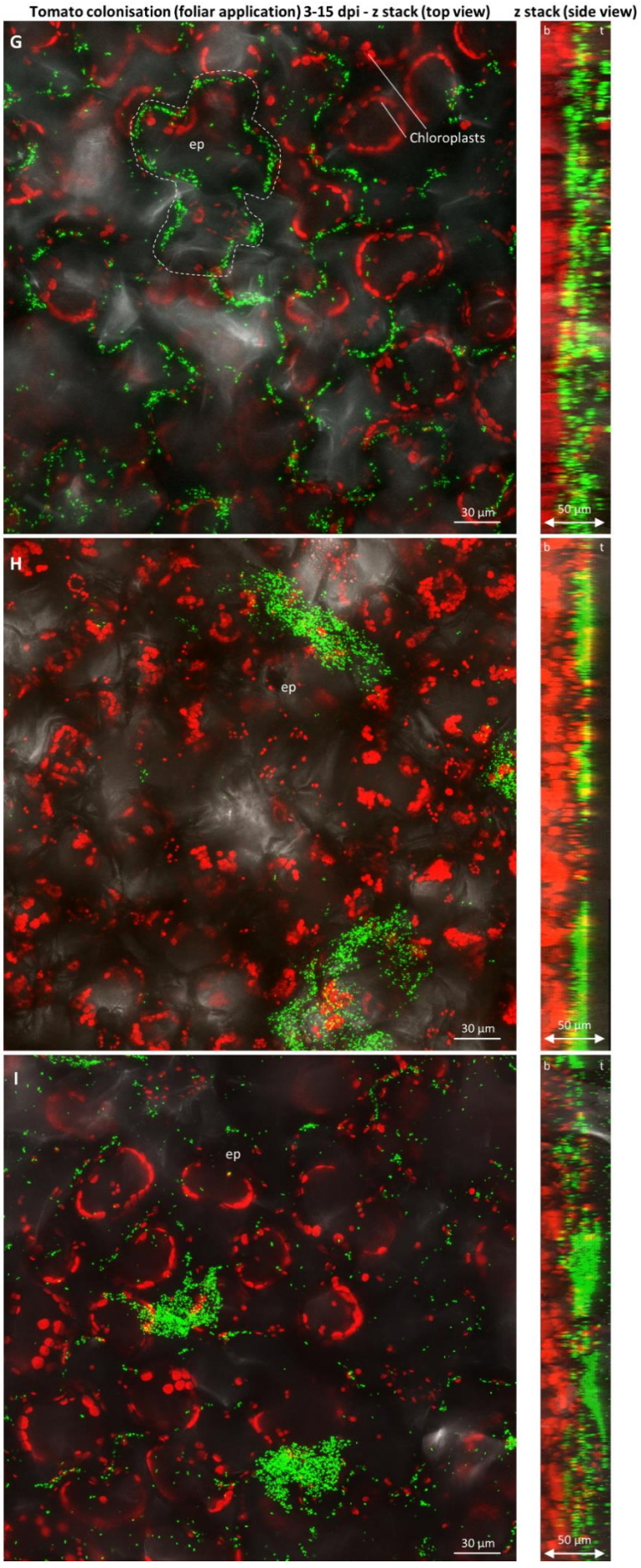

Tomato colonisation (foliar application) 3-15 dpi - z stack (top view)
z stack (side view)
G
ep
Chloroplasts
30 µm
b
t
50 µm
H
ep
30 µm
b
t
50 µm
I
ep
30 µm
b
t
50 µm

Fig. 4.64. Foliar application of GGG (10^7 CFU mL^{-1}, green) to tomato (A-C and G-I, red to purple for chlorophyll fluorescence under dsRed excitation light) and A. thaliana (D-F) leaves grown axenically in N-replete hydroponic setup or MS agar, respectively. (A, E, B) Adaxial epidermis showing cell wall invasion and dense colonisation (possibly endophytic white stars) of certain cells indicated by the white arrows and showed in detail in (B), fluorescence microscopy. (D) Abaxial epidermis of A. thaliana showing colonisation of stomata and subsidiary cells. (C, F) Colonisation of type II non glandular trichomes in A. thaliana (F) and tomato (C). (G-I) Maximum projection of 30 images z-stacks, for a total of 50 µm depth. On the right, the lateral view of the 3D modelling of the z-stack is included, with its right side corresponding to the top of the z-stack (leaf surface, t) and the left side corresponding to the z-stack bottom (leaf interior, b). In red are shown some chloroplasts as excited by a 633 nm laser that serve as a reference for evaluating the penetration of GGG cells into the root tissue. The closer to the left side of the 3D lateral view image, the deeper the penetration. One epidermal cell is delineated with white dashed lines to highlight the localisation of bacteria around the cell borders, between the walls of adjacent epidermal cells. Ab = abaxial leaf surface; Ad = adaxial leaf surface; ep = epidermal cell; NGD = non-glandular trichome (the type is indicated in brackets); S = stoma; SC = subsidiary cell.

4.3.2 Colonisation imaging in rice and colonisation model

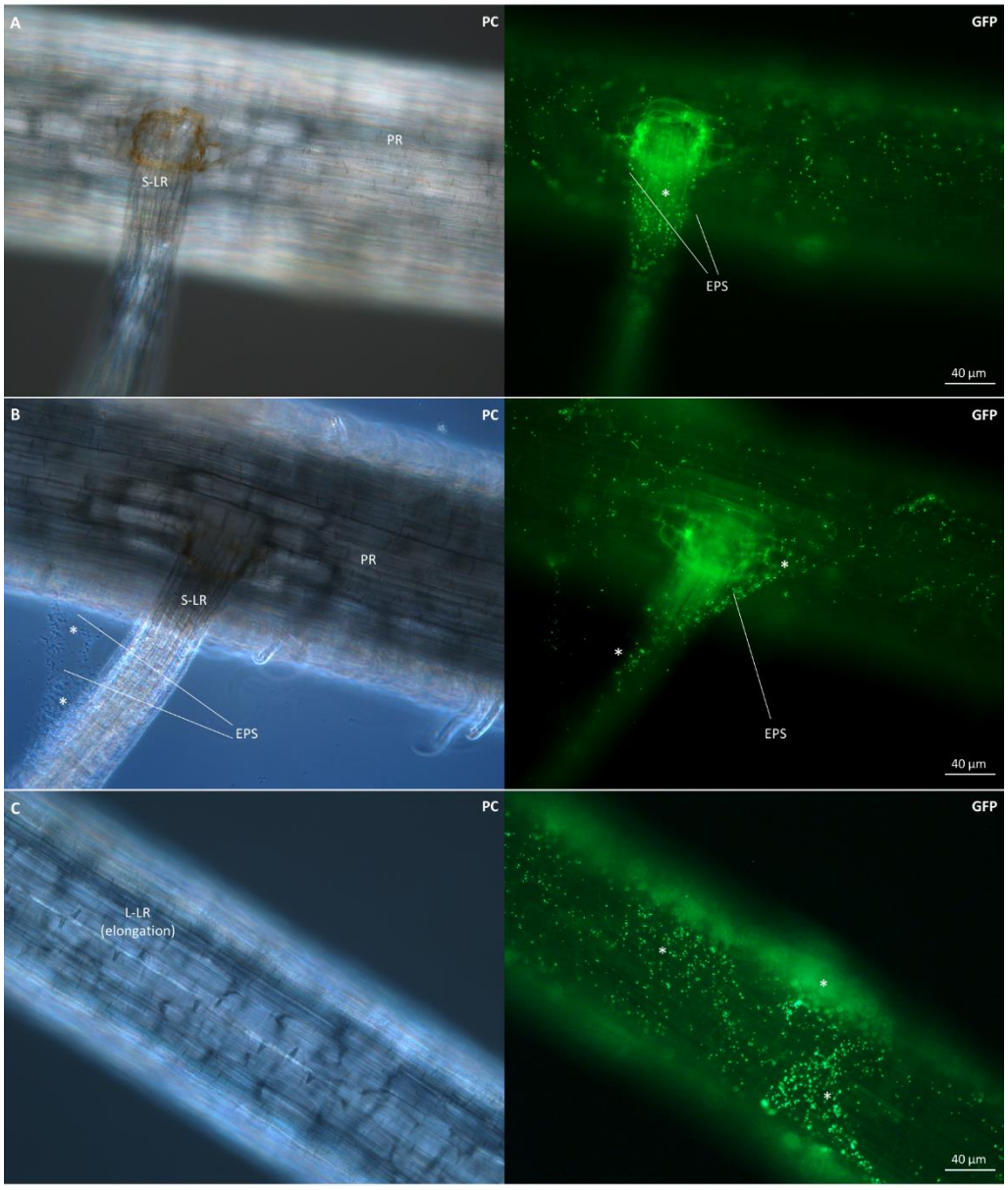
Compared to tomato, whose interactions with *G. diazotrophicus* was only investigated by an extremely limited number of preliminary studies, the literature on rice is more extensive (see section 4.1.2), due to the high commercial interest in this cereal and its natural association with diazotrophs. The first attempt of rice inoculation with *G. diazotrophicus* revealed bacteria in the root epidermis and aerenchyma, particularly along the grooves of the epidermal cells, and invasion of inter and intra cellular spaces of the cortex and xylem (depending on the variety) but with no shoot colonisation [97]. In a subsequent study, hydroponically grown rice treated with *gfpmut3* or *gus* tagged *G. diazotrophicus* Pal5 directly inoculated in N-free NS at a concentration of 10^4 CFU ml^{-1} exhibited bacterial aggregates and individual rod-shaped cells throughout the entire root axis; the GFP-tagged bacteria distribution was particularly prominent at sites of secondary root emergence and in the vicinity of the root apex, including root caps and root hairs, while endophytic GUS-tagged bacteria were found in the aerenchyma spaces and cortical parenchyma cells [526].

In the present study, rice seedlings of the BC15 variety were pregerminated until the emergence of a 1 to 2 cm-long radicle and 1 to 5 mm-long coleoptile. Seedling of the same developmental stage were then treated overnight through direct inoculation of 10^7 CFUs ml^{-1} of *GGG* and transferred in a hydroponic setup (see section 4.1.2b). Samples were collected at different intervals up until 30 dpi and analysed through fluorescent microscopy or light microscopy upon X-Gluc staining.

4.3.2a Rice colonisation in hydroponic setup - Root

First, treated rice seedlings were grown in N-free NS (Fig. 4.65). It appeared clear that, differently to what was observed in tomato, the secondary root emergence sites were among the preferred colonisation spots (Fig. 4.65a, b). As observed in the other model systems, individual bacterial cells covered the whole root surface on the longitudinal plane, but they did not seem to exhibit a marked predilection for epidermal cell wall junctions as often observed in tomato (Fig. 4.65c). Another interesting contrast with the dicot models investigated was the pronounced colonisation of lateral root apices (Fig. 4.65d, e). The radicle (or embryonic seminal root) and the shoot-borne crown roots of rice produce three types of lateral roots, named small lateral roots (or S-type), ranging from 50 to 60 μm in diameter, and two types of large lateral roots (thin and large L-type) ranging from 120 to 150 μm [542] [543]. They derive from the pericycle and endodermal cells of the main roots through a process controlled by auxin signalling [544]. A dense and consistent colonisation was observed along the S-type root axis and, most notably, at their apices. It is plausible that bacteria may colonise lateral root primordia along the main root may occur, and subsequently, "hitchhike" and accumulate on the advancing lateral root apex during its growth. This hypothesis was corroborated by the observation of *GGG* cells invading the tip of emerging lateral roots at 3 dpi and, simultaneously, entering through the cracks of the same roots (Fig. 4.66a, b). Interestingly, the bacterial biofilm transported by the elongating S-type root seemed to remain anchored to the main root surface through a mucous matrix, similar to a connective structure of bacterial origin bridging the spatial gap

between the two roots (Fig. 4.65b). This substance was initially considered an imaging artifact; however, it was observed in the majority of the colonised small lateral roots of plants grown in either zero-N (Fig. 4.65b) or in 2 mM KNO_3 NS (Fig. 4.66i-k) both through direct fluorescence microscopy and upon GUS staining. It is therefore possible that an EPS-based matrix formed by the bacteria over the root epidermis was lifted and eventually pierced by the advancing S-type root; however, the matrix (and the bacteria enmeshed in it) remained connected to the lateral root apex and continued stretching and growing in conjunction with the root as it moved away.



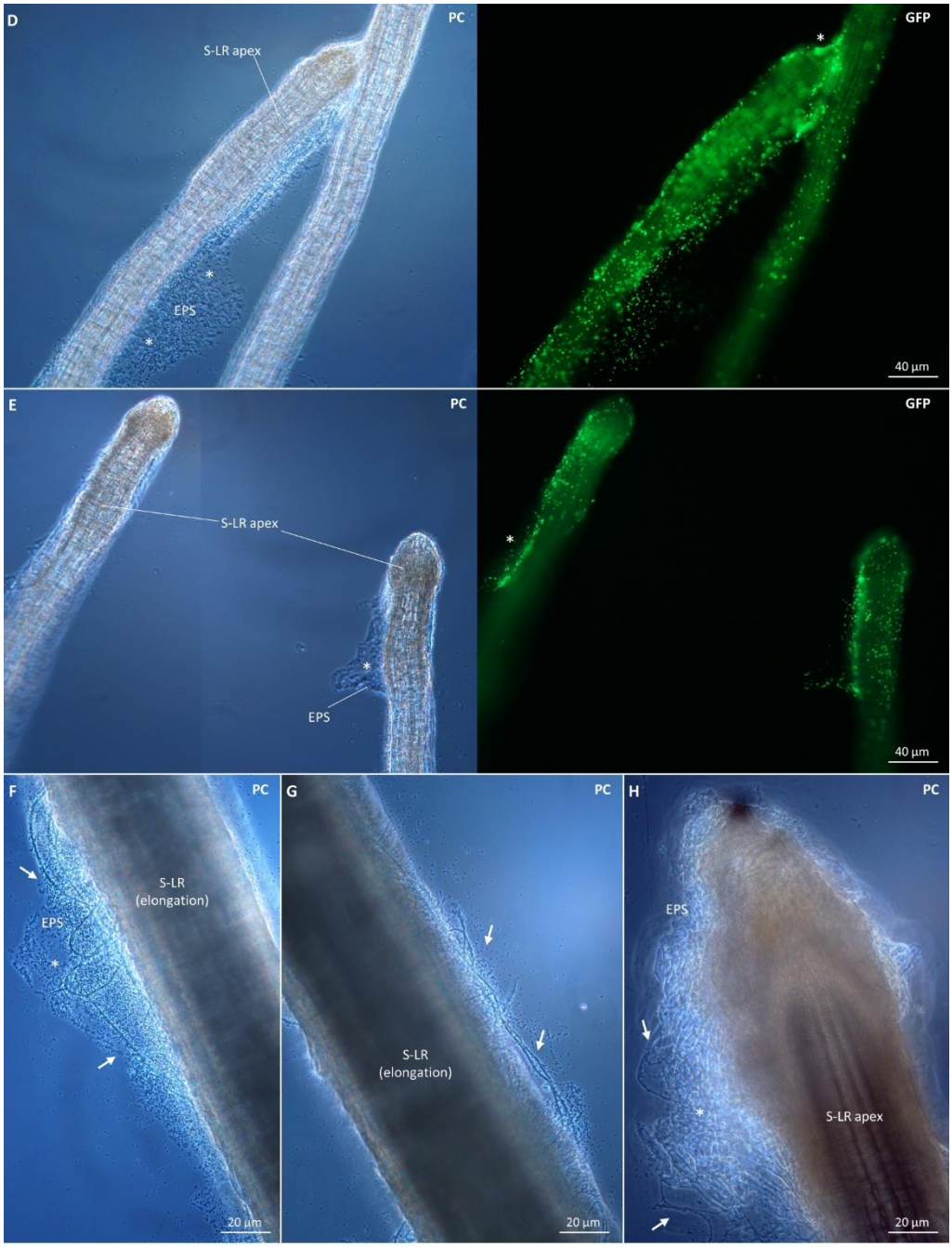


Fig. 4.65. Root colonisation of rice (cv. "BC15") grown hydroponically in zero-N NS upon overnight inoculation of the pregerminated seedling with GGG (green), longitudinal plane. Samples were collected at 15 dpi and analysed through fluorescence microscopy (GFP) (the corresponding phase contrast image is on the left image of each panel, labelled as PC). (A, B) Lateral root emergence site colonisation through putative EPS matrix with embedded bacteria (white stars). (C) Individual interspersed cells epiphytically colonising the root surface. (D-E) Colonisation of small lateral roots apices with traces of EPS embedded with bacteria. (F-H) Filamentous bacterial cells (white arrows) on the surface and apex of small lateral roots. EPS = putative EPS-based matrix; L-LR = large lateral roots (L-type); PR = primary root; S-LR = small lateral roots (S-type).

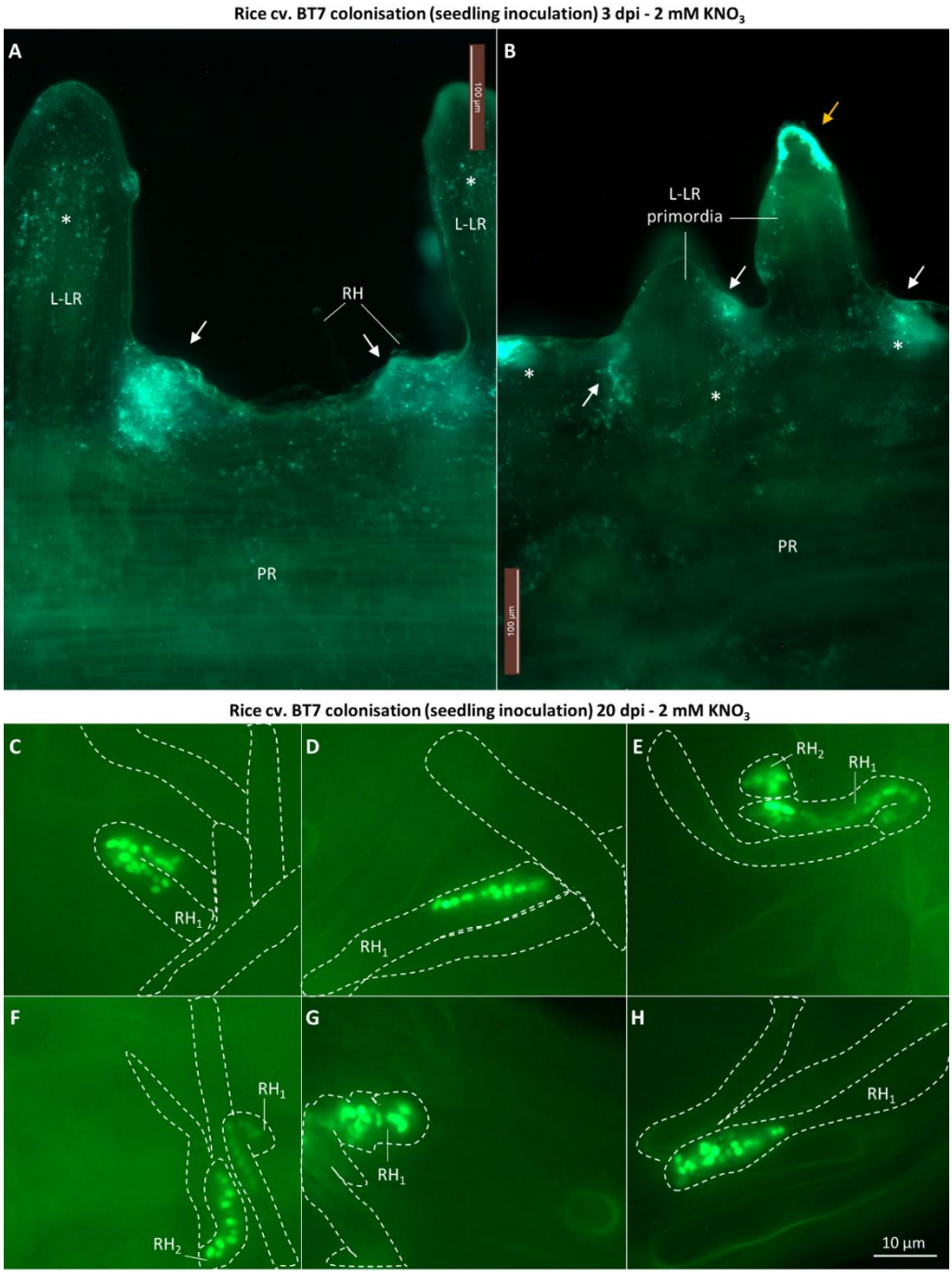
This "movement" of the putative EPS matrix is recognisable in the spiral-shaped biofilm depicted in Fig. 4.66c-e, which may be indicative of the matrix

being anchored to the S-type root apex while remaining free to rotate as the root developed.

Overall, regardless of the exact lateral root tip colonisation mechanism, the combined invasion of root apex and emergence crack appears advantageous: not only may this mechanism grant efficient endophytic colonisation of the lateral root itself, but, given its endodermal origin, it could also constitute a gate for stele colonisation. Interestingly, the tips and apices of L-type lateral roots were found to be colonised by filamentous cells (Fig. 4.65f-h) at higher ratios than what observed in other root regions, resembling the colonisation of *A. thaliana* grown on NH_4-free MS agar (Fig. 4.53d-f). It is possible that such morphological shift of bacteria may reflect a different metabolic state induced by higher root exudation and the presence of carbon-rich organic matter from the debris of the root cap (Fig. 4.65h).

Similarly to what observed in tomato, the analyses of treated rice samples grown in the same setup but with the addition of 2 mM KNO_3 in the hydroponic NS did not show significant mechanistic differences in the colonisation strategy (Fig. 4.66). At 7dpi, S-type roots exhibited the characteristic dense colonisation, particularly on the apex (Fig. 4.66l-n), and their invasion from the main root consistently involved the mucous matrix replete of bacterial cells which connected the two structures (Fig. 4.66i-k, black arrows). The spiralling, blue-stained EPS-based biofilm was distinguishable from the root emergence site to the apex (Fig. 4.66k-m). However, by comparing fluorescent images with their phase-contrast correspondents and observing the ratio of blue-stained cells to the total detectable bacterial cells upon X-Gluc staining, a high number of untagged bacteria were noted (e.g. in Fig. 4.65b and 4.65e note the amount of fluorescent cells in the EPS-connective material compared to the number of cells in the phase contrast image, and in Fig. 4.66o note the very limited extend of the blue staining in the biofilm covering the whole root). Two main hypotheses can be proposed to explain this observation. First, a higher and carbon-rich exudation from rice roots may induce a faster bacterial growth compared to tomato, resulting in an accelerated plasmid loss. Rice is known to produce carbohydrate-rich root exudates that, in the first two weeks, are

composed at 90% of glucose [267]. Furthermore, the starch-rich and voluminous rice seeds may contribute to a higher sugar availability; interestingly, the genome analyses of AZ0019 revealed the presence of an operon containing the genes *glgA*, *glgB*, *glgX*, *treZ*, *malQ* and *treY*, producing enzymes associated with glycogen or starch degradation and metabolism [545], as well as with desiccation and osmotic stress tolerance [546].



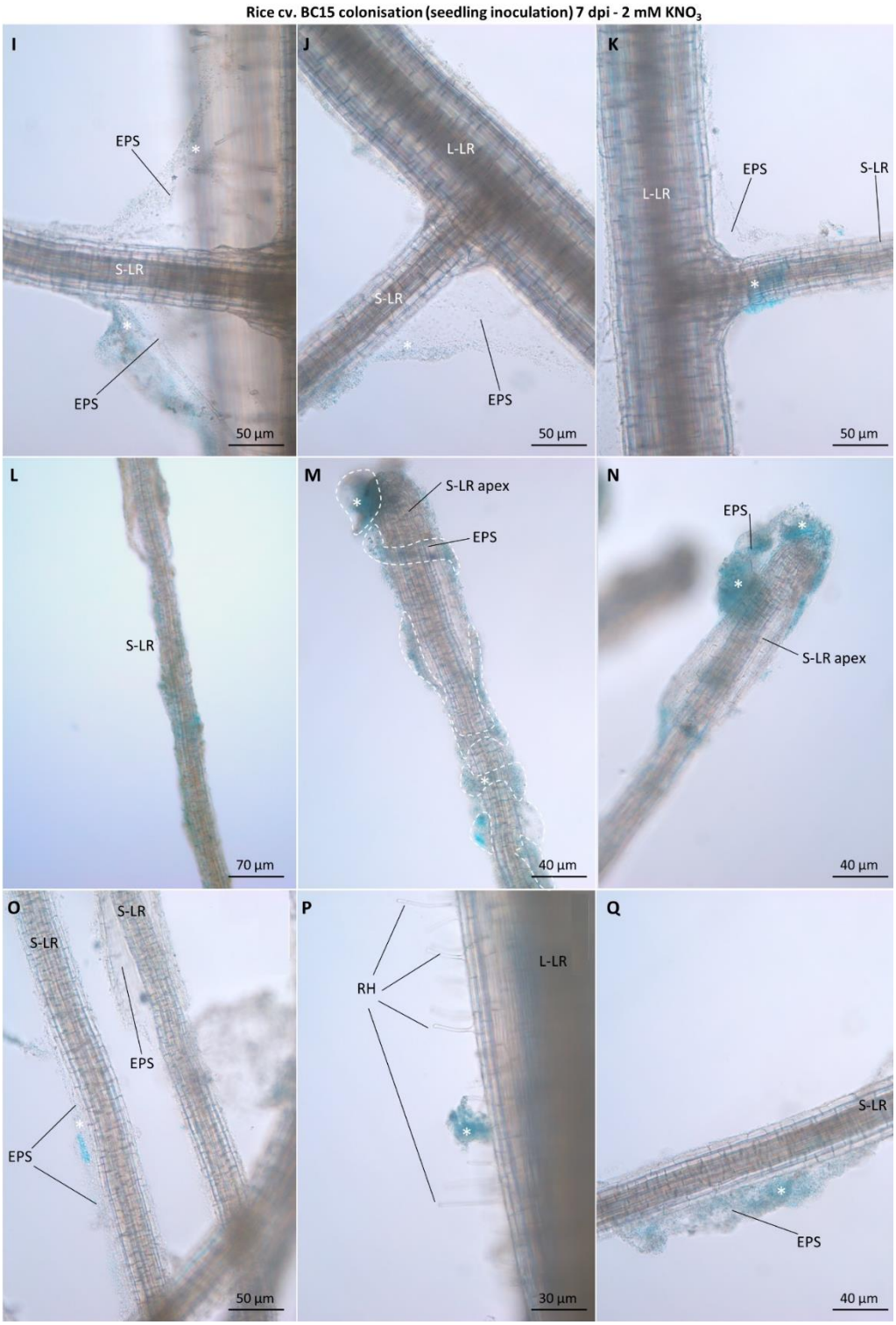


Fig. 4.66. Root colonisation of rice cv. "BT7" (A-H) and cv. "BC15" (I-Q) grown hydroponically in 2 mM KNO_3 NS upon overnight inoculation of the pregerminated seedling with GGG. BT7 samples were collected between 3 (A, B) and 20 (C-H) dpi and visualised through fluorescence microscopy, while BC15 samples were collected at 7 dpi and visualised through brightfield illumination upon X-Gluc staining. (A, B) Lateral root tips (orange arrow) and emergence cracks (white arrows) concomitant colonisation by biofilm and individual rod/coccoidal bacterial cells (white stars). (C-H) Root hairs colonisation by coccoid-shaped GGG cells, often disposed in single file (D-F) as in rhizobial infection threads. When multiple root hairs were present in the same image, they were demarcated individually with white dashed lines to facilitate precise identification and labelled as RH_n. (I-K) Colonisation through

putative EPS matrix at S-type lateral root junctions. (L-N) EPS biofilm extending in a spiral pattern along the lateral root (demarked in M with white dashed line), reaching up to the apices. (O-Q) Biofilm aggregates (white stars) epiphytically colonising the roots, often showing limited blue staining upon X-Gluc assay and scarce colonisation of root hairs in the main root (P). EPS = putative EPS-based matrix; L-LR = large lateral roots (L-type); PR = primary root; RH = root hair; S-LR = small lateral roots (S-type).

The presence of these genes suggests the genetic potential to directly access the carbon reservoirs of the seed.

Secondly, the abundant EPS-material observed may create an isolated low-oxygen microenvironment acidified by the metabolism of the bacterium, which would favour bacterial adhesion and nitrogen fixation while possibly inhibiting GFP maturation and reducing the X-Gluc staining solution penetration, as previously proposed in rice and sugarcane models [248]. EPS production was demonstrated to be involved in biofilm formation and root colonisation for many genera of endophytic diazotroph, including *Azoarcus*, *Azospirillum*, *Rhizobium*, *Sinorhizobium*, *Bradyrhizobium* and *Burkholderia* [184] [547]; these bacteria, as shown in *A. Brasiliense* [548], first form a weak contact with the root ("adsorption phase") and subsequently progress into an irreversible attachment ("anchoring phase") in which they become embedded in a self-produced matrix composed of proteins, nucleic acids and EPS [547]. In rhizobia, EPS is also associated with bacterial release from infection threads, bacteroid development, and resistance against plant antimicrobial metabolites [549]; furthermore, it is both responsible for eliciting a defence response by the plant [550] and for shielding the bacterium from such immune reaction [551]. In *G. diazotrophicus* Pal5, it has been demonstrated that EPS synthesis is driven by the *gum* operon and is essential for biofilm formation in hydroponically grown rice roots and for subsequent colonisation through lateral roots emergence sites, root epidermis and root hairs [184]. Although not explicitly mentioned, the microscopy analyses produced in that study show a colonisation phenotype similar to what observed in Fig. 4.65ib-e and Fig. 4.66i-q, with bacterial cell not strictly colocalising within the plant tissues but rather enmeshed in an EPS layer surrounding the roots in what the authors define "large aggregates with an apparently loose structure" [184]; this

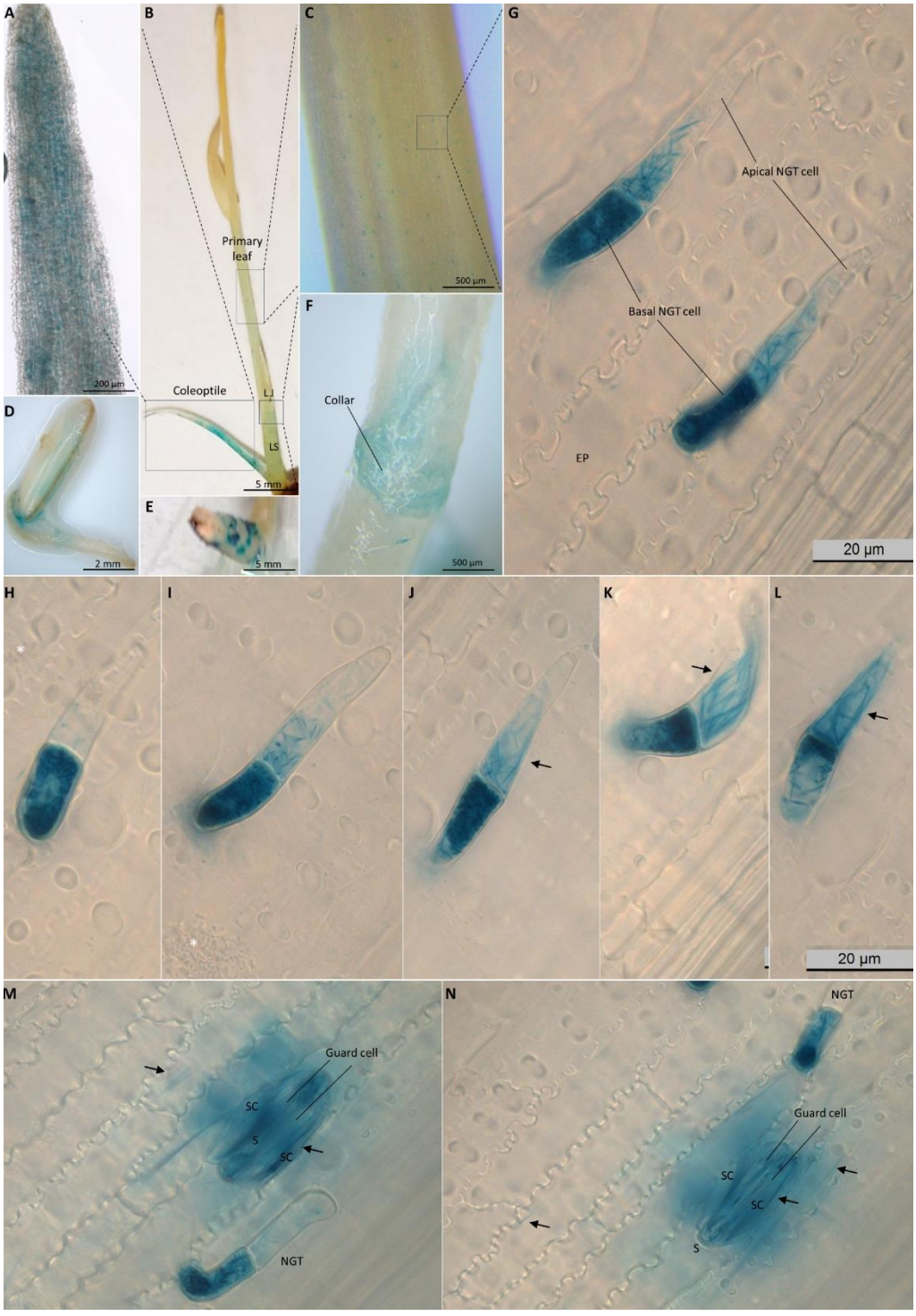
consistency suggest that a more substantial EPS production may be associated with rice or possibly with monocots in general, since electron transparent "haloes", proposed to be composed of EPS, were also reported by James et al. to surround *G. diazotrophicus* during sugarcane colonisation [221].

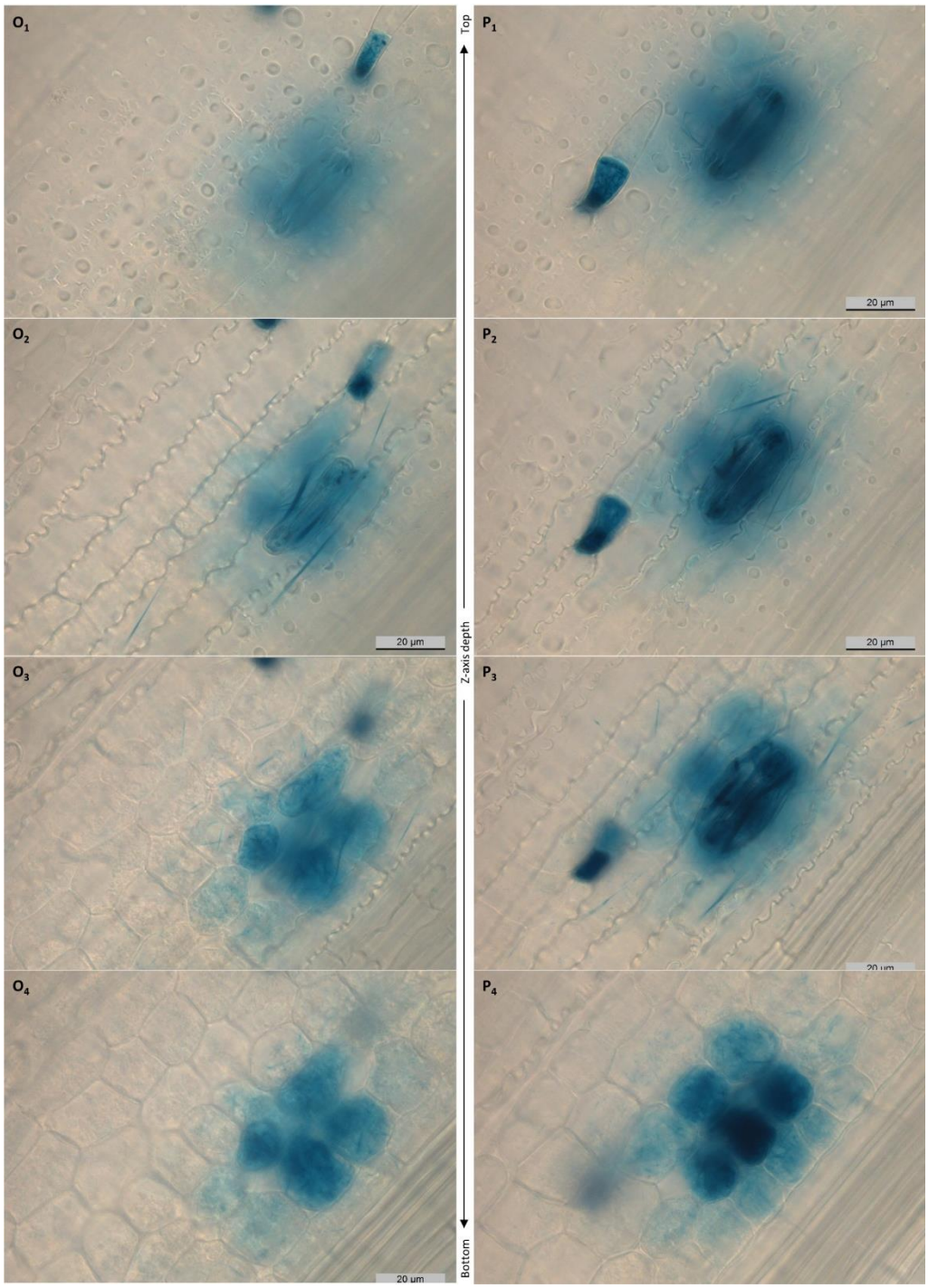
Apart from this EPS-based matrix, which was not seen in tomato and may depend on the substantial levels of carbohydrates exudated from the seed and root system [267], the other main colonisation mechanisms were similar to what described for the dicot systems, including colonisation of root surface in large aggregates (Fig. 4.66n-q) and targeting specific, possibly damaged, root cells as preferred entry point (Supplementary Video 1). One apparent difference was the relatively lower colonisation of root hairs (note the lack of bacterial cells in root hairs in Fig 4.66p), which, on the contrary, were found to be one of the preferred invasion sites for dicot models. However, when the same experiment was conducted using a different rice variety called BT7, on which *G. diazotrophicus* AZ0019 was recently evaluated for its PGP potential in field trials in Vietnam with positive results (unpublished data), root hair colonization was once again observed (Fig. 4.66c-h). An inconsistent root hair colonisation in rice was also reported by Sevilla et al. in early *G. diazotrophicus* colonisation studies in rice [248]. Coccoid-shaped *GGG* cells were found to endophytically colonise root hairs in a single-file manner, closely resembling rhizobial infection threads (Fig. 4.66d-f), in contrast to endophytic *GGG* within the longer and wider tomato root hairs which exhibited rod-elongated morphology. This difference may be attributed to the readjustment of the colonisation mechanisms in a plant variety-dependent manner (e.g., root hairs seemed shorter and thinner in the BC15 rice variety, making their colonisation less advantageous compared to S-type root invasion), but it may also depend on the inoculation method (rice seedling coating vs tomato direct inoculum in NS). Moreover, monocots and dicots exhibit different compositions in their root hair cytoplasmatic metabolites and cell wall polymers content, and root hair density and elongation can be affected by endophytic hosts and by nutrient availability [552], further complicating any biological interpretation.

4.3.2b Rice colonisation in hydroponic setup – Shoot

The analysis of X-Gluc stained shoots of BC15 rice samples, revealed a close resemblance to what observed in tomato: regardless of the nitrogen concentration applied, blue stains were predominantly observed around the seed (Fig. 4.67d-e), in the coleoptile, and in the leaf sheath, gradually diminishing in intensity towards the primary and secondary leaf (Fig. 4.67b). At 1 dpi, a prominent GUS stain was evident at the radicle emergence site, indicating a "crack entry" point for endophytic colonization (Fig. 4.67d).

The persistent presence of a bacterial layer around the seed throughout the entire duration of the experiment, but especially during the early colonisation stages (Fig. 4.67d, e), supports the hypothesis that *G. diazotrophicus* can directly utilize the carbohydrate reserves in the seed as a carbon source. The coleoptile exhibited diffuse blue staining (Fig. 4.67b), but bacterial cells could not be clearly distinguished within its tissues (Fig. 4.67a), suggesting that the GUS signal in this region may be caused by the acidification of the senescing coleoptile. A similar intense coleoptile staining pattern was observed in hydroponically grown rice inoculated with GUS-tagged *H. seropedicae* [254], indicating that this could either be a common colonization point for endophytic diazotrophs or, possibly, an artifact associated with rice; in fact, coleoptiles also showed some degree of staining in untreated controls, although not as pronounced as in the inoculated plants (not shown). Another intensely stained area was the lamina joint (an organ connecting the leaf blade to the sheath), which, speculatively, presented an ideal environment for endophytic shoot colonisation due to the presence of aerenchyma and vascular bundles [553], resulting in physical protection and cracks for accessing deeper plant tissues (Fig. 4.67b, f).


A
B
C
D
E
F
G
H
I
J
K
L
M
N
Primary leaf
Coleoptile
LJ
LS
Collar
Apical NGT cell
Basal NGT cell
EP
NGT
Guard cell
SC
S
200 µm
2 mm
5 mm
500 µm
20 µm


O1
P1
Top
20 µm
O2
P2
20 µm
20 µm
Z-axis depth
O3
P3
O4
P4
20 µm
Bottom

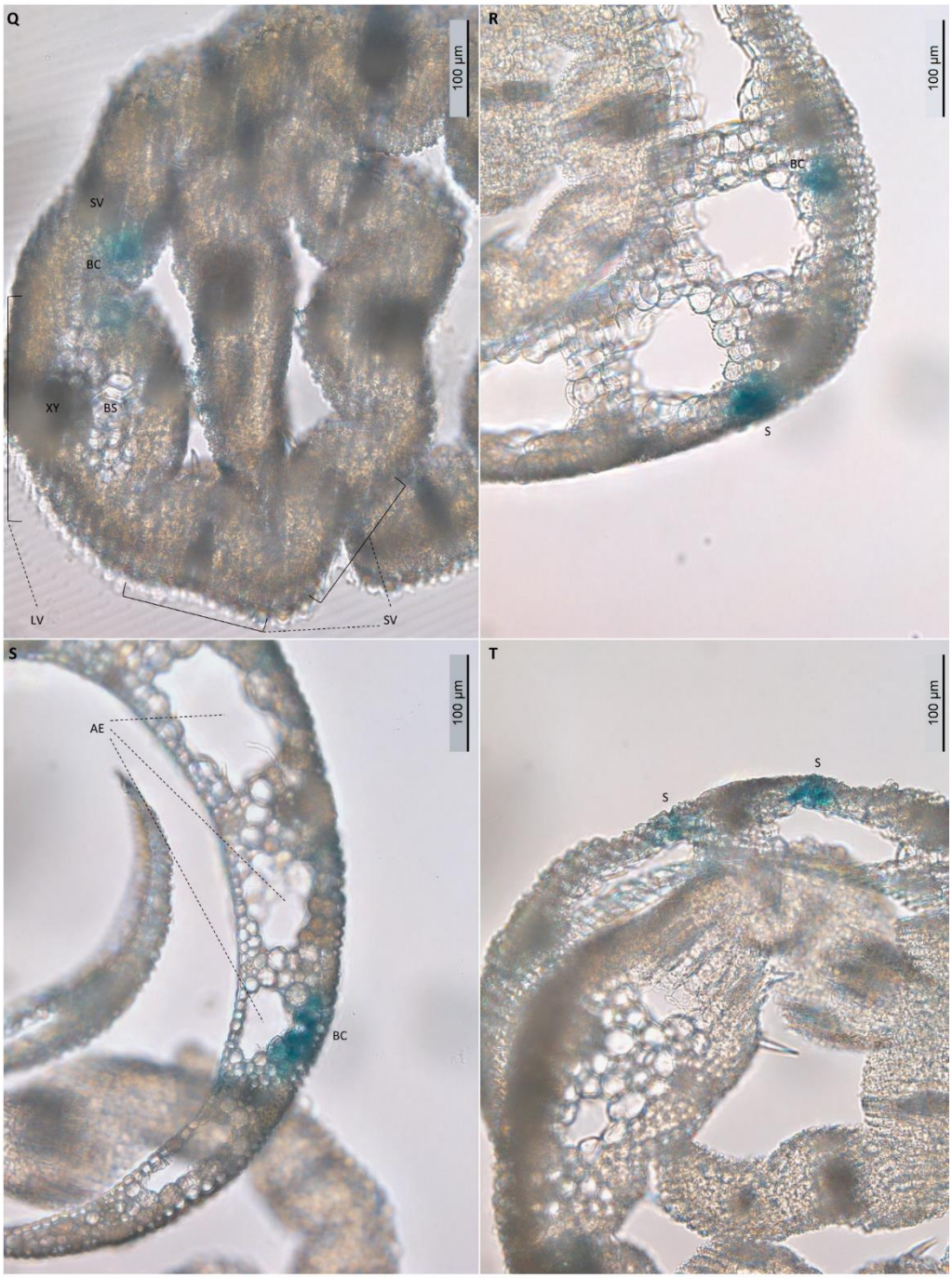


Fig. 4.67. Soot colonisation of rice cv. "BC15" grown hydroponically in zero N (A-F) or 2 mM KNO_3 (G-T) NS upon overnight inoculation of the pregerminated seedling with GGG. Samples were collected at 1 (D), 7 (A-C, E, F) and 20 (G-T) dpi and visualised through brightfield illumination upon X-Gluc staining. (A) 7 days-old coleoptile closeup, showing diffuse blue staining. (B) Rice shoot 7 dpi showing intense coleoptile and seed staining and milder sheath staining progressively degrading toward the secondary leaf tip. (C) Leaf sheath detail showing a high percentage of colonised trichomes. (D-E) 1 and 7 dpi seedling showing colonisation of seed tissues and crack entry in the radicle emergence junction. (F) Lamina joint showing high colonisation, especially in the collar. (G-L) Intracellularly colonised trichomes, showing the progressive movement and morphological differentiation of bacteria from the basal (rod shape) to the apical (filamentous, black arrows) trichome cell. The white stars indicate rod-shaped and untagged epiphytic bacteria found around trichomes. (M-N) Guard and subsidiary cell intracellularly colonised by filamentous GGG cells (black arrows).

(P_{1-4}, Q_{1-4}) Stomata and substomatal chamber intracellular colonisation, z-stack from top (X_1) to the bottom (X_4). (Q-T) Sheath bundles, aerenchyma, bulliform cell and stomata colonisation. EP = epidermal cell; LJ = lamina joint; LS = leaf sheath; SV = small vascular bundle; LV = large vascular bundle; BS = bundle sheath cell; BC, bulliform cell; XY, xylem; S = stomata; SC = subsidiary cell; AE = aerenchyma.

A closer examination of GUS-stained samples in the leaf sheath revealed bacterial cells intracellularly colonising the bicellular non-glandular trichomes (Fig. 4.67g-l). The percentage of colonised trichomes was, as in tomato, close to 100% in the culm/leaf sheath and primary leaf (Fig. 4.67c). The trichome colonisation seemed to originate from the mesophyll, passing through the apoplastic barrier that separates the basal trichome cell from the underlying epidermal cell and moving apically into the apical trichome cell (Fig. 4.67g-l). The trichome stalks were first colonised by rod-shaped bacteria, which seemed to multiply within the first trichome cell until completely occupying its volume (Fig. 4.67g, h); concomitantly, as cells were pushed (or actively swarmed) against the wall separating the apical trichome cell, some rod-shaped bacteria emerged on the apical cells and transitioned into the elongated morphology (Fig. 4.67h-i). In this movement toward the apex of the trichome, *G. diazotrophicus* seemed to follow the transport of solutes, which has been shown to flow unidirectionally from the mesophyll to the trichome apex through plasmodesmata-mediated symplastic route [554]. The vast majority of the trichomes observed at 20 dpi exhibited the conformation depicted in Fig. 4.67g, wherein the basal stalk cell is densely colonized by rod-shaped bacteria, while the apical cell contains a lower number of elongated/filamentous bacterial cells. This observation suggests that once this state is reached, it may remain stable over time, or that it may represent the homeostatic equilibrium of bacteria slowing moving to the upper trichome cell and possibly being secreted in the underlying epidermis while being replaced by other bacteria from the basal trichome cell. Indeed, it was noted that the proximity of colonised trichomes were occasionally occupied by unstained, seemingly epiphytic bacterial cells with rod-shape morphology (Fig. 4.67h, i, white stars) resembling what found on tomato leaf epidermis close to stomata.

Stomata represented another highly colonised site; in particular, guard and subsidiary cells were intracellularly colonised by filamentous bacteria, often as long as the entire length of the host plant cells (Fig. 4,67m, n). Furthermore, colonised stomata were often in proximity to colonised trichomes, suggesting either a cross contamination between bacteria emerged from these structures, or suggesting both trichomes and stomata to be the final recipients of a common stream of solutes and bacteria coming from the mesophyll via vascular sheath and bundles. A detailed examination of the stomata by imaging these structures along the z-axis revealed a dense colonization of the guard cells, subsidiary cells, and the entire substomatal chamber. Intracellular colonisation of all the parenchymatic cells surrounding the stomata by elongated rod-shaped bacteria was also observed, while subsidiary cells on the epidermis layer were colonised by filamentous *GGG* cells (Fig. 4,67o, p, Supplementary Videos 2.1, 2.2). Cross section of the leaf sheath confirmed the colonisation of substomatal chambers and parenchymal cells, particularly around vascular sheath and bundles, bulliform cells and aerenchyma (Fig. 4.67q-t). These areas are characterised by proficient solute and gas exchange, creating a mineral-rich environment and offering protection against desiccation; as a result, the surrounding tissues become favourable sites for bacterial accumulation upon transport via xylem sap. While previous reports failed to detect any shoot colonisation in inoculated rice [248], the findings presented in this study confirms that *G. diazotrophicus* is transported to the shoot via vascular bundles and accumulates in sugar and solute-rich organs such as stomata and trichomes.

4.3.3 *G. diazotrophicus* colonisation model and additional considerations

The inoculation of monocot and dicot model systems with various tagged mutant strains of *G. diazotrophicus* AZ0019 allowed an accurate assessment of the bacterium's colonisation process. The use of three different inoculation methods (treated seeds grown on MS agar, direct bacterium inoculation on hydroponically grown plants and foliar application) and two nitrogen

conditions (zero N and 2 mM KNO_3) revealed the existence of common colonisation patterns alongside species-specific variations.

The root system was found to host the majority of the bacteria, although efficient shoot colonisation was also observed as early as 1-2 dpi. This migration from the root system towards the aerial organs appears unlikely to occur solely by active chemotaxis through the apoplastic barriers in such short timeframe, suggesting the transport via xylem sap following endophytic invasion of plant tissues. Reaching the root vasculature shortly after the inoculation, although facilitated by crack entry through secondary root emergence sites, implies the ability to pass through cell walls, particularly in tomato in which lateral root junctions did not appear the main invasion sites.

The genome sequencing of AZ0019 enabled the identification of genes associated with plant wall degradation, belonging to the categories of cellulases (including endoglucanases, exoglucanases and β-glucosidases), hemicellulases (including xylanases and mannanases), pectinases (including pectinesterases, polygalacturonases and pectate lyases) and ligninases (including lignin peroxidases, manganese peroxidases and laccases). The only candidate found was a putative endoglucanase precursor (named *eglA* or GDI2537 in AM889285.1, GenBank accession number YP_001602781) which, interestingly, lies within the EPS-producing *gum* gene cluster, reinforcing the idea of EPS formation being essential for endophytic colonisation. The discovery of this single cell wall degrading gene confirmed what reported by Bertalan et al. during the first genome sequencing of Pal5, in which the authors noted that EPS production by the *gum* operon has been associated with the stabilization of hydrolytic enzyme activity [284] [555]. This apparent genetic scarcity of cell wall-degrading genes was also reported in the genus of the endophytic diazotrophs *Azoarcus*, in which only the strain BH72 was shown to possess *egl*, cellobiohydrolase and beta-glucosidase activities, catalysed by bacterial surface-associated enzymes expressed under microaerobic conditions [556] [557]. Similarly, diazotrophic *Klebsiella oxytoca VN 13* and *H. seropedicae* Z67 exhibited weak pectate lyase and cellulase activity [558] [254]. In general, an aggressive cell wall degrading activity is associated with phytopathogens and elicit a strong immune response

[222], while a weaker but sufficient lytic enzymes production may help non-pathogenic endophytes to evade plant's defences [254]. Furthermore, it has been demonstrated that the entry of *R. leguminosarum* through the infection thread is facilitated by self-plant cell wall rearrangement activity induced by *nod* factors [559], raising the intriguing question of whether a similar mechanism exists in *G. diazotrophicus* and other non-nodulating diazotrophs. This hypothesis was suggested by the expression of cell-wall loosening enzymes upon *G. diazotrophicus* inoculation in sugarcane [560]. Critically, however, the ability of *G. diazotrophicus* UAP5541 to produce endoglucanase, endopolymethylgalacturonase and endoxyloglucanase activities (catabolising cellulose, pectin and xyloglucan, respectively) was experimentally validated [561], further supporting the notion that this bacterium, like other beneficial endophytes [562], is capable of actively penetrating cell walls. Interestingly, the UAP4451 strain was shown to constitutively express these hydrolytic activities, while in Pal5 they were influenced by the sucrose concentration [561]. The ability of *G. diazotrophicus* to pass through cell wall, possibly by inducing plasmodesmata rearrangement, is supported by intracellular colonisation of epidermal, exodermal and cortical cells, and, most notably, by the migration from the basal to the apical cell of non-glandular trichomes. Furthermore, root hairs were also intracellularly colonised in both the monocot and dicot model systems investigated, suggesting an active wall penetration similar to rhizobial infection threads. Intriguingly, James et al. reported the presence of "infection thread-like structures" of intracellularly colonising *G. diazotrophicus* upon sugarcane inoculation [563]. Cell wall synthesis and elongation occur at the extreme root hair tip, where the intense vesicular trafficking [552] may both allow bacterial intracellular entry and subsequent endocytosis in the hair cytoplasm [98]. Root hairs are also known to be influenced in length and density by associative nitrogen fixers such as *A. brasiliense*, with implications on local proton efflux and subsequent increase in the uptake of nitrogenous compounds and other minerals [552]. Interestingly, root hair growth in *Arabidopsis* has been demonstrated to be stimulated by both pathogenic and PGP bacteria in an auxin-independent manner within the first 7 dpi, with concomitant inhibition of primary root elongation [564]. Furthermore, root hair and secondary root development can be influenced by

bacterial quorum-sensing signalling N-acyl-homoserine lactones (AHLs) [565], which *G. diazotrophicus* in known to produce [566]. Therefore, it is plausible to conclude that *G. diazotrophicus* possess the ability to exploit (and possibly actively modulate) root hair development to enhance bacterial access to the root system.

In general, roots were promptly colonised by bacterial aggregates or individual cells, part of which quickly found their way into the internal root regions and established themselves intracellularly. However, while the colonisation of grooves between epidermal wall junctions (previously reported in rice colonised by *G. diazotrophicus* [248]) and the massive invasion of specific, possibly lysogenic, epidermal cells was a process observed in all model systems, root hair entry was more commonly found in tomato, which only showed occasional root cap or columella colonisation; in contrast, rice exhibited a marked root tip and crack entry colonisation (also previously described in *G. diazotrophicus*-rice systems [248]), especially in the S-type secondary root caps. Nevertheless, these differences may be a species-specific variation of the same tendency to invade young, elongating root structures characterised by the presence of cracks, softer and less fibrous cellular tissues devoid of Casparian strips or suberized endodermis, and high exudation, as a result from the interplay between mechanical ease of root penetration and rhizogenic chemoattractant concentration. Root exudation/rhizodeposition patterns and composition are spatially and temporally heterogeneous, depending on plant developmental stage (sugar exudation in *Arabidopsis* decreases overtime, while amino acid and phenolic exudation increases [567]), genotype [568], root zone, nutrient availability, photosynthate production, transport and reabsorption from the substrate, and rhizobacterial metabolism [523], [569]. *Pseudomonas aeruginosa* PAO1, a human pathogen also associated with many plants, was reported to activate genes for chemotaxis, type III secretion, aromatic compound catabolism and energy generation in response to sugar beet exudates, in a cultivar-dependent manner [570]. Plants exude up to 15% of assimilated nitrogen and 20% of fixed carbon in the form of sugars, organic acids, secondary metabolites, and complex polymers such as mucilage [569]; however, root exudation is not a unidirectional flux, but

involves the reabsorption of exudated compounds [571]. Commonly, the root hair, collar, and tip zones, are characterised by high exudation [572], confirming the association between *G. diazotrophicus* and the root regions with the highest nutrients availability.

In *Arabidopsis*, root hairs have been shown to adsorb water and minerals such as phosphorus, iron, potassium and calcium, while secreting acid phosphatase, malate and citrate [573]. Root tips, which are often regarded as one of the main entry points for endophytic colonisation [569], shed border cells and secrete secondary metabolites and mucilage, i.e., hydrated polysaccharides, which are known to attract rhizobacteria [569]. Mucilage is composed of 95 to 97% sugars and 3 to 5% amino acids, and, in maize, it was estimated to represent 20 to 25% of the total released carbon [574]; certain plant beneficial *Azospirillum* strains have been shown to be attracted by mucilage of this monocot [575], suggesting a similar mechanism to occur in the matrix observed around rice secondary roots. Additionally, roots and particularly border cells exude protons, creating low pH niches ideal for bacteria like *G. diazotrophicus*, as well as malate, citrate, flavonoids, pectin and arabinogalactans that attract and trigger biofilm formation of rhizobacteria such as *B. subtilis* [569], [576], [577]. The lack of mucilage/bacterial EPS colonisation in tomato is likely due to the different exudate composition. The main sugars secreted by tomato roots are glucose (37% of the total exudates between 4 and 14 dps), fructose (50% at 4 dps and 10% at 14 dps) and maltose (23% at 4 dps and 9% at 14 dps) [578]; however, they were not found to have a significant impact on the growth of *Pseudomonas* biocontrol strains in the rhizosphere, and a very low concentration of glucose was estimated in tomato rhizosphere [578]. Interestingly, *G. diazotrophicus* is not able to use maltose as a C source and only exhibits moderate growth on fructose [83]. In contrast, hydroponically grown rice was reported to produce, between 7 and 28 days after sowing, 90% of glucose along with glucuronic acid, mannose, galactose and arabinose; these sugars were highly attractive for some natural rice endophytes but not for other PGPBs such *A. brasilense* [267], which, in turn, shows highest chemotaxis toward malate, succinate, and fructose [579]. *G. diazotrophicus* is known to have a high metabolic demand for glucose [111], but can also grow vigorously in arabinose and mannose, and moderately in galactose [83]. Ultimately,

different endophytic species exhibits very specific chemotaxis behaviours toward various C-sources, and *G. diazotrophicus* may find a better niche on the glucose-rich mucilage secreted by rice and wheat [267], explaining its high density in the polysaccharide matrix observed in the rice rhizosphere and around the starch-rich rice seed. Whether this substance is solely derived from plant mucilage or if it is formed by bacterial EPS, or both, requires further investigation. Its potential advantage in terms of endophytic colonization is not yet clear, since, while mucilage attracts some bacteria, it prevents the endophytic ingress of others [580]; bacterial counts obtained through the MPN technique were comparable between rice and tomato (see section 4.1). Interestingly, *B. subtilis* was found to produce an extracellular matrix crucial for root colonisation and biofilm formation made of polysaccharides and proteins in response to the exudation of specific plant polysaccharides, such as arabinogalactan, pectin, and xylan, which were also incorporated in the matrix [577].

As for the sporadic root epidermal cells that showed enhanced but localised intracellular colonisation (Fig. 4.58), they have also been reported as one of the main colonisation sites for *H. seropedicae* Z67 in both the roots and aerial parts of rice [254]. James et al. regarded them as lysigenous aerenchyma cells, i.e. cells committed to programmed death to create gaseous spaces and facilitate aeration of flooded organs (as discussed in section 4.3.1a); the presence of cracks in the cell walls could be exploited for apoplastic colonization, while the lack of functional cytoplasm may elicit a weak defence response, making these cells an ideal ecological niche. Similarly, large aerenchyma and bulliform cells near vascular bundles were found to be densely colonized in rice sheaths and primary leaves. This dynamic has also been observed in *Azoarcus* and *Serratia* spp. in rice and kallar grass roots and stems [375] [241]. James et al. raised the question of whether the bacterial invasion itself may be the cause of cell death, particularly in roots where these epidermal cells do not appear to be a result of programmed cell death but exhibit wild type phenotype; the high concentration of bacteria observed (Fig. 4.58g, Supplementary Video 1) would likely be incompatible with normal cellular functions. Similarly, James et al. reported the presence of intracellular

G. diazotrophicus only in sugarcane cells that appeared to be dead or damaged, without intact cytoplasm or organelles [221]. This scenario would not be necessarily damaging, as it has been proposed that the entire rice root epidermis layer acts as an extension of the rhizosphere and is eventually shed off [375]. It is plausible that *G. diazotrophicus* can act as a parasite to some extent, taking advantage of decaying plant tissues for nourishment. This putative behaviour could explain the occasional observation of stunted rice plantlets in the hydroponic system showing above-average bacteria counts through the MPN technique (not shown). However, rice inoculation with *G. diazotrophicus* WT consistently elicited an overall positive effect in hydroponic setups, suggesting this putative parasitic behaviour to be limited and circumstantial. Plausibly, the extensive invasion of these root epidermal cells may serve as a conduit for further endophytic colonisation, as also demonstrated in *H. seropedicae* B501 and *R. leguminosarum* [581] [582].

As a consequence of epiphytic colonisation upon root exudate chemotaxis and subsequent endophytic root invasion, bacteria accessed the xylem route to migrate into the shoot. Colonisation of root xylem vessels was a very rare occurrence, primarily observed in proximity to the root-shoot junctions (Fig. 4.61q), suggesting that bacteria travel through the xylem sap but do not accumulate in the vasculature: instead, they aggregate at plant junctures, such as the root-shoot junctions in tomato and the lamina joint in rice, which, due to rapid cell division, plant organ morphogenesis and nutrient flow, could likely create an environment used as transitional hub from which further progressing toward the shoot or re-entering the root tissues. Only a few bacteria can actively pass the endodermis, Casparian strip and pericycle via cell wall degrading enzymes, while most endophytes are thought to passively reach the stele by exploiting openings on the endodermal layer along secondary root emergence areas [583]. Once inside the xylem lumen, endophytes can spread to vegetative plants parts, passing from one xylem element to another through the perforated plates, whose holes have been reported to be wide enough for bacterial passage [584]. Ultimately, this study could not collect conclusive microscopic evidence to address the longstanding debate of whether *G. diazotrophicus* can actively penetrate xylem vessels [260] [221], but the data

collected strongly support that this bacterium can somehow access and move through plant vasculature.

All of the root colonisation strategies described in the present study and summarised in Fig. 4.68 and Fig. 4.69 present strong analogies with other non-nodulating diazotrophs. Several previous studies confirmed that lateral root emergence sites and root apices of rice are the preferred colonisation sites of phylogenetically distant endophytic diazotrophs such as *Azoarcus* spp. [375], *Herbaspirillum seropedicae* [254], *Burkholderia vietnamensis* [251], *Serratia marcescens* IRBG500 [241] and the Gram-positive *Bacillus megaterium C4* [585]. Similarly, *Azospirillum* strains preferentially invade lateral root emergence cracks and epidermal cell junctions in wheat [586], and *Pseudomonas fluorescens* A6RI shows a different spatial distribution overtime in different tomato root zones but privileges the junction between root epidermal cells [587].

The shoot colonisation, on the other hand, remains more elusive.

The consistent presence of *G. diazotrophicus* in non-glandular trichomes, both epiphytically and endophytically, indicates an active chemotaxis toward these structures rather than being the point of arrival of a passive apoplastic or symplastic flow of nutrients. In general, tomato trichomes store fatty acids, terpenoids (monoterpenoids and sesquiterpenoids), highly viscous acyl sugars, alkaloids and flavonoids, which are released under specific environmental conditions or following physical contact [533]. Glandular trichomes synthesise high quantities of secondary metabolites, including volatile compounds, with various functions related with biotic stress defence and interactions with the holobiont [588]. The glands of the type I, IV, and VI glandular trichomes of tomato contain acyl flavonoids, terpenoids, and sugars [534]; similarly, rice glandular trichomes store high amounts of terpenoids, most of which are known as insect repellents [589]. Non-glandular trichomes, or leaf hairs, are less metabolically active than the glandular ones, and are involved with resistance against abiotic stress (desiccation, temperature shock, UV-B radiation) and arthropod herbivores [590]; furthermore, they also contains photosynthates such as polysaccharide material and secondary metabolites

such as phenolics (particularly polyphenols and flavonoids including naringenin, apigenin, luteolin and chrysoeriol) and metals chelated by the phenolics [591]. Overall, the combination of glandular and non-glandular secretions is likely to permeate the trichome surroundings, driving *G. diazotrophicus* chemotaxis toward these and adjacent organs such as stomata. While some of these secondary metabolites such as luteolin are known to be endophyte attractants [592], other phenolics are known to have antimicrobial activity, making the presence of *G. diazotrophicus* in these structures particularly interesting and suggesting its adaptation to otherwise toxic compounds. As plants grow, however, the secondary metabolite concentrations in non-glandular trichomes decreases as their defence role is taken up by the developed epidermal cuticle [591], possibly explaining the high colonisation trichomes particularly at 20 dpi. Given the overlapping content and functions of glandular and non-glandular trichomes, it would be interesting to determine which molecule attracts *G. diazotrophicus* specifically in non-glandular trichomes, or what metabolites repels it from glands. Crucially, the stalk of trichomes contain no or very few chloroplasts [593], suggesting lower oxidative stress from photosynthetic reactions and, consequently, boosted nitrogenase activity. Moreover, trichomes are known to develop sulphur and glutathione-dependent defence mechanisms against oxidative stress responses [594], further contributing to nitrogenase protection. The colonisation of leaf hairs, as indicated by their name, appears to mirror the invasion of root hairs in a root-shoot symmetry that evidences the extreme adaptability of *G. diazotrophicus*' colonisation capability but also the existence of an innate preference for metabolite and nutrient-rich tubular plant organs (or possibly the presence of an unidentified chemoattractant in both structures). In rice, macro hairs (one of the three types of trichomes, together with micro and glandular hairs which are found along the stomata or beside motor cells) are located on silica cells over a thin vascular bundle [595], suggesting an entry point from the leaf vasculature. To the best of current knowledge, this work is the first to document trichome colonisation by *G. diazotrophicus*; in the past, such behaviour may have been overlooked due to the presence of occasional endogenous GUS activity in trichomes and stomata caused by their acidic environment (pH 4-5), which, however, can be prevented through adequately

buffered X-Gluc staining solutions at pH 7 [374]. In the present study, untreated plants never displayed any blue stain upon X-Gluc assay with a pH 7, 100 mM phosphate buffered solution.

Herbaspirillum seropedicae RAM10 also showed non-glandular and peltate scutiform trichome colonisation in pineapple from 7 dpi, although mostly epiphytically [516]. Baldotto and Olivares analysed epiphytic bacterial communities in a tropical agricultural system of 47 plant species, and reported colonisation at the bases and cell wall surfaces of both non-glandular and glandular trichomes, especially in plant species with trichomes associated with veins [596]. The epiphytic invasion of trichomes (and around stomata complexes, to a lesser extent) by diverse bacterial and fungal communities was found to be instrumental in phyllobacterial growth and establishment as biofilms, while plant species with epicuticular waxes was negatively correlated with bacterial presence [596]. Carbon availability, which is known to limit the establishment of phylloepiphytic populations together with its wettability and diffusion across the leaf surface [597], is probably as important in the phyllosphere as it is in the rhizosphere for *G. diazotrophicus* establishment, due to the high sugar metabolism of this bacterium. Notably, tomato trichomes have been shown to import sucrose from the leaf for their energetic metabolism, while using self-photogenerated reducing power (if any) to build secondary metabolites [598]. Therefore, trichome colonisation is likely the result of both active chemotaxis toward phenolic chemoattractants and bacterial concentration around C-rich areas. Intriguingly, trichome colonisation seemed to be regulated by a quorum sensing mechanism which maintained a dense bacterial concentration on the basal stalk cells while inducing the elongated morphology upon migration to the apical cell of a minority of cells, possibly indicating a nutrient micro gradient along the trichome stalk; this behaviour was particularly evident in rice due to their smaller and dyadic nature. In addition to trichomes, high exudation of sugars and aliphatic compounds is also known to occur in epidermal grooves and along leaf veins, which, together with stomata, are the region in which the highest number of phyllobacterial are found [31], explaining the epidermal cell junction colonisation obtained through foliar application (Fig. 4.64). Trichome colonisation was usually associated with epidermis and stomatal invasion, as

clearly observed in rice. Bacteria seemed to exhibit a dynamic mechanism of ingress/egress from trichomes or stomata (described in *Pseudomonas* invasion of sweet cherry leaf stomata [599]), colonising the shared epidermal region between these organs, and possibly re-entering both structures in a self-sustaining cyclic manner (Fig. 4.68, Fig. 4.69). Substomatal chambers, along with aerenchyma cell close to vasculature and the starch-rich bundle sheath cells, were found to host the vast majority, if not entirety, of phyllospheric *G. diazotrophicus*, especially in rice (Fig. 4.67) but also in tomato and *Arabidopsis* (Fig. 4.54e, f), regardless of the inoculation method and N condition. In their study on *G. diazotrophicus* Pal5 application to tomato [174], Luna et al. also reported sporadic colonisation of substomatal pits. Furthermore, the same pattern had been described in an early *G. diazotrophicus* study in sugarcane [221]. Pathogenic [600] and phyllospheric bacteria [601] have been known to exploit stomata for leaf invasion, due to the protection offered against the main abiotic stressors experienced by epiphytic bacteria on leaf surface, i.e., UV radiation [599] and desiccation, which are contrasted by the highly hydrophilic environment of stomatal chambers [602]. Nevertheless, these structures have rarely been identified as colonisation locations following inoculation with non-native PGPB [603]. In the tropical system investigated by Baldotto and Olivares, stomata seemed to play a secondary role as an anatomical structure for epiphytic bacteria establishment, with no differences in regard of abaxial and adaxial leaf surfaces [596]. *G. diazotrophicus* seems to be one of the few diazotrophic biostimulants capable of proficient stoma colonisation, along with *Herbaspirillum seropedicae* [516]. Guard cells were also densely colonised by filamentous/elongated *GGG* cells. When photosynthesis is active, guard cells accumulate sucrose and other sugars from the surrounding mesophyll and create an osmotic gradient that leads to water influx and subsequent turgor pressure, resulting in stomatal opening regulation [604]. Therefore, it seems plausible that *G. diazotrophicus* accumulates around stomata following the carbon flow within the leaf and consuming the sugars taken up in that vicinity. High wettability due to transpiration is also likely to favour bacterial presence [31]. It would be of interest to investigate how this interaction affects stomatal functions; a study on *Arabidopsis* reported increased water-use efficiency upon *G. diazotrophicus*

inoculation, attributed to reduced stomatal conductance [262]. In monocots, especially in sugarcane, the abundance of sugars raises the question of whether *G. diazotrophicus* has evolved to utilise sucrose from guard cells indefinitely, or if it can establish a non-detrimental equilibrium in plant species where sucrose availability is relatively lower. The latter hypothesis is supported by the positive results obtained in PGP evaluation in tomato and *Arabidopsis* model systems.

Among the investigated colonisation dynamics, bacterial elongation or filamentation was as fascinating as it was puzzling. Such morphology also appears in pictures from the work of Luna et al. on *G. diazotrophicus* UAP5541 inoculation in sorghum and wheat, although the phenomenon was not further examined [155]. Additionally, it was reported by Cocking et al. upon intracellular colonization of the root cortex of wheat by *G. diazotrophicus* [271]. As discussed in section 4.2.1c, Muthukumarasamy and colleagues investigated the occurrence of this phenotype *in vitro* and found a correlation with the ammonium concentration in the medium [134]. However, this strict correlation with ammonium was disproven upon observation of bacterial filamentation in media in which the N source was yeast extract (Fig. 4.31) in the rhizosphere of *Arabidopsis* grown in NH_4-free MS agar (Fig. 4.53) and in the phyllosphere of tomato and rice in hydroponic setups. Filamentation regulation in bacteria is unknown, but is commonly regarded as the disruption of cell division in response to different stimuli, including: 1) nutritional stress and stationary phase transition [349]; 2) glucose replete conditions; 3) abiotic stresses such as extremely low pH, low water conditions and high UV irradiance, none of which seem applicable in this study setups (for a detailed review see Karasz et al. [347]). The result is higher surface-to-volume ratio for enhanced nutrient uptake, promotion of surface motility and attachment even in hard surfaces, creation of a concentrated pressure force for burrowing into neighbouring materials or tunnelling into niches and semisolid environments, and spanning through redox gradients for differential respiratory rates in suboptimal oxygen conditions [349] [347]; moreover, bacteria with filamentation capability have been associated with lignin decomposition [347] and plant symbiosis (e.g. the filamentation of *Agrobacterium* in proximity of

different plant tissues [605]). Finally, elongation or filamentation are characteristic of swarming behaviour, in which a group of individual cells usually 5 to 300 μm long align themselves along their long axes and move together by coordinating the flagellar motions, initiating biofilm formation and colonisation of specific environmental niches [349]. As for non-nodulating diazotrophs, pleiomorphic elongated cells were reported for *Azospirillum* strains colonising the root surface of four-weeks-old rice grown hydroponically, and were speculated to be induced by nutritional stress [606]. All these traits appear advantageous within plant systems, but not necessarily *in vitro*. Interestingly, filamentation can also be induced by exogenous signalling compounds and nutrients [347], among which, glutamine is the strongest induction factor [607]. Glutamine is also known to induce swarming behaviour and to act as a strong chemoattractant in plant-microbial interaction, although the biological meaning of this mechanism is uncertain [608], [609]. Crucially, environmental and BNF-derived ammonium (upon protonation of the fixed ammonia in acidic environments) is assimilated by diazotrophic bacteria into glutamine [610] or glutamate by the glutamine synthetase (GS) and glutamine oxoglutarate aminotransferase (GOGAT), which have been characterised in *G. diazotrophicus* [121]. Therefore, it is tempting to speculate that the elongation phenotype observed may be induced by glutamine synthesis upon incorporation of glutamate or ammonium from the plant exudates. Glutamate is one of the most abundant amino acids in the rhizosphere, especially around the root tip, where it exerts an auxin-like regulation of root system architecture [611], and its efflux is stimulated by rhizobacteria [612]. Similarly, ammonium ad glutamine are both secreted by roots [613], suggesting the presence of glutamine or glutamine precursors in the rhizosphere of *Arabidopsis* grown in NH_4-free MS agar as well as in tomato and rice hydroponic setups. Most importantly, the elongated phenotype may reflect glutamine synthesis upon incorporation of BNF-derived ammonium. The low percentage of pleiomorphic cells observed by Muthukumarasamy et al. in potassium nitrate and urea may indicate a minority of bacteria incorporating glutamine upon N_2-fixation fuelled by traces of bioavailable nitrogen in the media, explain the complete lack of elongation in N-free substrate [134]. Similarly, elongated or filamentous *GGG* cells in the

trichomes and root epidermis may indicate a slow metabolic state acquired in carbon rich areas and characterised by nitrogen fixation.

However, one important element that must be taken into consideration in such speculations is the "choranaptyxic" nature of *G. diazotrophicus*, i.e., its ability to dramatically readjust its morphology in response to the available space, as underlined by the filamentous morphology in the long and narrow guard or root epidermis cells vs the ovoid morphology in the small rice root hairs; this dexterity may confer the ability to adapt to and navigate throughout differentially shaped plant organs, further complicating the biological interpretation of these observations. Ultimately, as previously noted, colonisation patterns depend on the combination of protection sites against abiotic stress and availability of nutrients and water [31] [462]. The lack of obvious colonisation differences upon *G. diazotrophicus* inoculation in plant hydroponically grown with different N conditions suggests that intrinsic plant or bacterial factors (such as cross-talk chemical signals) may be more relevant than the N availability in the medium, while carbon seemed to be crucial in driving bacterial chemotaxis, at least in aerial parts.

Another well-characterised shape transition in response to nitrogen fixation is the rhizobial bacteroid formation within the symbiosome, in which bacteria elongate in a non-motile and non-reproductive form upon stimulation by plants' nodule specific cysteine-rich peptides [614] [615]. Intriguingly, legumes control and modulate their symbiotic rhizobia populations through the use of nodule cysteine-rich (NCR) peptides, which have antimicrobial activity [615]: sublethal doses of antimicrobial compounds are known to induce filamentation in proteobacteria [347], suggesting the intriguing speculation of whether a similar mechanism may occur in *G. diazotrophicus* symbiosis, explaining the observed filamentation around highly exudating plant organs. In light of the microscopy analyses presented in this work, the analogies between rhizobial and *G. diazotrophicus* colonisation appear to exceed the conventional understanding.

On the other hand, among various non-nodulating diazotrophs, *Herbaspirillum seropedicae* showed the most striking similarity to the colonisation dynamics

described in this study: upon rice inoculation, the bacterium displayed cracks entry at lateral root junctions, stem and coleoptile colonisation, influx and/or efflux from stomata following epiphytic phyllosphere invasion resulting in large colonies in substomatal cavities, rare invasion of the stele with subsequent transport to the aerial parts via transpiration stream and aerenchyma colonisation [254]. In pineapple, *H. seropedicae* colonised epidermal cell wall junctions and periclinal walls, with a percentage of bacteria exhibiting filamentous or elongated morphology, root hairs, cortex (mostly apoplastically/intercellularly) upon lateral roots emergence crack entry and formation of an extracellular matrix, stomata and substomatal chambers and non-glandular or pelate scutiform trichomes [516].

Such remarkable similarities highlight the existence of common evolutionary adaptations and colonisation strategies which these generalist diazotrophic bacteria have adopted in response to specific plant anatomical and chemical features, contributing to their successful establishment and mutualistic interactions.

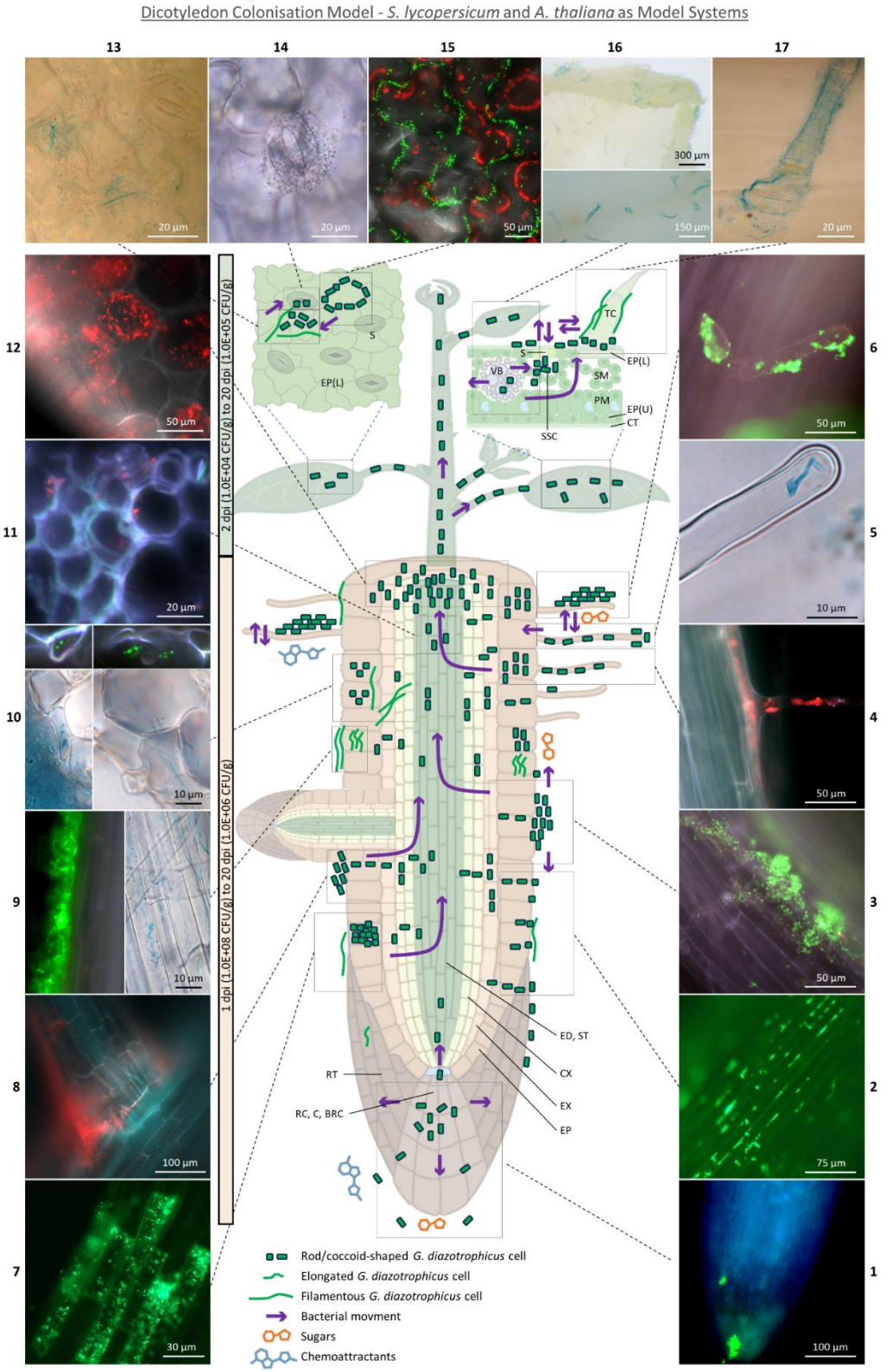


Fig. 4.68. Dicotyledon Colonisation Model - S. lycopersicum and A. thaliana as model systems. 1) Root tip colonisation. 2) Epiphytic colonisation of root epidermis cell wall junctions. 3) Epiphytic aggregates on root epidermis. 4) Concomitant trichoblast and root hair colonisation. 5) Root hair tip intracellular colonisation. 6) Root hair epiphytic colonisation. 7) Intracellular colonisation of lysogenic root epidermal cells. 8) Crack entry through secondary root emergence sites. 9) Filamentous bacterial cell epiphytically and intracellularly colonising root epidermal cells. 10) Elongated or filamentous bacteria intracellularly colonising epidermis, exodermis and cortex and putatively moving across cell walls. 11) Rare stele

colonisation by putative bacteria moving through xylem vasculature. 12) Dense cortex colonisation in the root-shoot junction. 13) Leaf epidermis colonisation by rod-shaed and filamentous bacteria around stomata. 14) Stomata colonisation. 15) Epiphytic colonisation of leaf epidermis cell wall junctions. 16) Abaxial and adaxial colonisation of trichomes, especially in correspondence of leaf vasculature. 17) Epiphytic and endophytic non-glandular trichome colonisation. On the left, a timescale (light orange for roots, light green for shoot) indicates the timeframe in which the summarised colonisation dynamic was observed, followed by the CFUs per gram of fresh tissue reisolated through the MPN method from hydroponic cultures grown under 2 mM KNO_3. BRC = border cells; C = columella; CT = cuticle; CX = cortex; ED = endodermis; EP = epidermis (L = lower, U = upper); EX = exodermis; PM = palisade mesophyll; RC = root cap; RT = root tip; S = stomata; SM = spongy mesophyll; SSC = substomatal chamber; ST = stele; TR = trichome; VB = vascular bundle.

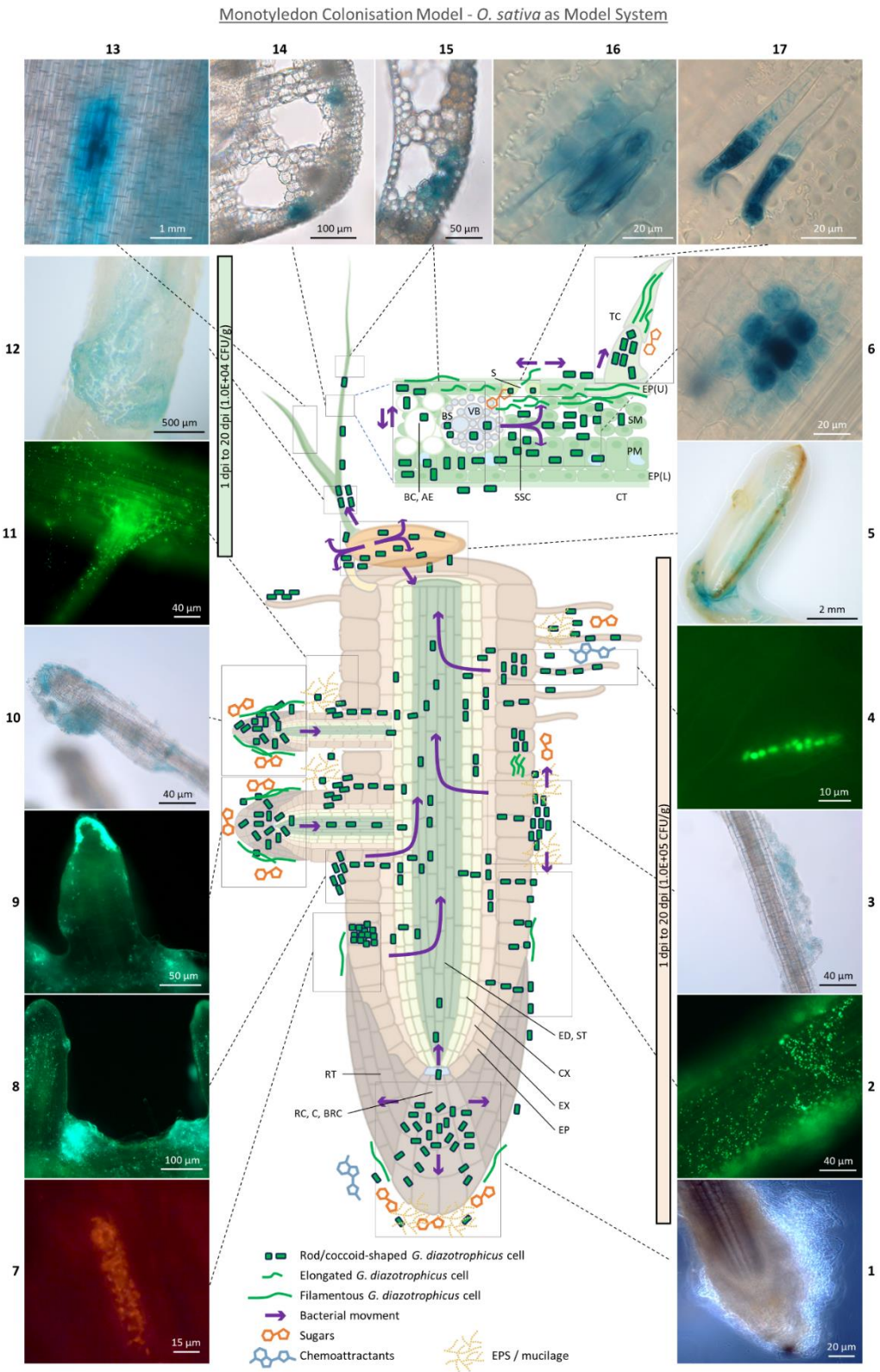


Fig. 4.68. Monocotyledon Colonisation Model – O. sativa as Model Systems. 1) Root tip colonisation by filamentous cells. 2) Epiphytic colonisation of root epidermis cell wall junctions. 3) Epiphytic aggregates on root epidermis. 4) Root hair colonisation. 5) Seed and radicle emergence site colonisation. 6) Substomatal chamber colonisation. 7) Intracellular colonisation of lysogenic root epidermal cells. 8) Crack entry through secondary root emergence sites. 9) L-type secondary root tip colonisation. 10) S-type secondary root tip colonisation. 11) Extracellular EPS matrix around lateral roots 12) Dense colonisation in the

collar-lamina joint. 13) Coleoptile staining. 14) Aerenchyma, bulliform cells, bundle sheath and stomata colonisation in proximity to leaf sheath vasculature. 15) Aerenchyma, bulliform cells, bundle sheath and stomata colonisation in proximity to primary leaf vasculature. 16) Guard and subsidiary cell colonisation by filamentous bacteria. 17) Endophytic non-glandular trichome colonisation. On the left, a timescale (light orange for roots, light green for shoot) indicates the timeframe in which the summarised colonisation dynamic was observed, followed by the CFUs per gram of fresh tissue reisolated through the MPN method from hydroponic cultures grown under 2 mM KNO_3. AE = aerenchyma; BC = bulliform cell; BRC = border cells; C = columella; CX = cortex; CT = cuticle; ED = endodermis; EP = epidermis (L = lower, U = upper); EX = exodermis; PM = palisade mesophyll; RC = root cap; RT = root tip; S = stomata; SM = spongy mesophyll; SSC = substomatal chamber; ST = stele; TR = trichome; VB = vascular bundle.

4.3.4 Cytoplasmic invasion in protoplast and callus systems

Following evidence from microscopy demonstrating intracellular colonisation and bacterial migration throughout both root and aerial plant organs, the specific ingress mechanism and fate of bacteria within plant cells remained to be further elucidated. Does intracellular colonisation involve bacterial uptake within the plant cytoplasm? If so, can bacteria be transmitted cytoplasmically to daughter cells in the meristem?

Cocking et al. proposed that, if *G. diazotrophicus* is able to locally degrade (or induce the rearrangement of the cell wall), it could be taken up in the cytoplasm into membrane-bounded vesicles [271]. Similarly, Mercado-Blanco and Prieto in their review of endophytic colonisation of root hairs, speculate that active endocytosis at the tip of growing hairs and subsequent trafficking of the endocytosed membranes may provide a route for intracellular colonisation [515]. These hypotheses are supported by the observation that protoplasts obtained by enzymatically removing the cell wall can endocytose rhizobia and cyanobacteria [616], [617].

As elaborated above, heterotrophic plant organs such as roots and fruits or cellular lineages such as trichomes and guard cells, are the recipient of a flow of C (mostly sucrose) and N-rich photoassimilates and secondary metabolites, which are stored in the vacuole. This nutrients flux does not solely occur apoplastically, but also via solute-filled vesicles trafficking, which can be transported directly into the vacuole and whose incorporation was found to increase as a function of external sucrose concentration [618]. Dong et al. measured the sucrose concentration in the apoplastic fluid of *G.*

diazotrophicus-colonised sugarcane to be around 12% [189], suggesting that this bacterium may have evolved benefitting from this sucrose-dependent endocytosis for intracellular establishment [98].

To investigate the ability of *G. diazotrophicus* to access the cell cytoplasm, tomato leaf samples inoculated through foliar application were used for protoplast isolation.

Briefly, strips of young, terminal leaves from tomato plants grown hydroponically in axenic condition were cut and incubated with *G. diazotrophicus* resuspended in water to the same OD_{600} applied in the hydroponic system (approximately 10^7 CFU mL^{-1}). After 5 hours of incubation at 28°C, the leaf strips were rinsed in sterile water and treated with a mix of Cellulase, Macerozyme R-10 and Viscozyme® L. When observed under the microscope, a fraction of the protoplasts showed the presence of rod-shaped bacterial cells, moving inside the plasma membrane (Fig. 4, Supplementary Video 3) and exhibiting the light blue coloration characteristic of *G. diazotrophicus* AZ0019 WT (Fig. 4.70). When the experiment was carried out using the *GGG* strain, no GFP fluorescence was detected from intraprotoplast bacteria, showing the plasmid loss or protein maturation issue discussed in previous sections (Fig. 4.70a, b). In contrast, some fluorescent bacteria were observed to interact with the protoplast plasma membrane extracellularly (Fig. 4.70c). Although no vesicle formation was observed directly, this result indicated the ability of the bacterium to reach and establish itself inside the cytoplasm, reinforcing the argument of the intracellular colonisation capability of *G. diazotrophicus* in non-sugarcane systems. Whether the intraprotoplast bacteria underlie bacterial intracellular ingress following foliar inoculation or whether the cell wall degrading enzymatic mix itself allowed the migration into the cytoplasm is difficult to establish, but the experiment demonstrate the existence of a mechanism that allows *G. diazotrophicus* passage through the plasma membrane, most likely through membrane invagination.

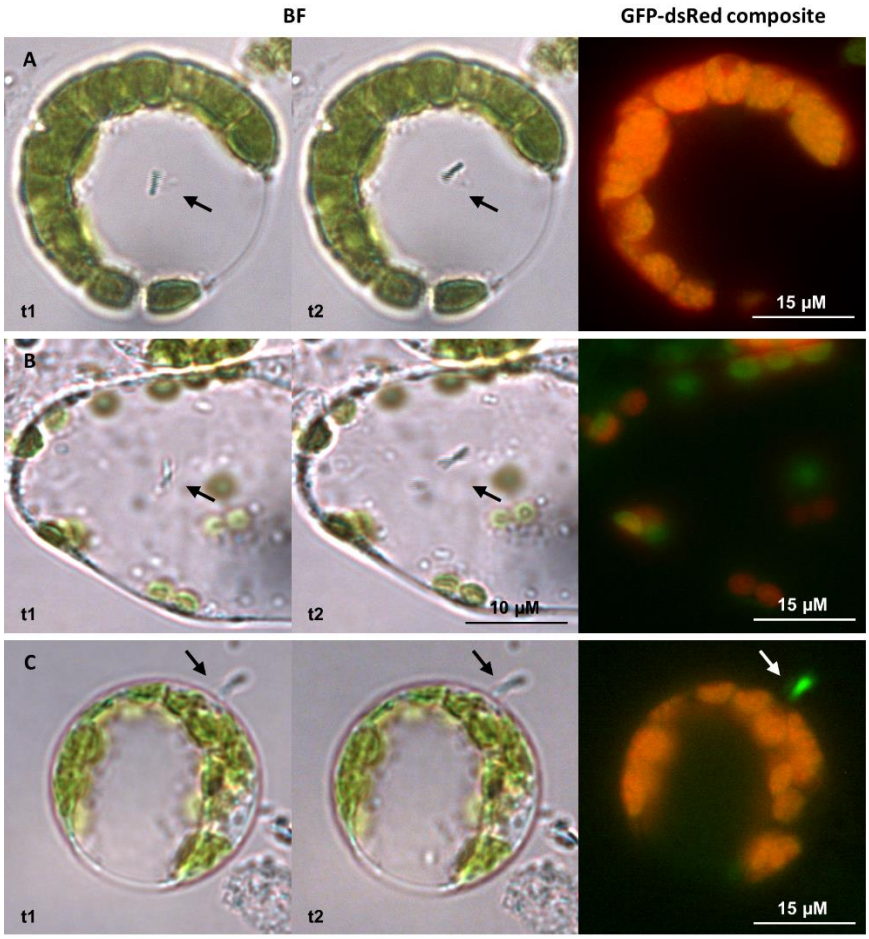


Fig. 4.70. Protoplast isolation from tomato leaf strips inoculated with GGG. After 5 hours of incubation of the leaf tissue with G. diazotrophicus, a fraction of the isolated protoplasts had one (A) to two (B) bacterial cells per protoplast, exhibiting swimming mobility in the cytosol. No GFP signal could be detected from intraprotoplast bacteria, while extracellular GGG cells interacting with the plasma membrane still exhibited GFP fluorescence (C). In both A and B images, the pictures on the left and on the right (t1 and t2) were taken with a 1 second interval to show the motion of the bacterium.

Next, the transmissibility of *G. diazotrophicus* was investigated in tobacco callus cultures. Like tomato, tobacco belongs to the family Solanaceae, and was chosen as a model system considering the availability of well-established callus generation protocols.

Tobacco leaves were inoculated through foliar application as described above and incubated overnight. Subsequently, some 5x5 mm squares were cut from treated apical leaves and grown on MS agar supplemented with indolacetic acid (IAA) and benzylaminopurine (BAP, a synthetic cytokinin) to induce callus formation and development. After 25 days of growth, the regenerated

plant tissues had massive epiphytic and endophytic colonisation, with elongated and filamentous *GGG* cells intracellularly occupying virtually the entirety of the callus except for some of the apical leaflet (Fig. 4.71a). The colonisation patterns observed in this experiment were consistent with previous findings, primarily occurring in the epidermal cells (Fig. 4.71d), stomata (Fig. 4.71e), guard cells (Fig. 4.71a) and trichomes (Fig. 4.71f). Notably, while the majority of bacteria exhibited the elongated morphology, the guard cells, characterized by a rounder shape and greater curvature compared to the slender and more elongated guard cells of rice, were found to be colonised by shorter, rod-shaped bacteria. This observation confirms the remarkable morphological adaptability of *G. diazotrophicus* in response to its surrounding environment. This experiment builds on the technique of in-vitro inoculation of micropropagated sugarcane plants developed by Reis et al. [231] and later employed by James et al. [563] and Oliveira et al. [619] to investigate sugarcane colonisation by *G. diazotrophicus* and other diazotrophic bacteria. The present work provides evidence showcasing the dissemination and transmission capacity of *G. diazotrophicus*, as it was observed to effectively spread intracellularly from the initial inoculated area of around 5 mm to the entire regenerated organism, proliferating within the host while targeting the same colonisation sites described in the other experimental systems. Bacteria were also found to partially colonise the regeneration medium (not shown), which contained 3% sucrose, but mostly remained localised within the callus. The presence of sucrose in the medium may have encouraged the robust colonisation, which seemed higher in the basal region of the callus that was directly in contact with the medium compared to the regenerated shoot (Fig. 4,71a); similarly, it is possible that high carbon levels induced the predominantly elongated morphology, possibly as result of BNF.

Consistent with previous reports by Thomas and Franco [620], callus culture presents a valuable approach for augmenting the current understanding of endophytic colonisation behaviour. In the context of *G. diazotrophicus* research, calli systems may enable rigorous monitoring of both plant cell division and bacterial cell replication and distribution over time within this staminal system, while also allowing to assess in which differentiated tissues

the endophyte establishes itself. The intracellular transmission capability observed in calli of tobacco (Fig. 4.71), along with the demonstrated evidence of cytoplasmic invasion in tomato protoplasts (Fig. 4.70), provides conclusive evidence that *G. diazotrophicus* is capable of multiplying inside cells and being transmitted during plant cell proliferation. This finding indicates a mechanism for bacterial spread within the plant host and highlights the profound adaptation of this organism to the plant cytoplasm environment.

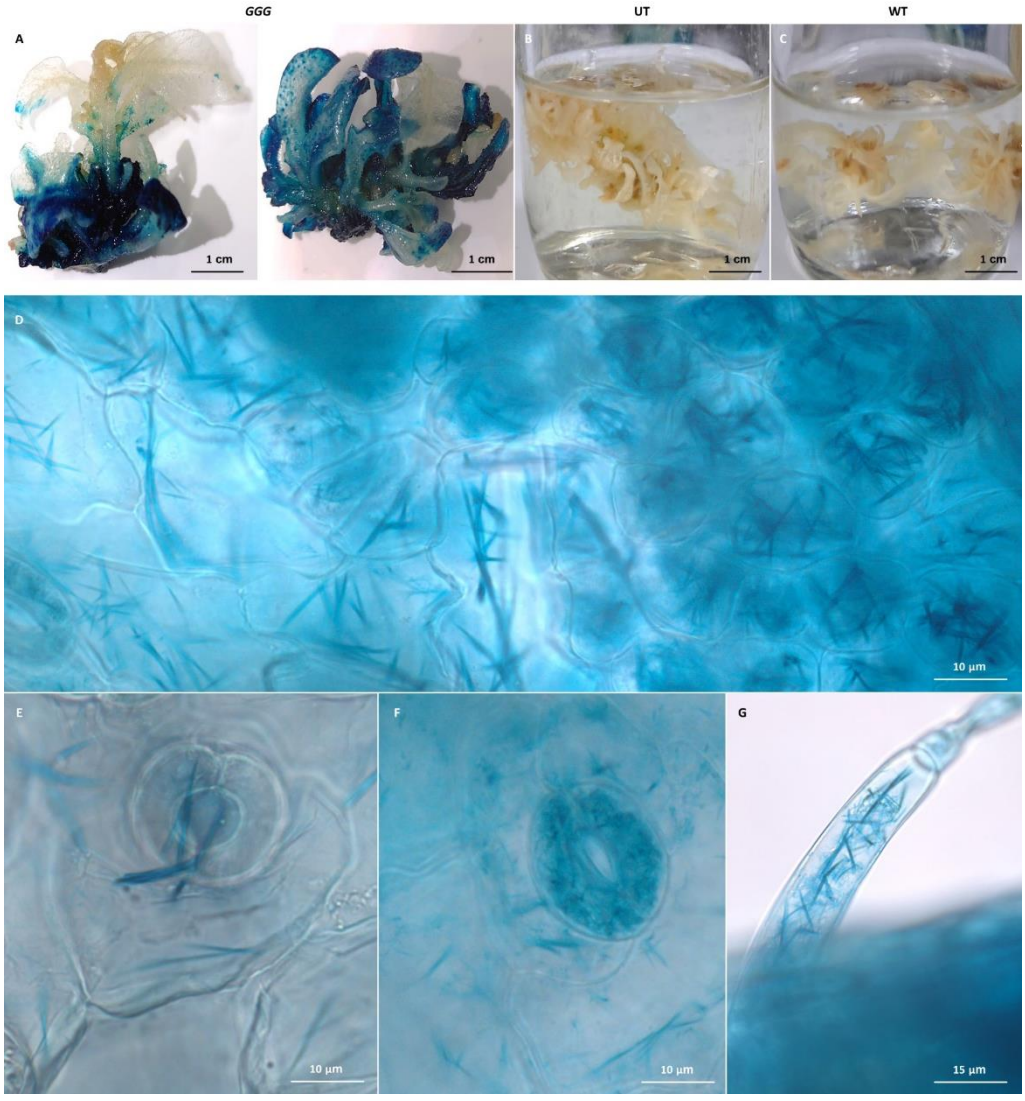


Fig. 4.71. Callus generation from tobacco plants inoculated with GGG resuspended in water t 10^7 CFUs mL^{-1} and incubated overnight, 25 dpi (A). (B, C) Untreated (UT) and G. diazotrophicus WT-treated callus upon X-Gluc assay showing no trace of blue staining. (D-G) intracellular colonisation of various callus organs by elongated GGG cells; in particular, epidermis colonisation (D), stomata invasion (E), guard cells colonisation (F) and trichome colonisation (G) are showed.

4.4 PGP metabolism investigation and engineering

To investigate the behaviour and PGP capabilities of *G. diazotrophicus*, the experimental observations outlined in sections 4.1 and 4.3 were tested making use of the mutant strains described in section 4.2. In particular, the symbiosis establishment, nitrogen metabolism and hormonal stimulation, which are widely regarded as critical factors contributing to the growth promotion effect, were further investigated under different nitrogen conditions. The nitrogen metabolism of *G. diazotrophicus* was kept at the centre of such investigations because, over the years, increasing evidence has highlighted its crucial role in the bacterium's symbiotic relationships with plants. This conception first arose from the observation by Fuentes-Ramirez et al. that the isolation frequency of *G. diazotrophicus* from sugarcane plants in Mexico diminished as the quantity of N-fertilisation in the field increased [100]. Later, similar observations were reported by Muthukumarasamy et al. from sugarcane plantations in India [84] and by Tapia-Hernandez et al. from pineapple [96]. Furthermore, Caballero-Mellando et al. suggested nitrogen to be a selective factor for *G. diazotrophicus* population diversity and establishment [621]. This hypothesis was confirmed by Muthukumarasamy et al. through *in vitro* inoculation experiments on sugarcane, that showed lower colonisation rates and nitrogenase activity *in planta* in the presence of high ammonium levels (25 mM ammonium chloride (NH_4Cl) or ammonium nitrate (NH_4NO_3)) as compared to 2 mM; no such effect was observed under cultivation with 25 mM potassium nitrate (KNO_3) or urea $\leq$ 500 µg mL^{-1} [134]. Similarly, no *G. diazotrophicus* UAP5541 cells could be reisolated from inoculated sugarcane grown in glasshouse condition in an inert substrate watered with 11 mM NH_4NO_3; nevertheless, 10 mM nitrate alone had no effect on bacterial growth or N-fixation capabilities [622]. These findings suggested that the different colonisation rates in field may depend on both bacterial metabolism and the plant physiological state in response to nitrogen nutrition [622], possibly because in mature sugarcane plants high nitrate doses were associated with a decrease in sucrose production [623]; alternatively, the out competition by other microorganisms feeding on nitrate may explain such behaviour [134]. Of

note, when KNO_3 concentration exceeded 60 mM or urea was higher than 600 µg mL^{-1}, a growth inhibition, and eventually growth suppression at 100 mM KNO_3, was observed, contributing to explaining the scarcity of *G. diazotrophicus* reisolation in highly urea and nitrate-fertilised soils [84]. In a similar *in vitro* setup, Muñoz-Rojas and Caballero-Mellado reported a dramatic decrease of the population of three *G. diazotrophicus* strains over time and dependently on the NH_4NO_3 level applied to five sugarcane cultivars, in a genotype-specific manner [624]; the same effect was observed upon the addition of ammonium sulphate or calcium nitrate in sugarcane grown in glasshouse conditions at 60 dpi, although with different outcome according to plant's genotype [623].

Following these preliminary observations about how the nitrogen nutrition in the plant-bacterium system affects the survival of the latter *in vivo*, the nitrogen metabolism of *G. diazotrophicus* has been further investigated through the characterisation of some elements of the *nif* regulon [129] [121] [123], but was never completely elucidated. Some of its aspects may be common to other bacteria (as shown by Kirchov et. al, who reported the same decrease of diazotroph populations in highly fertilised gramineous plants fields [625]), while other seem to be specific to this microorganism. As an instance, *Herbaspirillum* spp., another important non-nodulating diazotrophic endophyte which occurs in large numbers in sugarcane and fixes nitrogen under high sucrose, was reported by several studies to show a uniform isolation rate regardless of N applications [626] [84] [627].

In this study, the expression of seven bacterial genes was investigated through RT-qPCR analyses in the tomato model system. Four genes involved in BNF and nitrogen metabolism (*nifH*, *nifD*, *nifK*, *nrgA*), one gene involved in hormonal production (*cccA*), one involved in oxidative stress response (*katE*) and one in sucrose metabolism and biofilm formation (*lsdA*) were monitored in inoculated plants grown under different nitrogen conditions in order to detect the impact of nitrogen availability on the bacterium transcriptome *in planta*. Considering the centrality of the nitrogen metabolism in diazotrophic bacteria such as *G. diazotrophicus*, the exploration of its interplay with other PGP determinants like indoleacetic acid production and biofilm formation during

the symbiosis establishment are of utmost significance in the field of plant-microbe interactions: these analyses can allow to integrate the understanding of bacterial metabolism with the evaluation of its applicability in agricultural systems.

Briefly, tomato plants were grown hydroponically in the three nitrogen conditions described in previous sections (N-free, 2 mM KNO_3 or N-replete, and 2 mM KNO_3 + 0.4 millimoles of ammonium as bioavailable nitrogen for bacterial nutrition) and inoculated with *G. diazotrophicus* WT or *nifD*$^-$ strains to uncover any BNF-related transcriptional divergence. Root and shoot were analysed separately. To obtain the relative expression of each bacterial gene, the total RNA extracted from the inoculated plants was brought to the same concentration in each sample before the retrotranscription to cDNA, and the same concentration of cDNA was used as a template for every RT-qPCR reaction. To remove the variable of the different bacterial presence on the analysed plant tissues, the investigated genes were normalised on the constitutively expressed bacterial *rho* gene, encoding a Rho termination factor, which was previously validated as an optimal reference gene for *G. diazotrophicus* gene expression analyses [150].

4.4.1 Colonisation establishment

As discussed in section 4.1.2a, microbial assembly on plants is a process which consists in a standoff between the host immune response and the ability of the endophyte to evade such defence mechanism, in a dynamic equilibrium that ultimately shapes microbial communities [31]. Plants possess pattern recognition receptors (PRRs) that detect microbes through the recognition of microbe-associated molecular patterns (MAMPs) such as peptidoglycans, lipopolysaccharides and flagellin; recognition of MAMPs by PRRs leads to PAMP-triggered immunity (PTI), which serves as the first line of defence against non-adapted phytobacteria [46]. It is not clear how plants downregulate such mechanism to allow colonisation of beneficial bacteria [31], but it is generally accepted that beneficial endophytes elicit a milder immune response

compared to phytopathogens [41]. This weaker but detectable immune reaction was also observed during the colonisation of sugarcane plants by *G. diazotrophicus* [221].

Nevertheless, commensal endophytes and phytopathogens are eventually able to evade PTI by suppressing or modulating the host immune system or by modifying their MAMPs [46] and exploiting phase variation [628]. Early response to biotic stress usually involves an oxidative burst, i.e., the transient increase in reactive oxygen species (ROS) in the invasion site [629]. In addition to direct bacterial cell elimination by oxidative stress, ROS, which are produced by membrane-bound NADPH oxidases, also serve as secondary messengers to further elicit the activation of plant defence genes [630]. For instance, ROS are believed to function as priming signals upon SAR (systemic acquired resistance) activation, i.e., a long-lasting, acquired immune response that takes place in the days following the initial stress exposure and acts systemically [631].

Similarly to what was observed in plant inoculated with Rhizobia [256] or the pathogenic fungus *Ustilago maydis* [632], *G. diazotrophicus* was found to be able to survive the oxidative burst during rice root colonisation by upregulating ROS-detoxifying genes such as superoxide dismutase, glutathione reductase and catalase [257]. For this reason, these genes were found to be crucial for the colonisation establishment [257]. Furthermore, another study showed that these ROS-scavenging activities protect the nitrogenase from the elevated oxidative metabolic rates required by *G. diazotrophicus* to sustain BNF [110].

In the present study, the expression of a catalase-peroxidase gene (*katE*), already reported to be involved in oxidative burst protection during rice colonisation by *G. diazotrophicus* [257], was investigated at 1 and 20 dpi in hydroponically grown tomatoes. This ROS-scavenging gene, which catalyses the decomposition of hydrogen peroxide (H_2O_2) into water and oxygen, lies within an operon encoding a Cytochrome b561 and the glutathione transport proteins GsiA, GsiD, GsiC (belonging to the ABC transporters family). Cytochrome b561 is involved in Fe^{3+}-reductase activity and ascorbate regeneration, which is a central component of the redox network and act as electron donor in H_2O_2 scavenging reactions [633]. Similarly, glutathione and

its transport proteins play a leading role in bacterial protection against ROS [634], suggesting *katE* to be part of a regulon involved in redox balance and oxidative stress resistance.

In parallel, the expression of the *lsdA* gene, encoding a levansucrase, was monitored as an indicator of exudate/photoassimilate-dependent colonisation establishment. This enzyme is central in *G. diazotrophicus* metabolism since it is responsible for the bacterium ability to grow on sucrose [106]. The levansucrase is expressed as a polycistronic transcript including various pseudopilin genes [105] and is secreted extracellularly via periplasm by a signal-peptide-dependent pathway [635] due to the apparent inability of *G. diazotrophicus* to uptake sucrose intracellularly [119]. In the presence of low concentration of this sugar (< 0.1 M), LsdA primarily catalyses the hydrolysis of sucrose with subsequent release of glucose for energetic metabolism [636] and, presumably, for fuelling BNF [106]. At higher sucrose levels, it polymerises fructose molecules by 2,6-β-glycosidic linkages to form levan, a type of high-molecular-mass fructan (i.e., a polymer of fructose molecules) [104] first discovered in the fermentation of *nattō* [637]. In addition to transferring the fructosyl residue from sucrose to another fructose or fructan molecule, levansucrase can attach fructosyls to glucose or sucrose itself, creating different oligofructosides and levan polymers (mainly 1-ketose [106]) which are part of the bacterium EPS [104]. In fact, levan is the main EPS component in *G. diazotrophicus*, and is responsible for its characteristic mucoid phenotype when cultured in sucrose [107] and, particularly, in the presence of high phosphates [638]. The LsdA enzyme is not induced by sucrose but is constitutively expressed regardless of the carbon source, although mannitol induces the highest activity [106]. It was estimated to represents more than 70% of the total protein secreted by some *G. diazotrophicus* strains isolated from sucrose-rich hosts such as sugarcane [636], while strains isolated from coffee plants exhibit a lower enzymatic activity [106]. Levan was shown to be able to mediate wheat root colonisation by the diazotroph *Paenibacillus polymyxa* [639], and to inhibit the early plant defence response upon infection by the phytopathogens *Erwinia amylovora* and *Pseudomonas syringae* [106]; in general, levan is believed to both serve as

energy reserve for bacteria and to support their ecological adaptation by conferring biotic and abiotic stress resistance and colonisation competency in symbiotic associations [640]. Crucially, in *G. diazotrophicus*, levansucrase disruption was reported to affect the ability of the bacterium to adhere to surfaces and form cell aggregates and biofilm, confirming the role of LsdA as a colonisation factor, which was also demonstrated in other bacteria [107]. Moreover, levan was reported to serve as a mucous shield to protect *G. diazotrophicus* colonies against H_2O_2 peroxidation [638], suggesting an interesting link with KatE function.

gumD could have been another possible target due to its central role in EPS production and biofilm formation, making it an equally important gene for colonisation establishment [184]. However, it has already been shown that the deletion of this gene does not affect nitrogen fixation [184]; furthermore, sucrose, which is the substrate of LsdA, is the primary product of plant photosynthetic tissues and the primary sugar transported via phloem to heterotrophic sink organs in most plants [641], making the *lsdA* investigation particularly interesting as a link between colonisation establishment and dependency on the host plant photoassimilate availability.

In Fig. 4.72, the expression of the *katE* and *lsdA* genes is shown in comparison to qPCR data presented in section 4.3.1d and here regrouped in shoot (obtained by averaging the FC values of stem and leaves) and root (obtained by averaging the FC values of root-shoot junction, root maturation zone and root tip).

At 1 dpi, both *nifD*$^-$ and WT strains colonised the root system at similar levels and with the same pattern as a function of the N conditions, with the 2 mM KNO_3 system being associated with the highest bacterial density. This finding suggests that, on one hand, N-starved plants are less attractive for early bacterial colonisation and, on the other hand, the presence of free bioavailable ammonium in the medium may cause the partial uncoupling of the symbiosis, albeit minimal. At 20 dpi, the population decrease was more pronounced for the *nifD*$^-$ strain in the two N-replete conditions, while, in the absence of a nitrogen source, it was the WT bacterium to suffer the highest population

reduction. This dynamic seems to reflect that, in healthy plant systems which are replete of nitrogen and, consequently, of C-rich exudates, BNF capability may be an advantage in terms of colonisation efficiency, because it provides extra bioavailable nitrogen while being fuelled by non-limiting carbon sources from the environment. In contrast, the activation of the BNF machinery in the nutrient-poor rhizosphere of stunted plants may cause an unmet energy demand that constitutes a selective disadvantage and affect the long-term root colonisation capability of the WT bacterium, favouring the mutant. Possibly for the same reason, the *nifD*$^{-}$ strain had higher colonisation levels in the shoot of N-starved plants compared to the WT at 1 dpi, i.e., in nutrient-deprived plantlets with scarce photoassimilate availability in the aerial parts. Interestingly, at 20 dpi, the persistence of the two strains within the aerial parts was identical in both FC values and in terms of colonisation pattern across the different N conditions, similarly to what observed in the root tissues at 1 dpi. In the context of the shoot, the higher bacterial density of both strains in N-free conditions may have different explanations. In general, this finding is likely to reflect an enhanced NS uptake and xylemic sap flux from the rhizosphere in the attempt to compensate for the N scarcity. Additionally, as discussed in previous sections, this observation may indicate a parasitic behaviour of *G. diazotrophicus*, which may take advantage of the impaired immune modulation capability of stunted plants while still benefitting of the nutrient-rich environment of the autotrophic plant organs; in fact, although stressed and nutrient-deprived compared to plants grown under N-replete condition, a 25 day old plant grown on inoculated N-free NS, would still have stored enough photoassimilates for them not to be limiting factors for bacterial growth. Alternatively, it is possible that N-starved plants actively recruit the beneficial symbionts in the shoot by hormonal modulation to profit from their PGP properties where they are most needed. It is in fact known that microbial assembly on the rhizosphere is actively modulated by hormonal cascades [41], mostly involving jasmonic acid in monocotyledonous plants [642] and salicylic acid and ethylene in dicotyledonous plants [643], although this mechanism in the phyllosphere is less investigated.



Fig. 4.72. katE and lsdA expression from tomato plants grown under different N conditions in comparison to the bacterial abundance across the treatments. Bacterial abundance data are rearranged from Fig. 4.63 by averaging the fold change (FC) values of the root zones (Root) and of the aerial parts (Shoot): the FC reflect the enrichment of amplicons from G. diazotrophicus genome and are normalised against amplicons from the tomato genome as reference. The FC from the RT-qPCR analyses, on the other hand, indicate the enrichment in the transcript of the investigated bacterial genes and are normalised against the constitutive bacterial gene rho. The standard error of the mean between the three biological replicates is shown in the error bars. One-Way ANOVA analyses for statistical differences between the different conditions were conducted using Tukey's Honestly Significant Difference (HSD) test in R.

Overall, these data confirmed that the lack of a functional BNF machinery does not severely affect colonisation capability, as already reported in *H. seropedicae* [232]. The bacterial abundance across the N-conditions, however, showed no obvious correlation with the investigated genes.

In the root system, *katE* exhibited the same expression pattern between the WT and *niD*$^{-}$ strains, although the FC absolute values in the WT were higher compared to the mutant, especially at 1 dpi. The highest *katE* expression in both strains was induced at 1 dpi in the presence of 2 mM KNO_3; this is probably imputable by a stronger immune reaction in plants that were not nitrogen starved. The lower ROS-protection response in the ammonium-supplemented system may have been caused by the milder endophytic invasion due to partial uncoupling of the symbiosis discussed above and supported by the MPN data (Fig. 4.15). Furthermore, *katE* expression in N-deplete systems was generally low regardless of the strain, plant region or time-point, corroborating the idea of a scarce immune response in nitrogen-deprived plants; alternatively, the lower catalase expression may reflect a reduced bacterial oxidative metabolism due to photoassimilate scarcity. In the shoot, both strains exhibited mild *katE* expression. The most evident common trend, however, was a pronounced decrease in catalase expression at 20 dpi compared to 1 dpi, indicating that this protein is involved in escaping the oxidative burst in early colonisation stages, while its function seemed to diminish as the symbiotic relationship progressed; this may suggest that plants acclimate to the bacterial presence and downregulate the defence response. Overall, the BNF-impaired *G. diazotrophicus* strain and the wild-type showed only minimal variations in catalase expression when colonising the aerial parts, while the root colonisation exposed a higher demand for ROS-scavenging activity in the wild-type strain. Interestingly, *katE* showed some correlation with the nitrogenase gene expression profile, but mainly in the shoot and at 1 dpi, while the N-conditions associated with the highest nitrogenase transcription levels did not induce any concomitant catalase upregulation (see section 4.4.2); this observation suggests a limited involvement of *katE* in supporting BNF by ROS detoxification *in planta*. Intriguingly, White and colleagues proposed that the

oxidation observed around endophytes intracellularly colonising plant tissues may indicate the “digestion” of microbes as a nutritional source through peroxidation [520], suggesting another possible explanation for the observed *katE* expression profiles.

The *lsdA* transcript had the highest expression levels among all the genes analysed, thus confirming its central role in the metabolism of *G. diazotrophicus*. In general, its expression was higher in the root tissues compared to the aerial parts: this may suggest levansucrase involvement in both sucrose metabolism (observed in both root and shoot systems) and in the physical adherence to root tissues by EPS formation (observed mainly in the root and explaining the higher transcription level). The WT strain showed a high early *lsdA* expression regardless of the N condition, which decreased overtime except in the case of ammonium-amended medium; the *nifD*$^{-}$ mutant, on the other hand, maintained a consistent, lower transcription pattern across the different N conditions for the duration of the experiment, with the N-replete condition eliciting the highest *lsdA* expression and he ammonium-supplemented system inducing the lowest. A functional BNF-machinery is evidently required for full levansucrase transcription in the early root colonisation stages and, interestingly, the ammonium elicited an increase in *lsdA* expression in the WT while it induced its downregulation in the mutant strain. In the aerial parts at 1 dpi, the two strains exhibited the same levansucrase transcription levels in both N-free and 2 mM KNO_3 NS, with the latter condition eliciting the highest transcription possibly due to increased sucrose availability; however, similarly to what was observed in the roots, the presence of ammonium induced *lsdA* upregulation in the WT strain and its downregulation in the *nifD*$^{-}$ mutant in comparison to the other N-replete condition. These dynamics could reflect different metabolic states of the two *G. diazotrophicus* strains in response to the local sucrose availability and consequent nitrogen metabolism. The ammonium may have a direct effect on bacterial gene expression in the root system, but in the aerial parts it is likely to only affect the bacterial metabolism indirectly; this may happen by either modulating the plant metabolome or by allowing bacteria to accumulate extra nitrogen reserves before shoot colonisation, thus resulting in different

metabolic capabilities. For example, ammonium nutrition is known to increase phosphate uptake by the plant [644], and phosphates induce levan production in *G. diazotrophicus* [638], possibly explaining the augmented *lsdA* expression under ammonium-supplemented condition; however, the presence of a functional nitrogen regulon may be involved in this process, explaining the different *lsdA* expression profile between the two strains in the presence of ammonium.

Overall, these data highlight an extremely complex and diverse transcriptional response following the colonisation of plants grown in different nitrogen conditions, with no obvious consequence on the bacterial population distribution showed by the qPCR data (Fig. 4.72, top panel). Furthermore, despite of differential transcription profiles observed between the WT and the BNF-impaired mutant, neither the *katE* nor the *lsdA* expression pattern seemed to directly correlate with the expression of the *nifD* gene (see section 4.4.2).

4.4.2 Nitrogen metabolism

At the centre of the nitrogen regulation lies nitrogenase enzyme, a multisubunit complex composed by two main proteins: 1) the dinitrogenase or MoFe protein, a α2β2 heterotetramer produced by the *nifD* and *nifK* genes containing a molybdenum–iron cofactor that is the site of N_2 reduction; 2) the dinitrogenase reductase or Fe protein, encoded by the *nifH* gene, which transfers electrons to the MoFe protein [137] (Fig. 2.3b). Additionally, an extensive array of auxiliary proteins (such as the Fix family) is involved in the BNF machinery mechanism with diverse and often unidentified functions, including maturation, assembly and electron transfer [137]. In the bacterial chromosome, transcriptional regulatory networks of genes tend to be spatially associated in 1, 2 and 3-dimensions [645], thus conferring to the analyses of a genomic region a certain predictive value about its functions. In Fig. 4.73, the complete *nif* operon of *G. diazotrophicus* is depicted along with its genomic surroundings.

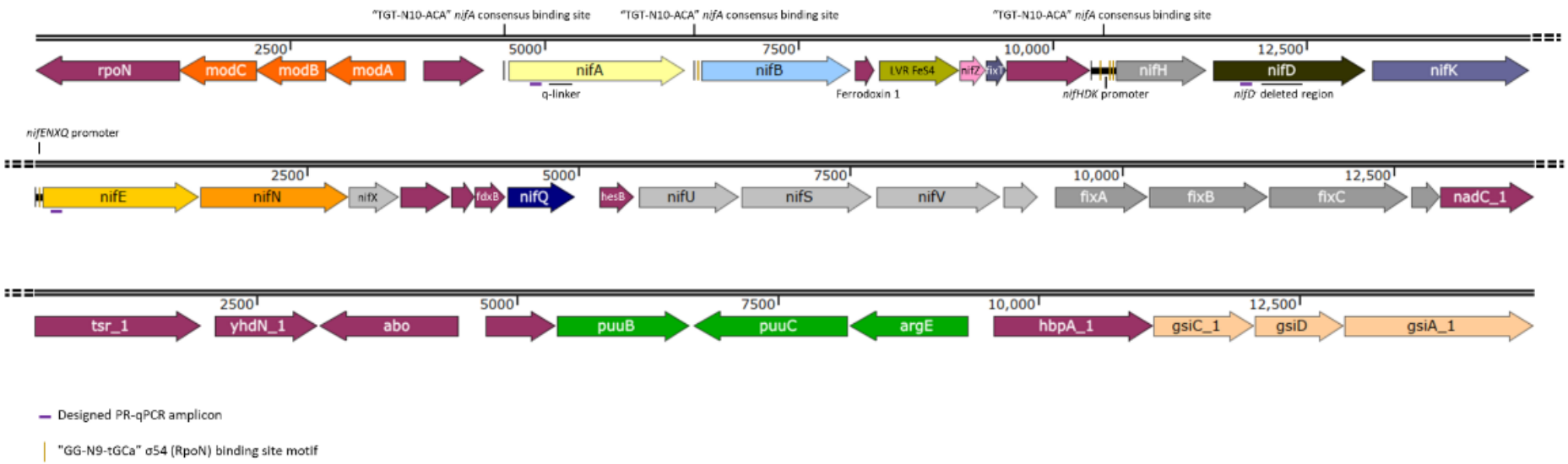


Fig. 4.73. Nif regulon in G. diazotrophicus AZ0019. A 118,493 bp region is depicted as sequenced and annotated in this study from the G. diazotrophicus AZ0019 WT strain. The designed amplicon for the RT-qPCR analysis (horizontal purple line), sigma factor RpoN (σ^{54}) binding motif (vertical yellow line) and NifA binding motif are highlithed where relevant for the purposes of this study.

When the *nif* cluster of this bacterium was first genetically characterised in 1999, it was described as the largest single grouping of genes required for nitrogenase structure and function found in any diazotroph so far studied [129]. Upstream of the positive regulator *nifA*, the *modABC* operon encodes a molybdate transport system [646] also found in *Azotobacter vinelandii* and most likely involved in the MoFe protein maturation [129]; in *G. diazotrophicus*, the operon also includes the RNA polymerase RpoN. Downstream the N-fixation cluster, other auxiliary genes appear to be part of the endophytic metabolism network: the nicotinate-nucleotide pyrophosphorylase *nadC* and 4-methylaminobutanoate oxidase *abo* suggest the involvement in the catabolism of nicotine or other plant aromatic compounds with a pyrrolidine ring [647]. The presence of the glutathione transport genes *gsiADC* discussed above suggests ROS protection for preserving BNF function. In proximity to the *gsiADC* operon, the gamma-glutamylputrescine oxidoreductase *puuB*, aldehyde dehydrogenase *puuC* and acetylornithine deacetylase *argE* are involved in the metabolism of polyamines, which are signalling molecules produced by plants to regulate their nitrogen metabolism in response to microbial interactions [648], [649].

Among this large and complex regulon, three genes were selected for transcriptional analyses: *nifD*, *nifA* and *nifE*. *nifD*, which is transcribed as a polycistronic *nifHDK* unit [129], was selected as an indicator of the nitrogenase production. To detect the expression of this transcript in the *nifD*$^{-}$ mutant strain and unveil any self-modulation in response to the nitrogenase disruption, the amplicon of *nifD* was designed upstream the deletion cassette (Fig. 4.73); however, it must be emphasised that any detected transcriptional activity would not result in the presence of a functional BNF machinery. Similarly, the *nifE* gene, that in *G. diazotrophicus* is expressed as a separate polycistronic transcript ranging from *nifE* up until *nifQ* [129], is believed to be involved along with the other genes of its operon in FeMo-co synthesis/scaffolding [137]. The expression of NifA was investigated as it transcriptionally activates the *nifHDK* operon in response to the environmental conditions; specifically, this protein responds to NH_4 supply and oxygen level, due to the inherent sensitivity to oxygen damage of a Cys-aa4-Cys motif in its

interdomain linker region [128]. Finally, the expression of the *nrgA* gene, encoding an ammonium channel, was investigated as part of the nitrogen metabolism regulation. In the genome of *G. diazotrophicus*, two NH_4^+ transporters are present, named *nrgA* and *amtB*, both linked in a bicistronic operon with a P_{II} nitrogen regulatory protein GlnK [124]. Normally, the ammonium flux through the channel is modulated by the bifunctional uridylyltransferase/uridylyl-removing protein GlnD, which, under high NH_4^+ levels, deuridylylates GlnK that in turn binds to NrgA/AmtB and induces the channel closure [118]. In previous research, the combined deletion of the GlnK1 protein (associated with the NrgA channel) and GlnK2 protein (associated with the AmtB channel) resulted in the partial expression of the nitrogenase complex even under high ammonium, and upon the deletion of a third P_{II} protein (GlnB), the nitrogenase was fully expressed as in N-fixing conditions [124]. This observation, also reported in *Azorhizobium caulinodans* [650], indicates the importance of functional ammonium-sensing/transport machinery for BNF regulation.

The transcription data (Fig. 4.74) highlighted a complex BNF dynamic *in planta*, with significant variation across the different nitrogen conditions. The *nifENXQ* and the *nifHDK* transcripts exhibited grossly the same expression pattern in both strains across the different treatments, with the exception of the root system at 20 dpi, where the ammonium induced the downregulation of *nifE* and the upregulation of *nifD* in the WT bacterium. However, the FC of the *nifE* gene were higher compared to *nifD*, suggesting that both operons respond to the same activation stimulus, but the *nifENXQ* transcript is magnified by some feedback mechanism.

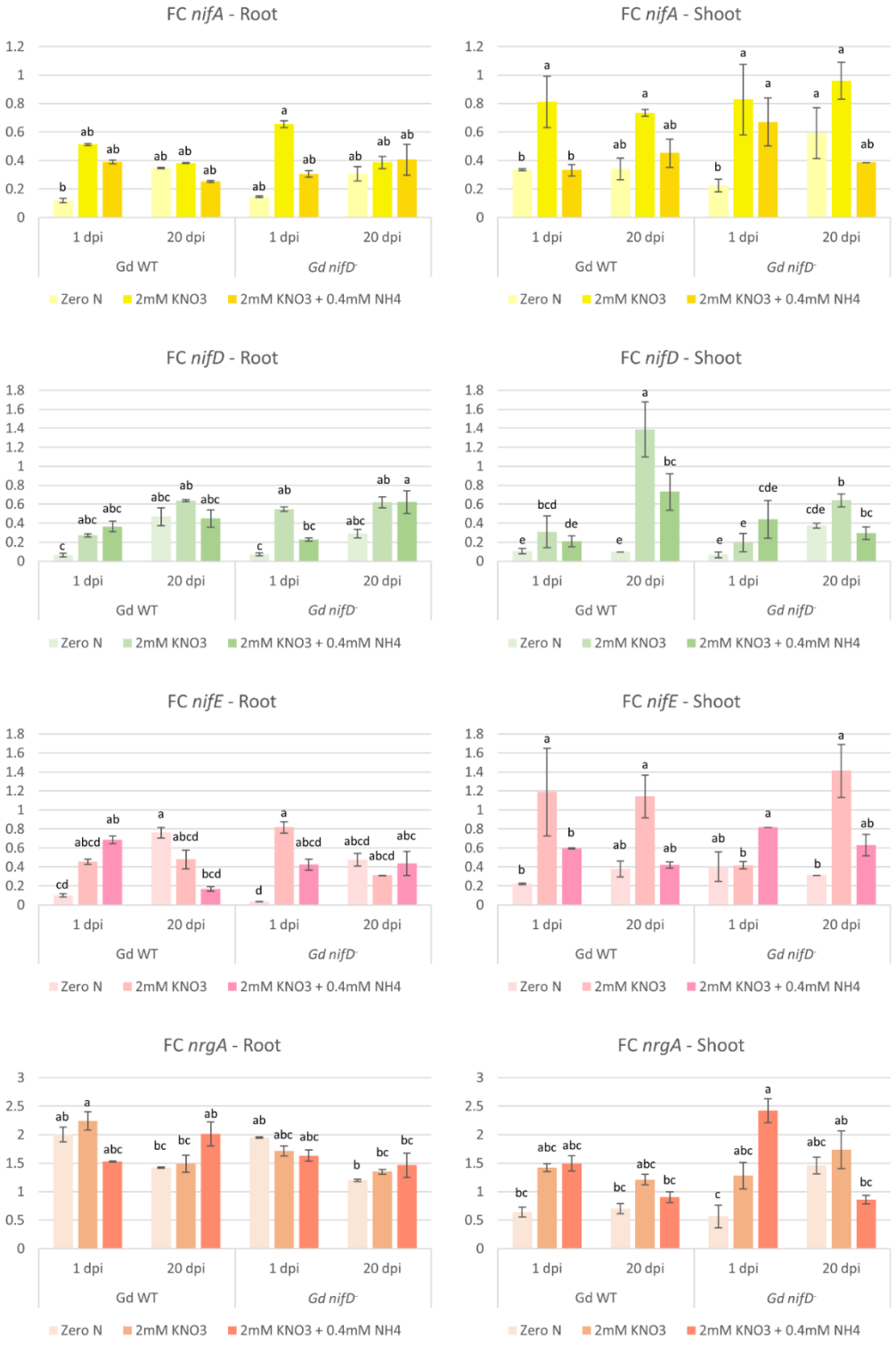


Fig. 4.74. nifA, nifD, nifE and nrgA expression from tomato plants grown under different N conditions. The FC are normalised on the constitutive bacterial gene rho. The standard error of the mean between the three biological replicates is shown in the error bars. One-Way ANOVA analyses for statistical differences between the different conditions were conducted using Tukey's Honestly Significant Difference (HSD) test in R.

In the experimental setup employed, all three nitrogen conditions were predicted to support BNF; in particular, as discussed in previous sections, the addition of 2 mM KNO_3 was expected to enhance root exudation/nutrient availability and, consequently, to boost the bacterial metabolism and BNF capability. In contrast, the addition of 0.4 mmol of bioavailable NH_4 on top of 2 mM KNO_3 could, on one hand, potentially facilitate the initiation of a self-sustaining BNF cycle, or, on the other hand, lead to the uncoupling of the symbiosis. These hypotheses were partially confirmed. At 20 dpi, there was an upregulation of *nifD* compared to 1 dpi, except in the shoot of N-starved plants treated with the WT bacterium, possibly due to the proposed disadvantage of spending energy for activating BNF in nutrient-poor environments. Interestingly, in plants grown under N-replete conditions, there was a pronounced upregulation of the nitrogenase in the shoot at 20 dpi, indicating that the photossimilate-rich aerial parts support the highest nitrogen fixation rates in colonised tomato plants. In the root system, the *nifHDK* upregulation overtime was more modest, although this result may be affected by the lack of aeration and water circulation in the hydroponic system.

As for the *nifA* gene, its expression profile grossly matched *nifD*, with some exceptions: the *nifA* expression level in the shoot of plants grown under 2 mM KNO_3, which showed the highest FC, did not change over time in either strain. This consistency does not reflect the *nifD* modulation observed over time in the correspondent N conditions; similarly, in the root system, a consistently high *nifA* expression did not seem to correlate with a more modest transcription of *nifD*. These findings suggest a dynamic in which, in the presence of photoassimilate-rich environments, the NifA is constitutively expressed, and translational modification such as oxygen damage or direct interaction with other P_{II} proteins (such as GlnK or GlnB) are responsible for NifA activity modulation [128]. These two proteins appear as the best candidates for NifA regulation by N-terminal GAF domain binding [118], especially considering the lack of both the NtrB-NtrC regulatory proteins and of the anti-activator NifL in *G. diazotrophicus*. In general, however, the fold change of *nifA* had lower magnitude compared to *nifD* and *nifE*, which is in

line with the amplification cascade expected from a transcriptional activator compared to its target genes. NifA was reported to bind a "TGT-N10-ACA" motif located around 100 bp upstream of its target [128]. This motif was identified in *G. diazotrophicus* AZ0019 within the *nifHDK* promoter, 140 bp from the *nifH* TSS (Fig. 4.73); interestingly, it was also discovered in an intergenic region 104 bp upstream of the FeMo cofactor biosynthesis gene *nifB* and within the promoter of *nifA* itself, suggesting the existence of a positive autoregulation (PAR) mechanism. PAR occurs when a transcription factor enhances its own rate of transcription, and, although slower than other transcription activation strategies, it increases cell–cell variability and can lead to a bimodal distribution of the gene activation profile, resulting in bacterial populations that maintain a mixed phenotype to better respond to complex and variable environments [651]. This characteristic seems advantageous considering the multiplicity of colonisation strategies and plant compartments occupied by the bacterium and discussed in section 4.3.

In addition, the GG-N9-tGCa binding site motif of the σ^{54} factor [128] (also named RpoN and formerly known as NtrA or GlnF) was found in the promoter of *nifB*, *nifHDK* and *nifENXQ* (Fig. 4.73), confirming that this polymerase is responsible for the transcription of nitrogen-fixation genes in *G. diazotrophicus* as it is in other diazotrophs [652]. Once bound to the consensus motif, the core RNA-polymerase-σ^{54} complex needs the action of an activator, which usually recognise enhancer-like sequences located 80-150 bp upstream of the targeted promoter; in the genomic context of the *nif* regulon, NifA activates σ^{54} c-dependent transcription, acting as a bacterial enhancer binding protein [653], [654].

The observations from gene expression analyses suggest that, under C-replete conditions (i.e. in plants grown in the presence of nitrogen), NifA may be constitutively expressed, although with variable intensity within the same endophytic population due to a PAR dynamic; the existence of a mixed bacterial population expressing different *nifA* levels may speculatively also explain the high error of the FC resulting from the average of three biological replicates, observed in *nifA* as well as in *nifD* and *nifE*, as if this variability was transmitted from the regulator to its target genes (Fig. 4.74).

NrgA had a stable and high expression across the treatments, with increased expression in the root system of N-starved plants at 1 dpi and downregulation upon addition of ammonium, suggesting the modulation of this gene according to extracellular ammonium concentrations. This expression pattern in N-deplete vs NH_4 conditions was equivalent between the two strains. In the shoot, the N-deplete system induced the lowest *nrgA* transcription, in a pattern that grossly resembled the *nifD* expression profile. This general downregulation of nitrogen metabolism genes in the aerial parts of N-deprived plants may reveal a quiescent state of reduced metabolic activity to minimise energy expenditure in response to nutrient-poor conditions. The most evident *nrgA* upregulation in the shoot was observed in the mutant strain at 1 dpi in the NH_4-supplemented system, possibly disclosing an attempt to increase nitrogen uptake to compensate from the lack of BNF-derived ammonia.

In order to further elucidate this extremely complex picture, *G. diazotrophicus* was decoupled from the plant system and investigated in solid or semisolid medium through the use of the *nif* reporter strains described in sections 4.2.1b and 4.2.2c. Four strains were employed in a complementary way. The *Gd_nifHDK::GFP* strain, with a promoterless *gfp* cassette integrated downstream of the *nifHDK* operon, was predicted to allow the bacterium visualisation with minimal disturbance of the *nif* regulatory network; however, the presence of a single-copy GFP complicated the imaging due to modest fluorescence and prevented the identification of bacteria in non-fixing conditions. Therefore, *Gd_nifHDK::GFP* was transformed with the pICH47751_DsRed vector for constitutive tagging, giving origin to the *GdRed_nifHDK::GFP* strain. Alternatively, when *in vivo* visualisation was not strictly required, the *Gd_nifHDK::GUS* mutant was employed.

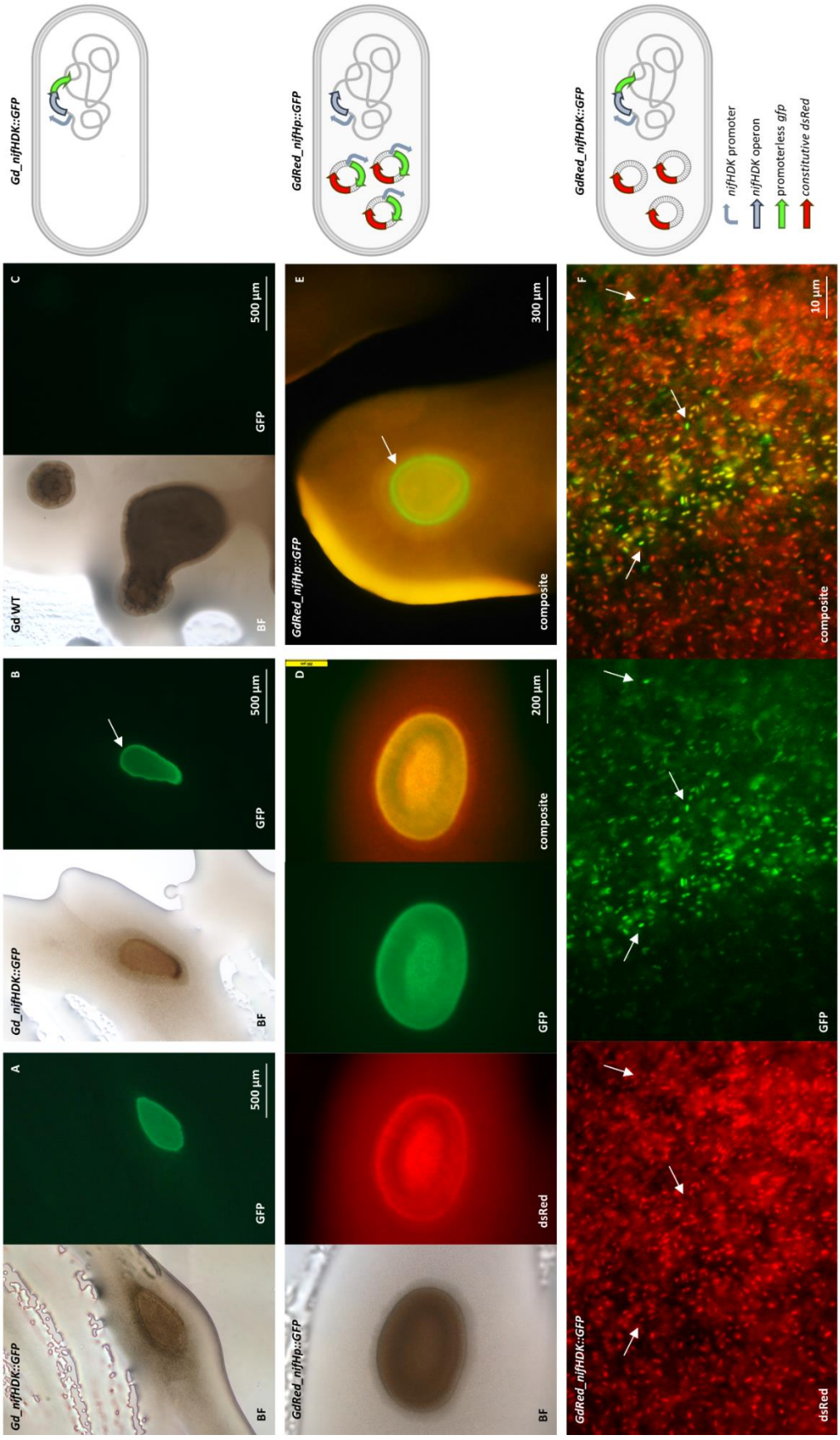


Fig. 4.75. nif-reporter strains in zero N ATGUS medium (i.e. yeast extract free) 48 hours after being restreaked from complete ATGUS medium. (A, B) Gd_nifHDK::GFP strain exhibiting nifHDK-driven fluorescence from the denser pre-colony. (C) Wild-type strain showing the

same morphology without GFP expression. (D, E) GdRed_nifHp::GFP strain, exhibiting a diffuse and weaker red signal from the constitutive dsRed in the mucoid matrix compared to the intensely fluorescent and GFP-expressing pre-colony. The white arrows indicate the pre-colony border showing a particularly high nifHDK-driven fluorescence. (F) GdRed_nifHDK::GFP strain from the interface between the pre-colony border and its outside, showing colocalization of GFP and dsRed signals in some cells (yellow), while some of the bacteria with the brightest GFP signal (white arrows) exhibited minimal dsRed fluorescence. In correspondence of each strain, a schematic representation of the relevant genotype is depicted.

In addition to *GdRed_nifHDK::GFP*, the *GdRed_nifHp::GFP* strain, carrying a promoterless *gfp* under the control of the *nifHDK* promoter in a constitutive plasmid, was used; the advantage of moving the reporter gene in a high copy plasmid is the amplification of the fluorescent GFP signal, but it must be taken into consideration that increasing the number of promoters of the investigated gene inside a cell could potentially affect the gene expression, for example by competing for the activator with the genomic promoter. Furthermore, the presence of a constitutive plasmid may represent an additional energetic burden with possible implications in the overall metabolic regulation. Considering these limitations, the different strains were used in parallel and compared among each other to reduce observation biases.

First, it was noted that all three GFP-tagged strain exhibited the fluorescent signal only when restreaked from a complete medium (such as ATGUS, DYGS or LIGP) to a N-free medium, such as ATGUS or DYGS devoid of yeast extract (Fig. 4.75). In this condition, bacteria formed rarefied colonies made of a transparent mucoid matrix amidst which, after around 48 hours of growth, arose smaller and denser bacterial aggregates with discrete boundaries and seemingly stochastic distribution (already observed in Fig. 4.39h). This phenotype was consistent in all the strain tested when streaked from a rich to a N-deplete medium, included the WT (Fig. 4,75b). Interestingly, in the *nif*-reporter strains, the detectable GFP signal derived exclusively from these internal subcolonies (Fig. 4.75a, b, d, e). In Fig. 4.75d the red signal from the constitutive DsRed protein highlights the lower bacterial concentration within the mucoid matrix compared to the densely populated internal nucleus. Inside this N-fixing region, the GFP signal was particularly intense in the ring corresponding to the nucleus border (Fig. 4.75b, e, white arrows).

It is known that the growth of a colony is determined by local concentration and diffusion rate of substrates or bacterial end-products; most notably, oxygen has a limited penetration through the colony volume, while glucose is rapidly consumed from the central and older colony compartment, with a consequent pH decrease [181]. Furthermore, it has been proven that even colonies of genetically identical cells undergo spatial function partitioning and naturally engage in cooperative crossfeeding in response to the local microenvironment [655], [656]. Previous research proposed that *G. diazotrophicus* uses the path length of the colony mucilage to reduce or modulate the O_2 diffusion as a strategy to solve the paradox of requiring high oxidative respiration rates to fuel a BNF which is sensitive to ROS [112]. Therefore, it is plausible that these discrete N-fixing aggregates benefit from O_2-limited niches for BNF preservation, or, alternatively, highlight an increased local nutrient availability.

To investigate this phenotype under different nitrogen conditions, the *GdRed_nifHp::GFP* strain was restreaked from either N-free or complete ATGUS into N-free ATGUS supplemented with diverse nitrate or ammonium sources (Fig. 4.76a). Interestingly, the absence of a nitrogen source prevented the growth of bacteria deriving from N-free medium. Conversely, upon the addition of just 0.1 mmol of ammonium, nitrogen-starved bacteria exhibited growth level and *nifHDK* expression phenotype comparable to those of bacteria transferred from complete to N-free ATGUS. This observation suggests the existence of a minimal threshold of bioavailable nitrogen which, in addition to a carbon source, is required for initiating BNF, and is in accordance with what reported by Flores-Encarnación et al., who noted lack of growth in zero N and thereby added 1 mM ammonium to prompt bacterial growth in bioreactors [111]. In solid medium, this threshold could apparently be met either through nitrogen carryover from previous rich media, or by the presence of ammonium in the growth medium. However, at higher ammonium levels (2 mM) the two distinct bacterial phenotypes (the dense nuclei and the sparsely populated transparent matrix), transitioned and converged into the homogeneous colony morphology normally observed in full ATGUS or DYGS, while the GFP signal diffused and eventually faded away (Fig. 4.76a). During this transition, the denser aggregates expanded across the matrix and

eventually represented the whole colony biomass, suggesting their function as nutrient-rich "pre-colonies" in which bacteria concentrate resources and perform spatially restricted and energetically demanding metabolic processes while wating for more favourable conditions. It is not clear whether the colony would actively concentrate nutrients in a confined area or if the pre-colonies arise on stochastically distributed nutrient-rich spots derived from uneven medium blending. Nevertheless, this finding confirms that: 1) in C-rich and N-limited environments, performing BNF still offer a selective advantage despite of its energetic requirement. In other words, *G. diazotrophicus* will activate BNF as soon as it encounters the minimal requirements of C and N needed to fuel such process, which will then be downregulated when higher extracellular ammonium concentrations are reached. Most likely, the minimal threshold of bioavailable nitrogen required for BNF activation reflects the fact that, in complete absence of a N source, the bacterium would enter a quiescent phenotype induced by starvation. 2) in solid medium, the task of nitrogen fixation task can be performed by a subcomponent of the colony, indicating a capability of function partitioning that may also be critical *in planta*.

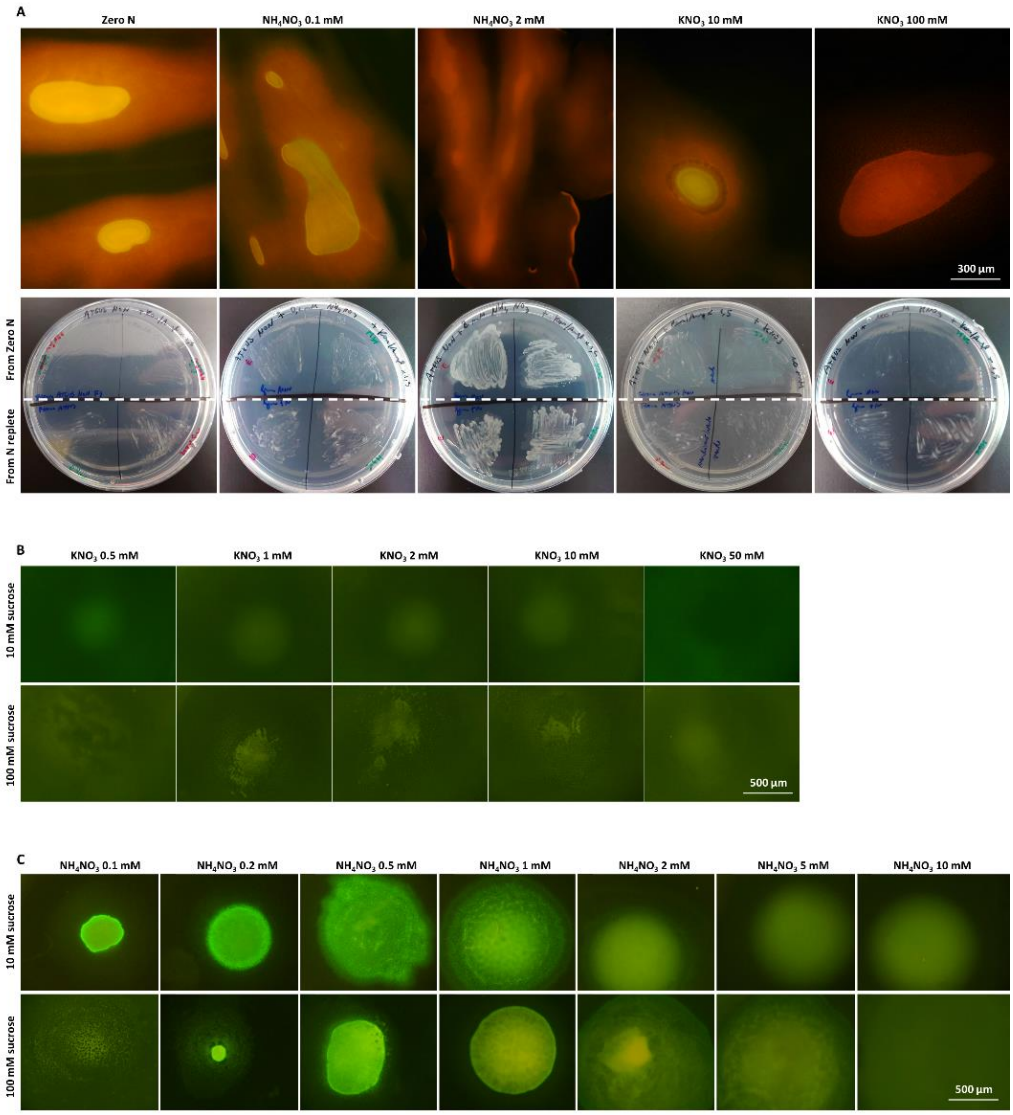


Fig. 4.76. nif-reporter strains in different N conditions after 48 hours of growth. (A) GdRed_nifHp::GFP restreaked from either complete ATGUS ("from N replete", bottom plate half) or from yeast extract-free ATGUS ("from zero N", top plate half). (B, C) Gd_nifHDK::GFP strain grown in complete ATGUS, washed in water to remove EPS carryover and inoculated in 96-well plates at the same concentration (10 µL of bacteria resuspended in water at OD_{600} = 0.1) in 150 µL of semisolid LGIP medium supplemented with different carbon and nitrogen sources. Each image is representative of a biological triplicate.

In this scenario, the intensely fluorescent ring of at the pre-colony edge may indicate fast-growing cells with higher metabolic rates and enough oxygen consumption to maximise BNF production, while the slightly dimmer pre-colony centre may indicate partial resources depletion leading to BNF deceleration. However, it must be remembered that this fluorescence profiles

reflect nitrogenase expression but not its activity or persistence in the medium. Moreover, this simplified setup does not take into account other N sources, such as amino acids, that would be present *in planta*. Nevertheless, it can offer a simplified model of nitrogenase activation *in vivo*. This relatively narrow window of bioavailable nitrogen in which BNF seems to occur, may reflect natural conditions found in plant tissues. The presence of free ammonium was estimated in different plant species to range between 1 and 25 mmol per kg of dry mass, suggesting that bacteria are surrounded by micromolar concentration of ammonium and non-limiting carbon sources [657]. However, it should be emphasised that ammonium concentration in plant tissues varies according to the N-source assimilated, and the ammonium-ammonia balance (with the latter being toxic for plants even at low levels) is modulated according to the local pH condition [658].

Restreaking the bacterium in 10 mM nitrate led to the same phenotype of zero-to-0.1 ammonium, i.e., scarce growth with *nifHDK*-expressing nuclei (Fig. 4.76a), as expected from a bacterium incapable of using nitrate as a N source and therefore virtually "blind" to its presence. Unexpectedly, however, under 100 mM KNO_3 condition, bacteria from N-replete media exhibited a higher growth rate compared to N-free, 0.1 mM NH_4^+ and 10 mM KNO_3 conditions, and the pre-colonies, although present, did not exhibited any green-fluorescent signal. This observation indicates a direct BNF inhibition by high nitrate levels and, possibly, the vestigial capacity to sense and respond to high doses of this nutrient. In fact, although *G. diazotrophicus* lacks a nitrate reductase [83], and is unaffected by up to 25 mM nitrate in solid medium [134], its growth and BNF rate *in planta* were found to be affected by nitrate over 60 mM [84], which is consistent with the low reisolation rates of this bacterium in highly fertilised soils [100], [84], [96]. Furthermore, the analyses of AZ0019 genome revealed the presence of an operon encoding for the putative nitrate transport protein NrtA (Gdia_0857), putative nitrate transport permease NrtB (Gdia_0858) and putative nitrate transport ATP-binding protein NrtC (Gdia_0859), with 70-to-75% amino acid identity with the NrtA protein of *Komagataeibacter sucrofermentans*, *Acetobacter aceti*, *Gluconobacter frateurii*, and *Gluconobacter japonicus*. More exhaustive bioinformatic

analyses and experimental validations such as *ntr* genes knock-out will be necessary to test the activity of this system.

When the bacteria were washed in water before inoculation in LGIP medium supplemented with different KNO_3 conditions, to remove any nitrogen residues embedded in the EPS matrix, no growth or BNF were observed regardless of the sucrose concentration (Fig. 4.76b), remarking the importance of a minimal N source to trigger self-sustaining ammonium production. In contrast, under growing concentrations of ammonium, the fluorescent pre-colony expanded and lost GFP signal at different rates in 10 vs 100 mM sucrose, with the latter causing a delay in the pre-colony maturation cycle. In both conditions, however, the reporter fluorescence became indistinguishable from the background levels at around 2 mM NH_4^+, likely due to BNF suppression but also to the mucoid colony phenotype and pH decrease of fast-growing cultures that were already reported to cause GFP quenching (see section 4.2.1c).

Considering the nifHDK expression profiles revealed by RT-qPCR data and by growth in solid medium, the *GdRed_nifHDK::GFP* strain was inoculated to *Arabidopsis* through seed vacuum-infiltration, and plants were grown in agarised nutrient solution in zero N vs 2 mM KNO_3 + 0.4 mM NH_4^+ (Fig. 4.77). Ammonium was included in the experiment as it induced the highest expression of *nif* genes in the tomato root system at 1 dpi (Fig. 4.74), although in the aboveground parts it elicited lower expression levels compared to the 2 mM KNO_3 condition. However, the diffusion of nutrients in agar medium is constrained compared to aqueous solutions, resulting in a significantly lower ammonium concentration sensed by the host-endophyte system in agarised NS in respect to the hydroponic setup.

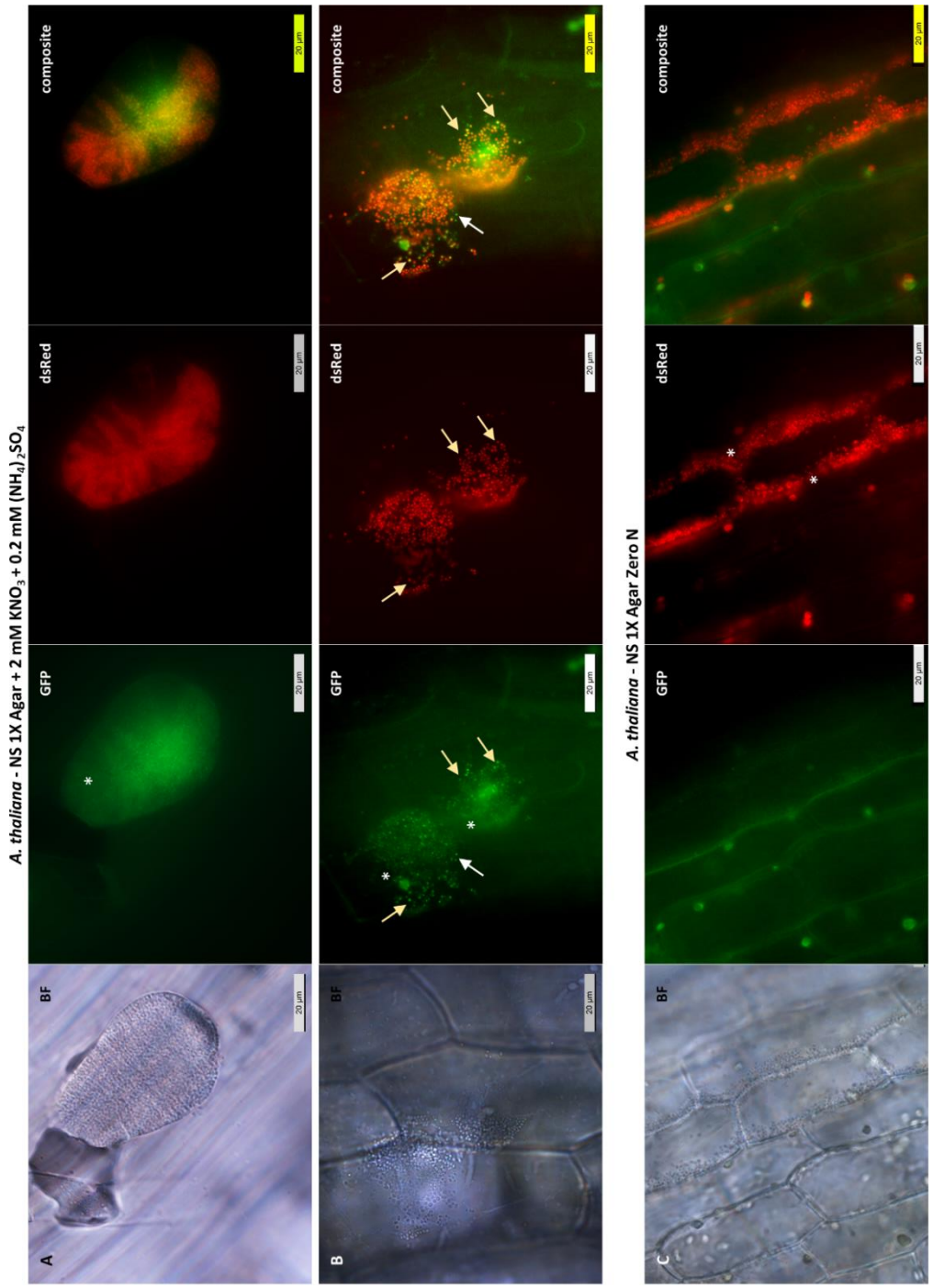


Fig. 4.77. GdRed_nifHDK::GFP strain grown in liquid ATGUS and inoculated onto A. thaliana seeds at OD_{600} = 0.1 for two hours through vacuum infiltration. Plants were grown in agarised 1x NS in either zero N (C) or 2 mM KNO_3 + 0.2 mM $(NH_4)_2SO_4$ (A, B). Samples were collected at 7 dps and analysed through fluorescence microscopy. Bacterial aggregates are labelled with white stars. Bacterial cells with high GFP fluorescence (resulting in a green signal when merged with the dsRed channel) are indicated by white arrows; bacterial cells with medium GFP fluorescence (resulting in a yellow signal when merged with the dsRed channel) are indicated by yellow arrows.

GFP-tagged bacteria colocalising with dsRed signal were found in the shoot of *Arabidopsis* supplemented with ammonium (Fig. 4.77a) and, amidst the root system, inside the spherical biofilm (Fig. 4.77b) previously described (Fig. 4.54b, c). However, such bacterial phenotype was discovered with low frequency, and no GFP signal could be detected from plants grown in the absence of a N source (Fig. 4.77c), nor in rice or tomato plants treated and grown in the same setup (not shown). This finding does not necessarily indicate lack of *nifHDK* transcription, but rather the technically challenging detection of the weak fluorescent signal on top of plant autofluorescence and dsRed fluorescence. The only GFP-expressing bacteria, in fact, were visualised in thin, semi-transparent *Arabidopsis* tissues, in which the dim background and favourable transmittance conditions allowed a sufficient green signal detection. To further complicate this picture, the microscopy analysis of the GFP-expressing border of pre-colonies grown on N-free ATGUS medium revealed that the bacterial cells exhibiting the highest GFP fluorescence had lost the red signal, possibly to mitigate the BNF energy burden (Fig. 4.75f, 4.77b, white arrows).

Therefore, the *Gd_nifHDK::GUS* was employed to facilitate the imaging process. The strain was tested in hydroponic setups, for both rice and tomato. The NS was kept at zero N or supplemented with 2 mM KNO_3 (Fig. 4.78); however, instead of investigating the ammonium variable, which proved elusive *in planta* and, ultimately, seemed to negatively affect the PGP phenotype (Fig. 4.14), the effect of an external carbon source was tested. This factor had never been evaluated so far due to the attempt of maintaining a closed system in which both organisms were mutually dependent, thus proving the capability of *G. diazotrophicus* to establish an active symbiosis upon inoculation in non-sugarcane, artificial setups. However, in soil, the rhizospheric bacteria would be in contact with abundant and diverse carbon sources, with potentially significant impact on the BNF capability. Therefore, 1 mM sucrose was added to N-replete NS to investigate the response in terms of *nifHDK* expression (Fig. 4.79, 4.80).

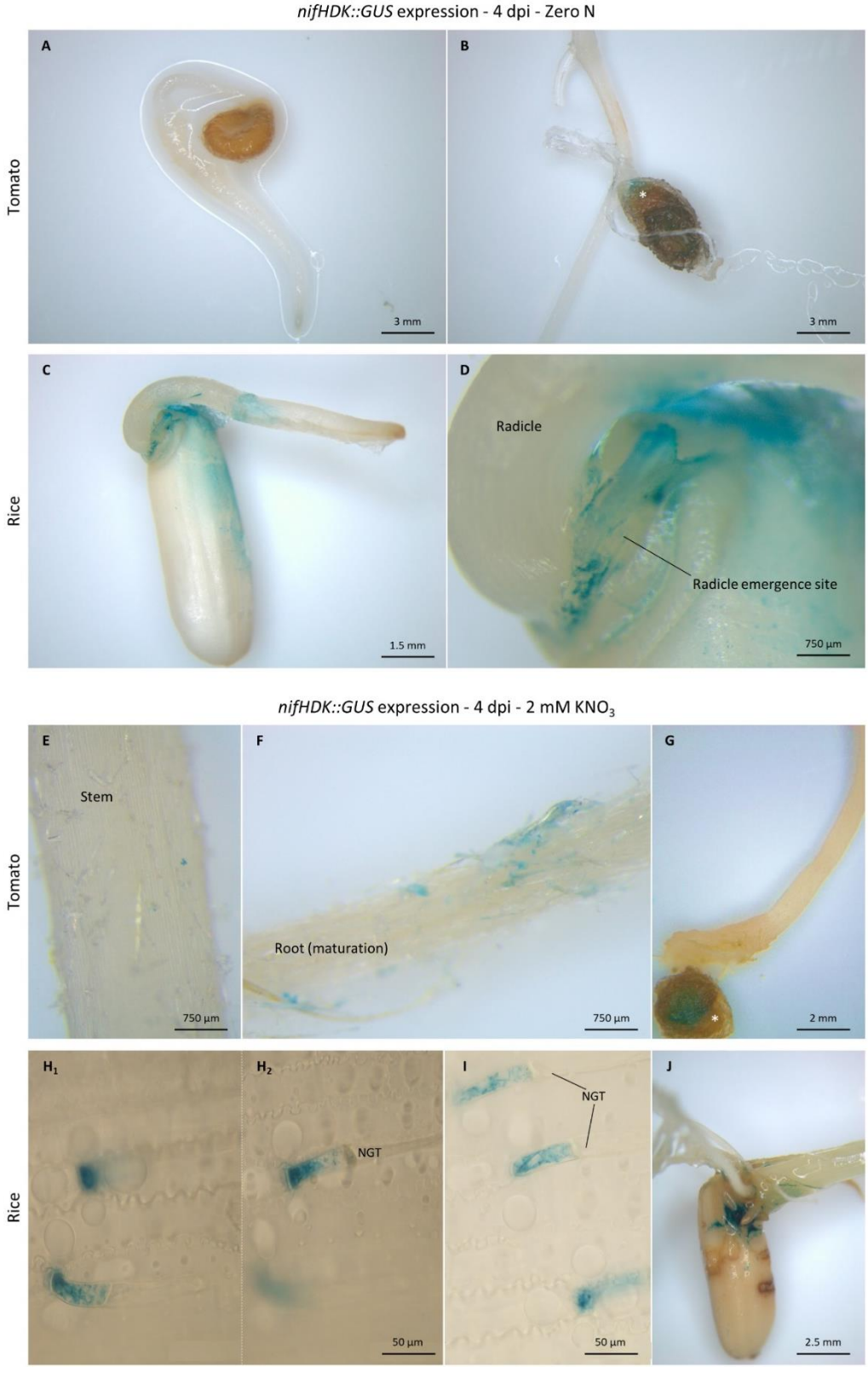


Fig. 4.78. Gd_nifHDK::GUS colonisation of tomato and rice hydroponically grown in zero N (A-D) or 2 mM KNO3 (E-J) conditions, 4 dpi. (A-B) Tomato plants showing minimal staining on the seed nearby radicle emergence site (white star). (C, D) Rice seedlings revealing nifHDK expression on the starch-rich seed surface and radicle emergence site. (E-G) nifHDK-driven GUS activity in tomato stem trichomes (E), root and root hairs (F) and seed (G). (H_1-

H_2) different z-planes of a colonised rice trichome, showing the entrance of bacteria through the vasculature at the base of the first trichome stalk cell. (I-J) nifHDK-driven GUS activity in elongated Gd_nifHDK::GUS cells occupying the basal trichome cell of rice (I) and showing localised BNF on the seed surface around the radicle emergence site (J). NGT = Non-glandular trichome.

Fig. 4.78 displays tomato and rice plantlets stained in X-Gluc solution after 4 days of growth in inoculated hydroponic systems. No blue staining was ever observed in untreated controls. In N-free condition, tomato plantlets did not show any sign of *nifHDK* expression except for a restricted area in the seed around the radicle emergence site (Fig. 4.78b). Rice seedlings, on the other hand, exhibited BNF-driven GUS activity on the seed surface, radicle (Fig. 4.78c) and, principally, radicle emergence site (Fig. 4.78d) confirming both the importance of a carbon-rich substrates for nitrogen fixation, and reinforcing the radicle emergence site as a favoured rout for systemic endophytic colonisation.

In the presence of 2 mM KNO3, GUS activity was also detected in tomato, mainly on trichomes (Fig. 4.78e), root hairs (Fig. 4.78f) and seed (Fig. 4.78g). Similarly, rice exhibited *nifHDK*-driven GUS expression from colonised trichomes on the leaf sheath (Fig. 4.78h-i) and seed surface/adventitious roots (Fig. 4.78j).

However, the most significant BNF activation was observed in plants grown in the presence of exogenous sucrose (Fig. 4.79, 4.80). It was not determined whether this enhanced GUS activity was the direct result of enhanced nitrogenase expression, or if it reflected an increase on the bacterial population, (most likely both). Nevertheless, the stained bacteria matched exactly the colonisation dynamic described in section 4.3, including endophytic and epiphytic invasion of trichomes, stomata, guard cells and subsidiary cells, root hairs and epidermal root cells. Rice samples exhibited a particularly intense *nifHDK*-driven coloration (Fig. 4.80), especially around radicle and coleoptile emergence sites. The blue staining derived mostly from elongated *Gd_nifHDK::GUS* cells (Fig. 4.79b-d, Fig. 4.80a, d, j-l), but, to a lesser extent, also some of the coccoidal cells exhibited blue coloration (Fig. 4.7k-l, Fig. 4.80c, d, i, k).

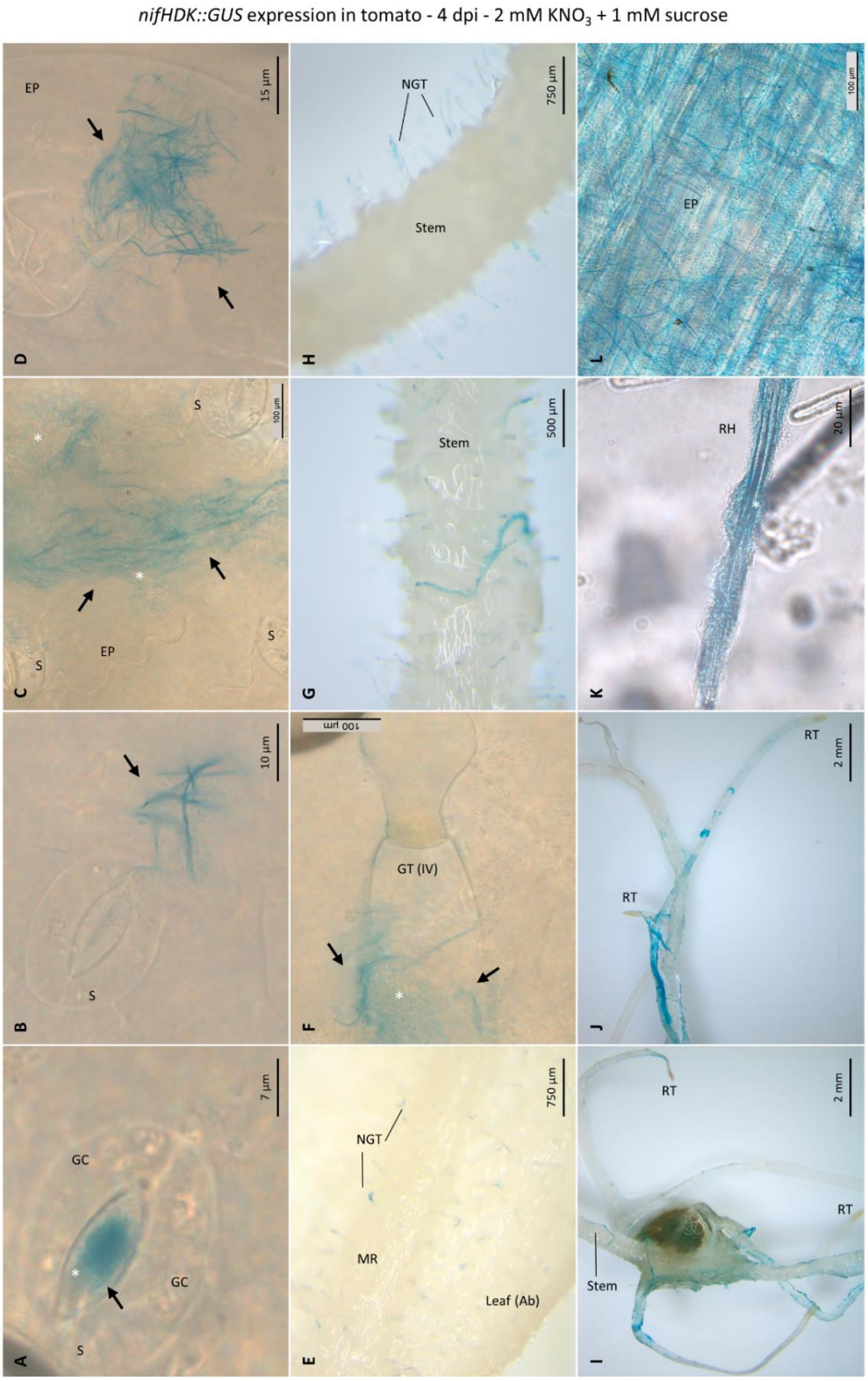


Fig. 4.79. Gd_nifHDK::GUS colonisation of tomato hydroponically grown in 2 mM KNO_3 + 1 mM sucrose, 4 dpi. (A-D) Elongated bacterial cells (black arrows) entering stomata and epiphytically colonising their surroundings. (E-H) nifHDK-driven GUS activity in bacteria colonising trichomes in leaves (E, F) and stem (G, H). (I-K) BNF in the root system, mainly among root hairs (K) and root epidermal cells, which were colonised by a mixed population of elongated and coccoidal cell (L, white stars). Note the lack of blue staining in the root tips. EP = epidermis; GC = guard cells; GT = glandular trichome; MR = midrib; RH = root hair; RT = root tip; S = stoma.

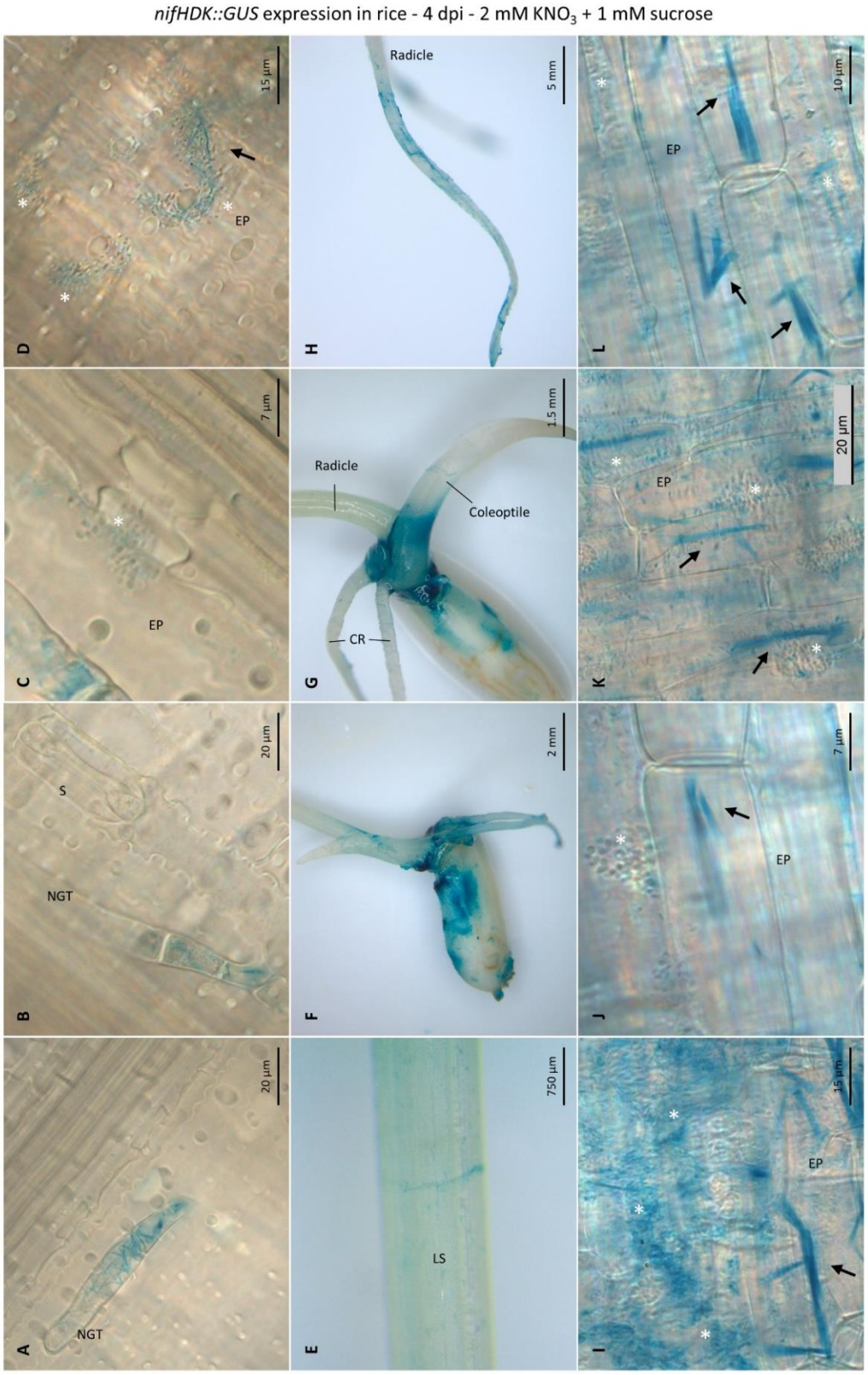


Fig. 4.80. Gd_nifHDK::GUS colonisation of rice hydroponically grown in 2 mM KNO_3 + 1 mM sucrose, 4 dpi. (A-D) Elongated (black arrow) and coccoidal (white stars) bacterial cells endophytically colonising trichomes (A, B), guard cells (B), stomata (C, black arrow) and epiphytically colonising their surroundings (D), mainly in the primary leaf sheath (E). (F-H) nifHDK-driven GUS activity on the seed surface, coleoptile and radicle (H), with particularly intense staining around the emergence site of these organs. (I-K) BNF in the root system epidermis, which was colonised by a mixed population of elongated and coccoidal cell (black

arrow) with distinct ratios in different root zones. EP = epidermis; CR = crown roots; NGT = non-glandular trichome; LS = leaf sheath; S = stoma.

Overall, the addition of an exogenous carbon source significantly boosted the nitrogenase expression *in planta*, as detected through the *nif* reporter systems, highlighting this element as the main BNF regulator over nitrogen. The high number of bacterial cells expressing the *nifHDK* transcript may also be the result of increased colonisation due to the carbon source. This finding is consistent with early studies reporting a significant increase in nitrogenase activity when *G. diazotrophicus* was cultured in sugar-rich media (10% sucrose) [232]. Similar conclusions were drawn upon the investigation of *H. seropedicae* in gramineous plants; the authors noted that the weak, although consistent, expression of *nifHDKENX* transcript, as visualised through a similar GUS reporter system, depended on the lack of a carbon source in the *in vitro* system, and that several studies have demonstrated that *in vivo* BNF is only achievable upon the addition of an external carbon source [233].

Under C-replete conditions, which might not have been met in the hydroponic setups without sugar amendments, *G. diazotrophicus* consistently expressed the nitrogenase genes in virtually all the plant niches and organs that were previously identified as colonisation targets. This finding supports the notion that in natural settings, biological nitrogen fixation may occur constitutively; however, such a hypothesis would require experimental validation through RT-qPCR and microscopy analyses in different soils.

4.4.3 IAA production and PGP metabolism overview

During the early studies on *G. diazotrophicus*, several researchers independently reached the conclusion that nitrogen nutrition was not the main benefit provided by the bacterium to its host, but rather that it was just a component of a wider PGP effect that, most notably, included indoleacetic acid production [233] [100]. Indole-3-acetic acid (IAA), as the predominant form of

auxin, not only holds a central position in plant physiology, but is instrumental in shaping plant-bacterial interaction [659], to the point that the acronym IAA has been referred to as molecule that "Influences Almost Anything" [660]. Following the characterisation of IAA production by *G. diazotrophicus* in culture media [100] [101], the gene involved in its biosynthesis were identified by Rodrigues et al. in an operon comprising the genes *lao* (GDI2456), *cccA* (GDI2455) and *ridA* (GDI2454), encoding, respectively, a L-amino-acid oxidase, a putative alcohol dehydrogenase cytochrome c subunit and a reactive intermediate deaminase A [661]. The authors found IAA production and the relative operon transcription to be dependent on the addition of L-tryptophan in the medium, in accordance with previous studies which indicated this amino acid as the IAA precursor via IPyA biosynthetic pathway.

As a marker of IAA production *in planta*, *cccA* transcription was monitored through RT-qPCR analyses. The results are presented in Fig. 4.81 in comparison with *nifHDK* expression. IAA and nitrogen metabolism are connected by the tryptophan biosynthesis: under ammonium-replete concentrations, this cation is incorporated in glutamine [610] which, in turn, serves as precursor for tryptophan synthesis via chorismic acid pathway [662]. Furthermore, tryptophan is a non-limiting organic molecule in the rhizosphere; in *Avena barbata*, this amino acid was found to be the most abundant exudate from the root maturation zone, where it played a key role in microbial interactions [663], suggesting that endophytic bacteria could exploit this molecule as a precursor of growth regulators [523].

In the model system of hydroponically grown tomatoes, there was not obvious correlation between *cccA* and *nifD* expression profiles (Fig. 4.81a). CccA was primarily upregulated in the root, in accordance with its implication in root architecture modulation. Such increase was more obvious at 1 dpi and in the WT strain, while the *nifD*$^{-}$ mutant seemed unable to drive the same *cccA* transcription rates. While this finding may suggest that BNF favours higher IAA production levels, no concomitant nitrogenase upregulation was observed during the peak of *cccA* transcription, thus implying a more complex regulatory mechanism. Interestingly, in the aerial parts at 20 dpi, while the WT strain exhibited the highest *nifHDK* operon expression, it concomitantly

showed low *cccA* transcription; in contrast, the BNF-impaired mutant, under the same condition, exhibited the highest *cccA* transcription level. This counterintuitive result may indicate that, due to the lack of an active BNF machinery, the *nifD*$^{-}$ mutant colonising the N and C-rich environment of plant shoots may be able to redirect part of its energetic capabilities in the production of IAA, possibly in response to a different metabolomic plant profile that the mutant itself elicited in the plant. The WT strain, on the other hand, seemed to invest on BNF, whose activity may confer a long-term advantage in unstable environments.

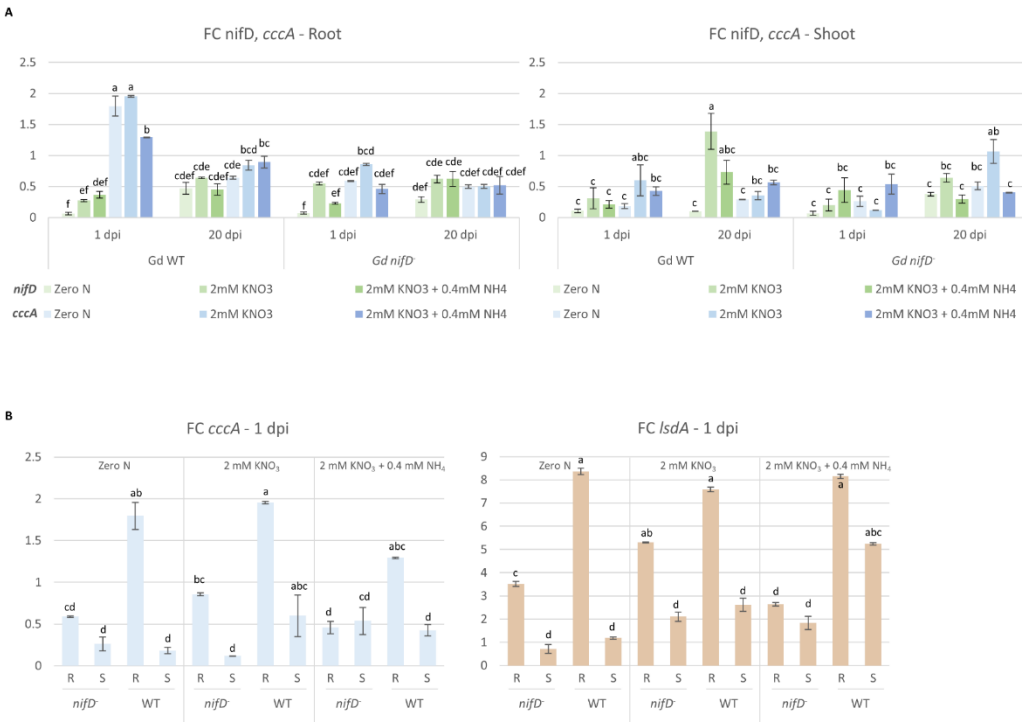


Fig. 4.81. (A) nifD and cccA expression from tomato plants grown under different N conditions. (B) cccA expression compared to the lsdA transcript. The FC are normalised on the constitutive bacterial gene rho. The standard error of the mean between the three biological replicates is shown in the error bars. One-Way ANOVA analyses for statistical differences between the different conditions were conducted using Tukey's Honestly Significant Difference (HSD) test in R.

Unexpectedly, among the investigated genes, *lsdA* was the only one to show a very similar expression profile compared to the *cccA* gene at 1 dpi, with the higher expression being in the root system regardless of the N condition (Fig. 4.81b).

This finding may be explained by the biological function of auxin in bacteria. IAA production, which is common to many PGPB, confers bacterial survival benefits against various stresses, including acidity, osmotic shock, UV irradiation, and heat shock; furthermore, this molecule can act as a signal to increase antibiotic production, inhibiting competing microbes, and mediates quorum sensing, chemotaxis and motility in plant tissues [659]. Crucially, IAA have also been reported to enhance EPS production. Imperlini et al. reported increased biofilm, EPS, and lipopolysaccharide production in a IAA-overexpressing strain of *Sinorhizobium meliloti*, leading to better adherence to root surfaces and protection against desiccation and antibacterial compounds [664]; the same effect was observed upon the addition of exogenous IAA [665]. Similarly, pre-treating *Bradyrhizobium japonicum* with IAA increased EPS and biofilm production as well as the ability of the bacterium to tolerate oxidative damage and various abiotic stressors [666]. Even in the field of *G. diazotrophicus* research, when investigating its application to rice, Rolfe et al. reported that the exogenous addition of the synthetic auxin 2,4-dichlorophenoxyacetic acid in the system led to an increased root-bacteria association, with stronger PGP in the long term compared to auxin uninoculated controls [247].

Overall, the ability of IAA to enhance EPS production, biofilm formation, and oxidative stress protection contributes to bacterial survival and adaptation in plant environments, which, in the context of the presented RT-qPCR data, may suggest that the *nifD*$^{-}$ mutant strain upregulates IAA production to compensate for the putative advantage conferred by an active BNF.

However, RT-qPCR data, that reflect complex interactions largely dependent on the environmental context and account for gene expression rather than enzymatic activities, did not ultimately answer the question of whether there is a direct link between IAA production and BNF *G. diazotrophicus*. To explore this possible connection, the plant-bacterial system was once again decoupled, and the IAA production was investigated in bacteria cultured in liquid media under different nutrient conditions (Fig. 4.82). IAA production was directly measured through the Salkowski assay. This colorimetric method allows the detection of indole-3-acetic acid upon its reaction with a mixture of FeCl3 and

perchloric acid (Salkowski reagent), which under acidic conditions induce the formation of a red or pink-coloured compound that can be quantified spectrophotometrically. Although this assay was found to be imprecise in determining the absolute values of detected IAA, it remains a valid method for assessing the relative ratio of IAA production under different conditions [667].

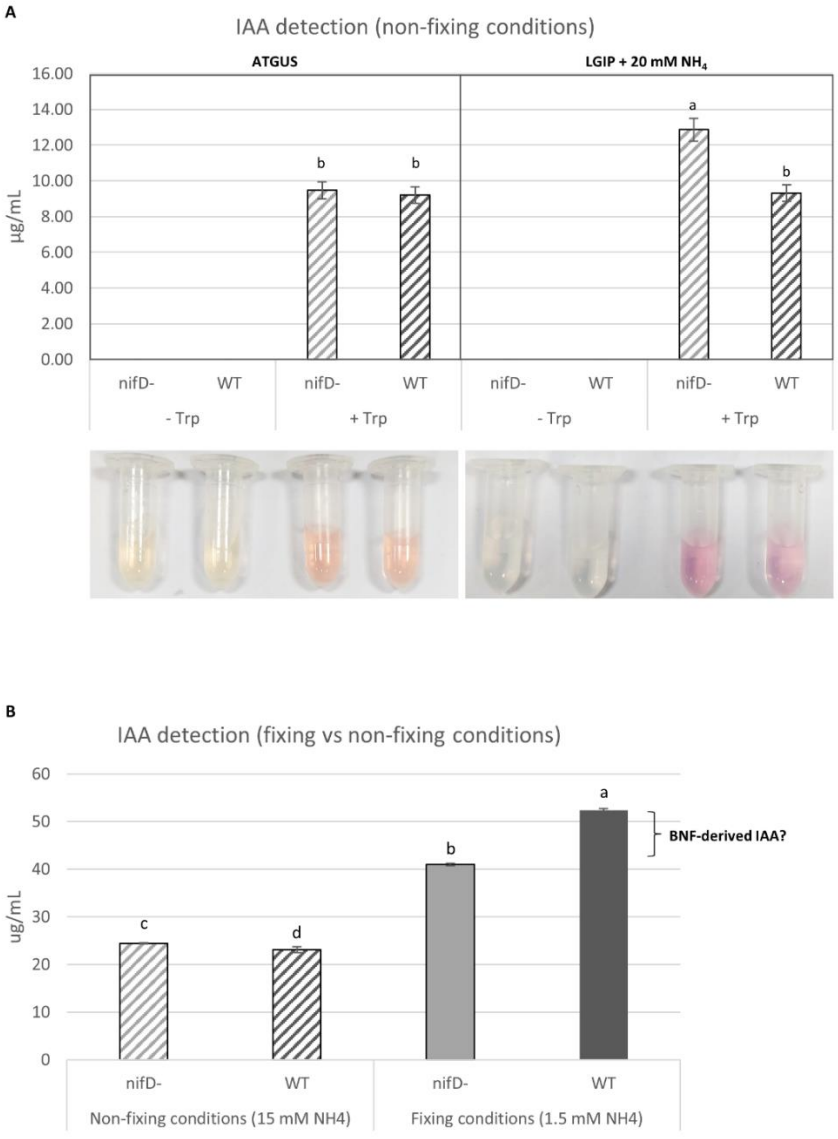
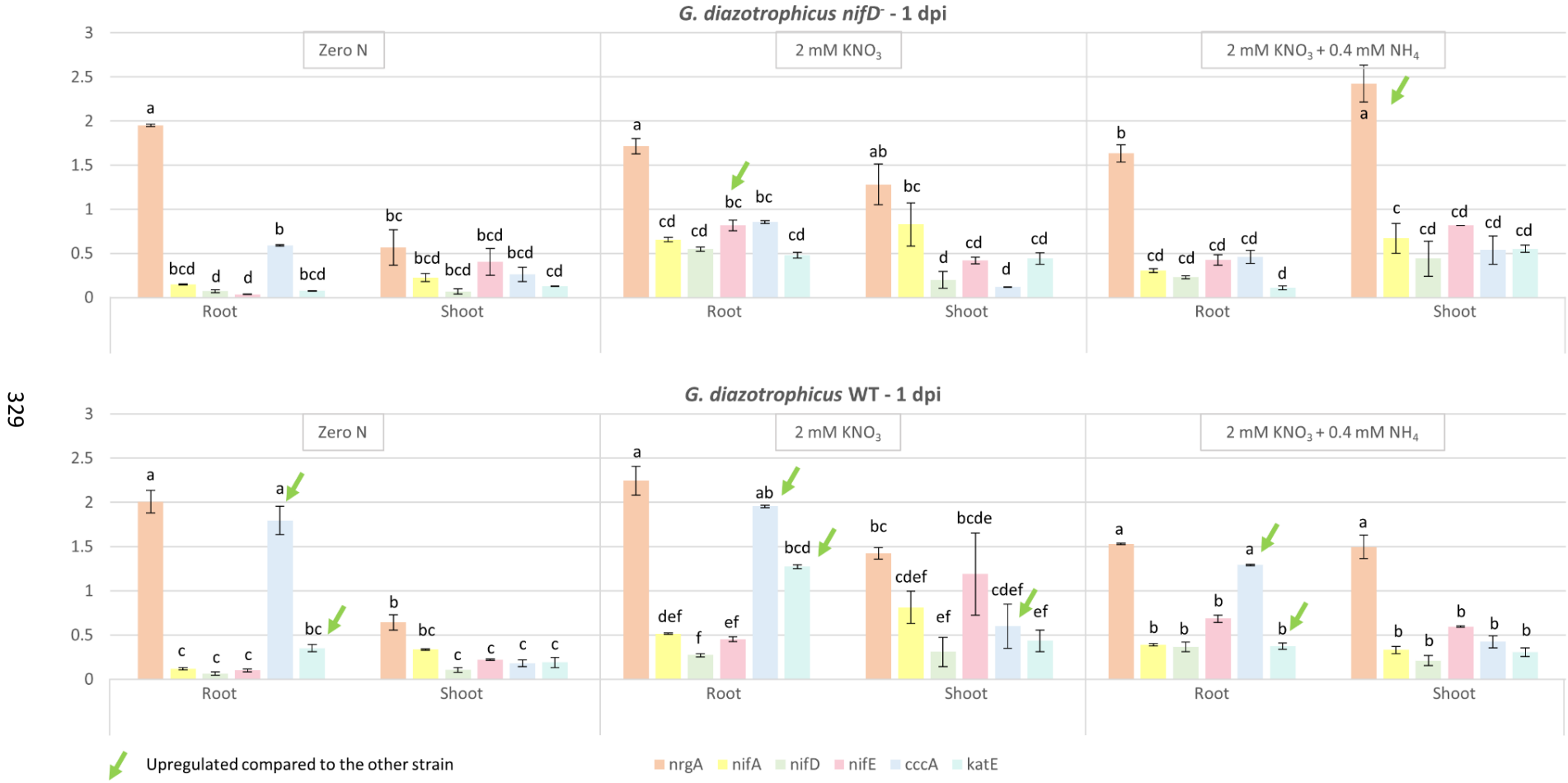


Fig. 4.82. IAA production detection through Salkowski assay in WT vs nifD$^-$ mutant strains. (A) IAA detection in ATGUS vs LGIP medium supplemented with sucrose 292 mM and NH_4Cl 20 mM. IAA production was only obtained upon the addition of 100 µg mL^{-1} tryptophan. (B) IAA detection in fixing (1.5 mM NH_4Cl) vs non-fixing (15 mM NH_4Cl) conditions. These ammonium concentrations were chosen in accordance with previous papers [100] *and based on the nifHDK activation pattern described in Fig. 4.76, showing expression up to 2 mM NH_4. The bacterial cultures were grown in gentle agitation at 28 °C until exponential phase. Experiments were carried out in triplicate and samples were brought to the same OD before measurement. The standard deviation and statistical significance according to Tukey's Honestly Significant Difference (HSD) test are shown.*

When cultured in complete ATGUS or LGIP medium amended with 20 mM NH_4Cl, i.e., in non-fixing conditions, both strains produced similar levels of IAA, although the *nifD*$^-$ mutant showed an increased IAA concentration in LGIP medium (Fig. 4.82a), which is a mineral medium depleted of yeast extract and supplemented with 10% sucrose as the sole source of carbon. This medium was selected to further simplify the system by removing any organic molecule apart from sucrose as a C source and ammonium as a N source. Moreover, the presence of 0.008 mM molybdate and of 292 mM sucrose, which is the sugar concentration eliciting the strongest nitrogenase activity [232] and highest IAA production [101], makes this setup ideal for highlighting any BNF contribution.

Next, bacteria were grown in the same LGIP medium under different N concentration, corresponding to 15 mM NH_4^+ (BNF-off state) [83] and 1.5 mM NH_4^+ (BNF-on state) [206]. The spectrophotometric quantification revealed that, under non-fixing condition, both strains produced similar IAA levels, although the BNF-impaired mutant demonstrated a statistically significant increase in IAA compared to the WT. Interestingly, under fixing-conditions, both strains exhibited an upregulation of IAA production, indicating the existence of a connection in the regulation of these two mechanisms. Furthermore, the WT strain produced significantly more IAA than the mutant, leading to the conclusion that such difference may be caused by the direct utilisation of BNF-derived ammonium for hormonal production, possibly via glutamine increase and enhanced tryptophan production.

Based on these findings, the overall transcriptome analyses of G. diazotrophicus are summarised in Fig. 4.83. The treatments are presented separately to better compare the gene expression differences relative to the nitrogen condition, time point, and bacterial strain investigated.


G. diazotrophicus nifD- - 1 dpi
Zero N
2 mM KNO3
2 mM KNO3 + 0.4 mM NH4
Root
Shoot
G. diazotrophicus WT - 1 dpi
Upregulated compared to the other strain
nrgA
nifA
nifD
nifE
cccA
katE

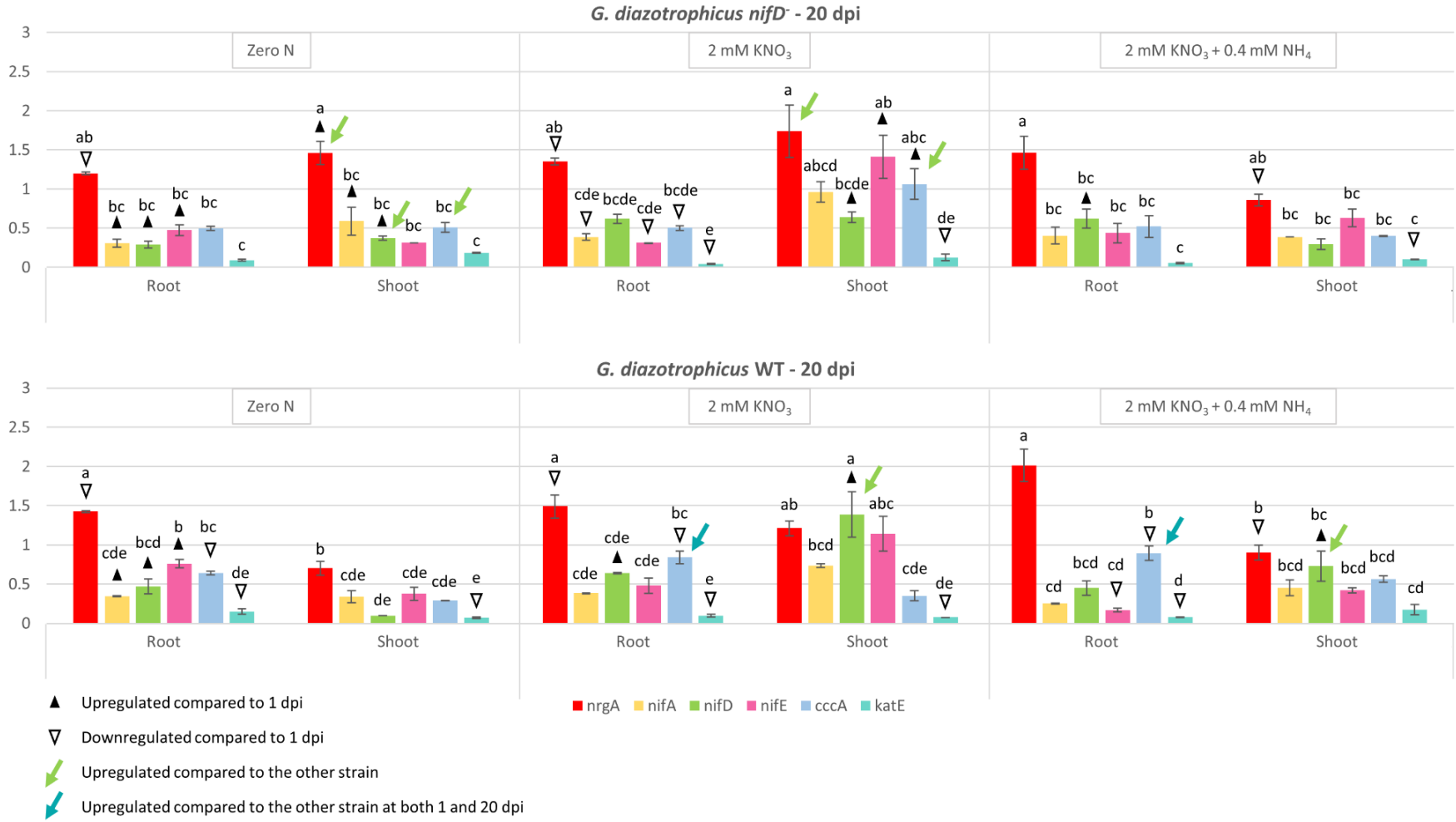

G. diazotrophicus nifD- - 20 dpi
Zero N
2 mM KNO3
2 mM KNO3 + 0.4 mM NH4
Root
Shoot
G. diazotrophicus WT - 20 dpi
nrgA nifA nifD nifE cccA katE
Upregulated compared to 1 dpi
Downregulated compared to 1 dpi
Upregulated compared to the other strain
Upregulated compared to the other strain at both 1 and 20 dpi

Fig. 4.83. Gene expression from tomato plants grown under different N conditions. Genes involved in nitrogen metabolism, oxidative damage protection and hormonal production are grouped together to highlight individual FC variation in the comprehensive outlook. The FC are normalised on the constitutive bacterial gene rho. The standard error of the mean between the three biological replicates is shown in the error bars. One-Way ANOVA analyses for statistical differences between the different genes were conducted using Tukey's Honestly Significant Difference (HSD) test in R.

Overall, the expression levels and profiles were remarkably consistent among the two strains, indicating that the highly complex environmental context of plant tissues was more impactful in shaping the bacterial physiology than the strain genetic backgrounds; in other words, in spite of lacking a functional BNF machinery, the mutant responded similarly to the WT to the environment. However, some notable differences were observed. At 1 dpi, the WT strain upregulated hormonal and ROS-scavenging genes in the root system, indicating a turbulent interaction: the bacterium responded to the plant oxidative burst not only by increasing peroxidase gene expression, but also by upregulating levansucrase and IAA production, which, as discussed above, enhance environmental adaptation, ROS resistance and biofilm formation on plant tissues. Additionally, IAA production may indicate the attempt of forcing root entry by exploiting the cell wall loosening activity of this hormone [668]. The BNF-impaired strain, in contrast, did not boost the same physiological traits: instead, an upregulation in ammonium channel genes was observed, possibly to compensate a lower intracellular concentration of bioavailable nitrogen. There was no apparent correlation between the upregulation of *katE* and *nifHDK* transcripts, revealing a less obvious dynamic *in planta* compared to culture media, in which the catalase was shown to protect the nitrogenase against oxidative damage [110]. At 20 dpi, while still upregulating ammonium channels, the *nifD*$^{-}$ strains exhibited the most relevant difference from the WT, i.e., the upregulation of IAA synthesis gene. In the correspondent inoculation, the WT strain upregulated the nitrogenase genes whilst reducing hormonal production. Although unexpected, this behaviour mimicked what observed in culture medium under non-fixing conditions, where the mutant produced more IAA (Fig. 4.82). Culture media and plant tissues share very few similarities. The "N-replete" condition used in LGIP medium (15 mM NH_4^+) corresponds to BNF suppression in culture media; plant shoot, on the other hand, also

contain non-limiting C and N sources to sustain the growth of the relatively low *G. diazotrophicus* population in aboveground parts (between 10.000 and 1,000,000 cells per fresh plant gram, Fig. 4.15), but, being at much lower concentrations, would likely still allow for BNF activation. Nevertheless, the fact that the mutant strain exhibited increased IAA production both in non-fixing solid medium and in plant aerial tissues, may reflect two scenarios: 1) this molecule may be produced to mitigate some nutritional stress in the BNF-impaired bacterium; 2) in C and N-replete environments like plant shoots, the lack of the energetic burden from BNF may induce the bacterium to devolve part of the assimilated resources to hormonal production, possibly to facilitate endophytic colonisation. This could explain the beneficial effect provided by the *nifD*$^{-}$ strain in hydroponic systems (see section 4.1.1b). In other words, under N-replete condition and even in non-fixing environments, the mutant strain may have a larger energy reserve saved on untranslated and generally downregulated *nif* genes, which would fuel other metabolic pathways such as IAA synthesis. In support of this theory, in N-limited environments such as the roots of tomato grown under zero N at 1 dpi, the mutant strain exhibited a much lower *cccA* transcription compared to the WT, and maintained a consistently low expression up to 20 dpi. As for the WT strain, it appeared to balance BNF and hormonal production over time across different plant compartments: at early colonisation stages, *cccA* was upregulated in the root system and progressively decreased, while *nif* genes were progressively upregulated in the roots and, primarily, in the shoot. In simpler terms, the energy investment of the bacterium shifted from early hormonal stimulation performed mainly in the root system, to later nitrogen fixation in the aboveground organs. Unexpectedly and in contrast with previous literature, a recent study reported that rice root architecture modification and development observed upon inoculation with by *G. diazotrophicus* was not mediated by IAA synthesis, suggesting this hormone to be potentially more impactful as a signalling or colonisation-promoting molecule [669].

This simplified view, however, was complicated by the role of carbon availability, which was only marginally investigated in the present work. The addition of 1 mM sucrose in the NS of hydroponic setups greatly enhanced the

expression of the GUS reporter system in comparison to bacteria colonising plants grown in zero N or 2 mM KNO_3 conditions. When grown in sucrose rich medium (292 mM) and under limiting ammonium concentration compatible with BNF, both strains increased IAA production, but this increase was significantly higher in the WT, suggesting the potential for directing employing BNF-derived ammonium in hormonal biosynthesis. However, this condition may have never been met in hydroponically grown tomato, with the possible exception of micro-niches such as the metabolite-rich trichomes; in fact, in the absence of an external carbon source, only the starch-rich surface of rice seeds was observed to sustain substantial *nifHDK* expression (Fig. 4.78). Similarly, studies conducted on *Herbaspirillum seropedicae* revealed negligible BNF in rice except when exogenous carbon (5 mM sodium malate) was added [254]. The same conclusion was reported in *Serratia marcescens* on rice [241], *Azospirillum brasilense* on wheat [670] and *Klebsiella pneumoniae* on maize [671].

Such high demand for carbon by these non-nodulating diazotrophs may explain the natural association between *G. diazotrophicus* and sugarcane and the BNF rates observed in that species [216], although even in sugarcane some reports observed only minimal expression of nitrogenase [221]. These data suggest that a carbon-rich formulation strategy may encourage nitrogen fixation in crops inoculated with this bacterium. Furthermore, it is acknowledged that different fertilisation inputs affect the exudate composition in plants; for example, ammonium nutrition significantly enhanced sugar exudation compared to nitrate fertilisation in kallar grass [672]. This suggests that additional modulation of BNF can potentially be achieved by carefully considering the plant growth parameters in relationship to their influence on bacterial growth.

4.4.4 PGP engineering

As previously discussed, the lack of the NtrB-NtrC two-component system in *G. diazotrophicus* suggests that most of the nitrogen-sensing and BNF regulation relies on the master regulator NifA and its interactors GlnK1, Glnk2 and GlnB

[118] [124]. In *Azotobacter vinelandii*, the inactivation of the NifA anti-activator *nifL* (not present in *G. diazotrophicus*), drives constitutive nitrogenase activity, although the consequent excess NH_3 production triggers a feedback mechanism which reduce ammonium assimilation by glutamine synthetase activity [673].

In the present study, to test whether in *G. diazotrophicus* the nitrogenase regulation could be overdriven by the simple overexpression (OE) of its positive regulator, NifA was cloned from the genome of AZ0019 and inserted into the pICH47751_DsRed plasmid in place of the *dsRed-Express2* protein, under the strong constitutive P_c promoter. The plasmid was then transformed in the *Gd_nifHDK::GUS* mutant, giving origin to the *GdnifAoe_nifHDK::GUS* reporter strain.

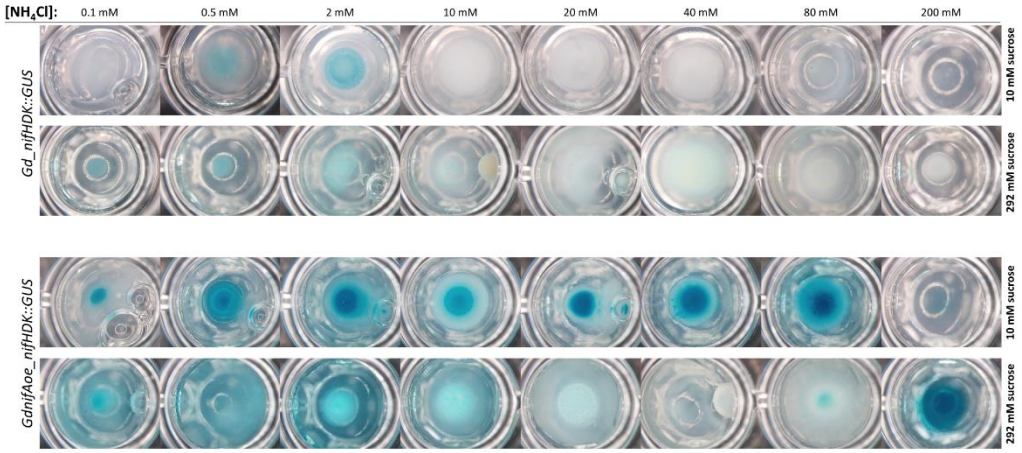


Fig. 4.84. Growth comparison of *Gd_nifHDK::GUS and GdnifAoe_nifHDK::GUS in LGIP semisolid medium supplemented with sucrose 10 mM or 292 mM (10%) under increasing levels of NH_4Cl. The X-Gluc reagent was incorporated in the medium at the concentration of 130 ug/mL. The images were taken after 5 days of growth and are representative of the overall progression of the reporter activation.*

The OE strain was tested in LGIP semisolid medium under different ammonium and sucrose conditions and compared to *Gd_nifHDK::GUS*, which retains a wild-type BNF regulation (Fig. 4.84). The *Gd_nifHDK::GUS* strain exhibited a similar nitrogenase activation profile to what was observed with the *Gd_nifHDK::GFP* reporter system (Fig. 4.76), in which BNF is activated between the interval of 0.1 to 2 mM ammonium. The X-Gluc staining circumvented the issue with GFP

quenching in the mucoid medium, and revealed traces of nitrogenase activity up to 40 mM ammonium under 292 mM sucrose condition. In contrast, at the lower sugar concentration, the *nifHDK* transcription was abolished at 2 mM ammonium, highlighting again the centrality of carbon in BNF regulation. Remarkably, the OE strain was able to perform BNF up to ammonium 80 mM under sucrose 10 mM and even under 200 mM ammonium in the presence of 10% sucrose. This noteworthy result also indicates that, as in other bacterial species [117], *G. diazotrophicus* is resistant to high ammonium levels; however, it was previously reported that in the presence of 10% sucrose, ammonium assimilation by the bacterium is reduced by 65% compared with growth in 1% sucrose [674], suggesting that a reduced ammonium uptake in high sugars may explain the lack of toxicity. Unexpectedly, under 10% sucrose some of the central ammonium values (20 to 80 mM) caused a reduction of the reporter activation, which then recovered in ammonium 200 mM. This puzzling dynamic may reflect an imbalance in the oxidative metabolism due to BNF regulation disruption, although it is not clear why such mechanism reverted at even higher ammonium concentrations. Overall, the lower C condition seemed to elicit a more balanced equilibrium between growth in semisolid medium and BNF activation in response to NifA deregulation, underlining the intimate connection between carbon and nitrogen metabolism.

The constitutive expression of the nitrogenase in the OE strain was also observed upon growth in solid DYGS medium (Fig. 4.85a), demonstrating the efficacy of this system even in the context of a protein and amino acid rich substrate with diverse N and C sources. Finally, the strain was preliminary tested on *Arabidopsis* plantlets, that were treated through vacuum infiltration and grown in ammonium-free MS agar supplemented with 1 mM NH_4Cl and 1 mM sucrose. In contrast to what previously observed in rice and tomato, at 4 dpi no GUS activity was detected in *Gd_nifHDK::GUS*-treated *Arabidopsis* plantlets, possibly due to the lower diffusion of sucrose in agarised medium as compared to hydroponic systems. Nevertheless, the OE strain exhibited some blue staining in the roots and seed, possibly in correspondence to C-rich niches.

In conclusion, although only preliminarily investigated, the overexpression of NifA has demonstrated promising biotechnological potential for *in vivo* applications of the OE mutant. Moreover, the combination of NifA overexpression

with the deletion of other genes involved in nitrogen metabolism may constitute a valid tool for elucidating the function of the other players in the BNF regulation. The creation of this engineered strain opens the way for exciting experimentations in field, although further research is needed to fully harness the benefits of the *G. diazotrophicus* and NifA OE strains in enhancing crop productivity and reducing environmental impacts of intensive agricultural practices.

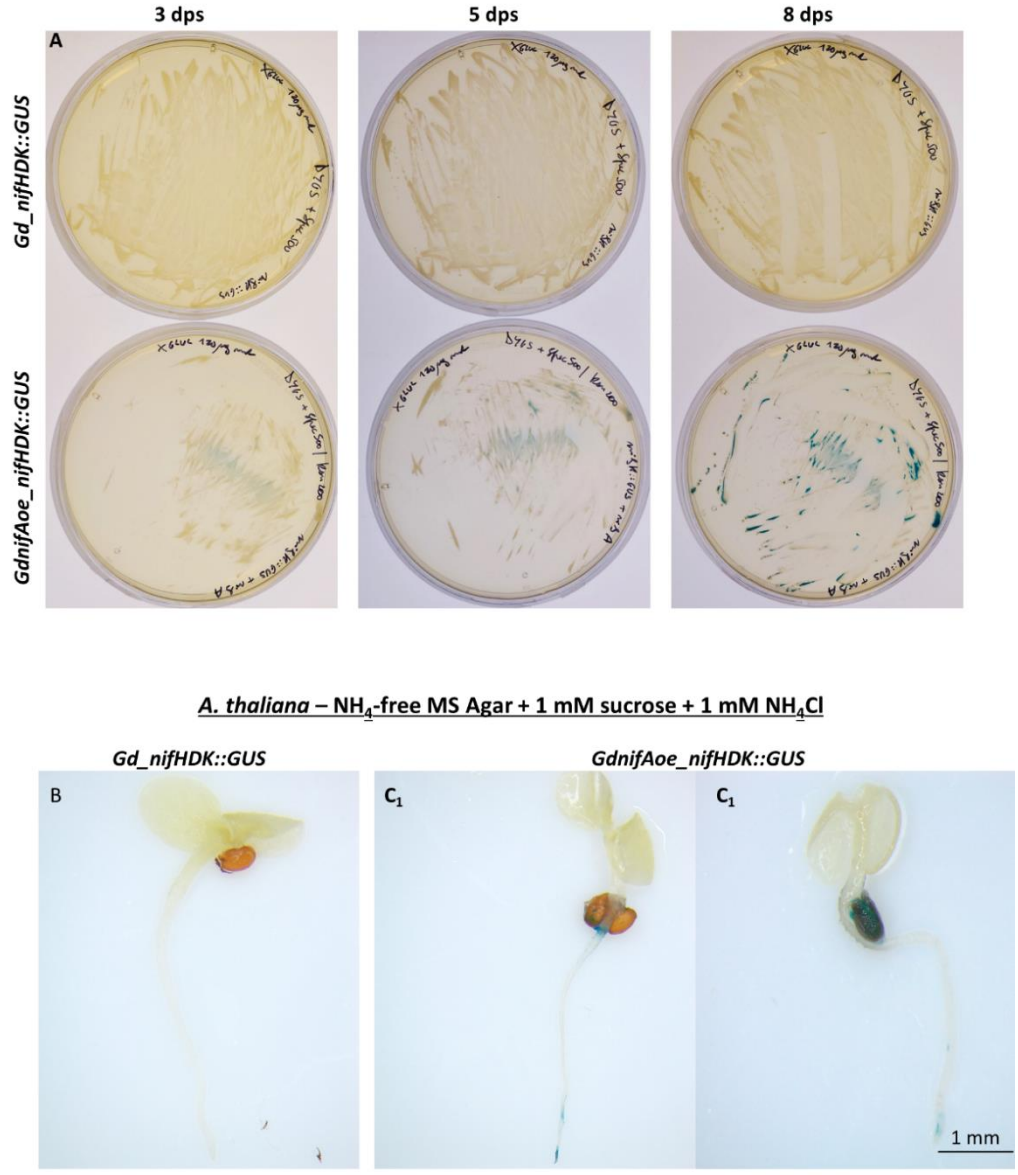


Fig. 4.85. (A) Growth comparison of Gd_nifHDK::GUS and GdnifAoe_nifHDK::GUS in DYGS medium. The X-Gluc reagent was incorporated in the medium at the concentration of 130 ug/mL. The images were taken with 3-day intervals (dps = days post streaking). (B-C) X-Gluc staining of Arabidopsis grown for 3 days after germination in ammonium-free MS agar supplemented with 1 mM sucrose and 1 mM ammonium, seed vacuum infiltration treatment with of Gd_nifHDK::GUS vs GdnifAoe_nifHDK::GUS resuspended in water at OD_{600} = 0.1 for 1 hour.

5. CONCLUSIONS AND FUTURE PERSPECTIVES

The exchange of carbon for fixed nitrogen between legumes and rhizobia has long been recognised as a remarkable evolutionary adaptation that has profoundly shaped the anthroposphere as we know it. However, free-living and non-nodulating symbiotic diazotrophs and cyanobacteria have been carrying out the same task since much older times [33], albeit in a more subtle but inexorable way, permeating every ecological niche with bioavailable nitrogen [35] [675]. Artificial experimental settings, which often involve simplified and time-limited experiments, do not fully capture the magnitude and gradual impact of this remarkable biological force. This work focused on the study and description of the colonisation and PGP properties of the non-nodulating diazotroph *G. diazotrophicus* following its application in tomato, rice, and *Arabidopsis* systems. Different inoculation methods were evaluated in order to establish a scalable working protocol for bacterial application. Seed coating or seed vacuum infiltration followed by in soil growth generated promising results in terms of biomass increase and fruit yield, although in a genotype-specific manner. The comparison of different inoculation strategies revealed the existence of a window in which the bacterium was sufficiently concentrated for eliciting significant PGP effect without causing a growth reduction due to biotic stress response in early plant developmental stage. This optimal bacterial load was modulable by adjusting either the inoculum density, the application time, or the sugar supply in the carrier. However, these results should be considered as preliminary, and field trials including more accurate phenotypic investigations under different soil conditions will be required to obtain a more statistically robust assessment of the PGP effect. Specifically, the quantification of shoot and root length, as well as biomass accumulation measured in both dry and fresh weights of plant tissues, should be conducted at various time points over the entire growing season, in order to monitor the impact of bacterial inoculation in field from the sowing to the harvesting stage. Similarly, parameters such as leaf area and leaf number, chlorophyll content, and photosynthetic rate, along with stomatal conductance and water use efficiency, should be measured in both hydroponic and soil setups to assess the

bacterial impact on above-ground plant organs and, to some extent, as indicators of direct BNF-derived nitrogen exchange. However, the verification of this phenomenon should be rigorously conducted through experiments involving 15/14N isotope labelling (see section 4.1.1d). Furthermore, it remains to be established whether the shoot biomass accumulation is a direct effect of nitrogen exchange with the bacterium or if it results from enhanced nutrient uptake due to a larger root system induced by hormonal stimulation. To address this inquiry, the root architecture modification (in terms of length, density, and branching) should be accurately monitored through CT-scanning. Finally, pathogen resistance and abiotic stress tolerance (such as drought, salinity, or heavy metals) should be evaluated to provide a complete picture of the bacterial effect on plant growth in field.

In contrast to in soil growth, MS agar and hydroponic systems offered a stable setup which provided more consistent results, as thoroughly discussed elsewhere [208]. These cultivation techniques confirmed the existence of an optimal concentration of bacteria to maximise their PGP capability, which should be assessed in relationship to the nutrient profile (primarily carbon and nitrogen) of the substrate. In particular, the presence of ammonium had the capacity to negatively affect both plant growth and bacteria establishment. The BNF-impaired *G. diazotrophicus* mutant was still capable of eliciting growth promotion to some extent, although not as pronounced as in the WT. However, ^{15}N isotope dilution analyses failed to detect significant amount of fixed nitrogen in the chlorophyll of treated tomato, suggesting some flow in the setup employed (such as lack of aeration and of carbon in the substrate or the choice of an unrepresentative N-sink) or the presence of other mechanisms underlying the observed PGP effect. Nevertheless, this and previous studies [208] have shown that under appropriate N conditions it is possible to obtain a long-lasting PGP upon one single initial application of *G. diazotrophicus* in hydroponic systems, which are a modern, sustainable, and easily scalable cultivation method.

Transcriptomic analyses and BNF evaluations under different N and C sources using reporter systems highlighted the need of a minimal threshold of

bioavailable nitrogen to trigger the self-sustaining nitrogen fixation cycle, as well as non-limiting carbon sources to fuel such process. These conditions are more likely to be met in plants grown under nitrate-replete substrate, which induced a more stable and beneficial symbiosis. In this context, while the addition of external ammonium is unnecessary and potentially disadvantageous, as micromolar concentration of bioavailable nitrogen in the shoot and root of plants will be enough to initiate nitrogen-fixation, the addition of an external carbon source in the medium could greatly boost BNF. On the other hand, bacterial inoculation could also greatly improve the growth of severely N-starved plants, but it was not sufficient per se to induce normal plant growth; however, this extreme setup would arguably never be met under natural field conditions. Interestingly, IAA production was more relevant in early colonisation stages within the root system and was later superseded by BNF in the shoots (Fig. 5.1); however, the BNF-impaired mutant was able to compensate the lack of this process by boosting its hormonal production, revealing a remarkable adaptation capability as well as the importance of IAA synthesis in the overall PGP effect. This ability may explain why the two strain could colonise their host at comparable levels, although with slightly different distribution across plant's organ. Nevertheless, considering the different nitrogen conditions tested and the differences in gene expression between the WT and the *nifD*$^{-}$ strains, the presence of a functional BNF machinery in the root system seemed to be correlated with the transcription of genes involved in the colonisation establishment and EPS production (*lsdA*) and in IAA synthesis since the early colonisation stages (Fig. 5.1, 1 dpi). IAA synthesis may promote root development and cell wall rearrangement to facilitate bacterial penetration in deeper root tissues, possibly in concert with BNF-derived tryptophan biosynthesis (Fig. 5.1, 1 dpi): after fixed ammonium is incorporated into glutamine [610], glutamine can be used as the precursor for tryptophan synthesis via chorismic acid pathway [662]. Speculatively, the increased concentration of intracellular glutamine in N-fixing bacteria may explain the transition into elongated or filamentous morphology [607] observed in some bacterial cells colonising the shoot (Fig. 5.1, 20 dpi) and expressing the *nifHDK* transcript (as evidenced through the *Gd_nifHDK::GUS* reporter strain, Fig. 4.78, 4.79).

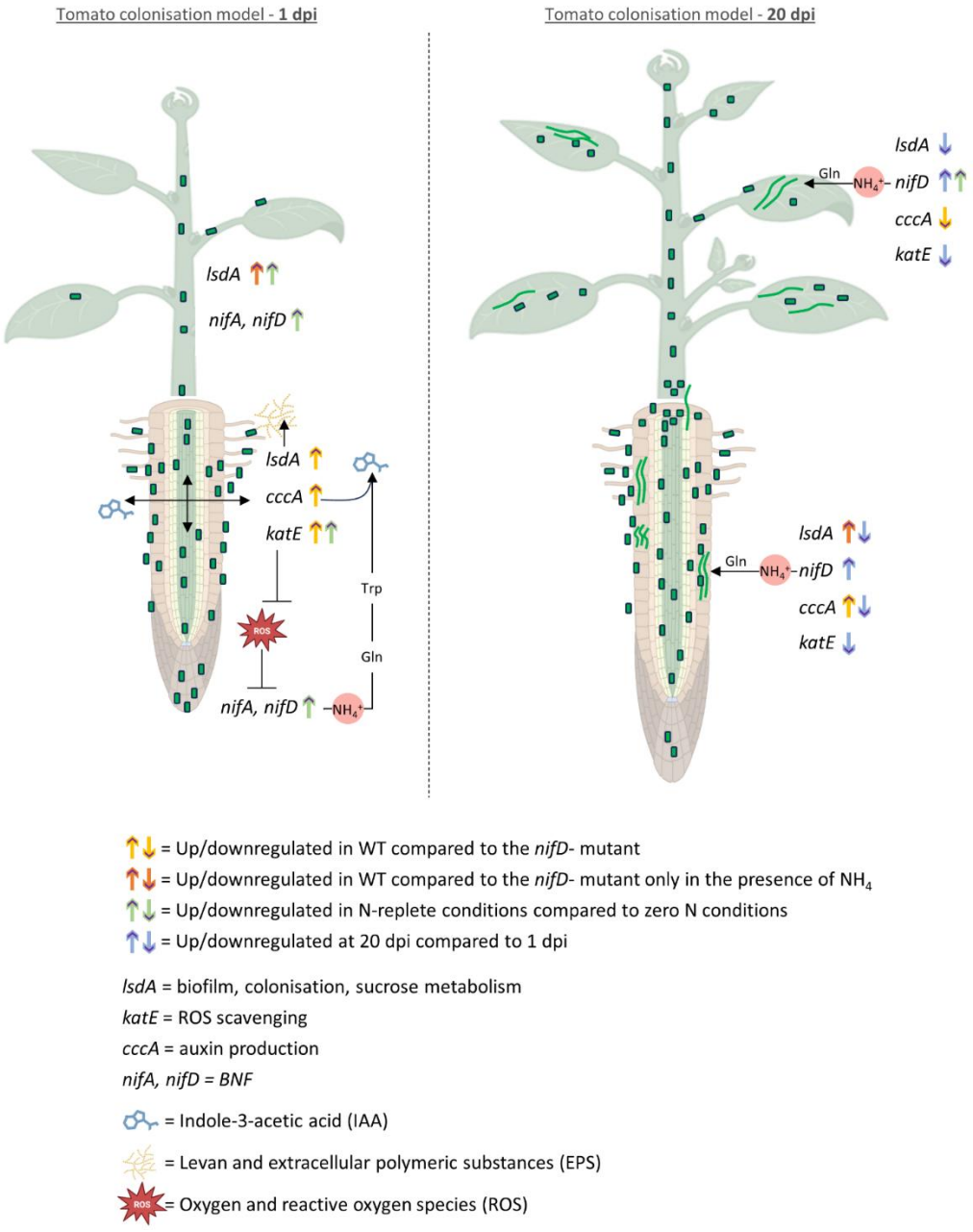


Fig. 5.1. Colonisation model of G. diazotrophicus interacting with tomato, summarised from transcriptomic and microscopy data. Yellow arrows indicate gene up or down regulation of the WT strain compared to the nifD- mutant strain; orange arrows indicate gene up or down regulation of the WT strain compared to the nifD- mutant strain only under NH_4 condition; blue arrow indicate gene up or down regulation at 20 dpi compared to 1 dpi; green arrows indicate gene up or down regulation in N-replete conditions compared to zero N condition. The black cross arrows in the root system at 1 dpi indicate the root development and cell wall loosening promoted by bacterial IAA production.

The action of the ROS-scavenging gene *katE* in the root system at 1 dpi is likely to protect the bacterium from the oxidative burst produced by the plant as an immune response during the early colonisation stages; furthermore, its

overexpression in the WT strain compared to the *nifD*$^{-}$ mutant may indicate its role in protecting the nitrogenase enzyme and its activator NifA, although no correlation between *katE* and *nifD* transcription patterns were observed (Fig. 4.81a). The downregulation of *katE* at 20 dpi reflects the establishment of the bacterium with consequent decrease of the immune response (Fig. 5.1, 20 dpi). For the same reason, the *lsdA* was mostly expressed at 1 dpi and was later downregulated (Fig. 5.1, 1 dpi); unexpectedly, however, its transcription compared to the *nifD*$^{-}$ mutant increased in the presence of external ammonium at 1 dpi in the shoot and at 20 dpi in the roots (Fig. 5.1), although plants grown in ammonium were normally found to be colonised by a lower number of bacteria (Fig. 4.15), suggesting a direct effect of the plant nutritional status on levan production and sucrose metabolism. In general, *lsdA* was more expressed in plants grown under N-replete condition compared to zero N, and so were *nifD* and *nifA* (Fig. 5.1, 1 dpi), likely reflecting that severely nitrogen starved plants cannot sustain a fully functional symbiosis due to the limited energetic reserves. In N-replete conditions, the expression of *nifA* was consistent over time, implying its regulation (and, consequently, the regulation of BNF) to be mostly contingent upon oxygen levels and post-transcriptional mechanisms. However, the transcription of *nifD* increased in shoot and roots at 20 dpi, while the IAA producing gene *cccA* was downregulated, suggesting the progressive establishment of a N-fixing symbiosis (as evidenced by the *Gd_nifHDK::GUS* reporter strain, Fig. 4.78, 4.79) and the production of IAA to be mostly required in early colonisation stages.

The various colonisation strategies observed during plant tissue invasion uncovered a generalist approach which allows the bacteria to exploit different anatomical features of the plants, including root hair, lateral root emergence site, lysogenic cells and cell wall junctures. Following endophytic root colonisation, *G. diazotrophicus* was able to reach the aerial parts via xylem flow in just 24 hours (possibly less), where it established itself within nutrient and water rich interfaces to the external environment such as stomata and trichomes. Whether this localisation was the result of passive phloem and xylem transport or if there was an active chemotaxis toward favourable niches remains to be established through time-lapse microscopy and chemotaxis

assays evaluating the movement of bacteria in response to key molecules found in the trichomes such as terpenoids. Crucially, the bacterium was observed to express BNF genes in the colonised plant compartments; furthermore, it was proven for the first time to be able to pass through the plasma membrane and establish itself within the cytoplasm, from which it seemed to be able to be transmitted in dividing plant cells.

These characteristics confirm *G. diazotrophicus* as a highly promising PGPB in agricultural applications. Moreover, genetically engineered strains can be exploited to unlock the full potential of this bacterium, although careful consideration and optimisation of the overall bacterial physiology and energy balance should be addressed before in field applications. The genetic manipulation tools described in this study may contribute to expedite metabolic engineering, thus opening exciting opportunities for both basic research and biotechnological bacterial amelioration. However, the utilisation of genome-edited strains should be confined solely to controlled and enclosed artificial settings, such as hydroponic setups, while avoiding any introduction into natural ecosystems.

In conclusion, while addressing some specific issues about the bacterium's physiology, the present study rather provides a holistic view of *G. diazotrophicus*-plant interaction and offers new stimuli for research that will require further investigation. The natural continuation of this work would involve the exploration of bacterial ammonium sensing and extracellular release, in order to combine nitrogenase overexpression with increased ammonium nutrition [673], although the plant assimilation of fixed nitrogen will also need to be re-evaluated with different techniques. Furthermore, a rigorous evaluation of the interaction between *G. diazotrophicus* and the microbiota of plants in soil through metagenomic and metatranscriptomic approaches, as well as via functional microbial consortia studies, will be instrumental in determining the efficacy of this bacterium in field. Alternatively, the cytoplasmic transmission capability of this bacterium in callous culture suggests the intriguing possibility of producing pre-colonised micro-propagated calli for different biotechnological applications.

6. ACKNOWLEDGEMENTS

My thanks go to all the people that have been involved in shaping this project and provided valuable suggestion along the journey: Rupert, Phil, Michele, Ramdane, Adriana, Gabriel, Thomas, Ute, my colleagues and friends fellows PhD students.

Many thanks to Chris Hayes and Matt Ford for the ^{15}N analyses.

Grazie a mia madre per avermi dato la possibilità di diventare quello che sono ed avermi sempre ascoltato. Grazie al resto della mia famiglia, in particolare ai Brandi ed allo zione, per il più che benvenuto contributo di pazzia e saggezza e per il supporto emotivo.

Grazie al BT per non avere mai mancato di farmi notare quando, per alleviare lo stress, condividevo una quantità di meme esagerata.

Soprattutto grazie a Marti, a cui devo, in ordine sparso, metà buona dei dati di questo progetto, più della metà della sanità mentale sopravvissuta a questa esperienza, la metà migliore di me e la consapevolezza di muovermi verso una meta.

In memory of Ted Cocking, who pioneered the academic research on *G. diazotrophicus* at the University of Nottingham.

7. REFERENCES

[1] O. Christen, “DEVELOPMENT ISSUES IN FOOD AND AGRICULTURE,” *UNESCO-EOLSS*, vol. I.

[2] “Map of the Month: How Many People Work in Agriculture? - Resource Watch Blog.” Accessed: Feb. 01, 2021. [Online]. Available: https://blog.resourcewatch.org/2019/05/30/map-of-the-month-how-many-people-work-in-agriculture/

[3] EEA, *The State of Nature in the European Union - Results from reporting under the nature directives 2007–2012*, no. 2. 2015. doi: COM(2015) 219 final.

[4] P. M. Vitousek and R. W. Howarth, “Nitrogen limitation on land and in the sea: How can it occur?,” *Biogeochemistry*, vol. 13, no. 2, pp. 87–115, 1991, doi: 10.1007/BF00002772.

[5] G. J. Leigh, “Dinitrogen Chemistry,” in *Nitrogen Fixation at the Millennium*, Elsevier, 2002, pp. 299–332. doi: 10.1016/b978-044450965-9/50011-2.

[6] C. Smith, A. K. Hill, and L. Torrente-Murciano, “Current and future role of Haber-Bosch ammonia in a carbon-free energy landscape,” *Energy Environ Sci*, vol. 13, no. 2, pp. 331–344, 2020, doi: 10.1039/c9ee02873k.

[7] J. W. Erisman, M. A. Sutton, J. Galloway, Z. Klimont, and W. Winiwarter, “How a century of ammonia synthesis changed the world,” *Nat Geosci*, vol. 1, no. 10, pp. 636–639, 2008, doi: 10.1038/ngeo325.

[8] “The Haber-Bosch Reaction: An Early Chemical Impact On Sustainability.” Accessed: Mar. 30, 2021. [Online]. Available: https://cen.acs.org/articles/86/i33/Haber-Bosch-Reaction-Early-Chemical.html

[9] “Global ammonia annual production capacity | Statista.” Accessed: Jul. 29, 2023. [Online]. Available: https://www.statista.com/statistics/1065865/ammonia-production-capacity-globally/

[10] C. Lu and H. Tian, “Global nitrogen and phosphorus fertilizer use for agriculture production in the past half century: Shifted hot spots and nutrient imbalance,” *Earth Syst Sci Data*, vol. 9, no. 1, pp. 181–192, 2017, doi: 10.5194/essd-9-181-2017.

[11] R. W. Howarth, “Coastal nitrogen pollution: A review of sources and trends globally and regionally,” *Harmful Algae*, vol. 8, no. 1, pp. 14–20, 2008, doi: 10.1016/j.hal.2008.08.015.

[12] P. M. Vitousek *et al.*, “Human alteration of the global nitrogen cycle: Sources and consequences,” *Ecological Applications*, vol. 7, no. 3, pp. 737–750, 1997, doi: 10.1890/1051-0761(1997)007[0737:HAOTGN]2.0.CO;2.

[13] A. Soumare *et al.*, “Exploiting biological nitrogen fixation: A route towards a sustainable agriculture,” *Plants*, vol. 9, no. 8, pp. 1–22, 2020, doi: 10.3390/plants9081011.

[14] D. Tilman, K. G. Cassman, P. A. Matson, R. Naylor, and S. Polasky, “Agricultural sustainability and intensive production practices,” *Nature*, vol. 418, no. 6898, pp. 671–677, 2002, doi: 10.1038/nature01014.

[15] P. Omara *et al.*, “World Cereal Nitrogen Use Efficiency Trends: Review and Current Knowledge,” *Agrosystems, Geosciences & Environment*, vol. 2, no. 1, pp. 1–8, Jan. 2019, doi: 10.2134/AGE2018.10.0045.

[16] E. W. Boyer, R. W. Howarth, J. N. Galloway, F. J. Dentener, P. A. Green, and C. J. Vörösmarty, “Riverine nitrogen export from the continents to the coasts,” *Global Biogeochem Cycles*, vol. 20, no. 1, Mar. 2006, doi: https://doi.org/10.1029/2005GB002537.

[17] R. W. Howarth, E. W. Boyer, W. J. Pabich, and J. N. Galloway, “Nitrogen use in the United States from 1961-2000 and potential future trends.,” *Ambio*, vol. 31, no. 2, pp. 88–96, Mar. 2002, doi: 10.1579/0044-7447-31.2.88.

[18] J. N. Galloway *et al.*, “Transformation of the nitrogen cycle: Recent trends, questions, and potential solutions,” *Science (1979)*, vol. 320, no. 5878, pp. 889–892, 2008, doi: 10.1126/science.1136674.

[19] P. J. Crutzen, “The Role of NO and NO2 in the Chemistry of the Troposphere and Stratosphere,” *Annu Rev Earth Planet Sci*, pp. 443–472, 1979, doi: 10.1146/ANNUREV.EA.07.050179.002303.

[20] T. J. Griffis *et al.*, “Nitrous oxide emissions are enhanced in a warmer and wetter world,” *Proc Natl Acad Sci U S A*, vol. 114, no. 45, pp. 12081–12085, Nov. 2017, doi: 10.1073/PNAS.1704552114/-/DCSUPPLEMENTAL.

[21] J. W. Erisman *et al.*, “Consequences of human modification of the global nitrogen cycle,” *Philosophical Transactions of the Royal Society B: Biological Sciences*, vol. 368, no. 1621, 2013, doi: 10.1098/rstb.2013.0116.

[22] J. A. Downing *et al.*, “Library of Congress Cataloging in Publication Data Gulf of Mexico Hypoxia: Land and Sea Interactions Council for Agricultural Science and Technology Task Force Members ii,” 1999.

[23] R. H. Whitbeck, “Chilean Nitrate and the Nitrogen Revolution,” *Econ Geogr*, vol. 7, no. 3, pp. 273–283, Oct. 1931, doi: 10.2307/140893.

[24] “Fertiliser and food prices could be high for years - Oxford Analytica Daily Brief.” Accessed: Nov. 15, 2022. [Online]. Available: https://dailybrief.oxan.com/Analysis/DB268415/Fertiliser-and-food-prices-could-be-high-for-years

[25] “Russia-Ukraine Crisis Ignites Fertilizer Prices at Critical Time for World Crops.” Accessed: Oct. 11, 2022. [Online]. Available: https://gro-intelligence.com/insights/russia-ukraine-crisis-ignites-fertilizer-prices-at-critical-time-for-world-crops

[26] N. Boivin and A. Crowther, “Mobilizing the past to shape a better Anthropocene,” *Nat Ecol Evol*, vol. 5, no. 3, pp. 273–284, 2021, doi: 10.1038/s41559-020-01361-4.

[27] J. Pretty, “Agricultural sustainability: Concepts, principles and evidence,” *Philosophical Transactions of the Royal Society B: Biological Sciences*, vol. 363, no. 1491, pp. 447–465, 2008, doi: 10.1098/rstb.2007.2163.

[28] P. Brown and S. Saa, “Biostimulants in agriculture,” *Front Plant Sci*, vol. 6, no. AUG, 2015, doi: 10.3389/fpls.2015.00671.

[29] J. W. Kloepper and C. J. Beauchamp, “A review of issues related to measuring colonization of plant roots by bacteria,” *Can J Microbiol*, vol. 38, no. 12, pp. 1219–1232, 1992, doi: 10.1139/M92-202.

[30] S. Bukhat, A. Imran, S. Javaid, M. Shahid, A. Majeed, and T. Naqqash, “Communication of plants with microbial world: Exploring the regulatory networks for PGPR mediated defense signaling,” *Microbiol Res*, vol. 238, Sep. 2020, doi: 10.1016/J.MICRES.2020.126486.

[31] N. Sivakumar, R. Sathishkumar, G. Selvakumar, R. Shyamkumar, and K. Arjunekumar, “Phyllospheric Microbiomes: Diversity, Ecological Significance, and Biotechnological Applications,” *Plant Microbiomes for Sustainable Agriculture*, vol. 25, p. 113, 2020, doi: 10.1007/978-3-030-38453-1_5.

[32] M. A. Santana, K. Pihakaski-Maunsbach, N. Sandal, K. A. Marcker, and A. G. Smith, “Evidence that the Plant Host Synthesizes the Heme Moiety of Leghemoglobin in Root Nodules,” *Plant Physiol*, vol. 116, no. 4, p. 1259, 1998, doi: 10.1104/PP.116.4.1259.

[33] J. I. Sprent, “60Ma of legume nodulation. What’s new? What’s changing?,” *J Exp Bot*, vol. 59, no. 5, pp. 1081–1084, Mar. 2008, doi: 10.1093/JXB/ERM286.

[34] W. Remy, T. N. Taylor, H. Hass, and H. Kerp, “Four hundred-million-year-old vesicular arbuscular mycorrhizae.,” *Proc Natl Acad Sci U S A*, vol. 91, no. 25, p. 11841, Dec. 1994, doi: 10.1073/PNAS.91.25.11841.

[35] C. Santi, D. Bogusz, and C. Franche, “Biological nitrogen fixation in non-legume plants,” *Ann Bot*, vol. 111, no. 5, pp. 743–767, May 2013, doi: 10.1093/AOB/MCT048.

[36] E. Hugoson, A. Guliaev, T. Ammunet, and L. Guy, “Host Adaptation in Legionellales Is 1.9 Ga, Coincident with Eukaryogenesis,” *Mol Biol Evol*, vol. 39, no. 3, Mar. 2022, doi: 10.1093/MOLBEV/MSAC037.

[37] G. E. D. Oldroyd, “Speak, friend, and enter: signalling systems that promote beneficial symbiotic associations in plants,” *Nat Rev Microbiol*, vol. 11, no. 4, pp. 252–263, Apr. 2013, doi: 10.1038/NRMICRO2990.

[38] F. Thiebaut, M. C. de O. Urquiaga, A. C. Rosman, M. L. da Silva, and A. S. Hemerly, “The Impact of Non-Nodulating Diazotrophic Bacteria in Agriculture: Understanding the Molecular Mechanisms That Benefit Crops,” *Int J Mol Sci*, vol. 23, no. 19, Oct. 2022, doi: 10.3390/IJMS231911301.

[39] P. Xu and E. Wang, “Diversity and regulation of symbiotic nitrogen fixation in plants,” *Current Biology*, vol. 33, no. 11, pp. R543–R559, Jun. 2023, doi: 10.1016/J.CUB.2023.04.053.

[40] A. Muangthong, S. Youpensuk, and B. Rerkasem, “Isolation and Characterisation of Endophytic Nitrogen Fixing Bacteria in Sugarcane,” *Trop Life Sci Res*, vol. 26, no. 1, p. 41, 2015, Accessed: Apr. 23, 2023. [Online]. Available: /pmc/articles/PMC4437324/

[41] S. Compant, C. Clément, and A. Sessitsch, “Plant growth-promoting bacteria in the rhizo- and endosphere of plants: Their role, colonization, mechanisms involved and prospects for utilization,” *Soil Biol Biochem*, vol. 42, no. 5, pp. 669–678, May 2010, doi: 10.1016/J.SOILBIO.2009.11.024.

[42] M. Böhm, T. Hurek, and B. Reinhold-Hurek, “Twitching motility is essential for endophytic rice colonization by the N2-fixing endophyte Azoarcus sp. strain BH72,” *Mol Plant Microbe Interact*, vol. 20, no. 5, pp. 526–533, May 2007, doi: 10.1094/MPMI-20-5-0526.

[43] M. Z. Tadra-Sfeir *et al.*, “Naringenin regulates expression of genes involved in cell wall synthesis in Herbaspirillum seropedicae,” *Appl Environ Microbiol*, vol. 77, no. 6, pp. 2180–2183, Mar. 2011, doi: 10.1128/AEM.02071-10.

[44] S. Compant, M. C. Cambon, C. Vacher, B. Mitter, A. Samad, and A. Sessitsch, “The plant endosphere world – bacterial life within plants,” *Environ Microbiol*, vol. 23, no. 4, pp. 1812–1829, 2021, doi: 10.1111/1462-2920.15240.

[45] Y. Bashan, “Inoculants of plant growth-promoting bacteria for use in agriculture,” *Biotechnol Adv*, vol. 16, no. 4, pp. 729–770, Jul. 1998, doi: 10.1016/S0734-9750(98)00003-2.

[46] M. Greco, A. Chiappetta, L. Bruno, and M. B. Bitonti, “Microbial recognition and evasion of host immunity,” *J Exp Bot*, vol. 64, no. 5, pp. 1237–1248, Mar. 2013, doi: 10.1093/JXB/ERS262.

[47] B. H. Jenkins *et al.*, “Emergent RNA–RNA interactions can promote stability in a facultative phototrophic endosymbiosis,” *Proc Natl Acad Sci U S A*, vol. 118, no. 38, p. e2108874118, Sep. 2021, doi: 10.1073/PNAS.2108874118/SUPPL_FILE/PNAS.2108874118.SD05.XLSX.

[48] E. H. Verbon and L. M. Liberman, “Beneficial microbes affect endogenous mechanisms controlling root development,” *Trends Plant Sci*, vol. 21, no. 3, p. 218, Mar. 2016, doi: 10.1016/J.TPLANTS.2016.01.013.

[49] N. O. Igiehon and O. O. Babalola, “Rhizosphere microbiome modulators: Contributions of nitrogen fixing bacteria towards sustainable agriculture,” *Int J Environ Res Public Health*, vol. 15, no. 4, Apr. 2018, doi: 10.3390/IJERPH15040574/IJERPH_15_00574_PDF.PDF.

[50] Y. Ma, M. N. V. Prasad, M. Rajkumar, and H. Freitas, “Plant growth promoting rhizobacteria and endophytes accelerate phytoremediation of metalliferous soils,” *Biotechnol Adv*, vol. 29, no. 2, pp. 248–258, 2011, doi: 10.1016/j.biotechadv.2010.12.001.

[51] A. M. Castiglione, G. Mannino, V. Contartese, C. M. Bertea, and A. Ertani, “Microbial Biostimulants as Response to Modern Agriculture Needs: Composition, Role and Application of These Innovative Products,” *Plants*, vol. 10, no. 8, Aug. 2021, doi: 10.3390/PLANTS10081533.

[52] V. C. S. Pankievicz, T. B. Irving, L. G. S. Maia, and J. M. Ané, “Are we there yet? The long walk towards the development of efficient symbiotic associations between nitrogen-fixing bacteria and non-leguminous crops,” *BMC Biol*, vol. 17, no. 1, Dec. 2019, doi: 10.1186/S12915-019-0710-0.

[53] M. R. Wagner *et al.*, “Microbe-dependent heterosis in maize,” *Proc Natl Acad Sci U S A*, vol. 118, no. 30, p. e2021965118, Jul. 2021, doi: 10.1073/PNAS.2021965118/SUPPL_FILE/PNAS.2021965118.SAPP.PDF.

[54] N. Christian, B. K. Whitaker, and K. Clay, “Microbiomes: unifying animal and plant systems through the lens of community ecology theory,” *Front Microbiol*, vol. 6, no. SEP, 2015, doi: 10.3389/FMICB.2015.00869.

[55] J. E. Pérez-Jaramillo, R. Mendes, and J. M. Raaijmakers, “Impact of plant domestication on rhizosphere microbiome assembly and functions,” *Plant Mol Biol*, vol. 90, no. 6, pp. 635–644, Apr. 2016, doi: 10.1007/S11103-015-0337-7.

[56] C. N. Jack, R. H. Petipas, T. E. Cheeke, J. L. Rowland, and M. L. Friesen, “Microbial Inoculants: Silver Bullet or Microbial Jurassic Park?,” *Trends Microbiol*, vol. 29, no. 4, pp. 299–308, 2021, doi: 10.1016/j.tim.2020.11.006.

[57] M. Ricci, L. Tilbury, B. Daridon, and K. Sukalac, “General Principles to Justify Plant Biostimulant Claims,” *Front Plant Sci*, vol. 10, Apr. 2019, doi: 10.3389/FPLS.2019.00494.

[58] Y. Ma, “Seed coating with beneficial microorganisms for precision agriculture,” *Biotechnol Adv*, vol. 37, no. 7, p. 107423, 2019, doi: 10.1016/j.biotechadv.2019.107423.

[59] R. A. Date, “Advances in inoculant technology: A brief review,” *Aust J Exp Agric*, vol. 41, no. 3, pp. 321–325, 2001, doi: 10.1071/EA00006.

[60] Y. Bashan, L. E. de-Bashan, S. R. Prabhu, and J. P. Hernandez, “Advances in plant growth-promoting bacterial inoculant technology: Formulations and practical perspectives (1998-2013),” *Plant Soil*, vol. 378, no. 1–2, pp. 1–33, 2014, doi: 10.1007/s11104-013-1956-x.

[61] M. S. Santos, M. A. Nogueira, and M. Hungria, “Microbial inoculants: reviewing the past, discussing the present and previewing an outstanding future for the use of beneficial bacteria in agriculture,” *AMB Express*, vol. 9, no. 1, 2019, doi: 10.1186/s13568-019-0932-0.

[62] M. Hungria, D. de S. Andrade, L. M. de O. Chueire, A. Probanza, F. J. Guttierrez-Mañero, and M. Megías, “Isolation and characterization of new efficient and competitive bean (Phaseolus vulgaris L.) rhizobia from Brazil,” *Soil Biol Biochem*, vol. 32, no. 11, pp. 1515–1528, 2000, doi: https://doi.org/10.1016/S0038-0717(00)00063-8.

[63] P. J. Riggs, M. K. Chelius, A. L. Iniguez, S. M. Kaeppler, and E. W. Triplett, “Enhanced maize productivity by inoculation with diazotrophic bacteria,” *Aust J Plant Physiol*, vol. 28, no. 9, pp. 829–836, 2001, doi: 10.1071/pp01045.

[64] M. del C. Rivera-Cruz, A. Trujillo Narcía, G. Córdova Ballona, J. Kohler, F. Caravaca, and A. Roldán, “Poultry manure and banana waste are effective biofertilizer carriers for promoting plant growth and soil sustainability in banana crops,” *Soil Biol Biochem*, vol. 40, no. 12, pp. 3092–3095, 2008, doi: https://doi.org/10.1016/j.soilbio.2008.09.003.

[65] P. Singleton, H. Keyser, and E. Sande, “Development and Evaluation of Liquid Inoculants,” Jan. 2002.

[66] Y. Bashan, “Inoculants of plant growth-promoting bacteria for use in agriculture,” *Biotechnol Adv*, vol. 16, no. 4, pp. 729–770, 1998, doi: https://doi.org/10.1016/S0734-9750(98)00003-2.

[67] T. J. Schulz and K. D. Thelen, “Soybean Seed Inoculant and Fungicidal Seed Treatment Effects on Soybean,” *Crop Sci*, vol. 48, no. 5, pp. 1975–1983, Sep. 2008, doi: https://doi.org/10.2135/cropsci2008.02.0108.

[68] Y. Ma, “Seed coating with beneficial microorganisms for precision agriculture,” *Biotechnol Adv*, vol. 37, no. 7, p. 107423, 2019, doi: 10.1016/j.biotechadv.2019.107423.

[69] L. G. Moretti *et al.*, “Can Additional Inoculations Increase Soybean Nodulation and Grain Yield?,” *Agron J*, vol. 110, no. 2, pp. 715–721, Mar. 2018, doi: https://doi.org/10.2134/agronj2017.09.0540.

[70] M. Evenari, “THE HISTORY OF GERMINATION RESEARCH AND THE LESSON IT CONTAINS FOR TODAY,” *Isr J Plant Sci*, vol. 29, no. 1–4, pp. 4–21, 1980, doi: https://doi.org/10.1080/0021213X.1980.10676873.

[71] A. J. Deshmukh, R. S. Jaiman, R. P. Bambharolia, and V. A. Patil, “Seed Biopriming– A Review,” *International Journal of Economic Plants*, vol. 7, no. 1, pp. 038–043, 2020, doi: 10.23910/2/2020.0359.

[72] H. R. El-Ramady *et al.*, “Plant Nutrition: From Liquid Medium to Micro-farm BT - Sustainable Agriculture Reviews 14: Agroecology and Global Change,” H. Ozier-Lafontaine and M. Lesueur-Jannoyer, Eds., Cham: Springer International Publishing, 2014, pp. 449–508. doi: 10.1007/978-3-319-06016-3_12.

[73] W. F. Gericke, “HYDROPONICS--CROP PRODUCTION IN LIQUID CULTURE MEDIA.,” *Science*, vol. 85, no. 2198, pp. 177–178, Feb. 1937, doi: 10.1126/science.85.2198.177.

[74] N. Engler and M. Krarti, “Review of energy efficiency in controlled environment agriculture,” *Renewable and Sustainable Energy Reviews*, vol. 141, p. 110786, 2021, doi: https://doi.org/10.1016/j.rser.2021.110786.

[75] A. A. Stegelmeier, D. M. Rose, B. R. Joris, and B. R. Glick, “The Use of PGPB to Promote Plant Hydroponic Growth,” *Plants*, vol. 11, no. 20, 2022, doi: 10.3390/plants11202783.

[76] A. Anzalone *et al.*, “Soil and Soilless Tomato Cultivation Promote Different Microbial Communities That Provide New Models for Future Crop Interventions,” *Int J Mol Sci*, vol. 23, no. 15, 2022, doi: 10.3390/ijms23158820.

[77] D. Handy, M. E. Hummerick, A. R. Dixit, A. M. Ruby, G. Massa, and A. Palmer, “Identification of Plant Growth Promoting Bacteria Within Space Crop Production Systems,” *Frontiers in Astronomy and Space Sciences*, vol. 8, no. October, pp. 1–10, 2021, doi: 10.3389/fspas.2021.735834.

[78] E. Lima, R. M. Boddey, and J. Döbereiner, “Quantification of biological nitrogen fixation associated with sugar cane using a 15N aided nitrogen balance,” *Soil Biol Biochem*, vol. 19, no. 2, pp. 165–170, 1987, doi: 10.1016/0038-0717(87)90077-0.

[79] S. Urquiaga, K. H. S. Cruz, and R. M. Boddey, “Contribution of nitrogen fixation to sugar cane. Nitrogen-15 and nitrogen-balance estimates,” *Soil Science Society of America Journal*, 1992, doi: 10.2136/sssaj1992.03615995005600010017x.

[80] J. Dobereiner, “Nitrogen-fixing bacteria of the genus Beijerinckia Derx in the rhizosphere of sugar cane,” *Plant Soil*, 1961, doi: 10.1007/BF01400455.

[81] R. M. Boddey, S. Urquiaga, V. Reis, and J. Döbereiner, “Biological nitrogen fixation associated with sugar cane,” *Plant Soil*, 1991, doi: 10.1007/BF02187441.

[82] J. Dobereiner, “Nitrogenase activity in the rhizosphere of sugar cane and some other tropical grasses,” *Plant Soil*, vol. 196, pp. 191–196, 1972.

[83] V. A. Cavalcante and J. Dobereiner, “A new acid-tolerant nitrogen-fixing bacterium associated with sugarcane,” *Plant Soil*, vol. 108, no. 1, pp. 23–31, 1988, doi: 10.1007/BF02370096.

[84] R. Muthukumarasamy, G. Revathi, and C. Lakshminarasimhan, “Influence of N fertilisation on the isolation of Acetobacter diazotrophicus and Herbaspirillum spp. from Indian sugarcane varieties,” *Biol Fertil Soils*, vol. 29, no. 2, pp. 157–164, 1999, doi: 10.1007/s003740050539.

[85] Y. Yamada, K. Hoshino, and T. Ishikawa, “The phylogeny of acetic acid bacteria based on the partial sequences of 16S ribosomal RNA: the elevation of the subgenus Gluconoacetobacter to the generic level.,” *Biosci Biotechnol Biochem*, vol. 61, no. 8, pp. 1244–1251, Aug. 1997, doi: 10.1271/bbb.61.1244.

[86] “Genus: Gluconacetobacter.” Accessed: Nov. 23, 2022. [Online]. Available: https://lpsn.dsmz.de/genus/gluconacetobacter

[87] V. M. Reis and K. R. dos S. Teixeira, “Nitrogen fixing bacteria in the family Acetobacteraceae and their role in agriculture,” *J Basic Microbiol*, vol. 55, no. 8, pp. 931–949, 2015, doi: 10.1002/jobm.201400898.

[88] “Family: Acetobacteraceae.” Accessed: Nov. 19, 2022. [Online]. Available: https://lpsn.dsmz.de/family/acetobacteraceae

[89] P. Raspor and D. Goranovič, “Biotechnological applications of acetic acid bacteria,” *Crit Rev Biotechnol*, vol. 28, no. 2, pp. 101–124, 2008, doi: 10.1080/07388550802046749.

[90] J. Möllerová, “Nitrogen fixation: Hundred years after,” *Folia Geobotanica et Phytotaxonomica*, vol. 25, no. 3, p. 256, 1990, doi: 10.1007/BF02913022.

[91] M. A. Paula, S. Urquiaga, and J. O. Siqueira, “Synergistic effects of vesicular-arbuscular mycorrhizal fungi and diazotrophic bacteria on nutrition and growth of sweet potato (Ipomoea batatas),” pp. 61–66, 1992.

[92] R. P. Li and I. C. Macrae, “Specific association of diazotrophic acetobacters with sugarcane,” *Soil Biol Biochem*, vol. 23, no. 10, pp. 999–1002, 1991, doi: 10.1016/0038-0717(91)90181-I.

[93] R. Li and I. C. MacRae, “Specific identification and enumeration of Acetobacter diazotrophicus in sugarcane,” *Soil Biol Biochem*, vol. 24, no. 5, pp. 413–419, 1992, doi: https://doi.org/10.1016/0038-0717(92)90203-A.

[94] T. Jimenez-Salgado, L. E. Fuentes-Ramirez, A. Tapia-Hernandez, M. A. Mascarua-Esparza, E. Martinez-Romero, and J. Caballero-Mellado, “Coffea arabica L., a New Host Plant for Acetobacter diazotrophicus, and Isolation of Other Nitrogen-Fixing Acetobacteria,” 1997.

[95] P. Loganathan, R. Sunita, A. K. Parida, and S. Nair, “Isolation and characterization of two genetically distant groups of Acetobacter diazotrophicus from a new host plant Eleusine coracana L.,” *J Appl Microbiol*, vol. 87, no. 1, pp. 167–172, Jul. 1999, doi: 10.1046/J.1365-2672.1999.00804.X.

[96] A. Tapia-Hernandez, M. Bustillos, T. Jiménez-Salgado, J. Caballero-Mellado, and L. Fuentes-Ramirez, “Natural Endophytic Occurrence of Acetobacter diazotrophicus in Pineapple Plants,” *Microb Ecol*, vol. 39, pp. 49–55, Jan. 2000, doi: 10.1007/s002489900190.

[97] P. Loganathan and S. Nair, “Crop-specific endophytic colonization by a novel, salt-tolerant, N2-fixing and phosphate-solubilizing Gluconacetobacter sp. from wild rice,” *Biotechnol Lett*, vol. 25, no. 6, pp. 497–501, 2003, doi: 10.1023/A:1022645124506.

[98] D. Dent, “Non-nodular Endophytic Bacterial Symbiosis and the Nitrogen Fixation of Gluconacetobacter diazotrophicus,” in *Symbiosis*, InTech, 2018. doi: 10.5772/intechopen.75813.

[99] J. M. Crespo, J. L. Boiardi, and M. F. Luna, “Mineral phosphate solubilization activity of gluconacetobacter diazotrophicus under P-limitation and plant root environment,” *Agricultural sciences*, vol. 02, no. 01, pp. 16–22, 2011, doi: 10.4236/AS.2011.21003.

[100] L. E. Fuentes-Ramirez, T. Jimenez-Salgado, I. R. Abarca-Ocampo, and J. Caballero-Mellado, “Acetobacter diazotrophicus, an indoleacetic acid producing bacterium isolated from sugarcane cultivars of México,” *Plant Soil*, vol. 154, no. 2, pp. 145–150, 1993, doi: 10.1007/BF00012519.

[101] F. Bastián, A. Cohen, P. Piccoli, V. Luna, R. Baraldi, and R. Bottini, “Production of indole-3-acetic acid and gibberellins A1 and A3 by Acetobacter diazotrophicus and Herbaspirillum seropedicae in chemically-defined culture media,” *Plant Growth Regul*, vol. 24, no. 1, pp. 7–11, 1998, doi: 10.1023/A:1005964031159/METRICS.

[102] R. Silva *et al.*, “Gluconacetobacter diazotrophicus changes the molecular mechanisms of root development in Oryza sativa L. growing under water stress,” *Int J Mol Sci*, vol. 21, no. 1, Jan. 2020, doi: 10.3390/ijms21010333.

[103] L. E. Contreras-Llano, M. A. Guerrero-Rubio, J. D. Lozada-Ramírez, F. García-Carmona, and F. Gandía-Herrero, “First Betalain-Producing Bacteria Break the Exclusive Presence of the Pigments in the Plant Kingdom,” *mBio*, vol. 10, no. 2, Mar. 2019, doi: 10.1128/MBIO.00345-19.

[104] C. Martínez-Fleites *et al.*, “Crystal structure of levansucrase from the Gram-negative bacterium Gluconacetobacter diazotrophicus,” *Biochemical Journal*, vol. 390, no. Pt 1, p. 19, Aug. 2005, doi: 10.1042/BJ20050324.

[105] J. G. Arrieta *et al.*, “A Type II Protein Secretory Pathway Required for Levansucrase Secretion by Gluconacetobacter diazotrophicus,” *J Bacteriol*, vol. 186, no. 15, p. 5031, Aug. 2004, doi: 10.1128/JB.186.15.5031-5039.2004.

[106] L. Hernández *et al.*, “Structural levansucrase gene (lsdA) constitutes a functional locus conserved in the species Gluconacetobacter diazotrophicus,” *Arch Microbiol*, vol. 174, no. 1–2, pp. 120–124, 2000, doi: 10.1007/S002030000173.

[107] M. L. Velázquez-Hernández *et al.*, “Gluconacetobacter diazotrophicus levansucrase is involved in tolerance to NaCl, sucrose and desiccation, and in biofilm formation,” *Arch Microbiol*, vol. 193, no. 2, pp. 137–149, 2011, doi: 10.1007/s00203-010-0651-z.

[108] M. L. Galar and J. L. Boiardi, “Evidence for a membrane-bound pyrroloquinoline quinone-linked glucose dehydrogenase in Acetobacter diazotrophicus,” *Appl Microbiol Biotechnol*, vol. 43, no. 4, pp. 713–716, 1995, doi: 10.1007/BF00164778/METRICS.

[109] M. M. Attwood, J. P. van Dijken, and J. T. Pronk, “Glucose metabolism and gluconic acid production by Acetobacter diazotrophicus,” *J Ferment Bioeng*, vol. 72, no. 2, pp. 101–105, Jan. 1991, doi: 10.1016/0922-338X(91)90317-A.

[110] S. M. C. Alquéres *et al.*, “Antioxidant pathways are up-regulated during biological nitrogen fixation to prevent ROS-induced nitrogenase inhibition in Gluconacetobacter diazotrophicus,” *Arch Microbiol*, vol. 192, no. 10, pp. 835–841, 2010, doi: 10.1007/s00203-010-0609-1.

[111] M. Flores-Encarnación, M. Contreras, S. Lucía, G. R. Aguilar, B. Baca, and J. Escamilla, “The Respiratory System and Diazotrophic Activity of Acetobacter diazotrophicus PAL5,” *J Bacteriol*, vol. 181, pp. 6987–6995, Dec. 1999, doi: 10.1128/JB.181.22.6987-6995.1999.

[112] Z. Dong *et al.*, “Evidence for protection of nitrogenase from O(2) by colony structure in the aerobic diazotroph Gluconacetobacter diazotrophicus,” *Microbiology (Reading)*, vol. 148, no. Pt 8, pp. 2293–2298, 2002, doi: 10.1099/00221287-148-8-2293.

[113] J. Caballero-Mellado and E. Martínez-Romero, “Limited Genetic Diversity in the Endophytic Sugarcane Bacterium Acetobacter diazotrophicus,” *Appl Environ Microbiol*, vol. 60, pp. 1532–1537, Jun. 1994, doi: 10.1128/AEM.60.5.1532-1537.1994.

[114] R. Gupta and N. Gupta, “Nitrogen Assimilation and Dissimilation,” 2021, pp. 431–464. doi: 10.1007/978-981-16-0723-3_16.

[115] A. Kamp, D. De Beer, J. L. Nitsch, G. Lavik, and P. Stief, “Diatoms respire nitrate to survive dark and anoxic conditions,” *Proc Natl Acad Sci U S A*, vol. 108, no. 14, p. 5649, Apr. 2011, doi: 10.1073/PNAS.1015744108.

[116] P. Stief *et al.*, “Dissimilatory nitrate reduction by Aspergillus terreus isolated from the seasonal oxygen minimum zone in the Arabian Sea,” *BMC Microbiol*, vol. 14, no. 1, Feb. 2014, doi: 10.1186/1471-2180-14-35.

[117] T. Müller, B. Walter, A. Wirtz, and A. Burkovski, “Ammonium toxicity in bacteria,” *Curr Microbiol*, vol. 52, no. 5, pp. 400–406, May 2006, doi: 10.1007/S00284-005-0370-X.

[118] L. F. Huergo, G. Chandra, and M. Merrick, “P(II) signal transduction proteins: nitrogen regulation and beyond,” *FEMS Microbiol Rev*, vol. 37, no. 2, pp. 251–283, Mar. 2013, doi: 10.1111/J.1574-6976.2012.00351.X.

[119] B. Alvarez and G. Martinez-Drets, “Metabolic characterization of Acetobacter diazotrophicus,” *Can J Microbiol*, vol. 41, no. 10, pp. 918–924, 1995, doi: 10.1139/M95-126.

[120] C. Feehily and K. A. G. Karatzas, “Role of glutamate metabolism in bacterial responses towards acid and other stresses,” *J Appl Microbiol*, vol. 114, no. 1, pp. 11–24, 2013, doi: 10.1111/J.1365-2672.2012.05434.X.

[121] A. Ureta and S. Nordlund, “ Glutamine synthetase from Acetobacter diazotrophicus : properties and regulation ,” *FEMS Microbiol Lett*, vol. 202, no. 2, pp. 177–180, Aug. 2001, doi: 10.1111/j.1574-6968.2001.tb10800.x.

[122] K. Forchhammer, “Glutamine signalling in bacteria,” *Front Biosci*, vol. 12, no. 1, pp. 358–370, 2007, doi: 10.2741/2069.

[123] O. Perlova, R. Nawroth, E. M. Zellermann, and D. Meletzus, “Isolation and characterization of the glnD gene of Gluconacetobacter diazotrophicus, encoding a putative uridylyltransferase/uridylyl-removing enzyme,” *Gene*, vol. 297, no. 1–2, pp. 159–168, Sep. 2002, doi: 10.1016/S0378-1119(02)00881-8.

[124] O. Perlova, A. Ureta, S. Nordlund, and D. Meletzus, “Identification of three genes encoding PII-like proteins in Gluconacetobacter diazotrophicus: Studies of their role(s) in the control of nitrogen fixation,” *J Bacteriol*, vol. 185, no. 19, pp. 5854–5861, Oct. 2003, doi: 10.1128/JB.185.19.5854-5861.2003.

[125] Y. Zhang, E. L. Pohlmann, C. M. Halbleib, P. W. Ludden, and G. P. Roberts, “Effect of P(II) and its homolog GlnK on reversible ADP-ribosylation of dinitrogenase reductase by heterologous expression of the Rhodospirillum rubrum dinitrogenase reductase ADP-ribosyl transferase-dinitrogenase reductase-activating glycohydrolase regulatory system in Klebsiella pneumoniae,” *J Bacteriol*, vol. 183, no. 5, pp. 1610–1620, 2001, doi: 10.1128/JB.183.5.1610-1620.2001.

[126] B. Masepohl and K. Forchhammer, “Chapter 9 - Regulatory Cascades To Express Nitrogenases,” in *Biology of the Nitrogen Cycle*, Elsevier, 2007, pp. 131–145. doi: 10.1016/B978-044452857-5.50010-2.

[127] D. Meletzus *et al.*, “Characterization of Genes Involved in Regulation of Nitrogen Fixation and Ammonium Sensing in Acetobacter diazotrophicus, an Endophyte of Sugarcane,” in *Biological Nitrogen Fixation for the 21st Century*, Springer, Dordrecht, 1998, pp. 125–126. doi: 10.1007/978-94-011-5159-7_41.

[128] K. R. S. Teixeira *et al.*, “Molecular analysis of the chromosomal region encoding the nifA and nifB genes of Acetobacter diazotrophicus,” *FEMS Microbiol Lett*, vol. 176, no. 2, pp. 301–309, 1999, doi: 10.1016/S0378-1097(99)00249-9.

[129] L. Sunhee, R. Alexander, M. Dietmar, S. Myrna, and K. Christina, “Characterization of a Major Cluster of nif,fix, and Associated Genes in a Sugarcane Endophyte,Acetobacter diazotrophicus,” *J Bacteriol*, vol. 182, no. 24, pp. 7088–7091, Dec. 2000, doi: 10.1128/JB.182.24.7088-7091.2000.

[130] A. Pawlowski *et al.*, “Yeast Two-Hybrid Studies on Interaction of Proteins Involved in Regulation of Nitrogen Fixation in the Phototrophic Bacterium Rhodobacter capsulatus,” *J Bacteriol*, vol. 185, no. 17, p. 5240, Sep. 2003, doi: 10.1128/JB.185.17.5240-5247.2003.

[131] V. M. Reis and J. Döbereiner, “Effect of high sugar concentration on nitrogenase activity of Acetobacter diazotrophicus,” *Arch Microbiol*, vol. 171, no. 1, pp. 13–18, 1998, doi: 10.1007/s002030050672.

[132] B. O. Pan and J. K. Vessey, “Response of the Endophytic Diazotroph Gluconacetobacter diazotrophicus on Solid Media to Changes in Atmospheric Partial O2 Pressure,” *Appl Environ Microbiol*, vol. 67, no. 10, pp. 4694–4700, 2001, doi: 10.1128/AEM.67.10.4694-4700.2001.

[133] M. P. Stephan, M. Oliveira, K. R. S. Teixeira, G. Martinez-Drets, and J. Döbereiner, “Physiology and dinitrogen fixation of Acetobacter diazotrophicus,” *FEMS Microbiol Lett*, vol. 77, no. 1, pp. 67–72, 1991, [Online]. Available: https://www.sciencedirect.com/science/article/pii/0378109791900153

[134] R. Muthukumarasamy, G. Revathi, and P. Loganathan, “Effect of inorganic N on the population, in vitro colonization and morphology of Acetobacter diazotrophicus (syn. Gluconacetobacter diazotrophicus),” *Plant Soil*, vol. 243, no. 1, pp. 91–102, 2002, doi: 10.1023/A:1019963928947.

[135] A. Wen *et al.*, “Enabling Biological Nitrogen Fixation for Cereal Crops in Fertilized Fields,” *ACS Synth Biol*, vol. 10, no. 12, pp. 3264–3277, Dec. 2021, doi: 10.1021/acssynbio.1c00049.

[136] A. K. Garcia, H. McShea, B. Kolaczkowski, and B. Kaçar, “Reconstructing the evolutionary history of nitrogenases: Evidence for ancestral molybdenum-cofactor utilization,” *Geobiology*, vol. 18, no. 3, p. 394, May 2020, doi: 10.1111/GBI.12381.

[137] L. M. Rubio and P. W. Ludden, “Maturation of Nitrogenase: a Biochemical Puzzle,” *J Bacteriol*, vol. 187, no. 2, p. 405, 2005, doi: 10.1128/JB.187.2.405-414.2005.

[138] C. P. Owens and F. A. Tezcan, *Conformationally Gated Electron Transfer in Nitrogenase. Isolation, Purification, and Characterization of Nitrogenase From Gluconacetobacter diazotrophicus*, 1st ed., vol. 599. Elsevier Inc., 2018. doi: 10.1016/bs.mie.2017.09.007.

[139] G. Xu, X. Fan, and A. J. Miller, “Plant nitrogen assimilation and use efficiency,” *Annu Rev Plant Biol*, vol. 63, pp. 153–182, Jun. 2012, doi: 10.1146/ANNUREV-ARPLANT-042811-105532.

[140] T. Hachiya and H. Sakakibara, “Interactions between nitrate and ammonium in their uptake, allocation, assimilation, and signaling in plants,” *J Exp Bot*, vol. 68, no. 10, pp. 2501–2512, May 2017, doi: 10.1093/JXB/ERW449.

[141] Y. Zhu *et al.*, “Appropriate NH4+/NO3– Ratio Triggers Plant Growth and Nutrient Uptake of Flowering Chinese Cabbage by Optimizing the pH Value of Nutrient Solution,” *Front Plant Sci*, vol. 12, p. 656144, Apr. 2021, doi: 10.3389/FPLS.2021.656144/BIBTEX.

[142] S. Ishii, S. Ikeda, K. Minamisawa, and K. Senoo, “Nitrogen Cycling in Rice Paddy Environments: Past Achievements and Future Challenges,” *Microbes Environ*, vol. 26, no. 4, pp. 282–292, 2011, doi: 10.1264/JSME2.ME11293.

[143] T. Näsholm, K. Kielland, and U. Ganeteg, “Uptake of organic nitrogen by plants,” *New Phytologist*, vol. 182, no. 1, pp. 31–48, Apr. 2009, doi: 10.1111/J.1469-8137.2008.02751.X.

[144] C. Paungfoo-Lonhienne *et al.*, “Plants can use protein as a nitrogen source without assistance from other organisms,” *Proc Natl Acad Sci U S A*, vol. 105, no. 11, pp. 4524–4529, Mar. 2008, doi: 10.1073/PNAS.0712078105.

[145] J. K. Schjoerring, S. Husted, G. Mäck, and M. Mattsson, “The regulation of ammonium translocation in plants,” *J Exp Bot*, vol. 53, no. 370, pp. 883–890, Apr. 2002, doi: 10.1093/JEXBOT/53.370.883.

[146] R. Tischner, “Nitrate uptake and reduction in higher and lower plants,” *Plant Cell Environ*, vol. 23, no. 10, pp. 1005–1024, Oct. 2000, doi: 10.1046/J.1365-3040.2000.00595.X.

[147] C. H. Loh, B. S. Inbaraj, M. H. Liu, and B. H. Chen, “Determination of chlorophylls in Taraxacum formosanum by high-performance liquid

chromatography-diode array detection-mass spectrometry and preparation by column chromatography," *J Agric Food Chem*, vol. 60, no. 24, pp. 6108–6115, Jun. 2012, doi: 10.1021/JF301422M.

[148] J. A. Atkinson and D. M. Wells, "An updated protocol for high throughput plant tissue sectioning," *Front Plant Sci*, vol. 8, p. 294406, Oct. 2017, doi: 10.3389/FPLS.2017.01721/BIBTEX.

[149] H. Banani *et al.*, "Characterization of resistance mechanisms activated by Trichoderma harzianum T39 and benzothiadiazole to downy mildew in different grapevine cultivars," *Plant Pathol*, vol. 63, no. 2, pp. 334–343, Apr. 2014, doi: 10.1111/PPA.12089.

[150] P. S. Galisa *et al.*, "Identification and validation of reference genes to study the gene expression in Gluconacetobacter diazotrophicus grown in different carbon sources using RT-qPCR," *J Microbiol Methods*, vol. 91, no. 1, pp. 1–7, 2012, doi: 10.1016/j.mimet.2012.07.005.

[151] P. Stothard, "The sequence manipulation suite: JavaScript programs for analyzing and formatting protein and DNA sequences," *Biotechniques*, vol. 28, no. 6, 2000, doi: 10.2144/00286IR01.

[152] M. A. Paula, V. M. Reis, and J. Döbereiner, "Interactions of Glomus clarum with Acetobacter diazotrophicus in infection of sweet potato (Ipomoea batatas), sugarcane (Saccharum spp.), and sweet sorghum (Sorghum vulgare)," *Biol Fertil Soils*, vol. 11, no. 2, pp. 111–115, 1991, doi: 10.1007/BF00336374.

[153] G. Tian, P. Pauls, Z. Dong, L. M. Reid, and L. Tian, "Colonization of the nitrogen-fixing bacterium Gluconacetobacter diazotrophicus in a large number of Canadian corn plants," *Canadian Journal of Plant Science*, vol. 89, no. 6, pp. 1009–1016, 2009, doi: 10.4141/CJPS08040.

[154] J. Caballero-Mellado, E. Martínez-Romero, P. Estrada de los Santos, and L. E. Fuentes-Ramírez, "Maize Colonization by Acetobacter diazotrophicus BT - Biological Nitrogen Fixation for the 21st Century: Proceedings of the 11th International Congress on Nitrogen Fixation, Institut Pasteur, Paris, France, July 20–25, 1997," C. Elmerich, A. Kondorosi, and W. E. Newton, Eds., Dordrecht: Springer Netherlands, 1998, pp. 381–382. doi: 10.1007/978-94-011-5159-7_228.

[155] M. F. Luna, M. L. Galar, J. Aprea, M. L. Molinari, and J. L. Boiardi, "Colonization of sorghum and wheat by seed inoculation with Gluconacetobacter diazotrophicus," *Biotechnol Lett*, vol. 32, no. 8, pp. 1071–1076, 2010, doi: 10.1007/s10529-010-0256-2.

[156] V. Yoon *et al.*, "Colonization efficiency of different sorghum genotypes by Gluconacetobacter diazotrophicus," *Plant Soil*, vol. 398, no. 1–2, pp. 243–256, 2016, doi: 10.1007/s11104-015-2653-8.

[157] Y. Ríos Rocafull, B. Dibut Álvarez, M. Rojas Badía, M. Ortega García, N. Arozarena Daza, and J. Rodríguez Sánchez, "Interacción de la bacteria

Gluconacetobacter diazotrophicus y hortalizas de raíz," *Cultivos tropicales*, vol. 37, no. 2, pp. 28–32, 2016, doi: 10.13140/RG.2.1.2799.0640.

[158] M. Pellegrini, G. Pagnani, M. Rossi, S. D'egidio, M. Del Gallo, and C. Forni, "Article daucus carota l. Seed inoculation with a consortium of bacteria improves plant growth, soil fertility status and microbial community," *Applied Sciences (Switzerland)*, vol. 11, no. 7, pp. 1–18, 2021, doi: 10.3390/app11073274.

[159] P. Delaporte-Quintana, M. Grillo-Puertas, N. C. Lovaisa, K. R. Teixeira, V. A. Rapisarda, and R. O. Pedraza, "Contribution of Gluconacetobacter diazotrophicus to phosphorus nutrition in strawberry plants," *Plant Soil*, vol. 419, no. 1–2, pp. 335–347, 2017, doi: 10.1007/s11104-017-3349-z.

[160] E. A. P. Lopes, A. D. A. Da Silva, A. C. D. E. S. Mergulhão, E. V. N. Da Silva, A. D. Santiago, and M. D. V. B. Figueiredo, "Co-Inoculation of growth promoting bacteria and glomus clarum in micropropagated cassava plants," *Revista Caatinga*, vol. 32, no. 1, pp. 152–166, 2019, doi: 10.1590/1983-21252019v32n116rc.

[161] T. R. A. de Oliveira *et al.*, "The performance of bean pod lineage inoculated with Gluconacetobacter diazotrophicus PAL5," *Sci Hortic*, vol. 249, no. January, pp. 65–70, 2019, doi: 10.1016/j.scienta.2019.01.044.

[162] R. L. Sebring, S. W. Duiker, R. D. Berghage, J. M. Regan, J. D. Lambert, and R. B. Bryant, "Gluconacetobacter diazotrophicus Inoculation of Two Lettuce Cultivars Affects Leaf and Root Growth under Hydroponic Conditions," *Applied Sciences (Switzerland)*, vol. 12, no. 3, 2022, doi: 10.3390/app12031585.

[163] E. K. James, V. M. Reis, F. L. Olivares, J. I. Baldani, and J. Döbereiner, "Infection of sugar cane by the nitrogen-fixing bacterium Acetobacter diazotrophicus," 1994. [Online]. Available: https://about.jstor.org/terms

[164] "FAOSTAT." Accessed: Oct. 28, 2022. [Online]. Available: https://www.fao.org/faostat/en/#compare

[165] "Global Consumption of Tomato Products 2018 / 2019 Edition Written by Françis-Xavier Branthôme (Editor , Tomato News) with funding from WPTC," no. January, 2020.

[166] "World - Tomato - Market Analysis, Forecast, Size, Trends and Insights." Accessed: Oct. 28, 2022. [Online]. Available: https://www.researchandmarkets.com/reports/4701312/world-tomato-market-analysis-forecast-size

[167] "Hydroponics: tomato crop market share by region worldwide 2017-2022 | Statista." Accessed: Nov. 15, 2022. [Online]. Available: https://www.statista.com/statistics/879885/global-hydroponic-growth-tomato-crops-market-share-by-region/

[168] E. Costa, Miguel & Huevelink, "Today 's worldwide tomato production," *International Suppliers Guide*, no. January, pp. 2006–2008, 2007.

[169] Y.-D. Du, W.-Q. Niu, X.-B. Gu, Q. Zhang, and B.-J. Cui, “Water- and nitrogen-saving potentials in tomato production: A meta-analysis,” *Agric Water Manag*, vol. 210, pp. 296–303, 2018, doi: https://doi.org/10.1016/j.agwat.2018.08.035.

[170] R. Poudel, A. Jumpponen, M. M. Kennelly, C. L. Rivard, L. Gomez-Montano, and K. A. Garrett, “Rootstocks shape the rhizobiome: Rhizosphere and endosphere bacterial communities in the grafted tomato system,” *Appl Environ Microbiol*, vol. 85, no. 2, Jan. 2019, doi: 10.1128/AEM.01765-18.

[171] S. A. Lee *et al.*, “A preliminary examination of bacterial, archaeal, and fungal communities inhabiting different rhizocompartments of tomato plants under real-world environments,” *Sci Rep*, vol. 9, no. 1, Dec. 2019, doi: 10.1038/s41598-019-45660-8.

[172] J. Caballero-Mellado, J. Onofre-Lemus, P. Estrada-De Los Santos, and L. Martínez-Aguilar, “The tomato rhizosphere, an environment rich in nitrogen-fixing Burkholderia species with capabilities of interest for agriculture and bioremediation,” *Appl Environ Microbiol*, vol. 73, no. 16, pp. 5308–5319, Aug. 2007, doi: 10.1128/AEM.00324-07.

[173] M. Madhaiyan *et al.*, “Occurrence of Gluconacetobacter diazotrophicus in tropical and subtropical plants of Western Ghats, India,” *Microbiol Res*, vol. 159, no. 3, pp. 233–243, 2004, doi: 10.1016/j.micres.2004.04.001.

[174] M. F. Luna, J. Aprea, J. M. Crespo, and J. L. Boiardi, “Colonization and yield promotion of tomato by Gluconacetobacter diazotrophicus,” *Applied Soil Ecology*, vol. 61, pp. 225–229, 2012, doi: 10.1016/j.apsoil.2011.09.002.

[175] A. L. Botta, A. Santacecilia, C. Ercole, P. Cacchio, and M. del Gallo, “In vitro and in vivo inoculation of four endophytic bacteria on Lycopersicon esculentum,” *N Biotechnol*, vol. 30, no. 6, pp. 666–674, 2013, doi: 10.1016/j.nbt.2013.01.001.

[176] G. Restrepo, O. Sánchez, S. Marulanda Moreno, N. Galeano, and G. Taborda, “African Journal of Biotechnology Evaluation of plant-growth promoting properties of Gluconacetobacter diazotrophicus and Gluconacetobacter sacchari isolated from sugarcane and tomato in West Central region of Colombia,” *Afr J Biotechnol*, vol. 16, pp. 1619–1629, Jul. 2017, doi: 10.5897/AJB2017.16016.

[177] D. Uddin, H. Ahmad, M. Hassan, S. Mahbuba, and M. Z. K. Roni, “EFFECTS OF Trichoderma SPP. ON GROWTH AND YIELD CHARACTERS OF BARI TOMATO-14,” *INTERNATIONAL JOURNAL OF BUSINESS, SOCIAL AND SCIENTIFIC RESEARCH*, vol. 4, pp. 117–122, Jan. 2016.

[178] M. De Palma, R. Scotti, N. D’Agostino, M. Zaccardelli, and M. Tucci, “Phyto-Friendly Soil Bacteria and Fungi Provide Beneficial Outcomes in the Host Plant by Differently Modulating Its Responses through (In)Direct Mechanisms.,” *Plants (Basel)*, vol. 11, no. 20, Oct. 2022, doi: 10.3390/plants11202672.

[179] K. Velmourougane, R. Prasanna, G. Chawla, L. Nain, A. Kumar, and A. K. Saxena, “Trichoderma-Azotobacter biofilm inoculation improves soil nutrient availability and plant growth in wheat and cotton.,” *J Basic Microbiol*, vol. 59, no. 6, pp. 632–644, Jun. 2019, doi: 10.1002/jobm.201900009.

[180] V. de A. Moreira *et al.*, “Inoculation with Trichoderma harzianum and Azospirillum brasilense increases nutrition and yield of hydroponic lettuce,” *Arch Microbiol*, vol. 204, no. 7, p. 440, 2022, doi: 10.1007/s00203-022-03047-w.

[181] S. Jeanson, J. Floury, V. Gagnaire, S. Lortal, and A. Thierry, “Bacterial Colonies in Solid Media and Foods: A Review on Their Growth and Interactions with the Micro-Environment,” *Front Microbiol*, vol. 6, no. December, 2015, doi: 10.3389/fmicb.2015.01284.

[182] L.-S. A, G.-L. Gao, G.-D. Ding, Y. Zhang, H.-Y. Cao, and Y.-J. DU, “[Eco-physiological functions of soil microbial biofilms: A review].,” *Ying Yong Sheng Tai Xue Bao*, vol. 33, no. 7, pp. 1885–1892, Jul. 2022, doi: 10.13287/j.1001-9332.202207.006.

[183] R. V. Serrato *et al.*, “Structural studies of an exopolysaccharide produced by Gluconacetobacter diazotrophicus Pal5,” *Carbohydr Polym*, vol. 98, no. 1, pp. 1153–1159, 2013, doi: 10.1016/j.carbpol.2013.07.025.

[184] C. H. S. G. Meneses, L. F. M. Rouws, J. L. Simões-Araújo, M. S. Vidal, and J. I. Baldani, “Exopolysaccharide production is required for biofilm formation and plant colonization by the nitrogen-fixing endophyte Gluconacetobacter diazotrophicus,” *Molecular Plant-Microbe Interactions*, vol. 24, no. 12, pp. 1448–1458, 2011, doi: 10.1094/MPMI-05-11-0127.

[185] P. T. Cong *et al.*, “Inoculant plant growth-promoting microorganisms enhance utilisation of urea-N and grain yield of paddy rice in southern Vietnam,” *Eur J Soil Biol*, vol. 45, no. 1, pp. 52–61, 2009, doi: https://doi.org/10.1016/j.ejsobi.2008.06.006.

[186] R. Deaker and A. C. for I. A. Research, Eds., *Practical methods for the quality control of inoculant biofertilisers / Rosalind Deaker ... [et al.]*. in ACIAR monograph series ; no. 147. Canberra: Australian Centre for International Agricultural Research, 2011.

[187] P. A. Wani, M. S. Khan, and A. Zaidi, “Effect of metal tolerant plant growth promoting Bradyrhizobium sp. (vigna) on growth, symbiosis, seed yield and metal uptake by greengram plants.,” *Chemosphere*, vol. 70, no. 1, pp. 36–45, Nov. 2007, doi: 10.1016/j.chemosphere.2007.07.028.

[188] C. K. Nielsen, J. Kjems, T. Mygind, T. Snabe, and R. L. Meyer, “Effects of Tween 80 on Growth and Biofilm Formation in Laboratory Media.,” *Front Microbiol*, vol. 7, p. 1878, 2016, doi: 10.3389/fmicb.2016.01878.

[189] Z. Dong *et al.*, “A Nitrogen-Fixing Endophyte of Sugarcane Stems’ A New Role for the Apoplast,” 1994.

[190] J. Lynch, P. Marschner, and Z. Rengel, “Chapter 13 - Effect of Internal and External Factors on Root Growth and Development,” P. B. T.-M. M. N. of H. P. (Third E. Marschner, Ed., San Diego: Academic Press, 2012, pp. 331–346. doi: https://doi.org/10.1016/B978-0-12-384905-2.00013-3.

[191] J. Muñoz-Rojas and J. Caballero-Mellado, “Population Dynamics of Gluconacetobacter diazotrophicus in Sugarcane Cultivars and Its Effect on Plant Growth,” *Microb Ecol*, vol. 46, no. 4, pp. 454–464, 2003, doi: 10.1007/s00248-003-0110-3.

[192] T. L. G. Carvalho, A. C. Rosman, C. Grativol, E. de M. Nogueira, J. I. Baldani, and A. S. Hemerly, “Sugarcane Genotypes with Contrasting Biological Nitrogen Fixation Efficiencies Differentially Modulate Nitrogen Metabolism, Auxin Signaling, and Microorganism Perception Pathways,” *Plants*, vol. 11, no. 15. 2022. doi: 10.3390/plants11151971.

[193] E. French, T. Tran, and A. S. Iyer-Pascuzzi, “Tomato genotype modulates selection and responses to root microbiota,” *Phytobiomes J*, vol. 4, no. 4, pp. 314–326, 2020, doi: 10.1094/PBIOMES-02-20-0020-R.

[194] J. Taffner, A. Bergna, T. Cernava, and G. Berg, “Tomato-Associated Archaea Show a Cultivar-Specific Rhizosphere Effect but an Unspecific Transmission by Seeds,” *Phytobiomes J*, vol. 4, no. 2, pp. 133–141, Apr. 2020, doi: 10.1094/PBIOMES-01-20-0017-R.

[195] A. F. Bent, “Arabidopsis in Planta Transformation. Uses, Mechanisms, and Prospects for Transformation of Other Species1,” *Plant Physiol*, vol. 124, no. 4, pp. 1540–1547, Dec. 2000, doi: 10.1104/pp.124.4.1540.

[196] J. M. van der Wolf *et al.*, “Virulence of Pectobacterium carotovorum subsp. brasiliense on potato compared with that of other Pectobacterium and Dickeya species under climatic conditions prevailing in the Netherlands,” *Plant Pathol*, vol. 66, no. 4, pp. 571–583, May 2017, doi: https://doi.org/10.1111/ppa.12600.

[197] C. Jiang, M. Johkan, M. Hohjo, S. Tsukagoshi, and T. Maruo, “A correlation analysis on chlorophyll content and SPAD value in tomato leaves,” *HortResearch*, vol. 71, pp. 37–42, Mar. 2017, doi: 10.20776/S18808824-71-P37.

[198] O. A. de O. Maria, M. de F. A. Sueli, de F. M. F. Elaine, F. L. de F. Hiago, and F. L. Cristiane, “Relative chlorophyll index on doses of nitrogen fertilization for cherry tomato culture,” *Afr J Agric Res*, vol. 12, no. 39, pp. 2946–2953, 2017, doi: 10.5897/ajar2016.12051.

[199] I. Prsa, F. Stampar, D. Vodnik, and R. Veberi\vc, “Influence of nitrogen on leaf chlorophyll content and photosynthesis of ‘Golden Delicious’ apple,” *Acta Agric Scand B Soil Plant Sci*, vol. 57, pp. 283–289, 2007.

[200] D. Yan, L. Duermeyer, C. Leoveanu, and E. Nambara, “The Functions of the Endosperm During Seed Germination,” *Plant Cell Physiol*, vol. 55, no. 9, pp. 1521–1533, Sep. 2014, doi: 10.1093/pcp/pcu089.

[201] A. L. Botta, A. Santacecilia, C. Ercole, P. Cacchio, and M. del Gallo, “In vitro and in vivo inoculation of four endophytic bacteria on Lycopersicon esculentum,” *N Biotechnol*, vol. 30, no. 6, pp. 666–674, Sep. 2013, doi: 10.1016/j.nbt.2013.01.001.

[202] B. Li, M. K. Shukla, and T. Du, “Combined environmental stresses induced by drip irrigation positively affect most solar greenhouse grown tomato fruit quality,” *Sci Hortic*, vol. 288, p. 110334, 2021, doi: https://doi.org/10.1016/j.scienta.2021.110334.

[203] N. I. Kolev, “Solubility of O2, N2, H2 and CO2 in water BT - Multiphase Flow Dynamics 4: Turbulence, Gas Adsorption and Release, Diesel Fuel Properties,” N. I. Kolev, Ed., Berlin, Heidelberg: Springer Berlin Heidelberg, 2012, pp. 209–239. doi: 10.1007/978-3-642-20749-5_11.

[204] “The Hoaglands Solution for Hydroponic Cultivation – Science in Hydroponics.” Accessed: Nov. 17, 2022. [Online]. Available: https://scienceinhydroponics.com/2009/02/the-hoaglands-solution-for-hydroponic-cultivation.html

[205] O. Achilea and U. Kafkafi, “Enhanced Performance of Processing Tomatoes by Potassium Nitrate based Nutrition,” *Acta Hortic*, vol. 613, Jan. 2003, doi: 10.17660/ActaHortic.2003.613.8.

[206] M. P. Stephan, M. Oliveira, K. R. S. Teixeira, G. Martinez-Drets, and J. Döbereiner, “Physiology and dinitrogen fixation of Acetobacter diazotrophicus,” *FEMS Microbiol Lett*, vol. 77, no. 1, pp. 67–72, 1991, doi: 10.1111/j.1574-6968.1991.tb04323.x.

[207] L. E. Fuentes-Ramírez, J. Caballero-Mellado, J. Sepúlveda, and E. Martínez-Romero, “Colonization of sugarcane by Acetobacter diazotrophicus is inhibited by high N-fertilization,” *FEMS Microbiol Ecol*, vol. 29, no. 2, pp. 117–128, 1999, doi: 10.1016/S0168-6496(98)00125-1.

[208] M. Franchini, “Investigations on the interactions between the endophyte nitrogen fixing bacterium Gluconacetobacter diazotrophicus and tomato plants.,” *PhD thesis - University of Nottingham*, no. September, 2021.

[209] M. H. Jensen and A. J. Malter, “Protected Agriculture: A Global Review. World Bank Technical Paper No. 251.,” *Exp Agric*, vol. 32, no. 2, pp. 233–234, 1995, doi: DOI: 10.1017/S0014479700026193.

[210] D. Neocleous, G. Nikolaou, G. Ntatsi, and D. Savvas, “Nitrate supply limitations in tomato crops grown in a chloride-amended recirculating nutrient solution,” *Agric Water Manag*, vol. 258, p. 107163, 2021, doi: https://doi.org/10.1016/j.agwat.2021.107163.

[211] J. I. Baldani, V. M. Reis, S. S. Videira, L. H. Boddey, and V. L. D. Baldani, “The art of isolating nitrogen-fixing bacteria from non-leguminous plants using N-free semi-solid media: a practical guide for microbiologists,” *Plant Soil*, vol. 384, no. 1–2, pp. 413–431, Oct. 2014, doi: 10.1007/s11104-014-2186-6.

[212] J. Döbereiner, V. M. Reis, M. A. Paula, and F. Olivares, “Endophytic Diazotrophs in Sugar Cane, Cereals and Tuber Plants,” in *New Horizons in Nitrogen Fixation: Proceedings of the 9th International Congress on Nitrogen Fixation, Cancún, Mexico, December 6–12, 1992*, R. Palacios, J. Mora, and W. E. Newton, Eds., Dordrecht: Springer Netherlands, 1993, pp. 671–676. doi: 10.1007/978-94-017-2416-6_55.

[213] L. Silva, R. Boddey, and V. Reis, “Quantification of natural populations of Gluconacetobacter diazotrophicus and Herbaspirillum spp. In sugar cane (Saccharum spp.) Using differente polyclonal antibodies,” *Braz J Microbiol*, vol. 40, pp. 866–878, Oct. 2009, doi: 10.1590/S1517-838220090004000018.

[214] G. Tcherkez, “Natural 15N/14N isotope composition in C3 leaves: are enzymatic isotope effects informative for predicting the 15N-abundance in key metabolites?,” *Functional Plant Biology*, vol. 38, p. 1, Jan. 2011, doi: 10.1071/FP10091.

[215] D. Neocleous, G. Nikolaou, G. Ntatsi, and D. Savvas, “Nitrate supply limitations in tomato crops grown in a chloride-amended recirculating nutrient solution,” *Agric Water Manag*, vol. 258, p. 107163, 2021, doi: https://doi.org/10.1016/j.agwat.2021.107163.

[216] N. Eskin, K. Vessey, and L. Tian, “Research progress and perspectives of nitrogen fixing bacterium, gluconacetobacter diazotrophicus, in monocot plants,” *International Journal of Agronomy*, vol. 2014, 2014, doi: 10.1155/2014/208383.

[217] J. K. Vessey and B. Pan, “Living a Grounded Life: Growth and Nitrogenase Activity of Gluconacetobacter diazotrophicus on Solid Media in Response to Culture Conditions,” 2003.

[218] Y. Liu, N. Lai, K. Gao, F. Chen, L. Yuan, and G. Mi, “Ammonium Inhibits Primary Root Growth by Reducing the Length of Meristem and Elongation Zone and Decreasing Elemental Expansion Rate in the Root Apex in Arabidopsis thaliana,” *PLoS One*, vol. 8, no. 4, pp. e61031-, Apr. 2013, [Online]. Available: https://doi.org/10.1371/journal.pone.0061031

[219] D. Marino and J. F. Moran, “Can Ammonium Stress Be Positive for Plant Performance?,” *Front Plant Sci*, vol. 10, Sep. 2019, doi: 10.3389/fpls.2019.01103.

[220] M. Sevilla, R. H. Burris, N. Gunapala, and C. Kennedy, “Comparison of benefit to sugarcane plant growth and 15N2 incorporation following inoculation of sterile plants with acetobacter diazotrophicus wild-type and Nif- mutant strains,” *Molecular Plant-Microbe Interactions*, vol. 14, no. 3, pp. 358–366, 2001, doi: 10.1094/MPMI.2001.14.3.358.

[221] E. K. James, F. L. Olivares, A. L. M. de Oliveira, F. B. dos Reis Jr, L. G. da Silva, and V. M. Reis, “Further observations on the interaction between sugar cane and Gluconacetobacter diazotrophicus under laboratory and greenhouse conditions1,” *J Exp Bot*, vol. 52, no. 357, pp. 747–760, Apr. 2001, doi: 10.1093/jexbot/52.357.747.

[222] J. Hallmann, A. Quadt-Hallmann, W. F. Mahaffee, and J. W. Kloepper, “Bacterial endophytes in agricultural crops,” *Can J Microbiol*, vol. 43, no. 10, pp. 895–914, Oct. 1997, doi: 10.1139/m97-131.

[223] M. Sevilla, A. de Oliveira, I. Baldani, and C. KENNEDYl, “Contributions of the Bacterial Endophyte Acetobacter diazotrophicus to Sugarcane Nutrition: A Preliminary Study,” 1998.

[224] D. Barraclough, “15N isotope dilution techniques to study soil nitrogen transformations and plant uptake,” *Fertilizer research*, vol. 42, no. 1, pp. 185–192, 1995, doi: 10.1007/BF00750513.

[225] E. Lima, R. M. Boddey, and J. ~xbereiner, “QUANTIFICATION OF BIOLOGICAL NITROGEN FIXATION ASSOCIATED WITH SUGAR CANE USING A 15N AIDED NITROGEN BALANCE,” 1987.

[226] S. Urquiaga, K. H. S. Cruz, and R. M. Boddey, “Contribution of Nitrogen Fixation to Sugar Cane: Nitrogen-15 and Nitrogen-Balance Estimates.”

[227] D. Xiong *et al.*, “SPAD-based leaf nitrogen estimation is impacted by environmental factors and crop leaf characteristics,” *Sci Rep*, vol. 5, no. 1, p. 13389, 2015, doi: 10.1038/srep13389.

[228] K. Zhang, Y. Wu, and H. Hang, “Differential contributions of NO3−/NH4+ to nitrogen use in response to a variable inorganic nitrogen supply in plantlets of two Brassicaceae species in vitro,” *Plant Methods*, vol. 15, no. 1, Jul. 2019, doi: 10.1186/S13007-019-0473-1.

[229] M. A. Paula, S. Urquiaga, J. O. Siqueira, and J. D6bereiner, “Biology and Fe~ty of Soils Synergistic effects of vesicular-arbuscular mycorrhizal fungi and diazotrophic bacteria on nutrition and growth of sweet potato (Ipomoea batatas),” 1992.

[230] M. Shinohara *et al.*, “Microbial mineralization of organic nitrogen into nitrate to allow the use of organic fertilizer in hydroponics,” *Soil Sci Plant Nutr*, vol. 57, no. 2, pp. 190–203, 2011, doi: 10.1080/00380768.2011.554223.

[231] V. M. Reis, F. L. Olivares, A. L. M. de Oliveira, F. Bueno dos Reis Junior, J. I. Baldani, and J. Döbereiner, “Technical approaches to inoculate micropropagated sugar cane plants were Acetobacter diazotrophicus,” *Plant Soil*, vol. 206, no. 2, pp. 205–211, 1999, doi: 10.1023/A:1004436611397.

[232] E. H. Cojho, V. M. Reis, A. C. G. Schenberg, and J. Döbereiner, “Interactions of Acetobacter diazotrophicus with an amylolytic yeast in nitrogen-free batch culture,” *FEMS Microbiol Lett*, vol. 106, no. 3, pp. 341–346, Feb. 1993, doi: 10.1111/j.1574-6968.1993.tb05986.x.

[233] L. D. B. Roncato-Maccari *et al.*, “Endophytic Herbaspirillum seropedicae expresses nif genes in gramineous plants,” *FEMS Microbiol Ecol*, vol. 45, no. 1, pp. 39–47, Jul. 2003, doi: 10.1016/S0168-6496(03)00108-9.

[234] N. K. Fukagawa and L. H. Ziska, “Rice: Importance for Global Nutrition.,” *J Nutr Sci Vitaminol (Tokyo)*, vol. 65, no. Supplement, pp. S2–S3, 2019, doi: 10.3177/jnsv.65.S2.

[235] “Types of rice | The Rice Association.” Accessed: Nov. 19, 2022. [Online]. Available: https://www.riceassociation.org.uk/types-of-rice

[236] L. J. Ding, H. L. Cui, S. A. Nie, X. E. Long, G. L. Duan, and Y. G. Zhu, “Microbiomes inhabiting rice roots and rhizosphere,” *FEMS Microbiol Ecol*, vol. 95, no. 5, pp. 1–13, 2019, doi: 10.1093/femsec/fiz040.

[237] L.-J. Ding, X.-L. An, S. Li, G.-L. Zhang, and Y.-G. Zhu, “Nitrogen Loss through Anaerobic Ammonium Oxidation Coupled to Iron Reduction from Paddy Soils in a Chronosequence,” *Environ Sci Technol*, vol. 48, no. 18, pp. 10641–10647, Sep. 2014, doi: 10.1021/es503113s.

[238] A. A. APP, I. WATANABE, T. S. VENTURA, M. BRAVO, and C. D. JUREY, “THE EFFECT OF CULTIVATED AND WILD RICE VARIETIES ON THE NITROGEN BALANCE OF FLOODED SOIL,” *Soil Sci*, vol. 141, no. 6, 1986.

[239] M. Engelhard, T. Hurek, and B. Reinhold-Hurek, “Preferential occurrence of diazotrophic endophytes, Azoarcus spp., in wild rice species and land races of Oryza sativa in comparison with modern races.,” *Environ Microbiol*, vol. 2, no. 2, pp. 131–141, Apr. 2000, doi: 10.1046/j.1462-2920.2000.00078.x.

[240] M. GILLIS *et al.*, “Polyphasic Taxonomy in the Genus Burkholderia Leading to an Emended Description of the Genus and Proposition of Burkholderia vietnamiensis sp. nov. for N2-Fixing Isolates from Rice in Vietnam,” *Int J Syst Bacteriol*, vol. 45, no. 2, pp. 274–289, Apr. 1995, doi: 10.1099/00207713-45-2-274.

[241] P. Gyaneshwar, E. K. James, N. Mathan, P. M. Reddy, B. Reinhold-Hurek, and J. K. Ladha, “Endophytic colonization of rice by a diazotrophic strain of Serratia marcescens.,” *J Bacteriol*, vol. 183, no. 8, pp. 2634–2645, Apr. 2001, doi: 10.1128/JB.183.8.2634-2645.2001.

[242] Y. G. Yanni *et al.*, “Natural endophytic association between Rhizobium leguminosarum bv. trifolii and rice roots and assessment of its potential to promote rice growth,” *Plant Soil*, vol. 194, no. 1, pp. 99–114, 1997, doi: 10.1023/A:1004269902246.

[243] T. Ueda, Y. Suga, N. Yahiro, and T. Matsuguchi, “Remarkable N2-fixing bacterial diversity detected in rice roots by molecular evolutionary analysis of nifH gene sequences.,” *J Bacteriol*, vol. 177, no. 5, pp. 1414–1417, Mar. 1995, doi: 10.1128/jb.177.5.1414-1417.1995.

[244] T. L. G. Carvalho, E. Balsemão-Pires, R. M. Saraiva, P. C. G. Ferreira, and A. S. Hemerly, “Nitrogen signalling in plant interactions with associative and endophytic diazotrophic bacteria,” *J Exp Bot*, vol. 65, no. 19, pp. 5631–5642, 2014, doi: 10.1093/jxb/eru319.

[245] J. Edwards *et al.*, “Structure, variation, and assembly of the root-associated microbiomes of rice,” *Proc Natl Acad Sci U S A*, vol. 112, no. 8, pp. E911–E920, Feb. 2015, doi: 10.1073/pnas.1414592112.

[246] P. Malarvizhi and J. K. Ladha, “Influence of Available Nitrogen and Rice Genotype on Associative Dinitrogen Fixation,” *Soil Science Society of America Journal*, vol. 63, no. 1, pp. 93–99, Jan. 1999, doi: https://doi.org/10.2136/sssaj1999.03615995006300010015x.

[247] B. G. Rolfe *et al.*, “Root morphogenesis in legumes and cereals and the effect of bacterial inoculation on root development BT - Opportunities for Biological Nitrogen Fixation in Rice and Other Non-Legumes: Papers presented at the Second Working Group Meeting of the Frontier Project on Nitrogen Fixation in Rice held at the National Institute for Biotechnology and Genetic Engineering (NIBGE), Faisalabad, Pakistan, 13–15 October 1996,” J. K. Ladha, F. J. de Bruijn, and K. A. Malik, Eds., Dordrecht: Springer Netherlands, 1997, pp. 131–144. doi: 10.1007/978-94-011-7113-7_13.

[248] M. Sevilla, Kennedy. C., J. K. (Jagdish K. Ladha, P. M. Reddy, and P. Working Group Meeting on Assessing Opportunities for Nitrogen Fixation in Rice (3rd : 1999 : Los Baños, *Colonization of rice and other cereals by Acetobacter diazotrophicus an endophyte of sugarcane (from “The quest for nitrogen fixation in rice”)*. International Rice Research Institute, 2000.

[249] R. Muthukumarasamy *et al.*, “Natural association of Gluconacetobacter diazotrophicus and diazotrophic Acetobacter peroxydans with wetland rice,” *Syst Appl Microbiol*, vol. 28, no. 3, pp. 277–286, 2005, doi: 10.1016/j.syapm.2005.01.006.

[250] R. Muthukumarasamy *et al.*, “Enumeration, isolation and identification of diazotrophs from Korean wetland rice varieties grown with long-term application of N and compost and their short-term inoculation effect on rice plants,” *J Appl Microbiol*, vol. 102, no. 4, pp. 981–991, Apr. 2007, doi: 10.1111/j.1365-2672.2006.03157.x.

[251] M. Govindarajan, J. Balandreau, S. W. Kwon, H. Y. Weon, and C. Lakshminarasimhan, “Effects of the inoculation of Burkholderia vietnamensis and related endophytic diazotrophic bacteria on grain yield of rice,” *Microb Ecol*, vol. 55, no. 1, pp. 21–37, 2008, doi: 10.1007/S00248-007-9247-9.

[252] B. Wang and S. Sugiyama, “Phylogenetic signal of host plants in the bacterial and fungal root microbiomes of cultivated angiosperms,” *Plant Journal*, vol. 104, no. 2, pp. 522–531, 2020, doi: 10.1111/tpj.14943.

[253] H. Gamal-Eldin and K. Elbanna, “Field evidence for the potential of Rhodobacter capsulatus as Biofertilizer for flooded rice.,” *Curr Microbiol*, vol. 62, no. 2, pp. 391–395, Feb. 2011, doi: 10.1007/s00284-010-9719-x.

[254] E. K. James *et al.*, “Infection and Colonization of Rice Seedlings by the Plant Growth-Promoting Bacterium Herbaspirillum seropedicae Z67,” *https://doi.org/10.1094/MPMI.2002.15.9.894*, vol. 15, no. 9, pp. 894–906, Feb. 2007, doi: 10.1094/MPMI.2002.15.9.894.

[255] J. K. BARIK, P. K. MOHAPATRA, S. K. PRADHAN, and E. KARIALI, “De-hulling facilitates seed germination and ethylene production in dormant and non-dormant rice genotypes,” *J Agric Sci*, vol. 155, no. 10, pp. 1508–1519, 2017, doi: DOI: 10.1017/S0021859617000697.

[256] R. Santos, D. Hérouart, A. Puppo, and D. Touati, “Critical protective role of bacterial superoxide dismutase in Rhizobium-legume symbiosis,” *Mol Microbiol*, vol. 38, no. 4, pp. 750–759, 2000, doi: 10.1046/j.1365-2958.2000.02178.x.

[257] S. Alquéres *et al.*, “The bacterial superoxide dismutase and glutathione reductase are crucial for endophytic colonization of rice roots by Gluconacetobacter diazotrophicus PAL5,” *Molecular Plant-Microbe Interactions*, vol. 26, no. 8, pp. 937–945, Aug. 2013, doi: 10.1094/MPMI-12-12-0286-R.

[258] L. Filgueiras, R. Silva, I. Almeida, M. Vidal, J. I. Baldani, and C. H. S. G. Meneses, “Gluconacetobacter diazotrophicus mitigates drought stress in Oryza sativa L.,” *Plant Soil*, vol. 451, no. 1–2, pp. 57–73, Jun. 2020, doi: 10.1007/s11104-019-04163-1.

[259] E. de Matos Nogueira *et al.*, “Expression of sugarcane genes induced by inoculation with Gluconacetobacter diazotrophicus and Herbaspirillum rubrisubalbicans.” [Online]. Available: http://sucest.lad.ic.unicamp.br/en/

[260] Z. DONG, M. E. McCULLY, and M. J. CANNY, “Does Acetobacter diazotrophicus Live and Move in the Xylem of Sugarcane Stems? Anatomical and Physiological Data,” *Ann Bot*, vol. 80, no. 2, pp. 147–158, 1997, [Online]. Available: http://www.jstor.org/stable/42765472

[261] M. V. Rodriguez *et al.*, “Anatomical and Biochemical Changes Induced by Gluconacetobacter diazotrophicus Stand Up for Arabidopsis thaliana Seedlings From Ralstonia solanacearum Infection,” *Front Plant Sci*, vol. 10, Dec. 2019, doi: 10.3389/fpls.2019.01618.

[262] A. L. S. Rangel de Souza *et al.*, “Endophytic colonization of Arabidopsis thaliana by Gluconacetobacter diazotrophicus and its effect on plant growth promotion, plant physiology, and activation of plant defense,” *Plant Soil*, vol. 399, no. 1–2, pp. 257–270, Feb. 2016, doi: 10.1007/s11104-015-2672-5.

[263] J. D. Wang and P. A. Levin, “Metabolism, cell growth and the bacterial cell cycle,” *Nat Rev Microbiol*, vol. 7, no. 11, pp. 822–827, 2009, doi: 10.1038/nrmicro2202.

[264] M. Zakria, K. Udonishi, T. Ogawa, A. Yamamoto, Y. Saeki, and S. Akao, “Influence of inoculation technique on the endophytic colonization of rice by Pantoea sp. isolated from sweet potato and by Enterobacter sp. isolated from sugarcane,” *Soil Sci Plant Nutr*, vol. 54, no. 2, pp. 224–236, 2008, doi: 10.1111/j.1747-0765.2007.00233.x.

[265] M. S. Ngalimat *et al.*, “Plant growth-promoting bacteria as an emerging tool to manage bacterial rice pathogens,” *Microorganisms*, vol. 9, no. 4. MDPI AG, Apr. 01, 2021. doi: 10.3390/microorganisms9040682.

[266] H. Liu *et al.*, “Inner plant values: Diversity, colonization and benefits from endophytic bacteria,” *Frontiers in Microbiology*, vol. 8, no. DEC. Frontiers Media S.A., Dec. 19, 2017. doi: 10.3389/fmicb.2017.02552.

[267] M. Bacilio-Jiménez, S. Aguilar-Flores, E. Ventura-Zapata, E. Pérez-Campos, S. Bouquelet, and E. Zenteno, “Chemical characterization of root exudates from rice (Oryza sativa) and their effects on the chemotactic response of endophytic bacteria,” *Plant Soil*, vol. 249, no. 2, pp. 271–277, Feb. 2003, doi: 10.1023/A:1022888900465/METRICS.

[268] “Diminishing returns - Wikipedia.” Accessed: Jan. 18, 2023. [Online]. Available: https://en.wikipedia.org/wiki/Diminishing_returns

[269] X. Wang, P. Wu, M. Xia, Z. Wu, Q. Chen, and F. Liu, “Identification of genes enriched in rice roots of the local nitrate treatment and their expression patterns in split-root treatment,” *Gene*, vol. 297, no. 1, pp. 93–102, 2002, doi: https://doi.org/10.1016/S0378-1119(02)00870-3.

[270] Y. Wang, Y. Ohara, H. Nakayashiki, Y. Tosa, and S. Mayama, “Microarray Analysis of the Gene Expression Profile Induced by the Endophytic Plant Growth-Promoting Rhizobacteria, Pseudomonas fluorescens FPT9601-T5 in Arabidopsis,” *Molecular Plant-Microbe Interactions®*, vol. 18, no. 5, pp. 385–396, May 2005, doi: 10.1094/MPMI-18-0385.

[271] E. C. Cocking, P. J. Stone, and M. R. Davey, “Intracellular colonization of roots of Arabidopsis and crop plants by Gluconacetobacter diazotrophicus,” *In Vitro Cellular and Developmental Biology - Plant*, vol. 42, no. 1, pp. 74–82, Jan. 2006, doi: 10.1079/IVP2005716.

[272] T. C. dos Santos *et al.*, “Arabidopsis thaliana exudates induce growth and proteomic changes in Gluconacetobacter diazotrophicus,” *PeerJ*, vol. 8, 2020, doi: 10.7717/peerj.9600.

[273] A. Pinski, A. Betekhtin, K. Hupert-Kocurek, L. A. J. Mur, and R. Hasterok, “Defining the genetic basis of plant–endophytic bacteria interactions,” *Int J Mol Sci*, vol. 20, no. 8, 2019, doi: 10.3390/ijms20081947.

[274] P. G. Dennis, A. J. Miller, and P. R. Hirsch, “Are root exudates more important than other sources of rhizodeposits in structuring rhizosphere bacterial communities?,” *FEMS Microbiol Ecol*, vol. 72, no. 3, pp. 313–327, Jun. 2010, doi: 10.1111/j.1574-6941.2010.00860.x.

[275] S. Pierzynowski and K. Pierzynowska, “Alpha-ketoglutarate, a key molecule involved in nitrogen circulation in both animals and plants, in the context of human gut microbiota and protein metabolism,” *Advances in Medical Sciences*, vol. 67, no. 1. Medical University of Bialystok, pp. 142–147, Mar. 01, 2022. doi: 10.1016/j.advms.2022.02.004.

[276] T. Hachiya *et al.*, “Excessive ammonium assimilation by plastidic glutamine synthetase causes ammonium toxicity in Arabidopsis thaliana,” *Nat Commun*, vol. 12, no. 1, Dec. 2021, doi: 10.1038/s41467-021-25238-7.

[277] O. A. Koksharova, I. O. Butenko, O. v. Pobeguts, N. A. Safronova, and V. M. Govorun, “β-N-Methylamino-L-Alanine (BMAA) Causes Severe Stress in Nostoc sp. PCC 7120 Cells under Diazotrophic Conditions: A Proteomic Study,” *Toxins (Basel)*, vol. 13, no. 5, 2021, doi: 10.3390/toxins13050325.

[278] S. Hou *et al.*, “A microbiota–root–shoot circuit favours Arabidopsis growth over defence under suboptimal light,” *Nat Plants*, vol. 7, no. 8, pp. 1078–1092, Aug. 2021, doi: 10.1038/s41477-021-00956-4.

[279] Z. D. Blount, “The unexhausted potential of E. coli,” *Elife*, vol. 4, p. e05826, 2015, doi: 10.7554/eLife.05826.

[280] R. Borriss *et al.*, “Bacillus subtilis, the model Gram-positive bacterium: 20 years of annotation refinement,” *Microb Biotechnol*, vol. 11, no. 1, pp. 3–17, Jan. 2018, doi: https://doi.org/10.1111/1751-7915.13043.

[281] I. Cases and V. Lorenzo, “Genetically modified organisms for the environment: Stories of success and failure and what we have learned from them,” *Int Microbiol*, vol. 8, pp. 213–222, Oct. 2005.

[282] J. Armengaud, J. Trapp, O. Pible, O. Geffard, A. Chaumot, and E. M. Hartmann, “Non-model organisms, a species endangered by proteogenomics,” *J Proteomics*, vol. 105, pp. 5–18, 2014, doi: https://doi.org/10.1016/j.jprot.2014.01.007.

[283] L. A. Riley and A. M. Guss, “Approaches to genetic tool development for rapid domestication of non-model microorganisms,” *Biotechnol Biofuels*, vol. 14, no. 1, pp. 1–17, 2021, doi: 10.1186/s13068-020-01872-z.

[284] M. Bertalan *et al.*, “Complete genome sequence of the sugarcane nitrogen-fixing endophyte Gluconacetobacter diazotrophicus Pal5,” *BMC Genomics*, vol. 10, p. 450, Sep. 2009, doi: 10.1186/1471-2164-10-450.

[285] A. Giongo, H. L. Tyler, U. N. Zipperer, and E. W. Triplett, “Two genome sequences of the same bacterial strain, Gluconacetobacter diazotrophicus PAl 5, suggest a new standard in genome sequence submission,” *Stand Genomic Sci*, vol. 2, no. 3, pp. 309–317, 2010, doi: 10.4056/sigs.972221.

[286] X. Xia, Ed., “Contig assembly,” in *Bioinformatics and the Cell: Modern Computational Approaches in Genomics, Proteomics and Transcriptomics*, Boston, MA: Springer US, 2007, pp. 49–61. doi: 10.1007/978-0-387-71337-3_3.

[287] A. C. E. Darling, B. Mau, F. R. Blattner, and N. T. Perna, “Mauve: Multiple Alignment of Conserved Genomic Sequence With Rearrangements,” *Genome Res*, vol. 14, no. 7, pp. 1394–1403, Jul. 2004, [Online]. Available: http://genome.cshlp.org/content/14/7/1394.abstract

[288] N.-F. Alikhan, N. K. Petty, N. L. ben Zakour, and S. A. Beatson, “BLAST Ring Image Generator (BRIG): simple prokaryote genome comparisons,” *BMC Genomics*, vol. 12, no. 1, p. 402, 2011, doi: 10.1186/1471-2164-12-402.

[289] M. A. Schumacher, “Bacterial plasmid partition machinery: a minimalist approach to survival,” *Curr Opin Struct Biol*, vol. 22, no. 1, pp. 72–79, 2012, doi: https://doi.org/10.1016/j.sbi.2011.11.001.

[290] R. P. Novick, “Plasmid incompatibility,” *Microbiol Rev*, vol. 51, no. 4, pp. 381–395, Dec. 1987, doi: 10.1128/mr.51.4.381-395.1987.

[291] M. R. Green and J. Sambrook, “Transformation of Escherichia coli by Electroporation,” *Cold Spring Harb Protoc*, vol. 2020, no. 6, pp. 232–238, Jun. 2020, doi: 10.1101/pdb.prot101220.

[292] I. P. Sugar and E. Neumann, “Stochastic model for electric field-induced membrane pores electroporation,” *Biophys Chem*, vol. 19, no. 3, pp. 211–225, 1984, doi: https://doi.org/10.1016/0301-4622(84)87003-9.

[293] R. P. Joshi and K. H. Schoenbach, “Electroporation dynamics in biological cells subjected to ultrafast electrical pulses: a numerical simulation study,” *Phys Rev E Stat Phys Plasmas Fluids Relat Interdiscip Topics*, vol. 62, no. 1 Pt B, pp. 1025–1033, 2000, doi: 10.1103/physreve.62.1025.

[294] R. Antoine and C. Locht, “Isolation and molecular characterization of a novel broad-host-range plasmid from Bordetella bronchiseptica with sequence similarities to plasmids from Gram-positive organisms,” *Mol Microbiol*, vol. 6, no. 13, pp. 1785–1799, Jul. 1992, doi: https://doi.org/10.1111/j.1365-2958.1992.tb01351.x.

[295] M. Kovach, R. Phillips, P. Elzer, R. M. I. Roop, and K. M. Peterson, “pBBR1MCS: a broad-host-range cloning vector,” *Biotechniques*, vol. 16, pp. 800–802, Jun. 1994.

[296] H. Yano, M. Shintani, M. Tomita, H. Suzuki, and T. Oshima, “Reconsidering plasmid maintenance factors for computational plasmid design,” *Comput Struct Biotechnol J*, vol. 17, pp. 70–81, 2019, doi: https://doi.org/10.1016/j.csbj.2018.12.001.

[297] M. E. Kovach *et al.*, “Four new derivatives of the broad-host-range cloning vector pBBR1MCS, carrying different antibiotic-resistance cassettes,” 1995.

[298] P. M. Fricke, A. Klemm, M. Bott, and T. Polen, “On the way toward regulatable expression systems in acetic acid bacteria: target gene expression and use cases,” *Appl Microbiol Biotechnol*, vol. 105, no. 9, pp. 3423–3456, 2021, doi: 10.1007/s00253-021-11269-z.

[299] R. Silva-Rocha *et al.*, “The Standard European Vector Architecture (SEVA): a coherent platform for the analysis and deployment of complex prokaryotic phenotypes,” *Nucleic Acids Res*, vol. 41, no. D1, pp. D666–D675, Jan. 2013, doi: 10.1093/nar/gks1119.

[300] A. D. Buch, G. Archana, and G. Naresh Kumar, “Broad-host-range plasmid-mediated metabolic perturbations in Pseudomonas fluorescens 13525,” *Appl Microbiol Biotechnol*, vol. 88, no. 1, pp. 209–218, 2010, doi: 10.1007/s00253-010-2717-x.

[301] J. B. Andersen, C. Sternberg, L. K. Poulsen, S. P. Bjørn, M. Givskov, and S. Molin, “New unstable variants of green fluorescent protein for studies of transient gene expression in bacteria,” *Appl Environ Microbiol*, vol. 64, no. 6, pp. 2240–2246, 1998, doi: 10.1128/aem.64.6.2240-2246.1998.

[302] “GFP - OpenWetWare.” Accessed: Feb. 27, 2023. [Online]. Available: https://openwetware.org/wiki/GFP

[303] B. P. Cormack, R. H. Valdivia, and S. Falkow, “FACS-optimized mutants of the green fluorescent protein (GFP),” *Gene*, vol. 173, no. 1, pp. 33–38, 1996, doi: https://doi.org/10.1016/0378-1119(95)00685-0.

[304] “GFPmut3 :: Fluorescent Protein Database.” Accessed: Feb. 27, 2023. [Online]. Available: https://www.fpbase.org/protein/gfpmut3/

[305] E. Botella *et al.*, “pBaSysBioII: an integrative plasmid generating gfp transcriptional fusions for high-throughput analysis of gene expression in Bacillus subtilis,” *Microbiology (N Y)*, vol. 156, no. 6, pp. 1600–1608, Jun. 2010, doi: 10.1099/mic.0.035758-0.

[306] M. Lanzer and H. Bujard, “Promoters Largely Determine the Efficiency of Repressor Action,” *Proc Natl Acad Sci U S A*, vol. 85, no. 23, pp. 8973–8977, 1988, [Online]. Available: http://www.jstor.org/stable/32868

[307] D. Stüber, H. Matile, and G. Garotta, “8 - System for High-Level Production in Escherichia coli and Rapid Purification of Recombinant Proteins: Application to Epitope Mapping, Preparation of Antibodies, and Structure—Function Analysis,” in *Immunological Methods*, I. LEFKOVITS and B. PERNIS, Eds., Academic Press, 1990, pp. 121–152. doi: https://doi.org/10.1016/B978-0-12-442704-4.50014-1.

[308] Qiagen, “The QIAexpressionist ™ A handbook for high-level expression and purification of 6xHis-tagged proteins Fifth Edition,” 2003. [Online]. Available: www.qiagen.co.jpwww.qiagen.com

[309] H. Bujard *et al.*, “[26] A T5 promoter-based transcription-translation system for the analysis of proteins in Vitro and in Vivo,” in *Methods in Enzymology*, vol. 155, Academic Press, 1987, pp. 416–433. doi: https://doi.org/10.1016/0076-6879(87)55028-5.

[310] K. Thiel, E. Mulaku, H. Dandapani, C. Nagy, E.-M. Aro, and P. Kallio, “Translation efficiency of heterologous proteins is significantly affected by the genetic context of RBS sequences in engineered cyanobacterium Synechocystis sp. PCC 6803,” *Microb Cell Fact*, vol. 17, no. 1, p. 34, 2018, doi: 10.1186/s12934-018-0882-2.

[311] “SnapGene | Software for everyday molecular biology.” Accessed: Mar. 03, 2023. [Online]. Available: https://www.snapgene.com/

[312] van der W. M. W and B. A. J, “Phase and Antigenic Variation in Bacteria,” *Clin Microbiol Rev*, vol. 17, no. 3, pp. 581–611, Jul. 2004, doi: 10.1128/CMR.17.3.581-611.2004.

[313] B. Lau, P. Malkus, and J. Paulsson, “New quantitative methods for measuring plasmid loss rates reveal unexpected stability,” *Plasmid*, vol. 70, Sep. 2013, doi: 10.1016/j.plasmid.2013.07.007.

[314] “Part:BBa J95022 - parts.igem.org.” Accessed: Mar. 01, 2023. [Online]. Available: http://parts.igem.org/Part:BBa_J95022

[315] A. Hopes, V. Nekrasov, S. Kamoun, and T. Mock, “Editing of the urease gene by CRISPR-Cas in the diatom Thalassiosira pseudonana,” *Plant Methods*, vol. 12, no. 1, p. 49, 2016, doi: 10.1186/s13007-016-0148-0.

[316] E. Weber, C. Engler, R. Gruetzner, S. Werner, and S. Marillonnet, “A modular cloning system for standardized assembly of multigene constructs,” *PLoS One*, vol. 6, no. 2, 2011, doi: 10.1371/journal.pone.0016765.

[317] B. J. Bevis and B. S. Glick, “Rapidly maturing variants of the Discosoma red fluorescent protein (DsRed),” *Nat Biotechnol*, vol. 20, no. 1, pp. 83–87, 2002, doi: 10.1038/nbt0102-83.

[318] R. L. Strack *et al.*, “A noncytotoxic DsRed variant for whole-cell labeling,” *Nat Methods*, vol. 5, no. 11, pp. 955–957, 2008, doi: 10.1038/nmeth.1264.

[319] “DsRed-Express2 :: Fluorescent Protein Database.” Accessed: Mar. 09, 2023. [Online]. Available: https://www.fpbase.org/protein/dsred-express2/

[320] R. Wilton *et al.*, “A New Suite of Plasmid Vectors for Fluorescence-Based Imaging of Root Colonizing Pseudomonads,” *Front Plant Sci*, vol. 8, no. February, pp. 1–15, 2018, doi: 10.3389/fpls.2017.02242.

[321] X. Hai, D. Julian, and M. Vivian, “Molecular Characterization of Class 3 Integrons from Delftia spp,” *J Bacteriol*, vol. 189, no. 17, pp. 6276–6283, Sep. 2007, doi: 10.1128/JB.00348-07.

[322] R. M. Hall and C. M. Collis, “Antibiotic resistance in gram-negative bacteria: the role of gene cassettes and integrons,” *Drug Resistance Updates*, vol. 1, no. 2, pp. 109–119, 1998, doi: https://doi.org/10.1016/S1368-7646(98)80026-5.

[323] C. C. M, K. Mi-Jurng, P. S. R, H. W. Stokes, and H. R. M, “Characterization of the Class 3 Integron and the Site-Specific Recombination System It Determines,” *J Bacteriol*, vol. 184, no. 11, pp. 3017–3026, Jun. 2002, doi: 10.1128/JB.184.11.3017-3026.2002.

[324] X. Youqiang, T. Fei, M. Cuiqing, and X. Ping, “New Constitutive Vectors: Useful Genetic Engineering Tools for Biocatalysis,” *Appl Environ Microbiol*, vol. 79, no. 8, pp. 2836–2840, Apr. 2013, doi: 10.1128/AEM.03746-12.

[325] P. O. Olins, C. S. Devine, S. H. Rangwala, and K. S. Kavka, “The T7 phage gene 10 leader RNA, a ribosome-binding site that dramatically enhances the expression of foreign genes in Escherichia coli,” *Gene*, vol. 73, no. 1, pp. 227–235, 1988, doi: https://doi.org/10.1016/0378-1119(88)90329-0.

[326] N. Ryuichi, N. Akiyo, Y. Hisakazu, and O. Ryoichi, “Role of AmpR in the High Expression of the Plasmid-Encoded AmpC β-Lactamase CFE-1,” *mSphere*, vol. 2, no. 4, pp. e00192-17, Aug. 2017, doi: 10.1128/mSphere.00192-17.

[327] H. Yano *et al.*, “Host range diversification within the IncP-1 plasmid group,” *Microbiology (United Kingdom)*, vol. 159, no. PART11, pp. 2303–2315, Nov. 2013, doi: 10.1099/MIC.0.068387-0.

[328] H. Schwab, P. N. Saurugger, and R. M. Lafferty, “Occurrence of deletion plasmids at high rates after conjugative transfer of the plasmids RP4 and RK2 from Escherichia coli to Alcaligenes eutrophus H16,” *Arch Microbiol*, vol. 136, no. 2, pp. 140–146, 1983, doi: 10.1007/BF00404789.

[329] J. Haase, R. Lurz, A. Grahn, D. Bamford, and E. Lanka, “Bacterial conjugation mediated by plasmid RP4: RSF1010 mobilization, donor-specific phage propagation, and pilus production require the same Tra2 core components of a proposed DNA transport complex,” *J Bacteriol*, vol. 177, pp. 4779–4791, Sep. 1995, doi: 10.1128/jb.177.16.4779-4791.1995.

[330] H. Burkardt, G. Riess, and A. Puehler, “Relationship of group P1 plasmids revealed by heteroduplex experiments: RP1, RP4, R68 and RK2 are identical,” *J Gen Microbiol*, vol. 114, no. 2, pp. 341–348, Oct. 1979, doi: 10.1099/00221287-114-2-341/CITE/REFWORKS.

[331] A. Babic, A. M. Guérout, and D. Mazel, “Construction of an improved RP4 (RK2)-based conjugative system,” *Res Microbiol*, vol. 159, no. 7–8, pp. 545–549, Sep. 2008, doi: 10.1016/J.RESMIC.2008.06.004.

[332] C. M. Thomas, C. A. Smith, V. Shingler, M. A. Cross, A. A. K. Hussain, and M. Pinkney, “Regulation of Replication and Maintenance Functions of Broad Host-Range Plasmid RK2,” in *Plasmids in Bacteria*, D. R. Helinski, S. N. Cohen, D. B. Clewell, D. A. Jackson, and A. Hollaender, Eds., Boston, MA: Springer US, 1985, pp. 261–276. doi: 10.1007/978-1-4613-2447-8_21.

[333] M. Jahn, C. Vorpahl, T. Hübschmann, H. Harms, and S. Müller, “Copy number variability of expression plasmids determined by cell sorting and Droplet Digital PCR,” *Microb Cell Fact*, vol. 15, no. 1, p. 211, 2016, doi: 10.1186/s12934-016-0610-8.

[334] L. C. Dekkers, C. C. Phoelich, L. Van Der Fits, and B. J. J. Lugtenberg, “A site-specific recombinase is required for competitive root colonization by Pseudomonas fluorescens WCS365,” *Proc Natl Acad Sci U S A*, vol. 95, no. 12, pp. 7051–7056, Jun. 1998, doi: 10.1073/PNAS.95.12.7051/ASSET/0F43FEA0-9667-40F9-A6E2-0F61D78C51DF/ASSETS/GRAPHIC/PQ1080965002.JPEG.

[335] S. Mowade and P. Bhattacharyya, “Resistance of P-solubilizing Acetobacter diazotrophicus to antibiotics.,” *Curr Sci*, vol. 79, no. 11, pp. 1591–1594, 2000.

[336] J.-D. Pédelacq, S. Cabantous, T. Tran, T. C. Terwilliger, and G. S. Waldo, “Engineering and characterization of a superfolder green fluorescent protein,” *Nat Biotechnol*, vol. 24, no. 1, pp. 79–88, 2006, doi: 10.1038/nbt1172.

[337] “Codon Usage Database.” Accessed: Mar. 18, 2023. [Online]. Available: http://www.kazusa.or.jp/codon/

[338] K. Postle and R. F. Good, “A bidirectional rho-independent transcription terminator between the E. coli tonB gene and an opposing gene,” *Cell*, vol. 41, no. 2, pp. 577–585, Jun. 1985, doi: 10.1016/S0092-8674(85)80030-1.

[339] “Part:BBa K3395014 - parts.igem.org.” Accessed: Mar. 18, 2023. [Online]. Available: http://parts.igem.org/Part:BBa_K3395014

[340] A. OROSZ, I. BOROS, and P. VENETIANER, “Analysis of the complex transcription termination region of the Escherichia coli rrn B gene,” *Eur J Biochem*, vol. 201, no. 3, pp. 653–659, Nov. 1991, doi: https://doi.org/10.1111/j.1432-1033.1991.tb16326.x.

[341] “Part:BBa B0010 - parts.igem.org.” Accessed: Mar. 18, 2023. [Online]. Available: https://parts.igem.org/Part:BBa_B0010

[342] J. J. Dunn and F. W. Studier, “The transcription termination site at the end of the early region of bacteriophage T7 DNA,” *Nucleic Acids Res*, vol. 8, no. 10, pp. 2119–2132, May 1980, doi: 10.1093/nar/8.10.2119.

[343] “Bacterial Transformation Workflow–4 Main Steps - UK”, Accessed: Mar. 19, 2023. [Online]. Available: https://www.thermofisher.com/uk/en/home/life-science/cloning/cloning-learning-center/invitrogen-school-of-molecular-biology/molecular-cloning/transformation/bacterial-transformation-workflow.html

[344] T. Potočnik, D. Miklavčič, and A. Maček Lebar, “Effect of electroporation and recovery medium pH on cell membrane permeabilization, cell survival and gene transfer efficiency in vitro,” *Bioelectrochemistry*, vol. 130, p. 107342, 2019, doi: https://doi.org/10.1016/j.bioelechem.2019.107342.

[345] Y. Ma, Q. Sun, and S. C. Smith, “The mechanism of oxidation in chromophore maturation of wild-type green fluorescent protein: a theoretical study,” *Physical Chemistry Chemical Physics*, vol. 19, no. 20, pp. 12942–12952, 2017, doi: 10.1039/C6CP07983K.

[346] T. Trunk, H. S. Khalil, and J. C. Leo, “Bacterial autoaggregation,” *AIMS Microbiol*, vol. 4, no. 1, pp. 140–164, 2018, doi: 10.3934/microbiol.2018.1.140.

[347] D. C. Karasz, A. I. Weaver, D. H. Buckley, and R. C. Wilhelm, “Conditional filamentation as an adaptive trait of bacteria and its ecological significance in soils,” *Environ Microbiol*, vol. 24, no. 1, pp. 1–17, Jan. 2022, doi: 10.1111/1462-2920.15871.

[348] M. Gillis *et al.*, “Acetobacter diazotrophicus sp. nov., a nitrogen-fixing acetic acid bacterium associated with sugarcane,” *Int J Syst Bacteriol*, vol. 39, no. 3, pp. 361–364, 1989, doi: 10.1099/00207713-39-3-361.

[349] K. D. Young, “The Selective Value of Bacterial Shape,” *Microbiology and Molecular Biology Reviews*, vol. 70, no. 3, p. 660, Sep. 2006, doi: 10.1128/MMBR.00001-06.

[350] M. Regué, J. Enfedaque, S. Camprubi, and J. M. Tomás, “The O-antigen lipopolysaccharide is the major barrier to plasmid DNA uptake by Klebsiella pneumoniae during transformation by electroporation and osmotic shock,” *J Microbiol Methods*, vol. 15, no. 2, pp. 129–134, 1992, doi: https://doi.org/10.1016/0167-7012(92)90077-H.

[351] R. Miah *et al.*, “Major aldehyde dehydrogenase AldFGH of Gluconacetobacter diazotrophicus is independent of pyrroloquinoline quinone but dependent on molybdopterin for acetic acid fermentation,” *Appl Microbiol Biotechnol*, vol. 105, no. 6, pp. 2341–2350, Mar. 2021, doi: 10.1007/s00253-021-11144-x.

[352] https://www.btxonline.com/, “https://www.btxonline.com/media/wysiwyg/protocol_db/Electroporation_Optimization_Guide.pdf.” Accessed: Mar. 20, 2023. [Online]. Available: https://www.btxonline.com/media/wysiwyg/protocol_db/Electroporation_Optimization_Guide.pdf

[353] “Determining Electroporation Cuvette Gap Size - Universal Medical Blog.” Accessed: Mar. 22, 2023. [Online]. Available: https://blog.universalmedicalinc.com/determining-electroporation-cuvette-gap-size/

[354] K. Iwasaki, H. Uchiyama, O. Yagi, T. Kurabayashi, K. Ishizuka, and Y. Takamura, “Transformation of Pseudomonas putida by Electroporation,” *Biosci Biotechnol Biochem*, vol. 58, no. 5, pp. 851–854, Jan. 1994, doi: 10.1271/bbb.58.851.

[355] W. Huang and A. Wilks, “A rapid seamless method for gene knockout in Pseudomonas aeruginosa,” *BMC Microbiol*, vol. 17, no. 1, p. 199, 2017, doi: 10.1186/s12866-017-1112-5.

[356] E. Martínez-García, T. Aparicio, V. de Lorenzo, and P. I. Nikel, “New Transposon Tools Tailored for Metabolic Engineering of Gram-Negative Microbial Cell Factories,” *Front Bioeng Biotechnol*, vol. 2, 2014, [Online]. Available: https://www.frontiersin.org/articles/10.3389/fbioe.2014.00046

[357] X. Yin and G. Stotzky, “Gene Transfer Among Bacteria in Natural Environments,” in *Advances in Applied Microbiology*, vol. 45, S. L. Neidleman and A. I. Laskin, Eds., Academic Press, 1997, pp. 153–212. doi: https://doi.org/10.1016/S0065-2164(08)70263-6.

[358] C. Virolle, K. Goldlust, S. Djermoun, S. Bigot, and C. Lesterlin, “Plasmid transfer by conjugation in gram-negative bacteria: From the cellular to the community level,” *Genes*, vol. 11, no. 11. MDPI AG, pp. 1–33, Nov. 01, 2020. doi: 10.3390/genes11111239.

[359] G. Demarre, A. M. Guérout, C. Matsumoto-Mashimo, D. A. Rowe-Magnus, P. Marlière, and D. Mazel, “A new family of mobilizable suicide plasmids based

on broad host range R388 plasmid (IncW) and RP4 plasmid (IncPα) conjugative machineries and their cognate Escherichia coli host strains," *Res Microbiol*, vol. 156, no. 2, pp. 245–255, 2005, doi: 10.1016/j.resmic.2004.09.007.

[360] C. C. Brinton Jr., "THE STRUCTURE, FUNCTION, SYNTHESIS AND GENETIC CONTROL OF BACTERIAL PILI AND A MOLECULAR MODEL FOR DNA AND RNA TRANSPORT IN GRAM NEGATIVE BACTERIA*," *Trans N Y Acad Sci*, vol. 27, no. 8 Series II, pp. 1003–1054, Jun. 1965, doi: https://doi.org/10.1111/j.2164-0947.1965.tb02342.x.

[361] M. Llosa, F. X. Gomis-Rüth, M. Coll, and F. de la Cruz, "Bacterial conjugation: a two-step mechanism for DNA transport," *Mol Microbiol*, vol. 45, no. 1, pp. 1–8, Jul. 2002, doi: https://doi.org/10.1046/j.1365-2958.2002.03014.x.

[362] S. Samperio, D. L. Guzmán-Herrador, R. May-Cuz, M. C. Martín, M. A. Álvarez, and M. Llosa, "Conjugative DNA Transfer From E. coli to Transformation-Resistant Lactobacilli," *Front Microbiol*, vol. 12, 2021, [Online]. Available: https://www.frontiersin.org/articles/10.3389/fmicb.2021.606629

[363] C. Smillie, M. P. Garcillán-Barcia, M. V. Francia, E. P. C. Rocha, and F. de la Cruz, "Mobility of Plasmids," *Microbiology and Molecular Biology Reviews*, vol. 74, no. 3, pp. 434–452, Sep. 2010, doi: 10.1128/mmbr.00020-10.

[364] L. Ferrières *et al.*, "Silent mischief: Bacteriophage Mu insertions contaminate products of Escherichia coli random mutagenesis performed using suicidal transposon delivery plasmids mobilized by broad-host-range RP4 conjugative machinery," *J Bacteriol*, vol. 192, no. 24, pp. 6418–6427, Dec. 2010, doi: 10.1128/JB.00621-10.

[365] R. Simon, U. Priefer, and A. Pühler, "A Broad Host Range Mobilization System for In Vivo Genetic Engineering: Transposon Mutagenesis in Gram Negative Bacteria," *Bio/Technology*, vol. 1, no. 9, pp. 784–791, 1983, doi: 10.1038/nbt1183-784.

[366] R. Kolter, M. Inuzuka, and D. R. Helinski, "Trans-complementation-dependent replication of a low molecular weight origin fragment from plasmid R6K," *Cell*, vol. 15, no. 4, pp. 1199–1208, 1978, doi: https://doi.org/10.1016/0092-8674(78)90046-6.

[367] V. L. Miller and J. J. Mekalanos, "A novel suicide vector and its use in construction of insertion mutations: osmoregulation of outer membrane proteins and virulence determinants in Vibrio cholerae requires toxR," *J Bacteriol*, vol. 170, no. 6, pp. 2575–2583, Jun. 1988, doi: 10.1128/jb.170.6.2575-2583.1988.

[368] S. A. Rakowski and M. Filutowicz, "Plasmid R6K replication control," *Plasmid*, vol. 69, no. 3, pp. 231–242, 2013, doi: https://doi.org/10.1016/j.plasmid.2013.02.003.

[369] R. A. Jefferson, T. A. Kavanagh, and M. W. Bevan, "GUS fusions: beta-glucuronidase as a sensitive and versatile gene fusion marker in higher

plants.," *EMBO J*, vol. 6, no. 13, p. 3901, Dec. 1987, doi: 10.1002/J.1460-2075.1987.TB02730.X.

[370] M. Novel and G. Novel, "Regulation of β glucuronidase synthesis in Escherichia coli K 12: constitutive mutants specifically derepressed for uidA expression," *J Bacteriol*, vol. 127, no. 1, pp. 406–417, 1976, doi: 10.1128/jb.127.1.406-417.1976.

[371] W. J. Liang *et al.*, "The gusBC Genes of Escherichia coli Encode a Glucuronide Transport System," *J Bacteriol*, vol. 187, no. 7, p. 2377, Apr. 2005, doi: 10.1128/JB.187.7.2377-2385.2005.

[372] A. Guivarc'h, J. C. Caissard, A. Azmi, T. Elmayan, D. Chriqui, and M. Tepfer, "In situ detection of expression of the gus reporter gene in transgenic plants: Ten years of blue genes," *Transgenic Res*, vol. 5, no. 5, pp. 281–288, 1996, doi: 10.1007/BF01968938/METRICS.

[373] R. S. S. Datla, J. K. Hammerlindl, L. E. Pelcher, W. L. Crosby, and G. Selvaraj, "A bifunctional fusion between β-glucuronidase and neomycin phosphotransferase: a broad-spectrum marker enzyme for plants," *Gene*, vol. 101, no. 2, pp. 239–246, May 1991, doi: 10.1016/0378-1119(91)90417-A.

[374] L. Hodal, A. Bochardt, J. E. Nielsen, O. Mattsson, and F. T. Okkels, "Detection, expression and specific elimination of endogenous β-glucuronidase activity in transgenic and non-transgenic plants," *Plant Science*, vol. 87, no. 1, pp. 115–122, Jan. 1992, doi: 10.1016/0168-9452(92)90199-V.

[375] T. Hurek, B. Reinhold-Hurek, M. Van Montagu, and E. Kellenberger, "Root colonization and systemic spreading of Azoarcus sp. strain BH72 in grasses.," *J Bacteriol*, vol. 176, no. 7, p. 1913, 1994, doi: 10.1128/JB.176.7.1913-1923.1994.

[376] G. Van den Eede, R. Deblaere, K. Goethals, M. Van Montagu, and M. Holsters, "Broad host range and promoter selection vectors for bacteria that interact with plants," *Mol Plant Microbe Interact*, vol. 5, no. 3, pp. 228–234, 1992, doi: 10.1094/MPMI-5-228.

[377] D. Hébert, J. R. Kikkert, F. D. Smith, and B. I. Reisch, "Optimization of biolistic transformation of embryogenic grape cell suspensions," *Plant Cell Rep*, vol. 12, no. 10, pp. 585–589, Aug. 1993, doi: 10.1007/BF00233066.

[378] B. Hohn and K. Murray, "Packaging recombinant DNA molecules into bacteriophage particles in vitro.," *Proc Natl Acad Sci U S A*, vol. 74, no. 8, p. 3259, 1977, doi: 10.1073/PNAS.74.8.3259.

[379] G. Del Solar and M. Espinosa, "Plasmid copy number control: an ever-growing story," *Mol Microbiol*, vol. 37, no. 3, pp. 492–500, Aug. 2000, doi: 10.1046/J.1365-2958.2000.02005.X.

[380] J. Finnegan and D. Sherratt, "Plasmid ColE1 conjugal mobility: the nature of bom, a region required in cis for transfer," *Mol Gen Genet*, vol. 185, no. 2, pp. 344–351, Apr. 1982, doi: 10.1007/BF00330810.

[381] E. Murphy, “Nucleotide sequence of a spectinomycin adenyltransferase AAD(9) determinant from Staphylococcus aureus and its relationship to AAD(3") (9),” *Mol Gen Genet*, vol. 200, no. 1, pp. 33–39, Jun. 1985, doi: 10.1007/BF00383309.

[382] J. Leemans, J. Langenakens, H. De Greve, R. Deblaere, M. Van Montagu, and J. Schell, “Broad-host-range cloning vectors derived from the W-plasmid Sa,” *Gene*, vol. 19, no. 3, pp. 361–364, 1982, doi: 10.1016/0378-1119(82)90027-0.

[383] S. Heeb *et al.*, “Small, stable shuttle vectors based on the minimal pVS1 replicon for use in gram-negative, plant-associated bacteria,” *Mol Plant Microbe Interact*, vol. 13, no. 2, pp. 232–237, 2000, doi: 10.1094/MPMI.2000.13.2.232.

[384] E. L. Lagendijk, S. Validov, G. E. M. Lamers, S. De Weert, and G. V. Bloemberg, “Genetic tools for tagging Gram-negative bacteria with mCherry for visualization in vitro and in natural habitats, biofilm and pathogenicity studies,” *FEMS Microbiol Lett*, vol. 305, no. 1, pp. 81–90, Apr. 2010, doi: 10.1111/J.1574-6968.2010.01916.X.

[385] F. Bolivar, “Construction and characterization of new cloning vehicles III. Derivatives of plasmid pBR322 carrying unique Eco RI sites for selection of Eco RI generated recombinant DNA molecules,” *Gene*, vol. 4, no. 2, pp. 121–136, Oct. 1978, doi: 10.1016/0378-1119(78)90025-2.

[386] V. Solovyev and A. Salamov, “Automatic Annotation of Microbial Genomes and Metagenomic Sequences 3 MATERIAL AND METHODS Learning Parameters and Prediction of Protein-Coding Genes,” 2013.

[387] “BPROM - Prediction of bacterial promoters.” Accessed: Apr. 01, 2023. [Online]. Available: http://www.softberry.com/berry.phtml?topic=bprom&group=programs&subgroup=gfindb

[388] R. A. Jefferson, S. M. Burgess, and D. Hirsh, “beta-Glucuronidase from Escherichia coli as a gene-fusion marker.,” *Proc Natl Acad Sci U S A*, vol. 83, no. 22, p. 8447, 1986, doi: 10.1073/PNAS.83.22.8447.

[389] V. de Lorenzo and K. N. Timmis, “Analysis and construction of stable phenotypes in gram-negative bacteria with Tn5- and Tn10-derived minitransposons,” *Methods Enzymol*, vol. 235, no. C, pp. 386–405, Jan. 1994, doi: 10.1016/0076-6879(94)35157-0.

[390] B. Wilbanks and C. T. Trinh, “Comprehensive characterization of toxicity of fermentative metabolites on microbial growth,” *Biotechnol Biofuels*, vol. 10, no. 1, p. 262, Nov. 2017, doi: 10.1186/S13068-017-0952-4.

[391] S. Gómez-Manzo *et al.*, “The Oxidative Fermentation of Ethanol in Gluconacetobacter diazotrophicus Is a Two-Step Pathway Catalyzed by a Single Enzyme: Alcohol-Aldehyde Dehydrogenase (ADHa),” *Int J Mol Sci*, vol. 16, no. 1, p. 1293, Jan. 2015, doi: 10.3390/IJMS16011293.

[392] X. Didelot, G. Méric, D. Falush, and A. E. Darling, “Impact of homologous and non-homologous recombination in the genomic evolution of Escherichia coli,” *BMC Genomics*, vol. 13, no. 1, pp. 1–15, Jun. 2012, doi: 10.1186/1471-2164-13-256/FIGURES/8.

[393] S. C. Kowalczykowski, D. A. Dixon, A. K. Eggleston, S. D. Lauder, and W. M. Rehrauer, “Biochemistry of homologous recombination in Escherichia coli.,” *Microbiol Rev*, vol. 58, no. 3, p. 401, Sep. 1994, doi: 10.1128/MR.58.3.401-465.1994.

[394] G. W. Blakely, A. O. Davidson, and D. J. Sherratt, “Binding and cleavage of nicked substrates by site-specific recombinases XerC and XerD,” *J Mol Biol*, vol. 265, no. 1, pp. 30–39, Jan. 1997, doi: 10.1006/jmbi.1996.0709.

[395] D. Zahradka, K. Zahradka, M. Petranović, D. Dermić, and K. Brčić-KostićK., “The RuvABC resolvase is indispensable for recombinational repair in sbcB15 mutants of Escherichia coli,” *J Bacteriol*, vol. 184, no. 15, pp. 4141–4147, 2002, doi: 10.1128/JB.184.15.4141-4147.2002.

[396] N. Handa, K. Morimatsu, S. T. Lovett, and S. C. Kowalczykowski, “Reconstitution of initial steps of dsDNA break repair by the RecF pathway of E. coli,” *Genes Dev*, vol. 23, no. 10, p. 1234, May 2009, doi: 10.1101/GAD.1780709.

[397] D. Kidane and P. L. Graumann, “Intracellular protein and DNA dynamics in competent Bacillus subtilis cells,” *Cell*, vol. 122, no. 1, pp. 73–84, Jul. 2005, doi: 10.1016/j.cell.2005.04.036.

[398] S. Geng, Q. Tian, S. An, Z. Pan, X. Chen, and X. Jiao, “High-Efficiency, Two-Step Scarless–Markerless Genome Genetic Modification in Salmonella enterica,” *Curr Microbiol*, vol. 72, no. 6, pp. 700–706, Jun. 2016, doi: 10.1007/S00284-016-1002-3/FIGURES/4.

[399] L. A. Riley and A. M. Guss, “Approaches to genetic tool development for rapid domestication of non-model microorganisms,” *Biotechnology for Biofuels 2021 14:1*, vol. 14, no. 1, pp. 1–17, Jan. 2021, doi: 10.1186/S13068-020-01872-Z.

[400] N. Philippe, J. P. Alcaraz, E. Coursange, J. Geiselmann, and D. Schneider, “Improvement of pCVD442, a suicide plasmid for gene allele exchange in bacteria,” *Plasmid*, vol. 51, no. 3, pp. 246–255, May 2004, doi: 10.1016/J.PLASMID.2004.02.003.

[401] J.-M. Reyrat, V. Pelicic, B. Gicquel, and R. Rappuoli, “Counterselectable Markers: Untapped Tools for Bacterial Genetics and Pathogenesis,” *Infect Immun*, vol. 66, no. 9, p. 4011, Sep. 1998, doi: 10.1128/IAI.66.9.4011-4017.1998.

[402] S. Klumpp and T. Hwa, “Traffic patrol in the transcription of ribosomal RNA,” *RNA Biol*, vol. 6, no. 4, p. 392, 2009, doi: 10.4161/RNA.6.4.8952.

[403] K. H. McClean *et al.*, “Quorum sensing and Chromobacterium violaceum: exploitation of violacein production and inhibition for the detection of N-

acylhomoserine lactones," *Microbiology (Reading)*, vol. 143 (Pt 12), no. 12, pp. 3703–3711, 1997, doi: 10.1099/00221287-143-12-3703.

[404] R. Y. Tsien, "The green fluorescent protein," *Annu Rev Biochem*, vol. 67, pp. 509–544, 1998, doi: 10.1146/ANNUREV.BIOCHEM.67.1.509.

[405] T. M. Roberts *et al.*, "Identification and Characterisation of a pH-stable GFP," *Scientific Reports 2016 6:1*, vol. 6, no. 1, pp. 1–9, Jun. 2016, doi: 10.1038/srep28166.

[406] "GFPmut3 :: Fluorescent Protein Database." Accessed: Apr. 05, 2023. [Online]. Available: https://www.fpbase.org/protein/gfpmut3/

[407] M. M. Oliveira, E. T. A. Ramos, M. M. Drechsel, M. S. Vidal, S. Schwab, and J. I. Baldani, "Gluconacin from Gluconacetobacter diazotrophicus PAL5 is an active bacteriocin against phytopathogenic and beneficial sugarcane bacteria," *J Appl Microbiol*, vol. 125, no. 6, pp. 1812–1826, Dec. 2018, doi: 10.1111/JAM.14074.

[408] M. J. Shepherd, J. S. Horton, and T. B. Taylor, "A Near-Deterministic Mutational Hotspot in Pseudomonas fluorescens Is Constructed by Multiple Interacting Genomic Features," *Mol Biol Evol*, vol. 39, no. 6, Jun. 2022, doi: 10.1093/MOLBEV/MSAC132.

[409] A. J. Forsberg, G. D. Pavitt, and C. F. Higgins, "Use of transcriptional fusions to monitor gene expression: a cautionary tale.," *J Bacteriol*, vol. 176, no. 7, p. 2128, 1994, doi: 10.1128/JB.176.7.2128-2132.1994.

[410] W. S. Reznikoff, I. Y. Goryshin, and J. J. Jendrisak, "Tn5 as a molecular genetics tool: In vitro transposition and the coupling of in vitro technologies with in vivo transposition," *Methods Mol Biol*, vol. 260, pp. 83–96, 2004, doi: 10.1385/1-59259-755-6:083.

[411] I. Y. Goryshin, J. Jendrisak, L. M. Hoffman, R. Meis, and W. S. Reznikoff, "Insertional transposon mutagenesis by electroporation of released Tn5 transposition complexes," *Nat Biotechnol*, vol. 18, no. 1, pp. 97–100, 2000, doi: 10.1038/72017.

[412] L. F. M. Rouws, J. L. Simões-Araújo, A. S. Hemerly, and J. I. Baldani, "Validation of a Tn5 transposon mutagenesis system for Gluconacetobacter diazotrophicus through characterization of a flagellar mutant," *Arch Microbiol*, vol. 189, no. 4, pp. 397–405, 2008, doi: 10.1007/s00203-007-0330-x.

[413] B. Green, C. Bouchier, C. Fairhead, N. L. Craig, and B. P. Cormack, "Insertion site preference of Mu, Tn5, and Tn7 transposons," *Mob DNA*, vol. 3, no. 1, pp. 1–6, Feb. 2012, doi: 10.1186/1759-8753-3-3/FIGURES/3.

[414] P. Horvath and R. Barrangou, "CRISPR/Cas, the immune system of bacteria and archaea," *Science*, vol. 327, no. 5962, pp. 167–170, 2010, doi: 10.1126/SCIENCE.1179555.

[415] H. Deveau, J. E. Garneau, and S. Moineau, “CRISPR/Cas system and its role in phage-bacteria interactions,” *Annu Rev Microbiol*, vol. 64, pp. 475–493, Oct. 2010, doi: 10.1146/ANNUREV.MICRO.112408.134123.

[416] S. A. Jackson, R. E. McKenzie, R. D. Fagerlund, S. N. Kieper, P. C. Fineran, and S. J. J. Brouns, “CRISPR-Cas: Adapting to change,” *Science*, vol. 356, no. 6333, Apr. 2017, doi: 10.1126/SCIENCE.AAL5056.

[417] L. A. Marraffini and E. J. Sontheimer, “CRISPR interference: RNA-directed adaptive immunity in bacteria and archaea,” *Nat Rev Genet*, vol. 11, no. 3, p. 181, Mar. 2010, doi: 10.1038/NRG2749.

[418] I. Grissa, G. Vergnaud, and C. Pourcel, “The CRISPRdb database and tools to display CRISPRs and to generate dictionaries of spacers and repeats,” *BMC Bioinformatics*, vol. 8, no. 1, pp. 1–10, May 2007, doi: 10.1186/1471-2105-8-172/FIGURES/5.

[419] K. S. Makarova *et al.*, “Evolutionary classification of CRISPR–Cas systems: a burst of class 2 and derived variants,” *Nature Reviews Microbiology 2019 18:2*, vol. 18, no. 2, pp. 67–83, Dec. 2019, doi: 10.1038/s41579-019-0299-x.

[420] K. S. Makarova *et al.*, “Evolution and classification of the CRISPR–Cas systems,” *Nature Reviews Microbiology 2011 9:6*, vol. 9, no. 6, pp. 467–477, May 2011, doi: 10.1038/nrmicro2577.

[421] D. Couvin *et al.*, “CRISPRCasFinder, an update of CRISRFinder, includes a portable version, enhanced performance and integrates search for Cas proteins,” *Nucleic Acids Res*, vol. 46, no. W1, pp. W246–W251, Jul. 2018, doi: 10.1093/NAR/GKY425.

[422] J. L. McKenzie *et al.*, “A VapBC Toxin-Antitoxin Module Is a Posttranscriptional Regulator of Metabolic Flux in Mycobacteria,” *J Bacteriol*, vol. 194, no. 9, p. 2189, May 2012, doi: 10.1128/JB.06790-11.

[423] X. Y. You *et al.*, “Genomic analysis of Acidianus hospitalis W1 a host for studying crenarchaeal virus and plasmid life cycles,” *Extremophiles*, vol. 15, no. 4, p. 487, Jul. 2011, doi: 10.1007/S00792-011-0379-Y.

[424] M. Li *et al.*, “Toxin-antitoxin RNA pairs safeguard CRISPR-Cas systems,” *Science*, vol. 372, no. 6541, Apr. 2021, doi: 10.1126/SCIENCE.ABE5601.

[425] T. Flusche and R. Rajan, “Molecular Details of DNA Integration by CRISPR-Associated Proteins During Adaptation in Bacteria and Archaea,” *Adv Exp Med Biol*, vol. 1414, 2023, doi: 10.1007/5584_2022_730.

[426] Y. Dhingra, S. K. Suresh, P. Juneja, and D. G. Sashital, “PAM binding ensures orientational integration during Cas4-Cas1-Cas2-mediated CRISPR adaptation,” *Mol Cell*, vol. 82, no. 22, pp. 4353-4367.e6, Nov. 2022, doi: 10.1016/J.MOLCEL.2022.09.030.

[427] K. H. Nam *et al.*, “Cas5d protein processes pre-crRNA and assembles into a cascade-like interference complex in subtype I-C/Dvulg CRISPR-Cas system,”

Structure, vol. 20, no. 9, pp. 1574–1584, Sep. 2012, doi: 10.1016/J.STR.2012.06.016.

[428] T. M. McBride, E. A. Schwartz, A. Kumar, D. W. Taylor, P. C. Fineran, and R. D. Fagerlund, "Diverse CRISPR-Cas Complexes Require Independent Translation of Small and Large Subunits from a Single Gene," *Mol Cell*, vol. 80, no. 6, pp. 971-979.e7, Dec. 2020, doi: 10.1016/J.MOLCEL.2020.11.003.

[429] R. E. O'Brien, J. P. K. Bravo, D. Ramos, G. N. Hibshman, J. T. Wright, and D. W. Taylor, "Structural snapshots of R-loop formation by a type I-C CRISPR Cascade," *Mol Cell*, vol. 83, no. 5, pp. 746-758.e5, Mar. 2023, doi: 10.1016/J.MOLCEL.2023.01.024.

[430] M. L. Hochstrasser, D. W. Taylor, J. E. Kornfeld, E. Nogales, and J. A. Doudna, "DNA Targeting by a Minimal CRISPR RNA-Guided Cascade," *Mol Cell*, vol. 63, no. 5, p. 840, Sep. 2016, doi: 10.1016/J.MOLCEL.2016.07.027.

[431] E. R. Westra *et al.*, "CRISPR immunity relies on the consecutive binding and degradation of negatively supercoiled invader DNA by Cascade and Cas3," *Mol Cell*, vol. 46, no. 5, pp. 595–605, Jun. 2012, doi: 10.1016/J.MOLCEL.2012.03.018.

[432] Y. Xiao, M. Luo, A. E. Dolan, M. Liao, and A. Ke, "Structure basis for RNA-guided DNA degradation by Cascade and Cas3," *Science*, vol. 361, no. 6397, Jul. 2018, doi: 10.1126/SCIENCE.AAT0839.

[433] Y. Zheng *et al.*, "Endogenous Type I CRISPR-Cas: From Foreign DNA Defense to Prokaryotic Engineering," *Front Bioeng Biotechnol*, vol. 8, p. 62, Mar. 2020, doi: 10.3389/FBIOE.2020.00062/BIBTEX.

[434] M. L. Hochstrasser *et al.*, "CasA mediates Cas3-catalyzed target degradation during CRISPR RNA-guided interference," *Proc Natl Acad Sci U S A*, vol. 111, no. 18, pp. 6618–6623, May 2014, doi: 10.1073/PNAS.1405079111/SUPPL_FILE/PNAS.201405079SI.PDF.

[435] T. Sinkunas, G. Gasiunas, C. Fremaux, R. Barrangou, P. Horvath, and V. Siksnys, "Cas3 is a single-stranded DNA nuclease and ATP-dependent helicase in the CRISPR/Cas immune system," *EMBO J*, vol. 30, no. 7, pp. 1335–1342, Apr. 2011, doi: 10.1038/EMBOJ.2011.41.

[436] E. Semenova *et al.*, "Interference by clustered regularly interspaced short palindromic repeat (CRISPR) RNA is governed by a seed sequence," *Proc Natl Acad Sci U S A*, vol. 108, no. 25, pp. 10098–10103, Jun. 2011, doi: 10.1073/PNAS.1104144108/-/DCSUPPLEMENTAL.

[437] E. R. Westra *et al.*, "Type I-E CRISPR-Cas Systems Discriminate Target from Non-Target DNA through Base Pairing-Independent PAM Recognition," *PLoS Genet*, vol. 9, no. 9, Sep. 2013, doi: 10.1371/JOURNAL.PGEN.1003742.

[438] M. M. Jore *et al.*, "Structural basis for CRISPR RNA-guided DNA recognition by Cascade," *Nature Structural & Molecular Biology 2011 18:5*, vol. 18, no. 5, pp. 529–536, Apr. 2011, doi: 10.1038/nsmb.2019.

[439] S. Nimkar and B. Anand, “Cas3/I-C mediated target DNA recognition and cleavage during CRISPR interference are independent of the composition and architecture of Cascade surveillance complex,” *Nucleic Acids Res*, vol. 48, no. 5, pp. 2486–2501, Mar. 2020, doi: 10.1093/NAR/GKZ1218.

[440] D. Couvin *et al.*, “CRISPRCasFinder, an update of CRISRFinder, includes a portable version, enhanced performance and integrates search for Cas proteins,” *Nucleic Acids Res*, vol. 46, no. W1, pp. W246–W251, Jul. 2018, doi: 10.1093/NAR/GKY425.

[441] T. Künne, D. C. Swarts, and S. J. J. Brouns, “Planting the seed: target recognition of short guide RNAs,” *Trends Microbiol*, vol. 22, no. 2, pp. 74–83, Feb. 2014, doi: 10.1016/J.TIM.2013.12.003.

[442] V. Kunin, R. Sorek, and P. Hugenholtz, “Evolutionary conservation of sequence and secondary structures in CRISPR repeats,” *Genome Biol*, vol. 8, no. 4, p. R61, Apr. 2007, doi: 10.1186/GB-2007-8-4-R61.

[443] S. Van Houte *et al.*, “The diversity-generating benefits of a prokaryotic adaptive immune system,” *Nature 2016 532:7599*, vol. 532, no. 7599, pp. 385–388, Apr. 2016, doi: 10.1038/nature17436.

[444] F. J. M. Mojica, C. Díez-Villaseñor, J. García-Martínez, and E. Soria, “Intervening sequences of regularly spaced prokaryotic repeats derive from foreign genetic elements,” *J Mol Evol*, vol. 60, no. 2, pp. 174–182, Feb. 2005, doi: 10.1007/S00239-004-0046-3.

[445] S. F. Altschul, W. Gish, W. Miller, E. W. Myers, and D. J. Lipman, “Basic local alignment search tool,” *J Mol Biol*, vol. 215, no. 3, pp. 403–410, 1990, doi: 10.1016/S0022-2836(05)80360-2.

[446] A. Biswas, J. N. Gagnon, S. J. J. Brouns, P. C. Fineran, and C. M. Brown, “CRISPRTarget: bioinformatic prediction and analysis of crRNA targets,” *RNA Biol*, vol. 10, no. 5, pp. 817–827, 2013, doi: 10.4161/RNA.24046.

[447] M. F. Hasan, M. A. Islam, and B. Sikdar, “First report of Serratia marcescens associated with black rot of Citrus sinensis fruit , and evaluation of its biological control measures in Bangladesh,” *F1000Res*, vol. 9, p. 1371, Mar. 2020, doi: 10.12688/F1000RESEARCH.27657.2.

[448] L. E. Casida, “Bacterial Predators of Micrococcus luteus in Soil,” *Appl Environ Microbiol*, vol. 39, no. 5, pp. 1035–1041, May 1980, doi: 10.1128/AEM.39.5.1035-1041.1980.

[449] G. C. Zhou *et al.*, “Biodegradation of the neonicotinoid insecticide thiamethoxam by the nitrogen-fixing and plant-growth-promoting rhizobacterium Ensifer adhaerens strain TMX-23,” *Appl Microbiol Biotechnol*, vol. 97, no. 9, pp. 4065–4074, May 2013, doi: 10.1007/S00253-012-4638-3.

[450] D. I. Walitang, K. Kim, M. Madhaiyan, Y. K. Kim, Y. Kang, and T. Sa, “Characterizing endophytic competence and plant growth promotion of bacterial endophytes inhabiting the seed endosphere of Rice,” *BMC*

Microbiol, vol. 17, no. 1, pp. 1–13, Oct. 2017, doi: 10.1186/S12866-017-1117-0/FIGURES/4.

[451] I. Kim, G. Chhetri, Y. So, Y. Jung, S. Park, and T. Seo, "Sphingomonas liriopis sp. nov., Sphingomonas donggukensis sp. nov., and Sphingomonas tagetis sp. nov., isolated from Liriope platyphylla fruit, soil, and Tagetes patula roots," *Arch Microbiol*, vol. 205, no. 1, Jan. 2022, doi: 10.1007/S00203-022-03360-4.

[452] Y. Luo *et al.*, "Sphingomonas sp. Cra20 increases plant growth rate and alters rhizosphere microbial community structure of Arabidopsis thaliana under drought stress," *Front Microbiol*, vol. 10, no. JUN, p. 1221, 2019, doi: 10.3389/FMICB.2019.01221/FULL.

[453] V. Vives-Peris, A. Gómez-Cadenas, and R. M. Pérez-Clemente, "Salt stress alleviation in citrus plants by plant growth-promoting rhizobacteria Pseudomonas putida and Novosphingobium sp," *Plant Cell Rep*, vol. 37, no. 11, pp. 1557–1569, Nov. 2018, doi: 10.1007/S00299-018-2328-Z.

[454] A. M. Smit, T. J. Strabala, L. Peng, P. Rawson, G. Lloyd-Jones, and T. W. Jordan, "Proteomic phenotyping of Novosphingobium nitrogenifigens reveals a robust capacity for simultaneous nitrogen fixation, polyhydroxyalkanoate production, and resistance to reactive oxygen species," *Appl Environ Microbiol*, vol. 78, no. 14, pp. 4802–4815, Jul. 2012, doi: 10.1128/AEM.00274-12.

[455] V. Van Tran, P. Mavingui, O. Berge, J. Balandreau, and T. Heulin, "Burkholderia vietnamiensis, a new nitrogen-fixing species associated with rice roots, isolated from an acid sulphate soil in Vietnam: plant-growth-promoting effects on rice," *Biological Nitrogen Fixation Associated with Rice Production*, pp. 181–190, 1996, doi: 10.1007/978-94-015-8670-2_20.

[456] D. Scudeletti *et al.*, "Inoculation with Azospirillum brasilense as a strategy to enhance sugarcane biomass production and bioenergy potential," *European Journal of Agronomy*, vol. 144, p. 126749, Mar. 2023, doi: 10.1016/J.EJA.2023.126749.

[457] A. D. Arencibia *et al.*, "Gluconacetobacter diazotrophicus Elicits a Sugarcane Defense Response Against a Pathogenic Bacteria Xanthomonas albilineans," *Plant Signal Behav*, vol. 1, no. 5, p. 265, 2006, doi: 10.4161/PSB.1.5.3390.

[458] S. A. Shmakov, V. Sitnik, K. S. Makarova, Y. I. Wolf, K. V. Severinov, and E. V. Koonin, "The CRISPR Spacer Space Is Dominated by Sequences from Species-Specific Mobilomes," *mBio*, vol. 8, no. 5, Sep. 2017, doi: 10.1128/MBIO.01397-17.

[459] Y. Tang and Y. Fu, "Class 2 CRISPR/Cas: an expanding biotechnology toolbox for and beyond genome editing," *Cell & Bioscience 2018 8:1*, vol. 8, no. 1, pp. 1–13, Nov. 2018, doi: 10.1186/S13578-018-0255-X.

[460] Y. Zhang *et al.*, "Processing-independent CRISPR RNAs limit natural transformation in Neisseria meningitidis," *Mol Cell*, vol. 50, no. 4, pp. 488–503, May 2013, doi: 10.1016/J.MOLCEL.2013.05.001.

[461] A. Mir, A. Edraki, J. Lee, and E. J. Sontheimer, “Type II-C CRISPR-Cas9 Biology, Mechanism, and Application,” *ACS Chem Biol*, vol. 13, no. 2, pp. 357–365, Feb. 2018, doi: 10.1021/ACSCHEMBIO.7B00855/ASSET/IMAGES/MEDIUM/CB-2017-00855B_0003.GIF.

[462] S. H. Sternberg, H. Richter, E. Charpentier, and U. Qimron, “Adaptation in CRISPR-Cas Systems,” *Mol Cell*, vol. 61, no. 6, pp. 797–808, Mar. 2016, doi: 10.1016/J.MOLCEL.2016.01.030.

[463] K. Selle and R. Barrangou, “Harnessing CRISPR-Cas systems for bacterial genome editing,” *Trends Microbiol*, vol. 23, no. 4, pp. 225–232, Apr. 2015, doi: 10.1016/J.TIM.2015.01.008.

[464] E. Deltcheva *et al.*, “CRISPR RNA maturation by trans-encoded small RNA and host factor RNase III,” *Nature 2011 471:7340*, vol. 471, no. 7340, pp. 602–607, Mar. 2011, doi: 10.1038/nature09886.

[465] A. R. Gruber, R. Lorenz, S. H. Bernhart, R. Neuböck, and I. L. Hofacker, “The Vienna RNA Websuite,” *Nucleic Acids Res*, vol. 36, no. Web Server issue, p. W70, Jul. 2008, doi: 10.1093/NAR/GKN188.

[466] M. Jinek, K. Chylinski, I. Fonfara, M. Hauer, J. A. Doudna, and E. Charpentier, “A programmable dual-RNA-guided DNA endonuclease in adaptive bacterial immunity,” *Science*, vol. 337, no. 6096, pp. 816–821, Aug. 2012, doi: 10.1126/SCIENCE.1225829.

[467] G. Gasiunas, R. Barrangou, P. Horvath, and V. Siksnys, “Cas9-crRNA ribonucleoprotein complex mediates specific DNA cleavage for adaptive immunity in bacteria,” *Proc Natl Acad Sci U S A*, vol. 109, no. 39, Sep. 2012, doi: 10.1073/PNAS.1208507109/-/DCSUPPLEMENTAL/PNAS.201208507SI.PDF.

[468] C. Anders, O. Niewoehner, A. Duerst, and M. Jinek, “Structural basis of PAM-dependent target DNA recognition by the Cas9 endonuclease,” *Nature 2014 513:7519*, vol. 513, no. 7519, pp. 569–573, Jul. 2014, doi: 10.1038/nature13579.

[469] Y. Zhang, R. Rajan, H. S. Seifert, A. Mondragón, and E. J. Sontheimer, “DNase H Activity of Neisseria meningitidis Cas9,” *Mol Cell*, vol. 60, no. 2, pp. 242–255, Oct. 2015, doi: 10.1016/J.MOLCEL.2015.09.020.

[470] G. Gasiunas, R. Barrangou, P. Horvath, and V. Siksnys, “Cas9-crRNA ribonucleoprotein complex mediates specific DNA cleavage for adaptive immunity in bacteria,” *Proc Natl Acad Sci U S A*, vol. 109, no. 39, Sep. 2012, doi: 10.1073/PNAS.1208507109/-/DCSUPPLEMENTAL/PNAS.201208507SI.PDF.

[471] Z. Hou *et al.*, “Efficient genome engineering in human pluripotent stem cells using Cas9 from Neisseria meningitidis,” *Proc Natl Acad Sci U S A*, vol. 110, no. 39, pp. 15644–15649, Sep. 2013, doi: 10.1073/PNAS.1313587110/SUPPL_FILE/SD03.DOCX.

[472] M. Naville, A. Ghuillot-Gaudeffroy, A. Marchais, and D. Gautheret, “ARNold: a web tool for the prediction of Rho-independent transcription terminators,” *RNA Biol*, vol. 8, no. 1, pp. 11–13, 2011, doi: 10.4161/RNA.8.1.13346.

[473] E. Kim *et al.*, “In vivo genome editing with a small Cas9 orthologue derived from Campylobacter jejuni,” *Nature Communications 2017 8:1*, vol. 8, no. 1, pp. 1–12, Feb. 2017, doi: 10.1038/ncomms14500.

[474] S. Ashrafi *et al.*, “Two New Rhizobiales Species Isolated from Root Nodules of Common Sainfoin (Onobrychis viciifolia) Show Different Plant Colonization Strategies,” *Microbiol Spectr*, vol. 10, no. 5, Oct. 2022, doi: 10.1128/SPECTRUM.01099-22.

[475] B. Román-Ponce *et al.*, “Rhizobium acidisoli sp. nov., isolated from root nodules of Phaseolus vulgaris in acid soils,” *Int J Syst Evol Microbiol*, vol. 66, no. 1, pp. 398–406, Jan. 2016, doi: 10.1099/IJSEM.0.000732.

[476] K. da Silva, L. A. Florentino, K. B. da Silva, E. de Brandt, P. Vandamme, and F. M. de Souza Moreira, “Cupriavidus necator isolates are able to fix nitrogen in symbiosis with different legume species,” *Syst Appl Microbiol*, vol. 35, no. 3, pp. 175–182, May 2012, doi: 10.1016/J.SYAPM.2011.10.005.

[477] F. Jiang and J. A. Doudna, “CRISPR-Cas9 Structures and Mechanisms,” *Annu Rev Biophys*, vol. 46, pp. 505–529, May 2017, doi: 10.1146/ANNUREV-BIOPHYS-062215-010822.

[478] F. J. M. Mojica, C. Díez-Villaseñor, J. García-Martínez, and C. Almendros, “Short motif sequences determine the targets of the prokaryotic CRISPR defence system,” *Microbiology (Reading)*, vol. 155, no. Pt 3, pp. 733–740, 2009, doi: 10.1099/MIC.0.023960-0.

[479] G. Gasiunas, R. Barrangou, P. Horvath, and V. Siksnys, “Cas9-crRNA ribonucleoprotein complex mediates specific DNA cleavage for adaptive immunity in bacteria,” *Proc Natl Acad Sci U S A*, vol. 109, no. 39, pp. E2579–E2586, Sep. 2012, doi: 10.1073/PNAS.1208507109/SUPPL_FILE/PNAS.201208507SI.PDF.

[480] S. Shuman and M. S. Glickman, “Bacterial DNA repair by non-homologous end joining,” *Nature Reviews Microbiology 2007 5:11*, vol. 5, no. 11, pp. 852–861, Nov. 2007, doi: 10.1038/nrmicro1768.

[481] Y. Wang *et al.*, “Bacterial Genome Editing with CRISPR-Cas9: Deletion, Integration, Single Nucleotide Modification, and Desirable ‘Clean’ Mutant Selection in Clostridium beijerinckii as an Example,” *ACS Synth Biol*, vol. 5, no. 7, pp. 721–732, Jul. 2016, doi: 10.1021/ACSSYNBIO.6B00060.

[482] J. M. Vento, N. Crook, and C. L. Beisel, “Barriers to genome editing with CRISPR in bacteria,” *J Ind Microbiol Biotechnol*, vol. 46, no. 9–10, pp. 1327–1341, Oct. 2019, doi: 10.1007/S10295-019-02195-1.

[483] M. L. Luo, R. T. Leenay, and C. L. Beisel, “Current and future prospects for CRISPR-based tools in bacteria,” *Biotechnol Bioeng*, vol. 113, no. 5, pp. 930–943, May 2016, doi: 10.1002/BIT.25851.

[484] Y. Jiang, B. Chen, C. Duan, B. Sun, J. Yang, and S. Yang, “Multigene editing in the Escherichia coli genome via the CRISPR-Cas9 system,” *Appl Environ Microbiol*, vol. 81, no. 7, pp. 2506–2514, 2015, doi: 10.1128/AEM.04023-14.

[485] T. Wang *et al.*, “Pooled CRISPR interference screening enables genome-scale functional genomics study in bacteria with superior performance,” *Nature Communications 2018 9:1*, vol. 9, no. 1, pp. 1–15, Jun. 2018, doi: 10.1038/s41467-018-04899-x.

[486] K. Labun, T. G. Montague, M. Krause, Y. N. Torres Cleuren, H. Tjeldnes, and E. Valen, “CHOPCHOP v3: expanding the CRISPR web toolbox beyond genome editing,” *Nucleic Acids Res*, vol. 47, no. W1, pp. W171–W174, Jul. 2019, doi: 10.1093/NAR/GKZ365.

[487] M. Stemmer, T. Thumberger, M. Del Sol Keyer, J. Wittbrodt, and J. L. Mateo, “CCTop: An Intuitive, Flexible and Reliable CRISPR/Cas9 Target Prediction Tool,” *PLoS One*, vol. 10, no. 4, p. e0124633, Apr. 2015, doi: 10.1371/JOURNAL.PONE.0124633.

[488] S. Cho, D. Choe, E. Lee, S. C. Kim, B. Palsson, and B. K. Cho, “High-Level dCas9 Expression Induces Abnormal Cell Morphology in Escherichia coli,” *ACS Synth Biol*, vol. 7, no. 4, pp. 1085–1094, Apr. 2018, doi: 10.1021/ACSSYNBIO.7B00462.

[489] S. A. Lynch, S. K. Desai, H. K. Sajja, and J. P. Gallivan, “A high-throughput screen for synthetic riboswitches reveals mechanistic insights into their function,” *Chem Biol*, vol. 14, no. 2, pp. 173–184, Feb. 2007, doi: 10.1016/J.CHEMBIOL.2006.12.008.

[490] I. C. Cañadas, D. Groothuis, M. Zygouropoulou, R. Rodrigues, and N. P. Minton, “RiboCas: A Universal CRISPR-Based Editing Tool for Clostridium,” *ACS Synth Biol*, vol. 8, no. 6, pp. 1379–1390, Jun. 2019, doi: 10.1021/acssynbio.9b00075.

[491] S. Fischer *et al.*, “An archaeal immune system can detect multiple protospacer adjacent motifs (PAMs) to target invader DNA,” *J Biol Chem*, vol. 287, no. 40, pp. 33351–33365, Sep. 2012, doi: 10.1074/JBC.M112.377002.

[492] B. Csörgő *et al.*, “A compact Cascade–Cas3 system for targeted genome engineering,” *Nature Methods 2020 17:12*, vol. 17, no. 12, pp. 1183–1190, Oct. 2020, doi: 10.1038/s41592-020-00980-w.

[493] Y. Tong, P. Charusanti, L. Zhang, T. Weber, and S. Y. Lee, “CRISPR-Cas9 Based Engineering of Actinomycetal Genomes,” *ACS Synth Biol*, vol. 4, no. 9, pp. 1020–1029, Sep. 2015, doi: 10.1021/ACSSYNBIO.5B00038/SUPPL_FILE/SB5B00038_SI_001.PDF.

[494] Y. Jiang *et al.*, “CRISPR-Cpf1 assisted genome editing of Corynebacterium glutamicum,” *Nature Communications 2017 8:1*, vol. 8, no. 1, pp. 1–11, May 2017, doi: 10.1038/ncomms15179.

[495] M. E. Pyne, M. R. Bruder, M. Moo-Young, D. A. Chung, and C. P. Chou, “Harnessing heterologous and endogenous CRISPR-Cas machineries for

efficient markerless genome editing in Clostridium," *Scientific Reports 2016 6:1*, vol. 6, no. 1, pp. 1–15, May 2016, doi: 10.1038/srep25666.

[496] T. Künne *et al.*, "Cas3-Derived Target DNA Degradation Fragments Fuel Primed CRISPR Adaptation," *Mol Cell*, vol. 63, no. 5, pp. 852–864, Sep. 2016, doi: 10.1016/J.MOLCEL.2016.07.011.

[497] R. Tan *et al.*, "Cas11 enables genome engineering in human cells with compact CRISPR-Cas3 systems," *Mol Cell*, vol. 82, no. 4, p. 852, Feb. 2022, doi: 10.1016/J.MOLCEL.2021.12.032.

[498] R. T. Leenay *et al.*, "Identifying and visualizing functional PAM diversity across CRISPR-Cas systems," *Mol Cell*, vol. 62, no. 1, p. 137, Apr. 2016, doi: 10.1016/J.MOLCEL.2016.02.031.

[499] E. Semenova, M. Nagornykh, M. Pyatnitskiy, I. I. Artamonova, and K. Severinov, "Analysis of CRISPR system function in plant pathogen Xanthomonas oryzae," *FEMS Microbiol Lett*, vol. 296, no. 1, pp. 110–116, Jul. 2009, doi: 10.1111/J.1574-6968.2009.01626.X.

[500] D. Gleditzsch *et al.*, "PAM identification by CRISPR-Cas effector complexes: diversified mechanisms and structures," *RNA Biol*, vol. 16, no. 4, pp. 504–517, Apr. 2019, doi: 10.1080/15476286.2018.1504546.

[501] G. E. Crooks, G. Hon, J. M. Chandonia, and S. E. Brenner, "WebLogo: a sequence logo generator," *Genome Res*, vol. 14, no. 6, pp. 1188–1190, Jun. 2004, doi: 10.1101/GR.849004.

[502] A. E. Dolan *et al.*, "Introducing a spectrum of long-range genomic deletions in human embryonic stem cells using Type I CRISPR-Cas," *Mol Cell*, vol. 74, no. 5, p. 936, Jun. 2019, doi: 10.1016/J.MOLCEL.2019.03.014.

[503] A. E. Stachler and A. Marchfelder, "Gene Repression in Haloarchaea Using the CRISPR (Clustered Regularly Interspaced Short Palindromic Repeats)-Cas I-B System," *J Biol Chem*, vol. 291, no. 29, pp. 15226–15242, Jul. 2016, doi: 10.1074/JBC.M116.724062.

[504] K. M. Esvelt, P. Mali, J. L. Braff, M. Moosburner, S. J. Yaung, and G. M. Church, "Orthogonal Cas9 proteins for RNA-guided gene regulation and editing," *Nature Methods 2013 10:11*, vol. 10, no. 11, pp. 1116–1121, Sep. 2013, doi: 10.1038/nmeth.2681.

[505] N. Amrani *et al.*, "NmeCas9 is an intrinsically high-fidelity genome-editing platform Jin-Soo Kim," *Genome Biol*, vol. 19, no. 1, pp. 1–25, Dec. 2018, doi: 10.1186/S13059-018-1591-1/FIGURES/1.

[506] O. Pines, H. J. Yoon, and M. Inouye, "Expression of double-stranded-RNA-specific RNase III of Escherichia coli is lethal to Saccharomyces cerevisiae.," *J Bacteriol*, vol. 170, no. 7, p. 2989, 1988, doi: 10.1128/JB.170.7.2989-2993.1988.

[507] C. M. Nowak, S. Lawson, M. Zerez, and L. Bleris, “Guide RNA engineering for versatile Cas9 functionality,” *Nucleic Acids Res*, vol. 44, no. 20, pp. 9555–9564, 2016, doi: 10.1093/NAR/GKW908.

[508] R. Xu *et al.*, “Genome editing with type II-C CRISPR-Cas9 systems from Neisseria meningitidis in rice,” *Plant Biotechnol J*, vol. 20, no. 2, pp. 350–359, Feb. 2022, doi: 10.1111/PBI.13716.

[509] Z. Hou *et al.*, “Efficient genome engineering in human pluripotent stem cells using Cas9 from Neisseria meningitidis,” *Proc Natl Acad Sci U S A*, vol. 110, no. 39, pp. 15644–15649, Sep. 2013, doi: 10.1073/PNAS.1313587110/SUPPL_FILE/SD03.DOCX.

[510] R. Muthukumarasamy, G. Revathi, S. Seshadri, and C. Lakshminarasimhan, “Gluconacetobacter diazotrophicus (syn. Acetobacter diazotrophicus), a promising diazotrophic endophyte in tropics,” *Curr Sci*, vol. 83, no. 2, pp. 137–145, 2002, [Online]. Available: http://www.jstor.org/stable/24106216

[511] J. Vasse, F. De Billy, S. Camut, and G. Truchet, “Correlation between ultrastructural differentiation of bacteroids and nitrogen fixation in alfalfa nodules.,” *J Bacteriol*, vol. 172, no. 8, p. 4295, 1990, doi: 10.1128/JB.172.8.4295-4306.1990.

[512] O. A. Gorelova, “Surface ultrastructure of the heteromorphic cells of Nostoc muscorum CALU 304 in a mixed culture with the Rauwolfia callus tissue,” *Microbiology (N Y)*, vol. 70, no. 3, pp. 285–294, 2001, doi: 10.1023/A:1010447109864/METRICS.

[513] M. Melotto, W. Underwood, J. Koczan, K. Nomura, and S. Y. He, “Plant stomata function in innate immunity against bacterial invasion,” *Cell*, vol. 126, no. 5, pp. 969–980, Sep. 2006, doi: 10.1016/J.CELL.2006.06.054.

[514] F. Mignolli, J. S. Todaro, and M. L. Vidoz, “Internal aeration and respiration of submerged tomato hypocotyls are enhanced by ethylene-mediated aerenchyma formation and hypertrophy,” *Physiol Plant*, vol. 169, no. 1, pp. 49–63, May 2020, doi: 10.1111/PPL.13044.

[515] L. E. B. Baldotto, F. L. Olivares, and R. Bressan-Smith, “Structural Interaction Between GFP-Labeled Diazotrophic Endophytic Bacterium Herbaspirillum seropedicae RAM10 and Pineapple Plantlets ‘VitóRia,’” *Brazilian Journal of Microbiology*, vol. 42, no. 1, p. 114, 2011, doi: 10.1590/S1517-83822011000100015.

[516] J. Mercado-Blanco and P. Prieto, “Bacterial endophytes and root hairs,” *Plant Soil*, vol. 361, no. 1–2, pp. 301–306, Nov. 2012, doi: 10.1007/S11104-012-1212-9/FIGURES/1.

[517] P. Prieto, E. Schilirò, M. M. Maldonado-González, R. Valderrama, J. B. Barroso-Albarracín, and J. Mercado-Blanco, “Root Hairs Play a Key Role in the Endophytic Colonization of Olive Roots by Pseudomonas spp. with Biocontrol Activity,” *Microb Ecol*, vol. 62, no. 2, p. 435, Aug. 2011, doi: 10.1007/S00248-011-9827-6.

[518] J. F. White *et al.*, “Disease protection and allelopathic interactions of seed-transmitted endophytic pseudomonads of invasive reed grass (Phragmites australis),” *Plant Soil*, vol. 422, no. 1–2, pp. 195–208, Jan. 2018, doi: 10.1007/S11104-016-3169-6/TABLES/4.

[519] H. R. Shehata, C. Dumigan, S. Watts, and M. N. Raizada, “An endophytic microbe from an unusual volcanic swamp corn seeks and inhabits root hair cells to extract rock phosphate,” *Scientific Reports 2017 7:1*, vol. 7, no. 1, pp. 1–13, Oct. 2017, doi: 10.1038/s41598-017-14080-x.

[520] S. K. Verma, K. Kingsley, I. Irizarry, M. Bergen, R. N. Kharwar, and J. F. White, “Seed-vectored endophytic bacteria modulate development of rice seedlings,” *J Appl Microbiol*, vol. 122, no. 6, pp. 1680–1691, Jun. 2017, doi: 10.1111/JAM.13463.

[521] J. Fournier *et al.*, “Remodeling of the infection chamber before infection thread formation reveals a two-step mechanism for rhizobial entry into the host legume root hair,” *Plant Physiol*, vol. 167, no. 4, pp. 1233–1242, Apr. 2015, doi: 10.1104/PP.114.253302.

[522] S. R. Long, “SnapShot: Signaling in Symbiosis,” *Cell*, vol. 167, no. 2, pp. 582-582.e1, Oct. 2016, doi: 10.1016/J.CELL.2016.09.046.

[523] H. P. Bais, T. L. Weir, L. G. Perry, S. Gilroy, and J. M. Vivanco, “The role of root exudates in rhizosphere interactions with plants and other organisms,” *Annu Rev Plant Biol*, vol. 57, pp. 233–266, 2006, doi: 10.1146/annurev.arplant.57.032905.105159.

[524] K. Herburger, S. Schoenaers, K. Vissenberg, and J. Mravec, “Shank-localized cell wall growth contributes to Arabidopsis root hair elongation,” *Nat Plants*, vol. 8, no. 11, pp. 1222–1232, Nov. 2022, doi: 10.1038/S41477-022-01259-Y.

[525] C. Paungfoo-Lonhienne, S. Schmidt, and T. Lonhienne, “Rhizophagy-A New Dimension of Plant-Microbe Interactions,” in *Molecular Microbial Ecology of the Rhizosphere*, vol. 2, 2013. doi: 10.1002/9781118297674.ch115.

[526] L. F. M. Rouws, C. H. S. G. Meneses, H. V. Guedes, M. S. Vidal, J. I. Baldani, and S. Schwab, “Monitoring the colonization of sugarcane and rice plants by the endophytic diazotrophic bacterium Gluconacetobacter diazotrophicus marked with gfp and gusA reporter genes,” *Lett Appl Microbiol*, vol. 51, no. 3, pp. 325–330, Sep. 2010, doi: 10.1111/j.1472-765X.2010.02899.x.

[527] J. Y. Lee and H. Lu, “Plasmodesmata: the battleground against intruders,” *Trends Plant Sci*, vol. 16, no. 4, pp. 201–210, Apr. 2011, doi: 10.1016/J.TPLANTS.2011.01.004.

[528] A. W. Robards, “Plasmodesmata,” *Annu Rev Plant Physiol*, vol. 26, no. 1, pp. 13–29, Jun. 1975, doi: 10.1146/annurev.pp.26.060175.000305.

[529] Z. P. Li, A. Paterlini, M. Glavier, and E. M. Bayer, “Intercellular trafficking via plasmodesmata: molecular layers of complexity,” *Cellular and Molecular Life Sciences*, vol. 78, no. 3, p. 799, Feb. 2021, doi: 10.1007/S00018-020-03622-8.

[530] J. P. Knox and Y. Benitez-Alfonso, “Roles and regulation of plant cell walls surrounding plasmodesmata,” *Curr Opin Plant Biol*, vol. 22, pp. 93–100, Dec. 2014, doi: 10.1016/J.PBI.2014.09.009.

[531] K. Aung *et al.*, “Pathogenic Bacteria Target Plant Plasmodesmata to Colonize and Invade Surrounding Tissues,” *Plant Cell*, vol. 32, no. 3, pp. 595–611, 2020, doi: 10.1105/TPC.19.00707.

[532] Z. Li, H. Variz, Y. Chen, S. L. Liu, and K. Aung, “Plasmodesmata-Dependent Intercellular Movement of Bacterial Effectors,” *Front Plant Sci*, vol. 12, p. 640277, Mar. 2021, doi: 10.3389/FPLS.2021.640277/BIBTEX.

[533] E. T. McDowell *et al.*, “Comparative Functional Genomic Analysis of Solanum Glandular Trichome Types,” *Plant Physiol*, vol. 155, no. 1, pp. 524–539, Jan. 2011, doi: 10.1104/PP.110.167114.

[534] Y. Zhang *et al.*, “The Roles of Different Types of Trichomes in Tomato Resistance to Cold, Drought, Whiteflies, and Botrytis,” *Agronomy 2020, Vol. 10, Page 411*, vol. 10, no. 3, p. 411, Mar. 2020, doi: 10.3390/AGRONOMY10030411.

[535] J. Gershenzon and N. Dudareva, “The function of terpene natural products in the natural world,” *Nature Chemical Biology 2007 3:7*, vol. 3, no. 7, pp. 408–414, Jun. 2007, doi: 10.1038/nchembio.2007.5.

[536] Y. Taheri *et al.*, “Myricetin bioactive effects: moving from preclinical evidence to potential clinical applications,” *BMC Complementary Medicine and Therapies 2020 20:1*, vol. 20, no. 1, pp. 1–14, Aug. 2020, doi: 10.1186/S12906-020-03033-Z.

[537] C. Preininger, U. Sauer, A. Bejarano, and T. Berninger, “Concepts and applications of foliar spray for microbial inoculants,” *Appl Microbiol Biotechnol*, vol. 102, no. 17, pp. 7265–7282, Sep. 2018, doi: 10.1007/S00253-018-9173-4.

[538] P. Sudhakar, G. N. Chattopadhyay, S. K. Gangwar, and J. K. Ghosh, “Effect of foliar application of Azotobacter, Azospirillum and Beijerinckia on leaf yield and quality of mulberry (Morus alba),” *J Agric Sci*, vol. 134, no. 2, pp. 227–234, Mar. 2000, doi: 10.1017/S0021859699007376.

[539] A. Efthimiadou, N. Katsenios, S. Chanioti, M. Giannoglou, N. Djordjevic, and G. Katsaros, “Effect of foliar and soil application of plant growth promoting bacteria on growth, physiology, yield and seed quality of maize under Mediterranean conditions,” *Sci Rep*, vol. 10, no. 1, p. 11080, Dec. 2020, doi: 10.1038/S41598-020-78034-6.

[540] B. R. Pati and A. K. Chandra, “Effect of spraying nitrogen-fixing phyllospheric bacterial isolates on wheat plants,” *Plant Soil*, vol. 61, no. 3, pp. 419–427, Oct. 1981, doi: 10.1007/BF02182022/METRICS.

[541] S. Ahmadi-Rad, M. Gholamhoseini, A. Ghalavand, A. Asgharzadeh, and A. Dolatabadian, “Foliar application of nitrogen fixing bacteria increases growth

and yield of canola grown under different nitrogen regimes," *Rhizosphere*, vol. 2, pp. 34–37, Dec. 2016, doi: 10.1016/J.RHISPH.2016.08.006.

[542] S. Henry *et al.*, "Immunoprofiling of rice root cortex reveals two cortical subdomains," *Front Plant Sci*, vol. 6, no. JAN2016, p. 172279, Jan. 2016, doi: 10.3389/FPLS.2015.01139/BIBTEX.

[543] T. Kawai *et al.*, "WUSCHEL-related homeobox family genes in rice control lateral root primordium size," *Proc Natl Acad Sci U S A*, vol. 119, no. 1, p. e2101846119, Jan. 2022, doi: 10.1073/PNAS.2101846119/SUPPL_FILE/PNAS.2101846119.SD04.XLSX.

[544] T. Kawai *et al.*, "Auxin Distribution in Lateral Root Primordium Development Affects the Size and Lateral Root Diameter of Rice," *Front Plant Sci*, vol. 13, p. 834378, Apr. 2022, doi: 10.3389/FPLS.2022.834378/BIBTEX.

[545] D. Dauvillée *et al.*, "Role of the Escherichia coli glgX Gene in Glycogen Metabolism," *J Bacteriol*, vol. 187, no. 4, p. 1465, Feb. 2005, doi: 10.1128/JB.187.4.1465-1473.2005.

[546] S. D. Woodcock *et al.*, "Trehalose and α-glucan mediate distinct abiotic stress responses in Pseudomonas aeruginosa," *PLoS Genet*, vol. 17, no. 4, Apr. 2021, doi: 10.1371/JOURNAL.PGEN.1009524.

[547] D. N. Rodríguez-Navarro, M. S. Dardanelli, and J. E. Ruíz-Saínz, "Attachment of bacteria to the roots of higher plants," *FEMS Microbiol Lett*, vol. 272, no. 2, pp. 127–136, Jul. 2007, doi: 10.1111/J.1574-6968.2007.00761.X.

[548] K. W. Michiels, C. L. Croes, and J. Vanderleyden, "Two different modes of attachment of Azospirillum brasilense Sp7 to wheat roots," *J Gen Microbiol*, vol. 137, no. 9, pp. 2241–2246, Sep. 1991, doi: 10.1099/00221287-137-9-2241/CITE/REFWORKS.

[549] A. Skorupska, M. Janczarek, M. Marczak, A. Mazur, and J. Król, "Rhizobial exopolysaccharides: genetic control and symbiotic functions," *Microb Cell Fact*, vol. 5, p. 7, Feb. 2006, doi: 10.1186/1475-2859-5-7.

[550] A. Milling, L. Babujee, and C. Allen, "Ralstonia solanacearum extracellular polysaccharide is a specific elicitor of defense responses in wilt-resistant tomato plants," *PLoS One*, vol. 6, no. 1, 2011, doi: 10.1371/JOURNAL.PONE.0015853.

[551] L. V. Rinaudi and W. Giordano, "An integrated view of biofilm formation in rhizobia," *FEMS Microbiol Lett*, vol. 304, no. 1, pp. 1–11, Mar. 2010, doi: 10.1111/J.1574-6968.2009.01840.X.

[552] R. L. Peterson and M. L. Farquhar, "Root hairs: Specialized tubular cells extending root surfaces," *The Botanical Review 1996 62:1*, vol. 62, no. 1, pp. 1–40, 1996, doi: 10.1007/BF02868919.

[553] R. Wang, C. Liu, Q. Li, Z. Chen, S. Sun, and X. Wang, "Spatiotemporal Resolved Leaf Angle Establishment Improves Rice Grain Yield via Controlling Population

Density," *iScience*, vol. 23, no. 9, p. 101489, Sep. 2020, doi: 10.1016/J.ISCI.2020.101489.

[554] N. M. Christensen, C. Faulkner, and K. Oparka, "Evidence for Unidirectional Flow through Plasmodesmata," *Plant Physiol*, vol. 150, no. 1, pp. 96–104, May 2009, doi: 10.1104/PP.109.137083.

[555] M. C. Roper, L. C. Greve, J. G. Warren, J. M. Labavitch, and B. C. Kirkpatrick, "Xylella fastidiosa Requires Polygalacturonase for Colonization and Pathogenicity in Vitis vinifera Grapevines," *https://doi.org/10.1094/MPMI-20-4-0411*, vol. 20, no. 4, pp. 411–419, Mar. 2007, doi: 10.1094/MPMI-20-4-0411.

[556] A. Krause *et al.*, "Complete genome of the mutualistic, N2-fixing grass endophyte Azoarcus sp. strain BH72," *Nat Biotechnol*, vol. 24, no. 11, pp. 1385–1391, Nov. 2006, doi: 10.1038/NBT1243.

[557] B. Reinhold-Hurek, T. Hurek, M. Claeyssens, and M. Van Montagu, "Cloning, expression in Escherichia coli, and characterization of cellulolytic enzymes of Azoarcus sp., a root-invading diazotroph," *J Bacteriol*, vol. 175, no. 21, pp. 7056–7065, 1993, doi: 10.1128/JB.175.21.7056-7065.1993.

[558] G. Kovtunovych, O. Lar, S. Kamalova, V. Kordyum, D. Kleiner, and N. Kozyrovska, "Correlation between pectate lyase activity and ability of diazotrophic Klebsiella oxytoca VN 13 to penetrate into plant tissues," *Plant Soil*, vol. 215, no. 1, pp. 1–6, 1999, doi: 10.1023/A:1004790122353/METRICS.

[559] P. C. van Spronsen, R. Bakhuizen, A. V. van Brussel, and J. Kijne, "Cell wall degradation during infection thread formation by the root nodule bacterium Rhizobium leguminosarum is a two-step process.," *Eur J Cell Biol*, 1994.

[560] E. M. De Nogueira *et al.*, "Expression of sugarcane genes induced by inoculation with Gluconacetobacter diazotrophicus and Herbaspirillum rubrisubalbicans," *Genet Mol Biol*, vol. 24, no. 1–4, pp. 199–206, Dec. 2001, doi: 10.1590/S1415-47572001000100027.

[561] M. Adriano-Anaya, M. Salvador-Figueroa, J. A. Ocampo, and I. García-Romera, "Plant cell-wall degrading hydrolytic enzymes of Gluconacetobacter diazotrophicus.," *Symbiosis (Rehovot)*, vol. 40, no. 3, pp. 151–156, 2005.

[562] J. M. Igual, E. Velázquez, P. F. Mateos, C. Rodríguez-Barrueco, E. Cervantes, and E. Martínez-Molina, "Cellulase isoenzyme profiles in Frankia strains belonging to different cross-inoculation groups," *Plant Soil*, vol. 229, no. 1, pp. 35–39, 2001, doi: 10.1023/A:1004835313723/METRICS.

[563] E. K. James, V. M. Reis, F. L. Olivares, J. I. Baldani, and J. Döbereiner, "Infection of sugar cane by the nitrogen-fixing bacterium Acetobacter diazotrophicus," *J Exp Bot*, vol. 45, no. 6, pp. 757–766, Jun. 1994, doi: 10.1093/JXB/45.6.757.

[564] T. Pečenková, M. Janda, J. Ortmannová, V. Hajná, Z. Stehlíková, and V. Žárský, "Early Arabidopsis root hair growth stimulation by pathogenic strains of Pseudomonas syringae," *Ann Bot*, vol. 120, no. 3, p. 437, Sep. 2017, doi: 10.1093/AOB/MCX073.

[565] R. Ortíz-Castro, M. Martínez-Trujillo, and J. López-Bucio, “N-acyl-L-homoserine lactones: a class of bacterial quorum-sensing signals alter post-embryonic root development in Arabidopsis thaliana,” *Plant Cell Environ*, vol. 31, no. 10, pp. 1497–1509, 2008, doi: 10.1111/J.1365-3040.2008.01863.X.

[566] E. V. Bertini, C. G. Nieto Peñalver, A. C. Leguina, V. P. Irazusta, and L. I. C. De Figueroa, “Gluconacetobacter diazotrophicus PAL5 possesses an active quorum sensing regulatory system,” *Antonie Van Leeuwenhoek*, vol. 106, no. 3, pp. 497–506, 2014, doi: 10.1007/S10482-014-0218-0.

[567] J. M. Chaparro, D. V. Badri, and J. M. Vivanco, “Rhizosphere microbiome assemblage is affected by plant development,” *The ISME Journal 2014 8:4*, vol. 8, no. 4, pp. 790–803, Nov. 2013, doi: 10.1038/ismej.2013.196.

[568] S. Monchgesang *et al.*, “Natural variation of root exudates in Arabidopsis thaliana-linking metabolomic and genomic data,” *Sci Rep*, vol. 6, Jul. 2016, doi: 10.1038/SREP29033.

[569] J. Sasse, E. Martinoia, and T. Northen, “Feed Your Friends: Do Plant Exudates Shape the Root Microbiome?,” *Trends Plant Sci*, vol. 23, no. 1, pp. 25–41, Jan. 2018, doi: 10.1016/J.TPLANTS.2017.09.003.

[570] G. L. Mark *et al.*, “Transcriptome profiling of bacterial responses to root exudates identifies genes involved in microbe-plant interactions,” *Proc Natl Acad Sci U S A*, vol. 102, no. 48, p. 17454, Nov. 2005, doi: 10.1073/PNAS.0506407102.

[571] D. L. Jones, C. Nguyen, and R. D. Finlay, “Carbon flow in the rhizosphere: Carbon trading at the soil-root interface,” *Plant Soil*, vol. 321, no. 1–2, pp. 5–33, 2009, doi: 10.1007/S11104-009-9925-0.

[572] S. J. Grayston, D. Vaughan, and D. Jones, “Rhizosphere carbon flow in trees, in comparison with annual plants: the importance of root exudation and its impact on microbial activity and nutrient availability,” *Applied Soil Ecology*, vol. 5, no. 1, pp. 29–56, Jan. 1997, doi: 10.1016/S0929-1393(96)00126-6.

[573] N. Tanaka *et al.*, “Characteristics of a root hair-less line of Arabidopsis thaliana under physiological stresses,” *J Exp Bot*, vol. 65, no. 6, pp. 1497–1512, 2014, doi: 10.1093/JXB/ERU014.

[574] E. M. Knee *et al.*, “Root mucilage from pea and its utilization by rhizosphere bacteria as a sole carbon source,” *Mol Plant Microbe Interact*, vol. 14, no. 6, pp. 775–784, 2001, doi: 10.1094/MPMI.2001.14.6.775.

[575] G. Mandimba, T. Heulin, R. Bally, A. Guckert, and J. Balandreau, “Chemotaxis of free-living nitrogen-fixing bacteria towards maize mucilage,” *Plant Soil*, vol. 90, no. 1–3, pp. 129–139, Feb. 1986, doi: 10.1007/BF02277392/METRICS.

[576] M. Vicré, C. Santaella, S. Blanchet, A. Gateau, and A. Driouich, “Root border-like cells of Arabidopsis. Microscopical characterization and role in the interaction with rhizobacteria,” *Plant Physiol*, vol. 138, no. 2, pp. 998–1008, 2005, doi: 10.1104/PP.104.051813.

[577] P. B. Beauregard, Y. Chai, H. Vlamakis, R. Losick, and R. Kolter, “Bacillus subtilis biofilm induction by plant polysaccharides,” *Proc Natl Acad Sci U S A*, vol. 110, no. 17, pp. E1621–E1630, Apr. 2013, doi: 10.1073/PNAS.1218984110/SUPPL_FILE/PNAS.201218984SI.PDF.

[578] B. J. Lugtenberg, L. V. Kravchenko, and M. Simons, “Tomato seed and root exudate sugars: composition, utilization by Pseudomonas biocontrol strains and role in rhizosphere colonization,” *Environ Microbiol*, vol. 1, no. 5, pp. 439–446, 1999, doi: 10.1046/J.1462-2920.1999.00054.X.

[579] I. B. Zhulin, S. E. Tretyakova, and V. V. Ignatov, “Chemotaxis of Azospirillum brasilense towards compounds typical of plant root exudates,” *Folia Microbiol (Praha)*, vol. 33, no. 4, pp. 277–280, Aug. 1988, doi: 10.1007/BF02925621/METRICS.

[580] S. N. Humphris *et al.*, “Root cap influences root colonisation by Pseudomonas fluorescens SBW25 on maize,” *FEMS Microbiol Ecol*, vol. 54, no. 1, pp. 123–130, Sep. 2005, doi: 10.1016/J.FEMSEC.2005.03.005.

[581] J. Prayitno *et al.*, “Interactions of rice seedlings with bacteria isolated from rice roots,” *Aust J Plant Physiol*, vol. 26, no. 6, pp. 521–535, 1999, doi: 10.1071/PP98090.

[582] A. Elbeltagy *et al.*, “Endophytic colonization and in planta nitrogen fixation by a Herbaspirillum sp. isolated from wild rice species,” *Appl Environ Microbiol*, vol. 67, no. 11, pp. 5285–5293, 2001, doi: 10.1128/AEM.67.11.5285-5293.2001.

[583] F. A. Smith, “Plant roots. Growth, activity and interaction with soils,” *Ann Bot*, vol. 100, no. 1, p. 151, Mar. 2007, doi: 10.1093/AOB/MCM099.

[584] “Internalization and Infiltration,” *Microbiology of Fruits and Vegetables*, pp. 91–110, Aug. 2005, doi: 10.1201/9781420038934-8.

[585] X. Liu, H. Zhao, and S. Chen, “Colonization of maize and rice plants by strain Bacillus megaterium C4,” *Curr Microbiol*, vol. 52, no. 3, pp. 186–190, Mar. 2006, doi: 10.1007/S00284-005-0162-3.

[586] R. De Oliveira Pinheiro, L. H. Boddey, E. K. James, J. I. Sprent, and R. M. Boddey, “Adsorption and anchoring of Azospirillumstrains to roots of wheat seedlings,” *Plant and Soil 2002 246:2*, vol. 246, no. 2, pp. 151–166, Oct. 2002, doi: 10.1023/A:1020645203084.

[587] E. Gamalero, G. Lingua, F. G. Caprì, A. Fusconi, G. Berta, and P. Lemanceau, “Colonization pattern of primary tomato roots by Pseudomonas fluorescens A6RI characterized by dilution plating, flow cytometry, fluorescence, confocal and scanning electron microscopy,” *FEMS Microbiol Ecol*, vol. 48, no. 1, pp. 79–87, Apr. 2004, doi: 10.1016/J.FEMSEC.2003.12.012.

[588] R. Schuurink and A. Tissier, “Glandular trichomes: micro-organs with model status?,” *New Phytologist*, vol. 225, no. 6, pp. 2251–2266, Mar. 2020, doi: 10.1111/NPH.16283.

[589] P. Khetnon *et al.*, “Mechanisms of Trichomes and Terpene Compounds in Indigenous and Commercial Thai Rice Varieties against Brown Planthopper,” *Insects*, vol. 13, no. 5, p. 427, May 2022, doi: 10.3390/INSECTS13050427/S1.

[590] A. Tissier and A. Tissier, “Trichome Specific Expression: Promoters and Their Applications,” *Transgenic Plants - Advances and Limitations*, Mar. 2012, doi: 10.5772/32101.

[591] G. Karabourniotis, G. Liakopoulos, D. Nikolopoulos, and P. Bresta, “Protective and defensive roles of non-glandular trichomes against multiple stresses: structure–function coordination,” *J For Res (Harbin)*, vol. 31, no. 1, pp. 1–12, Feb. 2020, doi: 10.1007/S11676-019-01034-4/FIGURES/2.

[592] G. Caetano-Anollés, D. K. Crist-Estes, and W. D. Bauer, “Chemotaxis of Rhizobium meliloti to the plant flavone luteolin requires functional nodulation genes,” *J Bacteriol*, vol. 170, no. 7, pp. 3164–3169, 1988, doi: 10.1128/JB.170.7.3164-3169.1988.

[593] R. Laterre, M. Pottier, C. Remacle, and M. Boutry, “Photosynthetic Trichomes Contain a Specific Rubisco with a Modified pH-Dependent Activity,” *Plant Physiol*, vol. 173, no. 4, p. 2110, Apr. 2017, doi: 10.1104/PP.17.00062.

[594] E. Harada, J. A. Kim, A. J. Meyer, R. Hell, S. Clemens, and Y. E. Choi, “Expression profiling of tobacco leaf trichomes identifies genes for biotic and abiotic stresses,” *Plant Cell Physiol*, vol. 51, no. 10, pp. 1627–1637, Oct. 2010, doi: 10.1093/PCP/PCQ118.

[595] S. Fei, M. Wenbin, W. Hao, X. Furong, X. Chunyan, and W. Jianfei, “Paper New Allele of HL6 Regulates Trichome Elongation in Rice,” *Rice Sci*, vol. 27, no. 6, pp. 480–492, Nov. 2020, doi: 10.1016/J.RSCI.2020.09.005.

[596] L. E. B. Baldotto and F. L. Olivares, “Phylloepiphytic interaction between bacteria and different plant species in a tropical agricultural system,” *Can J Microbiol*, vol. 54, no. 11, pp. 918–931, Nov. 2008, doi: 10.1139/W08-087.

[597] J. Mercier and S. E. Lindow, “Role of leaf surface sugars in colonization of plants by bacterial epiphytes,” *Appl Environ Microbiol*, vol. 66, no. 1, pp. 369–374, 2000, doi: 10.1128/AEM.66.1.369-374.2000.

[598] G. U. Balcke *et al.*, “Multi-Omics of Tomato Glandular Trichomes Reveals Distinct Features of Central Carbon Metabolism Supporting High Productivity of Specialized Metabolites,” *Plant Cell*, vol. 29, no. 5, pp. 960–983, May 2017, doi: 10.1105/TPC.17.00060.

[599] I. M. M. Roos and M. J. Hattingh, “Scanning Electron Microscopy of Pseudomonas syringae pv, morsprunorum on Sweet Cherry Leaves,” *Journal of Phytopathology*, vol. 108, no. 1, pp. 18–25, Sep. 1983, doi: 10.1111/J.1439-0434.1983.TB00559.X.

[600] M. Melotto, W. Underwood, and Y. H. Sheng, “Role of stomata in plant innate immunity and foliar bacterial diseases,” *Annu Rev Phytopathol*, vol. 46, pp. 101–122, 2008, doi: 10.1146/ANNUREV.PHYTO.121107.104959.

[601] B. Normander, B. B. Christensen, S. Molin, and N. Kroer, “Effect of Bacterial Distribution and Activity on Conjugal Gene Transfer on the Phylloplane of the Bush Bean (Phaseolus vulgaris),” *Appl Environ Microbiol*, vol. 64, no. 5, p. 1902, 1998, doi: 10.1128/AEM.64.5.1902-1909.1998.

[602] S. E. Lindow, “Determinants of Epiphytic Fitness in Bacteria,” in *Microbial Ecology of Leaves*, J. H. Andrews and S. S. Hirano, Eds., New York, NY: Springer New York, 1991, pp. 295–314.

[603] S. Compant, B. Reiter, A. Sessitsch, J. Nowak, C. Clément, and E. A. Barka, “Endophytic Colonization of Vitis vinifera L. by Plant Growth-Promoting Bacterium Burkholderia sp. Strain PsJN,” *Appl Environ Microbiol*, vol. 71, no. 4, p. 1685, Apr. 2005, doi: 10.1128/AEM.71.4.1685-1693.2005.

[604] Y. Kang, W. H. Outlaw, G. B. Fiore, and K. A. Riddle, “Guard cell apoplastic photosynthate accumulation corresponds to a phloem-loading mechanism,” *J Exp Bot*, vol. 58, no. 15–16, pp. 4061–4070, Dec. 2007, doi: 10.1093/JXB/ERM262.

[605] K. R. Finer, K. M. Larkin, B. J. Martin, and J. J. Finer, “Proximity of Agrobacterium to living plant tissues induces conversion to a filamentous bacterial form,” *Plant Cell Rep*, vol. 20, no. 3, pp. 250–255, Feb. 2001, doi: 10.1007/S002990100315/METRICS.

[606] G. Y. Zhu, S. Dobbelaere, and J. Vanderleyden, “Use of green fluorescent protein to visualize rice root colonization by Azospirillum irakense and A. brasilense,” *Funct Plant Biol*, vol. 29, no. 11, pp. 1279–1285, 2002, doi: 10.1071/FP02120.

[607] M. G. Rizzo *et al.*, “Glutamine-induced filamentous cells of Pseudomonas mediterranea CFBP-5447T as producers of PHAs,” *Appl Microbiol Biotechnol*, vol. 103, no. 21–22, pp. 9057–9066, Nov. 2019, doi: 10.1007/S00253-019-10144-2.

[608] C. Allison, H. -C Lai, D. Gygi, and C. Hughes, “Cell differentiation of Proteus mirabilis is initiated by glutamine, a specific chemoattractant for swarming cells,” *Mol Microbiol*, vol. 8, no. 1, pp. 53–60, 1993, doi: 10.1111/J.1365-2958.1993.TB01202.X.

[609] M. S. Thilakarathna and M. N. Raizada, “A biosensor-based assay (GlnluX-Agar) shows defoliation triggers rapid release of glutamine from nodules and young roots of forage legumes,” *Phytobiomes J*, vol. 3, no. 2, pp. 85–91, Jun. 2019, doi: 10.1094/PBIOMES-03-19-0014-R/ASSET/IMAGES/LARGE/PBIOMES-03-19-0014-RF2.JPEG.

[610] B. do Carmo Dias, F. F. da Mota, D. Jurelevicius, and L. Seldin, “Genetics and regulation of nitrogen fixation in Paenibacillus brasilensis PB24,” *Microbiol Res*, vol. 243, Feb. 2021, doi: 10.1016/J.MICRES.2020.126647.

[611] A. Canarini, C. Kaiser, A. Merchant, A. Richter, and W. Wanek, “Root exudation of primary metabolites: Mechanisms and their roles in plant

responses to environmental stimuli," *Front Plant Sci*, vol. 10, p. 422679, Feb. 2019, doi: 10.3389/FPLS.2019.00157/BIBTEX.

[612] D. A. Phillips, T. C. Fox, M. D. King, T. V. Bhuvaneswari, and L. R. Teuber, "Microbial Products Trigger Amino Acid Exudation from Plant Roots," *Plant Physiol*, vol. 136, no. 1, p. 2887, 2004, doi: 10.1104/PP.104.044222.

[613] F. Paynel, P. J. Murray, and J. Bernard Cliquet, "Root exudates: A pathway for short-term N transfer from clover and ryegrass," *Plant Soil*, vol. 229, no. 2, pp. 235–243, 2001, doi: 10.1023/A:1004877214831/METRICS.

[614] B. Alunni and B. Gourion, "Terminal bacteroid differentiation in the legume−rhizobium symbiosis: nodule-specific cysteine-rich peptides and beyond," *New Phytologist*, vol. 211, no. 2, pp. 411–417, Jul. 2016, doi: 10.1111/NPH.14025.

[615] H. Pan and D. Wang, "Nodule cysteine-rich peptides maintain a working balance during nitrogen-fixing symbiosis," *Nature Plants 2017 3:5*, vol. 3, no. 5, pp. 1–6, May 2017, doi: 10.1038/nplants.2017.48.

[616] M. R. Davey and J. B. Power, "Polyethylene glycol-induced uptake of micro-organisms into higher plant protoplasts: An ultrastructural study," *Plant Sci Lett*, vol. 5, no. 4, pp. 269–274, Oct. 1975, doi: 10.1016/0304-4211(75)90022-X.

[617] M. R. Davey and E. C. Cocking, "Uptake of Bacteria by Isolated Higher Plant Protoplasts," *Nature 1972 239:5373*, vol. 239, no. 5373, pp. 455–456, 1972, doi: 10.1038/239455b0.

[618] E. Etxeberria, E. Baroja-Fernandez, F. J. Muñoz, and J. Pozueta-Romero, "Sucrose-inducible Endocytosis as a Mechanism for Nutrient Uptake in Heterotrophic Plant Cells," *Plant Cell Physiol*, vol. 46, no. 3, pp. 474–481, Mar. 2005, doi: 10.1093/PCP/PCI044.

[619] A. L. M. Oliveira, M. Stoffels, M. Schmid, V. M. Reis, J. I. Baldani, and A. Hartmann, "Colonization of sugarcane plantlets by mixed inoculations with diazotrophic bacteria," *Eur J Soil Biol*, vol. 45, no. 1, pp. 106–113, Jan. 2009, doi: 10.1016/J.EJSOBI.2008.09.004.

[620] P. Thomas and C. M. M. Franco, "Intracellular bacteria in plants: Elucidation of abundant and diverse cytoplasmic bacteria in healthy plant cells using in vitro cell and callus cultures," *Microorganisms*, vol. 9, no. 2, pp. 1–27, Feb. 2021, doi: 10.3390/microorganisms9020269.

[621] J. Caballero-Mellado, L. E. Fuentes-Ramirez, V. M. Reis, and E. Martinez-Romero, "Genetic Structure of Acetobacter diazotrophicus Populations and Identification of a New Genetically Distant Group," 1995.

[622] L. E. Fuentes-Ramírez, J. Caballero-Mellado, J. Sepúlveda, and E. Martínez-Romero, "Colonization of sugarcane by Acetobacter diazotrophicus is inhibited by high N-fertilization," *FEMS Microbiol Ecol*, vol. 29, no. 2, pp. 117–128, 1999, doi: 10.1016/S0168-6496(98)00125-1.

[623] A. F. A. Medeiros, J. C. Polidoro, and V. M. Reis, “Nitrogen source effect on Gluconacetobacter diazotrophicus colonization of sugarcane (Saccharum spp.),” *Plant Soil*, vol. 279, no. 1–2, pp. 141–152, Feb. 2006, doi: 10.1007/s11104-005-0551-1.

[624] J. Muñoz-Rojas and J. Caballero-Mellado, “Population Dynamics of Gluconacetobacter diazotrophicus in Sugarcane Cultivars and Its Effect on Plant Growth,” *Microb Ecol*, vol. 46, no. 4, pp. 454–464, 2003, doi: 10.1007/s00248-003-0110-3.

[625] G. Kirchhof, V. M. Reis, J. I. Baldani, B. Eckert, J. Döbereiner, and A. Hartmann, “Occurrence, physiological and molecular analysis of endophytic diazotrophic bacteria in gramineous energy plants,” *Plant Soil*, vol. 194, no. 1, pp. 45–55, 1997, doi: 10.1023/A:1004217904546.

[626] F. L. Olivares, V. L. D. Baldani, V. M. Reis, J. I. Baldani, and J. Döbereiner, “Occurrence of the endophytic diazotrophs Herbaspirillum spp. in roots, stems, and leaves, predominantly of Gramineae,” *Biol Fertil Soils*, vol. 21, no. 3, pp. 197–200, 1996, doi: 10.1007/BF00335935.

[627] F. Bueno dos Reis Junior, V. Massena Reis, S. Urquiaga, and J. Döbereiner, “Influence of nitrogen fertilisation on the population of diazotrophic bacteria Herbaspirillum spp. and Acetobacter diazotrophicus in sugar cane (Saccharum spp.),” *Plant Soil*, vol. 219, no. 1, pp. 153–159, 2000, doi: 10.1023/A:1004732500983.

[628] W. Achouak, S. Conrod, V. Cohen, and T. Heulin, “Phenotypic variation of Pseudomonas brassicacearum as a plant root-colonization strategy,” *Mol Plant Microbe Interact*, vol. 17, no. 8, pp. 872–879, 2004, doi: 10.1094/MPMI.2004.17.8.872.

[629] M. A. Torres and J. L. Dangl, “Functions of the respiratory burst oxidase in biotic interactions, abiotic stress and development,” *Curr Opin Plant Biol*, vol. 8, no. 4, pp. 397–403, Aug. 2005, doi: 10.1016/J.PBI.2005.05.014.

[630] M. A. Torres, J. D. G. Jones, and J. L. Dangl, “Reactive oxygen species signaling in response to pathogens,” *Plant Physiol*, vol. 141, no. 2, pp. 373–378, 2006, doi: 10.1104/PP.106.079467.

[631] A. Baxter, R. Mittler, and N. Suzuki, “ROS as key players in plant stress signalling,” *J Exp Bot*, vol. 65, no. 5, pp. 1229–1240, Mar. 2014, doi: 10.1093/JXB/ERT375.

[632] L. Molina and R. Kahmann, “An Ustilago maydis gene involved in H2O2 detoxification is required for virulence,” *Plant Cell*, vol. 19, no. 7, pp. 2293–2309, 2007, doi: 10.1105/TPC.107.052332.

[633] H. Asard, R. Barbaro, P. Trost, and A. Bérczi, “Cytochromes b561: ascorbate-mediated trans-membrane electron transport,” *Antioxid Redox Signal*, vol. 19, no. 9, pp. 1026–1035, Sep. 2013, doi: 10.1089/ARS.2012.5065.

[634] H. Suzuki, T. Koyanagi, S. Izuka, A. Onishi, and H. Kumagai, “The yliA, -B, -C, and -D Genes of Escherichia coli K-12 Encode a Novel Glutathione Importer

with an ATP-Binding Cassette," *J Bacteriol*, vol. 187, no. 17, p. 5861, Sep. 2005, doi: 10.1128/JB.187.17.5861-5867.2005.

[635] L. Hernández *et al.*, "Levansucrase from Acetobacter diazotrophicus SRT4 is secreted via periplasm by a signal-peptide-dependent pathway," *Curr Microbiol*, vol. 39, no. 3, pp. 146–152, 1999, doi: 10.1007/S002849900436.

[636] L. Hernandez *et al.*, "Isolation and enzymic properties of levansucrase secreted by Acetobacter diazotrophicus SRT4, a bacterium associated with sugar cane.," *Biochemical Journal*, vol. 309, no. Pt 1, p. 113, Jul. 1995, doi: 10.1042/BJ3090113.

[637] E. T. Öner, L. Hernández, and J. Combie, "Review of Levan polysaccharide: From a century of past experiences to future prospects," *Biotechnol Adv*, vol. 34, no. 5, pp. 827–844, Sep. 2016, doi: 10.1016/J.BIOTECHADV.2016.05.002.

[638] N. Idogawa, R. Amamoto, K. Murata, and S. Kawai, "Phosphate enhances levan production in the endophytic bacterium Gluconacetobacter diazotrophicus Pal5," no. June, pp. 173–179, 2014.

[639] S. Bezzate, S. Aymerich, R. Chambert, S. Czarnes, O. Berge, and T. Heulin, "Disruption of the Paenibacillus polymyxa levansucrase gene impairs its ability to aggregate soil in the wheat rhizosphere," *Environ Microbiol*, vol. 2, no. 3, pp. 333–342, 2000, doi: 10.1046/J.1462-2920.2000.00114.X.

[640] L. D. Wilson *et al.*, "Recent Developments and Applications of Microbial Levan, A Versatile Polysaccharide-Based Biopolymer," *Molecules 2023, Vol. 28, Page 5407*, vol. 28, no. 14, p. 5407, Jul. 2023, doi: 10.3390/MOLECULES28145407.

[641] O. Stein and D. Granot, "An overview of sucrose synthases in plants," *Front Plant Sci*, vol. 10, p. 435701, Feb. 2019, doi: 10.3389/FPLS.2019.00095/BIBTEX.

[642] L. Miché, F. Battistoni, S. Gemmer, M. Belghazi, and B. Reinhold-Hurek, "Upregulation of jasmonate-inducible defense proteins and differential colonization of roots of Oryza sativa cultivars with the endophyte Azoarcus sp," *Mol Plant Microbe Interact*, vol. 19, no. 5, pp. 502–511, May 2006, doi: 10.1094/MPMI-19-0502.

[643] A. L. Iniguez, Y. Dong, H. D. Carter, B. M. M. Ahmer, J. M. Stone, and E. W. Triplett, "Regulation of enteric endophytic bacterial colonization by plant defenses," *Mol Plant Microbe Interact*, vol. 18, no. 2, pp. 169–178, Feb. 2005, doi: 10.1094/MPMI-18-0169.

[644] H. Zeng *et al.*, "Stimulation of phosphorus uptake by ammonium nutrition involves plasma membrane H+ ATPase in rice roots," *Plant Soil*, vol. 357, no. 1, pp. 205–214, Aug. 2012, doi: 10.1007/S11104-012-1136-4.

[645] L. Tian, T. Liu, K. J. Hua, X. P. Hu, and B. G. Ma, "The Spatial Organization of Bacterial Transcriptional Regulatory Networks," *Microorganisms*, vol. 10, no. 12, Dec. 2022, doi: 10.3390/MICROORGANISMS10122366/S1.

[646] H. Neubauer, I. Pantel, P. E. Lindgren, and F. Götz, “Characterization of the molybdate transport system ModABC of Staphylococcus carnosus,” *Arch Microbiol*, vol. 172, no. 2, pp. 109–115, 1999, doi: 10.1007/S002030050747.

[647] Z. Zhang *et al.*, “Nicotine metabolism pathway in bacteria: mechanism, modification, and application,” *Appl Microbiol Biotechnol*, vol. 106, no. 3, pp. 889–904, Feb. 2022, doi: 10.1007/S00253-022-11763-Y/METRICS.

[648] J. F. Jiménez-Bremont *et al.*, “Physiological and molecular implications of plant polyamine metabolism during biotic interactions,” *Front Plant Sci*, vol. 5, no. MAR, p. 81717, Mar. 2014, doi: 10.3389/FPLS.2014.00095/BIBTEX.

[649] K. Paschalidis *et al.*, “The Interplay among Polyamines and Nitrogen in Plant Stress Responses,” *Plants*, vol. 8, no. 9, Sep. 2019, doi: 10.3390/PLANTS8090315.

[650] N. Michel-Reydellet and P. A. Kaminski, “Azorhizobium caulinodans PII and GlnK Proteins Control Nitrogen Fixation and Ammonia Assimilation,” *J Bacteriol*, vol. 181, no. 8, p. 2655, 1999, doi: 10.1128/JB.181.8.2655-2658.1999.

[651] U. Alon, “Network motifs: theory and experimental approaches,” *Nature Reviews Genetics 2007 8:6*, vol. 8, no. 6, pp. 450–461, Jun. 2007, doi: 10.1038/nrg2102.

[652] B. Dombrecht, K. Marchal, J. Vanderleyden, and J. Michiels, “Prediction and overview of the RpoN-regulon in closely related species of the Rhizobiales,” *Genome Biol*, vol. 3, no. 12, p. research0076.1, 2002, doi: 10.1186/GB-2002-3-12-RESEARCH0076.

[653] M. Bush and R. Dixon, “The Role of Bacterial Enhancer Binding Proteins as Specialized Activators of σ54-Dependent Transcription,” *Microbiol Mol Biol Rev*, vol. 76, no. 3, p. 497, Sep. 2012, doi: 10.1128/MMBR.00006-12.

[654] D. K. Berger, F. Narberhaus, and S. Kustu, “The isolated catalytic domain of NIFA, a bacterial enhancer-binding protein, activates transcription in vitro: activation is inhibited by NIFL,” *Proc Natl Acad Sci U S A*, vol. 91, no. 1, pp. 103–107, Jan. 1994, doi: 10.1073/PNAS.91.1.103.

[655] A. Dal Co, M. Ackermann, and S. Van Vliet, “Metabolic activity affects the response of single cells to a nutrient switch in structured populations,” *J R Soc Interface*, vol. 16, no. 156, 2019, doi: 10.1098/RSIF.2019.0182.

[656] J. A. Cole, L. Kohler, J. Hedhli, and Z. Luthey-Schulten, “Spatially-resolved metabolic cooperativity within dense bacterial colonies,” *BMC Syst Biol*, vol. 9, no. 1, pp. 1–17, Mar. 2015, doi: 10.1186/S12918-015-0155-1/FIGURES/6.

[657] I. Novozamsky and V. J. G. Houba, “Determination of free ammonium in plant tissue,” *Netherlands Journal of Agricultural Science*, vol. 25, pp. 26–31, 1977.

[658] C. Frerichs, D. Daum, and A. S. Pacholski, “Ammonia and Ammonium Exposure of Basil (Ocimum basilicum L.) Growing in an Organically Fertilized Peat Substrate and Strategies to Mitigate Related Harmful Impacts on Plant

Growth," *Front Plant Sci*, vol. 10, p. 484665, Feb. 2020, doi: 10.3389/FPLS.2019.01696/BIBTEX.

[659] D. R. Duca and B. R. Glick, "Indole-3-acetic acid biosynthesis and its regulation in plant-associated bacteria," *Appl Microbiol Biotechnol*, vol. 104, no. 20, pp. 8607–8619, Oct. 2020, doi: 10.1007/S00253-020-10869-5.

[660] S. Paque and D. Weijers, "Q&A: Auxin: The plant molecule that influences almost anything," *BMC Biol*, vol. 14, no. 1, pp. 1–5, Aug. 2016, doi: 10.1186/S12915-016-0291-0/FIGURES/2.

[661] E. P. Rodrigues *et al.*, "Identification of genes involved in indole-3-acetic acid biosynthesis by Gluconacetobacter diazotrophicus PAL5 strain using transposon mutagenesis," *Front Microbiol*, vol. 7, no. OCT, pp. 1–12, 2016, doi: 10.3389/fmicb.2016.01572.

[662] J. Kagan, I. Sharon, O. Beja, and J. C. Kuhn, "The tryptophan pathway genes of the Sargasso Sea metagenome: new operon structures and the prevalence of non-operon organization," *Genome Biol*, vol. 9, no. 1, p. R20, Jan. 2008, doi: 10.1186/GB-2008-9-1-R20.

[663] C. H. Jaeger, S. E. Lindow, W. Miller, E. Clark, and M. K. Firestone, "Mapping of sugar and amino acid availability in soil around roots with bacterial sensors of sucrose and tryptophan," *Appl Environ Microbiol*, vol. 65, no. 6, pp. 2685–2690, 1999, doi: 10.1128/AEM.65.6.2685-2690.1999.

[664] E. Imperlini *et al.*, "Effects of indole-3-acetic acid on Sinorhizobium meliloti survival and on symbiotic nitrogen fixation and stem dry weight production," *Appl Microbiol Biotechnol*, vol. 83, no. 4, pp. 727–738, Jun. 2009, doi: 10.1007/S00253-009-1974-Z.

[665] C. Bianco, E. Imperlini, and R. Defez, "Legumes like more IAA," *Plant Signal Behav*, vol. 4, no. 8, p. 763, 2009, doi: 10.4161/PSB.4.8.9166.

[666] A. J. Donati, H. I. Lee, J. H. J. Leveau, and W. S. Chang, "Effects of indole-3-acetic acid on the transcriptional activities and stress tolerance of Bradyrhizobium japonicum," *PLoS One*, vol. 8, no. 10, Oct. 2013, doi: 10.1371/JOURNAL.PONE.0076559.

[667] A. Crozier,', P. Arruda, J. M. Jasmim, A. M. Monteiro, and G. Sandberg4, "Analysis of Indole-3-Acetic Acid and Related Indoles in Culture Medium from Azospirillum lipoferum and Azospirillum brasilense," *Appl Environ Microbiol*, vol. 54, no. 11, p. 2833, Nov. 1988, doi: 10.1128/AEM.54.11.2833-2837.1988.

[668] M. Majda and S. Robert, "The Role of Auxin in Cell Wall Expansion," *Int J Mol Sci*, vol. 19, no. 4, Apr. 2018, doi: 10.3390/IJMS19040951.

[669] M. S. R. de A. da Silva *et al.*, "Stimulatory effects of defective and effective 3-indoleacetic acid-producing bacterial strains on rice in an advanced stage of its vegetative cycle," *Brazilian Journal of Microbiology*, vol. 53, no. 1, pp. 281–288, Mar. 2022, doi: 10.1007/s42770-021-00651-8.

[670] A. Vande Broek, " Spatial-Temporal Colonization Patterns of Azospirillum brasilense on the Wheat Root Surface and Expression of the Bacterial nifH Gene during Association ," *Molecular Plant-Microbe Interactions*, vol. 6, no. 5, p. 592, 1993, doi: 10.1094/MPMI-6-592.

[671] M. K. Chelius and E. W. Triplett, "Immunolocalization of dinitrogenase reductase produced by Klebsiella pneumoniae in association with Zea mays L," *Appl Environ Microbiol*, vol. 66, no. 2, pp. 783–787, Feb. 2000, doi: 10.1128/AEM.66.2.783-787.2000.

[672] T. Mahmood, M. Woitke, H. Gimmler, and W. M. Kaiser, "Sugar exudation by roots of kallar grass [Leptochloa fusca (L.) Kunth] is strongly affected by the nitrogen source," *Planta*, vol. 214, no. 6, pp. 887–894, 2002, doi: 10.1007/S00425-001-0697-X.

[673] T. L. Haskett, R. Karunakaran, M. B. Batista, R. Dixon, and P. S. Poole, "Control of nitrogen fixation and ammonia excretion in Azorhizobium caulinodans," *PLoS Genet*, vol. 18, no. 6, Jun. 2022, doi: 10.1371/journal.pgen.1010276.

[674] E. James, F. Olivares, and J. Sprent, "Infection and Colonization of Sugar Cane and Other Graminaceous Plants by Endophytic Diazotrophs," *CRC Crit Rev Plant Sci*, vol. 50, pp. 77–119, Jan. 1997, doi: 10.1080/07352689891304195.

[675] E. S. Boyd and J. W. Peters, "New insights into the evolutionary history of biological nitrogen fixation," *Front Microbiol*, vol. 4, no. AUG, p. 54696, Aug. 2013, doi: 10.3389/FMICB.2013.00201/BIBTEX.